The Dissertation Committee for Frederick Bynum Closmann Certifies that this is the approved version of the following dissertation:

Oxidation and thermal degradation of methyldiethanolamine/piperazine in CO_2 capture

Committee:

Gary T. Rochelle, Supervisor

John G. Ekerdt

C. Grant Willson

Desmond F. Lawler

Stephen A. Bedell

Oxidation and thermal degradation of methyldiethanolamine/piperazine in CO_2 capture

by

Frederick Bynum Closmann, B.S.; M.S.E.

Dissertation

Presented to the Faculty of the Graduate School of

The University of Texas at Austin

in Partial Fulfillment

of the Requirements

for the Degree of

Doctor of Philosophy

The University of Texas at Austin

December 2011

Dedication

To Kat, Molly and Nero.

Acknowledgements

I would like to thank my wife Kat who has supported me in this endeavor. She has been patient, and provided me with much good advice over the years. Not too many people would understand why their husbands would quit a perfectly good job in a bad economy to seek out higher learning.

My family has been supportive, and my Dad was there when I needed assistance with intractable mathematics problems. Seems like the problems get a little harder with each degree I obtain, yet my Dad still handles them like they are introductory math lessons.

I would like to thank Dr. Rochelle for taking me into the group in 2007. I wasn't really sure what I was getting into, but he knew. He may not have known what he was getting into when he accepted a slightly older student, but it all worked out, thanks largely to his patience.

A big thanks goes out to Stephanie Freeman, many years my junior, but no less wiser. Stephanie was always willing to assist when I needed it, and was a life saver when it came to managing life with Dionex equipment. I was fortunate to start my graduate studies at the same time as Stephanie, and quickly learned to value her assistance.

I would also like to thank a handful of chemical engineering professors who have helped me when I needed it the most. They include Buddie Mullins, who was supportive every step of the way, and encouraged me to seek out assistance within and outside the department from any source necessary. Buddie let me audit his transport class, and I learned how to teach this class if asked one day. I would also like to thank Dr. Sanchez and Dr. Ekerdt, both of whom allowed me to audit their classes. I would like to think I took auditing classes to a new level. Both professors allowed me to sit for exams as an

auditing student. This was an essential part of my "relearning" chemical engineering after many years away.

I would like to thank Stephen Bedell, PhD, of Alstom Power, Inc. for assistance with organic chemistry questions related to solvent degradation. Many of the conclusions regarding degradation pathways and mechanisms were reviewed with Steve before committed to paper. I was fortunate to have access to such a seasoned chemist like Steve.

Oxidation and thermal degradation of methyldiethanolamine/piperazine in CO_2 capture

Frederick Bynum Closmann, Ph.D.

The University of Texas at Austin, 2011

Supervisor: Gary T. Rochelle

The solvent 7 molal (m) methyldiethanolamine (MDEA)/2 m piperazine (PZ) presents an attractive option to industry standard solvents including monoethanolamine (MEA) for carbon dioxide (CO_2) capture in coal-fired power plant flue gas scrubbing applications. The solvent was tested under thermal and oxidizing conditions, including temperature cycling in the Integrated Solvent Degradation Apparatus (ISDA), to measure rates of degradation for comparison to other solvents. Unloaded 7 m MDEA/2 m PZ was generally thermally stable up to 150 °C, exhibiting very low loss rates. However, at a loading of 0.25 mol CO_2/mol alkalinity, loss rates of 0.17 ± 0.21 and 0.24 ± 0.06 mM/hr, respectively, for MDEA and PZ were measured. No amine loss was observed in the unloaded blend. Thermal degradation was modeled as first-order in [$MDEAH^+$], and a universal E_a for amine loss was estimated at 104 kJ/mol.

An oxidative degradation model for 7 m MDEA was developed based on the ISDA data. From the model, the rate of amine loss in 7 m MDEA/2 m PZ was estimated at 1.3 X 10^5 kg/yr, based on a 500 MW power plant and 90% CO_2 capture. In terms of

amine loss, the solvent can be ranked with other cycled solvents from greatest to least as follows: 7 m MDEA>7 m MDEA/2 m PZ>8 m PZ.

Thermal degradation pathways and mechanisms for 7 m MDEA/2 m PZ include S_N2 substitution reactions to form diethanolamine (DEA), methylaminoethanol (MAE), 1-methylpiperazine (1-MPZ), and 1,4-dimethylpiperazine (1,4-DMPZ). The formation of the amino acids bicine and hydroxyethyl sarcosine (HES) has been directly tied to the formation of DEA and MAE, respectively, through oxidation.

As a result of the construction and operation of the ISDA for cycling of solvents from an oxidative reactor to a thermal reactor, several practical findings related to solvent degradation were made. The ISDA results demonstrated that increasing dissolved oxygen in solvents leaving the absorber will increase the rate of oxidation. A simple N_2 gas stripping method was tested and resulted in a reduction to $1/5^{th}$ the high temperature oxidation rate associated with dissolved oxygen present in the higher temperature regions of an absorber/stripper system. The ISDA experiments also demonstrated the need to minimize entrained gas bubbles in absorber/stripper systems to control oxidation. When the ISDA was modified to intercept entrained gas bubbles, the oxidation rate was reduced 2 to 3X.

Table of Contents

List of Tables

List of Figures

Chapter 1 - Introduction

1.1 NEED FOR SCRUBBING TECHNOLOGY

Alkanolamines have seen extensive use in the oil and gas industry for acid gas treatment for many years. Their use for CO_2 scrubbing of flue gases has been identified as a leading approach to curb CO_2 emissions in coal fired power plants in any future effort to mitigate climate change (Rochelle, 2009). Should global agreements and resulting cap and trade legislation force the power generation or petroleum refining industries to curtail CO_2 emissions in the future, the use of amines to scrub CO_2 from flue gases would likely become a key tool in their effort to meet greenhouse gas emissions reduction requirements. The potential exists that a new generation of power plants incorporating flue gas CO_2 absorption/stripping systems will become the industry standard. The possible wide-spread use of this technology presents new challenges to the power generation industry looking for more reliable and cost-effective process designs.

The U.S. Energy Information Administration (EIA) estimated the Demonstrated Reserve Base of coal to be 489 billion short tons (2009). The current U.S. power generation mix includes coal-fired power generation at 45% of total power consumption. The current domestic energy consumption rate (as of 2008) and the Demonstrated Reserve Base equate to a 234 year supply of coal for power generation. With a 0.6% annual increase in energy consumption, that base would be exhausted in 146 years if no new coal reserves are added. Given this large domestic supply of coal and the drive for domestic energy security, the operation of coal-fired power plants for electric power generation in the near and distant future is a reality. This reality of domestic and

worldwide dependence on coal for electric power generation reinforces the need to search for reliable CO_2 scrubbing technologies.

On December 23, 2010, the U.S. Environmental Protection Agency (EPA), at the direction of the administration of President Barack Obama, announced that it had entered into two proposed settlement agreements that will address greenhouse gas (GHG) emissions from certain fossil fuel-fired power plants, electric power generation units, and refineries (EPA Fact Sheet, 2010). The EPA Fact Sheet states that the settlement agreement stipulates that for natural gas, oil and coal-fired electric generating units, these rules would establish new source performance standards (NSPS) for new and modified electric generating units, and emission guidelines for existing electric generating units. The Fact Sheet also states that under the agreement, the EPA would commit to issuing proposed regulations by July 26, 2011, and final regulations by May 26, 2012. Finally, the Fact Sheet states:

> "This schedule provides a measureable and sensible path forward that will allow the agency to address GHG pollution that threatens the health and welfare of Americans, and contributes to climate change. These standards are part of EPA's common-sense approach to addressing GHG from the largest industrial emissions sources."

That announcement did not provide specifics on the level of CO_2 emissions that must be achieved by these industries, but any proposed restrictions on CO_2 emissions will likely be tied to best available control technologies. It can be expected that proposed regulatory emissions limits would be achievable and standardized to the use of the amine scrubbing technology, further securing its place in the market as a key technology in efforts to curb CO_2 emissions and combat climate change.

1.2 Overview of CO_2 Scrubbing Technology

The alkanolamine absorption/stripping process has been used extensively for over 70 years for removal of acid gases in produced gas streams. The basic process (Figure 1.1) was first patented in December 1930 by Robert Roger Bottoms (Bottoms, 1930). That patent utilized the same basic configuration under refinement today for CO_2 absorption from flue gases (Rochelle, 2009). The process includes the absorption of CO_2 into aqueous solutions of either primary (1°), secondary (2°), or tertiary (3°) amines in a column absorber with dumped packing in a reversible reaction. As stated in the Bottoms patent, the reaction of acid gases such as CO_2, H_2S and SO_2 will form products which are soluble in water and whose formation is easily reversed. This "rich" amine is heated to reverse the reaction with the CO_2 in a steam stripper, yielding the acid gases and undestroyed amine.

The currently modeled process looks remarkably similar to the one described in the Bottoms patent. Modifications to the process do not alter the basic approach wherein acid gases such as CO_2 are alternately absorbed into the amine in the packed absorber, and desorbed from the amine in a steam stripper or "regenerator." Certain modifications do improve the overall performance of the process by reducing the energy required to absorb and strip CO_2 from flue gas. Absorber intercooling will improve the absorption of CO_2 into the amine by minimizing the negative impact of an absorber "pinch" by reducing the temperature in the absorber where a temperature bulge is most prominent (Kvamsdal, 2008). Single or two-stage flash configurations have been modeled and pilot tested to reduce the amount of stripping steam needed to desorb CO_2 from the amine (Van Wagener, 2011). The advantage of a two-stage flash configuration is not only to improve energy performance, but to simplify the mechanical requirements of steam stripping, thereby reducing capital requirements of the overall process. Finally, novel

solvents are being continuously tested to identify solvents that are inexpensive, provide excellent energy performance, are resistant to degradation and have low impact on the environment.

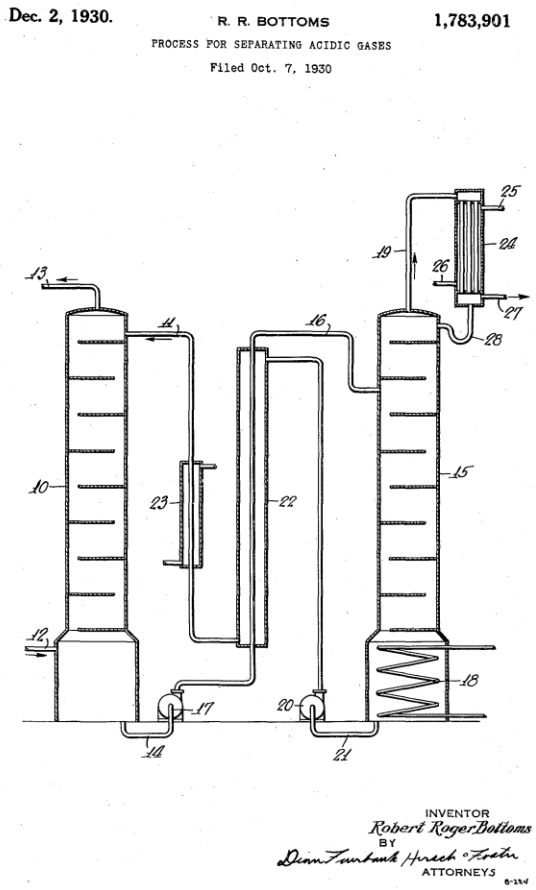

Figure 1.1: Bottoms (1930) absorber/stripper system

1.3 SOLVENT SELECTION

The Bottoms patent provides some detail as to the proper selection of an amine, with the presence of an alcohol group as part of an R-group aliphatic substitution on the nitrogen being an appropriate chemical solvent. In particular, the use of

monoethanolamine (MEA) and diethanolamine (DEA) are mentioned in the patent as appropriate compounds for acid gas scrubbing purposes. In all cases, the patented process utilizes an amine which replaces typical absorbants of the day such as sodium carbonate, providing faster rates and higher capacity to absorb gases, resulting in the absorption of large amounts of acid gas with small amounts of regenerated solvent. The concept of heat integration was incorporated into the Bottoms design, with a heat exchanger for heat removal from the regenerated solvent, and a trim cooler for additional cooling of amine before returning to the absorber. Finally, the basic design includes a condenser for liquids removal including amine from the vapor exiting the top of the regenerator (steam stripper).

Key performance considerations in the selection of an amine solvent for CO_2 capture purposes include CO_2 reaction rate, capture capacity, mass transfer characteristics, degradation resistance, corrosivity and foaming potential. The sum of these operational considerations determines how well a solvent will perform, but in practice, the screening and characterization of solvent degradation potential (oxidative and thermal) has emerged as a critical step in the early stages of solvent selection.

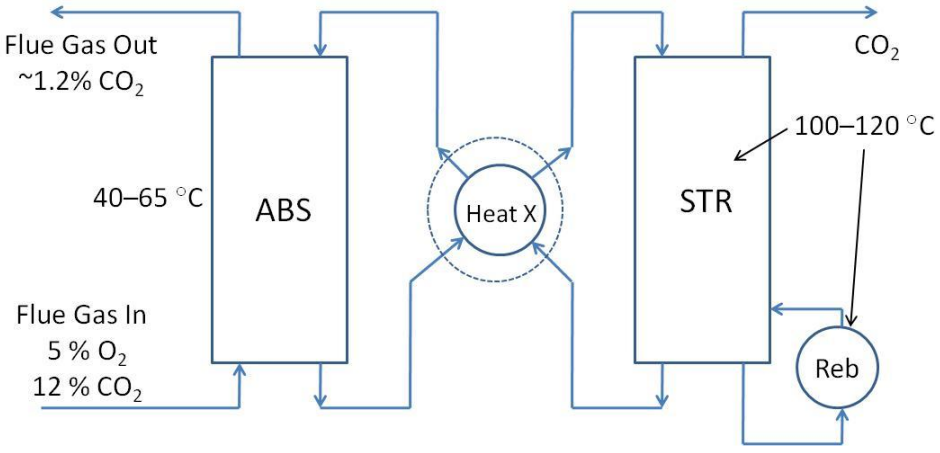

Figure 1.2: Typical absorber/stripper system

Predicting how a solvent will degrade in a system designed for CO_2 capture from flue gas streams requires an understanding of a typical absorber/stripper configuration. Figure 1.2 presents a process flow diagram for an absorber/stripper system intended for CO_2 removal from flue gas. Flue gas enters the absorber with approximately 7.5% O_2, 13.5% CO_2 and a temperature of 60 °C (Fayette Power Plant Unit 3, LCRA, June 2008). The flue gas is counter-currently contacted with the lean amine for CO_2 absorption in the reversible reaction. Absorber design generally includes a hold-up section sized for approximately five minutes of solvent retention time. After passing through a cross exchanger, the CO_2-rich amine enters a steam stripper for reversal of the CO_2 absorption process. Steam stripping increases the amine temperature to 120 °C or greater for desorption and removal of CO_2 for subsequent dehumidification and sequestration. Typical absorber operating conditions for MEA include a temperature of 55 to 60 °C with a potential temperature bulge of up to 74 °C (Kvamsdal and Rochelle, 2008). The steam stripper (regenerator) would be operated at 1 atm, and temperature in the range of 100 to 120 °C (Aaron, and Tsouris, 2007).

Current efforts to reduce the energy requirements of CO_2 scrubbing systems and improve overall performance have included the consideration of novel system configurations and operating conditions including higher stripper temperature (>120 °C) and pressure (>1.5 bar). Additionally, the presence of a high concentration of oxygen in the gas phase provides greater opportunity for dissolution of oxygen into the amine when compared to typical acid gas treatment applications where produced gases are involved. These fundamental operational changes in temperature, pressure and dissolved oxygen content generally result in a harsher environment for the amines, leading to degradation and loss of CO_2 capture capacity.

The prevailing degradation mechanism(s) in the absorber and absorber hold-up follow oxidative pathways, with some oxidation of solvents continuing to occur in the cross-exchanger as dissolved and entrained O_2 is depleted. In contrast, it has been assumed that in the stripper, a high-temperature and oxygen-depleted environment would exist, resulting in chemical degradation processes including disproportionation and polymerization of carbamate structures (Rochelle, 2001); the latter mechanism occurs with amines that form carbamates (primary and secondary). Thermal degradation will occur in the rich amine as it is heated in the cross-exchanger before entering the steam stripper. The extent to which dissolved or entrained oxygen is carried over to the stripper resulting in an oxidative environment at higher temperatures has generally been assumed to be low. Flashing of dissolved oxygen from the solvent at stripper pressures (~1 bar) is likely, leading to low oxygen content in amines passing through the stripper. However, due to a general lack of pilot or full-scale data from flue gas CO_2 capture systems, the extent of entrainment or dissolution of O_2 in these applications is generally unknown; typical acid gas treatment feed gases in the oil and gas industry have less than 1% O_2 (Astarita et al., 1983). Figure 1.3 depicts the locations and types of degradation that are anticipated in a typical absorber/stripper system with cross exchange for heat recovery.

Since the Bottoms patent in 1930, the primary (1°) amine MEA has become the solvent of choice, exhibiting fast reaction kinetics, high CO_2 cyclic capacity, and a high heat of absorption. Its fast reaction with CO_2 is generally due to its formation of an MEA-carbamate. A study performed by the National Energy Technology Laboratory (NETL) (Ramezan, 2007) focused on the use of MEA as a scrubbing solvent for an absorption/stripping retrofit at the AEP Conesville, OH power plant. Assuming a 90% removal of CO_2 from coal-fired power plant flue gas, the study estimated the cost of CO_2 avoided at 89$/ton CO_2. The report cites efficiency improvements in solvent

regeneration and utilized a solvent regeneration energy of 1,550 Btu/lbm-CO_2 versus a value of 2,350 Btu/lbm-CO_2 used in a 2001 study performed by the same authors. Given the relatively low cost of MEA and its availability on the chemical market, MEA has become the solvent against which all others are compared.

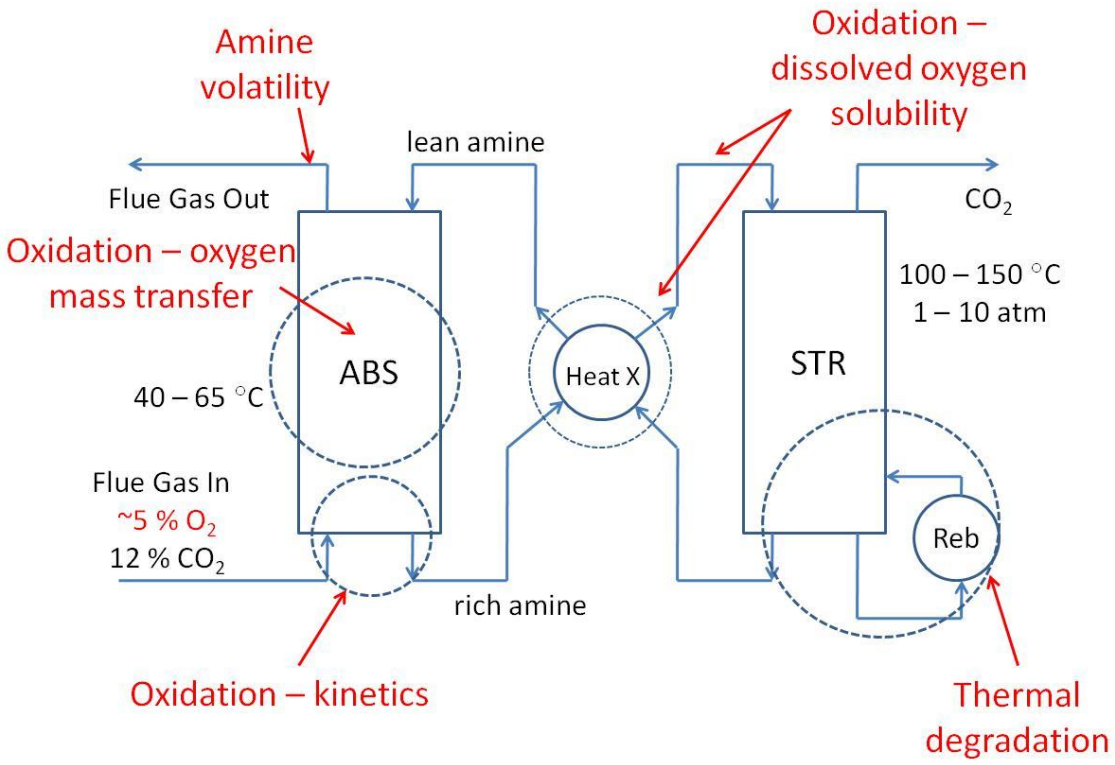

Figure 1.3: Degradation processes in an absorber/stripper

MEA is known to degrade in acid gas field applications. After studying degraded field samples of MEA, Polderman et al. (1955) reported that MEA breaks down at elevated temperatures to form 2-oxazolidone and 1-(2-hydroxyethyl)-2-imidazolidone (HEIA). Davis (2009) reported that MEA thermally degrades with a rate constant of 0.021 wk^{-1} at 120 °C, and will preferentially degrade in blended amine systems. MEA will also degrade oxidatively to form heat stable salts including acetate, formate and

glycolate, as reported by Rooney et al. (1998). Sexton (2009) found that as much as 70 % MEA was lost after ten days when degraded oxidatively at 55 °C. The overall effect of this solvent degradation is to diminish CO_2 absorption capacity.

1.4 SOLVENT BLENDS INCLUDING MDEA/PZ

Because of performance characteristics that limit their effectiveness for CO_2 capture, most amines provide a less-than ideal alternative for CO_2 capture in coal-fired power plant flue gas streams. One approach to solvent selection is the use of blends of solvents already in use (Appl et al., 1990). A common approach is to promote an inexpensive amine with poor absorption characteristics with a fast reacting amine to create a blend with optimized performance in terms of reaction rates (k_g'), cyclic capacity, and degradation resistance. One such blend is the tertiary amine methyldiethanolamine (MDEA) promoted with the fast reacting cyclic diamine piperazine (PZ). When combined at a ratio of 7 m (molal, or mol/kg water) MDEA and 2 m PZ, the faster reacting PZ ($k_{298} \sim 0.2$ gmol/L-s vs. 0.02 - 0.2 gmol/L-s for MDEA) (Rochelle et al., 2001) ensures that the overall rate of reaction of CO_2 in the blend will be as good or better as in single amines already in use (i.e., MEA or MDEA). The presence of 7 m MDEA improves capacity to absorb CO_2 by behaving as a sink for protons through formation of protonated MDEA ($MDEAH^+$). Using AspenPlus, Rochelle (2011) reported that at a lean CO_2 loading of 0.1 mol CO_2/mol alkalinity, the concentration of $MDEAH^+$ exceeds that of PZH^+, indicating that the MDEA actively functions as a proton sink as the solvent is absorbing CO_2 in the absorber. While functioning as a proton sink, the MDEA enables the blend to function with kinetics similar to that of 8 m PZ by allowing the PZ to react with CO_2 and form a carbamate.

The reactions that are used to model the absorption of CO_2 into aqueous amine solutions of MDEA/PZ (Rochelle, 2010) are listed below as 1.1 through 1.5. The first three reactions are kinetically controlled reactions, while the last two are equilibrium reactions.

$$MDEA + CO_2 + H_2O \rightarrow MDEAH^+ + HCO_3^- \quad (1.1)$$

$$PZ + CO_2 + MDEA \rightarrow MDEAH^+ + PZCOO^- \quad (1.2)$$

$$PZCOO^- + CO_2 + MDEA \rightarrow MDEAH^+ + PZ(COO)_2^{2-} \quad (1.3)$$

$$MDEA + PZH^+ \Leftrightarrow MDEAH^+ + PZ \quad (1.4)$$

$$H^+PZCOO^- + MDEA \Leftrightarrow MDEAH^+ + PZCOO^- \quad (1.5)$$

Reaction 1.1 involves the protonation of MDEA in aqueous CO_2-loaded solution to also form bicarbonate (HCO_3^-); this reaction will be in competition with the reaction of PZ with CO_2 to form the carbamate of PZ (PZCOOH). The relatively high pK_{1a} (9.83) (Vahidi et al., 2009) of PZ results in Reaction 1.2 occurring fast as loading occurs, also resulting in the protonatation of MDEA (pK_a ~ 8.56, Hamborg, 2009). The PZ serves to "promote" the overall solvent reaction rate, while MDEA allows the faster reaction resulting in the formation of $PZCOO^-$ to occur without consuming the PZ through protonation. The presence of ~41.5 wt % MDEA provides a large "sink" for protons, making more of the nitrogen sites on PZ available for absorption of CO_2. The presence of this proton sink results in both greater CO_2 cyclic capacity and a high liquid side mass transfer coefficient when compared to commonly used tertiary amines (Table 1.1). At a partial pressure of CO_2 of 5 kPa, the liquid side mass transfer coefficient (k_g') for 7 m MDEA/2 m PZ is comparable to that for 8 m PZ, and much higher than the measured rate for 7 m MEA.

Table 1.1: Common amine performance comparison

Amine	Conc	CO_2 Capacity @ $P_{CO2,lean}$ = 0.5 kPa	kg' @ P_{CO2} = 5 kPa	ΔH_{abs} @ P_{CO2} = 1.5 kPa
Units	m	mol/(kg water + Am)	$\times 10^7$ mol/s*Pa*m^2	kJ/mol
PZ	8	0.79	5.3	70
MDEA/PZ	7/2	0.8	5.2	68
MEA	7	0.47	3.1	82
AMP	4.8	0.96	1.7	73

Despite its performance advantages over non-blend solvents, early degradation studies determined that 7 m MDEA/2 m PZ is only thermally stable up to ~130 °C (Rochelle, 2009), with severe degradation occurring at 135 °C and above in thermal degradation experiments. The protonation of MDEA upon loading with CO_2 has proven to provide an avenue for degradation of the blend, as the reactivity of PZ results in interaction of the two amines at high temperatures.

Thermal degradation prevents the use of optimal absorber/stripper conditions for CO_2 capture in carbon capture and sequestration (CCS) applications. For example, to take full advantage of the blend's relatively high heat of absorption ($\Delta H \sim 68$ kJ/mol), the stripper temperature would typically be 150 °C or greater. There is an energy benefit to creating a CO_2 stream at a higher pressure because steam stripping can be characterized as a thermal swing operation. A greater steam stripper temperature results in a greater pressure for recovered CO_2, reducing the compression requirement for the recovered CO_2 to be sequestered. An additional benefit of the higher stripper operating temperature is a more optimal separation of CO_2 in the recovered stream from water vapor.

1.5 Review of Relevant Literature

The published work on thermal degradation of amines generally relies on batch experimentation using a single autoclave or multiple sample cylinders for rapid screening of multiple solvents, as in use at The University of Texas at Austin (Freeman, 2011). The bulk of that work focused on MEA and PZ, but data relevant to the MDEA/PZ blend has been published. This section reviews the relevant work.

Polderman (1955) studied MEA solutions from acid gas treatment systems to understand why most operations undergo a gradual loss in capture capacity. The authors reported the presence of MEA degradation products including 2-oxazolidone and the urea 1-(2-hydroxyethyl) imidazolidone (HEIA). They also reported that HEIA undergoes hydrolysis to N-(2-hydroxyethyl) ethylenediamine (HEEDA). The HEIA contributes no basicity or acid gas absorbing capacity, whereas hydrolysis of the HEIA to HEEDA restores part of the lost alkalinity and acid gas absorption capacity.

Chakma and Meisen (1988) degraded MDEA in an autoclave for 144 hours at 180 °C and a CO_2 partial pressure of 2.59 MPa, and utilized gas chromatography-mass spectrometry (GC-MS) methods to identify degradation products. In doing so, they reported the presence of several compounds, most notably ethylene glycol, dimethylaminoethanol (DMAE), 1,4-dimethylpiperazine (1,4-DMPZ), N-(hydroxyethyl)methylpiperazine (HEMP), triethanolamine (TEA), and N,N-bis(hydroxyethyl)piperazine (bHEP). They also identified 3-(hydroxyethyl)-2-oxazolidone (HEOD) and N,N,N-tris-(hydroxyethyl)ethylenediamine (THEED) in degraded MDEA samples. Later, the same authors (1997) report that MDEA will degrade at 200 °C to form several products including N,N-dimethylethanamine (DMEA), DMAE, diethanolamine (DEA) and bHEP. Their work suggested that DMAE and TEA were intermediate products under thermal degradation conditions. Using the same GC-

MS techniques, Dawodu and Meisen (1996) reported the presence of many of the same compounds as well as methylaminoethanol (MAE), which they termed a reactive intermediate in the thermal degradation of MDEA/MEA and MDEA/DEA blends.

Polderman (1956), and later Kennard and Meisen (1980), suggested that the pathway for thermal degradation of DEA involved the formation of the oxazolidone of DEA (HEOD), and subsequent formation of bHEP (Figure 1.4). Their work was followed by that of Kim and Sartori (1984) wherein a kinetic model was derived based on degradation studies of CO_2 loaded solutions. The authors reported that the presence of CO_2 in aqueous DEA solutions was necessary to catalyze the degradation process. They reported a similar pathway for degradation of DEA involving the formation of HEOD, which degrades to THEED, then bHEP and other products.

Holub and Critchfield (1998) reported that when they analyzed acid gas field samples where DEA and MDEA had been in service, the primary degradation products they saw were the substituted ethylenediamines including THEED. In one case, they reported that approximately 25% of the original DEA was converted to THEED in only six months of acid gas treatment operation. They also note that, as in laboratory studies of the same solvents, they detected bHEP in field samples, but at far lower concentrations. Critchfield and Jenkins (1999) reported the presence of secondary amines including DEA and MAE, and heat stable salts in degraded MDEA samples from tail gas treating units (TGTUs). The authors also reported the presence of the amino acids bicine and hydroxyethyl sarcosine (HES) in the same degraded samples.

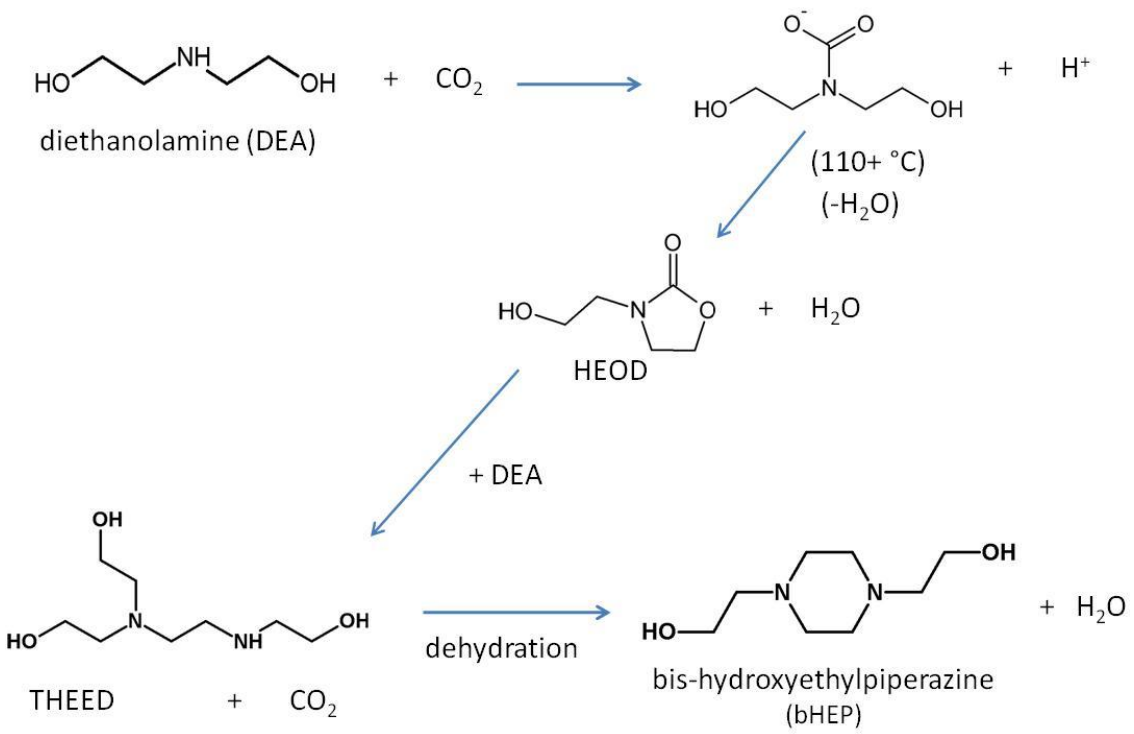

Figure 1.4: Pathway for thermal degradation (Polderman, 1956)

Using GC-MS, Lepaumier et al. (2009) degraded DEA at 140 °C in a 100-mL stainless steel reactor for 15 days and observed that the vast majority of degradation occurred due to ring closure after the DEA forms a carbamate. The DEA-carbamate will undergo ring closure to the oxazolidone structure (HEOD) easier than it will undergo an addition reaction. The authors also note that oxazolidones are very sensitive to nucleophilic reactions and react easily with another amine, resulting in addition products (dimers).

1.5.1 Oxidative Degradation

In 1950, the Girdler Corporation (1950) reported a series of accelerated oxidative screening studies designed to determine the relative resistance of amines and amine blends to oxidative degradation. Based on free amine concentration before and after

oxidation, the authors reported that tertiary amines such as MDEA, as a group, are the most resistant to oxidation, whereas the primary amines (MEA) are the most susceptible to oxidation. The authors also reported that MEA degrades to form appreciable amounts of non-alkaline corrosive products.

In 1956, Hofmeyer et al. reported that up to 40% of basicity loss in MEA can be attributed to oxidative deamination to form ammonia. They also note that the balance of basicity loss is due principally to the tie-up of MEA by other products including formic acid, a carbonyl compound, a high molecular weight polymer, and mono- and di-substituted amides. Blachly and Ravner (1964) reported that when CO_2 free air was passed through 4N MEA at 131 °F (55 °C) for several days, no perceptible degradation occurred. However, the presence of just 1% CO_2 resulted in almost instantaneous degradation, as evidenced by the generation of ammonia and peroxide. The authors also reported that N,N-diethanolglycine (VFS) (bicine) can be used as an anti-oxidant to reduce the peroxide and prevent further degradation of MEA.

Rooney et al. (1998) studied the oxidative degradation of various amines including MDEA, MEA, DEA and DGA, and reported the presence of acetate, formate, and glycolate in each of these solvents after only 7 days. They also reported the presence of DEA in degraded MDEA solutions, but when the same experiments were conducted with a nitrogen blanket, no DEA was detected. The latter observation was noted as evidence of the role oxygen plays in the degradation of MDEA at elevated temperatures. The authors proposed pathways for the sequential oxidative degradation of MEA to end products including formic acid, acetic acid, and oxalic acid (Figure 1.5).

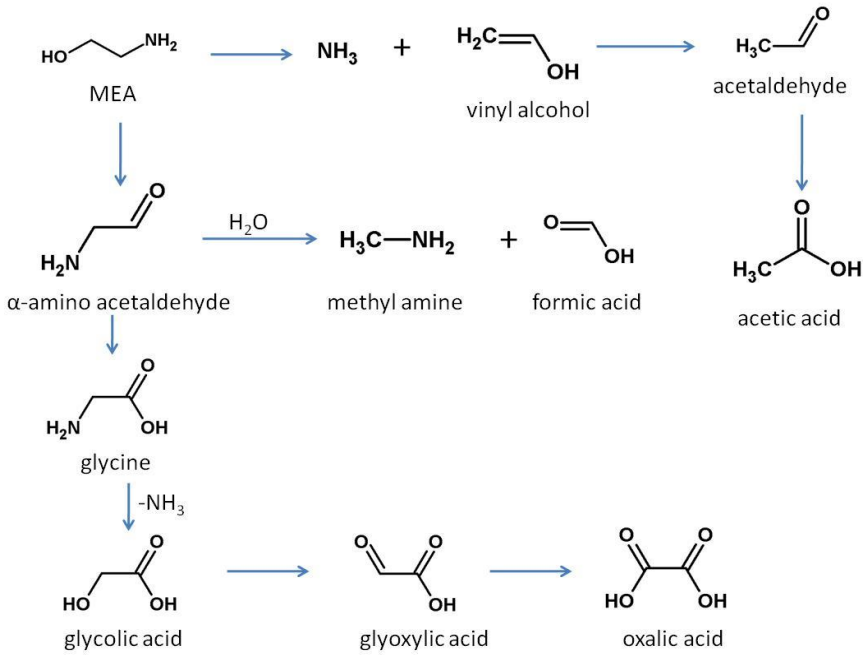

Figure 1.5: Oxidative Pathways of MEA (Rooney, 1998)

Strazisar et al. (2003) attempted to develop a fundamental understanding of the degradation pathways associated with MEA by studying samples collected from the IMC Chemicals facility in Trona CA which uses MEA for scrubbing CO_2. Using GC methods, the authors analyzed process samples including reclaimer bottoms to quantify degradation products. They reported that carbamate dimerization of MEA resulting in oxazolidone formation was not a significant pathway. The authors proposed that an alternate pathway wherein MEA reacts with acetic acid to form N-acetylethanolamine occurs. They also reported that the latter compound reacts with MEA to form an acetamide compound, which may then form a six-membered ring compound by internally eliminating water to form 1-hydroxyethyl-2-piperazinone or 4-hydroxyethyl-2-piperizinone.

CO_2 loaded solutions of 7 m MDEA/2 m PZ (~3.8 M MDEA/1.1 M PZ) with dissolved metals are fairly resistant to oxidative degradation at 55 °C. For example,

when 7 m MDEA/2 m PZ at an initial loading of 0.30 moles CO_2/mole alkalinity and 1 mM Fe^{2+} was degraded in the Low-gas reactor, a formate production rate of 0.011 mM/hr at 55 °C was measured, with very little production of other heat stable salts. This rate is over an order of magnitude lower than that observed at the same conditions for MEA (0.39 mM/hr) (Sexton, 2008). Importantly, very little loss of total alkalinity and total MDEA or PZ concentrations were observed in the oxidatively degraded blend, whereas, at the same conditions, significant loss of 7 m MEA was observed (Figure 1.6). Using the same experimental apparatus, Freeman (2010) attempted to oxidize 10 m PZ with various metals for catalyst, but reported a similarly low production of formate, and very little loss of PZ as evidenced by alkalinity and IC measurement methods.

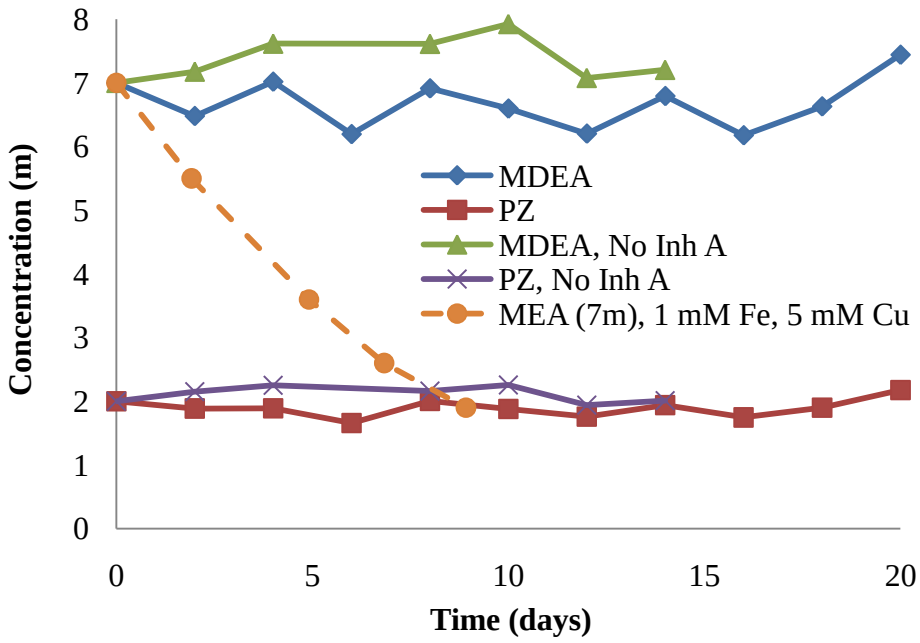

Figure 1.6: Oxidatively degraded solvents; 1 mM Fe^{2+}, 100 mM Inh A, 7 m MEA data from Sexton (2008)

From MEA oxidative degradation studies, Sexton (2008) reported that the formation of heat stable salts can be followed by a reaction with MEA and the production of amides; formamide will be the product of a reaction between formic acid and MEA. Formamide can be converted back to formate through a simple hydrolysis step using 5N NaOH, and quantified through comparison of formate measured in hydrolyzed versus unhydrolyzed samples. This hydrolysis step was performed on 7 m MDEA samples degraded in a solvent cycling apparatus (discussed below) for 60 hours, resulting in the production of as much as 37 mM formamide. When degraded in the Low-gas reactor, approximately 7 mM formamide was observed after 192 hours of degradation. Because amides are not formed from tertiary amines (Morrison and Boyd, 1973), the presence of amides in degraded MDEA is likely the result of amide formation from 1° and 2° amine degradation products in the degraded MDEA, including MEA and DEA.

Davis (2009) reported that blends of solvents tended to thermally degrade the individual solvent components at rates in excess of those measured for the solvents when degraded in non-blend form. For example, Davis reported that in a thermally (135 °C) degraded blend of MEA and PZ, the PZ experienced a 77% loss, whereas as a standalone solvent (8 m), PZ loss was immeasureable. In that same experiment, the MEA loss was 62%, which is approximately the same loss observed when 7 m MEA is degraded at 135 °C, indicating that the degradation processes in the blend allow the participation of the PZ in the degradation mechanisms, but do not accelerate the MEA loss.

Later work (presented in Chapter 7) determined that 7 m MDEA/2 m PZ will oxidatively degrade in an oxidative environment, with accelerated degradation occurring at higher temperatures (>100 °C). A complicating factor in understanding the degradation of the 7 m MDEA/2 m PZ blend is the likelihood that secondary reactions between MDEA and PZ occur in CO_2-loaded solvents once degradation is initiated. For

example, early thermal studies with this solvent determined that PZ participates in the degradation mechanisms once MDEA degrades, leading to the production of a number of degradation compounds indicative of PZ loss.

1.6 Research Objectives

1.6.1 Degradation Mechanisms in MDEA/PZ (Primary Objective)

The degradation behavior of MDEA/PZ presented the motivation for the investigative work completed in fulfillment of this doctoral degree. The primary objective of the research was to develop a fundamental understanding of the degradation mechanisms that occur in 7 m MDEA/2 m PZ when used for CO_2 capture from flue gas feed streams. Emphasis has been placed on 7 m MDEA/2 m PZ because of its commercial use. Degradation products of this solvent are identified, and an understanding of degradation mechanisms is sought so that methods for preventing degradation can be determined. This work determined that 7 m MDEA/2 m PZ is limited to an operating temperature of no more than 117 °C with a simple absorber/stripper configuration. A novel alternative includes the use of a two-stage flash. Under this approach, the first flash vessel is operated at no more than 100 °C, allowing the flashing of dissolved oxygen and some CO_2, while the second vessel is operated at much higher temperatures (~140 °C). This configuration should allow the use of 7 m MDEA/2 m PZ as long as the residence time of solvent in the second flash stage is minimized.

MDEA is known to thermally degrade to DEA and MAE, with further degradation to other products well documented. Secondary reactions with PZ in the MDEA/PZ blend have been confirmed through targeted experiments, and detection of products such as methyl piperazine (1-MPZ), 1,4-DMPZ, and the amino acids bicine and

HES. An understanding of the mechanisms leading to these secondary reactions is important to the understanding of blend degradation. Important degradation mechanisms have been postulated based on the identification of products using MS methods on thermal and cycling degradation samples. These postulated mechanisms have wide applicability to other amine blends including a secondary or tertiary amine blended with a cyclic diamine such as PZ.

1.6.2 Investigating Effects of Solvent Cycling (Secondary Objective)

The subject research focused on the combined effects of oxidative and thermal degradation occurring in cycled solvents. To date, the published data have typically been generated by performing isolated batch experiments wherein the thermal and oxidative degradation effects are studied separately. The research presented in this dissertation entailed the construction and utilization of the Integrated Solvent Degradation Apparatus (ISDA). The ISDA continuously cycles a single charge of solvent through oxidative and thermal degradation conditions to mimic the degradation environment of an absorber/stripper system. The ISDA does not achieve CO_2 absorption and stripping as in a true absorber/stripper configuration. Instead, the ISDA cycles solvents at a preselected CO_2 loading, corresponding to either the rich or lean end of expected conditions.

1.7 SCOPE OF RESEARCH

The scope of this research included the use of already existing methods of degradation to oxidize and thermally degrade 7 m MDEA/2 m PZ. Several experiments were conducted with the Swagelok® thermal cylinders and the Low-gas oxidative degradation apparatus to degrade 7 m MDEA, 8 m PZ, and 7 m MDEA/2 m PZ. The

data from these experiments were used to construct a basic understanding of how the blend degrades.

The scope also included the construction and use of the ISDA for degradation of solvents. The ISDA represented a completely new method for degrading samples, integrating the oxidation effects of the Low-gas reactor with those of the thermal cylinders in a single system. The new data generated from experiments conducted with the ISDA complimented the data from Low-gas and thermal cylinder experiments.

This work also focused on a solvent (7 m MDEA/2 m PZ) for which little degradation data existed. Unlike MEA and DEA which have been studied since the 1950s (Polderman, 1955), 7 m MDEA/2 m PZ has previously only been studied and understood from the standpoint of the individual amines themselves. This work utilized the three degradation methods (Low-gas, thermal cylinders, and the ISDA) to better understand the degradation of 7 m MDEA, 8 m PZ, then the blend. Towards this end, separate experiments with 7 m DEA and 7 m MAE and blends of these 2° amines were performed to clarify the role of intermediate degradation products in the overall degradation of 7 m MDEA/2 m PZ. Finally, this work incorporated the extensive use of high performance liquid chromatography (HPLC) and ion chromatography (IC) coupled to mass spectrometry (MS), and an HPLC amino acid method.

Chapter 2 – Methods

The methods utilized in the work and described in this dissertation fall into two general categories: (1) degradation methods to create representative samples, and (2) analytical methods used to understand the types and rates of degradation of the studied amines. The following discussion covers both of these general method areas as well as basic solvent preparation and sample handling methods in necessary detail.

2.1 Solvent Batch Preparation and CO_2 Loading

Solvents were prepared using gravimetric methods developed at The University of Texas at Austin over the past ten years (Hilliard, 2008, Sexton, 2008, Freeman 2011). Each solvent batch was prepared gravimetrically on a molal (moles/kg water) basis. For example, a 7 m MDEA solution was prepared by adding seven moles of MDEA to one kg water in a large glass jar. The 7 m MDEA/2 m PZ blend was prepared in the same fashion by adding seven moles of MDEA and two moles of PZ to one kg water. When creating the 7 m MDEA/2 m PZ blend, the MDEA was first added to water, followed by the PZ, avoiding concerns related to the aqueous solubility of concentrated PZ (Freeman, 2011) in unloaded solutions at room temperature. The solvents studied create heat upon mixing with water, which is indicative of the heat of mixing of aqueous solutions of amine solvents.

The MDEA utilized for all of the degradation studies discussed in this dissertation was supplied by Huntsman Chemical Company in 5-gallon lots, and was of 95-99.99% purity (Lot No. EO717). IC work determined that impurities in the MDEA included water, and the secondary (2°) amines DEA and MAE. However, based on analyses of

undegraded samples, these 2° amine comprise less than 0.35% of total sample mass. The PZ utilized in these studies was supplied by Sigma Aldrich as dry PZ flakes, and was of >99 % purity. Unless otherwise noted, the water utilized for the creation of all aqueous solutions was deionized using a Millipore Direct-Q UV system at a standard of 18 megaohm*cm (at 25 °C) (referred to as DDI).

The loading of solvents with CO_2 was performed gravimetrically, but on the basis of the amount of moles of CO_2 loaded or reacted, ratioed to the amount of alkalinity in the solvent. In this work, alkalinity is defined by the number of active nitrogen atoms in a molecule of the solvent. For example, the MDEA molecule has one nitrogen atom which protonates upon reaction with CO_2 and, therefore, has one mol of alkalinity per mol of MDEA. In a similar fashion, the PZ molecule has two active nitrogen atoms and its loading is performed based on having two moles of alkalinity per mol of PZ.

The gravimetric loading of solvents was performed in a 1 L Wilmad LabGlass cylindrical column (14 ¾" X 2 ½") with an impinger inserted into the column, reaching approximately ¼ inch from the bottom of the loader. At the bottom of the impinger was mounted a round fritted stone through which fine CO_2 gas bubbles were sparged. The CO_2 was supplied by Matheson TriGas in 1A or 1L steel bottles, and was listed as CP Grade with a purity of 99.6%.

The glass loading column was placed on a bench balance (Mettler Toledo PB8001-S/FACT model) with a precision of 0.1 g, and flexible plastic tubing was connected to an inlet aperture at the top of the loader column through which CO_2 was passed. A second flexible plastic tube or vent line was connected to an outlet at the top of the loader column which allowed gas to escape during the loading process. After the balance was tared, a Swagelok® metering valve was opened allowing CO_2 to pass into the loader column through the flexible inlet line and out through the fritted stone at the

bottom. As the CO_2 passed upward through the column of solvent, it reacted. The reaction of most alkanolamine solvents with CO_2 is exothermic, resulting in the generation of heat as loading proceeds. For this reason, the CO_2 purge rate was regulated through the metering valve to control the reaction rate and minimize solvent heating. The loading of CO_2 into the solvent was monitored by an increase in weight registered on the balance. After reaching the pre-calculated target mass for loading the solvent, the metering valve was closed and a final mass recorded which corresponded to the total mass of CO_2 loaded into the amine. The plastic inlet and vent lines were then removed from the top of the loader column, and the solvent poured into a separate glass storage jar until use in a degradation study.

The loading of 7 m MDEA/2 m PZ resulted in the development of a reaction layer as the CO_2 passed into the zone of solvent immediately surrounding the fritted stone. The reaction zone was prominent in 7 m MDEA/2 m PZ when loaded with this system, indicating the presence of a layer of reacted solvent wherein some of the PZ was in the form of PZ-carbamate ($PZCOO^-$) and some of the MDEA was present in protonated form ($MDEAH^+$), changing the overall liquid density. Figure 2.1 is a plot of the predicted speciation of MDEA, PZ, and CO_2 species in a solution of the blend as the CO_2 loading proceeds from zero to 0.4 mol CO_2/mol alkalinity. This plot was created by the Aspen model of Frailie (2011). Even at a lean loading of 0.1 mol CO_2/mol alkalinity, $PZCOO^-$ and H^+PZCOO^- are both present at concentrations nearly equal to that of free PZ, changing the characteristics of the solvent. In the loader column method described where complete mixing is not occurring, it was expected that a zone of highly loaded solvent develops, which is concentrated in the carbamate and protonated species. However, this zone simply progressed upward in the column of solvent as loading proceeded, and did

not prevent loading to rich conditions (0.25 mol CO_2/mol alkalinity) in the 7 m MDEA/2 m PZ.

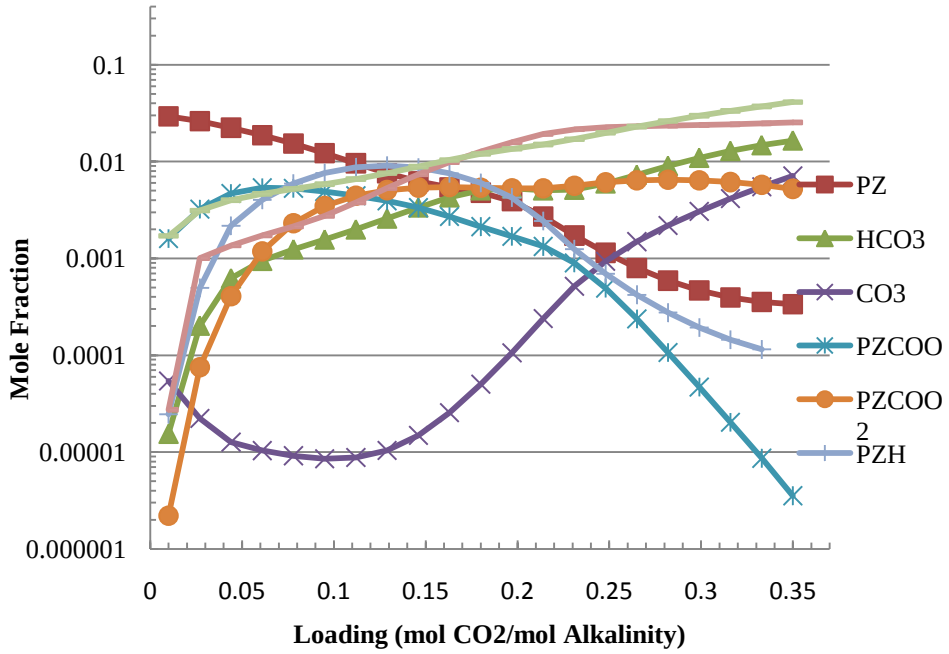

Figure 2.1 Speciation in 7 m MDEA/2 m PZ (Frailie, 2011)

2.2 STANDARD BATCH DEGRADATION METHODS

All three degradation methods utilized in this body of work were of batch design. The first two methods (Swagelok® cylinders and Low-gas reactor) discussed in this section were designed to isolate thermal or oxidative degradation processes in solvents. The third method (ISDA) integrated both thermal and oxidative degradation processes in a single system to more closely approach conditions observed in a scaled-up absorber/stripper system.

2.2.1 Thermal Cylinders

Batch thermal degradation studies were conducted using 316 stainless steel Swagelok® sample cylinders with a nominal internal volume of 10 mL (Figure 2.2). The batch cylinders were charged with solvent(s) and placed in vented forced convection ovens maintained at controlled temperatures for various lengths of time. Several hundred sample cylinders were utilized for the collection of thermally degraded samples. Utilizing numerous cylinders for each experiment allowed the simultaneous and rapid evaluation of solvents at various conditions including initial amine concentration, CO_2 loading, and temperature.

Figure 2.2: Swagelok® Thermal Cylinders

Sample cylinders were constructed in our laboratory with 1/2-inch diameter 316 stainless steel tubing manufactured by Swagelok® (Part No. SS-T8-S-035-8), and compression fitting endcaps (Part No. SS-810-C). The tubes with endcaps are approximately 4.5 inches in length, and as noted, have an approximate capacity of 10 mL. Compression fitting endcaps were permanently set at both ends of each section of tubing using Swagelok® specifications which recommended tightening the endcap 1 and ¼ turn, which set the front and back ferrule of each endcap permanently in-place on the tubing. When the endcap compression fittings were properly sealed, they were rated to

approximately 2,000 psi burst pressure. When solvents were charged to the sample cylinders for each experiment, the endcaps required a ¼ turn past finger tight to ensure a proper seal for each experiment.

Cylinder failure occurred on ~25% of charged cylinders for 7 m MDEA and 7 m MDEA/2 m PZ thermal degradation experiments. No pattern or cause for failure was elucidated throughout the course of these studies with MDEA and the blend. However, cylinder failure occurred at a much lower frequency in experiments conducted with most other solvents studied. The high failure rate may have been due to the evolution of volatile species and resulting high pressures from thermally degraded 7 m MDEA and 7 m MDEA/2 m PZ.

Before solvent was transferred to the sample cylinders, the dry weight of each cylinder + endcaps was weighed. A single endcap was then tightened onto the cylinder ¼ turn past finger tight to ensure proper seal. While held in a vertical position in a vise, approximately 10 mL of solvent was transferred into the Swagelok® cylinders by Eppendorf Research pipette (pipetter). The second endcap (open end) of the Swagelok® cylinder was then sealed with the same method and torque as the first, providing a completely sealed sample. After the sealed sample cylinders were prepared, they were again weighed to determine the starting mass of solvent sample plus cylinder. Upon removal of each cylinder from the ovens following the degradation period at elevated temperature, they were immediately weighed to determine whether solvent loss occurred, and confirm the continued integrity of the cylinder seals. A <10% solvent mass loss standard was generally applied to samples from each experiment to ensure that analytical results were not skewed by preferential loss of volatile constituents.

Placing 10 mL of solvent into each Swagelok® cylinder allowed for less than 1 mL of headspace in each cylinder, minimizing the effects of headspace gases dissolving

into the solvent during the thermal degradation process. However, in Thermal No. 13, samples were transferred into cylinders and the cylinders sealed under an N_2 gas blanket inside a glove bag. The latter experiment was intended to create an inert headspace and eliminate the effect of having small amounts of oxygen available to the solvent as it thermally degraded.

After being weighed, the newly charged cylinders were placed in forced convection ovens for sample degradation. Cylinders were typically removed from the ovens for each sample series at one day, three days, seven days, fourteen days, and greater time intervals to ensure collection of adequate analytical data during the initial period of degradation, while also providing data at greater times to ensure that long-term solvent resistance to thermal degradation was understood. This sample scheme allowed evaluation of initial degradation rates, rate constants, and long-term degradation trends for each data series.

A typical thermal degradation experiment entailed the use of several (>6) sample cylinders charged with solvent for each series studied. For example, in Thermal No. 16, sample cylinders were charged with 7 m MDEA/2 m PZ at three different loadings (0.0, 0.1 and 0.25 mol CO_2/mol alk), and placed in forced convection ovens maintained at three different temperatures (120, 135, and 150 °C), providing a total of nine solvent series. With a minimum of eight cylinders utilized in each series, Thermal No. 16 utilized over 70 sample cylinders. Individual sample cylinders for each series were removed over time, and the cylinders were opened so that the samples could be recovered for subsequent analyses. For some series, cylinder failure occurred to the extent that only a few samples were obtained.

Upon opening the cylinders, the liquid solvent was poured directly into borosilicate glass vials for preservation, and diluted for analyses. Sample dilution was

typically performed within 24 hours of opening the sample cylinder, but in some cases to accommodate work flow, either the sample was not diluted immediately upon opening, or the Swagelok® cylinder was left unopened for a period of days or weeks at room temperature until a sufficient number had accumulated. In the latter case, the cylinders were opened, and the samples were recovered and diluted at one time to ensure consistency in results. Subsequent analyses were performed as described later in this chapter. The Swagelok® cylinders were cleaned between each use with a detergent soap, scrub brush and distilled water. Each cylinder was rinsed a minimum of three times with distilled water before being placed in a 100 °C oven for drying and reuse.

2.2.2 Low-gas Oxidative Reactor

The oxidative degradation of solvents was studied using a jacketed glass reactor with a nominal working volume of ~375 mL (Figure 2.3). This system was utilized extensively by Sexton (2008) and Freeman (2011), both of whom provide thorough descriptions of the system. Basic dimensions included an internal diameter of 80 mm and a height of 160 mm. The reactor and ancillary equipment were situated in a fume hood for health and safety purposes. Water was circulated through the outside sealed jacket with a Lauda E100 water bath to maintain temperature control of the solvent charge on the inside of the low-gas reactor. In these studies, a solvent temperature of either 55 or 70 °C was maintained over the course of the experiments. The Low-gas reactor, therefore, isolated low temperature oxidative degradation effects in the solvents.

A rubber stopper was placed in the open top of the reactor, through which an impeller shaft and purge gas line were inserted. The impeller shaft had a 5.5-cm diameter four-point impeller blade which reached approximately ½-inch off the reactor bottom.

The impeller was turned at ~1,440 rpm for the duration of the low-gas experiments by a ThermoFisher Steadystir analog stir motor assembly.

Figure 2.3: Low-gas reactor with Teflon lid (TOR)

A 100 mL/min gas was fed to the headspace of the low-gas reactor above the liquid level. The purge gas was a mixture of oxygen and CO_2 at a partial pressure of CO_2 selected to match the equilibrium condition of CO_2 in the solvent at 55 °C. For example, for 7 m MDEA at 55 °C, the purge gas was a mixture of 98% O_2/2% CO_2. Gases were

provided to the low-gas reactor by either using a pre-mixed gas blend purchased from Matheson TriGas, or mixing pure oxygen and CO_2 with Brooks 5850E mass flow controllers connected to a four-channel Brooks 5878 central control box. The mixed gas was passed through a water saturator vessel with fritted stone before being fed to the headspace of the reactor. The saturator was immersed in a water bath maintained at approximately the same temperature as the oxidative reactor (55 ± 3 °C). The saturation step was necessary to minimize the dehydration of the solvent over the course of the experiment.

Five-mL samples were collected from the reactor vessel on a daily basis using a pipetter, and placed directly into Fisher 4-Dr borosilicate glass vials (4-Dr vials). The level of liquid solvent in the reactor was noted at the start of the experiment, and after the daily shut-down of the impeller shaft to allow sample collection. A drop in the liquid level was interpreted as a loss in water from the solvent. DDI was added to make-up the liquid volume and bring the liquid level back to the last level noted on the outside of the reactor. The impeller shaft was then turned for approximately ten seconds to ensure complete mixing of the make-up water, and a sample was collected with a fresh disposable plastic tip and pipetter. Immediately after sample collection, a new mark was placed on the outside of the reactor vessel noting the new liquid level; the slight liquid level drop over the course of the experiment was due to the removal of solvent samples. To minimize effects associated with a drop in liquid level, samples were collected every other day after the first four days of most experiments. Finally, the liquid level in the saturator dropped over the course of each experiment, and was routinely refilled with DDI, and the amount of water added noted for water balance purposes.

A modified Low-gas oxidative reactor system was developed (Freeman, 2011) and utilized in the last four Low-gas experiments discussed in this dissertation (OD-6

through OD-9). In these experiments, a jacketed glass reactor vessel was constructed by UT's glass fabrication facility located in the Chemistry Department. Freeman (2011) provides a full discussion of those reactor construction specifications. The main element of this modified reactor is the use of a Teflon® (Polytetrafluorethylene) (PTFE) lid with pre-drilled NPT fitting apertures in place of the black rubber stopper lid. The PTFE lid was fitted to the reactor with a flange connection and O-ring seal. This design achieved better water balance performance over the course of each experiment when compared to the original low-gas oxidative reactor design. This reactor design is referred to as the Teflon Oxidative Reactor (TOR).

2.3 THE INTEGRATED SOLVENT DEGRADATION APPARATUS (ISDA)

The degradation methods described in section 2.2 generally isolate oxidative or thermal degradation behavior. Solvents were also degraded in the Integrated Solvent Degradation Apparatus (ISDA) (Figure 2.4), which alternately and continuously exposed solvents to oxidative and thermal degradation conditions in a single system. This is a new apparatus and method designed and constructed for this research. The ISDA mimicked degradation conditions observed in an absorber/stripper configuration designed for CO_2 capture. The ISDA allowed the evaluation of carryover of dissolved oxygen into the thermal reactor on overall degradation rates. The products of oxidative degradation were exposed to high temperature conditions in the thermal reactor, while the products of thermal degradation in the thermal reactor were exposed to dissolved oxygen as a result of being cycled through the oxidative reactor.

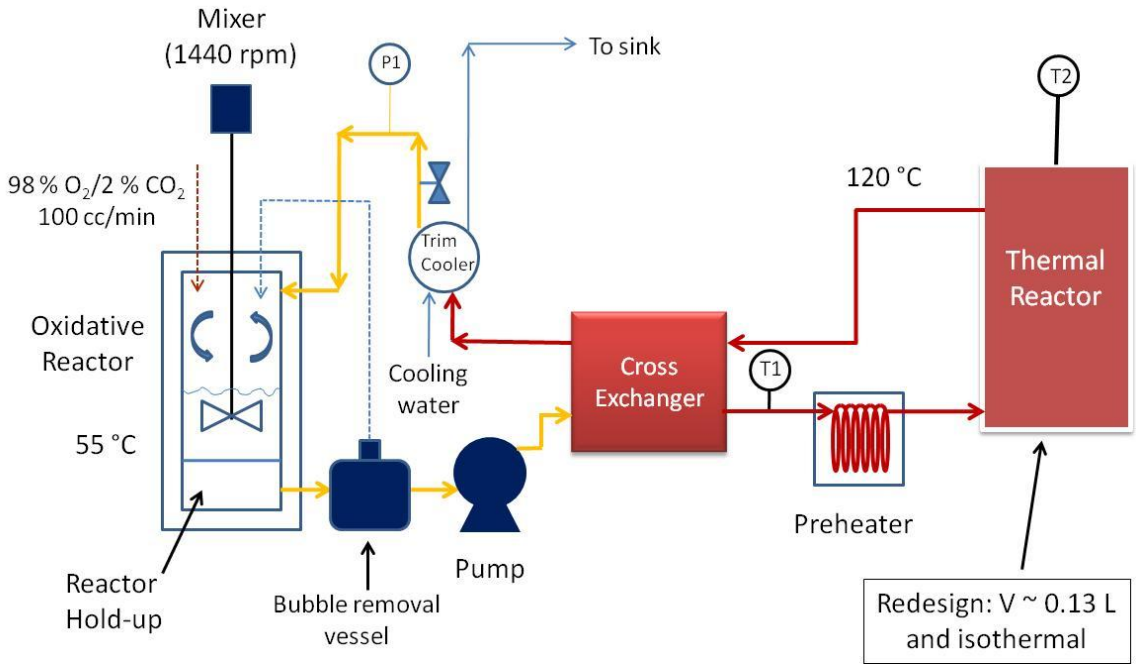

Figure 2.4: The Integrated Solvent Degradation Apparatus (ISDA)

2.3.1 System Description

This section describes the ISDA as it currently exists with minor exceptions. The ISDA is a circulating batch system with the three main elements typically expected in a true absorber/stripper system: (1) an oxidative reactor which mimics conditions observed in absorber packing, (2) a cross exchanger for heat integration, and (3) a thermal reactor which mimics conditions observed in a steam stripper. Nominal volumes for the oxidative and thermal reactors are 0.750 and 1.12 L, respectively. Solvents are generally circulated at 200 mL/min, providing approximate residence times of 3.75 and 6.5 minutes, respectively, for the oxidative and thermal reactors. In November 2010, the thermal reactor was redesigned to be $1/9^{th}$ of the original reactor volume (0.13 L) in order to ensure that experiments were conducted in a kinetically limited fashion. This change is discussed in detail in Chapters 3 and 5.

The major components for the ISDA are listed in Table 2.1, including manufacturer, part number, and basic specifications. Unless otherwise noted, materials of construction consist of 316 stainless steel tubing, plastic tubing (NYLO-SEAL Nylon 11, 44N-1/4"), and glass. All transfer tubing for pressurized and/or hot solvent was ¼-inch Swagelok® 316 stainless steel. All major and minor components of the ISDA are wrapped in thermal insulation designed for domestic hot water heater service and purchased at a local Home Depot store. This insulation is necessary to prevent heat losses to the surroundings, and allows the ISDA to achieve thermal reactor temperatures of 130 °C in select experiments.

Table 2.1: Major components in the ISDA

Equipment	Type	Manufacturer	Model	Specifications
Pump	Positive Displacement	Cole-Parmer	Micropump, No. 75211	50-5,000 mL/min
Cross-Exchanger	Tube-in-tube	Exergy	No. 00413	316 SS, 240-inch length
Pre-heaters	Coiled tube	UT ChE Fabrication	-	316 SS, 40 and 70 inch lengths
Trim Cooler	Tube-in-tube	Exergy	No. 00517-2	316 SS, 60-inch length
Oxidative Reactor	CSTR	UT Glass Fab Shop	-	0.4 L Top Section/0.33 L Bottom Section
Thermal Reactor	Tube-in-tube Heat-X	UT ChE Fabrication	-	316 SS, 1.12 L
Tubing	316 SS	Swagelok®	-	1/4-inch OD
Heat Baths	Water/Oil Circulation	Lauda	E100, E200, and E300	Up to 2.25 kW

2.3.1.1 ISDA Oxidative Reactor

The oxidative reactor of the ISDA was constructed by UT's glass fabrication facility with similar internal dimensions as the Low-gas oxidative reactor so that the overall gas-liquid mass transfer characteristics of both reactors would be similar. The

ISDA oxidative reactor is constructed of 80-mm inner diameter glass tubing, and has a total volume of 750 mL. Solvents pass through a top section of approximately 165 mm in height, through 3 mm diameter holes in a fused glass plate, and into the bottom section of the reactor which is intended to mimic the hold-up section of a typical absorber. The top section has a working volume of approximately 400 mL, resembling the Low-gas reactor. When in operation, the bottom section has a volume of 330 mL and no void space. The separator plate between the top and bottom sections is intended to prevent agitation energy from reaching the solvent after it has passed into the hold-up region (bottom) of the reactor to minimize bubble entrainment effects.

The oxidative reactor temperature is maintained at 55 °C for the duration of each cycling experiment through circulation of dimethyl silicone oil (DMSO) supplied by Krayden (Denver, CO) on the jacket side of the reactor. The top section of the reactor is fitted with a rubber stopper with several apertures for accessing the actively stirred reactor section. A K-type Omega Engineering thermowell is inserted through one of these apertures, and is immersed a minimum of two inches into the solvent for accurate temperature acquisition during each experiment. Temperature is acquired on an Omega Engineering Model No. 199 multi-channel digital readout device. The top section of the oxidative reactor is exposed to the atmosphere, as the apertures are not sealed from the surrounding environment. Importantly, this is the only point in the entire cycling system which is exposed to atmospheric pressure.

A four-point impeller blade (5.5 cm diameter) at the end of a 34.5-cm long impeller shaft is stirred at 1,440 rpm by a ThermoFisher Steadystir analog stir motor assembly. This high agitation rate provides a high level of oxygen mass transfer by vortexing the solution. Exceptions to that stir rate were studied using 7 m MDEA (experiments C-4, C-5 and C-9) to understand the effects of stir rate on bubble

entrainment and mass transfer limitations in the ISDA. Those experiments elucidated the role of mass transfer of oxygen into the solvent through increased bubble entrainment, as discussed in Chapter 3.

A 100 mL/min purge gas is introduced to the top section of the oxidative reactor by inserting a ¼-inch plastic line through a hole in the rubber stopper which is fitted to the top of the oxidative reactor. The plastic line is inserted to a depth of approximately one inch from the inside top of the rubber stopper, but at least one inch from the surface of the vortexing liquid. The possibility of short-circuiting of liquid from the inlet line to the reactor headspace outlet at the annular region around the stir shaft exists. However, its impact is assumed to be minimal due to the well mixed gas headspace environment resulting from the large liquid surface vortex (~2 inches). The purge gas is typically a 98% O_2/2% CO_2 mixture. As described in Section 2.2, cycling experiments are designed to match the partial pressure of CO_2 in the purge gas to that partial pressure expected from the equilibrium solubility condition based on initial solvent loading in each experiment. For example, for an initial loading of 0.14 mol CO_2/mol alkalinity in 7 m MDEA/2 m PZ, the expected partial pressure of CO_2 in the headspace gas is 2% (2 kPa) CO_2, with the remainder of the gas consisting of O_2 (98 kPa or 98%). The proper gas mixture is created by either using a pre-mixed gas blend purchased from Matheson TriGas, or mixing pure O_2 and CO_2 with Brooks 5850E mass flow controllers and a Brooks 5878 central control box. The CO_2 and O_2 gases are supplied by Matheson TriGas and were of 99.6 and 99.5% purity, respectively. As with the low-gas reactor system, the 100 mL/min purge gas is passed through a vertical glass water saturator before passing into the headspace of the oxidative reactor. The saturator is immersed in a water bath maintained at approximately the same temperature as the oxidative reactor (55

± 3 °C). The saturator minimizes the dehydration of the solvent due to the 100 cc/min purge gas passing through the headspace of the oxidative reactor.

The composition of the headspace purge gas is changed to match the initial CO_2 solubility condition of each solvent being studied at 55 °C, and to study oxidative effects on cycled solvents. In two of the ISDA experiments, the purge gas mixture was 98% air/2% CO_2 gas, and in two other experiments, the mixture was 98% N_2/2% CO_2. The air/CO_2 mixture tested degradation when the O_2 content of the purge gas was approximately 20% overall, while the N_2/CO_2 purge gas experiments tested non-oxidative degradation effects including thermal degradation in cycled solvents. At a stir rate of 1,440 rpm with 98% O_2/2% CO_2 supplied as purge gas, it was estimated using Henry's Law that the dissolved oxygen mole fraction was ~1.6 x 10^{-5} mol O_2/mole solvent in 7 m MDEA as it exited the oxidative reactor at 55 °C (Perry's Handbook, 5th Ed). The purge gas flow rate is regulated in all experiments to 100 mL/min with a Cole-Parmer rotameter calibrated with N_2 gas.

Of note, the reason for utilizing a high O_2 purge gas composition is to accelerate oxidative degradation in the solvents studied. Using a solvent more closely resembling the composition of flue gas with respect to O_2 would be of very little value due to the long times necessary to achieve initial degradation rates, and overall useful results in terms of reaction pathways and mechanisms. Accelerating the oxidative degradation processes allows the implementation of a variety of solvents at a variety of conditions.

One other adaptation to the ISDA is the use of a tube specially constructed by the glass blower in the Chemistry Department at Welch Hall for the collection of condensate samples from the headspace of the oxidative reactor (Figure 2.5). The condensate tube design consists of ¼-inch S-shaped glass tube for saturated gases to pass through, allowing moisture and volatile species to condense and collect in a vertical glass shaft

which is enclosed at the bottom with an angled stopcock constructed of inert material. The tube is inserted into a hole in the rubber stopper sealing the top of the oxidative reactor, and during the course of the experiment, the 100 cc/min purge gas supplied to the headspace of the reactor forces saturated gas out the condensate tubing as well as other fitting openings (annular region around stir shaft). The volatile species and water vapor condense in the glass tubing which is nominally at ambient temperature, and collect in the vertical shaft. After sufficient condensate has collected in the vessel, a 4-Dr vial is placed under the stopcock and the stopcock is opened, releasing the condensate into the vial. Condensate samples are collected over the course of the experiment for subsequent analyses for degradation products.

Figure 2.5: Oxidative reactor condensate collection tube

2.3.1.2 Bubble Removal Vessel

Solvent is pumped from the oxidative reactor into a glass bubble removal vessel for interception and removal of entrained gas bubbles before passing through the pump and being transferred to the hotter section of the cycling system. This bubble removal vessel was installed as a modification to the ISDA shortly after its initial construction. From experiment C-6 through C-34, the bubble removal vessel described herein was a permanent part of the overall reactor system. The bubble removal system consists of a glass jar of 4 inches in diameter through which the solvent makes a single pass. The vessel contains a 1¼-inch layer of Pro-Pak Protruded Metal Distillation Packing (¼-inch diameter) through which the solvent passes; solvent enters at approximately ¾ inch off the bottom of the vessel. The solvent exits the vessel at a height of 2 and 3/4 inches from the bottom and is plumbed directly into the suction side of the Cole-Parmer pump. The glass jar is fitted with a thermoplastic polyester screw cap through which is bored a Swagelok® ¼-inch plastic compression fitting and line. This line is connected at the other end to the rubber stopper in the ISDA oxidative reactor to conduct gases being released from solvent in the bubble removal vessel back into the headspace of the oxidative reactor. This vent line is intended to minimize water vapor losses from the solvent at this point in the system. A typical experiment is conducted with a liquid height of approximately 3 inches and a flow rate of ~200 mL/min, providing a liquid residence time of approximately 3 minutes.

2.3.1.3 Cole-Parmer Variable Speed Pump

CO_2-loaded amine is continuously pumped from the bubble removal vessel through a Cole-Parmer variable speed gear pump (Micropump, Part No. 75211-10), and mounted magnetic pump head. This pump is rated to achieve pump rates of 2.5 to 5,450 mL/min, and a maximum head pressure of ~30 psig; all experimental work was

conducted at a solvent flow rate of 175-275 mL/min. The Micropump utilizes a Cole-Parmer A-mount pump head, with all wetted parts constructed of PTFE. The pump head connects to the front of the pump magnetic shaft mechanism with two screws and can be easily changed. The inlet and outlet ports to the pump head were 1/4-inch NPT fittings into which Swagelok® NPT-to-compression fitting adapters were mounted.

2.3.1.4 Cross Heat Exchanger

After exiting the pump, the solvent is passed through the shell side of a 316 stainless steel ¼-inch inner tubing diameter, 240-inch long tube-in-tube heat exchanger manufactured by Exergy (Part No. 00413) (Garden City, New York) to take on heat from solvent passing counter-currently from the thermal reactor. The solvent then makes a single pass through a series of two pre-heaters consisting of coiled 316 stainless steel tubing immersed in Lauda oil baths (Bath No.1: Lauda E200, and Bath No.2: Lauda E300) filled with DMSO. The first coil is approximately 44 inches in length, while the second coil is approximately 70 inches in length. The solvent then enters the internal section of a thermal reactor, which functions as a stainless steel tube-in-tube heat exchanger.

2.3.1.5 Thermal Reactor

The thermal reactor was fabricated in the Chemical Engineering shop on first floor of the Chemical and Petroleum Engineering (CPE) Building by Department of Chemical Engineering shop technicians. Materials were provided by Arthur Valve and Fittings (Swagelok® fittings) and Westbrook Metals of Austin, Texas (large diameter metal tubing). The outer tube of the original thermal reactor is fabricated of 4-inch diameter 304 stainless steel tubing and end sections; the outer tubing only contacts DMSO, allowing the use of 304 stainless steel instead of 316 stainless steel. The initial

design for the thermal reactor in the ISDA was a vertical 1.12 L tube-in-tube single-pass heat exchanger. Experiments C-1 through C-24 were conducted with this original thermal reactor design. The solvent passed through the internal tube of the reactor, while DMSO passed on the shell side. Liquids passed co-currently upward in the thermal reactor to ensure fully flooded flow. The external surface of this thermal reactor was completely covered in thermal insulation. This insulation was necessary to prevent heat losses to the surroundings. The redesigned thermal reactor has a volume of 0.13 L, and consists of ¾-inch Swagelok® stainless steel tubing (SS-1210-9) of approximately 21.5 inches in length, configured in a U-shape to allow immersion in DMSO in a Lauda E-300 heating bath for heat transfer into the solvent. Unlike the initial design, the redesigned thermal reactor is not a shell-in-tube design, but instead, a single stainless steel tube immersed in oil. The outer surface of this thermal reactor is in direct contact with the surrounding heating bath oil, and solvents make a single pass through the tube.

Temperature acquisition at the thermal reactor was achieved in the initial design through the insertion of an Omega Engineering K-type 12-inch long thermowell through a Swagelok ¼-inch bore-through fitting installed at the top of the reactor. This thermowell was inserted into the thermal reactor exit region and achieved bulk liquid temperature acquisition of the solvent at its exit point from the reactor. In the redesigned thermal reactor, two Omega Engineering K-type 6-inch long thermowells (Part No. KQSS-14U-6) are installed at the entry and exit to the reactor to provide accurate temperature acquisition. All temperatures are acquired on an Omega Engineering Model 199 multi-channel digital readout device. In the original thermal reactor design, inlet solvent bulk temperatures were not acquired during experiments. However, based on data acquired from the redesigned thermal reactor, it was generally believed that the solvent at the inlet was within five °C of the exit temperature.

The amine exits the thermal reactor and passes back through the tube side of the cross-exchanger where it provides heat to the amine passing counter-currently on the shell side. The amine is then passed through a heat exchanger (Exergy, Part No. 00517-2) installed for trim cooling before exiting through a back-pressure valve (¼-inch metering valve) to atmospheric pressure. At this point, the solvent is returned to the oxidative reactor through a ¼-inch aperture in the wall of the glass reactor located above the liquid surface.

2.3.1.6 Oxidation-Reduction Potential Sampling Loops

The ISDA was modified to include two oxidation-reduction potential (ORP) sampling loops, with one loop located just downstream of the discharge side of the pump (Point 1), and one loop located on the solvent return line downstream of the cross heat exchanger before the solvent is flashed to atmospheric pressure (Point 2); both of these locations were pressurized points of the system. These lines were installed with shut-in valves and a Swagelok® tee with reducers to control solvents. The tee included a ¾-inch NPT threaded opening to allow insertion of an ORP probe at either location. A Hanna Instruments platinum ORP probe (HI No. 6200405) designed for industrial applications was purchased for this application, and measurements were attempted. The probe is designed for continuous service at pressures of 87 psig and temperatures of 100 °C, and with a chemical resistant PVDF body.

The mechanical design of the system allowed for the same probe to be utilized for measurement at both points in immediate succession in order to ensure that the probe's reference point was the same. The intention was to measure and compare the ORP of solvents while cycling to assess whether the prevailing degradation mechanisms occurring in the solvent immediately after being oxygenated (Point 1) were characterized

by significantly higher ORP than after experiencing high temperatures in the thermal reactor (Point 2). This experimental approach was intended to confirm/refute that oxidative conditions prevailed in solvent in the absorber, absorber hold-up section, and heat exchanger, while reducing conditions prevailed in the stripper and piping leaving the stripper where the solvent is the hottest.

The lack of success in making ORP measurements was primarily due to the inability to achieve a good seal at the NPT fitting with the ORP probe. Because Points 1 and 2 are both pressurized, the poor seal resulted in excessive solvent loss in the system while trying to measure ORP. Further, it was unclear whether the current experimental equipment design would achieve fully flooded flow around the ORP probe, which was viewed as a requirement to get accurate measurements at either location.

2.3.2 Leak/Pressure test of the ISDA

Before conducting any cycling experiments with the ISDA, the system fittings were checked for tightness to prevent leakage; all compression fittings were installed, and the ferrules set according to Swagelok® guidelines (1/4 turn past hand-tight). The system was then pressure tested. The system was filled with tap water with the pump. The back-pressure valve was then shut with the pump running, allowing pressure to build up to 100+ psig in the pressurized part of the system. In this initial pressure test, the NPT fittings on the thermal reactor failed at pressures above 30 psig, prompting the welding of these fittings onto the thermal reactor. After re-installing the thermal reactor with the fittings welded in-place, the pressure test procedure with water was repeated, and the system held pressure up to 120 psig.

After conducting experiments C-1 through C-9, the system fittings were retightened to ensure that liquid losses when cycling solvents were not occurring due to

volatile or liquid losses at the pressurized fittings. The system was then pressure tested by two methods. In the first pressure test, 80 psig service air plumbed to the fume hood was connected to system and the back pressure valve was shut. The system was pressurized to 41 psig for a period of 5 minutes during which the pressure dropped to 40 psig. The pressure test was then repeated on the thermal reactor section of the system at 52 psig in order to isolate potential leaks. Several fittings were then tightened, and the system was filled with water and pressurized to 90 psig by applying service air. After 1 and ½ hours, the system pressure had dropped only slightly (87 psig). No visual evidence of leaks was noted at that time, and the system was readied for the next cycling experiment.

2.3.3 ISDA Operations

This section describes the start-up, operation, shut-down, and cleaning of the ISDA for a typical experiment where a solvent is cycled from 55 °C in the oxidative reactor to 120 °C in the thermal reactor.

2.3.3.1 ISDA Start-up

Start-up of the ISDA when cycling a solvent from 55 to 120 °C requires ½ day to achieve steady state conditions. The following description of system start-up is not to be interpreted as the only method for safely starting an experiment in the ISDA. However, the approach is considered the most tested and reliable method for achieving a safe and time-efficient start-up, while at the same time collecting accurate degradation data from the system.

All piping should be properly plumbed in the system, with the exception of the return line from the flash valve to the oxidative reactor, the gas purge line exiting the water saturator, and the headspace gas return line exiting the bubble removal vessel. The

solvent return line should be disconnected from the oxidative reactor to allow the removal of the initial volume (~250 mL) of solvent from the system during start-up. This return line is to be connected to the oxidative reactor following the charging of solvent to the system, and the flushing of the initial volume of solvent as described below. The black rubber stopper lid to the oxidative reactor will be installed towards the end of the start-up process, as will all appurtenances accessing the oxidative reactor through the rubber stopper. Finally, before solvent is transferred into the system for start-up, the 1/4-inch Swagelok® compression fitting plug is to be tightened onto the drain tee in the transfer line to the thermal reactor.

Start-up steps:

1) The back pressure valve located in the vertical ¼-inch stainless steel liquid line returning solvent to the oxidative reactor on the downstream side of the heat cross exchanger should be turned counter-clockwise until wide open,
2) Approximately 500 mL of fresh solvent is poured directly into the bubble removal,
3) Approximately 500 mL of fresh solvent is poured directly into the oxidative reactor, and the solvent is then stirred with a steel hand-held spatula to break a vapor lock created in the bottom section of the oxidative reactor until the bottom section has no gas pockets,
4) The pump should be turned on to initiate filling all liquid flow lines with solvent,
5) When solvent starts to exit the disconnected oxidative reactor return line, this initial volume of liquid is collected in a beaker for disposal;

approximately 250 mL of solvent should be collected, or until the solvent runs clear (whichever occurs first),

6) The pump is then stopped and the shut-in valve located just downstream from the flash valve is shut, stopping liquid flow,
7) The return line is connected to the oxidative reactor, and the shut in valve is opened, allowing solvent flow into the top section of the oxidative reactor,
8) The pump is then turned back on and set with tick mark as close to vertical as can be achieved without cavitating the pump as a result of the liquid level dropping below the pump inlet,
9) The black rubber stopper is installed onto the oxidative reactor with the stir shaft inserted and connected to the Fisher Steadystir analog stir motor, and the stir motor and stir shaft lowered into place approximately ½ inch above the bottom of the top section of the oxidative reactor (Caution: the motor is not to be turned at this point),
10) The 6-inch long Omega K-type thermowell is inserted through one of the holes in the rubber stopper and into place, seating onto the rubber stopper, checking that the thermowell does not reach the depth of the impeller blades at the end of the stir shaft,
11) The stir shaft length should be adjusted at the stir motor chuck to ensure clearance between the impeller blades and the thermowell, while still reaching the depth of ½ inch from the bottom of the top section of the oxidative reactor,
12) The Fisher Steadystir motor should be turned on and adjusted to 1,440 rpm; adjustments to the reactor alignment will be necessary to ensure

that the stir shaft does not contact the rubber stopper, causing friction and instability in the reactor operation,

13) The water bath should be set at ~58 °C, Oil Bath No. 1 should be set at ~138 °C, and Oil Bath No. 2 should be set at 134 °C for a typical experiment with 7 m MDEA/2 m PZ cycled from 55 to 120 °C in the oxidative and thermal reactors, respectively,

14) A single 5-mL solvent sample should be collected with a pipetter from the bubble removal chamber, and labeled Expt #-0a to denote the zeroth sample collected before significant cycling has occurred,

15) The end of the purge gas line exiting the water saturator should be inserted into a hole in the rubber stopper on the oxidative reactor far enough to reach approximately one inch below the lip of the oxidative reactor, but not into the liquid solvent (check line depth while solvent is being stirred),

16) As the solvent temperature exiting the thermal reactor approaches 100 °C, boiling will occur and the back-pressure valve (green handle) should be gradually closed (turned clockwise) to back-pressure the solvent and prevent boiling, and as the solvent approaches 120 °C, this valve should be closed sufficiently to reach a pressure of at least 35 psig (hot-side system pressure is acquired visually on a Swagelok® analog pressure gauge mounted downstream on the return line to the oxidative reactor),

17) As the solvent reaches its target T of 55 °C in the oxidative reactor (Channel 1 on the Omega digital readout device) and 120 °C at the exit to the thermal reactor (Channel 5), a 5 mL solvent sample should be

collected from the bubble removal vessel and labeled Expt No-0b to denote the zeroth (time zero) sample collected at the start of cycling,

18) The purge gas flow rate can now be accurately adjusted to 100 mL/min with the Cole-Parmer rotameter and a bubble column,

19) The glass condensate tube can be inserted into the remaining open hole in the runner stopper on the oxidative reactor, with the condensate drain valve closed to ensure collection of condensed liquids, and

20) A mark should be placed on the side of the oxidative reactor noting the liquid height when stirring, and a second mark made when not stirring; a mark should also be made on the side of the bubble removal vessel; both marks will be used over the course of the experiment to determine how much liquid loss is experienced due to water vapor escaping from the oxidative reactor.

After successfully completing the start-up process, minor adjustments to the temperature control baths will be necessary to reach target experimental temperatures. As the solvent degrades, its flow and mass transfer characteristics (viscosity) will change, requiring pump rate and temperature bath adjustments to meet all control targets.

Should the system experience a rapid increase in liquid level in the oxidative reactor, it is generally indicative of boiling in the thermal reactor because of insufficient pressure in this portion of the flow system. This type of upset will typically only occur during and immediately after start-up due to lack of back-pressure. The back-pressure valve should be closed a sufficient amount to achieve a back-pressure condition which exceeds the boiling pressure of the solvent at 120 °C. Should closing the valve alone not stop the boiling, the pump rate can be temporarily increased to maximum to achieve a greater differential pressure in the hot solvent. Once the solvent level in the oxidative

reactor returns to its original level, the pump rate should be returned to its set point. The back-pressure valve should then be established at a set-point which provides ample back-pressure in the solvent to prevent boiling, while not over-pressuring the pump. This set point will vary with solvent and loading.

2.3.3.2 ISDA Operations

The stir motor and shaft on the oxidative reactor should be stopped on a daily basis in order to determine liquid levels, and perform reactor maintenance. Five-mL solvent samples should be collected from the bubble removal vessel with a pipetter and fresh disposable tip each day within the first week of cycling; the frequency can be reduced to sampling every other day thereafter. A 5-mL aliquot of fresh solvent (undegraded) should then be transferred to the system. After checking liquid levels with respect to the original marks placed on the oxidative reactor and bubble removal vessel, DDI should be added to the bubble removal vessel as needed to restore the level to its starting point. A typical experiment requires approximately 5 mL of water addition per day. Condensate samples should be collected from the oxidative reactor on an as-produced basis from the glass condensate tube by opening the stop-cock and collecting the liquid sample directly into a 4-Dr vial. A typical cycling experiment will not generate sufficient condensate to allow collection more than once every two to three days, and in some cases, no more than one sample per week.

The water bath controlling the saturator and oxidative reactor temperature should be topped with water, and any adjustments made to control temperature of solvent in the oxidative reactor. The saturator should be topped with DDI, and the purge gas flow rate measured and readjusted to 100 mL/min if necessary with a soap bubble column. When using a pre-mixed gas such as the Matheson TriGas 98% O_2/2% CO_2 mixture, no other

gas adjustments are needed. However, should make-up of the purge gas require the use of mass flow controllers, adjustments to the flow controller settings may be necessary.

2.3.3.3 ISDA System Shutdown and Cleaning

This section provides a description of the necessary steps to shutdown and flush the ISDA in preparation for the next experiment. It is assumed that the final sample has been collected from the system before proceeding with the shutdown process.

Before initiating the first step in the shutdown of the ISDA, it is essential to measure the liquid flow rate while the solvent is still at its target temperatures, and not after cooling has been initiated; as the solvent is cooled, its viscosity increases, requiring the pumping rate to be reduced. The solvent pump should be turned off, and the shut-in valve temporarily closed to prevent loss of solvent. The return line connected to the top section of the oxidative reactor should be disconnected. The shut-in valve should be opened, and the pump turned back on with the solvent flow temporarily directed to a beaker to allow a short period of flow and return to steady state flow condition. The flow should then be directed into an empty 100-mL graduated cylinder or similar vessel, and using a stop-watch, the time required to discharge 100 mL of hot solvent measured. The solvent pump should then be turned off, the shut-in valve closed, and the solvent return line reconnected to the top section of the oxidative reactor. After opening the shut-in valve, the pump should be turned on and flow restored to the system for the cool-down process in the next few steps. The entire time taken to measure the flow rate should not exceed one minute, as the solvent is still hot and has a tendency to boil. With the pump turned off, the system has no ability to back-pressure the solvent.

The first step in the shutdown process is to reduce the set points on all three temperature control baths to ambient temperature or below while maintaining the solvent

circulation. It is recommended that the solvent is allowed to cool to less than 50 °C to minimize volatility of degradation species in the solvent, thereby minimizing exposure to volatile chemicals during the shut-down process. This initial cool-down process should require approximately one hour.

Once cooled, the solvent pump should be turned off, and the Swagelok® 1/4-inch compression fitting drain plug should be removed and a 3-foot long section of plastic 1/4-inch tubing (Drain Tubing) connected to the fitting. The shut-in valve located on the vertical solvent line returning solvent to the oxidative reactor should be closed. After directing the loose end of the Drain Tubing to a large container such as a glass jug for capture of the cycled solvent, the pump should be turned on and solvent pumped into the jug. This process will empty the glass bubble removal vessel. After turning off the pump, the ¼-inch plastic tubing connected to the bottom of the oxidative reactor should be disconnected from the bubble removal vessel and connected to the inlet side of the pump. The pump should again be turned on and the solvent in the oxidative reactor pumped into the jug. After emptying all solvent in this reactor, the pressurized service air connected to the fume hood should be connected to the ¼-inch stainless steel line directing solvent to the top of the oxidative reactor (return line outlet); the air line is plumbed with a Swagelok® compression fitting for this purpose. After opening the ¼-inch shut-in valve on the vertical return line and closing the ¼-inch shut-in valve on the inlet side of pump, the pressurized air should be delivered to the piping of the ISDA to push the remainder of the cycled solvent out the Drain Tubing and into the jug. The air should be allowed to flow through this line for approximately three minutes to ensure as much solvent is removed as is possible. After this period, the pressurized air should be shut off, and the air line disconnected from the outlet line.

After removing the cycled solvent from the ISDA, the system is now ready to be flushed with water. The drain plug should be reconnected and tightened, the inlet and outlet shut-in valves opened, and the service water line in the fume hood opened for filling of the oxidative reactor with water. The tap water should be continuously flowing to the glass reactor while the solvent pump is turned on, pumping solvent through the system and out the ¼-inch tubing which is normally used for directing solvent back to the oxidative reactor. While flushing the system, this line should be left disconnected from the oxidative reactor, and directed to the fume hood drain. The system should be continuously flushed in this fashion for a minimum of one hour.

When the flushing period is complete, the water line should be disconnected, and the drain plug removed once again. The pressurized air line should be reconnected to the return line, and the shut-in valve on the suction side to the pump closed. Air should be directed into the system to flush residual water directly out the drain line and into the fume hood. After blowing high pressure air through the system for approximately five minutes, the air line should disconnected from the discharge line and connected to the inlet to the pump (suction side). The inlet shut-in valve should be opened and return line shut-in valve closed. The air should be directed into the system for three minutes to flush the residual water out of the pump head and lines downstream of the pump. The air line can now be disconnected and the drain line plug can be left disconnected if the system is not going to be used for any length of time. If the system is going to be immediately charged with a new solvent for the next experiment, the drain plug should be reconnected one-quarter turn past finger tight to ensure it does not leak. The system is now ready for the next experiment.

As described, the bubble removal vessel was removed in the shut-down process. This vessel and the ProPak ¼-inch packing should be thoroughly rinsed with soapy

water, and flushed for a minimum of 15 minutes with running tap water. The packing should then be rinsed a minimum of three times with distilled water, and allowed to drain residual water before use in the next experiment. The impeller stir shaft, rubber stopper and oxidative reactor thermowell should all be rinsed of residual amine before the next experiment. The condensate tube should be thoroughly rinsed with tap water and distilled water with the stop-cock valve opened, and dried with compressed air blown through the tubing before use in the next experiment.

2.4 SAMPLE HANDLING METHODS

This section describes the basic methods used in the handling and preparation of samples for the analyses described in the sections that follow. All degraded solvent samples collected while implementing the experiments described in Section 2.3 are placed directly in Fisher glass 21 X 70 mm 4-Dr vials (4-Dr) with pulp/polyvinyl lined caps for short and long-term storage. The samples are stored at laboratory room temperature, and analyses with the standard analytical methods are generally implemented within three to seven days of completion of each experiment.

2.4.1 Sample Dilution

Neat samples are diluted for most analyses performed in this degradation work. Samples are diluted gravimetrically 10X, 100X, and 10,000X with DDI unless otherwise noted. Samples are typically diluted in 4-Dr vials unless larger quantities were needed for analytical work. All dilutions are prepared using pipetters with fresh disposable plastic tips. The laboratory stocks Eppendorfs Research pipetters with maximum volume ranges of 200 µl, 1 mL, and 10 mL.

After taring the balance, a 4-Dr vial is placed directly on a Mettler Model XS204 balance (220 g, d=0.1 mg), and DDI is transferred directly from an open top glass pitcher used specifically for DDI temporary storage into the vial. After recording the DDI mass and taring the balance, an aliquot of neat sample is transferred into the vial, and the mass again recorded. The dilution requirement dictates how much sample was transferred.

2.4.2 Sodium Hydroxide Treatment

In most experiments, neat degraded solvent samples are treated with 5N NaOH to reverse the formation of amide compounds through hydrolysis. Hydrolysis occurs in the presence of OH^-, and results in the amide rearranging to create an amine and a carboxylate ion, both of which can be measured with ion chromatography. Through this method, the concentration of amides is estimated. The hydrolysis treatments are made using a 1:1 ratio of neat sample to NaOH, with ~0.5 g of sample used. NaOH treatments are done on a gravimetric basis. Samples are treated with NaOH for a minimum of 24 hours, then diluted for subsequent analyses. Sample nomenclature for the NaOH treated samples follows a scheme: C-1-1+NaOH, which denoted cycling experiment no. 1, sample no. 1, treated with NaOH.

2.5 STANDARDS SYNTHESIS

The synthesis of compounds as standards for direct injection in the analytical methods used in this work was essential in the identification of unknowns. Synthesis of amino acids and amides was used, and the methods are described in the following section.

2.5.1 Amino Acid Synthesis

Synthesis of amino acids was either accomplished or attempted for four compounds suspected of being produced in degraded solvents in this work. Those compounds are depicted in Figure 2.6.

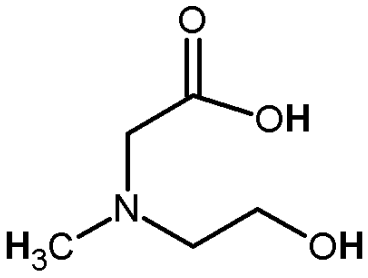

Hydroxyethyl sarcosine (HES)

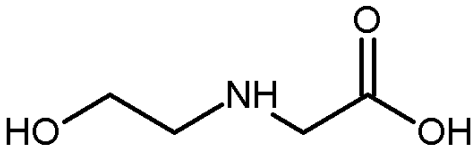

N-(2-hydroxyethyl)-glycine

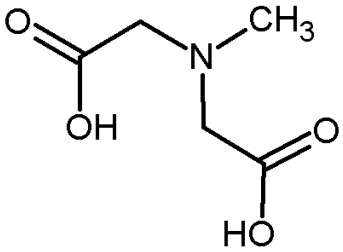

N-(carboxyethyl)-N-methyl glycine

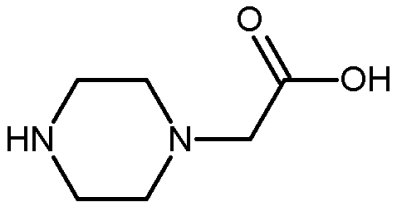

1-Piperazinecarboxylic acid

Figure 2.6: Synthesized Amino Acids

2.5.1.1 Hydroxyethyl sarcosine (HES) synthesis

Critchfield and Jenkins (1999) reported the presence of the amino acid HES, also known as N-(2-hydroxyethyl)-N-methyl-glycine (CAS No. 26294-19-9), in degraded MDEA samples from tail gas treating units (TGTU). The authors reported that MAE is an intermediate product in the degradation of MDEA, and will further oxidize to HES. In this work, the presence of MAE in degraded 7 m MDEA and 7 m MDEA/2 m PZ was confirmed. Using the Dionex AAA-Direct method for separation and detection of amino

acids, several unidentified peaks were observed in degraded sample chromatograms. Obtaining an HES standard for identification of this compound was difficult, with most fine chemical suppliers either not offering HES as a standard, or offering it at an excessively high price. In order to confirm the presence of HES in degraded samples, it was necessary to synthesize this amino acid.

HES was synthesized in experiment HE-Sarc-1 using a base-catalyzed reaction in aqueous solution. The synthesis steps included the following:

(1) A 0.2 M NaOH solution was created by adding 1.1 g Fisher 5 N NaOH (4.95 – 5.05 N grade) to 24 g DDI in an open beaker with a pipette;

(2) 1.9 g MAE (Acros Organics, 99% grade) was then added to the solution to bring the MAE concentration to 1 M;

(3) 0.26 g of monochloroacetic acid (MCAA) (Fisher, chlorides < 0.01%) was added to bring the MCAA concentration to 0.1 M; and

(4) the solution was stirred for four hours at approximately 60 °C to facilitate the substitution reaction between MAE and MCAA.

The solution was injected on the AAA-Direct system, and a single peak was observed at a retention time of 20.9 minutes (Figure 2.7). The 10 to 1 molar ratio of amine to MCAA was used to avoid the synthesis of products other than HES, based on the assumption that the most likely reaction to occur was the substitution reaction resulting in the loss of a proton on the nitrogen of MAE, and bond formation at the β-carbon on MCAA, and the formation of HES and HCl. No other peaks were observed in the synthesized solution injection chromatogram. The retention time for this peak corresponded to a peak in degraded 7 m MAE from the Low-gas reactor set-up (oxidation at 55 °C), which is also depicted in Figure 2.7. The most prominent amino acid peak expected in degraded MAE is HES. Direct injection of the synthesis solution on a

Thermo Finnigan TSQ® mass spectrometer was performed to confirm the presence of HES; a compound mass of 133.1 in this solution was observed, confirming the synthesis of HES. The synthesized HES solution chromatogram was then compared to sample chromatograms for 7 m MDEA and 7 m MDEA/2 m PZ from the AAA-Direct method, confirming the presence of amino acid in these samples.

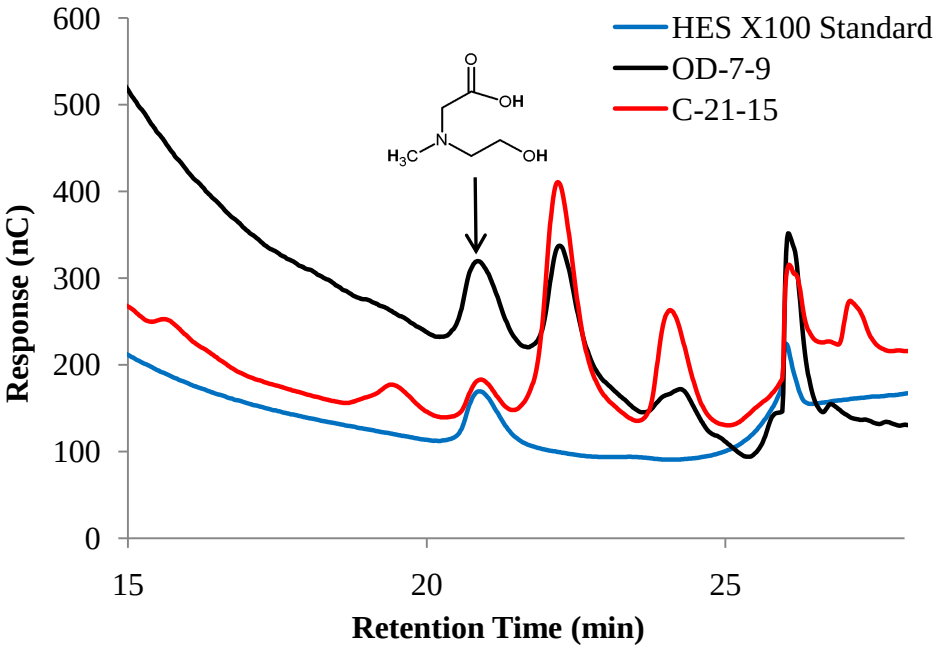

Figure 2.7: Amino acid chromatogram - synthesized HES (blue) and oxidized MAE (black)

The concentration of HES in the synthesis standard was estimated assuming the reaction between MCAA and MAE went to completion (all MCAA reacted with MAE to provide a concentration of 0.1 M HES). This solution was then diluted 20X, 50X, and 100X in ultrapure water, and analyzed using the AAA-Direct method to provide an HES standard curve. Using this method, the HES concentration was then estimated in degraded samples.

2.5.1.2 MEA Amino Acid

The presence of MEA in degraded 7 m MDEA/2 m PZ samples indicated the possible presence of an amino acid similar in structure to MEA, and the need to synthesize this compound. The base-catalyzed synthesis method used in the preparation of HES was used in experiment AA-2 for the preparation of N-(2-hydroxyethyl)-glycine (CAS No. 5835-28-9), an amino acid using MEA as a substrate (Figure 2.6). The following steps were followed:

(1) A 0.2 M NaOH solution was created by adding 1.1 g Fisher 5 N NaOH (4.95 – 5.05 N grade) to 28 g DDI in an open beaker with a pipette;

(2) 0.15 g MEA (Acros Organics) was then added to the solution to bring the MEA concentration to 0.1 M;

(3) 0.40 g of monochloroacetic acid (MCAA) (Fisher, chlorides < 0.01%) was added to bring the MCAA concentration to 0.2 M; and

(4) the solution was stirred for four hours at approximately 60 °C to facilitate the substitution reaction between MAE and MCAA.

The amino acid synthesis product was injected in the AAA-Direct amino acid method, and a double peak eluted at ~22.4 minutes. This peak corresponded to a peak of the same retention time observed in degraded 7 m MDEA samples, further supporting the hypothesis that an amino acid of MEA is formed in the degradation of MDEA (C-31-10). The synthesis product was analyzed through direct injection on the TSQ® mass spectrometer, and the presence of a compound with a molecular weight of 119.1 was observed, confirming the presence of N-(2-hydroxyethyl)-acetic acid. However, the compound produced a double peak, preventing the accurate estimation of the amino acid concentration.

2.5.1.3 Synthesis of substituted HES amino acid

Using the same base-catalyzed method for the preparation of HES, an attempt was made (experiment AA-3) to synthesize an amino acid corresponding to a single carboxyate arm substitution on sarcosine with a molecular weight of 147.1, as depicted in Figure 2.6. The amino acid is N-(carboxymethyl)-N-methyl glycine (CAS No. 4408-64-4). To a 0.2 M aqueous NaOH solution were added sarcosine and MCAA acid to get to concentrations of 1 M and 0.1 M, respectively. When injected in the AAA-Direct amino acid method, no clear peak was generated by the synthesis product solution.

2.5.1.4 Synthesis of PZ-amino acid

Using the same base-catalyzed method for the preparation of HES, an attempt was made (experiment AA-4) to synthesize an amino acid corresponding to a single carboxyate arm substitution on PZ. The compound, 1-piperazine acetic acid (CAS No. 37478-58-3), has a molecular weight of 144.1 and the structure depicted in Figure 2.6. To a 0.2 M aqueous NaOH solution were added PZ and MCAA to get to concentrations of 1 M and 0.1 M, respectively. The 10 to 1 ratio between PZ and MCAA was used to avoid a disubstitution reaction between the reagents. When injected in the AAA-Direct amino acid method, a broad and poorly defined peak was observed with an approximate retention time of 10.1 minutes. This retention time corresponded to time in the eluent ramp when the tail end of the unretained compounds elute from the column, preventing confirmation that the intended product was synthesized.

2.5.2 Amide Synthesis

Degraded 7 m MDEA/2 m PZ sample injections on the Dionex UltiMate 3000 HPLC system configured with the Polar Advantage II C18 column confirmed the presence of compounds with peak retention times of 4.3, 5.5, and 7.3 minutes. When

these same samples were hydrolyzed through the base-catalyzed hydrolysis process with NaOH, these peaks disappeared, indicating that these compounds were likely amide products. This observation prompted the need to obtain standards of amides of degradation products including MAE and DEA, neither of which were readily available from chemical reagent suppliers.

2.5.2.1 MAE-Amide

In experiment Amide-1, an amide of MAE (N-(2-hydroxyethyl)-N-methyl formamide, CAS No. 1590-50-7) was synthesized through the substitution reaction between MAE and formic acid to replace H^+ on the MAE-nitrogen with the carbonyl group. The synthesis was performed as follows:

(1) An aqueous solution of 1 MAE was created by adding 2.43 g MAE to 24.95 g DDI in an open beaker at room temperature;

(2) 0.65 g formic acid were added to bring the solution to 0.5 M formate;

(3) the solution was transferred to a Swagelok® sample cylinder, sealed, and placed in an oven at 135 °C (the 1 to 0.5 molar ratio between amine and formic acid was selected to ensure sufficient formic acid in solution to observe the nucleophilic substitution reaction); and

(4) after 72 hours, the cylinder was removed from the oven, and the solution was removed from the cylinder.

The sample was then diluted 1:1 with a 1 M ammonium carbonate buffer. The purpose of the buffer was two-fold: (1) to match the method eluent pH, and (2) to make the analytes more non-ionic and, therefore, more non-polar in the mobile phase. The effect of the buffer is to generally improve separation and response in the HPLC system. A 10,000X dilution of this synthesis product was injected on the cation IC system to

determine the loss of MAE, and the resulting conversion of MAE to the amide. With the conversion determined (29%), this solution was then diluted to 20X, 40X, and 100X and injected on the HPLC system to confirm the presence of a peak corresponding to N-(2-hydroxyethyl)-N-methyl formamide with a retention time of ~5.4 minutes (Figure 2.8). The synthesized standard was then used to confirm the presence and concentration of N-(2-hydroxyethyl)-N-methyl formamide in degraded samples through injection in the HPLC system.

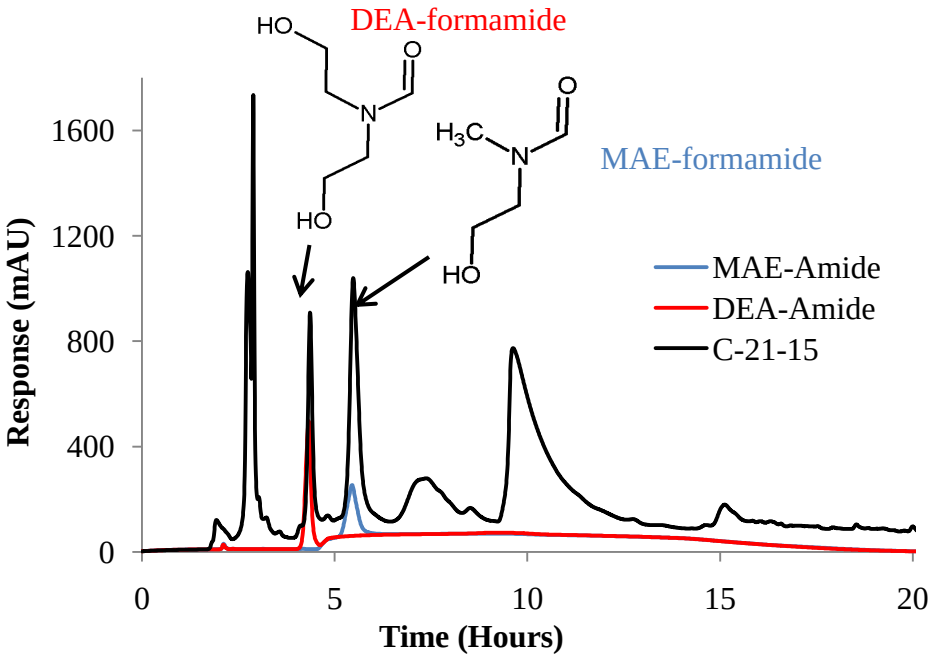

Figure 2.8: Amide Synthesis – comparison to C-21-15

2.5.2.2 DEA-Amide synthesis

In the same fashion as used in the synthesis of the MAE-amide, the DEA-amide (N,N-bis-(2-hydroxyethyl) formamide, CAS No. 25209-66-9) was synthesized in experiment Amide-2. The synthesis reaction involved the substitution reaction between

DEA and formic acid to replace H^+ on the DEA-nitrogen with the carbonyl group. The synthesis was performed as follows:

1) An aqueous solution of 1 DEA was created by adding 2.73 g of DEA to 25.23 g DDI in an open beaker at room temperature;
2) 0.65 g formic acid were added to bring the solution concentration to 0.5 M formate;
3) the solution was transferred to a Swagelok® sample cylinder, sealed, and placed in an oven at 135 °C; and
4) after 72 hours, the cylinder was removed from the oven, and the solution was removed from the cylinder.

The sample was diluted 1:1 with a 1 M ammonium carbonate buffer. A 10,000X dilution of this synthesis product was injected on the cation IC system to determine the loss of DEA, and the resulting conversion of DEA to the amide. With the conversion determined (34%), this solution was then diluted to 20X, 40X, and 100X and injected on the HPLC system to confirm the presence of a peak corresponding to N,N-bis-(2-hydroxyethyl) formamide with a retention time of ~4.4 minutes (Figure 2.8). The synthesized standard was then used to confirm the presence and concentration of N,N-bis-(2-hydroxyethyl) formamide in degraded samples.

2.6 Analytical Methods

This section covers the basic analytical methods used in this research. For a subset of the experiments conducted in this research, samples were collected in triplicate to allow the calculation of statistics.

2.6.1 Ion Chromatography

Ion chromatography methods were utilized in every degradation experiment conducted on amine solvents. The degradation of amines under oxidative conditions will result in the production of carboxylate ions which appear in degraded amine systems as heat stable salts. Rooney (1998) reported the presence of formate, acetate and glycolate in oxidatively degraded MEA. When 7 m MDEA/2 m PZ was degraded in a Low-gas oxidative reactor, formate production was observed. Under thermal degradation conditions, and to a lesser extent, oxidative conditions, solvents will degrade to other amine degradation products which can be separated and detected with cation chromatography (cation IC). All chromatography equipment used in this work was manufactured by Dionex Corporation (Sunnyvale, CA). Chromeleon proprietary software supplied by Dionex is used for all IC controls, data acquisition, and processing. All method programs for separation and detection of analytes are included in Appendix A.

2.6.1.1 Cation Chromatography

The cation IC system currently in use is a Dionex ICS-2100 RFIC system with an AS autosampler. The column is an IonPac CS17 analytical column (4 X 250 mm) and is used in conjunction with a guard column (IonPac CG17). This column is a carboxylate-functionalized cation-exchange medium which achieves separation of amines when eluted with a mobile phase consisting of ultrapure water and methanesulfonic acid (MSA). This column is recommended by Dionex for separation of polar amines including alkanolamines, methylamines, and moderately hydrophobic amines. The ICS-2100 utilizes an eluent generator to create the MSA concentration necessary for each sample sequence. The system is equipped with a Cationic Self-Generating Suppressor (CSRS-3000) for anion suppression/removal prior to passing eluted material through the

DSG conductivity detector. Samples are diluted in DDI 10,000X before being analyzed on this instrument.

The program used for analyzing degraded amine samples utilizes an eluent ramp where the initial MSA concentration is low (5.5 mM), but increases over the course of the program to 38.5 mM (See Jason3Auto_pgm, Appendix A). This program was developed by Davis (2009), and proved to be reliable at achieving amine degradation product separation in a short time when working with single monoamine solvents (MEA). The use of an eluent ramp allows the sequential separation of more strongly bound analytes from the separation column. Like ammonia, amines are polar compounds, exhibiting basicity associated with the lone electron pair on the nitrogen. The protonated form of the amines is retained on the separation column, and the mobile phase acid induces ion exchange, removing the amines from the column; as the mobile phase acid concentration is increased, the ion exchange process is increased, removing the more strongly retained amines including diamines and triamines.

The program for separating the degradation products of 7 m MDEA/2 m PZ was modified to achieve better separation. The method was lengthened in time to allow for a more gradual eluent ramp. FredAuto6_pgm is the original elution program utilized on a decommissioned IC system with isocratic pump, whereas Stephanie3Auto_pgm was developed by Freeman (2011) and utilized more recently for cation separations on a newer ICS-2100 RFIC system. Like FredAuto6_pgm, this program lengthened the separation time to 50 minutes, allowing more time for the mobile phase eluent to isocratically increase in acid concentration. Both programs are included in Appendix A.

Figure 2.9 depicts a typical cation chromatography result for cycled 7 m MDEA/2 m PZ, with monoamines including MDEA and MAE eluting from the column within 13 minutes, and diamines such as PZ eluting at ~33 minutes. Satisfactory separation of

monoamine and diamine products was achieved to allow quantification of major degradation products (DEA, FPZ, 1-MPZ, and 1,4-DMPZ) in this degraded solvent sample. Better separation of amines was attempted with earlier versions of this program, but the resolution (R) between neighboring eluites is not expected to improve based on thermodynamic effects preventing analyte bands from separating further (Small, 1989).

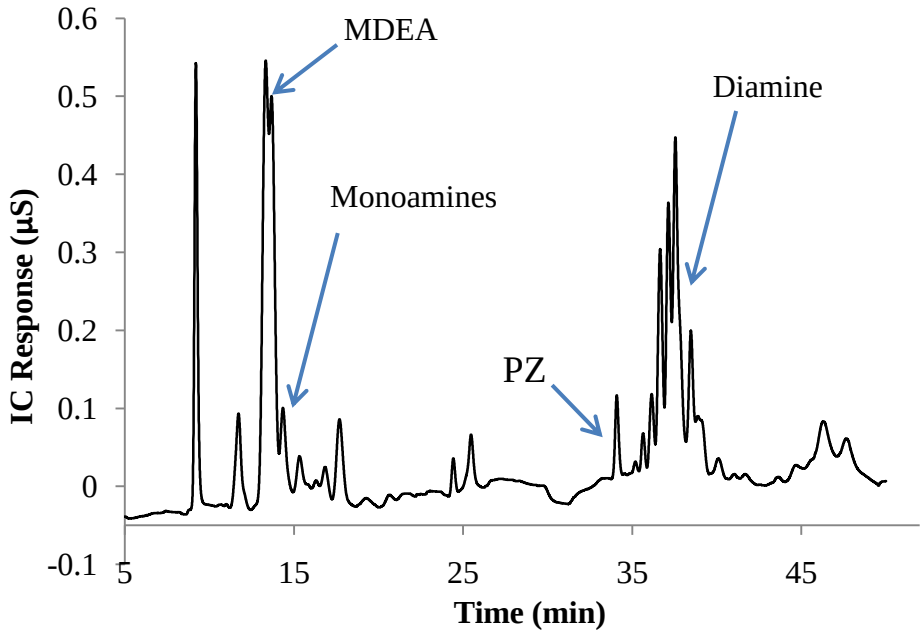

Figure 2.9: Cation IC chromatogram – thermally degraded 7 m MDEA/2 m PZ

The statistical quality of the data was tested for samples collected in thermal and cycling experiments. In both cases, samples were collected using the standard methods described, but in triplicate. All sample handling methods were repeated for each sample, including sample collection with pipettes, dilution, analyses with the instrumentation, and interpretation of data. A description of the sample and statistical results follows.

In experiment C-27, 7 m MDEA was cycled from 55 to 100 °C for 236 hours. The final sample (C-27-12) was collected in triplicate, and all analytical methods were repeated including cation and anion IC, amino acids, titrations and TIC.

A cation IC standard deviation for MDEA and MAE were calculated using the equation (Eq. 2.1) for a small data set (Skoog and West, 1979). This equation is valid for the calculation of standard of data sets consisting of two to five points.

$$s = \sqrt{\sum_{i=1}^{N} (x_i - \bar{x})^2 / (N-1)} \tag{2.1}$$

For C-27-12, the average and standard deviation of the MDEA and MAE concentrations were 2,571.3 ± 39.0 and 229.0 ± 3.0 mM, respectively. The value of performing these statistical analyses is to determine whether the determinate and indeterminate errors allow conclusions to be drawn about the magnitude of each data point. For example, the standard deviation associated with the cation data is 1.3 to 1.5% of the total concentration. This is an acceptable error for determining initial rates of degradation, and the extent of degradation.

For thermal degradation experiment Th. No. 16, thermal degradation cylinders samples were pulled from the ovens in triplicate on Day 113, and the three liquid samples recovered and diluted in an identical fashion. The average and standard deviation of cations were determined as described above. The MDEA concentration in this sample was completely degraded, but useful analysis can be extracted from cation degradation products including DEA and 1-MPZ. The average and standard deviation of these products were 23.7 ± 6.54 and 25.3 ± 13.4 mM, respectively. For 1,4-DMPZ, the average and standard deviation were 387.0 ± 20.4 mM. These standard deviations indicate that, at lower concentrations, the deviation in the data due to indeterminate errors becomes quite large (as much as 50% of the concentration). However, at larger

concentration (>250 mM), the error is much lower (~5%). The error associated with the cation IC measurements is acceptable for the determination of degradation rates of starting amine due to the inherent larger concentrations of initial amine. However, the formation rate of degradation products measured with cation IC should be used with caution due to the errors at the lower concentrations.

2.6.1.2 Anion Chromatography

Carboxylate ions form in the degradation of solvents, in particular, under oxidative degradation conditions (Chapter 1). These carboxylate ions can be separated as anions using ion chromatography. A Dionex Dual RFIC ICS-3000 ion chromatograph was used for anion separation and quantification in this work. Separations are achieved with an IonPac AS15 column (4 X 250 mm) column which is a hydroxide-selective anion exchange column. The column material consists of a cross-linked core and anion-exchange layer, with the column substrate consisting of a porous resin bead of 4 mm diameter of ethylvinylbenzene cross-linked with polyvinylbenzene (55%). The anion exchange layer is functionalized with alkanol quaternary ammonium groups, and the column was designed for isocratic separation methods. The instrument is equipped with an EGC III KOH eluent generator; the method currently in use for anion separations utilizes a KOH gradient in DDI. Separated samples are passed from the column through a 4-mm Anionic Self-Regenerating Suppressor (ASRS) device to remove cationic species. The system utilizes two carbonate removal devices to remove excess carbonate species from samples (Continuously Regenerated Anion Trap Column or CR-ATC), and a conductivity detector for anion quantification. All samples are run on this method at dilution factor of 100X.

The method (Anions_program) used for all analyses in this work is included in Appendix A. This method utilizes a KOH eluent ramp that starts at 2 mM KOH and increases to 45 mM within 25 minutes, with the eluent flow rate set at 1.6 mL/min. The column temperature is set at 30 °C. The total method time is 35 minutes. The anions chromatogram from sample C-21-15 is included as Figure 2.10, and demonstrates satisfactory separation between common analytes including glycolate (20.5 minutes), formate (21.4 minutes), and oxalate (28 minutes).

In sample C-27-12, the average and standard deviation of the formate concentration was 33.0 ± 0.33 mM. The standard deviation (s) is ~1% of the total, which is an acceptable deviation around the mean in terms of determining degradation rates and extent of degradation. In thermal degradation experiment Th. No. 16, the average and standard deviation of the formate concentration was measured in triplicate on Day 113, and determined to be 60.7 ± 3.62 mM. The standard deviation in anion IC measurements from thermal degradation experiments is also acceptable for determining product formation rates.

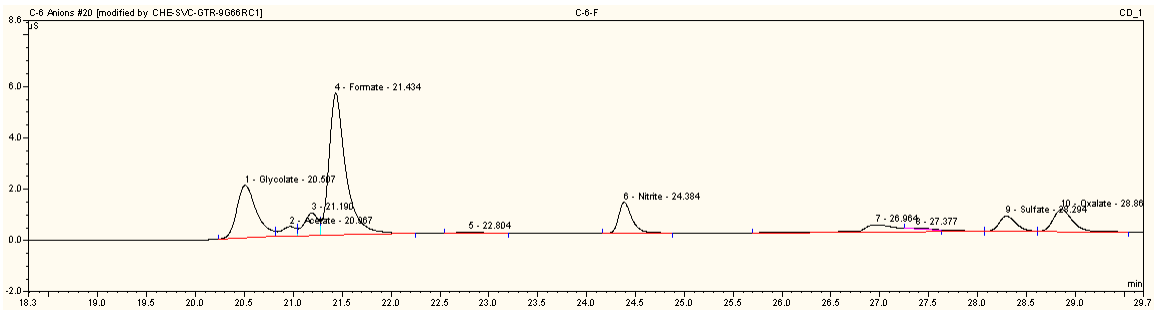

Figure 2.10: Anion IC chromatogram – 7 m MDEA degraded in the ISDA

2.6.2 Amino Acid (Dionex AAA-Direct™)

The Dionex ICS-3000 described in Section 2.6.1.2 is a dual-use system, allowing the simultaneous operation of an anion separation method and an HPLC method. The

Dionex AAA-Direct™ Amino Acid Analysis System was established for HPLC separations and detection, and is described in the document Product Manual AminoPac PA10 (Dionex, 2006). The system utilizes the AminoPac PA10 column which is a hydrophobic, polymeric, pellicular anion-exchange resin designed to be stable over a pH range of 0-14. Eluents include DDI, 250 mM NaOH, and 1 M sodium acetate. Samples are pumped under high pressure through the system with a DP-1 gradient pump during a 75 minute gradient program. The system utilizes a AAA-Certified Gold Working electrode for gold-oxide catalyzed oxidation of amino acids. The detection is achieved through Pulsed Electrochemical Detection in the detector compartment. Eluent preparation must be done manually for use of this system, and the methods for preparing them in DDI are described in detail in the Product Manual.

The amino acid program developed and used in the Rochelle laboratory is included in Appendix A (AminoAcid_program). Sodium acetate is increased to 70% at 42 minutes into the 75 minute program, replacing NaOH and DDI, and increasing the anion exchange of amino acids from the column. This method was used for analysis for amino acids in every sample collected during the latter stages of this research, and on a subset of samples collected prior to bringing this method on-line. Samples were diluted to 100X in DDI for these analyses. Figure 2.11 displays a typical chromatogram resulting from the analysis of sample C-21-15, and demonstrates the separation achieved between the amino acid hydroxyethyl sarcosine (HES) and bicine.

The average and standard deviation of the bicine concentration in C-27-12 were measured as 80.6 ± 0.93 mM, which represent an acceptable level of repeatability in amino acid measurement.

2.6.3 HPLC for non-polar compound analysis

HPLC was utilized to analyze degraded samples for non-polar products including ureas, oxazolidones, and amides. The system utilized in this work is a Dionex UltiMate 3000 modular system designed for rapid separations. This system has an integrated VWD-3100 variable wavelength detector which consists of dual-beam, variable wavelength photometer with one measureable and one internal reference beam. The light source is a deuterium lamp for ultraviolet detection. The system is also coupled to a separate Polymer Laboratories PL-ELS 2100 Evaporative Light Scattering Detector (ELSD) for detection of semi-volatile compounds which have no UV chromophore. An UltiMate 3000 autosampler module is included with this system which accepts Fisher borosilicate sample vials with pre-slit septa for auto-injection. All programming, sequence set-up, system control, and data acquisition and processing are done through Dionex Chromeleon 7 software.

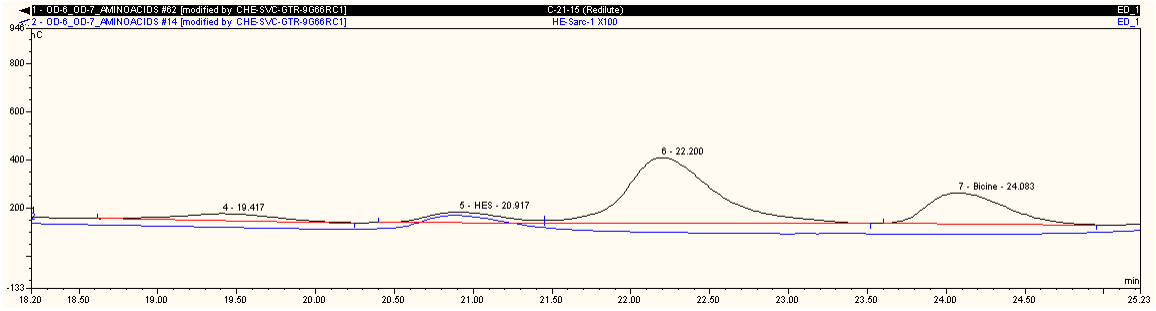

Figure 2.11: Amino acid chromatogram – HE-Sarc X100 and cycled 7 m MDEA/2 m PZ (C-21-15)

The column used for most of the reported work is a Dionex Acclaim PolarAdvantage II silica-based polar-embedded reversed-phase C18 column. This column is stable over a pH range 1.5 to 10. Eluents included water, methanol and

acetonitrile. Appendix A includes the program method for used for separations with the Polar Advantage II column.

2.6.4 Mass spectrometry

In addition to utilizing cation IC and HPLC methods as stand-alone tools for identification and quantification of degradation products, cation IC and HPLC coupled to a Thermo Finnigan TSQ® Quantum Discovery mass spectrometer (MS) in Civil Engineering were utilized. This work also utilized the Mass Spectrometry Laboratories operating out of the Chemistry Department in Welch Hall for gas chromatography (GC) coupled to MS (referred to as GC-MS). The GC-MS work was performed by technicians in Welch; no GC-MS method development was performed in this body of work. This section describes the IC-MS and LC-Ms methods in detail, and provides a brief overview of the GC-MS method used.

2.6.4.1 Cation IC-MS

A Dionex ICS-2000 coupled to the TSQ® MS was used to achieve cation IC separation and detection, and mass assignment to unknown degradation product peaks in degraded amine samples. An IonPac CS17 analytical column (4 X 250 mm) was used in conjunction with an IonPac CG17 guard column in the IC system. This system was similar to the system described in Section 2.6.1 for cation IC analysis, employing an EGC II for MSA eluent gradient generation. The cation IC separation program used in this analysis was the same method described in Section 2.6.1 and included in Appendix A.

As described in the document Finnigan TSQ® Quantum Discovery Hardware Manual (2003), the TSQ® consists of an atmospheric pressure ionization (API) source, ion guides, triple-stage mass analyzer, and ion detection system. Ionization of samples takes place in the API source, and the ions are transmitted by the ion guides into the mass

analyzer where they are separated according to the mass-to-charge ratio. The polarity of lenses in the API source can be configured to produce either positively charged or negatively charged ions which are then transmitted to the mass analyzer. All analytical work and measurements reported in this document are a result of positive ion polarity mode operation. The ions produced in the API source are filtered according to their mass-to-charge ratio, and in conventional mass analysis mode, mass analyzed in the first rod assembly. The mass selected ions are then transmitted through the second and third rod assemblies to the ion detection system. The TSQ® uses electrospray ionization (ESI) which can transform ions in solution into ions in gas phase. According to the TSQ® hardware manual (Thermo Finnigan, 2003), "ESI can be used to analyze any polar compound that makes a preformed ion in solution".

Sample eluent from the Dionex ICS-2000 was coupled directly to the TSQ® through PEEK tubing with a flow splitter valve to optimize the flow rate to the TSQ®. After analytes were separated in the ICS-2000 and sent to the conductivity detector, the mobile phase was sent to the TSQ® for analyte mass analysis. The coordination of the two instruments required the installation of a software module created by Dionex called DC-MS link. All sequence set-up and system deployment activities were controlled through Xcalibur®, and the DC-MS link software was a module selected in the System Configuration mode of Xcalibur® to create the linkage between the two instruments. When selected, the DC-MS link software controlled the ICS-2000, with Xcalibur® serving as the interface to all instrument functions for both instruments.

Samples were prepared in Dionex 5-mL PolyVials with filter caps and placed in a AS40 autosampler for automated delivery into the system per sequence set-up performed in Xcalibur®. Sample preparation for the IC-MS work reported in this document entailed dilutions in DDI at 500 or 1000X, depending on the extent of neat sample degradation.

2.6.4.2 LC-MS

HPLC coupled to MS was used as another technique for separating and assigning mass to analytes in degraded samples generated in this work. A Thermo Finnigan Surveyor HPLC (LC) system with a Surveyor PDA detector was coupled directly to the TSQ® described in the previous section. The mobile phase was pumped by a Surveyor MS Pump through the LC separation column, through the Surveyor PDA ultraviolet light (UV) detector, and through PEEK tubing to the TSQ®. Mobile phase eluents used in the LC separation method included methanol (A), DDI (B), 10 mM $NH_4^+CO_3^{2-}$ (C), and acetonitrile (D). The method used for separation directed the Surveyor Pump to create an eluent ramp for optimal separation of analytes. Sample preparation included dilution at 10X in DDI. The separation column used was a Shimadzu Premier C18 5µ 150 X 4.6 mm (Part No. 220-91199-12), which is designed for separations with polar compounds including amines and acids. Aqueous dilutions of samples were prepared in pre-slit injection vials and placed in the Surveyor autosampler tray for injection into the column and detector. The sample and mobile phase were plumbed directly from the PDA detector to the TSQ®. All sequence set-up and control was deployed with Xcalibur® software.

2.6.4.3 GC-MS

GC-MS services were provided by the Chemistry Department for a small number of key degradation samples generated in this work. The equipment employed included a TSQ® coupled to a Thermo TraceGC, and the carrier gas was helium. The TSQ® was typically operated in electron ionization mode (EI) with a 70 electron-volt setting, with a small subset of samples ionized in the TSQ® using chemical ionization (CI) for "softer" ionization and reduced fragmentation. The TSQ® was operated in full scan mode. With this mode of operation, all fragmentation of sample analytes occurs in the ionization

source. The eluent fragments were then mass analyzed in the detector. Samples were provided to the MS lab in neat form or as 10X aqueous dilutions, and typically diluted by the lab either 10X or 100X in DDI to ensure a net dilution of 100X.

Three different columns were used in the TraceGC for analyte separation, two of which were non-polar, and one which was a polar column. The non-polar columns were expected to perform better for separation of non-polar degradation products in samples, while the polar column was expected to perform better for separation of polar products. The non-polar columns included a Restek Rxi-5Sil MS (0.25 mm ID) (Cat. No. 13623) and a Restek Rtx-5 Amine (0.25 mm ID) (Cat. No. 12323), while the polar column was a Restek Stabilwax (0.25 mm ID) (Cat. No. 10623). While both polar and non-polar columns provided analyte separation and results, the non-polar columns provided the best separation. Results from the use of both columns are discussed in Chapters 4, 6, and 7.

The method developed and used for the separations is included in Appendix A. That method employs a column oven temperature ramp rate of 3 °C/min, starting at 60 °C and ending at 280 °C, for an approximate total ramp time of 73 minutes. The carrier gas initial flow rate is set at 1.5 mL/min, and the transfer line to the MS is set at 240 °C. The total run time for the hold, equilibration, and temperature ramp in the method is 84 minutes.

Most compounds will fragment in a unique mass pattern, which can then be compared to the fragmentation pattern of standards available in an electronic library. Using the Xcalibur® Qual Browser feature, mass fragmentation patterns for separated analytes of interest were matched against standards available in the National Institute of Standards and Technology (NIST) library (updated within last three years). The library match feature provides a list of probable compounds that match the mass of the parent compound, based on the fragmentation pattern of the parent. Each compound on the list

of matches is assigned a probability for an exact match. The selection of a match from the list is an imperfect process, requiring knowledge of likely structures, given that the NIST library returns many different compounds with the same mass. In many cases, the match listed with the highest probability of an exact match is not the likely candidate for the parent compound eluting at the selected retention time. Judgment in making a match is made based on the retention time of the peak on the LC column, as provided by the PDA UV chromatogram for each sample.

2.6.5 Titrations

Total alkalinity of samples was determined using a Titrando 835 autotitrator with 0.2 N H_2SO_4. A full description of the system including the deployment of the software (PC Control) can be found in Freeman (2011). Samples were prepared by placing a 0.4 g aliquot of degraded amine in a 100-mL beaker, and diluting 150X in DDI water. The beaker was placed on the 801 Stirrer, and using PC Control software on a dedicated PC, the autotitrator was deployed until titration to a pH of approximately 2 was completed.

As samples of 7 m MDEA and 7 m MDEA/2 m PZ are titrated, inflection points in the pH of solution are encountered. Figure 2.12 presents the pH plotted with volume of acid titrated for an undegraded 7 m MDEA/2 m PZ solvent sample. Two prominent inflection points correspond to the equivalence points of the solvent's alkalinity groups. MDEA has a pK_a of 8.56 (Hamborg, 2009), while PZ has two equivalence points (9.83 and 5.56 at 296 K) (Vahidi et al, 2009). The pK_a values are based on the ionization potentials (K_a) of the amines. Each of these equivalence points will cause an inflection in the titration result. In a degraded sample, additional inflection points may be observed. For example, the pH vs. volume acid plot (Figure 2.13) for a sample of cycled 7 m MDEA/2 m PZ has a different pH profile than presented in the undegraded sample plot

due to the presence of degradation products with pK_a values different from the parent amines in the solvent. As a solvent sample is titrated with H_2SO_4, amines, amino acids, carboxylate ions (formate), and other species are protonated, consuming acid. Certain species such as amides and ureas may not protonate, and will not consume acid in the titration. These species represent lost alkalinity, and do not show up in the total alkalinity calculation. The sample represented in Figure 2.13 was titrated to a pH of approximately 2.4 which is beyond the last inflection point detectable in this sample, allowing an estimation of the total alkalinity in the solvent.

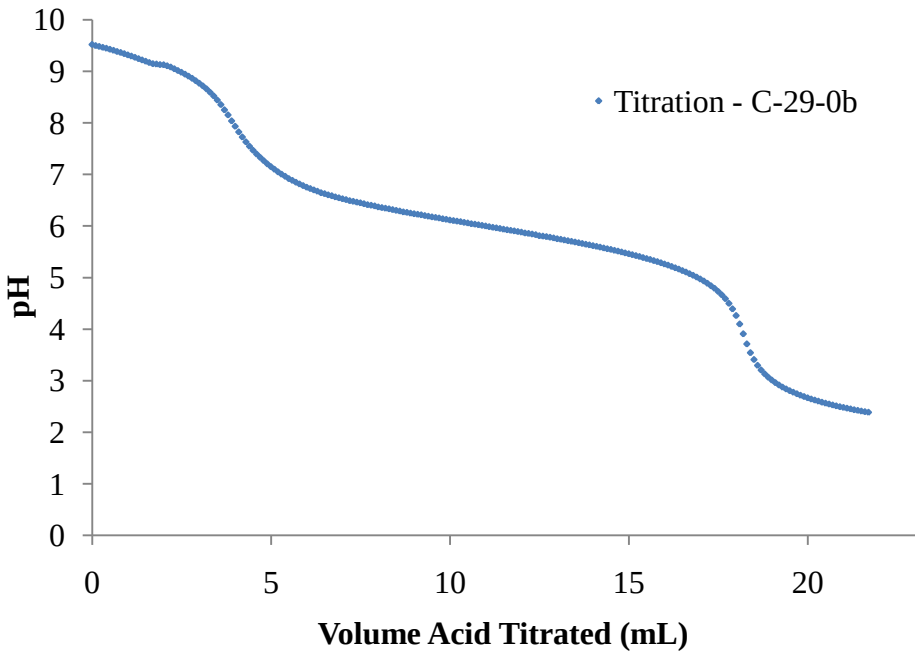

Figure 2.12: Acid titration plot – undegraded 7 m MDEA/2 m PZ

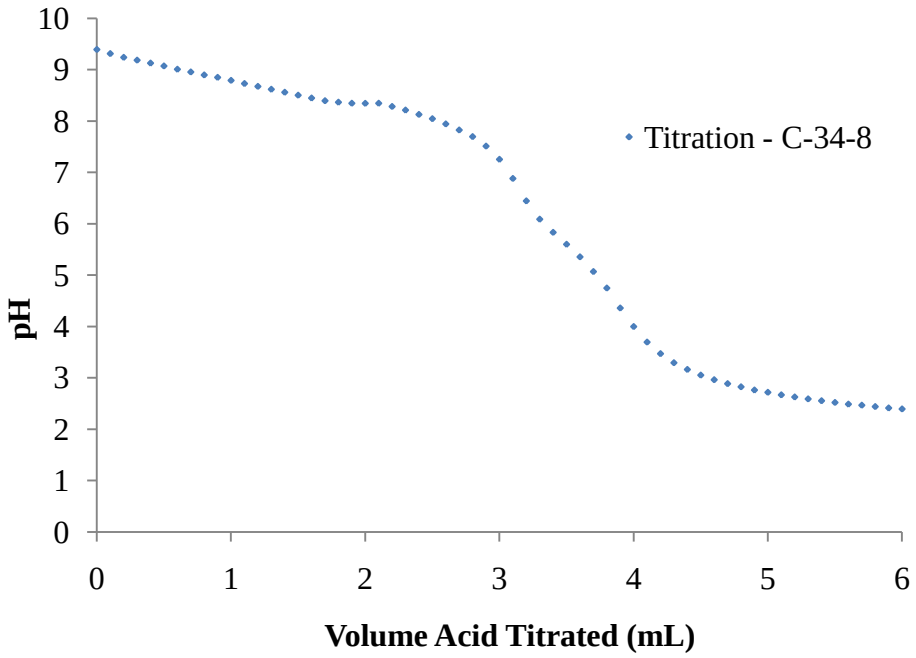

Figure 2.13: Acid titration plot – 7 m MDEA/2 m PZ cycled for 353 hours

The titration data is useful in the calculation of total alkalinity of solution. The calculation of alkalinity in titrated solvent is performed with Equation 2.2, which provides alkalinity in units of meq H^+/g solvent. For this work, meq H^+ is referred to as mol alkalinity.

$$\frac{(x\ ml\ H_2SO_4)\times\left(\frac{0.2\ meq\ H^+}{L\ acid}\right)\times\left(\frac{Lacid}{10^3\ mL\ acid}\right)}{y\ gm\ sample}=\frac{meq\ H^+}{gm\ sample} \qquad (2.2)$$

A determination of the effect of the build-up of carboxylate ions in solution was made in experiment Titration-1. In particular, we desired to test whether the presence of formic acid in a solvent such as 7 m MDEA would affect the overall amount of acid needed to titrate beyond this solvent's equivalence point(s) and, therefore, change the calculation of alkalinity. Starting with a neat, undegraded solution of 7 m MDEA (C-27 stock) previously loaded to 0.1 mol CO_2/mol alkalinity, subsequent additions of formic

acid (Fisher Brand, 88% purity) were made to the solvent, and the solvent was titrated after each addition. The additions were made to arrive at 20, 50, 200, and 350 mM formic acid. The tritations were carried out to a total pH of ~2.4, but the equivalence point (EP) for MDEA in this system (EP_2) was determined to be at an approximate pH of 4.8; EP_1 was the equivalence point for CO_2 species in solution. The total acid needed to titrate to EP_{MDEA} (EP_2) was used to determine the alkalinity at each level of formic acid addition. The amount of acid needed to titrate to each equivalence point with each addition of formic acid is plotted against total alkalinity in Figure 2.14. An analysis of the titration data elucidated that the formic acid additions had an approximate 1.25X neutralizing effect on the amount of alkalinity in solution as determined with 0.2N H_2SO_4 titration. The formic acid protonates functional groups exhibiting alkalinity as the solvent is titrated to its amine equivalence point(s), in this case to pH 4.8. With this in mind, the measurement of alkalinity in heavily degraded solvents will be affected when determined using sample titration to a pH=2. The measurement of alkalinity will be decreased by as much as 1.25X the formic acid concentration. It is unknown the extent to which other carboxylate ions (i.e., glycolate) will affect the titration method.

The error associated with the titration measurements was determined through the analyses of C-27-12 in triplicate. The average and standard deviation for this sample were 3,232 ± 46.2 mMol alk/kg solvent. At 1.5% of the total concentration, this standard deviation was acceptable for determining alkalinity loss rates.

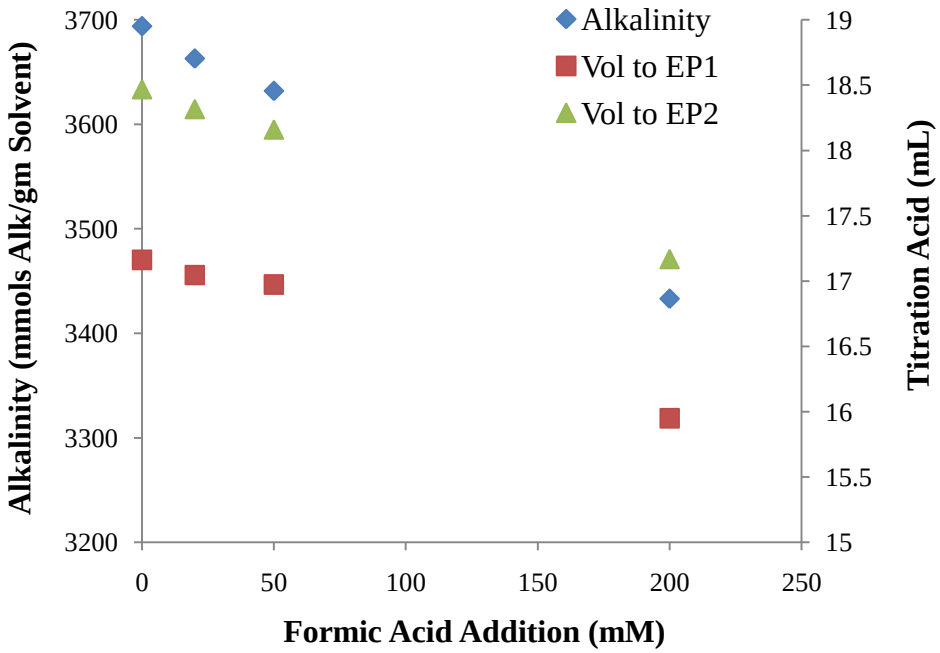

Figure 2.14 Titration test results with 7 m MDEA and formic acid additions

2.6.6 Total inorganic carbon analysis

Total inorganic carbon (TIC) analysis was performed using a method previously developed by Critchfield (1988). Hilliard (2008) provides a good description of the system componentry and method. The apparatus was reconstructed by Freeman in 2009. The apparatus for TIC measurement includes a N_2 gas supply, a Cole-Parmer rotameter for measuring gas flow rate, a glass purge trap vessel, two 6-inch glass tubes filled with a ~4-inch column of $MgClO_4$ dessicant connected in series, and an Horiba PIR 200 infrared (IR) detector. Samples are injected into the glass purge trap which holds 30 wt % H_3PO_4. CO_2 species in injected samples including CO_2, HCO_3^-, CO_3^{2-}, and carbamates are converted to gaseous CO_2 and swept from the purge trap vessel, through the dessicant material and into the IR detector where these species absorb an amount of IR energy depending on the concentration of CO_2. The absorption response is converted to a voltage which is recorded in Picolog software (Pico Technology, UK) deployed from a

dedicated PC. In addition to solvent samples, a 1,000 ppm standard is injected in triplicate at five different volumes to create a standard curve. The standard was supplied by RICCA Chemical Co. (1 mL = 1 mg C), and prepared with Primary Standard Grade Sodium Carbonate and ACS Reagent Grade Sodium Bicarbonate.

Setup of the TIC equipment for injection of a sample set is conducted as follows. Approximately 1.5 mL of 30 wt % H_3PO_4 is injected with a disposable hypodermic needle through a rubber septa into the glass purge vessel, and the dessicant tubes are filled with fresh dessicant material to create two ~4-inch columns to ensure no moisture is swept to the IR detector. The N_2 gas control valve is opened to allow N_2 gas to flow into the purge trap vessel, sweeping upward through the dessicant tubes, and into the IR detector. Picolog is opened and deployed for data acquisition. Depending on CO_2 loading, samples should generally be diluted 10 to 20X in DDI.

The sample injection process is performed as follows:

1) Samples are drawn into a syringe at a predetermined amount, typically between 10 and 50 uL in sample size,
2) The needle + sample is placed on the Mettler Toledo balance, and the balance tared,
3) The sample is then injected through the septa into the purge vessel for acidification,
4) The empty needle is placed back on the balance for weighing to determine the mass injected to 0.0001 g precision, and
5) The time corresponding to the mass first passing into the IR detector is recorded.

This process is repeated so that each sample is injected a total of three times. Injections of the 1,000 ppm total inorganic carbon standard are made in triplicate with

injection mass and time recorded in the same fashion. Five different TIC standard injection masses are selected such that the peak size recorded in Picolog for the smallest standard injection mass is smaller than the unknown sample peak sizes, and the largest is larger than the unknown peak sizes. The standard injection mass amounts are selected to ensure that the standard curve covers the same TIC mass range as exists in the samples. Once all samples and standards have been injected, the data is entered into a spreadsheet for injected mass integration, comparison to the standard curve, and calculation of CO_2 loading by mass in each sample.

The average and standard deviation of TIC measurements were determined for C-27-12 through analyses of the samples collected in triplicate. All three samples were collected, diluted, and injected in the TIC instrument as individual samples; the samples were injected in series in a single TIC analytical run. The average and standard deviation of the TIC measurements were 0.29 ± 0.0 mol CO_2/mol alk. The standard deviation of 0.0 is not surprising given that each individual TIC measurement is made in triplicate and averaged in the standard spreadsheet to provide the overall number. As such, three individual measurements are a result of making nine total (3 X 3) injections.

Chapter 3 - ISDA characterization with 7 m MDEA

This chapter describes the characterization of the ISDA with respect to degradation of 7 m MDEA, and complements the full description of the system provided in section 2.3. The ISDA characterization was conducted through the degradation of one solvent (7 m MDEA) in a series of experiments, starting with the initial design, and progressing through incremental modifications. Some of those modifications became permanent to the system and were, therefore, utilized in all subsequent cycling experiments. Other modifications were used in a subset of the experiments and subsequently discontinued. Some of the discussed experiments were simply conducted at modified conditions, and did not entail a change to the installed equipment. For example, bulk liquid temperature exiting the thermal reactor is one variable in system operations that is easily changed, and allows the evaluation of solvent oxidative degradation processes over a range of operational conditions. All cycling experiments entailed maintaining the oxidative reactor bulk liquid temperature at 55 °C.

The major components of the ISDA including their respective volumes and residence times based on a nominal liquid flow rate of 200 mL/min are listed in Table 3.1. The values are listed by the ISDA experiment according to major system changes. In Table 3.2, the experiments which will be discussed in this section are listed along with the basic equipment utilized, the modifications made to the system, and major ISDA operating conditions (thermal reactor temperature and purge gas make-up). The discussion is not intended to follow experiments in chronological order, but instead, to provide a coherent description of system function in terms of degrading solvents. Where applicable, data are compared to Low-gas experimental results.

Table 3.1: ISDA System Volumes and Retention Times

ISDA Expt No.	Units	1-4	5	6-24	25-34
Modification		Original Design	Bubble Removal Vessel – Vertical	Bubble Removal Vessel - Jar	Bubble Removal Jar + Redesigned Thermal Reactor
Oxid Rx V	mL	730	730	730	730
Oxid Rx RT	min	3.65	3.65	3.65	3.65
Bubble Rem V	mL	0	230	620	620
Bubble Rem RT	min	-	1.15	3.1	3.1
Heat-X Shell Side V	mL	378	378	378	378
Heat-X Shell Side RT	min	1.9	1.9	1.9	1.9
Heat-X Tube Side V	mL	100	100	100	100
Heat X Tube Side RT	min	0.5	0.5	0.5	0.5
Th Rx V	mL	1120	1120	1120	130
Th Rx RT	min	5.6	5.6	5.6	0.65
Heat Coil V	mL	48	48	48	48
Heat Coil RT	min	0.24	0.24	0.24	0.24
Transf Tubing	mL	45	45	45	45
Total Syst V	mL	2421	2651	3041	2051
Total Syst RT	min	12.1	13.3	15.2	10.3

All based on nominal liquid rate of 200 mL/min

3.1 SELECTION OF 7 m MDEA FOR CHARACTERIZATION

7 m MDEA at a nominal initial loading of 0.1 mol CO_2/mol alkalinity was the solvent utilized in all characterization experiments. A new solvent batch was created within 48 hours of the start of each experiment. An initial loading of 0.1 mol CO_2/mol alkalinity was utilized in all 7 m MDEA experiments. This loading matched the CO_2 solubility condition for this solvent at 55 °C when a purge gas of 98% O_2/2% CO_2 was used in the headspace of the oxidative reactor. The mixed gas was purchased from Matheson TriGas in 60 or 70-lb compressed gas bottles, which proved to be a convenient

method for consistently delivering the proper headspace purge gas mixture to the oxidative reactor in the ISDA.

Table 3.2: The ISDA characterization experiments

Expt No.	Thermal Rx Temp (°C)	Stir Rate - Oxidative Rx (rpm)	Purge Gas	System Modifications
C-1	120	1,440	98% O_2/2% CO_2	Initial Design
C-4	120	520	98% O_2/2% CO_2	-
C-5	120	1,000	98% O_2/2% CO_2	Vertical Bubble Removal Vessel
C-6	120	1,440	98% O_2/2% CO_2	Modified Bubble Removal Vessel
C-18	120	1,440	98% O_2/2% CO_2	2 L/min N_2 Gas Purge
C-13	120	1,440	98% Air/2% CO_2	Modified Bubble Removal Vessel
C-14	90	1,440	98% Air/2% CO_2	Modified Bubble Removal Vessel
C-12	90	1,440	98% O_2/2% CO_2	Modified Bubble Removal Vessel
C-8	90	1,440	98% N_2/2% CO_2	Modified Bubble Removal Vessel

With the exception of experiments C-1 and C-2, the 7 m MDEA stock solvent was augmented with a mixture of metal salts to mimic levels of dissolved metals that might be encountered in a solvent which had seen use in a scrubbing environment in stainless steel processing equipment. The metals were added as aqueous dissolved solutions of $FeSO_4 \cdot 7H_2O$, $Cr(SO_4)_3 \cdot 12H_2O$, and $NiSO_4 \cdot 6H_2O$ at concentrations of 0.4 mM Fe^{2+}, 0.1 mM Cr^{3+}, and 0.05 mM Ni^{2+}, respectively, to the stock solvent solutions in experiment C-3 through C-34. These solutions were dissolved in 0.1 mM HNO_3 to prevent precipitation in the stock solution. These dissolved metal salts were added to experiments with other solvents including 8 m PZ and 7 m MDEA/2 m PZ. Sexton (2008) reported that in the presence of iron, 7 m MEA degradation increased by a factor of 3X using the Low-gas degradation system. These studies corroborated studies conducted by the Girdler Corporation (1950) regarding metal ion catalysis of MEA

degradation. It was expected that these dissolved metal salts would serve to catalyze oxidative processes in the cycling environment created by the ISDA.

The selection of 7 m MDEA for characterization purposes was made to avoid the need to consider the more complicated degradation processes anticipated in 7 m MDEA/2 m PZ. Early thermal degradation experiments with the blend (Thermal No. 7) resulted in significant loss of both parent amines (MDEA and PZ), and the production of a number of degradation products including those resulting from arm-switching processes (Rochelle, 2009). These experiments were followed by additional cycling experiments with 8 m PZ and 7 m MDEA/2 m PZ. After making a final modification to the system by reducing the thermal reactor size, more cycling experiments (C-25 through C-34) were conducted in the ISDA with 7 m MDEA for comparison to the previous configuration with the larger reactor.

3.2 Assessment of Degradation Rates

3.2.1 Types of data used

Several different types of data were used in the assessment of degradation rates in 7 m MDEA as the initial design was tested and modified. Cation IC data were used to evaluate MDEA loss and amine degradation product formation (DEA and MAE). Anion IC data were used to evaluate carboxylate ions formation (formate). The AAA-Direct HPLC amino acid data provided bicine formation rates in 7 m MDEA. Finally, titration data were used to evaluate the loss of overall solvent alkalinity.

Most of the degradation data discussed in this section are generally characterized as indicators of oxidative degradation as opposed to thermal or CO_2-catalyzed degradation. Goff (2005) reported that formic acid is formed with a stoichiometric ratio

of 0.75 moles O_2 consumed per mole of formic acid produced in MEA; formic acid is measurable as formate using anion IC. Further supporting the use of formic acid as an indicator of oxidative degradation in the ISDA is the fact that the solvent spent less than 35% of the total cycling time at or near the bulk liquid thermal reactor temperature in the initial design, and was generally closer to 55 °C for the duration of each cycling experiment. After the thermal reactor was redesigned, this number was reduced to approximately 6% of total cycling time. In addition to formate and total formate production rates, the discussion in this section utilizes MDEA loss rates extracted from the cation IC data, and alkalinity loss rates extracted from titration data.

3.2.2 Extraction of linear initial rates

All data were plotted in Microsoft Excel, and initial rates extracted using the Excel least squares linear fit function. The ISDA characterization was made based on initial rates, requiring some judgment as to how much data to use in extracting a rate. Long-term degradation trends were used in other analyses to identify intermediate degradation products, and secondary effects including competition for oxygen in the solvent as product concentrations increased. Many data sets exhibited linearity over the course of the experiment, simplifying the evaluation of rates. However, some data sets exhibited one trend at the beginning of the experiment, and a different trend for the remainder of the experiment. For example, Figure 3.1 depicts the concentration of MDEA, PZ, formate, and other degradation products over the course of experiment C-34, and demonstrates how two trends can be extracted from the data. At approximately 100 hours, the rate of formate production decreased, perhaps indicating a competition for oxygen. As a point of emphasis, initial rates were used in this chapter for ISDA

characterization purposes and the following chapters to measure the degradation of 8 m PZ and 7 m MDEA/2 m PZ, and compare to data from Low-gas and thermal experiments.

All rates are absolute, based on cycling time in each respective experiment. The rates have not been corrected for any changes in total solvent inventory. Analysis of normalized rates is not presented in this section.

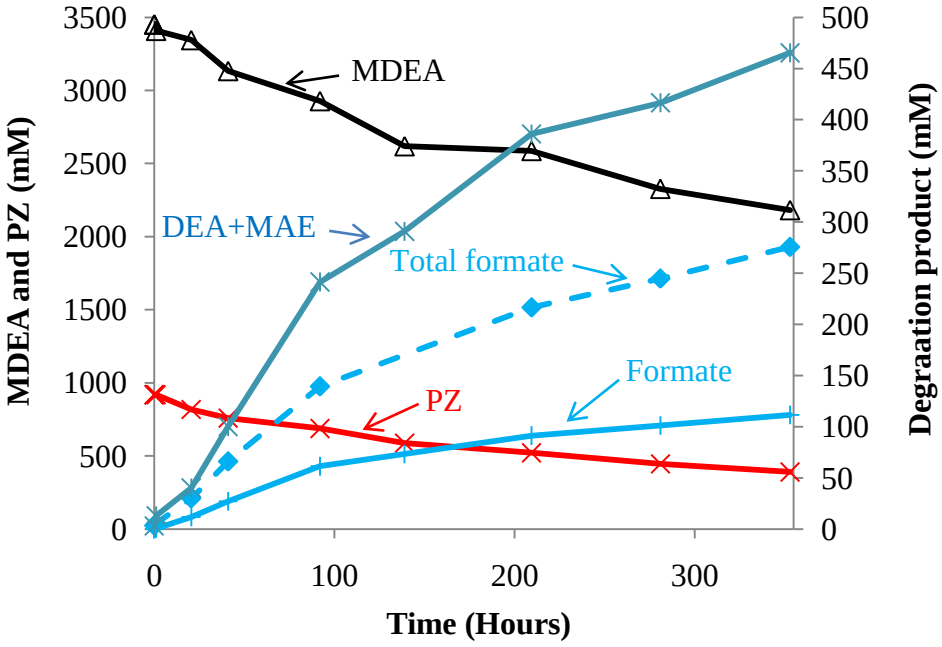

Figure 3.1: MDEA, PZ and degradation products in cycled 7 m MDEA/2 m PZ (C-34); solvent treated with 0.1 mol H^+/mol alkalinity and cycled 55 to 120 °C

3.2.3 Statistical error in data

To understand the error associated with the data and the estimates of degradation rates, the Linest function in Excel was used on a subset of data. For example, in C-27 for which samples were collected in triplicate (see section 2.6.1.1), the Linest function was utilized on the MDEA cation IC data. The average linear loss rate for MDEA using the entire data set was 2.94 ± 0.28 mM/hr with an R^2 of 0.91. The uncertainty in the slope or

linear loss rate was (0.28/2.94)*100% = ~9.6%. The average linear production rate for MAE using the entire data set (N-11) was 1.05 ± 0.045 mM/hr with an R^2 of 0.98. The uncertainty in the slope or linear loss rate was (0.045/1.05)*100% = ~4.3%. Recall from Section 2.6.1.1 that the error in the MDEA cation IC data was 1.3%, while for 1-MPZ the error was ~1.5%. Together these cation data suggest that even with low individual data error, the error associated with the linear rates can be as much as ± 5 to 10%.

Performing the same analysis with the formate data over the first 120 hours of cycling in C-27, the Linest linear production rate was 0.15 ± 0.008 mM/hr with an R^2 of 0.97. The error in the linear rate data was ~5%. Recall for the C-27 data that the formate concentration average and standard deviation were 33.0 ± 0.33 mM for the final sample (C-27-12). The error around the mean was 1%, which is much lower than the error in the Linest linear production rate (~5%). As with the cation data, the error associated with a single data point is acceptably small (~1%), while the error associated with the linear rate estimates can be 5%.

Further complicating the analysis of the linear rates is the more subjective issue of selecting the data most representative of "initial rates" as opposed to longer term rates. For example, for C-27, the first 213 hours of cycling were selected and Linest provided an average MDEA formation rate of 0.14 ± 0.009 mM/hr, and an R^2 of 0.96. Although not too different from the rate extracted from data through 120 hours, this analysis indicates that the initial rates used in the oxidative model in Chapter 5 are subject to the additional error associated with the user selecting the true initial rates as inputs to the model.

Finally, the amino acid data provide another challenge to the selection of the appropriate initial rate. For the first 42 hours in experiment C-27, bicine was undetectable. However, starting with sample C-27-4, bicine was detectable, increasing in

concentration in a near linear fashion through the end of the experiment. In this experiment, the initial rate was zero, but following the lag period, a linear production rate of 0.45 ± 0.016 mM/hr with an R^2 of 0.99 was calculated. The R^2 and overall error (3.6%) in the linear rate data suggest a very good fit to linearity. However, this linear rate is not truly representative of the initial rate unless the lag period is ignored altogether. This analysis highlights the subjectivity associated with selecting initial rates from the data.

3.2.4 Normalization of data to correct for liquid inventory changes

In the discussion that follows regarding rates of degradation in the ISDA, the rates have been extracted as discussed in section 3.2.2, but correction or normalization of the data to correct for liquid inventory changes after system modifications was not performed across the board on all data. For a subset of the data, correction for that portion of the inventory that was changed has been performed to normalize the data to a standard inventory, and allow direct comparison of rates. For example, following the redesign of the thermal reactor from 1.12 to 0.13 L in volume, the overall system inventory changed by ~33%. The residence time of solvent at the higher temperatures associated with each cycling experiment was reduced by far more than 33%, compounding the need to normalize the data in some cases to make direct comparisons. Normalization of data from a subset of experiments is performed in the discussions in Chapters 5 and 6.

3.2.5 Effect of On/Off operation (Experiments C-1 through C-3)

Up through cycling experiment C-3, the system was cooled down, and the pump shut down at the end of each work day. The solvent was left in the system overnight, and the ISDA was simply brought back on-line the next morning. This method allowed for approximately 7 to 8 hours of cycling degradation at full temperature each day, but also

allowed the solvent to remain in the system each night in a partially oxygenated state. The extent to which this start/stop operation impacted the overall degradation rates is undetermined, but any effect would likely cause the degradation rates to be higher. The degradation time used over the course of these first experiments was that time at which the target temperatures were achieved in both the thermal and oxidative reactors. Experiments C-4 through C-34 were all performed with continuous operation on a 24-hour per day basis.

3.3 INITIAL DESIGN OF THE ISDA

The initial design of the ISDA included the oxidative reactor, cross heat-exchanger, and large thermal reactor (1.12 L). The two preheater coils described in section 2.3.1.4 were also necessary for obtaining a temperature of 120 °C in the thermal reactor. The bubble removal vessel was not included in the system, nor was the larger heat bath (Lauda E300) which enabled higher temperatures (120+ °C) to be reached in the thermal reactor. As listed in Table 3.2, experiment C-1 was conducted with the thermal reactor bulk liquid temperature at 120 °C, the stir rate set at ~1,440 rpm, the nominal solvent flow rate set at 200 mL/min, and the 98% O_2/2% CO_2 purge gas in the headspace of the oxidative reactor.

Table 3.3 lists the rates of MDEA and alkalinity loss, and formate and total formate production in the experiments discussed in the following sections. The MDEA and alkalinity loss rates for C-1 were 8.8 and 5.2 mM/hr, respectively, while the formate and total formate production rates were 0.59 and 0.98 mM/hr, respectively. The error associated with these rates is in the range of 5 to 10%. These data were compared to the rate of formate production measured in Low-gas experiment OD-2 with 7 m MDEA (1

mM Fe^{2+}) conducted at 55 °C. The formate production rate in C-1 was approximately 25X the rate measured in OD-2, and approximately 2X the rate (0.24 mM/hr) measured in 7 m MEA in a Low-gas experiment (Sexton, 2008). Low-gas experiment OD-8 was conducted with 7 m MDEA. In that experiment, the formate production rate was 0.028 mM/hr, confirming that rates in the ISDA were 20 to 25X the rates measured in Low-gas experiments with 7 m MDEA.

Table 3.3: Initial degradation rates - 7 m MDEA in the ISDA (all rates mM/hr)

Expt No.	Th Rx T (°C)	Stir Rate (rpm)	Purge Gas (98% O_2/2% CO_2)	MDEA Loss Rate	Alk Loss Rate	Formate Production	Total Formate Production
C-1	120	1,440	98% O_2/2% CO_2	8.8	5.2	0.59	0.98
C-4	120	520	98% O_2/2% CO_2	3.4	2.5	0.17	0.15
C-5	120	1,000	98% O_2/2% CO_2	8.5	4.3	0.37	0.57
C-6	120	1,440	98% O_2/2% CO_2	4.6	4.9	0.28	0.34
C-18	120	1,440	98% O_2/2% CO_2	0	0.7	0.047	0.044
C-13	120	1,440	98% Air/2% CO_2	0.2	0.5	0.08	0.08
C-14	90	1,440	98% Air/2% CO_2	0.2	0.2	0.044	0.058
C-12	90	1,440	98% O_2/2% CO_2	2.9	2.2	0.12	0.15
C-8	90	1,440	98% N_2/2% CO_2	1.9	1.6	0.013	0
OD-2	-	1,440	98% O_2/2% CO_2	0.4	NM	0.013	0.026
OD-8	-	1,440	92.5% O_2/7.5% CO_2	0.4	0.1	0.028	0.03

Figure 3.2 provides the concentrations of the measured carboxylate ions (also referred to as heat stable salts) including formate, glycolate, and oxalate plotted over experimental time. The data indicate that formate is the only carboxylate ion formed in appreciable quantities in 7 m MDEA. For this reason, no other carboxylate ion data will be discussed in this section. The concentration of total formate, which as noted in section 2.4.1.2, is a measure of the formate concentration after samples are hydrolyzed with NaOH to reverse the formation of amides. The difference between total formate and

formate alone represents the approximate concentration of formyl-amides produced in the degradation of the solvent. The total formate concentrations indicate that amides are formed in the solvent, but at concentrations which are less than half those of formate without reversal of amide formation. The latter observation is a consistent trend observed in cycling experiments 7 m MDEA.

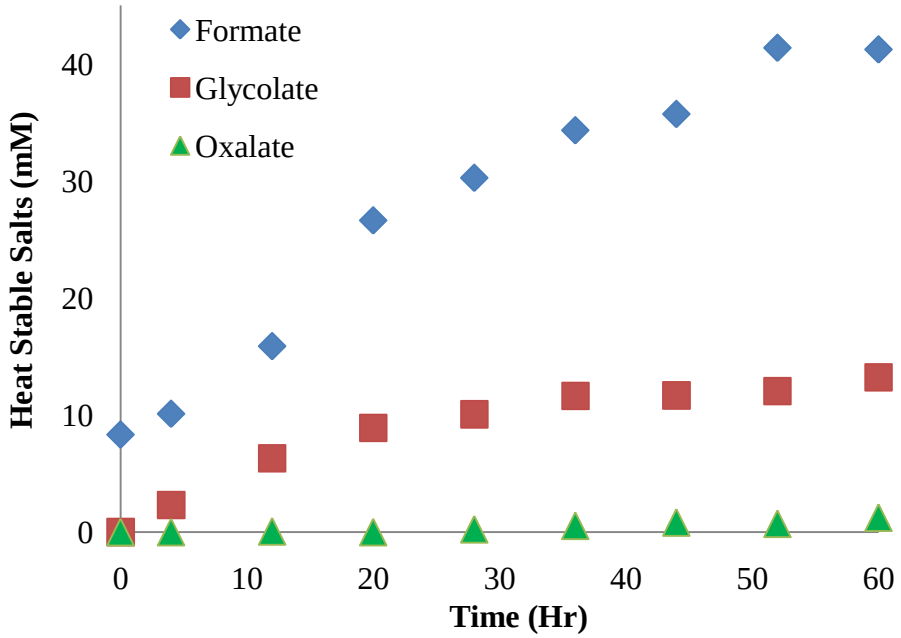

Figure 3.2: Heat stable salt formation in experiment C-1: 7 m MDEA cycled from 55 to 120 °C in original design of the ISDA

3.4 Effect of Bubble Entrainment

The direct comparison of formate production rates from the Low-gas (OD-2) and cycling (C-1) experiments indicates that one or more design issues were responsible for the accelerated rate measured in C-1. The visual observation of bubbles being entrained in the solvent as it passed through the reactor hold-up section (bottom) and passed out the

pump inlet tubing was coupled with the formate production measurements. The entrained bubbles represented a separate-phase oxygen supply in the solvent as dissolved oxygen was depleted through oxidative degradation processes in the solvent. At the higher stir rates experienced (>1000 rpm), these bubbles were likely sheared into smaller bubbles, enhancing the mass transfer of gas bubbles into the solvent. The bubble entrainment observed in solvent at the full stir rate of 1,440 rpm was believed to be a significant factor in the greater formate production rate measured in C-1 when compared to OD-2.

3.4.1 Stir rate reduction

In experiment C-4, 7 m MDEA with the dissolved metals salts was cycled from 55 to 120 °C. However, the stir rate in the oxidative reactor was set to 520 rpm to minimize the extent of bubble entrainment in this section of the ISDA. This rate was chosen based on a series of short tests where the solvent was brought to its experimental temperatures (55 and 120 °C), and the stir motor and impeller blade were turned on and set at half speed (720 rpm), then decreased again to 520 rpm. At 720 rpm, visual observation confirmed that a limited amount of gas bubbles was being entrained and carried through with the solvent to the pump, and subsequently to the thermal reactor. The stir rate was decreased again to 520 rpm to provide a factor of safety in terms of minimization of bubble entrainment.

Experiment C-4 was conducted with this decreased stir rate (520 rpm), and the formate production rate was measured as 0.17 mM/hr, with the total formate production rate 0.15 mM/hr. This rate represented a 70% decrease in formate production, with amide production (quantified as formate) decreased to an immeasurable rate. The initial rate of MDEA loss decreased from 8.8 mM/hr to 3.4 mM/hr, while the rate of alkalinity

loss was cut in half (2.46 vs. 4.78 mM/hr). With solvent exiting the thermal reactor at a bulk liquid temperature of 120 °C and the nominal liquid flow of 200 mL/min in both experiments, the residence time in the thermal reactor was also the same (~6.5 min), eliminating any effects associated with different thermal degradation behavior between the two experiments. These data indicate that the decrease in the oxidative reactor stir rate from 1,440 to 520 rpm resulted in a decrease in the amount of gas bubble entrainment in solvent exiting the oxidative reactor, providing a decreased MDEA degradation rate.

3.4.2 Bubble removal vessel

As with the Low-gas experimental reactor design, one objective of the ISDA system design was to ensure that solvent degradation occurred under kinetically-limited as opposed to mass transfer limited conditions. The design objective called for achieving dissolved oxygen saturation in the solvent as it leaves the oxidative reactor. This criterion required that the stir rate be increased and maintained at its original rate of 1,440 rpm, while bubble entrainment was kept at a minimum level. Cycling with this stir rate also ensured that comparable conditions were maintained in the Low-gas experiments and the oxidative reactor of the ISDA.

Before conducting experiment C-5, a vessel was constructed by the glass fabrication shop in the Chemistry Department for the purpose of intercepting and removing the entrained bubbles. A vertical glass vessel 11.5 inches in height and approximately 1.5 inches in diameter with a four-inch layer of loose ProPak 0.24-inch diameter distillation packing was installed in the ¼-inch tubing just downstream from the oxidative reactor, but immediately upstream of the liquid transfer pump. The solvent entered the vessel at a point above the liquid level and packing, and traveled downward to

a port near the bottom of the vessel where it exited and traveled to the pump inlet. The purpose of the packing was to intercept entrained bubbles at the packing surface, allowing smaller bubbles to contact each other and coalesce into larger bubbles which had a greater chance of escape from the solvent due to better gravity separation from the liquid. The stir rate in experiment C-5 was increased to 1,000 rpm to impart greater energy to the solvent in the oxidative reactor.

The formate and total formate production rates were 0.37 and 0.57 mM/hr, respectively, while the MDEA loss rate was 8.5 mM/hr (Table 3.3). These rates indicated a more than doubling of the degradation rates measured in C-4 wherein the stir rate was only 520 rpm in the oxidative reactor, and no bubble removal vessel was installed. Further, C-5 samples exhibited amide production, as evidenced by the total formate rate being almost double (0.57 vs 0.37 mM/hr) the formate production rate. These rates were indicative of two possible mechanical or chemical degradation effects: (1) the increase in stir rate to 1,000 rpm caused a general increase in the amount of oxygen being dissolved into the solvent and, therefore, available for oxidative degradation, and/or (2) the vertical bubble removal vessel was ineffective at intercepting and removing entrained bubbles from the solvent.

The bubble removal vessel was redesigned and constructed out of a 4-inch diameter glass jar as described in section 2.3.1.3. The ProPak distillation packing was dumped into the new vessel and covered the bottom in an approximately 1 and 1/4-inch layer. As the solvent entered a port near the bottom of the jar, it flowed directly into the packing, enhancing gas bubble contact and coalescence into larger bubbles, making it easier for bubbles to escape the solvent. Furthermore, the redesigned bubble removal vessel had a wider cross-sectional area and larger overall volume, providing a residence time of ~3 minutes. The liquid flow velocity at the midpoint in the wider vessel was

calculated as ~2.8 cm/sec, as compared to the average flow velocity in the previous design (vertical column) of ~17.5 cm/sec. The combined effect of greater residence time, reduced flow velocity, and immediate contact with the packing at the entry to the vessel provided more opportunity for bubbles to escape the solvent and reach the surface of the liquid. Once installed, visual observations made during preliminary tests confirmed that this bubble removal design was more effective than the previous at coalescing bubbles and allowing them to escape the solvent without getting caught in the flow path of solvent exiting the bubble removal vessel.

In cycling experiment C-6, 7 m MDEA was cycled from 55 to 120 °C with the newly designed bubble removal vessel installed. The stir rate in the oxidative reactor was increased to 1,440 rpm to ensure that the experimental conditions were not mass transfer controlled with respect to dissolved oxygen in solvent exiting the oxidative reactor. All other conditions of this experiment are listed in Table 3.2, while Table 3.3 lists the degradation rates.

Formate data are presented in Figure 3.3 for C-1, C-4, C-5, and C-6. The MDEA loss rate in C-6 was 4.6 versus 8.5 mM/hr in C-5. The formate and total formate production rates were 0.28 and 0.34 mM/hr, respectively. The only rate to exhibit an increase was the alkalinity loss rate, which increased to 4.93 mM/hr. In general, the rates were less than those rates measured in C-5, indicating that the newly designed bubble removal vessel was effective at minimizing gas bubble entrainment and the effect of those bubbles being carried over to higher temperature regions of the ISDA where accelerated oxidation could occur. Although the rates were not as low as those measured in experiment C-4 wherein the stir rate in the oxidative reactor was set to eliminate visual evidence of gas bubble entrainment, the rates measured in C-6 do indicate that those

same conditions were approached through installation of the redesigned bubble removal vessel.

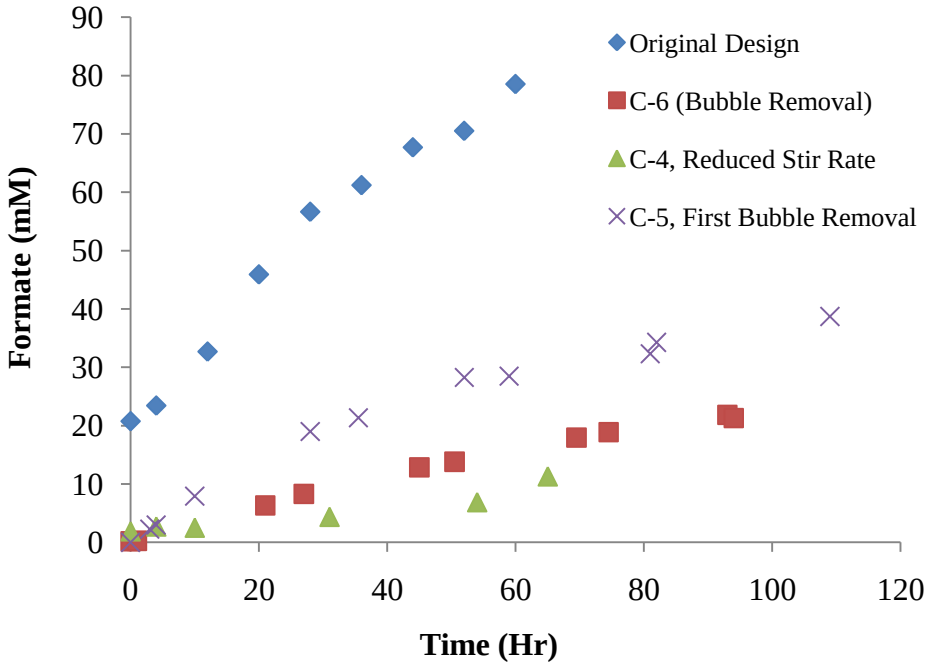

Figure 3.3: Formate (mM) measured in ISDA with bubble entrainment reductions

When compared to the degradation rates measured in Low-gas experiment OD-8 conducted at 70 °C, the rates measured in the ISDA were an order of magnitude higher. For example, the MDEA loss rate measured in OD-8 was 0.12 mM/hr, while the formate and total formate production rates were 0.028 and 0.03 mM/hr, respectively. The alkalinity loss rate in OD-8 was 0.37 mM/hr.

The measured degradation rates were normalized to the original system volume and compared to the original system design rate for MDEA loss (C-1). An assumption was made that experiment C-6, which was conducted with the large bubble removal vessel and a total system volume of 3.04 L, included 0.62 L of additional "cold" inventory when compared to the system design used in C-1 (V~2.42 L). This additional

inventory was generally depleted of entrained oxygen, but was saturated with dissolved oxygen. Assuming that the degradation rate at 55 °C is less than 1/100th the rate at 120 °C, the critical residence time will not include the bubble removal vessel volume. This last assumption regarding lower rates at lower temperatures is validated later in this chapter. With the nominal liquid flow rate approximately the same between these two experiments, the rate in C-6 was normalized to the rate from C-1 by multiplying it by a factor of 3.04/2.42 or ~1.25X. The normalized MDEA loss rate in C-6 is 1.25 X 4.6 mM/hr = 5.8 mM/hr. This rate is less than the rate measured in C-1 of 8.8 mM/hr, and indicates that normalization to the residence time of the original design does not fully account for the increased MDEA degradation when the bubble removal vessel is used.

Despite higher degradation rates with 7 m MDEA when compared to degradation of the same solvent in the Low-gas reactor, the ISDA system underwent no more permanent modifications until after experiment C-24, at which time the thermal reactor was redesigned to 1/9th its original volume. As such, with the exception of C-18, the basic design for experiments C-6 through C-34 included the 4-inch diameter bubble removal vessel with a 1 and ¼-inch layer of loose ProPak distillation packing for entrained bubble removal. In C-18, the vertical bubble removal vessel was retrofitted to allow insertion of a sparge stone for dissolved oxygen stripping for that single experiment. All other changes described in the following sections were changes to the system operating conditions as opposed to the hardware.

3.5 Effect of Dissolved oxygen

In experiment C-18, a modified bubble removal vessel was designed and installed to achieve both dissolved oxygen and entrained gas bubble removal. The modified

bubble removal vessel was 8 inches tall and ~2.4 inches in diameter, with a ¼-inch solvent inlet port at the bottom, and exit port closer to the top. A thermoplastic polyester screw cap was modified by tapping a bore-through Swagelok® plastic ¼-inch NPT-to-compression adapter into the middle. A ¼-inch glass tube with fritted stone was inserted into the fitting to within 1 inch of the bottom of the vessel. As the solvent was cycled in the ISDA, ~1 L/min of N_2 gas was sparged into the solvent in this modified vessel, effectively stripping dissolved and entrained gases from the solvent immediately after exiting the oxidative reactor. A ¼-inch plastic line was plumbed from the sparge vessel to the oxidative reactor headspace to return gases to this vessel.

The formate and total formate production rates were 0.047 and 0.044 mM/hr, respectively, while the MDEA loss rate was immeasurable. The alkalinity loss rate decreased to 0.73 mM/hr. These rates represented an order of magnitude decrease from the rates observed in C-6, and indicated that formyl-amide production was immeasurable. The inherent variability in the cation measurements did not allow estimation of losses in MDEA concentration in this experiment. A review of statistical analyses of cation IC and anion IC data collected from cycling experiments is presented in Chapter 4, providing an assessment of average and standard deviation data from the system. Although the sparge vessel design was used in a single experiment (C-18), the practical implications to this modification were significant, as discussed at the end of this chapter.

3.6 Effect of Headspace gas composition

The effect of the headspace gas composition on degradation rates was tested through a series of experiments where this gas composition was changed from the 98% O_2/2% CO_2 mixture used in all previous experiments. In experiments C-13 and C-14, the

headspace gas composition was changed to a mixture of 98% air/2% CO_2, which provided a CO_2 composition of 2%, an oxygen composition of approximately 20.5%, and the remaining 77.5% consisting of N_2, Ar, and other trace gases. The gas mixture was supplied by mixing compressed air supplied to the fume hood with CO_2 using Brooks flow controllers. During experiment C-13, 7 m MDEA was cycled from 55 to 120 °C. The degradation data collected in this experiment can be compared to the data from C-6 and other experiments where the bulk solvent temperatures in the two reactors were maintained at these temperatures. The expectation was that the rate of oxidation would decrease to one-fifth the rate measured in C-6.

The MDEA loss rate measured in C-13 was 0.24 mM/hr, which was $1/20^{th}$ the rate measured in C-6. The alkalinity loss rate was measured as 0.52 mM/hr, which was 1/10X the rate measured in C-6. The formate and total formate production rates were both 0.08 mM/hr. These rates were approximately 1/3X to 1/4X the rates measured in C-6, indicating that formate production is closely correlated with the amount of dissolved oxygen delivered to the solvent in the oxidative reactor.

In C-14, the thermal reactor bulk liquid temperature was maintained at 90 °C. No previous experiment with the thermal reactor set to this temperature has been discussed to this point. The experiment conducted at comparable thermal conditions, but utilizing a 98% O_2/2% CO_2 headspace gas, was C-12. The data listed in Table 3.3 indicate that the MDEA loss rate in C-14 was a full order of magnitude less than that measured in C-12 (0.22 vs. 2.87 mM/hr). The formate production rate in C-14 was 0.044 vs. 0.12 mM/hr in C-12, indicating a decrease to approximately 1/3X the rate measured when the headspace purge gas is 98% O_2/2% CO_2. A comparison of the total formate production rates indicates the same approximate ratios between the two experiments.

This close correlation between headspace gas O_2 composition and formate production also indicates that, when the headspace gas composition is constrained in O_2, oxidative degradation is kinetically limited overall. Mass transfer at the high stir rate (1,440 rpm) is adequate to achieve dissolved oxygen saturation in the solvent, and to achieve kinetically controlled oxidative degradation at these conditions.

In experiment C-8, 7 m MDEA was cycled from 55 to 120 °C with a headspace purge gas of 98% N_2/2% CO_2. This experiment was conducted to determine the extent of MDEA degradation that occurs in the extreme case of having no purge gas O_2 available. The absence of O_2 in the purge gas and, therefore, as dissolved oxygen in the solvent, was intended to place emphasis on thermal and CO_2-catalyzed degradation processes at temperatures above 55 °C. Recall that the solvent residence time at or near the thermal reactor temperature in the ISDA with the original thermal reactor is approximately 35% of the total residence time in the system. For example, over the course of the 167 hours of cycling in C-8, the solvent will have spent approximately 58 hours at the thermal reactor temperature setting, with limited additional time (~5% of total, or 8 hours) in between the oxidative reactor temperature (55 °C) and the thermal reactor temperature.

The rate of MDEA loss was ~1.9 mM/hr in C-8, while in C-6 where the 98% O_2/2% CO_2 headspace purge gas was used, the rate was 4.6 mM/hr. A comparable effect was measured in alkalinity loss rate, which decreased from 4.6 mM/hr to 1.6 mM/hr. The rates of formate and total formate production were 0.013 and 0.001 mM/hr, respectively. These rates including MDEA and alkalinity loss are representative of those rates to be expected with thermal degradation only. The formate and total formate production rates measured in C-6 were 0.28 and 0.34 mM/hr, respectively. The presence of oxygen in the headspace gas increased the formate production 20X, and the MDEA and alkalinity losses 2.5X and 3X, respectively.

Although thermal degradation experiment data are not generally relevant to the characterization of the ISDA, a better comparison of the rates of MDEA loss and formate production in C-8 is to the data from thermal degradation experiment Thermal No. 10. In that experiment, 7 m MDEA at a lean loading of 0.1 mol CO_2/mol alkalinity was thermally degraded at 120, 135 and 150 °C in Swagelok® cylinders. No dissolved metal salts were added to this solvent. As discussed in Chapter 2, the thermal degradation cylinders were charged with 10 mL of solvent, allowing for very little headspace gas and, therefore, very little dissolved oxygen. The rates of MDEA loss and formate production in Thermal No.10 at 120 °C were within the error of the measurement method. One possible explanation for why the MDEA loss in C-8 was 1.9 mM/hr accompanied by low amounts of formate production (0.013 mM/hr), while MDEA in the thermal experiment experienced essentially no loss and no formate production is the presence of dissolved metal salts in the cycled solvent. In MEA, these metals (added as salts) are known to catalyze oxidative degradation (Sexton, 2008). However, the possibility that oxygen gas is able to enter the headspace of the ISDA oxidative reactor is low due to a net positive pressure in the vessel created by the 100 mL/min purge gas; in C-8, that purge gas was 98% N_2/2% CO_2. It is likely that the solvent cycled under reduced conditions after the initial warm-up period (<1 hour) during which the small amount of dissolved oxygen in the stock solution was consumed. Additionally, Davis (2009) reported that 100 mM additions of Fe, Cr, Ni, Cu, and V in individual batch cylinder experiments did not increase the thermal degradation of 7 m MEA at 150 °C. The fact that cycled solvents undergo complete and continuous mixing for the duration of each experiment likely maximizes the potential for free radical mechanisms resulting from single electron abstraction processes in the presence of transition metals to occur, whereas the batch cylinder experiment is implemented under quiescent conditions.

One other possible explanation for the loss of MDEA in C-8 is the volatilization of the amine from the reactor over the course of the experiment. Recall that DDI was added to the reactor system each day based on the liquid level in the oxidative reactor. An assumption was made that liquid losses from the system through apertures in the oxidative reactor rubber stopper lid were primarily water. Subsequent experiments utilized the condensate tube described in Chapter 2. Analyses of liquid condensate samples from this tube determined that the more volatile species generated in each experiment did tend to collect in this liquid, verifying volatile losses. Although less volatile than DDI, MDEA losses can be expected due to this mechanism.

3.7 Effect of thermal reactor temperature

The ISDA oxidative reactor was designed to have the same geometry and mass transfer characteristics as the Low-gas reactor which had been in use in the Rochelle lab for over four years at the time of ISDA construction. The design similarities were purposeful; the ISDA data should be directly comparable to the Low-gas data in terms of oxidative reactor mass transfer and oxygen delivery characteristics. Given this design criterion, the standard operation of the ISDA was intended to include a 98% O_2/2% CO_2 headspace purge gas, and solvent agitation rate of 1,440 rpm in the oxidative reactor. The data presented in the previous sections indicate that these conditions will result in accelerated oxidative degradation when 7 m MDEA is cycled from 55 to 120 °C. The evidence for this conclusion includes MDEA loss rates, and formate and total formate production rates in experiments C-5 and C-6. It is important to better understand the effect of thermal reactor temperature on those rates in cycled 7 m MDEA.

Separate cycling experiments were conducted with 7 m MDEA in the ISDA with the thermal reactor bulk liquid temperature set at 55, 80, 90, 100, and 120 °C. All other solvent and operational conditions were held the same, including initial CO_2 loading (0.1 mol CO_2/mol alkalinity), stainless steel metals salts augmentation (0.4 mM Fe, 0.1 mM Cr, and 0.05 mM Ni), oxidative reactor bulk liquid temperature (55 °C), and solvent liquid flow rate (~200 mL/min). The data from these ISDA experiments are listed in Table 3.4, and can be utilized to understand the effect of temperature on oxidation rates in solvents. These data were also used to develop an oxidative degradation model for predictive purposes. The details and results of that model are discussed in Chapter 4.

Table 3.4: Formate Production (mM/hr) with thermal reactor varied 55 to 120 °C 7 m MDEA, Oxidative reactor – 55 °C, 98% O_2/2% CO_2

Expt No.	Thermal Reactor Temp (°C)	MDEA Loss Rate	Alk Loss Rate	Formate Production	Total Formate Production
C-3	55	0.9	0.9	0.005	0.01
C-11	80	0.9	1.0	0.034	0.039
C-12	90	2.9	2.2	0.12	0.15
C-10	100	4.1	3.1	0.18	0.31
C-6	120	4.6	4.9	0.28	0.34
OD-2	-	0.4	NM	0.013	0.026
OD-8	-	0.4	0.1	0.028	0.03

The thermal reactor was maintained at 55 °C in C-3 so that the solvent (7 m MDEA) was continuously cycled at 55 °C in the entire system. The data from this experiment can be compared directly to other data collected in the ISDA as well as data from two Low-gas experiments conducted with 7 m MDEA (OD-2 and OD-8). OD-2 was conducted with 7 m MDEA (1 mM Fe^{2+}) at 55 °C, while OD-8 was conducted with 7 m MDEA (0.4 mM Fe^{2+}, 0.1 mM Cr^{2+}, and 0.05 mM Ni) at 70 °C. Table 3.4 lists MDEA and alkalinity loss rates, and formate and total formate production rates from OD-2, OD-

8, and the series of cycling experiments with the thermal reactor set at increasing temperatures, starting with 55 °C in C-3.

The MDEA loss rate in C-3 was 0.9 mM/hr, which was double the rate measured in OD-2 (0.47 mM/hr). Using Linest, a linear fit of the formate concentration data in C-3 determined that the formate linear production rate was 0.005 ± 0.001 mM/hr. A linear formate production rate of 0.013 ± 0.001 mM/hr was calculated with Linest for OD-2. The formate production rate in C-3 can be normalized to the total volume of its own oxidative reactor (~0.73 L) to provide a more direct comparison of rates from these two experiments which were both conducted at 55 °C. The total system volume in the ISDA for C-3 was ~2.42 L, while the oxidative reactor alone was ~0.73 L. The C-3 formate production rate (0.005 mM/hr) was, therefore, multiplied by 2.42/0.73 (~3.3) to give a rate of ~0.017 mM/hr. This factor normalizes the rate to a "pseudo-saturation time" rate. This rate is comparable to the rate measured in OD-2 (0.013 mM/hr) because the Low-gas system has no system volume or residence time outside the oxidative reactor, and is saturated with dissolved oxygen 100% of the time. These results indicate that the Low-gas and the ISDA systems behave comparably in terms of formate production.

The formate production rate measured in OD-8 was 2X to 3X the rates measured in both C-3 and OD-2, reflecting the higher reactor temperature of 70 °C in OD-8 as compared to 55 °C in the other experiments. However, the MDEA and alkalinity loss rates measured in OD-8 were 0.37 and 0.12 mM/hr, respectively, and were both a fraction of the rates observed in either of the two other experiments.

One important difference in the operation of the two reactor systems (Low-gas vs. the ISDA) is relevant to this discussion. The only time that the solvent can be truly saturated with dissolved oxygen in the ISDA is the residence time in the oxidative reactor, which is ~3.75 min with reactor hold-up included; the hold-up section is likely

saturated because the solvent has not passed through the bubble removal vessel at this point in the system. After exiting the oxidative reactor, the solvent travels downstream while dissolved oxygen is consumed. The oxidative reactor time represented 100% X 0.73/2.42 ~30% of the total residence time in the ISDA based on the original design. This fact is in contrast to the solvent being saturated with dissolved oxygen for 100% of the time in Low-gas experiments. Based on this analysis, one would expect that the rate of degradation in C-3 would be a fraction of the rate measured in OD-2 or OD-8. Instead, the data indicate that the formate production rates are comparable, while the alkalinity and MDEA loss rates are at least 2X to 3X the rates measured in the Low-gas experiments. One possible explanation for the increased rates observed in C-3 is the presence of entrained oxygen. Recall that experiment C-3 was conducted prior to the installation of a bubble removal vessel, thus allowing entrained bubbles to pass through the pump and cross exchanger to the thermal reactor. Although the solvent never exceeded 55 °C in experiment C-3, the entrained bubbles were afforded plenty of opportunity to dissolve into the solvent, replenishing the dissolved oxygen on a continuous basis. As such, the solvent likely never depleted the dissolved oxygen at any point in the cycling process in experiment C-3.

The rates listed in Table 3.4 support the overall conclusion that MDEA degradation increased as the solvent was cycled to a higher temperature. MDEA and alkalinity loss rates increased with thermal reactor temperature, as did the rates of formate and total formate production. This trend supports the conclusion that degradation in the ISDA is a high-temperature oxidative process. However, the data also demonstrate that the increase in formate production between 100 and 120 °C is lower than the increase observed between 90 and 100 °C, indicating that the oxidation processes become dissolved oxygen limited between 100 and 120 °C.

Based on the individual degradation product formation rates for several products including formate, we developed a preliminary oxidative model based on a simple rate law relationship (Equation 3.1):

$$r = A \times \exp\left[- \frac{E_a}{RT} \right] \tag{3.1}$$

Using the production rates for formate over the temperature range of 55 to 120 °C for the thermal reactor and listed in Table 3.4, the activation energies for degradation products in the ISDA were estimated. Estimates for E_a and r_o used in the initial model were 45,640 J/mole and 0.12 mM/hr for formate. The measured and predicted rates for formate based on Arrhenius behavior and estimates of activation energy (E_a) and r_o are presented in Figure 3.4. The predicted values for the rate are greater than the measured values at higher temperatures based on E_a and r_o, indicating that the model over-predicts the production rate for formate at higher temperatures. This finding is consistent with the conclusion that, as temperature is increased to 120 °C in the thermal reactor in the ISDA, oxidative degradation is accelerated and all of the dissolved oxygen is consumed, creating a plateau in oxidative product formation rates. At thermal reactor temperature below 100 °C, not all of the dissolved oxygen is consumed before solvent is returned to the oxidative reactor. The thermal reactor was redesigned as discussed in Chapter 2 to enable the measurement of degradation rates in a kinetically controlled mode of operation. The following section reviews the results of that redesign. Additionally, the oxidative model was improved with the integration of a correction factor (S) to account for the consumption of oxygen with each pass through the system. The full discussion of the improved model is presented in Chapter 5.

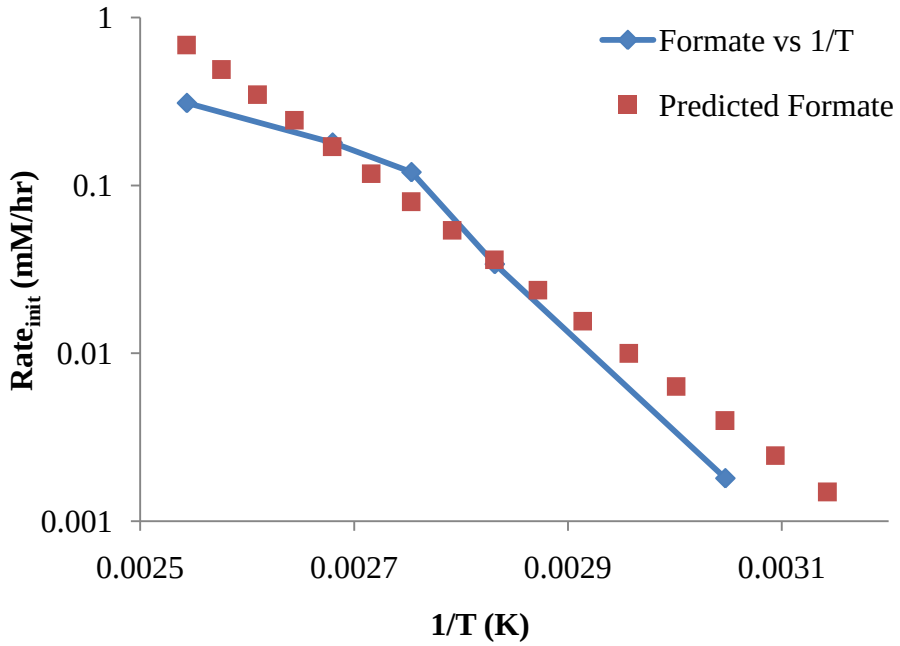

Figure 3.4: Initial rate of formate production for 7 m MDEA

3.8 EFFECT OF THERMAL REACTOR SIZE AND RESIDENCE TIME

The thermal reactor in the initial design had a nominal volume of 1.12 L. After completion of experiment C-24, this reactor was replaced with a thermal reactor with a volume of 0.13 L. The replacement was made in order to operate the ISDA in a kinetically controlled oxidative degradation mode as opposed to dissolved oxygen limited mode. Experiments C-25 through C-34 were implemented with the smaller reactor. At a nominal liquid flow rate of 200 mL/min, the residence time in the initial thermal reactor design was ~5.6 min, while in the newly designed reactor, the residence time was ~0.65 min. It was anticipated that, with the new smaller reactor, degradation rates would decrease due to the solvent spending a fraction of the original time at the higher temperatures associated with the thermal reactor.

A set of experiments with 7 m MDEA were conducted over a thermal reactor temperature range of 100 to 130 °C. In experiment C-25, the thermal reactor bulk liquid exit temperature was maintained at 120 °C, while in experiment C-27 that temperature was maintained at 100 °C. These experiments can be considered repeats of C-6 and C-10, respectively, given that the thermal reactor temperatures were the same as in the initial experiments with the larger reactor. In C-26, the thermal reactor bulk liquid exit temperature was maintained at 130 °C; this thermal reactor temperature was not possible with the initial design, so this experiment does not represent a repeat of another experiment. The rates of MDEA and alkalinity loss, and formate and total formate production for the related 7 m MDEA cycling experiments are included in Table 3.5 for direct comparison.

The decrease in thermal reactor size resulted in a decrease in MDEA and alkalinity loss rates of 23 to 39%, respectively, when the thermal reactor was set to 100 °C. The formate and total formate production rates decreased to 1/2X and 1/3X the rates measured in the initial reactor design. On the surface, these rates indicate that the lower residence time in the thermal reactor results in a decrease in oxidative degradation. However, when the thermal reactor was set at 120 °C, comparable MDEA and alkalinity loss rates were measured, but a nearly 2X increase in the rate of formate and 3X increase in rate of total formate production were observed. When the thermal reactor was set to 130 °C, the rate of MDEA loss was 3X any other rate measured including the rates measured in both 120 °C experiments (C-6 and C-25). However, the rate of alkalinity loss was approximately the same (3.67 mM/hr) as measured in the 120 °C experiments. Finally, the formate and total formate production rates were a fraction of the rates measured in C-25.

Table 3.5: Formate production (mM/hr) in 7 m MDEA – Original versus redesigned thermal reactor; rates listed in parentheses are the normalized rates based on thermal reactor volume

Expt No.	Thermal Reactor Vol (L)	Thermal Reactor T (°C)	MDEA Loss	Alk Loss	Formate Production	Total Formate Production
C-10	1.12	100	4.1	3.1	0.18	0.31
C-6	1.12	120	4.6	4.93	0.28	0.34
C-27	0.13	100	3.16 (22)	1.88 (13)	0.11 (0.76)	0.11 (0.76)
C-25	0.13	120	5.1 (35)	4.4 (30)	0.61 (4.2)	0.96 (6.6)
C-26	0.13	130	15.6 (107)	3.67 (25)	0.31 (2.1)	0.28 (1.9)

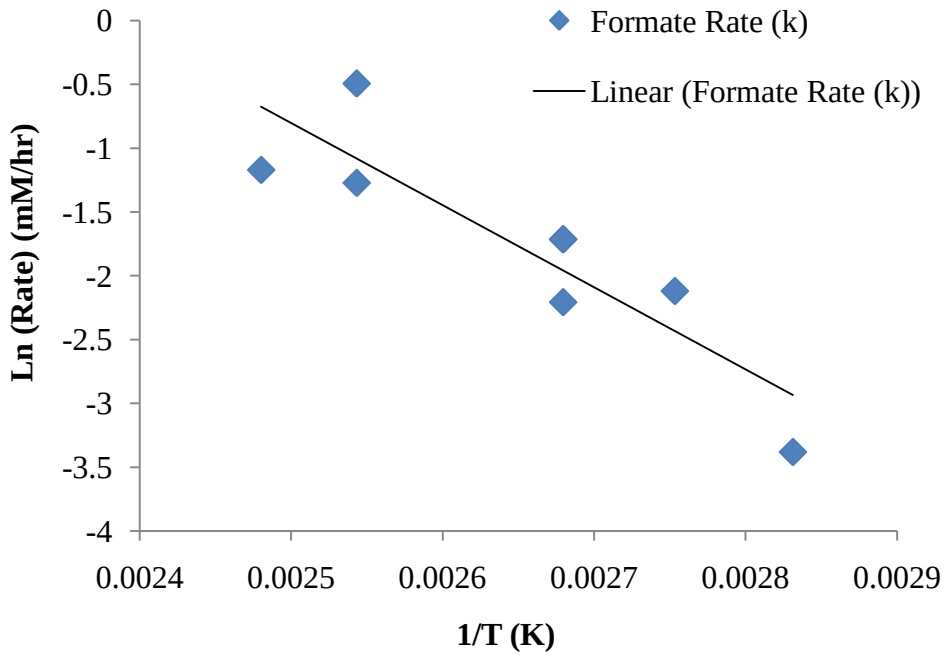

Figure 3.5: Formate initial rates over range of measured temperatures (both thermal reactors)

Figure 3.5 presents the $\ln(r_{formate})$ plotted against 1/T (K) for the temperature series experiments, including the three MDEA cycling experiments with the redesigned thermal reactor (C-25, C-26, and C-27). With the exception of a single rate measured at 120 °C

with the redesigned smaller thermal reactor, the initial formate production rates follow a discernible pattern, decreasing with thermal reactor temperature. Using the Arrhenius relationship and all rates represented in the figure, the energy of activation for the production of formate in 7 m MDEA was ~53.5 kJ/mol.

Based on the limited oxidative degradation measured in the ISDA when solvent was cycled at 55 °C throughout the system, an assumption can be made that the vast majority (>95%) of oxidation of 7 m MDEA occurs in the thermal reactor (see Table 3.4). Given this fact, normalization of both MDEA loss and degradation product formation rates for the redesigned reactor experiments (C-25 through C-27) requires dividing by a factor of 0.13/1.12 (0.12) to give rates comparable to those measured with the initial thermal reactor design in terms of thermal reactor residence time. Normalized rates are provided in parentheses () in Table 3.5. Those rates are generally an order of magnitude greater than those rates measured with the original thermal reactor. The normalized rates are well in excess of the rates measured with the original thermal reactor, and indicate that the assumption that dissolved oxygen was being completely consumed before existing the original reactor was likely correct. This observation supports a key assumption in the development of the oxidative reactor model discussed in Chapter 5.

A final comment regarding alkalinity measurements is essential before completing this chapter. As determined and discussed in Chapter 2, the measurement of alkalinity was affected by the presence of the heat stable salt formate. It was determined that formate will neutralize alkalinity by a factor of ~1.25, resulting in a lower overall alkalinity measurement. Because it is unknown to what extent other heat stable salts will affect the alkalinity measurements, the alkalinity loss rates have not been adjusted for the presence of formate or any other carboxylate ion in the analyses provided in this chapter.

3.9 REVIEW OF PRACTICAL IMPLICATIONS OF ISDA EXPERIMENTS

In testing and modifying the ISDA over the course of 34 cycling experiments, several practical observations were made relating to the degradation of alkanolamine solvents. Those observations have relevance to the operation of a true absorber/stripper system. This section reviews those important observations from the 7 m MDEA cycling experiments already reviewed.

3.9.1 Entrained bubble effects

The role of oxygen in the degradation of many alkanolamine solvents including MEA has been well documented for years (Girdler Corp., 1950, Rooney, 1998, and Sexton, 2008), but the role of entrained oxygen bubbles in causing oxidative degradation was observed and measured in the first five experiments with the ISDA. When entrained gas bubbles containing 98% O_2 were observed before the installation of an interception vessel, the rate of formate production was more than triple when compared to an experiment with minimal entrainment due to a stir rate reduction (C-4 vs. C-1 rates). However, the simple device consisting of a wide jar with loose distillation packing decreased the formate production by nearly 1/3 to 1/2X. These observations make it clear that gas bubble entrainment can create a continued supply of oxygen, particularly in a flue gas application where the feed gas may consist of as much as 12% O_2. However, the other practical observation that can be made from these initial experiments is that the bubble entrainment problem is easily solved from a design standpoint. A simple interception device with packing was sufficient to decrease degradation rates to one-half those observed without bubble removal. Of note, the use of packing to coalesce entrained

bubbles in the absorber hold-up may be sufficient to cause a decrease in bubble entrainment and the resulting oxidative degradation.

3.9.2 Dissolved oxygen effects

An experiment (C-18) involving the stripping of dissolved gases from the solvent with a 1 L/min N_2 gas purge in a modified bubble removal vessel demonstrated the role of dissolved oxygen in the degradation of 7 m MDEA. All rates indicative of MDEA degradation decreased by an order of magnitude when compared to the rates measured in a comparable cycling experiment (C-6) without the stripping device. C-18 demonstrated the positive effects of removing dissolved oxygen before the solvent increases in temperature in the stripper, thus preventing high temperature oxidation. This experimental work demonstrated that a simple stripping step is sufficient to cause an order of magnitude decrease in the rate of oxidative degradation in a cycling environment. The optimal stripping rate and conditions for stripping have not been evaluated, nor has the cost of operation of such a device. However, the simplicity and effectiveness of the stripping concept was demonstrated in C-18, warranting further consideration as an approach to minimizing oxidative degradation in full-scale systems. A patent relating to the stripping of dissolved oxygen from solvents to prevent degradation was issued for absorber/stripping systems (Chakravarti, 2001).

3.9.3 Gas Composition

The substitution of air for O_2 as the remaining 98% of gas composition to compliment the 2% CO_2 component reduced the degradation of 7 m MDEA, as measured by MDEA and alkalinity loss, to half the previous rates. The formate production rate decreased nearly an order of magnitude. When the headspace gas composition was reduced to zero oxygen by substitution with 98% N_2, the loss rates decreased another

order of magnitude. The implication for full-scale systems is that when treating a flue gas high in oxygen content (5-15 kPa), the rate of oxidative degradation can be expected to be much higher than in typical acid gas treating systems wherein the feed gas is likely to be <1% O_2. The designers of flue gas CO_2 scrubbing systems will need to consider the feed gas and appropriate solvent when specifying the conditions of operation.

3.9.4 High temperature oxidation effect

The ISDA characterization experiments demonstrated the effect of high temperature oxidation. Rates of oxidation, as evidenced by MDEA and alkalinity loss, increased by a factor of 5X when the thermal reactor temperature was increased from 55 to 120 °C. The rates of formate and total formate production increased nearly two orders of magnitude when the thermal reactor temperature was increased from 55 to 120 °C. These rate data indicate that, as steam stripper temperatures are increased to take advantage of the thermodynamic benefits of the thermal swing process when utilizing solvents with a high heat of absorption such as 7 m MDEA/2 m PZ ($\Delta H \sim 68$ kJ/mol*K), the carboxylate ion formation rates could increase by one to two orders of magnitude. Ultimately, the effect of increased carboxylate ions is to increase the need for reclaiming processes to maintain solvent scrubbing performance.

Chapter 4 – Degradation of 7 m MDEA

This chapter presents a detailed discussion of 7 m MDEA degradation, utilizing all relevant data collected with the batch methods described in Chapter 2 including the Swagelok® thermal cylinders, Low-gas reactors, and the ISDA solvent cycling system.

In Section 1.6, the research objectives of this body of work were outlined, with the main objective being to develop an understanding of 7 m MDEA/2 m PZ degradation behavior and rates. However, significant time and energy were committed towards understanding 7 m MDEA degradation. Fifteen cycling experiments with 7 m MDEA and three cycling experiments with 8 m PZ were conducted in the ISDA at varying conditions before 7 m MDEA/2 m PZ was cycled. Three additional cycling experiments were conducted with 7 m MDEA in the ISDA after cycling the blend and redesigning the thermal reactor. The purpose in separately studying MDEA and PZ was to understand the pathways, mechanisms, and initial rates of degradation of these individual amines before attempting to understand the second order effects and mechanisms associated with degradation of 7 m MDEA/2 m PZ. For reference, all 7 m MDEA experiments conducted in this body of work including the type of experiment, basic conditions for each, and initial MDEA loss rate are listed in Table 4.1.

7 m MDEA was generally found to degrade following similar pathways and mechanisms to those observed when this solvent is blended with PZ in 7 m MDEA/2 m PZ. However, as discussed in Chapter 7, PZ in the blend degrades under conditions ($T<130$ °C) where it does not degrade as 8 m PZ. This chapter reviews the 7 m MDEA degradation data, and compares amine loss rates and product formation rates to those rates measured in other key solvents including 7 m MEA and 8 m PZ. A list of the major

degradation products found in 7 m MDEA is provided in Table 4.2. That list includes the structures of those compounds for reference in this chapter. Degradation pathways and mechanisms are proposed in Chapters 8 and 9 based on the identified products in this solvent. The details associated with a 7 m MDEA oxidative model developed to predict the rates of degradation product formation over a range of measured temperatures (55 to 120 °C) are presented in Chapter 5.

Table 4.1: Experiments with 7 m MDEA

Expt. No.	Temp	Initial Loading	Stir Rate	Purge Gas		Other Condition(s)	Initial MDEA Loss Rate
	(°C)	mol CO_2/mol alk	Rpm	%/%	Y/N		mM/hr
Low-gas							
OD-2	55	0.1	1,440	98% O_2/2% CO_2	1 mM Fe	-	0.3
OD-8	70	0.14	1,440	98% O_2/2% CO_2	Y	-	0.1
Cycling							
C-1	55/120	0.1	1,440	98% O_2/2% CO_2	N	Base design	8.8
C-2	55/55	0.1	1,440	98% O_2/2% CO_2	N	"	0
C-3	55/55	0.1	1,440	98% O_2/2% CO_2	Y	Added ss metals	0.9
C-4	55/120	0.1	520	98% O_2/2% CO_2	Y	"	3.4
C-5	55/120	0.1	1,000	98% O_2/2% CO_2	Y	Added vertical bubble removal vessel	8.5
C-6	55/120	0.1	1,440	98% O_2/2% CO_2	Y	Redesigned bubble removal jar*	4.6
C-7	55/120	0.1	1,440	98% O_2/2% CO_2	Y	100 mM Inh A	5
C-8	55/120	0.1	1,440	98% N_2/2% CO_2	Y	-	1.9
C-9	55/120	0.1	0	98% N_2/2% CO_2	Y	-	4.1
C-10	55/100	0.1	1,440	98% O_2/2% CO_2	Y	-	4.1
C-11	55/80	0.1	1,440	98% O_2/2% CO_2	Y	-	0.9
C-12	55/90	0.1	1,440	98% O_2/2% CO_2	Y	-	2.9
C-13	55/120	0.1	1,440	98% Air/2% CO_2	Y	-	0.2
C-14	55/90	0.1	1,440	98% O_2/2% CO_2	Y	-	0.2
C-15	55/90	0.1	1,440	98% O_2/2% CO_2	Y	100 mM Inh A	2.4
C-25	55/120	0.1	1,440	98% O_2/2% CO_2	Y	Redesigned Th Rx	5.1
C-26	55/130	0.1	1,440	98% O_2/2% CO_2	Y	Redesigned Th Rx	15.6
C-27	55/100	0.1	1,440	98% O_2/2% CO_2	Y	Redesigned Th Rx	3.2
Thermal							
Th. No. 10	120/135/150	0.0/0.1/0.25	-	-	N		Various

*All subsequent ISDA expt utilized this jar.

4.1 LOW-GAS REACTOR EXPERIMENTS WITH 7 m MDEA

7 m MDEA was degraded in two Low-gas experiments, with the first experiment (OD-2) utilizing the original Low-gas reactor at 55 °C, and the second experiment (OD-8) utilizing the redesigned Low-gas reactor (TOR) (section 2.2) at 70 °C. The analytical methods utilized in the completion of OD-8 were more comprehensive, including extensive use of IC, MS and HPLC analysis for degradation product identification. The back-up data tables for basic analytical work performed on these experiments are included in Appendices B (ISDA), C (Low-gas), and D (Thermal cylinder). A master table with degradation rates is included in Appendix E.

In OD-2, 7 m MDEA at an initial loading of 0.1 mol CO_2/mol alkalinity was degraded in the Low-gas reactor for approximately 14 days at 55 °C. The headspace purge gas supplied to the reactor was 98% O_2/2% CO_2. The solvent was augmented with 1 mM Fe^{2+} ($FeSO_4 \cdot 7H_2O$) to catalyze oxidative degradation. OD-8 was conducted two and one-half years later in the TOR Low-gas reactor at 70 °C at an initial loading of 0.14 mol CO_2/mol alkalinity, with the headspace purge gas blended to ~92.5% O_2/7.5% CO_2 to match the equilibrium condition of this solvent at this temperature.

4.1.1 Overview of degradation products

The major degradation products of the Low-gas experiments with 7 m MDEA included the heat stable salts formate and glycolate, the secondary amines MAE and DEA, and the amino acids bicine and HES (Table 4.2). Because MAE and DEA have nearly the exact same retention time using cation IC and IonPac CS17 column, peak separation was not possible. Instead of expressing the concentration of these individual compounds, the combined concentration of both compounds will be expressed from this point onward as “DEA+MAE”. The average ratio of response factor between DEA and

MAE was ~1.35, so the combined concentration for both compounds is expressed after applying a factor of ~X1/1.17 to DEA data, and X1.17 to MAE data.

Table 4.2: Compounds detected in degraded 7 m MDEA

Product Name	Compound Class	MW	Analytical Method	Structure
Formate	Carboxylate ion	45	Anion IC	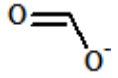
Glycolate	Carboxylate ion	75	Anion IC	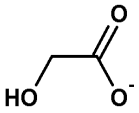
Acetate	Carboxylate ion	59	Anion IC	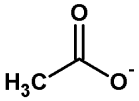
Oxalate	Carboxylate ion	88	Anion IC	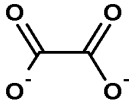
MEA	1 amine	61.1	Cation IC	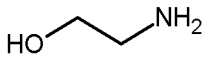
MAE	2 amine	75.1	Cation IC	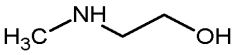
DEA	2 amine	105.1	Cation IC	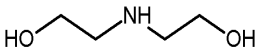
Bicine	Amino acid	163.1	HPLC	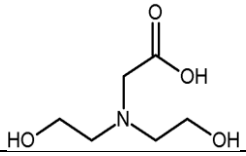
Glycine	Amino acid	75.1	HPLC	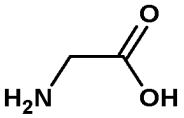
Hydroxyethyl sarcosine	Amino acid	133.1	HPLC	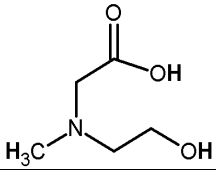

The formyl amides of MAE and DEA, N-(2-hydroxyethyl)-N-methyl formamide and N,N-bis-(2-hydroxyethyl) formamide, were not observed in OD-8 samples. The presence of ammonia in degraded amine was measured as ammonium ion (NH_4^+) using cation IC, but very little was detected in OD-8 samples. Acetate and oxalate were detected, but at a fraction of the concentration of formate. The structures of the heat stable salts, 2° amines, and amino acids are presented in Table 4.2.

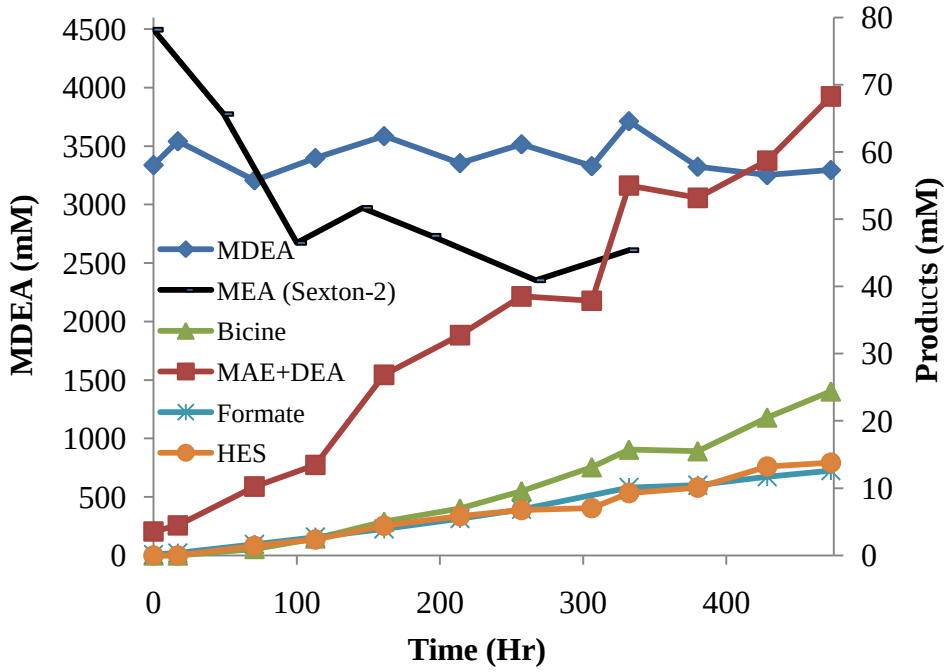

Figure 4.1: Degradation products in OD-8 (7 m MDEA in Low-gas at 70 °C) including MEA concentration in Low-gas (Sexton-2)

4.1.2 MDEA and alkalinity loss

The concentration of MDEA in OD-8 is plotted in Figure 4.1 along with major degradation products including DEA+MAE, bicine, HES, and formate. The initial MDEA loss was approximately 0.12 ± 0.3 mM/hr, while the alkalinity loss was 0.37 ± 0.21 mM/hr. This MDEA loss rate is in contrast to the initial loss rates of MEA of 6.9

and 11.7 mM/hr, respectively, measured in 7 m MEA in Sexton-1 and Sexton-2 (Sexton, 2008). MEA concentrations in Sexton-2 are also plotted in Figure 4.1. Note that Sexton-1 and Sexton-2 were conducted in the Low-gas reactor at 55 °C with 1 mM Fe and 0.6 mM Cr + 0.1 mM Ni as dissolved salts, respectively. OD-8 was conducted in the Low-gas reactor at 70 °C. Freeman (2011) conducted a Low-gas experiment with 8 m PZ at 55 °C in the presence of the stainless steel dissolved metal salts (0.4 mM Fe^{2+}, 0.1 mM Cr^{3+}, and 0.05 mM Ni^{2+}). The PZ loss was 0.02 mM/hr, while the alkalinity loss was 0.04 mM/hr, indicating that 8 m PZ generally degrades at 1/10X the rate of 7 m MDEA. These data indicate that amine and alkalinity loss in the Low-gas reactor both follow the order from greatest to least: 7 m MEA>7 m MDEA>8 m PZ.

4.1.3 Heat Stable Salts

In OD-8, formate and total formate were generated at initial rates of 0.028 ± 0.001 mM/hr and 0.035 ± 0.003 mM/hr, respectively (Figure 4.2). As noted in Chapter 2, when degraded samples contain amides, treatment with NaOH will reverse the formation of those amides to their respective amine and heat stable salts (i.e., formate) through hydrolysis, and allow the approximate quantification of the amides through measurement of the recovered heat stable salt. The production of amides is generally believed to be an oxidation process, and pathways for the generation of amides in MDEA are presented in Chapter 8 of this document. Sexton (2008) also measured the concentration of heat stable salts including formate in 7 m MEA at 55 °C in the Low-gas reactor. The concentrations of formate and total formate from OD-8 and Sexton-2 (7 m MEA) are presented in Figure 4.2 for comparison. Formate was produced at a rate of 0.27-0.29 mM/hr in the 7 m MEA experiments, which is a full order of magnitude greater than the rate measured in 7 m MDEA at 55 or 70 °C.

Formate and total formate production rates for MDEA from the relevant Low-gas and ISDA experiments are presented along with formate production rates for 7 m MEA in Low-gas experiments (Sexton-1 and Sexton-2) in Figure 4.2. These formate production rates compliment the rates measured in experiment OD-2 at 55 °C of 0.013 and 0.026 mM/hr, respectively, in the original Low-gas design. The rates listed in the table indicate that only after cycling 7 m MDEA to 120 °C in the ISDA thermal reactor, are formate production rates comparable to those measured in 7 m MEA observed.

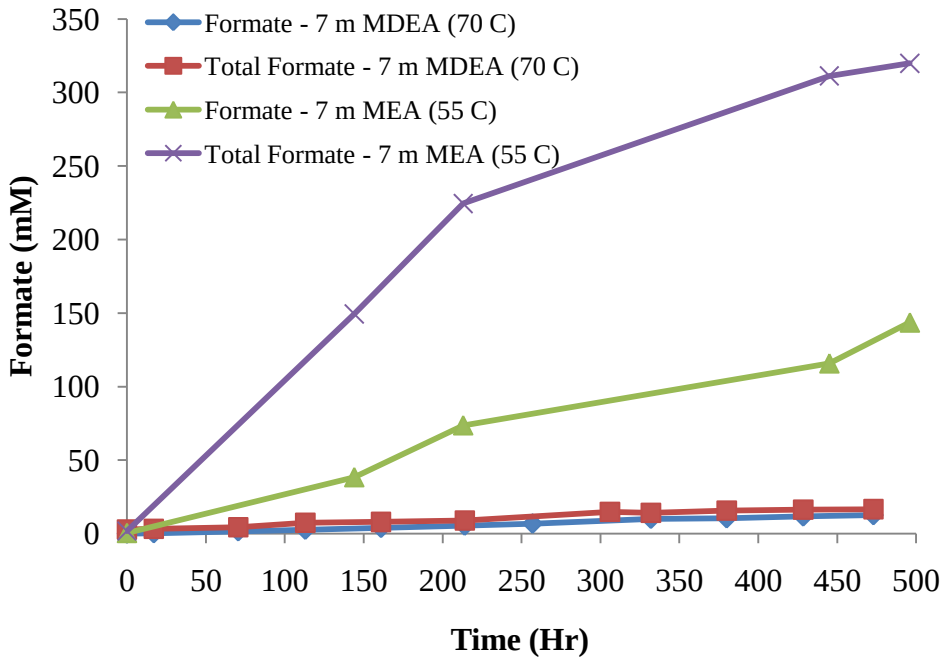

Figure 4.2: Formate comparison in Low-gas experiments – 7 m MDEA and 7 m MEA (Sexton, 2008)

Table 4.3 includes the formate and total formate production rates for Low-gas experiments with other solvents including 8 m PZ (Freeman, 2011), 7 m DEA, 7 m MAE and 7 m MDEA/2 m PZ. The linear fit and standard deviation of the slope for initial rate determinations are included in that table for a subset of the experiments. The 8 m PZ

experiment was conducted at 55 °C in the presence of the stainless steel dissolved metal salts (0.4 mM Fe^{2+}, 0.1 mM Cr^{3+}, and 0.05 mM Ni^{2+}). The rates were 0.005 and 0.014 mM/hr for formate and total formate, respectively, and represent the other end of the extreme in terms of heat stable salt production.

Table 4.3: Formate production in 7 m MDEA experiments; 7 m MEA Low-gas data (Sexton, 2008), 8 m PZ data (Freeman, 2011)

Expt No.	Solvent	T (°C)	Formate Production	Total Formate Production
OD-2	7 m MDEA	55	0.013	0.026
OD-8	7 m MDEA	70	0.028 ± 0.001	0.03 ± 0.003
C-6	7 m MDEA	55/120	0.28 ± 0.01	0.34 ± 0.006
C-25	7 m MDEA	55/120	0.61	0.96
C-26	7 m MDEA	55/130	0.31 ± 0.03	0.59 ± 0.06
Sexton-1	7 m MEA	55	0.27	1.04
Sexton-2	7 m MEA	55	0.29	0.67
OE18	8 m PZ	55	0.005	0.014
OD-6	7 m DEA	55	0.16	1.03
OD-7	7 m MAE	55	0.21	1.03
OD-9	7 m MDEA/2 m PZ	70	0.03	0.08

The formate and total formate production rates for 7 m DEA (OD-6) in the Low-gas system at 55 °C were 0.16 and 1.03 mM/hr, respectively. The formate and total formate rates for 7 m MAE (OD-7) were 0.21 and 1.03, respectively. 7 m DEA is a commercially viable solvent and used for CO_2 removal in natural gas applications, whereas 7 m MAE is less commercially relevant. Formate production in both of these 2° amines was relevant in the MDEA studies because both are considered degradation products or intermediates in the degradation of 7 m MDEA. These formate production rates indicate that the oxidation behavior of 2° amines is very similar to that of 1° amines, exhibiting faster oxidation when compared to the tertiary amine MDEA.

The rates of formate and total formate production in 7 m MDEA/2 m PZ measured in OD-9 were 0.03 and 0.08 mM/hr, respectively. This formate production rate is ~2X the rate measured in 7 m MDEA at 55 °C, and approximately the same as the rate measured in 7 m MDEA at 70 °C, indicating that the rate of oxidation is at least as fast in the blend when compared to 7 m MDEA. Solvents tested in this research using the Low-gas reactor adhere to the following relationship from greatest formate production to least: 7 m MEA>7m MAE>7 m DEA>7 m MDEA/2 m PZ≥7 m MDEA>8 m PZ.

As expected based on MDEA being a tertiary amine, the production of amides in 7 m MDEA was much lower than exhibited by any of the other solvents listed in Table 4.3 including 7 m MDEA/2 m PZ. The presence of amides in the blend was expected due to the formation of N-formyl piperazine (FPZ), and possibly also through the formation of amides from degradation intermediates including DEA and MAE. The amides of DEA and MAE were not observed in OD-8 (7 m MDEA) or OD-9 (7 m MDEA/2 m PZ), whereas FPZ and diformyl piperazine (DFPZ) were observed in OD-9. DFPZ was observed at a concentration of ~1 mM in the final sample from OD-9, indicating that it does form, but at a very low rate.

The concentration of total formate in the Low-gas experiments with 7 m DEA (OD-6) and 7 m MAE (OD-7) was much greater than the concentration of formate; recall that the difference between total formate and formate is generally considered the concentration of formyl amides, such as FPZ. Both DEA and MAE produced a high concentration of amides when compared to 7 m MDEA or 7 m MDEA/2 m PZ. Using HPLC, the formyl amide N,N-bis-(2-hydroxyethyl) formamide was detected at a concentration of ~242 mM in the final sample in OD-6, which can be compared to the formyl amide concentration of 240 mM determined through hydrolysis and formate/total

formate analysis of samples. These analyses indicate that the 2° amines, like the 1° amines, will produce a high concentration of formyl amides in an oxidizing environment.

In OD-8, the generation of heat stable salts other than formate was minimal, with glycolate being produced at the greatest concentration. Glycolate contains two carbon atoms as opposed to formate which contains one. The presence of glycolate in solution represents a two-carbon structure being lost from the parent amine, and is likely present as a result of a hydroxyethyl group loss from MDEA. The presence of formate represents the loss of a single carbon from MDEA, which may be the result of a methyl group loss. The ratio of formate to glycolate in OD-8 (Figure 4.3) experienced an initial drop from a value of 2.4 to 1 mmol formate/mmol glycolate within 17 hours of oxidation in the Low-gas reactor. From that point onward, the ratio increased in a linear fashion to a ratio of ~3 mmoles formate/mmol glycolate after 473 hours of oxidation. The ratio of total formate to total glycolate is also plotted in Figure 4.3, and indicates that when the samples are hydrolyzed with NaOH, the ratio increases as the length of the experiment increases, starting at ~3.5 and dropping to 2 for more than 200 hours before increasing to ~3.5 after 473 hours. The 200 hour lag time in the ratio of total formate to total glycolate indicates that formyl amide production is dependent on a factor such as formate concentration; the accumulation of sufficient formate is necessary for the formation of formyl-amides at greater concentrations than observed for glycol-amides.

In general, the significance of the ratio of formate to glycolate concentration lies in the fact that as MDEA degrades, one-carbon "leaving" groups are present in the degraded solvent to a much greater extent than two-carbon groups, indicating that MDEA loses methyl groups readily when compared to hydroxyethyl groups. Further, as degradation proceeds, the ratio increases, indicating that the loss of a hydroxyethyl group becomes less likely when compared to a methyl group loss. It is also probable that two-

carbon oxidized fragments such as glycolic acid may further degrade to produce two molecules of formate. However, these observations imply that the formation of DEA is more likely to occur than the formation of MAE as MDEA degrades in the presence of oxygen.

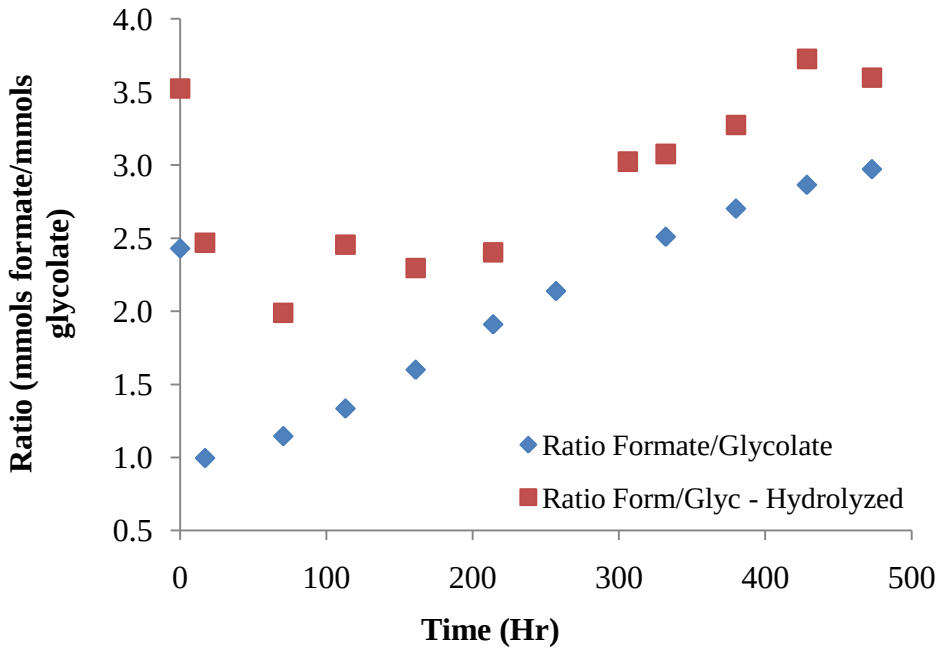

Figure 4.3: Ratio of formate/glycolate in 7 m MDEA (Low-gas)

4.1.4 Amine degradation products

The secondary (2°) amines DEA and MAE were measured in OD-8 samples, while other amines were generally not detected. Separation of DEA from MAE was not possible using cation IC with an IonPac CS17 column. When standards for DEA and MAE are injected on the cation IC system, a peak appears at approximately the same retention time for both compounds, preventing definitive quantification of either compound. However, when degraded 7 m MDEA samples from experiment C-1 were injected on the IC-MS system, a peak and mass for both compounds appear (75.1 for

MAE and 105.1 for DEA), confirming the presence of both compounds in degraded 7 m MDEA. When analyzed using LC-MS operated in reverse phase mode, samples from the same experiment provided a mass for both compounds, but at a retention time (~3.7-4 minutes) indicating poor retention on the LC column; it was anticipated that the amines would be poorly retained on the LC column when operating in reverse phase mode due to their inherent polarity. In summary, the most prominent amine products from 7 m MDEA degradation in the low gas system are DEA and MAE, and the quantification of these compounds has been handled as a single concentration for the combined mass of both in samples. The DEA+MAE formation rate in OD-8 was 0.14 mM/hr. Note that OD-8 samples were not analyzed with IC or LC-MS.

4.1.5 Amino acids

The amino acids bicine and HES were detected in degraded 7 m MDEA in Low-gas experiment OD-8. Glycine was not detected in OD-8. The initial rates of production of bicine and HES were 0.022 and 0.028 mM/hr, respectively. The data presented in Figure 4.1 do not indicate a lag time in HES production. However, for bicine, an apparent lag time exists for approximately 210 hours of oxidation in the reactor. This lag time is likely evidence of the need for the degradation intermediate DEA to accumulate in solution before bicine production occurs at the higher rate observed in the latter half of the experiment. Because the DEA concentration cannot be determined due to overlap with the MAE peak using cation IC, a direct correlation between the DEA and bicine concentrations is difficult to make.

A carbon and nitrogen balance was performed on the final sample from OD-8 to determine whether the carbon and nitrogen lost as MDEA loss was recovered. Because of the low MDEA loss rate measured in the experiment with cation IC, the moles of

carbon and nitrogen measured as recovered exceeded the measured loss of each as MDEA loss. Additionally, the methyl groups lost as MDEA loss were recovered in products including MAE, HES, formyl amides, and formate. When accounted for this way, more than 100% recovery of methyl groups was achieved.

4.2 THERMALLY DEGRADED 7 m MDEA

7 m MDEA was thermally degraded in three notable experiments utilizing the Swagelok® sample cylinders. In Th. No, 10, the solvent was loaded to 0.1 and 0.2 mol CO_2/mol alkalinity and thermally degraded at 120, 135, and 150 °C. In Th. No. 14, 7 m MDEA+0.35 m tetramethyl ammonium quaternary amine (quat) (added as tetramethyl ammonium chloride) was thermally degraded at 150 °C at initial loadings of 0.0 and 0.2 mol CO_2/mol alkalinity. Finally, in Th. No. 15, 7 m MDEA + 1 m quat was thermally degraded at 150 °C at an initial loading of 0.2 mol CO_2/mol alkalinity. Th. No. 10 was performed to obtain a baseline of MDEA thermal degradation. Th. No.s 14 and 15 were performed to understand the role of quaternary amines in initiating thermal degradation in MDEA through arm-switching following S_N2 substitution behavior, with Th. No. 15 performed at the higher quat concentration to facilitate a greater level of arm switching than observed in Th. No. 14. Finally, the sample cylinders in Th. No. 14 were filled with solvent in a sealed glove bag filled with N_2 gas to eliminate oxygen from the headspace of the sample cylinders during thermal degradation.

4.2.1 Degradation products observed in thermally degraded 7 m MDEA

The major products observed in thermally degraded 7 m MDEA include many of the compounds listed in Table 4.2, with the exception of MAE. Extensive IC and LC-MS analyses were performed on samples from Th. No. 10 and Th. No. 14, providing a list of

additional compounds, some of which have been identified with one or more analytical techniques, and others for which positive identification has not been achieved. A list of these additional compounds identified in 7 m MDEA by mass is provided in Table 4.4 with the analytical method used.

One notable exception to the list of compounds identified in thermally degraded 7 m MDEA is MAE. A single, relatively large peak for DEA+MAE was observed in nearly every thermally degraded 7 m MDEA sample. A cation chromatogram for Th. No. 15, sample FC-118 is provided as Figure 4.4. This sample was 7 m MDEA + 1 m quat thermally degraded at 150 °C for 63 days. As discussed above for oxidized 7 m MDEA, DEA and MAE were both typically observed in those samples. However, using MS methods, MAE was not detected in thermally degraded 7 m MDEA samples. DEA was observed in Th. No. 14 samples through MS methods.

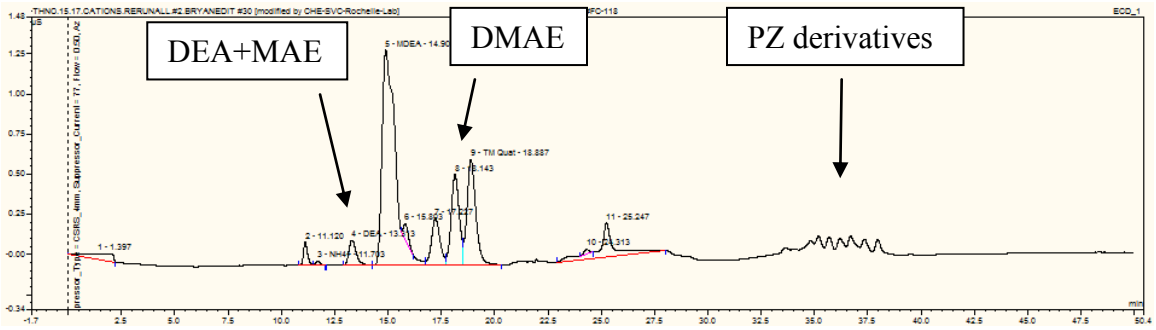

Figure 4.4: Cation IC chromatogram of Th. No. 15, No. FC-118, 7 m MDEA + 1 m Quat, α=0.2 mol CO_2/mol alkalinity, thermally degraded at 150 °C for 63 days

Table 4.4 Additional compounds identified in thermally degraded 7 m MDEA

Mass	Expt	Deg T (°C)	Full Method Used	Compound ID	Structure	Other Possible IDs
73.2	10	150	LC-MS IC-MS	DMEA	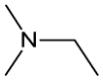	-
86.1	14	150	GC-MS	PZ	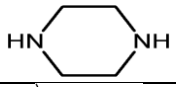	-
89.1	10, 14	150	LC-MS GC-MS	DMAE	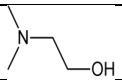	-
100.1	14	150	GC-MS	MPZ	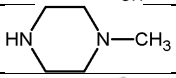	-
103.2	10	150	LC-MS IC-MS	MAE-Amide	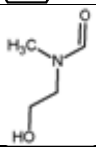	Diethylenetriamine
105.1	10, 14	150	LC-MS GC-MS	DEA	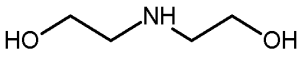	-
112.1	14	150	GC-MS	Triethylenediamine	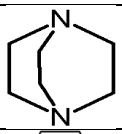	-
114.1	10	150	LC-MS	DMPZ	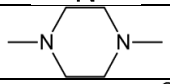	N-formyl PZ
130.1	14	150	GC-MS	HEP	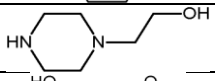	hydroxyethyl imidazolidone
131.1	14	150	GC-MS	HEOD	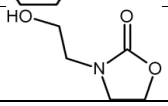	-
133.1	10	150	LC-MS IC-MS	DEA-Amide	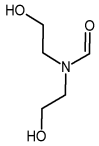	ethyldiethanolamine, HES
143.1	14	150	GC-MS	4-methyl-1-PZ ethanamine	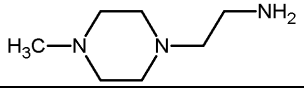	-
144.1	10, 14	150	LC-MS IC-MS GC-MS	HMP	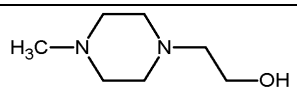	-

Table 4.4 Additional compounds identified in thermally degraded 7 m MDEA (continued)

146.1	14	150	GC-MS	N-methyl-N-(N,N-dimethylaminoethyl)-aminoethanol	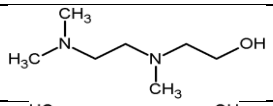	-
149.1	10, 14	150	IC-MS GC-MS	TEA	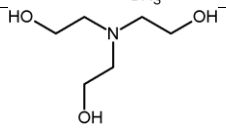	-
163.1	10	150	LC-MS	Bicine	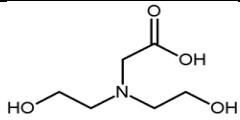	-
174.1	10, 14	150	LC-MS IC-MS GC-MS	bHEP	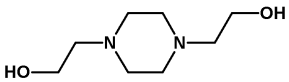	-
192.1	10	150	IC-MS	THEED	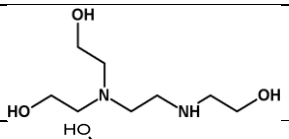	-
206.1	10	150	LC-MS IC-MS	MTHEED	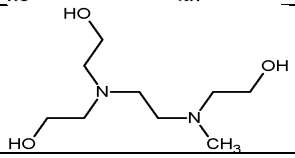	-

Even though a compound is listed in Table 4.4, it may not be a significant compound in terms of the overall understanding of MDEA degradation and/or accounting for mass loss due to MDEA degradation. Compounds are listed because they were identified by mass in one of the separation techniques mentioned in more than one sample. It is likely that many of these compounds were present at very low concentrations in terms of accounting for MDEA mass loss and are, therefore, not critical to the overall understanding of how MDEA/PZ degrades. For this reason, their presence in terms of concentration and pathways is not the focus of the following discussion in this chapter, or Chapter 9. The concentrations of DEA, 1-MPZ, 1,4-DMPZ, AEP, and bHEP were all determined in Th. No. 15 samples and will be discussed in terms of concentrations and rates. Amino acid analyses were performed on thermally degraded 7

m MDEA samples, but neither bicine nor HES, which are typically observed in oxidized MDEA, were observed.

4.2.2 Amine loss in thermally degraded 7 m MDEA

The MDEA loss rates and respective standard deviations for Th. No.s 10, 14, and 15 are listed in Table 4.5. From the results for Th. No. 10, MDEA loss was 1.2 mM/hr or less over the temperature range of 120 to 150 °C at a loading of 0.1 mol CO_2/mol alkalinity. However, at a loading of 0.2 mol CO_2/mol alkalinity, the loss rates ranged from 1.6 to 3.0 ± 0.7 mM/hr. Using the 0.2 mol CO_2/mol alkalinity data from Th. No. 10 only and Th. No. 15 (no quat), an energy of activation (E_a) for MDEA loss of ~60 kJ/mol was calculated. Freeman (2011) calculated an E_a of ~184 kJ/mol for thermal degradation of 8 m PZ at α=0.3 mol CO_2/mol alkalinity.

Based on the literature for MDEA degradation (Chakma and Meisen, 1997), an assumption was made that the thermal degradation of MDEA followed second-order behavior, with one mole of MDEA reacting with one mole of protonated MDEA in loaded solution. The degradation behavior would follow Equation 4.1:

$$-\frac{dC_{MDEA}}{dt} = k_2 \cdot [MDEA][MDEAH^+] \tag{4.1}$$

Solving this equation provides a relationship for the concentration of MDEA with time (t), and allows the determination of a second-order rate constant (k_2); the slope of a plot of 1/[MDEA] vs. time provides the second-order rate constant. However, when data for the thermal degradation of MDEA at 150 °C from two experiments (Th. No.s 10 and 15) with no quats and an initial loading of 0.2 mol CO_2/mol alkalinity were plotted, the linear fit to the data was poor. An assumption was then made that the thermal degradation of

MDEA followed first-order behavior. The degradation behavior would follow Equation 4.2:

$$-\frac{dC_{MDEA}}{dt} = k_1 \cdot C_{MDEA} \tag{4.2}$$

Solving this equation provides a relationship for the concentration of MDEA with time (t), and allows the determination of a first-order rate constant (k_1) through a semi-log plot of [MDEA] vs. time. Using the same 7 m MDEA data without the quat, the calculated first-order rate constant k_1 was 8.06 X 10^{-7} s^{-1}. Figure 4.5 is a semi-log plot of [MDEA] vs. time. PZ degrades nearly two orders of magnitude slower than MDEA. Freeman (2011) calculated a k_1 of ~6 X 10^{-9} s^{-1} for 8 m PZ at 150 °C and a loading of 0.3 mol CO_2/mol alkalinity.

Table 4.5 MDEA loss rates in thermally degraded 7 m MDEA

Expt.	Solvent	Loading	T	MDEA Loss Rate
		mol CO_2/mol alk	°C	mM/hr
Th. No. 10	7 m MDEA	0.1	120	0.0 ± 0.5
	7 m MDEA	0.1	135	0.5 ± 0.3
	7 m MDEA	0.1	150	1.2 ± 1.5
	7 m MDEA	0.2	120	1.6
	7 m MDEA	0.2	135	2.2
	7 m MDEA	0.2	150	3.0 ± 0.7
Th. No. 14*	7 m MDEA	0	150	0.0 ± 0.37
	7 m MDEA+0.35 m Quat	0	150	0.22 ± 0.21
	7 m MDEA+0.35 m Quat	0.2	150	0.94 ± 0.93
Th. No. 15	7 m MDEA+No Quat	0.2	150	2.9 ± 3.7
	7 m MDEA+1 m Quat	0.2	150	1.82

*Expt. Th. No. 14 cylinders filled with solvent under nitrogen gas blanket.

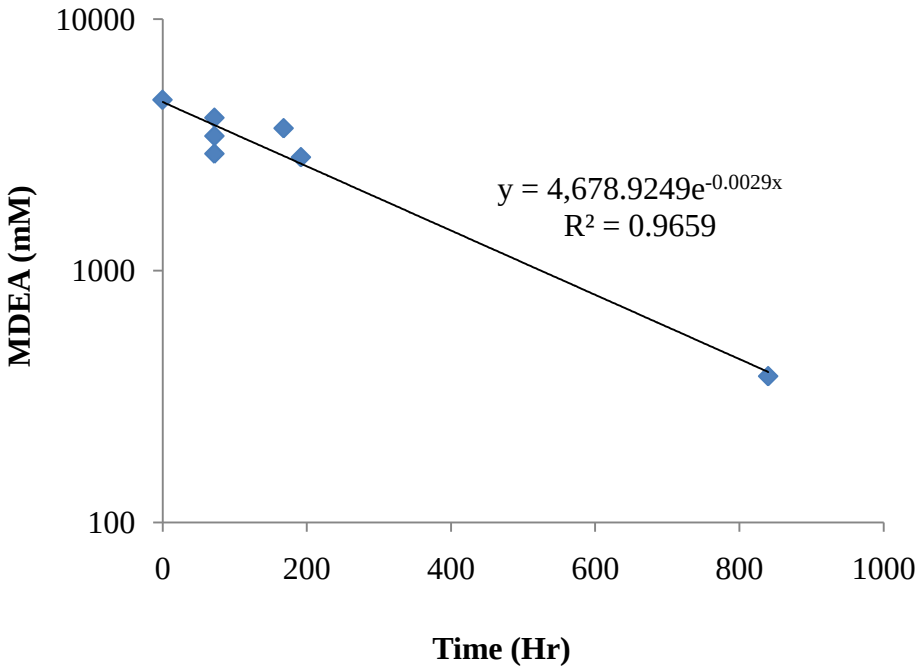

Figure 4.5: Determination of first-order rate constant from 7 m MDEA thermal degradation data collected at 150 °C

When compared to MDEA loss measured in Th. No. 10, the loss rates in Th. No. 14 which included an initial quat concentration of 0.35 m did not provide evidence of accelerated amine loss. For example, at a loading of 0.2 mol CO_2/mol alkalinity and degradation temperature of 150 °C, the loss rate with the quat was lower (0.94 ± 0.93 mM/hr) than the rate measured in Th. No. 10 (3.0 ± 0.7 mM/hr) without the quat. Assuming first-order behavior in [MDEA], the k_1 for MDEA+quat was calculated as 1.2 X 10^{-7} s^{-1}. The observation of a lower rate constant with an initial quat concentration of 0.35 m indicates that the quat inhibits the MDEA protonation and/or quat formation process, thus lowering the overall degradation rate. The quat is likely more reactive than MDEA itself as degradation proceeds, and its presence at a concentration of 0.35 m inhibits the participation of MDEA in degradation reactions until the quat is consumed. This observation is supported by a comparison of MDEA loss rates listed in Table 4.5

which reveals that the MDEA loss rate of both quat experiments (Th. No. 14 and 15) conducted at 150 °C and an initial loading of 0.2 mol CO_2/mol alkalinity are lower than the rate observed at 150 °C in the absence of the quat (Th. No. 10).

The absence of oxygen in headspace of Th. No. 14 cylinders may have played a role in reducing thermal degradation. However, in Th. No. 15, in which 7 m MDEA+1 m quat was thermally degraded at 150 °C at an initial loading of 0.2 mol CO_2/mol alkalinity, the thermal cylinders were not sealed under an N_2 blanket, thus providing a small amount of oxygen in the cylinder headspace. The MDEA loss rate of 1.82 mM/hr was 2X the rate measured with only 0.35 m quat, but a fraction of the rate measured in the absence of the quat in Th. No. 10.

Chakma and Meisen (1997) measured the degradation of 4.2 M MDEA over a range of loading and temperature, and measured first-order rate constants which they plotted. Rate constants (k_1) were extracted from Figure 12 of that paper at 140, 160, 180 and 200 °C, and replotted with the rate constant for thermal degradation of 7 m MDEA measured in this work at 150 °C (●). The partial pressure of CO_2 for 7 m MDEA and the experimental loading of this work was estimated by Frailie (2011) using an Aspen model. That plot is presented as Figure 4.6. The k_1 of 8.1 X 10^{-7} s^{-1} fits well with the interpolated data of Chakma and Meisen, with their measured data slightly underpredicting the rate constant at 150 °C. The k_1 measured in this work for thermal degradation of 7 m MDEA + 0.35 m quat at 150 °C is also presented (●) in Figure 4.6, and does not fit the data of Chakma and Meisen, indicating the suppression of degradation at 150 °C.

Chakma and Meisen (1997) presented a kinetic model to predict MDEA degradation. Equation (26) of that model involves the protonation of MDEA, while

Equation (27) entails the reaction of MDEA with $MDEAH^+$ to form DMAE, ethylene oxide (EO) and DEA. This is presumably an S_N2 substitution reaction, which by definition should follow second-order behavior. Convergence of their model requires knowledge of degradation product concentrations in solution. This work did not seek to determine 7 m MDEA degradation product concentrations. However, Chakma and Meisen (1997) estimated an E_a for the reaction of MDEA and $MDEAH^+$ (Equation 27 of the model) to be 57.4 kJ/mol, which is approximately the same as the E_a of 60 kJ/mol estimated in this work. This analysis and comparison confirms a general consistency between the two bodies of work in terms of measuring and modeling thermal degradation.

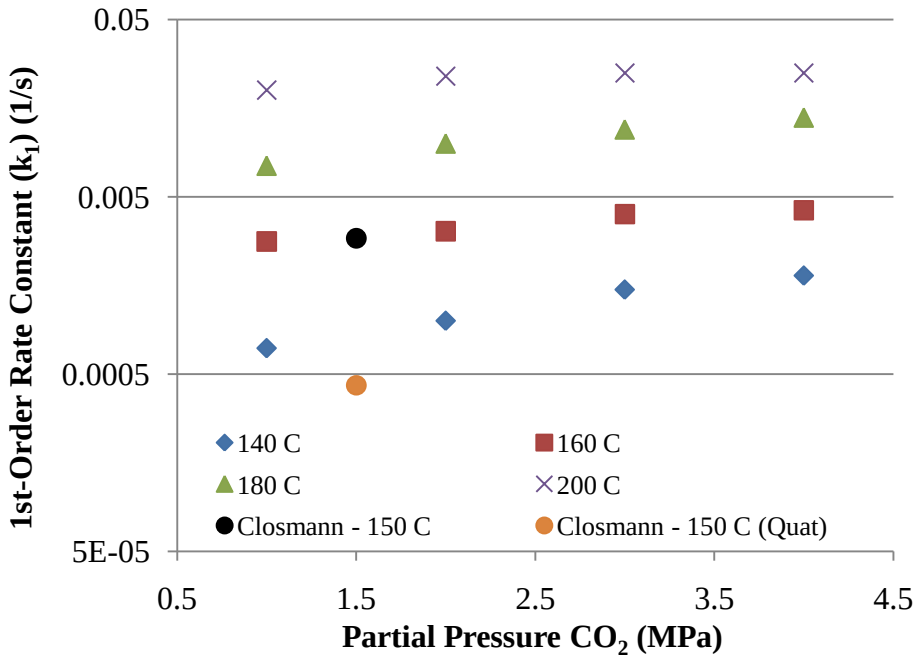

Figure 4.6: Rate constant for 7 m MDEA thermal degradation at 150 °C plotted against data from Chakma and Meisen (1997) for 4.2 M MDEA

4.2.3 Heat stable salts in thermally degraded 7 m MDEA

The concentration of formate was measured in Th. No. 15, and plotted in Figure 4.7. No other heat stable salt was detected above measurement background in this experiment. The formate concentration increases to ~60 mM after 500 hours, but then plateaus at this concentration for the remainder of the experiment. The CO_2 loading was also measured in Th. No. 15 samples and plotted in Figure 4.7. The data generally indicate that as the concentration of formate reaches a steady state, the loss of CO_2 loading stops.

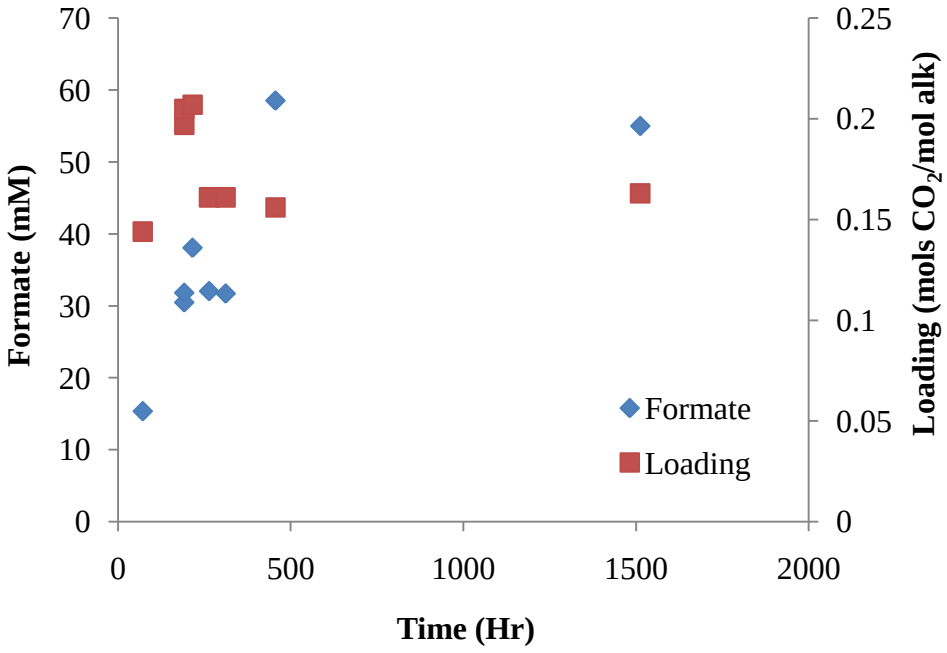

Figure 4.7: Formate concentration in thermally degraded 7 m MDEA (Th. No. 15)

4.2.4 Formation of other products in thermally degraded 7 m MDEA

The role of the quat was evaluated for its effect on creating more chemical mechanisms for degradation to occur in 7 m MDEA. For example, it was anticipated that the quat would facilitate the creation of arm-switching products other than those observed

in its absence, and increase the concentration of those products that were observed in its absence. Chakma and Meisen (1997) reported pathways for the formation of DEA, $DEACOO^-$, HEOD, and subsequent polymerization products in MDEA. Their proposed pathways were all based on the initial formation of a protonated amine such as MDEA or DMAE, with the subsequent formation of quaternary amines. The thermal experiments with the tetramethyl ammonium chloride quat were intended to verify these mechanisms.

The compounds listed in Table 4.4 include a number of PZ derivatives. As early as 1956, Polderman and Steele reported that DEA would react with CO_2 and thermally degrade through condensation polymerization to ultimately form bHEP. Kim and Sartori (1984) reiterated this pathway to explain the production of both THEED and bHEP. Both of these compounds were identified as reaction products in this work (see Table 4.4). The finding of PZ and several of its derivatives including 1-MPZ, 1,4-DMPZ, HEP, bHEP, AEP, triethylenediamine, HMP, and 4-methyl-1-PZ ethanamine confirms that the initial arm-switching behavior (S_N2 substitution reactions discussed in Chapter 9) was facilitated by the quat, with degradation continuing through the formation of several PZ derivatives. Some of these compounds were identified and quantified with cation IC, and some were identified with IC or LC-MS. In summary, these experiments indicate that the quaternary amine facilitates the formation of reaction intermediates such as DEA which will form its respective carbamate in CO_2-loaded solution ($DEACOO^-$ and ultimately undergo condensation polymerization to HEOD, which can react with another molecule of DEA to form bHEP. However, HEOD could just as easily react with another strong nucleophile such as MAE or PZ to form other dimers as confirmed in experiments RPN-1 and RPN-2 and discussed in Chapter 9.

The concentrations of DEA, 1-MPZ, 1,4-DMPZ, AEP, and HEP are plotted in Figure 4.8 to demonstrate the production of these MDEA degradation products when 7 m

MDEA+1 m quat at an initial loading of 0.2 mol CO_2/mol alkalinity was thermally degraded at 150 °C in Th. No. 15. In this experiment, the concentration of DEA was ~180 mM in the first few samples collected, indicating that the quaternary amine facilitated rapid arm switching. Because the route to bHEP formation starts with DEA production, bHEP is formed within 72 hours at a concentration of greater than 60 mM. The concentrations of both DEA and bHEP reach a plateau after ~450 hours of thermal degradation. Finally, PZ, 1-MPZ, and to a much lesser extent 1,4-DMPZ, are all produced, reaching an apparent plateau after 450 hours of thermal degradation. Freeman (2011) reported the presence of MPZ, 1,4-DMPZ and AEP when 8 m PZ was thermally degraded at temperatures of 165 °C and above. Chakma and Meisen (1997) reported that $DEACOO^-$ will react with MAE to form N,N-(hydroxyethyl)-methyl ethylenediamine (HEMED) which will then dehydrate to hydroxyethyl methyl piperazine (HMP). The formation of HMP could then result in arm switching on the PZ functional group to provide PZ and its derivatives. These data indicate that MDEA is being degraded in the presence of the quat as follows:

MDEA → DEA → $DEACOO^-$ → HEOD + HEMED → bHEP + HMP → PZ Der

This finding is in contrast to the anticipated result of more S_N2 arm switching products of MDEA including DMAE, MAE, MEA, DMEA, TMA and TEA.

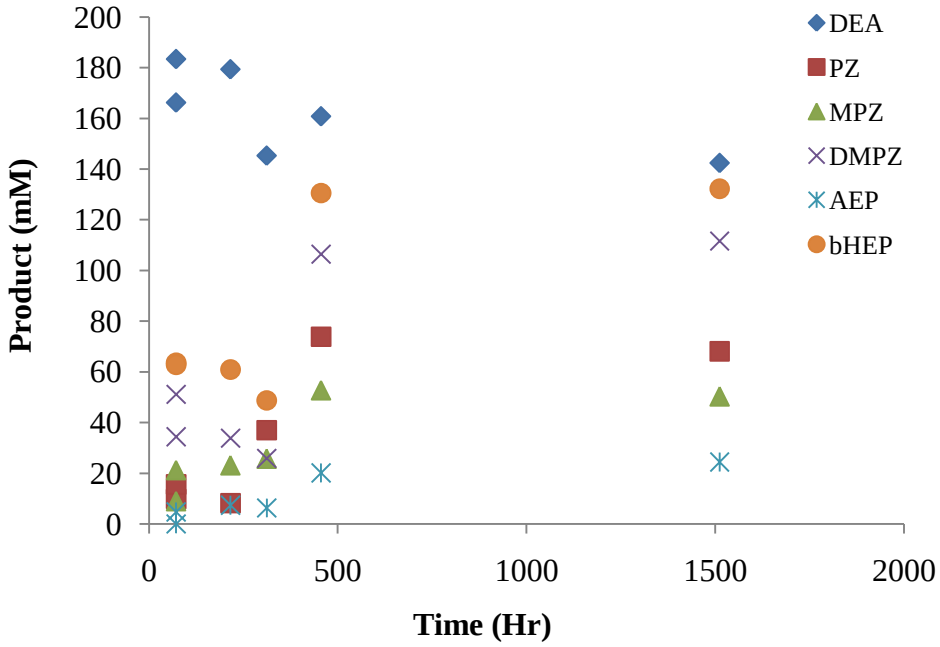

Figure 4.8: Thermal degradation products (150 °C) in 7 m MDEA + 1 m Quat

4.3 CYCLING DEGRADATION OF 7 m MDEA IN THE ISDA

This section reviews the degradation data generated through cycling of 7 m MDEA in the ISDA in the 18 separate experiments listed in Table 4.1. The characterization of the ISDA was performed with 7 m MDEA and discussed in detail in Chapter 3. The results from two of those experiments (C-6 and C-13) are utilized in this section to offer greater insight into 7 m MDEA degradation in the ISDA where needed. In addition to the 7 m MDEA cycling experiments, C-31 was conducted with 6 m MDEA + 1 m MAE, and C-32 was conducted with 6 m DEA + 1 m DEA. These experiments were designed to understand the role of DEA and MAE as reaction intermediates in the overall degradation of 7 m MDEA and 7 m MDEA/2 m PZ, and will be discussed as appropriate.

Experiment C-6 was conducted in the ISDA with 7 m MDEA at an initial loading of 0.1 mol CO_2/mol alkalinity. The solvent was cycled from 55 °C in the oxidative

reactor to 120 °C in the thermal reactor. The oxidative reactor headspace purge gas was 100 mL/min of 98% O_2/2% CO_2. Experiment C-13 was also conducted in the ISDA with 7 m MDEA at an initial loading of 0.1 mol CO_2/mol alkalinity. The solvent was cycled from 55 °C in the oxidative reactor to 120 °C in the thermal reactor, but the headspace purge gas was 98% Air/2% CO_2, providing an oxygen content of ~20%. C-13 was designed to understand the rate of MDEA degradation with ~1/5X the oxygen concentration in the headspace gas.

Before proceeding, the important conclusions from the ISDA characterization (Chapter 3) are reiterated here. 7 m MDEA degradation was determined to be dependent on: (1) the amount of dissolved oxygen delivered to the cycling system oxidative reactor through increased agitation rate and increased purge gas oxygen concentration, (2) the amount of undissolved gas bubble entrainment that occurred due to agitation and solvent viscosity effects as the solvent exited the oxidative reactor, (3) the thermal reactor temperature, and (4) the thermal reactor residence time.

4.3.1 Degradation products in cycled 7 m MDEA

The major degradation products observed in cycled 7 m MDEA are listed in Table 4.6. The degradation products observed in cycled 7 m MDEA fall into the same general categories as those observed with Low-gas and thermal degradation. The carboxylate ions formate and glycolate were observed, as well as the 2° amines DEA and MAE. As noted in previous sections, the separation of DEA and MAE is not possible using cation IC, but the presence of both compounds in cycled 7 m MDEA was confirmed using IC-MS. Other products observed in the cycled solvent were the 3° amine DMAE, the amide of DEA, N,N-bis-(2-hydroxyethyl)formamide, and the amino acids bicine and glycine. DMAE and the oxazolidone HEOD were both observed in degraded samples. HEOD is

known to form from $DEACOO^-$ which undergoes thermal degradation with condensation polymerization to the oxazolidone structure. The presence of HEOD in C-6 samples confirms the cation IC and IC-MS data indicating the presence of DEA in degraded 7 m MDEA in this work. Note that the last three compounds named were generally not observed in thermal degradation experiments, and are believed to require an oxidizing environment to form.

PZ derivatives were generally not observed using cation IC or MS methods in cycled 7 m MDEA samples. To confirm this finding, 7 m MDEA was cycled to 130 °C in the redesigned thermal reactor in C-26, but PZ derivatives were not observed using cation IC in this experiment either. The thermal reactor temperature of 130 °C was the highest thermal reactor temperature used in any cycling experiment in this work.

Table 4.6: Degradation products in cycled 7 m MDEA

Compound	MW	Expt	Method
Formate	45	Several	Anion IC
Glycolate	75	Several	Anion IC
DEA	105.1	Several	Cation IC, IC-MS
MAE	75.1	Several	Cation IC, IC-MS
DMAE	89.1	C-6	GC-MS
N,N-bis-(2-hydroxyethyl)formamide	133	C-1	IC-MS
Bicine	163.1	C-6	HPLC-AAA, IC-MS, GC-MS
Glycine	75.1	C-6	HPLC-AAA
HEOD	131	C-6	GC-MS

4.3.2 MDEA and alkalinity loss rates

The initial loss rates of MDEA and alkalinity are listed by cycling experiment number and conditions in Table 4.7 along with the loss rates measured in Low-gas experiment OD-8. The standard deviations of the rates were estimated with the Excel Linest function and are listed for a subset of the experiments. A more comprehensive

table listing degradation product formation rates in these experiments is provided in Appendix E. The loss of MDEA and alkalinity in experiment C-6 represents a baseline condition for understanding 7 m MDEA degradation in the cycling environment. Experiments C-25 through C-27 were conducted with the redesigned thermal reactor, and more advanced analytical techniques, providing more information regarding important and previously identified degradation products. The MDEA and alkalinity loss rates were measured as 4.6 and 4.9 mM/hr, respectively, in C-6. With the redesigned thermal reactor and same temperature targets for the oxidative (55 °C) and thermal reactor (120 °C) in C-25, the rates were 5.1 and 4.4 mM/hr, respectively.

4.3.3 MDEA loss rate constant determination

MDEA concentration data were tested to determine whether they follow first-order rate behavior. MDEA concentration data from C-6 and C-25 were plotted separately on semi-log plots to determine the goodness of fit, and whether the ISDA is characterized by first-order behavior. The C-6 first-order plot provided an R^2 value at 0.68 and a k_1 of 3.3 X 10^{-7} s^{-1}. C-25 provided an R^2 of 0.87 and a k_1 of 4.6 X 10^{-7} s^{-1}. The semi-log plot of [MDEA] vs. time is provided as Figure 4.9.

The data were also tested for adherence to second-order rate behavior using the relationship in Equation 4.3:

$$-\frac{dC_{MDEA}}{dt} = k \cdot [MDEA]^2 \tag{4.3}$$

An R^2 value at 0.68 and a k_2 of 8.3 X 10^{-11} $s^{-1}mM^{-1}$ were calculated for C-6, while an R^2 of 0.88 and a k_2 of 1.7 X 10^{-10} $s^{-1}mM^{-1}$ were calculated for C-25. Applying second-order rate behavior did not improve the fit in terms of the R^2. In summary, both rate expressions (first and second-order) provided relatively poor R^2 values.

Table 4.7: MDEA and alkalinity loss rates in 7 m MDEA experiments in the ISDA

Expt. No.	Temp	Stir Rate	Purge Gas	Metal Salts	Other Condition(s)	MDEA Loss Rate	Alk Loss Rate
	(°C)	rpm	%/%	Y/N		mM/hr	mM/hr
Low-gas							
OD-8	70	1,440	98% O_2/2% CO_2	Y	-	0.12 ± 0.3	0.37 ± 0.2
Cycling							
C-1	55/120	1,440	98% O_2/2% CO_2	N	Base design	8.8 ± 2.1	4.78 ± 0.4
C-2	55/55	1,440	98% O_2/2% CO_2	N	"	0 ± 4.7	0.5 ± 0.3
C-3	55/55	1,440	98% O_2/2% CO_2	Y	Added ss metals	0.9	0.91
C-4	55/120	520	98% O_2/2% CO_2	Y	"	3.4	2.46
C-5	55/120	1,000	98% O_2/2% CO_2	Y	Added vertical bubble removal vessel	8.5	3.95
C-6	55/120	1,440	98% O_2/2% CO_2	Y	Added redesigned bubble removal jar*	4.6 ± 1.9	4.7 ± 3.2
C-7	55/120	1,440	98% O_2/2% CO_2	Y	100 mM Inh A	5	5.03
C-8	55/120	1,440	98% N_2/2% CO_2	Y	-	1.9	1.57
C-9	55/120	0	98% N_2/2% CO_2	Y	-	4.1	2.62
C-10	55/100	1,440	98% O_2/2% CO_2	Y	-	4.1	3.1
C-11	55/80	1,440	98% O_2/2% CO_2	Y	-	0.91	0.97
C-12	55/90	1,440	98% O_2/2% CO_2	Y	-	2.9	2.19
C-13	55/120	1,440	98% Air/2% CO_2	Y	-	0.24	0.52
C-14	55/90	1,440	98% O_2/2% CO_2	Y	-	0.22	0.18
C-15	55/90	1,440	98% O_2/2% CO_2	Y	100 mM Inh A	2.37	1.63
C-25	55/120	1,440	98% O_2/2% CO_2	Y	Redesigned Th Rx	5.9 ± 4.2	4.4 ± 0.2
C-26	55/130	1,440	98% O_2/2% CO_2	Y	Redesigned Th Rx	15.6 ± 2.0	3.67 ± 0.4
C-27	55/100	1,440	98% O_2/2% CO_2	Y	Redesigned Th Rx	3.2	1.88

*All subsequent ISDA expt utilized this jar.

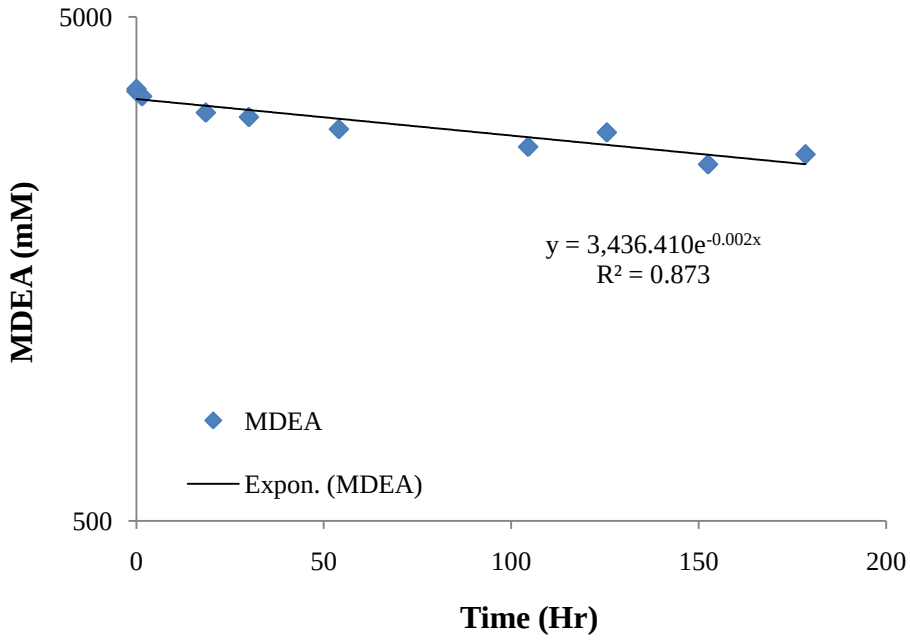

Figure 4.9: First-order degradation rate behavior test in 7 m MDEA cycled from 55 to 120 °C in the ISDA (loss rate 4.6 ± 1.9 mM/hr)

4.3.4 Temperature dependence of degradation rates

A series of experiments provided some insight as to how the oxidative degradation behaved with an increase in thermal reactor temperature in the ISDA. As discussed in section 3.7, experiments were performed with the thermal reactor varied from 55 to 130 °C, and several degradation parameters were measured. The MDEA loss rates from the combined data sets for degradation experiments (C-3, C-10, C-11, C-12, C-6, C-25, C-26, and C-27) with the original and redesigned thermal reactors were used to estimate the activation energy (E_a) for MDEA loss in the ISDA (Figure 4.10). The E_a for MDEA loss in the ISDA was estimated to be ~32 kJ/mol. The plotted data provided an R^2 of 0.73 which is poor, but the data sets from experiments conducted with both the original and redesigned thermal reactors are included in this regression.

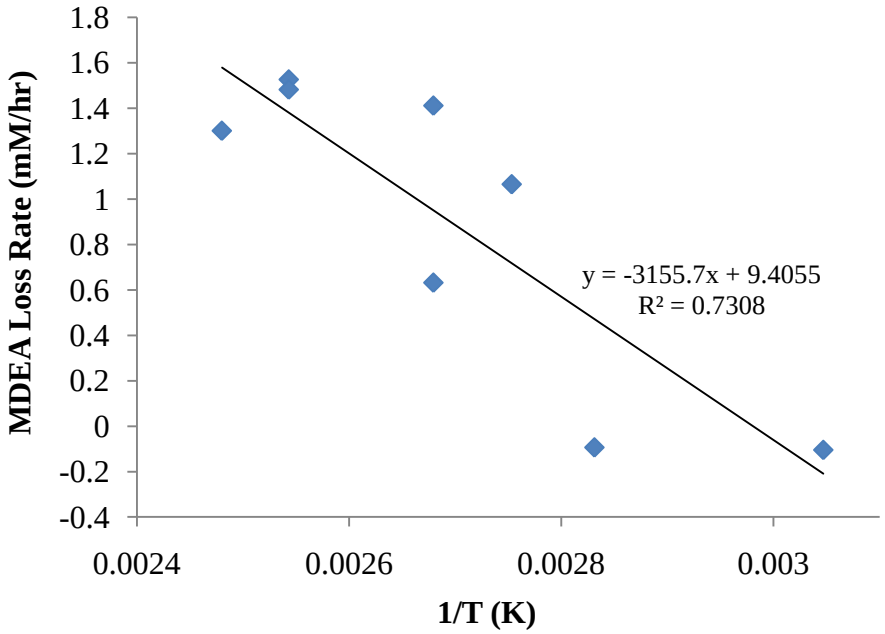

Figure 4.10: Estimation of activation energy from MDEA loss rates in the ISDA

The formate concentrations in the individual experiments are plotted in Figure 4.11 to demonstrate the effect of the thermal reactor temperature on oxidation rate. As the thermal reactor temperature was increased from 55 to 120 °C in this experimental series, formate production increased. From this series of experiments, an activation energy for formate production of ~46 kJ/mol was estimated.

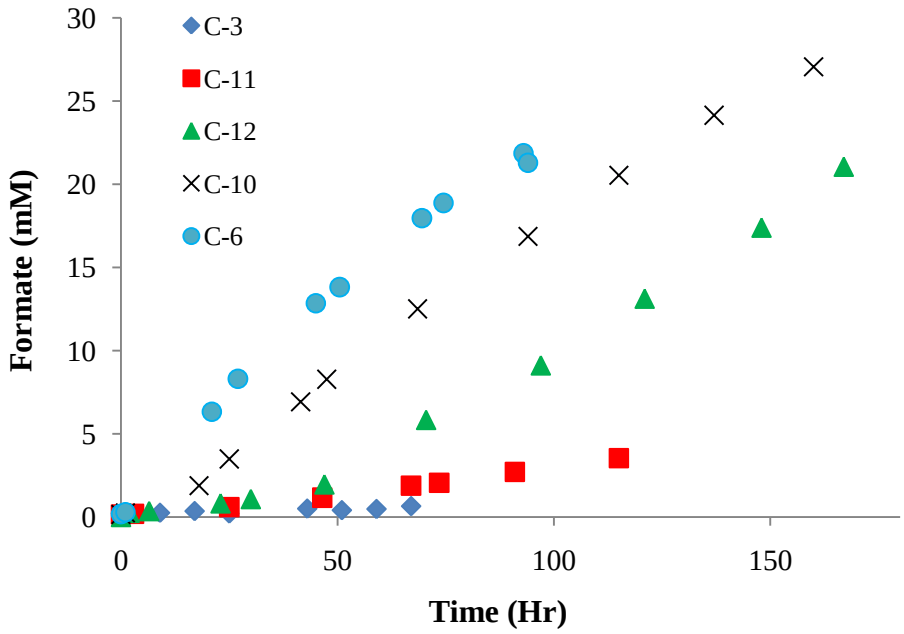

Figure 4.11: Formate concentration in cycled 7 m MDEA with thermal reactor temperature increased from 55 to 120 °C

In a similar fashion, the concentration of DEA+MAE was plotted vs. time as measured in this same series of experiments with 7 m MDEA (Figure 4.12). Note that the concentration of DEA+MAE was zero throughout experiments C-3 (thermal reactor at 55 °C) and C-11 (thermal reactor at 80 °C). In experiment C-12, the thermal reactor was set at 90 °C, and the concentration of DEA+MAE was ~zero for the first 70 hours of the experiment. However, after 70 hours of cycling from 55 to 90 °C, the DEA+MAE accumulated in solution at an initial rate of ~1.3 mM/hr. Aside from the lag time, the rate of accumulation or initial rate in this experiment after 70 hours of cycling is approximately the same as the initial rate of DEA+MAE formation in C-10 where the thermal reactor was maintained at 100 °C. This latter observation indicates that the accumulation of another product of degradation may be essential for the formation of DEA+MAE.

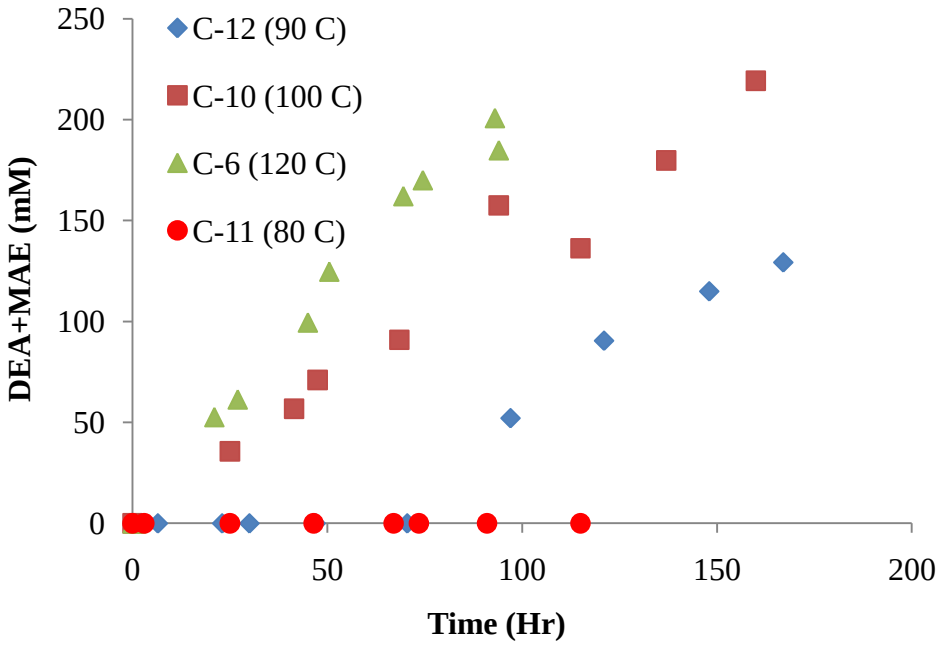

Figure 4.12: Production of DEA+MAE in cycled 7 m MDEA

A likely possible precursor to DEA+MAE production is a free radical fragment of MDEA. Chapter 8 reviews the oxidation of MDEA, and presents the initial abstraction of a proton from MDEA as an essential first step in the oxidation of MDEA in the presence of dissolved transition metal salts. Subsequent to this abstraction is the formation of a peroxy radical, then a peroxide molecule. The O–O bond of peroxides will undergo homolysis at temperatures between 50 and 150 °C, yielding two alkoxyl radicals (RO•) (Parsons, 2000). The lack of DEA+MAE formation at thermal reactor temperatures below 90 °C may be due to the inability to form these free radicals in appreciable concentrations to facilitate subsequent steps to lead to the formation of DEA and/or MAE. The pathway for formation of DEA from MDEA oxidation is presented as Figure 4.13.

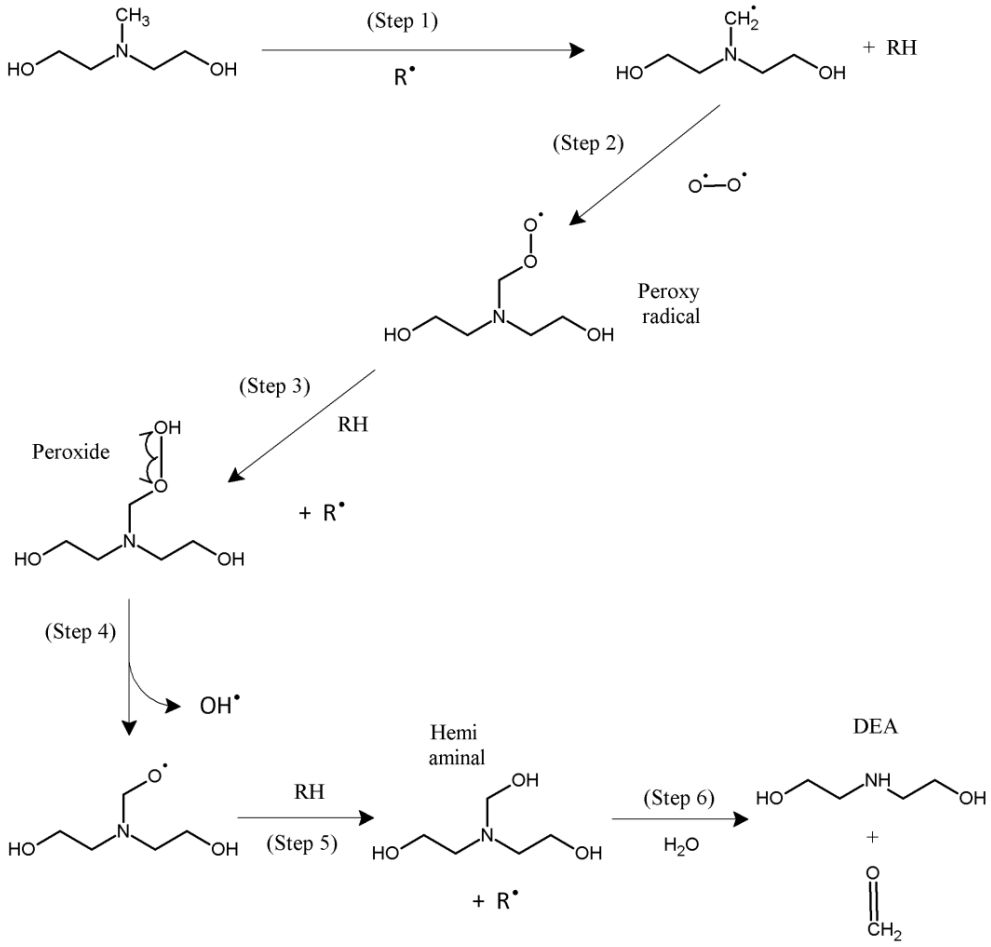

Figure 4.13: Pathway for oxidation of MDEA and formation of DEA with initial electron abstraction and free radical formation

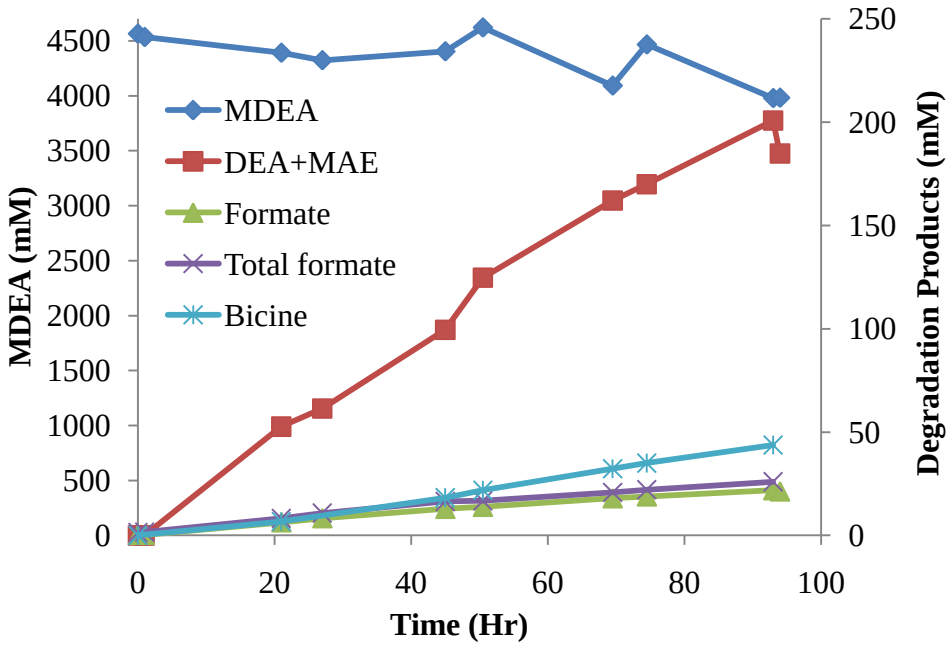

Figure 4.14: MDEA and degradation product concentrations in 7 m MDEA cycled from 55 to 120 °C in the ISDA (C-6)

4.3.5 Product formation trends

The concentration of MDEA and major degradation products of 7 m MDEA are presented in Figure 4.14. All products are formed without an apparent lag time. However, after approximately 50 hours of cycling, the increase in concentration of formate and total formate appears to fall off, indicating the possibility of reaching a steady state concentration after another 50 hours of cycling. In contrast, the concentration of bicine continues to increase in a linear fashion through the end of the experiment.

To provide more insight as to the relationship between bicine production and other products of degradation such as DEA+MAE, a plot of MDEA and degradation product concentrations in experiment C-13 is provided as Figure 4.15. Experiment C-13 was implemented for 450 hours with a 98% Air/2% CO_2 purge gas, and offers a better

assessment of long-term concentration trends. All rates of degradation in this experiment were lower than observed in C-6, but the long-term trends are more evident due to the length of the experiment.

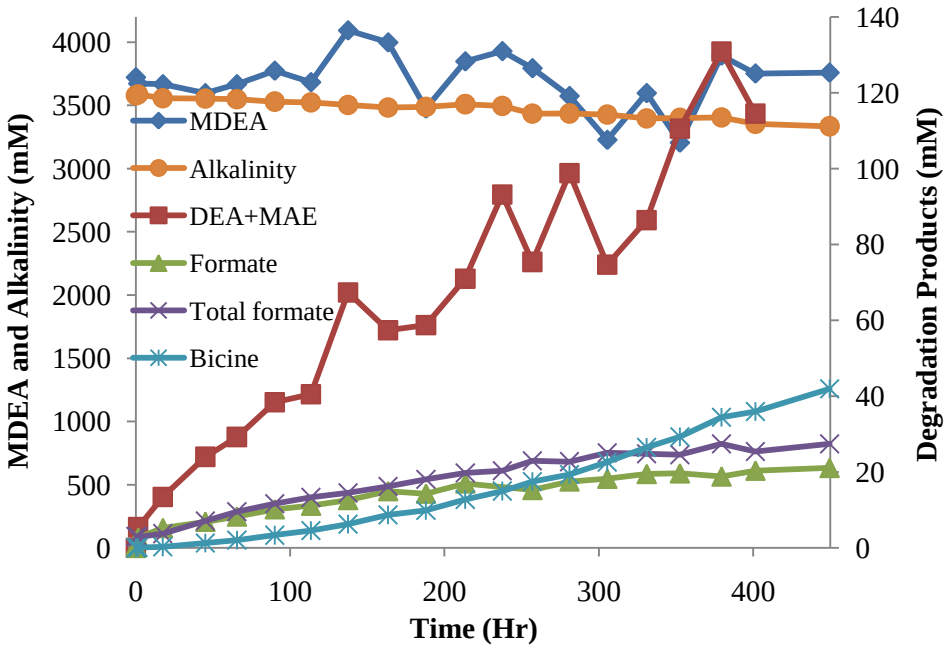

Figure 4.15: MDEA, alkalinity and degradation products in cycled 7 m MDEA cycled from 55 to 120 °C with 98% Air/2% CO_2

MDEA and alkalinity concentrations both experience loss in a generally linear fashion, and a linear trendline reveals the same rate of loss (~0.2 mM/hr). As with C-6, the production of DEA+MAE, formate and total formate do not pass through a lag period. All three parameters appear to decrease in production rate after approximately 175 hours of cycling, whereas at the same time, the bicine production rate increases. Critchfield and Jenkins (1999) reviewed degradation data from tail-gas treating units (TGTU) and discussed the production of DEA and MAE in degraded MDEA, with subsequent production of the amino acids bicine and HES from the further degradation of the 2°

amines. The data plotted in Figure 4.15 support this finding, with bicine being formed after DEA+MAE accumulates in the system for the first 175-200 hours. Following the lag period, the rate of DEA+MAE production decreases through the end of the experiment, while the bicine production rate increases, indicating a link between the two products. An oxidative pathway and accompanying set of mechanisms for the production of DEA as an intermediate, with subsequent degradation to bicine, is presented here as Figure 4.16 and in Chapter 8.

Another notable trend in Figure 4.15 is the apparent production of amides, quantifiable through the difference in total formate and formate. The difference between the two measurements is considered to be the approximate concentration of amides produced as the solvent degrades. The spread between the two concentrations increases as the experiment is carried through 450 hours of cycling. Although not evident through HPLC analyses of C-6 samples, amides of degradation products of MDEA are likely being formed. Of note, PZ was not detected through cation IC analyses of pre- and post-hydrolyzed samples.

4.3.6 Mass Balance in cycled 7 m MDEA

Using C-13, a molar balance in terms of carbon and nitrogen recovered as degradation products was performed on solvent samples. The moles of carbon and nitrogen that each degradation product comprises in the final sample from C-13 are listed in Table 4.8. The balance was performed using alkalinity measurements as a basis due to consistency of this data when compared to cation IC. The percent of carbon and nitrogen recovered in the final sample, based on initial alkalinity and final alkalinity measurements were 62 and 70 %, respectively. The degradation product comprising the largest amount of recovered carbon and nitrogen was DEA+MAE, at 35 and 50%,

respectively. Bicine is the next largest component, making up 22 and 18% of carbon and nitrogen loss, respectively. As a class, the carboxylate ions (formate+glycolate+oxalate) make up ~4% of carbon loss, and no nitrogen. The amino acids (bicine+glycine) as a class make up ~22% of carbon and ~18.5% of nitrogen.

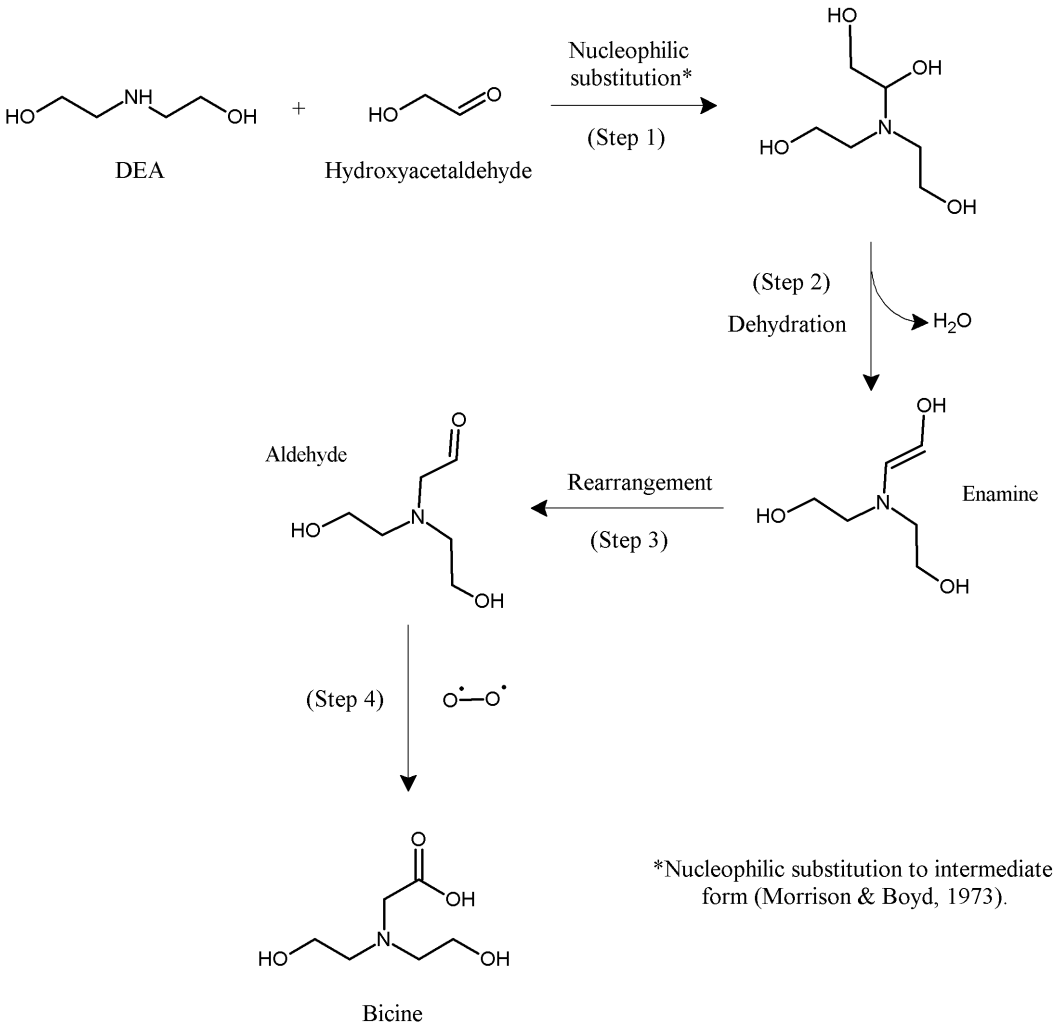

Figure 4.16: Proposed oxidative degradation pathway for production of bicine from DEA in degraded 7 m MDEA

Table 4.8: Percentage of carbon and nitrogen recovered in degradation products in cycled 7 m MDEA (C-13)

Compound	Concentration (mM)	% C	% N
Formate	19.9	1.6	0
Glycolate	11.7	1.9	0
Oxalate	2.8	0.5	0
Formyl amides	5.4	1.6	2.2
DEA+MAE	120.8	34.6	49.5
Bicine	44.2	21.7	18.1
Glycine	0.4	0.1	0.2
Total (%)	-	62	70

The degradation of MDEA has been found to lead to the production of other compounds with similar structures, but dissimilar behavior. The similarities in structure stem from arm switching, primarily of hydroxyethyl groups, but also methyl groups. The hydroxyethyl groups can be accounted for by adding the number of groups on MDEA and its products at the end of an experiment to determine whether major products of degradation have been accounted for. MDEA will have two hydroxyethyl groups, while bicine and glycine account for three and one, respectively, one of which is oxidized on both amino acids. DEA+MAE represents a compromise between two groups for DEA and one group for MAE, so the combined DEA+MAE is treated as representing 1.5 hydroxyethyl groups. Finally, the formyl amides are assumed to represent 1.5 hydroxyethyl groups, also as a compromise by considering them amides of MEA, MAE and DEA. The summation allows us to account for ~98% of mM hydroxyethyl groups.

4.4 INHIBITOR A IN CYCLED 7 m MDEA

A comparison of the MDEA loss rate measured in C-7 to the rate measured in C-6 demonstrates that 100 mM Inh A was ineffective in reducing the rate of high temperature

oxidation in the cycling environment. In both cycling experiments, the solvent was cycled from 55 to 120 °C, and the MDEA loss rates were generally measured as ~5 mM/hr. The only difference in the experiments was the addition of 100 mM Inh A to the solvent before initiation of cycling in C-7.

4.5 SUMMARY OF 7 m MDEA DEGRADATION

7 m MDEA was degraded using the Low-gas oxidative reactor, the Swagelok® thermal cylinders, and the ISDA cycling system. The major products of oxidative degradation included formate, formyl amides, DEA+MAE, bicine, and glycine. Other compounds that were detected at lesser concentrations in degraded samples included glycolate and the amino acid glycine. The oxidation rate measured as initial rate of MDEA loss in the Low-gas reactor was 0.12 ± 0.3 mM/hr, which can be compared to rates measured in 7 m MEA at comparable conditions of 6.9 to 11.7 mM/hr, and a rate for 8 m PZ of 0.02 mM/hr. The rate of oxidation in terms of amine loss followed: 7 m MEA>7 m MDEA>8 m PZ. Formate production was measured as 0.03 ± 0.003 mM/hr, which was $1/10^{th}$ the rate measured in 7 m MEA.

Thermal degradation products generally included the same products observed in oxidized 7 m MDEA with the addition of DMAE, HEOD and PZ derivatives. The E_a estimated for 7 m MDEA degradation was ~60 kJ/mol, which can be compared to the E_a estimated by Chakma and Meisen (1997) of 57.4 kJ/mol, and the E_a estimated by Freeman (2011) of 184 kJ/mol for 8 m PZ. The first-order rate constant for thermal degradation at 150 °C was measured as 8.1 X 10^{-7} s^{-1} which was over 100X the rate measured for 8 m PZ of 6 X 10^{-9} s^{-1}. The thermal degradation rates measured in this work are generally comparable to the rates reported by Chakma and Meisen (1997).

Finally, when 7 m MDEA was cycled in the ISDA from 55 to 120 °C, the MDEA loss rate was 4.6 ± 1.9 mM/hr, and the first-order rate constant was 3.3 X 10^{-7} s^{-1}. The E_a for degradation of MDEA was estimated as 32 kJ/mol. Pathways for the production of major degradation products became apparent from cycling the solvent, with the production of DEA and MAE viewed as intermediates in the further oxidation and production of the amino acids bicine from DEA and HES from MAE. Pathways have been proposed, which are covered in more detail in Chapters 8 and 9. The pathways entail free radical mechanisms for the initial abstraction of an electron, and the subsequent production of free radicals and degradation products. Approximately 60% of carbon loss as MDEA loss can be accounted for in the major degradation products, while approximately 70% of nitrogen can be accounted for.

Chapter 5 - MDEA Oxidative Model

This chapter presents a detailed discussion of an oxidative degradation model created to predict the concentration of key indicators of degradation in 7 m MDEA over a range of temperatures that may be encountered in an absorber/stripper (up to 130 °C). The model was developed from degradation data collected in the ISDA over the course of 18 separate experiments with 7 m MDEA. The behavior of the ISDA with respect to 7 m MDEA is discussed in detail in Chapter 3, and the data which provide the basis for the model are discussed further in Chapter 4.

5.1 Model Background and Underlying Assumptions

Solvent degradation in the ISDA occurs through oxidative processes when oxygen is introduced to the solvent as the headspace purge gas in the oxidative reactor. The data from the ISDA, therefore, provide the basis for modeling and predicting the rate of degradation. Indicators of oxidative degradation in 7 m MDEA include formate, total formate, and bicine, all of which are primarily formed under oxidative conditions. Other degradation products, including DEA+MAE, can be detected in thermally degraded 7 m MDEA, and are, therefore, not as useful for predicting oxidative degradation despite representing a substantial amount of the degraded amine.

Important assumptions were made to accurately model the ISDA reactor system. These assumptions, which will be covered in this section, include the following:

1) The system behaves as a plug-flow reactor (PFR);
2) The PFR operates approximately isothermally;

3) Very little degradation occurs at low temperatures, allowing the assumption that the PFR volume is that of the thermal reactor only; and
4) The solvent exits the oxidative reactor in an oxygen-saturated state.

5.1.1 PFR behavior

The assumption of the ISDA system behaving as a PFR is approximately met. Rawlings and Ekerdt (2002) state that:

> "Plug flow in a tube is an ideal-flow assumption in which the fluid is well mixed in the radial and angular directions. The fluid velocity is assumed to be function of only the axial position in the tube."

According to Holland and Anthony (1979):

> "The reacting stream flowing through a reactor is said to be in plug flow if the contents of the reactor are perfectly mixed in the radial direction while no mixing occurs in the axial direction (the direction of flow)."

The authors reiterate that the PFR design mixing assumptions are valid provided that the length-to-diameter ratio is greater than 50 and the Reynolds number of the flowing stream is greater than 10^4. The length of the redesigned thermal reactor is ~21.5 inches while the diameter is 0.65 inches, creating a length-to-diameter ratio of ~33. The length-to-diameter ratio of the hot-side system tubing within the heat exchanger and in heating coil tubing is >>50, creating overall plug-flow behavior in solvent before entering and after exiting the ISDA thermal reactor. However, the Reynolds number of a typical experiment with 7 m MDEA was calculated as ~500, which is $<10^4$ and suggests that some axial mixing may take place in the ISDA thermal reactor.

5.1.2 Isothermal behavior in thermal reactor

The assumption that the ISDA thermal reactor operates isothermally is approximately met. The redesigned thermal reactor was installed with two thermowells,

one at the entrance and one at the exit of the reactor. Oil bath settings in experiments were adjusted to maintain as close to isothermal operation as possible. For example, on Day 7 of experiment C-25, steady state conditions were met, and the entrance and exit thermal reactor temperatures were 116 and 120 °C, respectively. Temperature acquisition in the original thermal reactor was only achieved from a single thermowell installed to a depth of six inches from the exit of the reactor, providing knowledge of bulk liquid temperature at this location only. Bath settings were adjusted to achieve as close to isothermal operation as possible by maximizing the heat input to the solvent in heating coils upstream of the thermal reactor.

5.1.3 Degradation occurs primarily in thermal reactor

In experiments C-2 and C-3, both the oxidative and the thermal reactor were set to operate at a bulk solvent temperature of 55 °C. The alkalinity and MDEA loss rate in C-2 were 0.0 ± 4.7 and 0.5 ± 0.3 mM/hr, respectively, while in C-3 the measured rates for both were ~0.9 mM/hr. In the latter case, the formate production rate was 0.005 ± 0.001 mM/hr. These measured initial rates of degradation in 7 m MDEA indicate that very little degradation occurs in the solvent at lower temperature, allowing the approximation that all oxidative degradation occurs in the thermal reactor from an experimental standpoint. However, this assumption is not analogous to a true absorber/stripper system because the residence times for solvent in the heat exchanger and piping to the steam stripper are both significantly higher, allowing greater opportunity for oxidative processes to occur.

5.1.4 Solvent exits oxidative reactor in oxygen-saturated condition

The solvent exits the oxidative reactor in an oxygen saturated condition when the headspace purge gas contains 98% oxygen, and travels through a bubble removal vessel where entrained gas bubbles are allowed to aggregate and gravity separate from the solvent. The solvent is agitated at 1,440 rpm at 55 °C for the duration of typical experiments, creating a vortex and sufficient mass transfer as the solvent is intimately mixed with the headspace gas. As the solvent exits the top section of the oxidative reactor, entrained gas bubbles ensure that the solvent stays saturated for the period of time required for the solvent to pass through the bottom section of the oxidative reactor and exit to the bubble removal vessel. According to Rooney (1998), the C_{DO} in 7 m MDEA at 55 °C is approximately 5.85 mg/L, or 0.18 mM. However, no attempt was made to measure the concentration of dissolved oxygen in solvents in the ISDA.

5.2 MODEL DEVELOPMENT

When degradation rates from the ISDA were first plotted against thermal reactor temperature for each experiment, it was found that the rates did not adhere to the Arrhenius rate-law (Equation 5.1) relationship at higher temperature, indicating possible complete consumption of oxygen in the thermal reactor at these higher temperatures. A model relating the true degradation over the entire temperature region for experiments conducted in the ISDA was desired. The following discussion reviews the model development.

$$k = k_o * \exp\left[-\frac{E_a}{R}\left(\frac{1}{T}-\frac{1}{T_o}\right)\right] \tag{5.1}$$

The basic oxidation reaction for conversion of an amine was considered to occur as follows:

$$A + B \rightarrow C$$

where: A is MDEA, B is O_2, and C is Product. The reaction of solvent with oxygen is considered to be first-order in oxygen as follows:

$$R = -k_1 * C_B \tag{5.2}$$

Using the shell balance approach, the differential equation accounting for oxygen in a slice of solvent passing through the system is represented as follows:

$$\frac{\partial C_B}{\partial t} = -\frac{\partial (C_B v)}{\partial z} + R_B \tag{5.3}$$

where z is defined as being in the axial direction within the reactor system, and v is defined as solvent velocity in the z direction. If we assume the system is operating at steady state in terms of flow rate through the system, the left-hand side is zero, and the equation becomes the following:

$$\frac{\partial (C_B v)}{\partial z} = R_B \tag{5.4}$$

Now, assuming constant liquid density ρ and defining τ=V/Q, Q=A*v, and V=z*A, which can be substituted into the differential equation, we get the following equation:

$$\frac{\partial (C_B)}{\partial \tau} = R_B = -kC_B \tag{5.5}$$

Equation 5.5 can be separated and integrated as follows:

$$\int_{C_{B_{in}}}^{C_{B_{out}}} \frac{dC_B}{C_B} = -k \int_0^{\tau} d\tau \tag{5.6}$$

Equation 5.6 can be solved to give the following equation:

$$C_{B_{out}} = C_{B_{in}} \exp(-\frac{k_1 * V_{TR}}{Q}) \tag{5.7}$$

where $\tau = V_{TR}/Q$. Now, considering the amount of oxygen consumed per pass through the system as follows:

$$\frac{\Delta C_B}{Pass} = C_{B_{in}} - C_{B_{out}} \tag{5.8}$$

Making the proper substitution provides the following equation:

$$C_{B_{out}} = C_{B_{in}} \exp(-\frac{k_1 * V_{TR}}{Q}) \tag{5.9}$$

So, equating the consumption of oxygen per pass provides the following:

$$\frac{\Delta C_B}{Pass} = C_{B_{in}} (1 - \exp(-\frac{k_1 * V_{TR}}{Q})) \tag{5.10}$$

The number of passes that occur over the course of an experiment with time length t can be expressed as: no. passes=$Q*t/V_{tot}$ where V_{tot} is the ISDA total system volume. So, we can account for total oxygen consumption by multiplying the change in oxygen concentration per pass by the total number of passes, and substituting in the expression for number of passes in terms of flow rate (Q), and total reactor system volume (V_{tot}):

$$\left(\frac{\Delta C_B}{pass}\right)(No.passes) = C_{B_{in}} \left(1 - \exp(-\frac{k_1 * V_{TR}}{Q})\right)\left(\frac{Q*t}{V_{tot}}\right) \tag{5.11}$$

A relationship for conversion of amine (MDEA) to products by reaction with oxygen is necessary to relate the oxygen consumption to the conversion of amine into products:

$$MDEA + S*O_2 \rightarrow Products$$

where:

$$S = \frac{\Delta[Prod]}{\Delta[O_2]} \tag{5.12}$$

Manipulating this equation to express the change in concentration of products in terms of the stoichiometric ratio (S) and oxygen consumption, and substituting into Equation 5.11 provides the following expression:

$$\Delta[Prod] = \frac{C_{B_{in}} * S * Q * t}{V_{tot}} \left(1 - \exp(-\frac{k_1 * V_{TR}}{Q})\right) \tag{5.13}$$

The concentration of oxygen in solvent (C_{Bin}) is related to the concentration of oxygen in the headspace gas above the solvent in the oxidative reactor by Henry's Law which is expressed as: $P_{O2}=K_H*C_{O2}$. Substituting this expression into Equation 5.13 provides the PFR equation relating the first-order reaction behavior for oxygen consumption and production of degradation products in the ISDA:

$$\Delta[Prod] = \frac{P_{O_2} * S * Q * t}{K_H * V_{tot}} \left(1 - \exp(-\frac{k_1 * V_{TR}}{Q})\right) \tag{5.14}$$

A spreadsheet was created with Equation 5.14 and the Arrhenius equation (Equation 5.1) relating temperature behavior of the solvent degradation reactions for the production of major oxidative degradation products including formate, total formate, and bicine. The spreadsheet model was designed to converge to a solution that minimized the sum of the errors between the estimated value of product concentration from the Arrhenius equation and the modeled value for all measured temperatures over the range of 55 to 130 °C, with three floating parameters (E_a, k_1, and S). The Excel Solver add-in tool was used to converge to a solution for the three floating parameters through an optimization routine that minimized the sum of the errors.

5.3 MODEL INPUTS

The inputs to the oxidative model included the fixed parameters such as reactor volumes, the Universal Gas Constant R, and Henry's Law coefficient for oxygen at 55 °C. Dissolution of oxygen into the solvent occurs at 55 °C in the oxidative reactor, which limits how much oxygen is available in dissolved form as degradation occurs downstream of this reactor. The inputs also include the set of experiment specific parameters listed in Table 5.1. These parameters include the thermal reactor temperature, measured flow rate, initial rates and total accumulated concentration for formate, total formate, and bicine, and the total time from which the initial rate was estimated. The values for experiment C-12 (shaded in Table 5.1) were used as the basis for the initial guess in the Solver optimization routine.

Table 5.1: Experiment-specific input parameters; C-12 data (shaded) were used as the initial guess

		Experiment						
Input Parameter	Units	C-3	C-11	C-12	C-10	C-27	C-6	C-26
T_{th}	(°C)	55	80	90	100	100	120	130
Flow Rate	mL/min	200	265	206	181	272	200	213
Initial Rate – Formate	mM/hr	0.005	0.034	0.038	0.177	0.06	0.28	0.41
Initial Rate - Tot Formate	mM/hr	0	0.039	0.15	0.3	0.12	0.34	0.76
Initial Rate – Bicine	mM/hr	0.007	0.027	0.066	0.267	0	0.46	1.77
Time t	Hr	67	91	47	160	67	45	68
Δ[Formate]	mM	0.65	2.7	2	27.1	4.2	12.8	29.2
Δ[Tot Formate]	mM	2.2	5.1	7.7	48.1	8.75	16.4	50.5
Δ[Bicine]	mM	0.74	5.45	3.15	42.4	8	18.2	131.7

The time t used for each experiment was the approximate time over which an initial rate could be extracted for all of the degradation products. This time generally did not correspond to the experiment duration, but only to the time required to extract the

initial rate for the three degradation products. The accumulated concentration of formate, total formate, and bicine also corresponded to the concentration at the time t used for each experiment. This concentration was, therefore, not the concentration at the end of the experiment.

5.4 OXIDATIVE DEGRADATION MODEL RESULTS (7 m MDEA)

The 7 m MDEA oxidative model was used to converge to a set of parameters (E_a, k_o, and S) for formate, total formate, and bicine. Table 5.2 lists the values of k_o, E_a, and S for each degradation product. The first-order rate constants for consumption of oxygen in terms of each of three modeled products are derived from the data included in all of the ISDA experiments (data included in Appendix D).

Table 5.2: 7 m MDEA oxidative model results for formate, total formate, and bicine

Parameter	k_o (hr^{-1})	E_a (kJ/mol)	S (mol Prod/mol O_2)
Formate	2.6	151	0.09
Total formate	3.4	152	0.14
Bicine	0.32	244	0.35

Comparison of the activation energy E_a for formate production of 151 kJ/mol to the estimate of 46 kJ/mol from Chapter 4 indicates that when the stoichiometric ratio S of degradation product formation to oxygen consumption is accounted for, the activation energy is 3X. The value of S indicates that the production of one mol formate requires ~10 mol oxygen. With complete resaturation of the solvent upon each pass through the system, excess oxygen is available in the system. It is anticipated that the situation would be the same in an absorber/stripper system designed for CO_2 capture from flue gas streams where the oxygen concentration could be as high as 5%. The stoichiometric ratio

S for total formate production is 0.14, indicating that approximately 7.1 moles of oxygen are required for every mole of total formate produced.

The activation energies of formate and total formate are approximately the same from the model, indicating that mechanisms for production of amides are similar to those for formate production, and that they require approximately the same amount of energy. In contrast, the E_a for bicine production was estimated as ~244 kJ/mol, indicating that the production of this compound requires much more energy. As discussed in Chapter 4, the end concentration of bicine typically represented almost 15X the amount of lost carbon represented by the end concentrations of formate in cycled 7 m MDEA. This observation justifies the much larger S-value returned by Solver for bicine (0.35) when compared to the values for formate and total formate of 0.09 and 0.14, respectively.

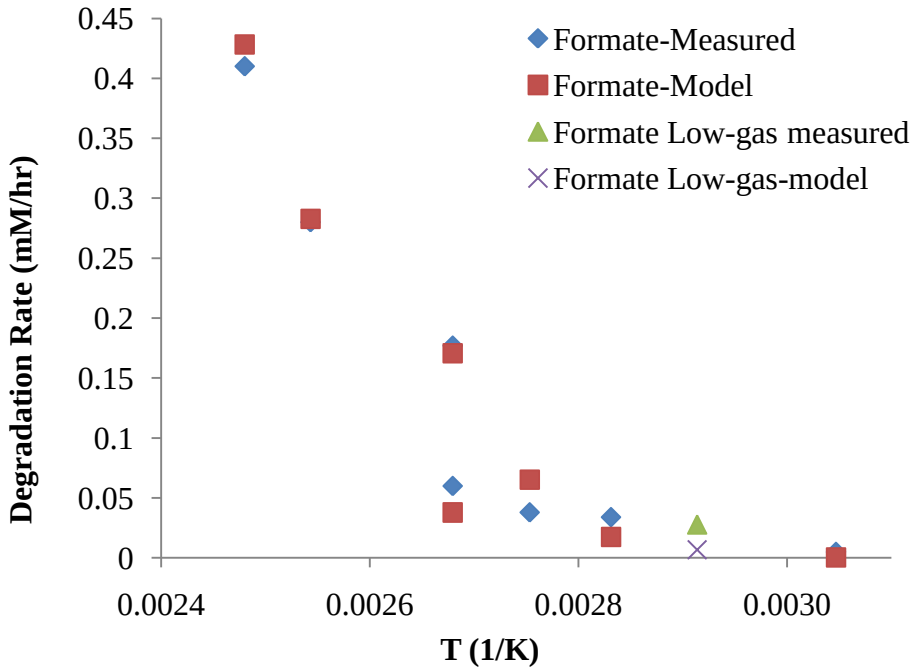

Figure 5.1: 7 m MDEA oxidative degradation model results for formate – comparison of measured and modeled formate concentration

The modeling results for formate production in 7 m MDEA are plotted with the measured rates of production in Figure 5.1. The modeled rates match the measured rates quite well over the entire range of measured and modeled temperatures (55 to 130 °C). The measured formate production rate from the Low-gas experiment (OD-8) conducted at 70 °C is presented along with the value predicted by the model at this temperature. The measured value appears to be slightly high in comparison to the measured and modeled values at other temperatures, and ~4X the value predicted by the model at 70 °C. In the Low-gas oxidative reactor, 100% of the experimental solvent is fully agitated for the duration of the experiment, potentially providing conditions more conducive to solvent degradation.

The measured and modeled total formate production rates over the experimental range of temperatures as 1/T (K) are presented as a semi-log plot in Figure 5.2. The predicted total formate production rates for the small thermal reactor design and for the large thermal reactor design are separately plotted in the figure. The solid filled symbols (♦) represent the measured rates of total formate production in the 7 m MDEA cycling experiments in the ISDA with the large thermal reactor, while the solid filled symbols (■) represent the measured rates of total formate production in the 7 m MDEA cycling experiments in the ISDA with the small thermal reactor. All rates have been corrected so that the thermal reactor residence time is normalized to the Low-gas reactor volume, putting the rates on the same basis as rates measured in the Low-gas reactor. The y-axis is plotted as Rate × (V_{Tot}/V_{TR}).

The model indicates that total formate production rates measured in the ISDA at the lower temperatures match for both the small and large thermal reactor designs. However, as the temperature rises beyond ~100 °C, the predicted rates for the two thermal reactor designs diverge, with the large thermal reactor predicting a lower rate of

total formate production. This divergence is a result of the oxygen solubility limited operation associated with the larger thermal reactor; at the greater residence times associated with the larger thermal reactor, insufficient dissolved oxygen is available to maintain a higher rate of total formate production. The smaller thermal reactor more accurately measures the degradation of 7 m MDEA in a kinetically controlled region. The two measured total formate production rates with the small reactor (■) match well with the oxidative model, while the measured rates with the large reactor (♦) match well at the higher temperatures, but diverge from the model at the lower temperature (55 °C). Because the measured and modeled rates have been normalized to reactor residence time in the Low-gas reactor, the total formate production rate measured in the Low-gas reactor at 70 °C falls in line with the modeled predicted rates in Figure 5.2.

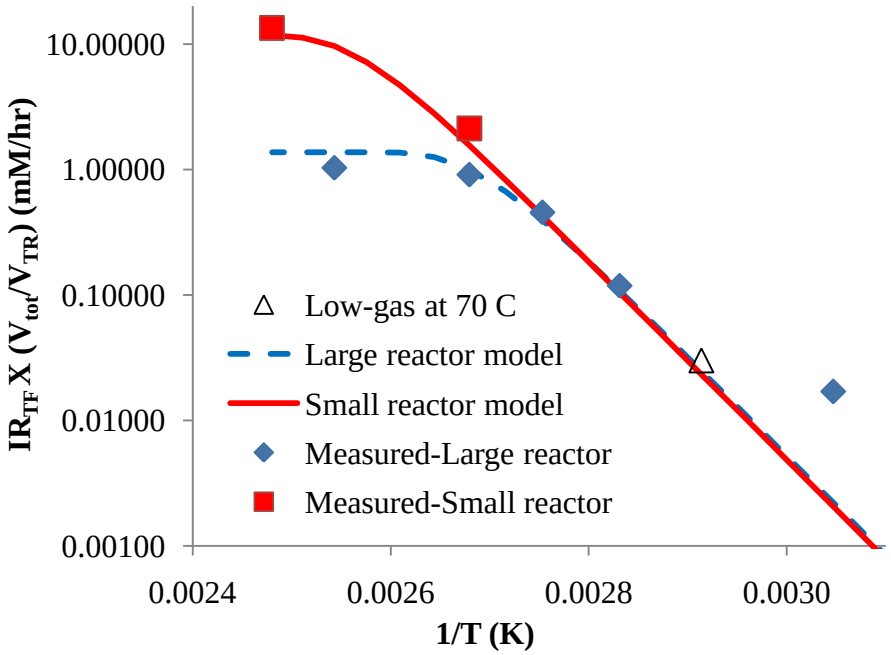

Figure 5.2: Initial rates of total formate production measured in 7 m MDEA in the ISDA; oxidative degradation model predicted values plotted for large thermal reactor (dashed blue line) and small thermal reactor (solid red line)

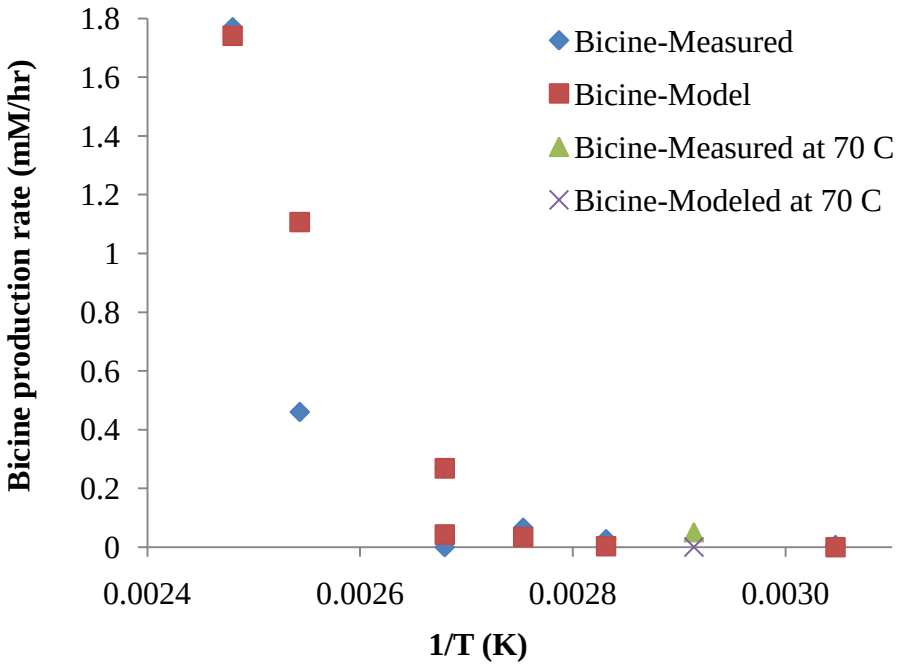

Figure 5.3: 7 m MDEA oxidative model – comparison between measured and modeled bicine production

The measured and modeled bicine production rates are plotted in Figure 5.3. The model fits the measured data over the entire range of measured values, and returned a bicine production rate of ~0.001 mM/hr at 70 °C. The bicine production measured in the ISDA at 55 °C was ~0 mM/hr, while the measured value at 80 °C was ~0.027 mM/hr. The bicine production rate measured in the Low-gas reactor at 70 °C was 0.05 mM/hr, indicating that the thorough agitation of all solvent for the duration of the experiment in the Low-gas reactor provides an environment more conducive to oxidative degradation.

5.5 PRACTICAL COMPARISONS OF TEMPERATURE TOLERANCE IN 7 m MDEA

It is useful to relate the production of oxidative degradation indicators such as total formate to a practical limit of oxidation. For example, if we consider a dissolved oxygen consumption limit in the piping passing through the heat exchanger and carrying solvent to the top of the stripper, we can relate this limit to a temperature limit for the solvent in this part of an absorber/stripper system. Equation 5.15 is the first-order relationship relating oxygen concentration in and out to the first-order rate constant and residence time. An assumption was made that the solvent passes through this portion of the system in ~30 seconds for each pass through the system. The upper limit of temperature tolerance at 10, 20 and 50% of dissolved oxygen consumption was calculated from the corresponding k_1 values returned by the model over the range of temperatures for formate, total formate, and bicine, and the temperature limits tabulated in Table 5.3.

$$\ln \frac{C_{in}}{C_{out}} = k(T) * t \tag{5.15}$$

Table 5.3: 7 m MDEA oxidative model temperature analysis assuming 30 seconds of residence time at temperature

	Temperature (°C)			
Oxygen Consumed (%)	Formate	Total formate	Bicine	Average
10	102	101	108	104
20	107	106	111	108
50	117	115	117	116

The results tabulated in Table 5.3 indicate that if we assume an oxygen consumption limit of 10% for each pass through the system for 7 m MDEA, the solvent can tolerate up to 102 °C in terms of formate production. For the 10% oxygen consumption, the average temperature limit for all three parameters is 104 °C. The

average temperature limit increases to 108 °C for a 20% oxygen consumption. If the oxygen consumption limit is increased to 50%, the average solvent temperature limit is 116 °C for 30 seconds.

The first-order rate constants for oxygen consumption and conversion of MDEA to each of the products can also be related to overall MDEA loss, and through an estimate of solvent CO_2 carrying capacity, the amount of MDEA loss per unit CO_2 captured. The analysis was performed based on total formate production at an average temperature of 100 °C and a flue gas oxygen concentration of 5 kPa (5%). Other calculation parameters included the stoichiometric ratio S returned by the oxidative model for total formate (0.14 mol total formate/mol oxygen) and the average solvent capacity of 0.5 mol CO_2/kg solvent. The rate of total formate production was calculated as follows:

$$rate = \left(\frac{13.0}{hr}\right)\left(0.14\,\frac{mol\,TF}{mol\ \ O_2}\right)\left(\frac{0.05\,atm\,O_2}{5.45E10^4\,atm\,O_2}\,\frac{gmol\,O_2}{gmol\,solv}\right)\left(\frac{10^3\,mmol\,TF}{gmol\,TF}\right)\left(35.6\,\frac{gmol\,solv}{Ls\,olv}\right)$$

$$rate = 0.0594\,\frac{mmol\,TF}{L * hr}$$

Using the calculated rate in terms of moles total formate and an estimate of 15 moles MDEA loss per mol total formate formed from the ISDA experiments, we can relate to the CO_2 capture rate per mass solvent:

$$rate = \left(0.0594\,\frac{mmol\ \ TF}{L\,solv * hr}\right)\left(\frac{kg\,solv}{0.5\,mols\,CO_2}\right)(30\,s)\left(\frac{hr}{3600s}\right)\left(\frac{15\,mmol\,MDEA\,lost/L}{mmol\,TF/L}\right)\left(\frac{L\,solv}{1.055\,kg\,solv}\right)$$

$$rate = \left(1.4E10^{-2}\,\frac{mmol\,MDEA\,Lost}{mol\,CO_2 Captured}\right)\left(\frac{mol\,MDEA\,Lost}{10^3\,mmol\,MDEA\,Lost}\right)$$

$$rate = \left(1.4E10^{-5} \frac{mol\ MDEA\ Lost}{mol\ CO_2 Captured} \right) \left(\frac{1\ mol\ CO_2}{44\ gm\ CO_2} \right) \left(\frac{454\ gm\ CO_2}{lb\ CO_2} \right) \left(\frac{2000\ lb\ CO_2}{ton\ CO_2} \right)$$

The final calculation provides a rate of 0.29 mol MDEA lost/ton CO_2 captured. The estimate of 0.5 mol CO_2 captured/kg solvent is based on a 90% CO_2 removal assumption. For a 500 MW power plant, if 90% CO_2 capture is assumed, the rate of CO_2 capture is estimated to be 1 ton CO_2/MW-hr. At 0.29 mol MDEA lost/ton CO_2 captured, the MDEA loss rate is estimated to be ~1.3 X 10^6 mol/year, or ~1.5 X 10^5 kg/year.

5.6 SUMMARY OF MODEL

A 7 m MDEA oxidative degradation model was developed based on the collection of degradation data from the ISDA. Model development was based on the key assumptions that the ISDA behaves as an isothermal PFR, solvent exits the oxidative reactor in an oxygen-saturated condition, and all degradation occurs in the thermal reactor. The model accurately predicts the concentration of key indicators of oxidative degradation including formate, total formate, and bicine over the range of experimental temperatures (55 to 130 °C). The E_a for formate, total formate, and bicine were 151, 152, and 244 kJ/mol, respectively.

The model was utilized to estimate the temperature limit for solvent exposure to high temperatures in the cross heat-exchanger and piping to the steam stripper. An assumption has been made that most of the dissolved oxygen will strip out of the solvent at the top of the stripper, thereby minimizing oxidation of the solvent after entering the stripper. A residence time of 30 seconds at high temperature was assumed, and the average temperature tolerance of 7 m MDEA was estimated to be ~104 °C for 10% oxygen consumption. If the oxygen consumption is allowed to increase to 20 and 50%, the temperature tolerance increases to 108 and 116 °C, respectively. Finally, using the

model results, an estimate for the amount of MDEA loss per tons CO_2 captured was made, assuming a CO_2 capture capacity for 7 m MDEA of 0.5 mol CO_2/kg solvent. That estimated amount was 0.29 mol MDEA loss/ton CO_2 captured. For a 500 MW power plant capturing 90% of CO_2, the MDEA loss rate is estimated to be 1.27×10^6 mol/year.

Chapter 6 - PZ Degradation

This chapter presents a discussion of the degradation of 8 m PZ in the ISDA, with comparisons made to degradation data collected in the Low-gas reactor by Freeman (2011). Freeman (2011) completed numerous experiments with PZ in the Low-gas reactor and the thermal cylinders. The purpose in conducting experiments with 8 m PZ in this body of work was to build an understanding of how this solvent degrades prior to attempting to fully understand how 7 m MDEA/2 m PZ degrades. In that sense, the 8 m PZ degradation studies serve to complement the ISDA experiments with 7 m MDEA, and provide a foundation for understanding how the blend degrades. Degradation of 7 m MDEA/2 m PZ is fully discussed in Chapter 7.

Table 6.1: Summary of 8 m PZ experiments in the ISDA

Expt No.	Thermal Rx Size	Thermal Reactor T	Flow Rate
	L	°C	mL/min
C-16	1.2	120	168
C-17	1.2	90	210
C-28	0.13	110	203
C-29	0.13	125	168

6.1 EXPERIMENTS WITH 8 m PZ IN THE ISDA

A total of four experiments were conducted in the ISDA with 8 m PZ, with two collected using the original thermal reactor (C-16 and C-17) with a volume of 1.12 L, and two collected with the redesigned thermal reactor (C-28 and C-29) with a volume of 0.13 L (Table 6.1). All of the experiments conducted in the ISDA utilized an oxidative reactor temperature of 55 °C, whereas the thermal reactor temperature ranged from 90 to 125 °C

as listed in the table. The initial CO_2 loading was gravimetrically performed as described in Chapter 2 to a nominal loading of 0.3 mol CO_2/mol alkalinity. The inlet gas to the oxidative reactor for all four experiments had CO_2 and O_2 concentrations of 2 and 98 kPa, respectively. All four experiments in the ISDA were conducted with the stainless steel metal salts which included 0.4 mM Fe^{2+}, 0.1 mM Cr^{3+}, and 0.05 mM Ni^{2+}, all added as sulfate salts. Tables summarizing the raw data for PZ, alkalinity, degradation product and CO_2 concentrations (loading) from cycling experiments are included in Appendix B.

Liquid samples were collected from the ISDA reactor system as described in Chapter 2. In addition, experiments C-28 and C-29 were conducted with the condensate tube in-place, allowing the collection of qualitative data regarding volatile species exiting the oxidative reactor in the ISDA. Reactor samples were subjected to the full suite of analyses including: cation IC for PZ and amine degradation products, anion IC for carboxylate ions (heat stable salts), HPLC AAA method for amino acids, titration for alkalinity, and TIC for CO_2 loading.

6.2 SUMMARY OF DEGRADATION PRODUCTS IN 8 m PZ

The major degradation products in the 8 m PZ cycling experiments in the ISDA included formate, total formate, oxalate, oxalyl amides, and ethylenediamine (EDA). The carboxylate ion glycolate was also detected in cycled 8 m PZ but at much lower concentrations than observed for formate. Additionally, the amino acid glycine was detected at low concentrations throughout the experiments, and does not represent a major degradation product, accumulating to only ~5 mM after 283 hours of cycling to 125 °C. Of the formyl amides, FPZ was detected in the ISDA experimental samples (C-

29). Using the HPLC method with UV detector on hydrolyzed and unhydrolyzed samples from experiment C-16, amides were not detected in this experiment.

Freeman (2011) consistently detected a similar mix of products in 8 m PZ degraded in the Low-gas reactor. Those products included formate, oxalate, formyl amides, oxalyl amides and EDA. As with 7 m MDEA degradation, the difference between total formate and formate concentrations is primarily considered to be amides of PZ such as FPZ, or amides of degradation products. Freeman also detected several different compounds in degraded 8 m PZ, but as with the ISDA findings, only a few of the detected compounds were of importance in terms of concentration and PZ losses. In all cases, Freeman was generally unable to account for more than 1% of lost PZ in Low-gas experiments. Freeman discussed the fact that the unidentified products of PZ oxidation are either volatile, ionic, or undetectable with IC methods due to their structure or stability. The author's analysis of volatility from the Low-gas reactor demonstrated that very little of the lost PZ could be accounted for through volatilization.

Table 6.2: Summary of rates measured in 8 m PZ experiments conducted in the ISDA (α=0.3 mol CO_2/mol alk, oxidative reactor T=55 °C)

Expt No.	T_{th} °C	Rates (mM/hr)						
		PZ loss	Alk loss	Formate prod	Total formate prod	EDA prod	FPZ prod	Glycine prod
C-17	90	0.11	0.087	0.013	0.038	0.07	NM	0.003
C-28	110	1.6	1	0.021	0.06	0	NM	0.005
C-16	120	1.1	0.91	0.046	0.13	0.17	NM	0.013
C-29	125	3.6	0.89	0.061	0.22	0.36		0.02
OE18*	55	0.017	0.041	0.0049	0.014	-	-	-
OE26*	70	1.29	1.15	0.0056	0.017	0.037	-	-

Experiments C-28 and C-29 (shaded) conducted with redesigned thermal reactor of 0.13 L volume. *Experiments performed by Freeman (2011).

6.2 DEGRADATION RATES MEASURED IN THE ISDA

The rates of degradation including PZ and alkalinity loss, and degradation product formation are listed in Table 6.2. As noted, the shaded data are for experiments conducted with the redesigned thermal reactor of 0.13 L volume. The data from two Low-gas experiments conducted by Freeman (2011) are included in the table and highlighted in yellow. OE18 was conducted in the redesigned Low-gas system known as the TOR at 55 °C, while OE26 was conducted in the TOR at 70 °C. Both Low-gas experiments included the addition of the stainless steel metals salts at the beginning. The formate, total formate, and glycine production rates all exhibited an increase with increase in the thermal reactor temperature. In contrast, the PZ and alkalinity loss rates did not adhere to the pattern of an increase with increasing thermal reactor temperature. Additionally, the EDA production rate in C-28 was ~0, which did not follow the pattern followed by the other three experiments.

Table 6.3: Initial degradation rate comparison between 7 m MDEA and 8 m PZ data collected in the ISDA at comparable conditions

Expt. No.	Amine	T_{Th} (°C)	Rates (mM/hr)				
			MDEA Loss	PZ Loss	Alk Loss	Formate prod	Total formate prod
C-6	7 m MDEA	120	4.6	-	4.9	0.28	0.34
C-16	8 m PZ	120	-	1.1	0.9	0.05	0.13
C-25	7 m MDEA	120	5.1	-	4.4	0.61	0.96
C-29	8 m PZ	125	-	3.64	0.89	0.06	0.22

Shaded experiments (C-25 and C-29) conducted with redesigned (0.13 L) thermal reactor.

A comparison of the measured degradation rates for 8 m PZ to comparable experimental rates for 7 m MDEA in the ISDA is presented in Table 6.3. The shaded entries are for data collected with the ISDA with the redesigned thermal reactor of 0.13 L volume. The amine loss rates for 7 m MDEA are greater than for 8 m PZ with both sets

of data. The alkalinity loss rates for 7 m MDEA are 5X the rates measured in 8 m PZ with both thermal reactor designs. Formate production rates in 7 m MDEA are 5 to 10X the rates observed in 8 m PZ, whereas the total formate production rates in 7 m MDEA are 3 to 5X the rates measured in 8 m PZ. These data highlight the overall greater tendency for MDEA to degrade than PZ under the conditions created by the ISDA.

6.2.1 Normalized rates and estimated activation energies

To compare the ISDA degradation rates to the rates from the Low-gas data collected at 55 and 70 °C, the ISDA rates were normalized to correct for the residence time in the ISDA system components other than the thermal reactor. For example, in experiments C-16 and C-17, the ISDA system total volume was ~3.4 L, while the thermal reactor volume was ~1.12 L or ~35% of total system volume. The rates collected in these two experiments were corrected by dividing by a factor of 1.12/3.4 (~0.35). For experiments C-28 and C-29, the total system and redesigned thermal reactor volumes were 2.3 and 0.13 L, respectively, so the rates were normalized by dividing by a factor of 0.13/2.3 (0.057).

In addition to normalizing the rates based on residence time in the thermal reactor, the rates were normalized to the partial pressure of oxygen in the headspace purge gas for each experiment. This adjustment was necessary because OE26 was conducted with a partial pressure of oxygen of 94 kPa and 6 kPa CO_2 to match the CO_2 solubility condition at 70 °C and a loading of 0.3 mol CO_2/mol alkalinity, whereas all other experiments were conducted with an oxygen partial pressure of 98 kPa. The normalized rates quoted in units of mM/hr-kPa O_2 X1000 are restated along with the Low-gas rates in Table 6.4, listing experiments from lowest to highest thermal reactor temperature, starting with the two Low-gas experiments conducted at 55 and 70 °C.

Table 6.4: Degradation and product formation rates for 8 m PZ, normalized to residence time of thermal reactor and partial pressure of O_2, compared to Low-gas data (OE18 and OE26) of Freeman (2011)

Expt No.	T_{th} °C	Rates (mM/hr-kPa O_2) X 1000					
		PZ loss	Alk loss	Formate prod	Total formate prod	EDA prod	Glycine prod
OE18	55	0.2	0.4	0.1	0.1	0.0	-
OE26	70	13.7	12.2	0.1	0.2	0.4	-
C-17	90	3.2	2.5	0.4	1.1	2.0	0.1
C-28	110	286.4	179.0	3.8	10.7	0.0	0.9
C-16	120	31.8	26.3	1.3	3.8	4.9	0.4
C-29	125	644.5	159.3	10.9	39.4	64.4	3.6

Shaded experiments (C-28 and C-29) conducted with redesigned thermal reactor (0.13 L).

The normalized ISDA and Low-gas rates of degradation measured as PZ and alkalinity loss were plotted in Figure 6.1 as natural log or ln(rate) versus 1/T (K) to determine whether the rates fit Arrhenius behavior. A linear fit was regressed to the data, and an activation energy E_a for PZ and alkalinity loss were estimated from the slope of each. The Arrhenius plot for formate and total formate is presented as Figure 6.2, and the Arrhenius plot for the amino acid glycine is presented as Figure 6.3. Note that the plot for glycine production does not include Low-gas data as this degradation product was not measured in Low-gas samples. The EDA production rate was generally low for most of the experiments, making the estimation of reliable rates from the cation IC data difficult. An E_a was estimated for EDA, but only after ignoring the rate measured at 55 °C in the Low-gas reactor because this point did not reflect the overall trend observed by plotting the rates estimated for the other five temperatures. The estimated E_a for amine and alkalinity loss and degradation product formation reactions for 8 m PZ and 7 m MDEA from Chapter 4 are presented in Table 6.5. The E_a for formate and total formate production predicted by the rigorous PFR model are listed in the last column.

The estimated activation energies listed in Table 6.5 reflect the faster (2X) degradation rates observed in 7 m MDEA in the ISDA and the Low-gas reactor under oxidizing conditions. The E_a for formate and total formate production estimated directly from the rate data are approximately 30% higher for 8 m PZ than 7 m MDEA, reflecting the greater resistance of 8 m PZ to oxidation to carboxylate ions and amides. However, the activation energies for formate and total formate production in 7 m MDEA predicted by the rigorous PFR model are 2.5X the E_a estimated directly from the raw rates, reflecting the effect of stoichiometric limitations of a limited oxygen concentration in the cycled 7 m MDEA at the higher temperatures.

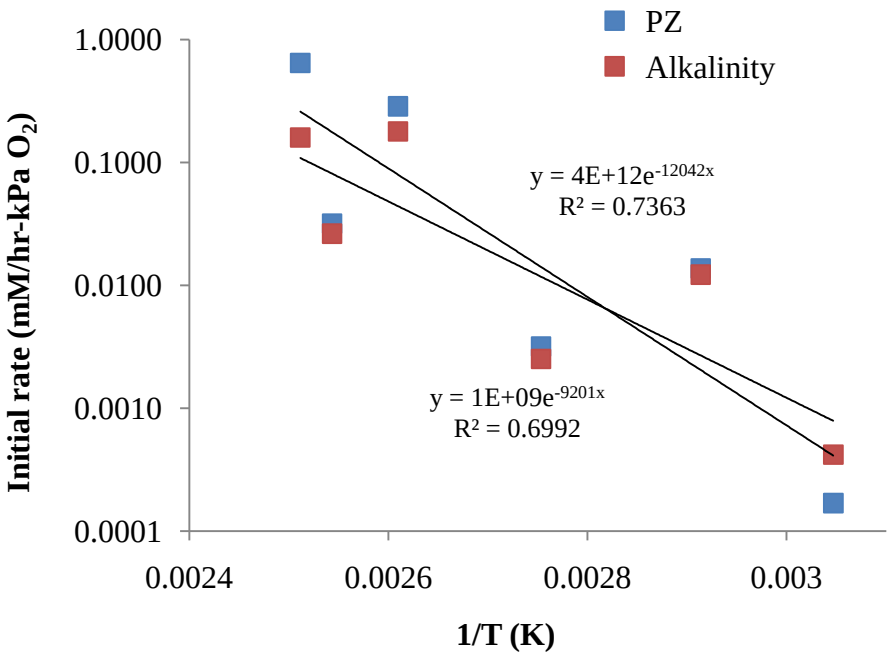

Figure 6.1: Arrhenius plot of PZ and alkalinity rates estimated from the ISDA and Low-gas experiments ranging from 55 to 125 °C with 8 m PZ

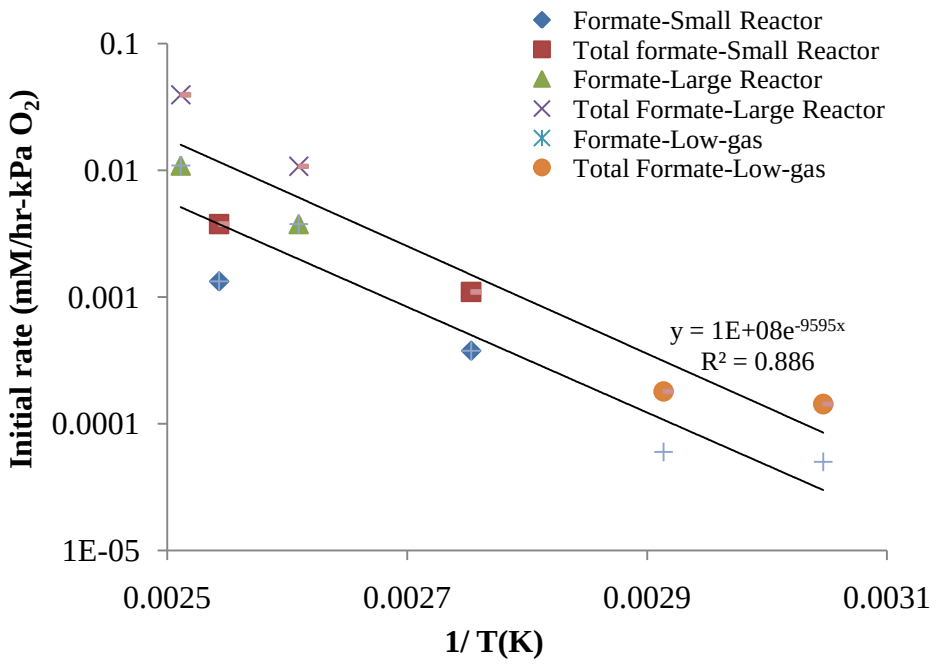

Figure 6.2: Arrhenius plot of formate and total formate production rates from the ISDA and Low-gas experiments ranging from 55 to 125 °C with 8 m PZ

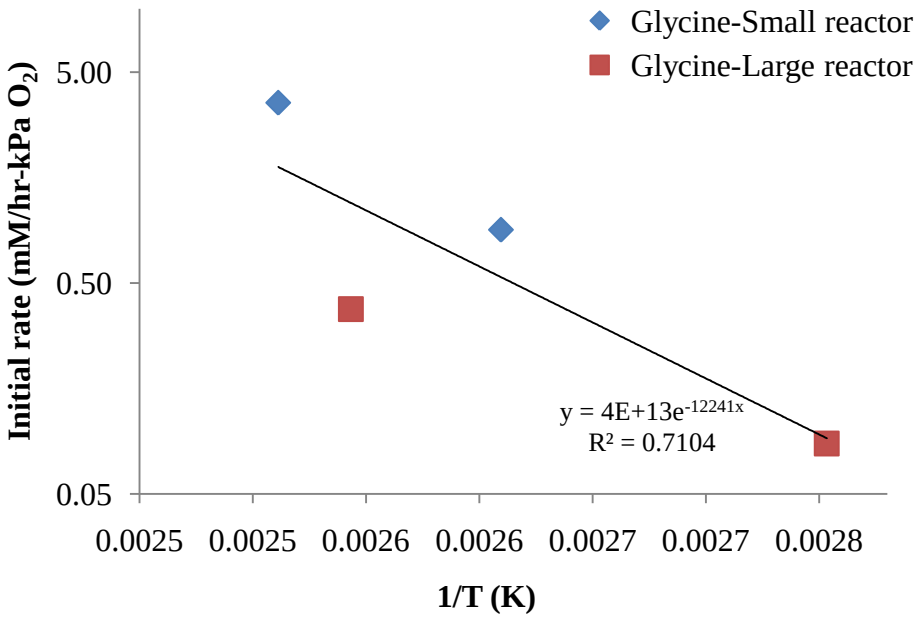

Figure 6.3: Arrhenius plot for the formation of glycine in 8 m PZ from data collected in the ISDA and Low-gas reactor experiments from 55 to 125 °C

Freeman (2011) reported that she was unable to identify the major degradation products of 8 m PZ, with formate and total formate comprising a very small portion of the overall lost carbon and nitrogen in the solvent. The ~3X activation energy for 8 m PZ (amine loss) likely reflects the difficulty in degrading PZ to compounds other than carboxyate ions and amides. For example, the production of EDA represents the most consistently observed amine degradation product of 8 m PZ in the Low-gas and the ISDA experiments; EDA production was not observed in 7 m MDEA. When the single rate measured at 55 °C in the Low-gas was ignored, an E_a of ~65 kJ/mol was estimated that reflects the activation energy for PZ degradation under oxidizing conditions. The formation of EDA requires that the PZ ring open, and is likely a more energy intensive degradation mechanism than the production of an amide through reaction of PZ and formate to form FPZ. The production of the amino acid glycine also represents the opening of the PZ ring, and reflects the requirement that additional energy is necessary to create this product when compared to formate and formyl amides. The activation energy of glycine formation is ~102 kJ/mol, which is in-line with the activation energy for amine loss in 8 m PZ. The unidentified PZ degradation products likely require the same chemical mechanism(s) for degradation and will have similar activation energies, driving up the E_a for PZ and alkalinity loss in 8 m PZ.

Table 6.5: Activation energies for 8 m PZ degradation reactions estimated from experiments in the ISDA and Low-gas reactor

	Activation Energy (kJ/mol)		
Parameter	8 m PZ	7 m MDEA	7 m MDEA PFR model
Amine loss	100	32	-
Alkalinity loss	76	27	-
Formate production	80	63	151
Total formate production	81	56	152
Glycine production	102	-	244
EDA	65	-	-

6.3 ESTIMATE OF TEMPERATURE TOLERANCE OF 8 m PZ IN TWO-STAGE STRIPPER

The calculation of activation energies for the formation of different degradation products in 8 m PZ allows the estimation of the rate of degradation of the solvent over a range of temperatures in an absorber/stripper system, up to the point when oxygen is flashed. In particular, it is of interest to know the oxidation rate that would be observed in the first stage of a two-stage flash configuration so that we can understand the temperature tolerance of the solvent for comparison to other solvents. The concept has been diagramed in Figure 6.4. CO_2-rich solvent exits the absorber, passes through the cross exchanger and piping to the first stage of a two-stage stripper system where the majority of the oxygen and a portion (<50%) of the CO_2 is flashed for separation, compression and sequestration. Steam is supplied to the first stage directly, but this stage does not utilize a reboiler. The partially stripped semi-rich solvent is then passed through a second flash or steam stripper for further CO_2 removal. The benefit of this configuration is the stripping of dissolved oxygen from the solvent in the first stage, thus minimizing the residence time of oxygen rich solvent at the higher temperatures expected in the second stage flash and associated piping of the absorber/stripper system and, therefore, minimizing the oxidation of the solvent. This configuration takes advantage of the high heat of absorption of 8 m PZ (~78 kJ/mol) through stripping of the majority of CO_2 at the higher temperature experienced in the second stage flash, thereby minimizing compression energy needed for sequestration. One drawback to this configuration is the need for a single stage compressor in service for the stripped CO_2 and O_2 coming off the first stage flash.

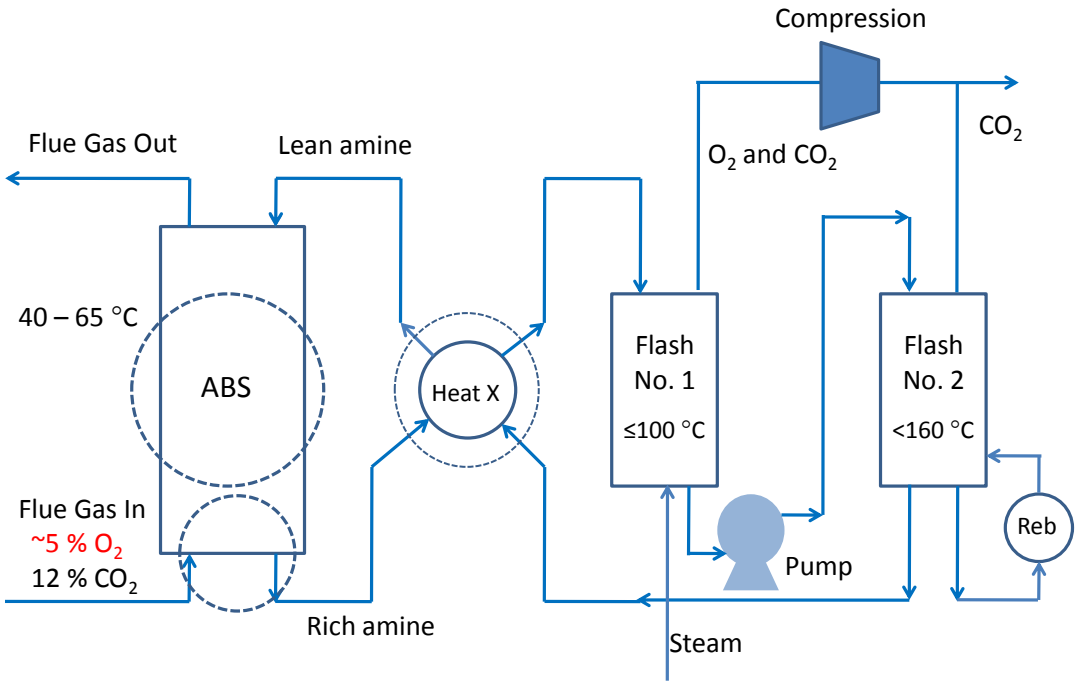

Figure 6.4: Two-stage flash configuration for 8 m PZ

The calculation of the temperature tolerance of 8 m PZ in the first stage of a two-stage flash configuration was performed as follows: (1) using the average temperature estimate of 104 °C from Chapter 5 for 7 m MDEA at the 10% oxygen consumption limit in a stripper, and the calculated correlation for amine loss rate/total formate production rate, an amine loss per pass was estimated, (2) assuming the amine loss per pass for 8 m PZ is the same as in 7 m MDEA, the total formate production rate was estimated from the correlation between PZ loss rate/total formate loss rate in the ISDA 8 m PZ experiments, and (3) using the Arrhenius relationship and a measured r_o at 90 °C from the ISDA, the rate (r) was plugged into Arrhenius to calculate the new temperature at which the rate is valid. Three important underlying assumptions to this calculation which are valid for the estimate for 7 m MDEA made in Chapter 5 are the following: (1) the incoming flue gas in contact with the solvent has an oxygen concentration of 5 kPa, (2) the solvent

residence time at the temperature limit is 30 seconds, and (3) the total formate production rate is a good indicator of overall oxidation in the solvent.

The estimated temperature tolerance for 8 m PZ is 112 °C, which is considerably higher than the average temperature limit of 104 °C calculated for 7 m MDEA using the same basis. A temperature limit can also be calculated for the 20% oxygen consumption basis as was performed for 7 m MDEA. That limit was 108 °C. Using the same set of assumptions, the limit calculated for 8 m PZ was ~123 °C. The estimated values are compared to the values calculated for 7 m MDEA in Table 6.6. The resistance to degradation of 8 m PZ is apparent in the considerably higher temperatures at all three oxygen consumption levels, with the estimated tolerance limit at 145 °C for the 50% oxygen consumption level. The practical upper limit of 112 °C estimated for the 10% oxygen consumption per pass likely represents an upper limit that would not be exceeded in the first stage of a two-stage flash configuration.

The first-order rate constant for oxygen consumption and conversion of PZ to total formate can be related to overall PZ loss at an operationally relevant temperature of 100 °C. This calculation considers a two-stage flash configuration wherein the first stage is set to 100 °C to provide a factor of safety in limiting solvent degradation in the overall absorber/stripper configuration. Through an estimate of solvent CO_2 carrying capacity, the amount of PZ loss per unit CO_2 captured can be estimated. The analysis was performed based on an average temperature of 100 °C and a flue gas oxygen concentration of 5 kPa (5%). Other calculation parameters included the stoichiometric ratio S returned by the oxidative model for total formate (0.14 mol total formate/mol oxygen) and the average solvent capacity of 0.79 mol CO_2/kg solvent. For the similar calculation with 7 m MDEA, an estimate of 15 mmol MDEA lost/mmol total formate produced was used, based on the average across all cycling experiments with that solvent.

Based on the cycling experiments with 8 m PZ, an estimate of 13 mmol PZ lost/mmol total formate produced was used. This calculation resulted in an estimate of 0.15 mol PZ lost/ton CO_2 captured, which is 1/2X the amount estimated for 7 m MDEA. For a 500 MW power plant and 90% CO_2 capture, the estimated PZ loss is ~6.7 X 10^5 mol/year, or 5.7 X 10^4 kg/year.

Table 6.6: Temperature tolerance comparison in 7 m MDEA and 8 m PZ based on total formate production in first stage of two-stage flash configuration

	Temperature (°C)	
Oxygen Consumed (%)	7 m MDEA	8 m PZ
10	101	112
20	106	123
50	115	145

6.4 SUMMARY OF 8 m PZ DEGRADATION IN THE ISDA

The rates of amine and alkalinity loss measured in 8 m PZ in the ISDA were 1/10 to 1/5X the rates measured in 7 m MDEA, while the rates of formate and total formate production measured in 8 m PZ were 1/10 to 1/3X the rates measured in 7 m MDEA. These rates reflect the findings of Freeman (2011) that 8 m PZ was generally resistant to oxidation when tested in the Low-gas reactor and compared to other solvents such as 7 m MEA and 7 m MDEA. When the rates of oxidation of 8 m PZ measured in the ISDA were normalized for time in the thermal reactor and partial pressure of oxygen in the headspace of the oxidative reactor to provide a comparable basis to rates measured in the Low-gas reactor, activation energies were estimated which were 3X the rates measured from the initial rate data for 7 m MDEA. The activation energies estimated for formate and total formate were ~30% higher than those rates measured from initial rate data collected in cycled 7 m MDEA. However, the activation energies for formate and total

formate in 7 m MDEA estimated by the PFR model were ~2X the rates in 8 m PZ. As discussed previously, the PFR model accounts for the stoichiometry of the oxidation reactions over the range of experimental temperatures, driving up the prediction of activation energy.

The activation energies were used to estimate the upper end temperature tolerance of 8 m PZ using the same basis as was used for 7 m MDEA in Chapter 5. A two-stage flash configuration was considered, with oxygen-rich solvent approaching the first flash at temperatures elevated to flash oxygen and CO_2 by its passage through the cross heat exchanger. An estimate of the upper limit of temperature that can be reached in this first stage was required for comparison to the estimate made for 7 m MDEA. The estimates were based on 30 seconds of residence time at the higher temperature and 10% of oxygen depletion due to oxidation of the solvent to produce total formate. The upper limit of temperature tolerance for 8 m PZ was ~112 °C at the 10% oxygen depletion level, which compared favorably to the 101 °C estimate made for 7 m MDEA; note that an overall average of 104 °C was considered for 7 m MDEA, based on the temperature tolerance for formate, total formate and bicine production. When the oxygen depletion level was allowed to increase to 20 and 50%, the temperature tolerance of 8 m PZ increased to 123 and 145 °C, respectively.

The PZ loss in a two-stage flash configuration was calculated based on the same assumptions made for 7 m MDEA, including the first-stage flash temperature limit of 100 °C and 30 seconds of residence time. Using a CO_2 capture capacity of 0.79 mol CO_2/kg solvent for 8 m PZ, the solvent loss rate was estimated to be 0.15 mol PZ loss/ton CO_2 captured. This amine loss rate was approximately 1/2X the rate estimated for 7 m MDEA (0.29 mol PZ lost/ton CO_2 captured) at the same conditions and 100 °C. This PZ loss rate translates to approximately 6.7 X 10^5 mol PZ/year, or 5.7 X 10^4 kg/year.

Chapter 7 - MDEA/PZ Degradation

This chapter presents a discussion of the degradation of 7 m MDEA/2 m PZ based on data collected in the Low-gas reactor, the Swagelok® thermal degradation cylinders, and the ISDA solvent cycling system. The discussions related to 7 m MDEA and 8 m PZ presented in previous chapters support the analysis and conclusions related to the blend presented in this chapter. Initial rates of degradation in terms of amine loss and degradation product formation are calculated, and comparisons are made to other solvents including 7 m MDEA, 8 m PZ, and 7 m MEA to benchmark the blend in terms of resistance to degradation of other well known and industrially relevant solvents. Comparisons of rates of degradation in 7 m MDEA to the blend are of particular interest because it is important to understand the role of PZ in the overall degradation, and whether PZ accelerates the degradation of the blend. Experiments useful in that determination were performed with all three degradation methods in the laboratory.

Several methods were utilized to identify degradation products in 7 m MDEA/2 m PZ including cation and anion IC, HPLC with UV detection to identify non-polar compounds, HPLC configured for amino acid analysis using the AAA-Direct method, and IC, LC and GC coupled to MS. A mass balance was performed on the degradation product data from the blend, including an assessment of the conservation of methyl and hydroxyethyl groups, and PZ rings.

The 7 m MDEA oxidative degradation model presented in Chapter 5 was utilized to make predictions of formate, total formate and bicine production in the blend. Two degradation models have been developed based on the thermal degradation data from experiments with the blend. A separate oxidative model for the blend was not created

due to a lack of degradation data for the blend in the ISDA over a wide range of temperatures.

A list of the experiments conducted with 7 m MDEA/2 m PZ is provided in Table 7.1. A total of five oxidation experiments were conducted in the Low-gas reactor system, with the first four conducted using the original Low-gas design at 55 °C, and the last oxidation experiment conducted with the TOR at 70 °C. The typical analytical suite utilized in those experiments included anion IC, with a check of initial CO_2 loading. However, starting in OD-5, cation IC was utilized to measure amine loss. Up to this point in time, Low-gas experiments were typically not performed with cation IC analyses due to very low amine loss rates exhibited by solvents in Low-gas experiments. The analytical suite utilized in OD-9 was more extensive than that used for all previous Low-gas experiments with this solvent. In that experiment, anion IC, cation IC, amino acid, HPLC and GC-MS methods were utilized on all samples in order to better understand the oxidation of 7 m MDEA/2 m PZ. Added emphasis will be placed on the data from this experiment in the ensuing discussion. The back-up data tables for basic analytical work performed on these experiments are included in Appendices B (ISDA), C (Low-gas), and D (Thermal cylinder). The master rate table is included in Appendix E.

A total of eight thermal degradation experiments were completed with the blend over a range of loading and temperature in the Swagelok® sample cylinders. The analysis of 7 m MDEA/2 m PZ thermal degradation is complemented by an understanding of how other solvents degrade, including 7 m MDEA, 7 m DEA and blends of DEA + PZ and DEA + 1-MPZ. The thermal experiments conducted with MDEA are fully reviewed in Chapter 4, but thermal degradation experiments (RPN-1 and RPN-2) with 7 m DEA and DEA blends are discussed in this chapter to facilitate a better understanding of the role of degradation intermediates in the blend.

Five cycling experiments were conducted with 7 m MDEA/2 m PZ in the ISDA at an initial loading of 0.14 mol CO_2/mol alkalinity, with the thermal reactor varied from 90 to 125 °C. A sixth and final experiment in the ISDA was conducted with 7 m MDEA/2 m PZ at zero CO_2 loading, but with acid treatment with H_2SO_4 at a concentration of 0.1 mol H^+/mol alkalinity. Other cycling experiments which are useful in understanding the degradation of the blend include C-24 (7 m MDEA + 100 mM DEA), C-31 (6 m MDEA + 1 m MAE), and C-32 (6 m MDEA + 1 m DEA). The data from these experiments will be reviewed where appropriate to add to the understanding of the degradation of 7 m MDEA/2 m PZ.

7.1 Oxidation of 7 m MDEA/2 m PZ in the Low-gas reactor

The oxidation products of 7 m MDEA/2 m PZ in the Low-gas reactor were primarily formate, formyl-amides, glycolate, glycol-amides, and bicine. Because of the low rates of degradation and overall amine loss in the Low-gas experiments, amine degradation products including PZ derivatives and EDA were not detected with cation IC. However, DEA+MAE was formed and quantified. Analysis of the Low-gas data will generally rely on the rates of formate, formyl amide, and bicine production. However, bicine data only exist for experiment OD-9 because the AAA-Direct amino acid method was not yet available during the timeframe when experiments OD-1 through OD-5 were run.

Table 7.1: Summary of experiments with 7 m MDEA/2 m PZ

Expt. No.	T (°C)	α (mol CO_2/mol alk)	Additives	Th Rx (L)
Low-gas				
OD-1	55	0.3	1 mM Fe^{2+}	-
OD-3	55	0.24	0.1 mM Fe2+, 0.6 mM Cr, 0.1 Ni	-
OD-4	55	0.23	0.1 mM Fe^{2+}, 5 mM Cu^{2+}	-
OD-5	55	0.24	1 mM Fe2+, 100 mM Inh A	-
OD-9	70	0.14	0.4 mM Fe^{2+}, 0.1 mM Cr^{3+}, 0.1 Ni^{2+}	-
Thermal				
Th. No. 1	100, 120	0.25, 0.23, 0.43	-	-
Th. No. 4	100, 120	0.1, 0.2	-	-
Th. No. 5	100, 120	0.18	1 mM Fe^{2+}	-
Th. No. 6	135	0.12, 0.23	-	-
Th. No. 7	135, 150	0.11, 0.26	-	-
Th. No. 8	135, 150	0.0, 0.02, 0.3	-	-
Th. No. 16	120, 135, 150	0.0, 0.1, 0.25	-	-
Th. No. 17	120, 135, 150	0.1 mol H^+/mol alk as TSA	-	-
ISDA				
C-21	55/120	0.14	SS metal salts	1.2
C-22	55/90	0.14	SS metal salts	1.2
C-23	55/100	0.14	SS metal salts	1.2
C-30	55/125	0.14	SS metal salts	0.13
C-33	55/90	0.14	SS metal salts	0.13
C-34	55/125	0.1 mol H^+/mol alk	SS metal salts	0.13

The concentration of formate was measured in samples from all five Low-gas experiments with 7 m MDEA/2 m PZ, but data from three of those experiments (OD-1, OD-3, and OD-4) were combined into a master file to determine an overall formate production rate. Formate concentration data are the only useful data obtained from these three experiments. The initial rates of formate, total formate and bicine production are listed in Table 7.2 for the combined data from OD-1/OD-3/D-4, listed as OD-Comb, and

from the two other experiments performed in the Low-gas reactor with the blend (OD-5, and OD-9). For reference, the rates of product formation for Low-gas experiments with 7 m MDEA (OD-2 and OD-8) and 7 m MEA (Sexton-1, Sexton, 2008) are listed in Table 7.2.

Table 7.2: Initial rates of formate, total formate, and bicine production in Low-gas experiments with 7 m MDEA/2 m PZ

Expts. No.	Solvent (m)	T (°C)	Amend (mM)	Other (mM)	Formate	Total formate	Bicine
OD-Comb	7 MDEA/ 2 PZ	55	Fe^{2+}, Cr^{3+}, Ni^{2+}	-	0.011 ± 0.002	-	-
OD-5	7 MDEA/ 2 PZ	55	1 Fe^{2+}	100 Inh A	0.009 ± 0.0004	0.083 ± 0.049	-
OD-9	7 MDEA/ 2 PZ	70	SS salts	-	0.031 ± 0.0003	0.075 ± 0.004	0.023 ± 0.001
OD-2	7 MDEA	55	1 Fe^{2+}	-	0.013	0.026	-
OD-8	7 MDEA	70	SS salts	-	0.028 ± 0.001	0.03 ± 0.003	0.022
Sexton-1	7 MEA	55	1 Fe^{2+}	-	0.27	1.04	-

The formate production rates for OD-Comb, OD-2, and Sexton-1 can be compared directly, as these Low-gas experiments were all conducted at 55 °C. Likewise, the formate production rates from OD-9 and OD-8 can be compared directly, as these Low-gas experiments were both conducted in the TOR low-gas reactors at 70 °C. The formate production rate in OD-Comb was 0.011 ± 0.002 mM/hr, which was approximately the same as measured in 7 m MDEA (OD-8), and an order of magnitude less than the rate measured in 7 m MEA of 0.27 mM/hr (Sexton-1). At 55 °C, the total formate production rate measured in 7 m MDEA/2 m PZ was 3X the rate measured in 7

m MDEA even when 100 mM Inhibitor A was added to the solvent before the start of the Low-gas experiment with the blend (OD-5). The formate production rate at 70 °C was ~3X the rate measured at 55 °C, and when compared to 7 m MDEA, the rate was approximately the same, at 0.031 ± 0.0003 mM/hr. The total formate production rate measured in 7 m MEA (Sexton-1) was ~12X the rate measured in the comparable 7 m MDEA/2 m PZ experiment at 55 °C. A direct comparison of the results of OD-Comb with OD-5 indicates that 100 mM Inhibitor A (OD-5) had little or no effect on the rate of oxidation of the solvent, as evidenced by a nearly equivalent formate production rate in the presence of the inhibitor (0.009 ± 0.0004 mM/hr). The bicine production rates measured in 7 m MDEA (OD-8) and 7 m MDEA/2 m PZ (OD-9) at 70 °C were approximately the same (~0.022 mM/hr). The solvents can be ranked in terms of the formate production rate from greatest to least as follows: 7 m MEA>7 m MDEA/2 m PZ=7 m MDEA.

In terms of total formate production, the solvents can be ranked from greatest to least as follows: 7 m MEA>7 m MDEA/2 m PZ>7 m MDEA. As discussed in previous chapters, the difference between the concentration of total formate and formate is generally considered to be the concentration of formyl amides. The formate and total formate production rates in 7 m MDEA/2 m PZ indicate that the blend has a greater tendency to produce formyl amides than 7 m MDEA. The formation of amides in tertiary amines is generally not possible (Morrison and Boyd, 1973), whereas the formation of amides in 1° and 2° amines is possible. The presence of a greater concentration of formyl amides in the degraded blend is likely the result of the presence of PZ which can form FPZ, and the formation of 1° and 2° amines as degradation products in the blend. The amine degradation products which are likely to form amides include DEA, MAE, and 1-MPZ. However, the cation IC data indicate that no 1-MPZ or FPZ were formed in the

oxidized blend at 70 °C in OD-9. Further, using the HPLC method described in Chapter 2, the amides of DEA and MAE were generally not detected in OD-9 samples. It is likely that amides are being formed in the oxidizing environment of the Low-gas reactor in 7 m MDEA/2 m PZ, but were not separated and detected with the HPLC method used. Finally, the rate of total formate production in OD-5 with 100 mM Inhibitor A exceeded the rate measured in OD-9 at 70 °C (0.083 vs. 0.075 mM/hr), indicating that the inhibitor had no effect on amide production in the blend.

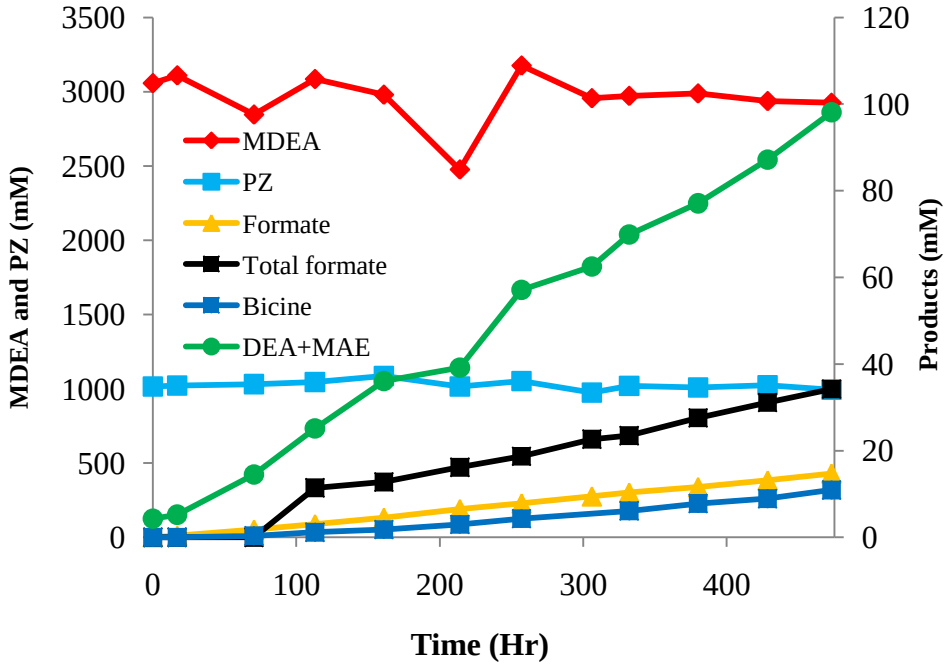

Figure 7.1: MDEA, PZ and degradation products in 7 m MDEA/2 m PZ oxidized in Low-gas reactor at 70 °C; initial loading of 0.14 mol CO_2/mol alkalinity

The concentrations of MDEA and PZ were plotted with degradation products including formate, total formate, DEA+MAE, and bicine measured in experiment OD-9 in Figure 7.1. The MDEA and PZ exhibited very little loss at 70 °C, with initial loss rates of 0.17 ± 0.35 and 0.07 ± 0.05 mM/hr, respectively. In terms of overall molar quantity,

DEA+MAE represented the largest degradation product, formed at a rate of 0.20 mM/hr. Total formate was the product formed at the second greatest concentration, at a ratio with formate of approximately 2.5/1. However, the total formate concentration experienced a lag in formation, only exceeding the formate concentration after 110 hours of oxidation. Neither formate nor bicine exhibited a lag time in formation as was observed with total formate.

The rate of MDEA, PZ and alkalinity loss for each of the Low-gas experiments with 7 m MDEA/2 m PZ, and select experiments with 7 m MDEA, 7 m MEA, and 8 m PZ are listed in Table 7.3. The amine and alkalinity loss rates were not measured in OD-Comb, so they are not included in this table. The concentrations of MDEA, PZ, and MEA were all measured with cation IC, and at the low loss rates observed in these oxidation experiments, the error associated with the linear regressions performed to obtain the loss rates can be relatively high. For example, in OD-5, regression of the data provided a loss rate of +0.4 ± 0.35 mM/hr. The MDEA loss rate is listed as 0.0 ± 0.35 mM/hr because we clearly did not produce more MDEA in the experiment, but the standard deviation returned by the Excel Linest regression was on the same order of magnitude as the absolute value of the slope.

At 55 °C (OD-5) with 100 mM Inh A, the loss of MDEA in the blend was ~0 mM/hr, while at 70 °C with the stainless steel metal salts (OD-9), the loss rate was 0.17 ± 0.35 mM/hr. In comparison, the MDEA loss rate in 7 m MDEA was 0.29 and 0.12 ± 0.3 mM/hr, respectively, at 55 °C (OD-2) and 70 °C (OD-8). The direct comparison of MDEA loss rates in OD-8 and OD-9 indicates that the blend exhibits slightly greater MDEA loss. In contrast, the alkalinity loss rate in 7 m MDEA was 0.37 mM/hr versus the rate of 0.17 mM/hr measured in 7 m MDEA/2 m PZ. The PZ loss rate measured in 8 m PZ (OE18) (Freeman, 2011) was 0.017 mM/hr, which is less than the rate measured in

the blend at 70 °C, but possibly on the same order of magnitude as the rate measured in OD-5. The alkalinity loss in the 8 m PZ experiment was 0.04 mM/hr, which was ¼X the rate measured in 7 m MDEA/2 m PZ at 70 °C in OD-9. In terms of amine loss rates, the opposite end of the spectrum is represented by the Low-gas experiment with 7 m MEA (Sexton-1) conducted with 1 mM Fe^{2+}, which exhibited an MEA loss rate of 6.9 mM/hr. In terms of amine loss rates, the solvents from these Low-gas experiments can be ranked from greatest to least as follows: 7 m MEA>7 m MDEA/2 m PZ>7 m MDEA>8 m PZ.

Table 7.3: Amine and alkalinity loss rates in Low-gas experiments with 7 m MDEA/2 m PZ and other solvents; 7 m MEA (Sexton, 2008), 8 m PZ (Freeman, 2011); SS - stainless steel metals – 0.4 mM Fe^{2+}, 0.1 mM Cr^{3+}, and 0.05 mM Ni^{2+}

				Rates (mM/hr)		
Expt No.	Solvent	T (°C)	Amendments	MDEA loss	PZ loss	Alk loss
OD-5	7 m MDEA/2 m PZ	55	1 mM Fe^{2+}, 100 mM Inh A	0.0 ± 0.35	0.0 ± 0.10	NM
OD-9	7 m MDEA/2 m PZ	70	SS metals	0.17 ± 0.35	0.06 ± 0.05	0.17
OD-2	7 m MDEA	55	1 mM Fe^{2+}	0.29	-	NM
OD-8	7 m MDEA	70	SS metals	0.12 ± 0.3	-	0.37
Sexton-1	7 m MEA	55	1 mM Fe^{2+}	6.9 (MEA)	-	-
OE18	8 m PZ	55	SS metals	-	0.017	0.04

NM denotes not measured.

7.2 THERMAL DEGRADATION OF 7 m MDEA/2 m PZ

The eight thermal degradation experiments listed in Table 7.1 vary from 100 to 150 °C and 0.0 to 0.43 mol CO_2/mol alkalinity. As discussed in Chapter 1, the lean and rich loadings of 7 m MDEA/2 m PZ for CO_2 capture purposes in a coal-fired power plant application are generally modeled as 0.1 and 0.25 mol CO_2/mol alkalinity, respectively. These lean and rich loadings are dictated by the CO_2 solubility in 7 m MDEA/2 m PZ at

absorber/stripper temperatures, and an assumption that 90% CO_2 is removed from the flue gas. These loadings are, therefore, the most relevant to this work, and were used in many of the experiments listed in Table 7.1. In addition to the lean and rich conditions, the degradation of the blend at α=0 was investigated in Th. No.s 8 and 16.

In Th. No. 17, CO_2 loading was replaced with acid treatment with toluene sulfonic acid (TSA) at a concentration equivalent to a lean loading (0.1 mol H^+/mol alkalinity) to assess the effect of protonation of MDEA on degradation of the blend in the absence of CO_2. 1° and 2° amines which were determined to be present in degraded MDEA (Chapter 4) will thermally degrade by undergoing carbamate polymerization reactions. The effect of protonation of MDEA in the absence of CO_2 on degradation of 7 m MDEA was investigated and discussed in Chapter 4, and the same concept was investigated in 7 m MDEA/2 m PZ in Th. No. 17.

The latter experiments, including Th. No.s 16 and 17, were performed using a wider suite of experimental methods including cation IC, anion IC, amino acids and HPLC because of a general improvement in the deployment of the tools available for investigating solvent degradation. The review of these latter experiments offers more to the understanding of how the blend degrades than review of the earlier experiments.

In Th. No. 16, a subset of thermal degradation cylinders was charged with solvent under a nitrogen gas blanket to eliminate the effect of having a small amount of oxygen present in the cylinder headspace. However, because these cylinders were charged and sealed in a glove bag, sufficient torque to seal the sample cylinders was likely not achieved in the cylinder preparation process, and these cylinders generally failed en masse, preventing the collection of data under these conditions.

7.2.1 Thermal degradation products in 7 m MDEA/2 m PZ

The thermal degradation products in 7 m MDEA/2 m PZ are similar to those observed in thermally degraded 7 m MDEA, with the addition of two PZ derivative compounds listed in red in Table 7.4. In addition to the positively identified products listed in the table, several unidentified products were determined to be present in multiple samples through one or more of the MS methods utilized, with the compound mass being the only identifier available. Those masses included the following: 128.1, 162.1, and 213.1 (IC-MS); 126.1 and 220.1 (LC-MS); and 176.1, 183.1, 201.1, and 226.1 (IC- and LC-MS). Only the GC-MS utilized in this work included a technical library to allow searches to match the fragmentation patterns exhibited by the compounds of interest. The LC- and IC-MS systems only allowed assignment of mass to separated peaks.

The compounds listed in Table 7.4 are likely produced as degradation products of the thermal degradation of 7 m MDEA/2 m PZ from the same chemical degradation mechanisms observed in 7 m MDEA, but with additional pathways and mechanisms occurring due to the presence of PZ in the starting solution. For example, it is believed that 1-MPZ is formed through an S_N2 substitution reaction between $MDEAH^+$ and PZ, with $MDEAH^+$ losing a methyl group to PZ to form DEA and 1-MPZ. In 7 m MDEA, $MDEAH^+$ would react with MDEA and 1° and 2° amines to form DEA plus other products. The basic mechanisms are presented in detail in Chapter 9. Some of the other products listed in the table including the amide of MAE with a mass of 133.1 have alternate and possible matches. For example, the amino acid hydroxyethyl sarcosine (HES) also has a mass of 133.1. Note that both the amide of MAE and HES are formed through a high temperature oxidative pathway as presented in Chapter 8 of this document, creating questions for how these compounds could be formed in thermally

degraded 7 m MDEA/2 m PZ in the general absence of oxygen. A peak with a mass of 133.1 is found in multiple samples of the thermally degraded blend.

Table 7.4: Compounds identified in thermally degraded 7 m MDEA/2 m PZ

Mass (g/mol)	Methods Used	Compound ID	Structure	Other Possible IDs
89.1	GC-MS, LC-MS	DMAE	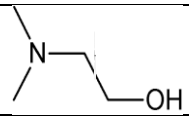	-
100.1	GC-MS, IC-MS, LC-MS	1-MPZ	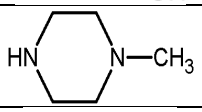	-
103.2	LC-MS	MAE-Amide	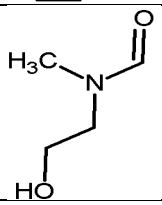	diethylenetriamine
105.1	IC-MS	DEA	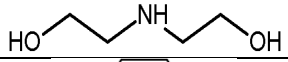	-
114.1	IC-MS	1,4-DMPZ	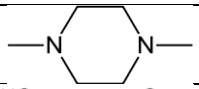	N-formyl PZ
131.1	GC-MS	HEOD	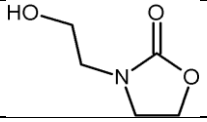	-
133.1	IC-MS, LC-MS	4-methyl-1-PZ ethanamine	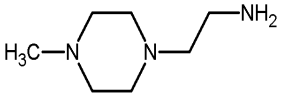	ethyldiethanolamine, HES
143.1	GC-MS	AEMP	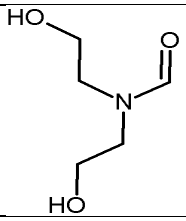	-
144.1	GC-MS, IC-MS, LC-MS	HMP	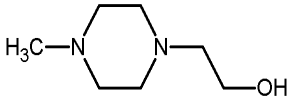	-

Table 7.4: Compounds identified in thermally degraded 7 m MDEA/2 m PZ (Continued)

Mass (g/mol)	Methods Used	Compound ID	Structure	Other Possible IDs
163.1	LC-MS	Bicine	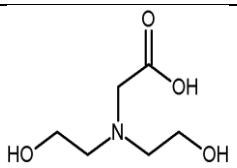	-
173.1	LC-MS	2-[[2-(1-piperazinyl)ethyl]amino]ethanol	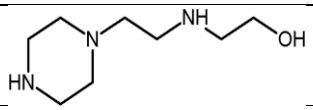	
174.1	GC-MS, LC-MS	bHEP	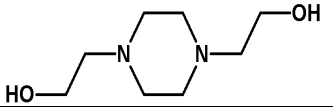	-
187.1	IC-MS, LC-MS	2-[[2-(4-methyl-1-piperazinyl)ethyl]amino]ethanol	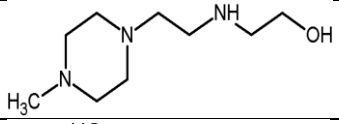	
206.1	IC-MS, LC-MS	MTHEED	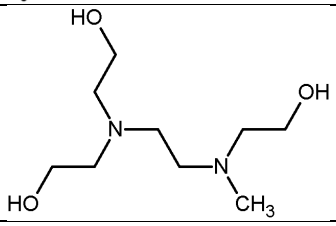	-

The compounds 2-[[2-(1-piperazinyl)ethyl]amino]ethanol and 2-[[2-(4-methyl-1-piperazinyl)ethyl]amino]ethanol are listed on Table 7.4 because they were identified with LC-MS in experimental samples of thermally degraded blends of DEA + PZ (Experiment RPN-2) and DEA + 1-MPZ (experiment RPN-1). Both experiments, which entailed the thermal degradation of these CO_2-loaded DEA blends, are discussed in Chapter 9. The underlying premise for these two experiments was that the initial S_N2 substitution reactions of MDEA and PZ will lead to the formation of 1° and 2° amines such as DEA and PZ derivatives, which will form $DEACOO^-$ in the presence of CO_2, which can then undergo condensation polymerization to form HEOD. As explained in Chapter 9, the strong nucleophile PZ (or 1-MPZ) will react with HEOD at the electron-deficient

carbonyl to open the oxazolidone structure and form the two long-chain ethanol compounds with masses of 173.1 and 187.1. Masses for both of these compounds have been observed in samples of thermally degraded 7 m MDEA/2 m PZ. It is believed that these compounds represent only a small portion of the overall carbon and nitrogen loss as MDEA and PZ loss, but verification of the pathways for the formation of these two compounds provides insight as to what types of thermal degradation reactions occur in the blend. The end result of the formation of these products is probable slower reaction rates with CO_2 for both compounds when compared to PZ, 1-MPZ, and DEA, thus reducing the effectiveness of the blend as a CO_2 capture solvent.

7.2.2 Thermal degradation loss rates of MDEA and PZ

The MDEA and PZ concentration data measured using cation IC in experiments Th. No. 7, Th. No. 8, and Th. No. 16 were collapsed into a combined data file, and the data were plotted separately for nominal loadings of 0.0, 0.1, and 0.25 mol CO_2/mol alkalinity. In Th. No. 8, a low loading series (0.016 mol CO_2/mol alkalinity) was created to examine the effect of small amounts of CO_2 on degradation, but at insufficient concentrations to create large quantities of polymerized products. The data from this loading series were combined with the data from the unloaded series (α=0).

As discussed in Chapter 3, the analysis of degradation experiment data is best performed through the evaluation of initial rates. The thermal degradation data of 7 m MDEA/2 m PZ creates a challenge when using this approach, as presented in Figure 7.2. In that figure, the concentrations of MDEA and PZ from multiple experiments (Th. No. 7, 8, and 16) for the 150 °C and $\alpha \approx 0.1$ loading series are plotted against time in the thermal degradation cylinders. The initial loss rate for MDEA and PZ can be estimated from approximately the first 20 days of thermal degradation. However, after that period of

time, the PZ concentration is approximately 0 mM/hr, and the loss rate of MDEA appears to decrease. In this case, the initial loss rate of MDEA (~1.7 ± 0.12 mM/hr) is much higher than the rate exhibited towards the end of the experiment (0.4 ± 0.08 mM/hr).

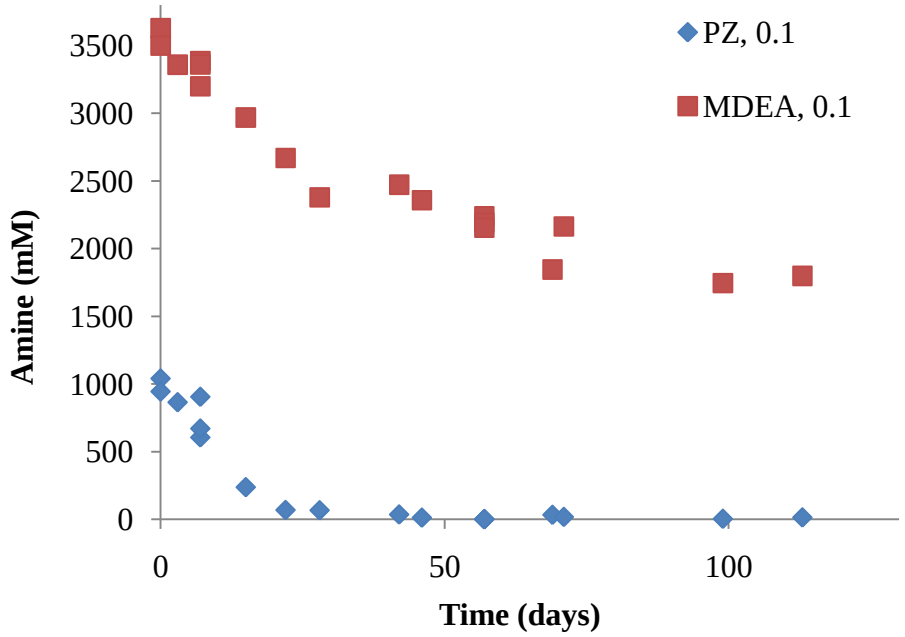

Figure 7.2: MDEA and PZ concentrations in thermally degraded 7 m MDEA/2 m PZ at 150 °C and an initial loading of 0.1 mol CO_2/mol alkalinity; data taken from multiple experiments (Th. No. 7, 8, and 16)

The pattern exhibited in Figure 7.2 presents some questions surrounding the degradation of 7 m MDEA/2 m PZ that will be investigated in depth in this chapter. The initial rates of MDEA and PZ over the first 28 days of data are 1.7 ± 0.1 and 1.6 ± 0.2 mM/hr, respectively. These rates are approximately the same, implying a one-to-one molar relationship between MDEA and PZ loss during this period of the experiment. This observation presents the question of whether the MDEA and PZ are interacting as the solvent generally degrades. During the latter period of the experiment (t>28 days), at

which time the PZ concentration has decreased to ~0 mM/hr, the MDEA loss rate appears to decrease from the initial rate of 1.7 mM/hr to ~0.4 ± 0.1 mM/hr, possibly indicating that the degradation of MDEA decreases once the PZ concentration is approximately zero. This observation is in line with the fact that PZ is the stronger nucleophile between the two amines, and may participate in or facilitate fast reaction(s) between the two amines, resulting in faster MDEA loss in the presence of PZ. If PZ is participating in reactions which convert it to other products such as 1-MPZ or 1,4-DMPZ, it likely results in products which are unable to cause the same fast rate of degradation, causing a slowdown in the MDEA degradation rate as the PZ is lost.

Another important question is whether the PZ is participating in reactions with amines other than MDEA that are present as degradation products, also resulting in PZ loss. The answer to this question is likely yes. This conclusion is supported by the observation of the two compounds with masses of 173.1 and 187.1 (see Table 7.4) in thermally degraded 7 m MDEA/2 m PZ (section 7.2). Thermal degradation experiments RPN-1 and RPN-2 targeted the pathways and degradation products of reactions between DEA, a thermal degradation product of MDEA, and PZ and 1-MPZ in CO_2-loaded solvent solutions. MS analytical results from those experiments provided evidence of these reactions between PZ functional groups and HEOD.

An additional question that must be answered is the role of CO_2 in catalyzing the degradation of 7 m MDEA/2 m PZ, as was observed in 7 m MDEA in Chapter 4. It will be shown that the blend, like 7 m MDEA, is generally thermally stable up to 150 °C in the absence of CO_2 loading. The CO_2-loaded solvent (0.25 mol CO_2/mol alkalinity) degrades in the Swagelok® thermal degradation cylinders at temperatures as low as 120 °C, with MDEA and PZ loss rates of 0.17 ± 0.21 and 0.24 ± 0.06 mM/hr, respectively at that temperature. The blend experienced approximately 50% loss of PZ within 75 days at

this loading. The loss rates were linear over the course of the entire experiment, indicating that as long as PZ was present in solution in significant quantities, the loss of each amine follows steady-state behavior. The MDEA and PZ concentrations are plotted in Figure 7.3. In subsequent sections, the accumulation of degradation products will be correlated with the loss rate of MDEA and PZ in an attempt to understand the types of reactions which are occurring.

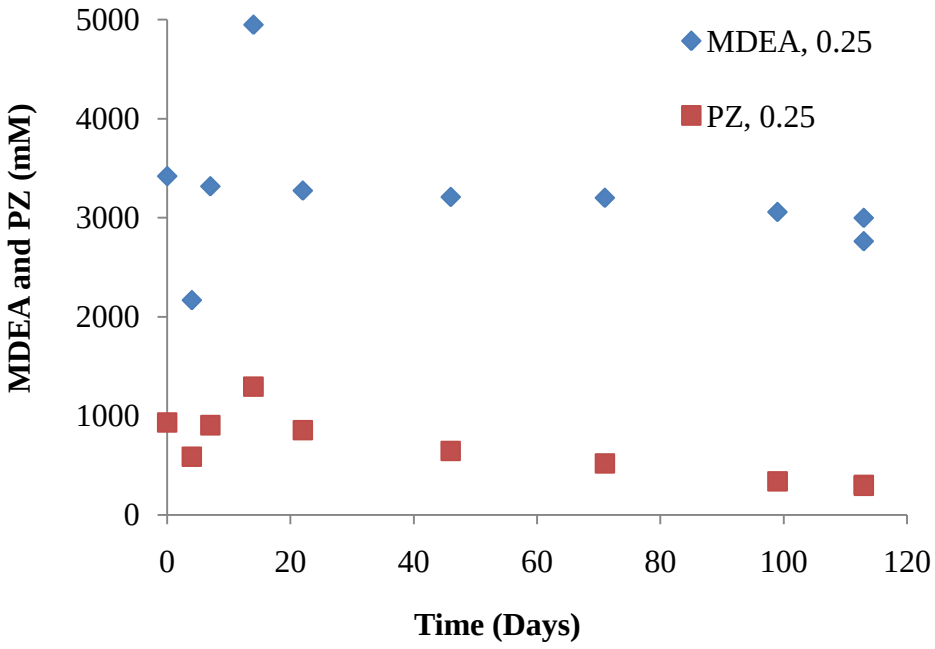

Figure 7.3: MDEA and PZ concentrations in 7 m MDEA/2 m PZ at initial loading of 0.25 mol CO_2/mol alkalinity, thermally degraded at 120 °C (Th. No. 16)

7.2.3 Comparison of rates to 7 m MDEA

In Chapter 4, the initial loss rates of amine in 7 m MDEA were presented from experiments Th. No. 10, 14 and 15. In particular, in Th. No. 10, the loss rate of MDEA at a temperature of 150 °C and an initial loading of 0.2 mol CO_2/mol alkalinity was ~3.0 ± 0.7 mM/hr, which compares to the initial rate of ~3.6 mM/hr measured over ~28 days in

7 m MDEA/2 m PZ at an initial loading of 0.26 mol CO_2/mol alkalinity and 150 °C. The solid black line in Figure 7.4 depicts the slope of the initial MDEA loss rate in the blend. Both sets of data are presented in the figure to illustrate and compare the degradation behavior of these solvents at 150 °C. The concentrations of PZ (▲) in the 7 m MDEA/2 m PZ experiment are also plotted in the figure.

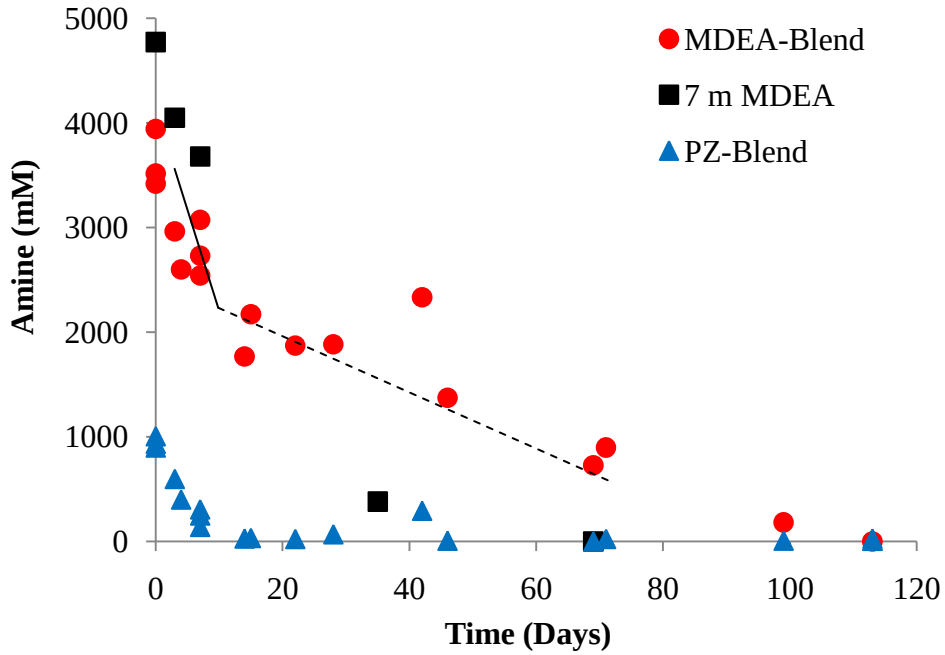

Figure 7.4: Comparison of MDEA concentrations in 7 m MDEA (■) and 7 m MDEA/2 m PZ (●) at an initial loading of ~0.25 mol CO_2/mol alkalinity thermally degraded at 150 °C; PZ concentrations in blend (▲)

The concentration of MDEA in the blend approached zero after approximately 120 days of thermal degradation, whereas in 7 m MDEA, the MDEA concentration decreased faster, approaching ~0 mM/hr after 70 days of thermal degradation. The loss rate of MDEA in 7 m MDEA/2 m PZ after the initial 28 days of degradation was ~1.0 mM/hr, as represented by the dashed line in Figure 7.4, which is <1/4X the loss rate (~3.6

mM/hr) measured over the first 28 days. One possibility is that the CO_2 is effectively taken out of solution in the process of degrading PZ and to some extent MDEA, creating a quasi-zero loaded solvent after the initial 28 days of degradation in the experiment. Another possibility is that the degradation products in the blend such as PZ derivatives inhibited the more rapid degradation and loss of MDEA observed in 7 m MDEA, and/or the absence of the strong nucleophile PZ in the latter part of the experiment results in a reduced rate of MDEA loss.

The MDEA and PZ concentrations were plotted for 7 m MDEA/2 m PZ and 7 m MDEA degraded at 135 °C at an initial loading of 0.2 to 0.25 mol CO_2/mol alkalinity in Figure 7.5. The MDEA loss rate decreased after the PZ concentration reached ~0 mM in the blend at ~45 days. However, the MDEA loss rate in the 7 m MDEA also decreased after approximately 45 days of thermal degradation at 135 °C, indicating that the loss mechanism was slowed or inhibited by the accumulation of degradation products and/or the depletion of $MDEAH^+$ in 7 m MDEA, thereby limiting the rate of further degradation. These results indicate conflicting conclusions between the amine concentration data collected at 150 °C (Figure 7.4) and the data collected at 135 °C (Figure 7.5).

Two thermal degradation models have been developed to predict the rate of degradation of 7 m MDEA/2 m PZ. The first model was developed based on the estimation of first-order rate constants for MDEA and PZ loss after normalizing the data based on the time required for PZ to disappear completely in each data set. This model is explained first. The second model was developed based on the estimation of a universal activation energy for all MDEA and PZ degradation over the range of experimental temperatures and CO_2 loadings. A key underlying assumption for this model is that the mechanisms for MDEA and PZ loss are first-order in $[MDEAH^+]$, and generally independent of [PZ].

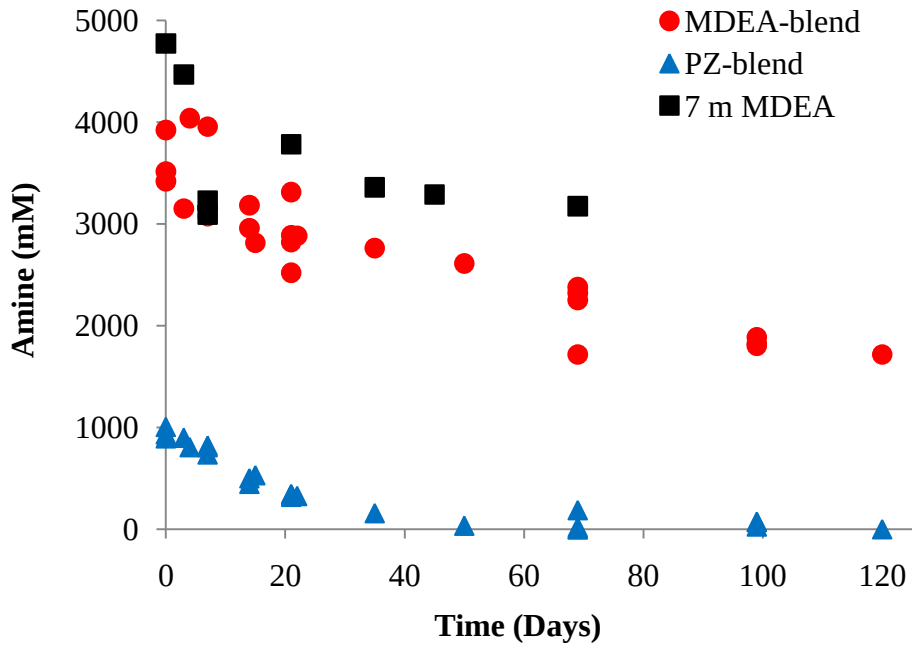

Figure 7.5: Comparison of MDEA concentrations in 7 m MDEA (■) and 7 m MDEA/2 m PZ (●) at an initial loading of 0.20-0.25 mol CO_2/mol alkalinity thermally degraded at 135 °C; PZ concentration in the blend (▲)

7.2.4 Thermal degradation models for 7 m MDEA/2 m PZ

7.2.4.1 Details of thermal degradation model using Arrhenius and "temperature-normalized" time

The first model was developed based on the estimation of first-order rate constants for MDEA and PZ loss from the solvent using the combined thermal degradation data of Th. No.s 7, 8 and 16, and regressing the data at each experimental loading. The individual data sets for each temperature were normalized based on the time required for PZ to disappear completely. From the rate constants over the temperature range of 120 to 150 °C, an activation energy was obtained for the MDEA and PZ loss mechanisms, assuming the mechanisms to be largely the same. However, a different activation energy was estimated for each of the two relevant loadings (0.1 and 0.25 mol CO_2/mol alkalinity). The data were then combined into plots based on

"temperature-normalized" time of degradation, and a common E_a was estimated for MDEA and PZ at each of the two relevant loadings. The model provided a set of equations for estimating the rate constants for MDEA and PZ loss at these two loadings based on the Arrhenius equation for estimating the change in rate constant with temperature.

Details associated with the development of the thermal degradation model using a temperature-normalized time include the following:

1) Using initial rates of degradation at temperatures of 120, 135 and 150 °C, the E_a for MDEA and PZ loss were both estimated;
2) The raw MDEA and PZ concentration vs. time data were normalized to the time required for the PZ concentration to reach ~0 mM/hr at each loading at 135 °C;
3) The raw concentration data for MDEA and PZ were then plotted against normalized time for all three experimental temperatures, and nominal loadings of 0.1 and 0.25 mol CO_2/mol alkalinity;
4) From the combined MDEA and PZ plots described above, a rate constant for 135 °C (408 K) was estimated for the loss of each amine at each experimental loading;
5) With an estimate for the activation energy E_a (kJ/mol) and the rate constant k_{408} (hr^{-1}) for the MDEA and PZ loss reactions, the rate constants at other temperatures were then estimated using the Arrhenius expression for variation in k_1 with temperature (Equation 7.1) for both amines;
6) A "temperature-normalized" time was then calculated for all experimental data as $t_T*(k_T/k_{408})$, and the raw MDEA and PZ

concentration data were plotted versus this normalized time for loadings of 0.1 and 0.25 mol CO_2/mol alkalinity to demonstrate goodness of fit of the model towards predicting the concentration of MDEA and PZ in the blend with time over the range of experimental temperatures (120 to 150 °C); and

7) From the plot of the data, the optimal E_a for MDEA and PZ loss was estimated based on the collapse of the combined data to the best fit possible; this process was repeated at each of the two relevant (experimental) loadings (0.1 and 0.25 mol CO_2/mol alkalinity).

$$k_1 = k_{408} * \exp\left\{\frac{E_a}{R} * \left(\frac{1}{408} - \frac{1}{T_1}\right)\right\} \tag{7.1}$$

The collapse of all thermal data serving as inputs to the model over the range of experimental temperatures (135 to 150 °C) is demonstrated in Figure 7.6, which is the plot of raw amine concentration versus the normalized time for the thermal degradation of 7 m MDEA/2 m PZ at an initial experimental loading of 0.1 mol CO_2/mol alkalinity. The experimental data from three different experiments at two different temperatures (135 and 150 °C) are included in this plot; recall that data at an initial loading of 0.1 mol CO_2/mol alkalinity are not available for 120 °C from the experiments. The amine concentrations generally follow a single pattern, exhibiting a decrease in concentration of both MDEA and PZ with time. However, the PZ concentrations from the 150 °C series data exhibited more variability than data collected at other temperatures, particularly at the longer times (>3500 hr).

The same plot was generated for the thermal degradation data collected in these experiments at a nominal initial loading of 0.25 mol CO_2/mol alkalinity. For this loading,

amine concentration data were generated at all three experimental temperatures (120, 135, and 150 °C). That plot, presented as Figure 7.7, demonstrates better goodness of fit in terms of all data adhering to a single pattern for both MDEA and PZ. More data exist for short times, creating difficulty in assessing the fit of the normalized data to a single trend. A replot of the same data covering only the initial 2,500 hours (normalized time) is presented as Figure 7.8. The overall collapse of the data into a single trend is more evident in this plot.

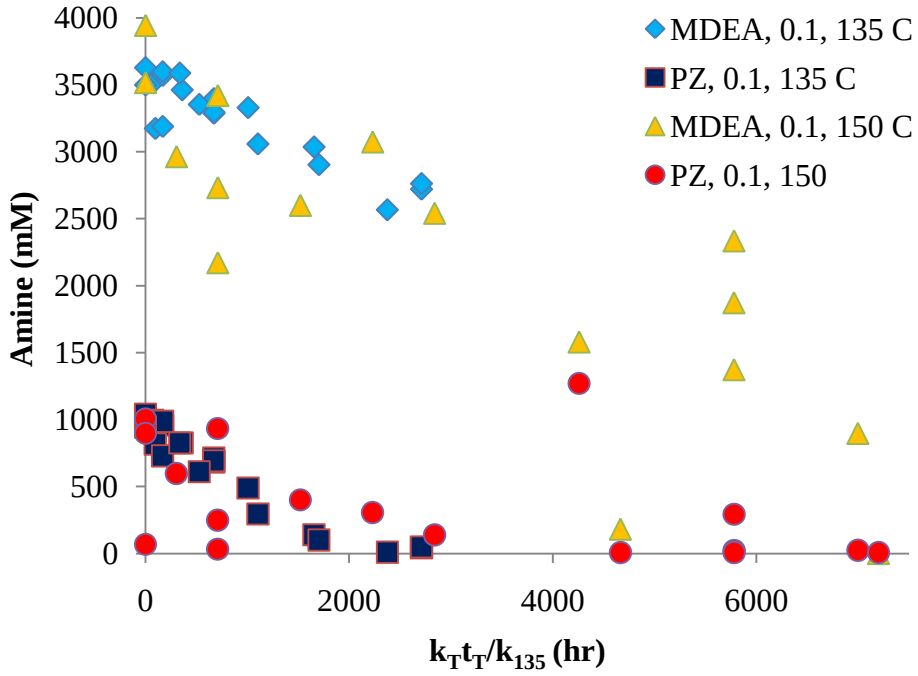

Figure 7.6: Amine concentration plotted with temperature-normalized time in thermally degraded 7 m MDEA/2 m PZ at nominal initial loading of 0.1 mol CO_2/mol alkalinity; experimental temperature range 135 to 150 °C

Step (7) above entails the collapse of the amine concentration data in the temperature-normalized plots (Figure 7.6 and Figure 7.7) through adjustment of the activation energy (E_a) to give the best possible fit to both the MDEA and PZ data at both

loadings. The resulting E_a for both MDEA and PZ loss at a loading of 0.1 mol CO_2/mol alkalinity was ~138 kJ/mol. The resulting E_a for both MDEA and PZ loss at a loading of 0.25 mol CO_2/mol alkalinity was ~95 kJ/mol. In both cases, the complete collapse of amine concentration data was not possible.

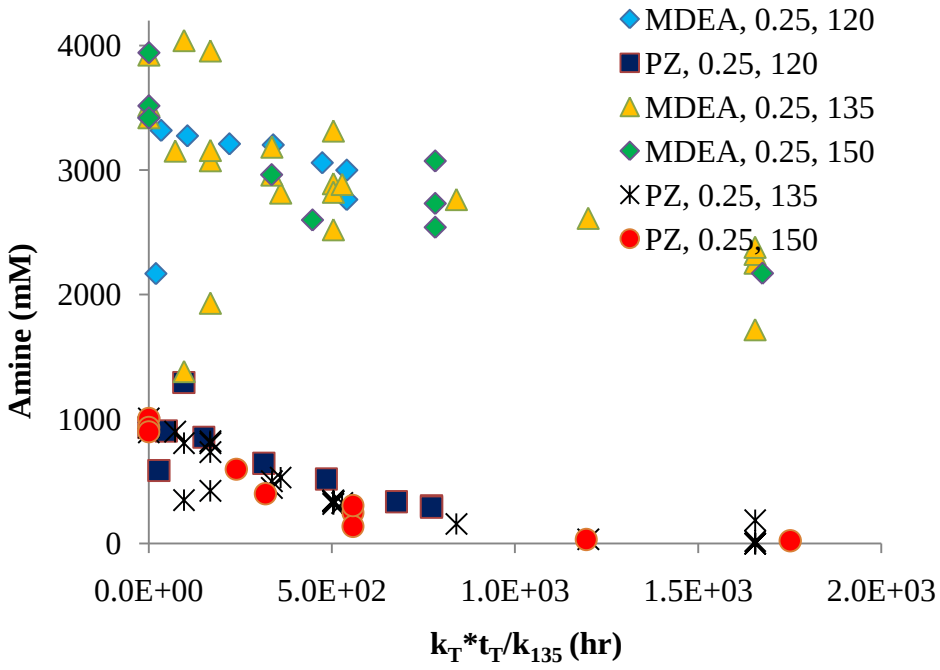

Figure 7.7: Amine concentrations plotted with temperature-normalized time in thermally degraded 7 m MDEA/2 m PZ at a nominal initial loading of 0.25 mol CO_2/mol alkalinity; experimental temperature range 120 to 150 °C

With an estimate of the activation energy for both MDEA and PZ loss at each of the two loadings considered (0.1 and 0.25 mol CO_2/mol alkalinity), and an estimate of the k_{408} for MDEA and PZ loss mechanisms, an expression for amine loss was developed from Arrhenius for MDEA (Equation 7.2) and PZ (Equation 7.3) at a nominal loading of 0.1 mol CO_2/mol alkalinity as follows:

$$k_{MDEA} = 7.8X10^{-5}(1/hr) * \exp\left\{\frac{138\frac{kJ}{mol} * \frac{1000J}{kJ}}{8.314\frac{J}{mol*K}} * \left(\frac{1}{408K} - \frac{1}{T_1}\right)\right\} \quad (7.2)$$

$$k_{PZ} = 9.7X10^{-4}(1/hr) * \exp\left\{\frac{138\frac{kJ}{mol} * \frac{1000J}{kJ}}{8.314\frac{J}{mol*K}} * \left(\frac{1}{408K} - \frac{1}{T_1}\right)\right\} \quad (7.3)$$

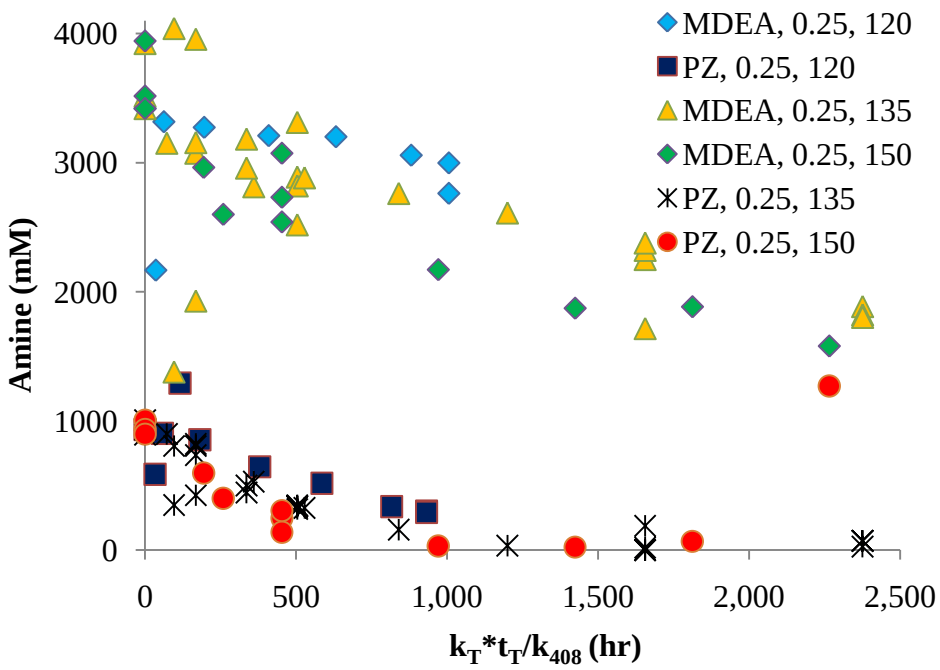

Figure 7.8: Collapse of MDEA and PZ data over initial 2,500 hours in thermally degraded 7 m MDEA/2 m PZ over temperature range of 120 to 150 °C at a loading of 0.25 mol CO_2/mol alkalinity; amine concentration data plotted against temperature normalized time

The model was used to estimate the rate constants for MDEA and PZ loss at 150 °C at the nominal initial loading of 0.1 mol CO_2/mol alkalinity for comparison to the

experimental data from this condition. The predicted concentrations for MDEA from the model-predicted rates constants (Equation 7.2 and Equation 7.3) are plotted in Figure 7.9. The plot includes the measured amine concentrations from the combined data set created with Th. No.s 7, 8, and 16, but plotted based on temperature-normalized time. The model does a good job of predicting MDEA concentration, but the scatter in experimental data is a source of discrepancy between the modeled and measured values for both amines. Further, the model fit is sensitive to the choice of E_a to match both MDEA and PZ loss.

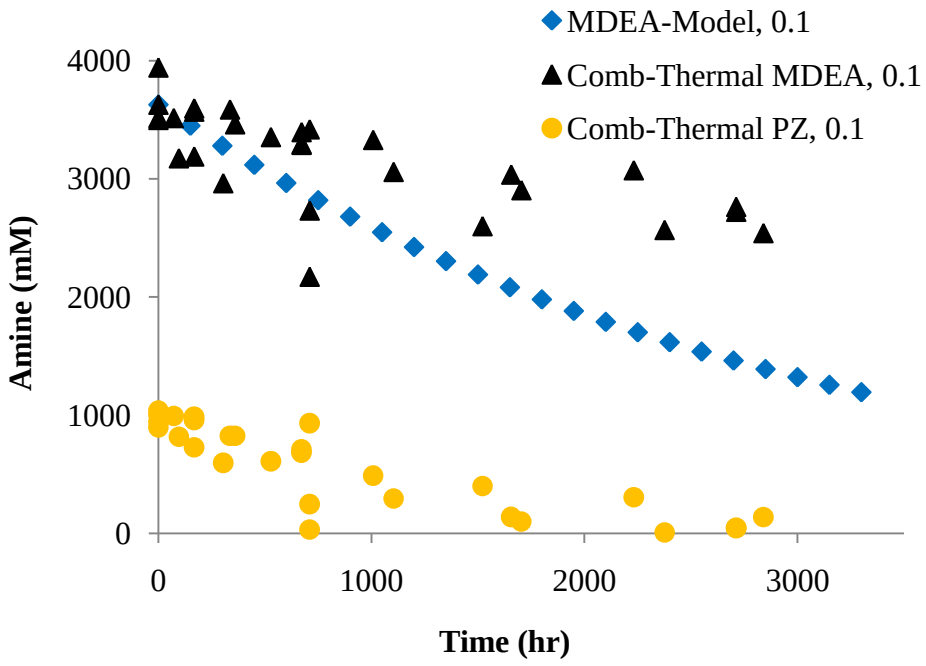

Figure 7.9: Amine concentrations in thermally degraded 7 m MDEA/2 m PZ predicted by the model at 150 °C, and measured in Th. No. 7, 8, and 16, all at nominal initial loading of 0.1 mol CO_2/mol alkalinity

Arrhenius expressions were developed for the MDEA and PZ rate constants at a nominal initial loading of 0.25 mol CO_2/mol alkalinity, and are presented as Equation 7.4 and Equation 7.5:

$$k_{MDEA} = 2.4X10^{-4}(1/hr) * \exp\left\{\frac{95\frac{kJ}{mol} * \frac{1000J}{kJ}}{8.314\frac{J}{mol*K}} * \left(\frac{1}{408K} - \frac{1}{T_1}\right)\right\} \quad (7.4)$$

$$k_{PZ} = 3.1X10^{-3}(1/hr) * \exp\left\{\frac{95\frac{kJ}{mol} * \frac{1000J}{kJ}}{8.314\frac{J}{mol*K}} * \left(\frac{1}{408K} - \frac{1}{T_1}\right)\right\} \quad (7.5)$$

The model was used to estimate the rate constants for MDEA and PZ loss at 150 °C at the nominal initial loading of 0.25 mol CO_2/mol alkalinity for comparison to the experimental data from this condition. The predicted concentrations for MDEA from the model-predicted rate constants (Equation 7.4 and Equation 7.5) are plotted in Figure 7.10. The plot also includes the measured amine concentrations from the combined data set created with Th. No.s 7, 8, and 16. Because of the general scatter in the measured amine concentration data, it is difficult to assess the fit of the model prediction for the MDEA data. Further, the model is sensitive to the selection of E_a, and the predicted MDEA concentration can be adjusted upward or downward by changing this parameter. However, given that the combined temperature-normalized data collapsed the best at an E_a of 95 kJ/mol, this number was used in the final model equations. Because this model requires a set of equations for each CO_2 loading, and does not provide a fully adequate match for amine concentration with time, the development of a universal model was necessary, which is described in the next section.

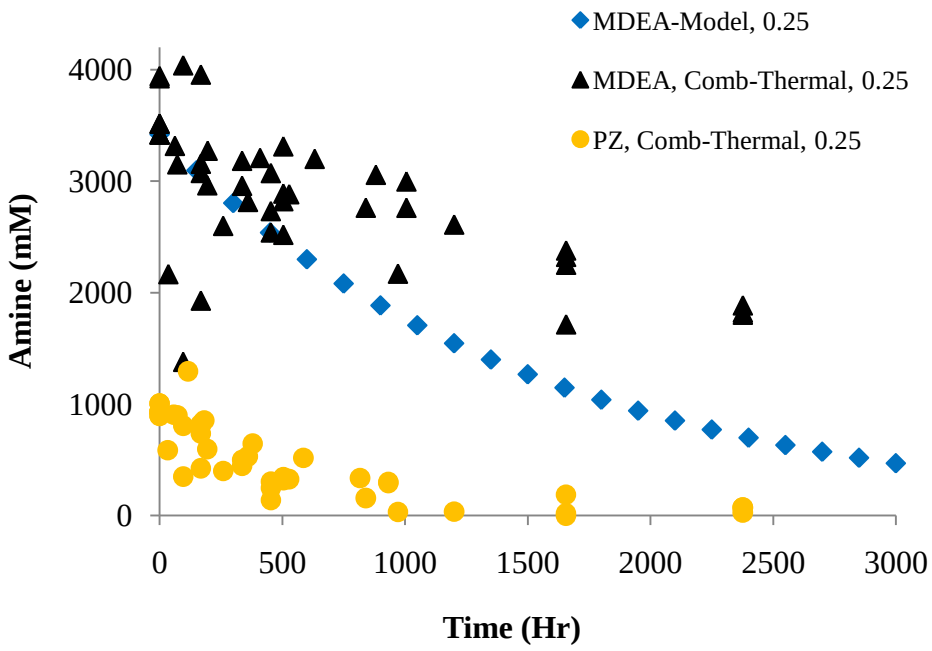

Figure 7.10: Amine concentrations in thermally degraded 7 m MDEA/2 m PZ predicted by the model at 150 °C, and measured in Th. No. 7, 8, and 16, all at nominal initial loading of 0.25 mol CO_2/mol alkalinity

7.2.4 Universal activation energy model

A universal thermal degradation model based on a single or simplified degradation mechanism was developed. This model is a "universal activation energy model". A single E_a for overall degradation of 7 m MDEA/2 m PZ was estimated based on rate constants regressed for all experimental temperatures and loadings from the combined thermal degradation data set. The model developed for this purpose has some simplifying assumptions including the underlying hypothesis that the rate-limiting step in degradation of the blend is first-order in [$MDEAH^+$]. Another simplifying assumption is that the overall degradation rate is generally independent of the concentration of PZ.

Equation 7.6 describes the reaction resulting in the loss of MDEA:

$$\frac{d[MDEA]}{dt} = -k_{1,MDEAH^+}(T)[MDEAH^+] \tag{7.6}$$

Although MDEA loss is considered independent of [PZ] in this model, the loss of PZ in the blend can be related to the MDEA loss rate constant by Equation 7.7 as follows:

$$\frac{d[PZ]}{dt} = -S * k_{1,MDEAH^+}(T)[MDEAH^+] \tag{7.7}$$

where S is a stoichoimetric factor which relates the loss of both amines as follows: S=d[PZ]/dt/d[MDEA]/dt, or d[PZ]/d[MDEA]. The rate constant for MDEA loss can be related to CO_2/H^+ loading as follows:

$$k_{1,MDEA}(T) = k_{1,MDEAH^+}(T) * \alpha_{acid} \tag{7.8}$$

We can also say:

$$S * k_{1,MDEA}(T) = S * k_{1,MDEAH^+}(T) * \alpha_{acid} \tag{7.9}$$

Equation 7.9 can be rearranged into another useful form:

$$S * k_{1,MDEAH^+} = \frac{S * k_{1,MDEA}}{\alpha_{acid}} \tag{7.10}$$

Using initial rates of degradation for MDEA and PZ loss, a value of the stoichiometric relationship for initial rate of PZ loss and initial rate of MDEA loss, expressed as S_j, can be calculated for each experiment at each condition as follows:

$$S_j = \frac{InitialRate_{PZLoss}}{InitialRate_{MDEALoss}} \tag{7.11}$$

The objective of evaluating S_j for each experiment is to calculate the average across all experimental temperatures and loadings. Using the Th. No. 7, 8, and 16 initial rates at all temperature series and loadings, an average S (S_{avg}) was calculated as ~1.13.

The rate constants calculated for MDEA and PZ loss at all temperatures and loadings (♦) were then normalized and combined into a single spreadsheet as k_U. Normalization of MDEA rate constants was performed by multiplying by 1/α.

Normalization of PZ rate constants was performed as follows: (1) multiplying by the stoichiometric factor S_{avg}, (2) dividing by α, and (3) multiplying by initial [PZ]/[MDEA], or 2/7. A plot of k_U versus 1/T (K) was then created (Figure 7.11). The average slope for this curve provided the universal activation energy (E_a) for MDEA and PZ loss in the blend. The overall average E_a for MDEA and PZ loss was ~104 kJ/mol, which is between the two values estimated in the development of the temperature-normalized model (95 and 138 kJ/mol for PZ and MDEA loss, respectively) in Section 7.2.4.1.

The first-order rate constants estimated from the acid-treated experimental series (Th. No. 17) are also plotted in the figure (■) to demonstrate the similarity in degradation behavior when 7 m MDEA/2 m PZ is loaded with CO_2, and when the solvent is protonated with an acid in the absence of CO_2. The rate constants measured at all three temperatures collapsed onto the rate constants measured in the CO_2-loaded blend. Note that the rate constants for MDEA and PZ loss at 135 °C were approximately the same in the acid treatment experiment, reflecting one-to-one molar rate loss behavior at this temperature.

With an estimate for the stoichiometric ratio (S~1.13) of PZ loss rate to MDEA loss rate, and a regressed value for the global activation energy for the loss of MDEA and PZ (E_a~104 kJ/mol), a universal model expressing the rate constant for MDEA loss can be written as Equation 7.12:

$$\frac{d[MDEA]}{dt} = -k_U(T) * [MDEA]_T * \alpha \tag{7.12}$$

Where $k_U = k_1(T)*(1/\alpha)$, and:

$$k_U(T) = k_{408}(1/hr) * \exp\left\{-\frac{104{,}300 J/mol}{8.314 J/mol - K}\left(\frac{1}{408K} - \frac{1}{T_U}\right)\right\} \tag{7.13}$$

The rate loss equation can also be expressed in terms of PZ loss as:

$$\frac{d[PZ]}{dt} = 1.13 * \frac{d[MDEA]}{dt} \tag{7.14}$$

Finally, we can express the loss of [PZ] as:

$$\frac{d[PZ]}{dt} = -1.13 k_U(T) * [MDEA]_T * \alpha \tag{7.15}$$

Where $k_U = k_1(T)*(2/7)*(1/\alpha)$.

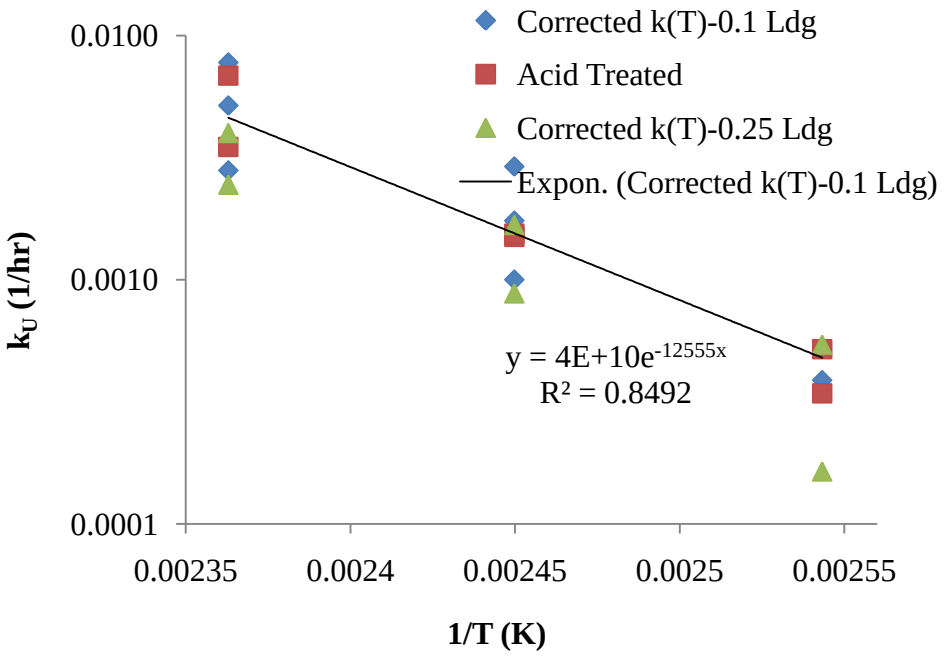

Figure 7.11: Corrected rate constants (k_{corr}) measured from MDEA and PZ loss in 7 m MDEA/2 m PZ thermally degraded at 120 to 150 °C at loadings of 0.0, 0.1 and 0.25 mol CO_2/mol alkalinity; rate constants corrected for loading, initial amine concentration, initial rates of amine loss, and S_{avg}, and expressed as: $k*\{[PZ]/[MDEA]*[IR_{PZ}/IR_{MDEA}]*(1/\alpha)*S_{avg}$

7.2.5 Degradation product formation trends

The concentrations of degradation products were measured in Th. No. 16 and Th. No. 17. These experiments can be viewed as companion experiments for comparison

because the former was conducted with 7 m MDEA/2 m PZ at 120, 135 and 150 °C with CO_2-loaded solutions, while the latter was performed with the blend at these same temperatures, but with acid treatment (0.1 mol H^+/mol alkalinity added as TSA). The product accumulation data from these two experiments are compared in this section. Products of interest from these experiments include DEA+MAE, 1-MPZ, 1,4-DMPZ, AEP, formate, and ammonia (measured as NH_4^+ with cation IC).

7.2.5.1 Trends in CO_2-loaded 7 m MDEA/2 m PZ

In order to better understand degradation mechanisms in the blend, amine degradation products, which represent the majority of the lost carbon and nitrogen in thermally degraded 7 m MDEA/2 m PZ, were plotted in Figure 7.12. These include DEA+MAE, 1-MPZ, 1,4-DMPZ, and AEP. Ammonium ion (NH_4^+) was also plotted in the figure. The degradation product data series are represented by dashed lines, while MDEA and PZ are represented with solid lines. Data from the same experiment are plotted in Figure 7.13, but covering only the first 25 days to allow evaluation of the degradation behavior during the initial period of degradation.

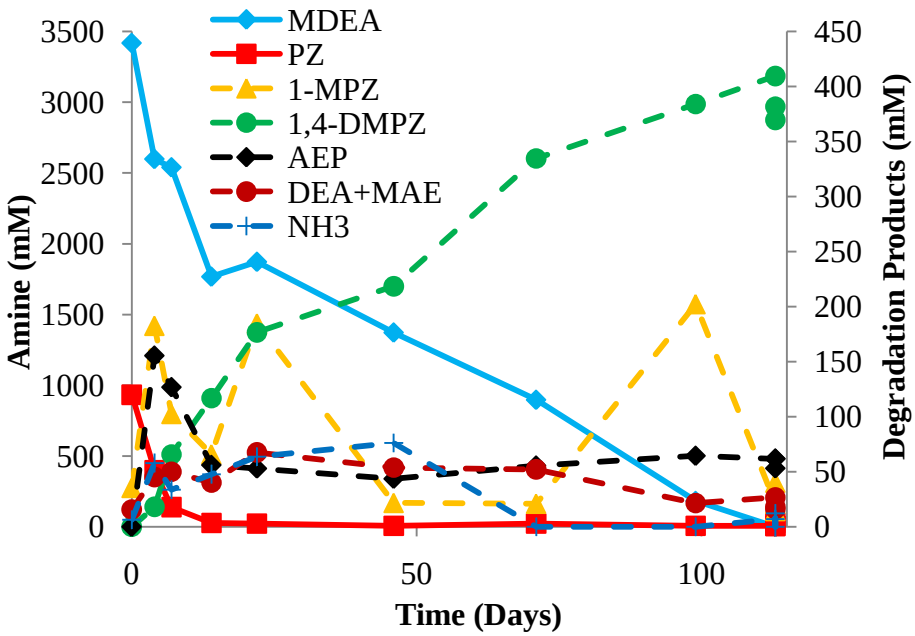

Figure 7.12: Concentration of MDEA, PZ and amine degradation products in thermally degraded (150 °C) 7 m MDEA/2 m PZ at an initial loading of 0.25 mol CO_2/mol alkalinity

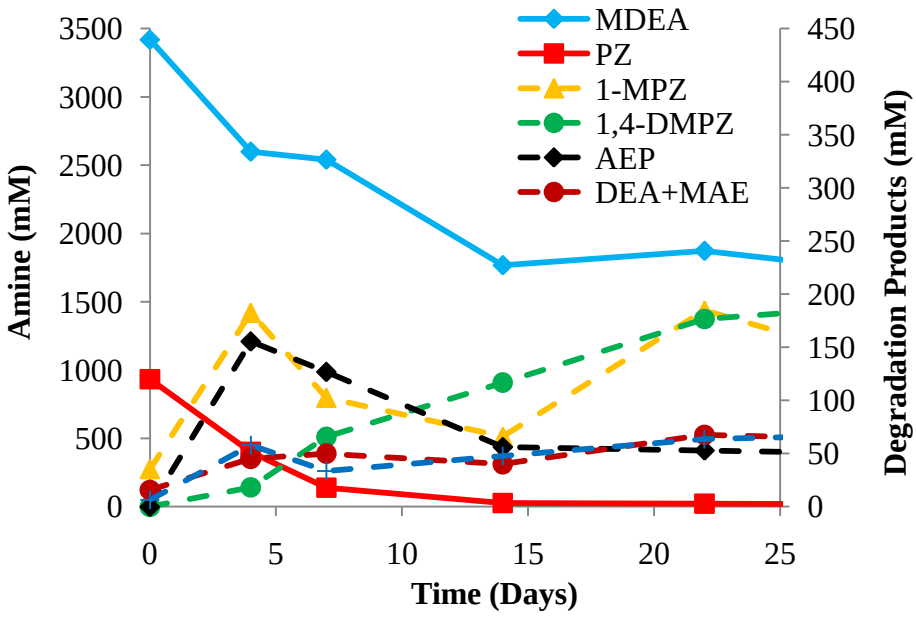

Figure 7.13: Concentration of MDEA, PZ and amine degradation products in thermally degraded (150 °C) 7 m MDEA/2 m PZ at an initial loading of 0.25 mol CO_2/mol alkalinity; 0 to 25 days of degradation

In the plotted series in Figure 7.12 and Figure 7.13, it is evident that the concentration of PZ decreases to ~0 mM/hr within 15-20 days, accompanied by a steady decrease in the MDEA concentration. At Day 4, the approximate total PZ derivative concentration (1-MPZ, 1,4-DMPZ, and AEP) is 325 mM, versus the approximate loss of PZ of 650 mM. Some of the PZ ring loss is likely due to ring opening, but additional loss is also likely the result of degradation products which have not been identified. The concentration of 1,4-DMPZ exhibits a steady increase through the end of the experiment, but the other PZ derivatives quantified in the experiment including 1-MPZ and AEP experienced an initial increase within the first ten days of the experiment, followed by a decrease through the end of the experiment. The rapid increase in concentration of both 1-MPZ and AEP coincided with the period of rapid loss of PZ and MDEA. It is likely that S_N2 substitution reactions are occurring in the solvent (section 9.3.1), as presented here in Figure 7.14. The reactivity of the unreacted nitrogen on 1-MPZ allows 1-MPZ to continue to undergo an additional S_N2 reaction until most or all of the 1-MPZ is converted to 1,4-DMPZ. As a result of this behavior, the 1,4-DMPZ concentration exhibited an increase through the end of the experiment. A similar effect was observed for AEP, which also has one unreacted nitrogen capable of undergoing further S_N2 substitution with $MDEAH^+$, or any other protonated 1° or 2° amine. For example, after the initial S_N2 substitution reaction between $MDEAH^+$ and PZ occurs, $DEAH^+$ could also react with PZ or 1-MPZ. In fact, the S_N2 reactions which may occur include those between strong nucleophiles such as PZ and its derivatives, and protonated amines. The exception to this effect is the formation of 1,4-DMPZ which no longer has an available amine group for S_N2 substitution reaction. As a result, it accumulates in the degraded solvent, as was observed in Figure 7.12.

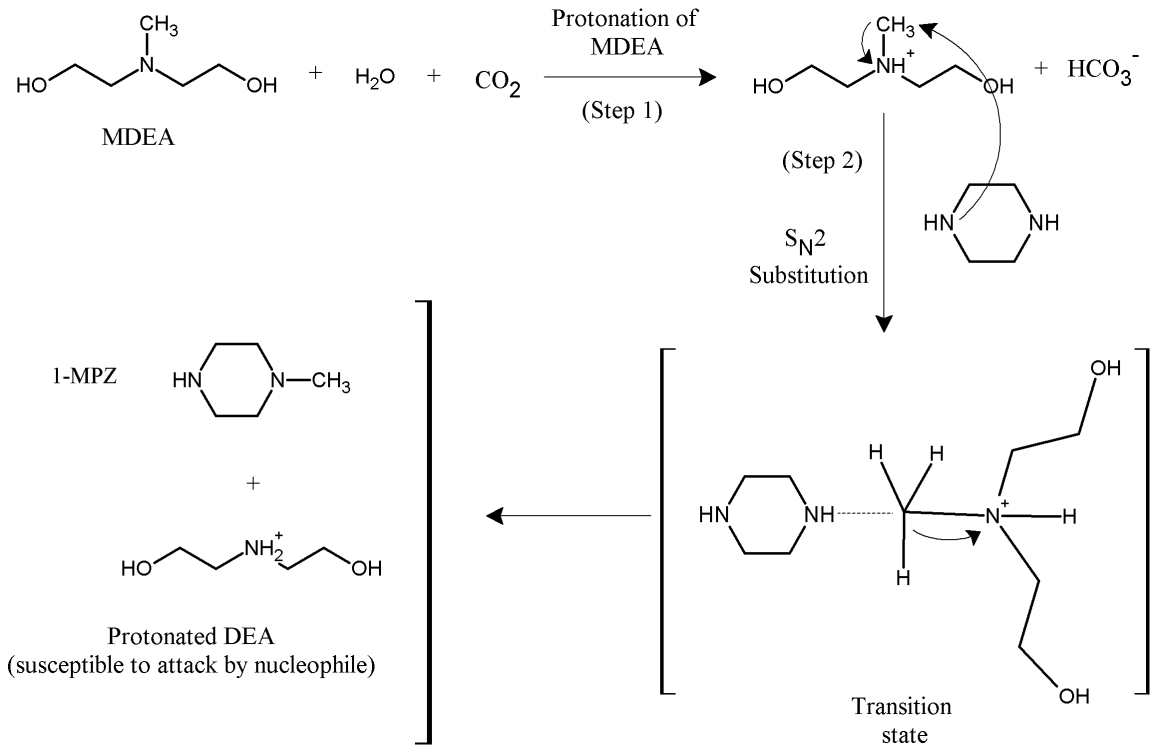

Figure 7.14: Proposed S_N2 substitution reaction and pathway for thermal degradation of 7 m MDEA/2 m PZ and production of 1-MPZ and DEA in CO_2-loaded solvent

The behavior of DEA+MAE is similar to 1-MPZ and AEP, experiencing an increase, but leveling off at a concentration of ~50 mM for most of the experiment before decreasing after ~75 days of degradation. The initial formation followed by loss of DEA+MAE over the course of the experiment is likely a result of the same effect observed for PZ derivatives. DEA and MAE will both undergo S_N2 substitution reactions with PZ and 1-MPZ, leading to the formation of MEA and methyl amine. The concentration of DEA+MAE reaches a steady-state after the initial period of degradation, but then decreases as less MDEA is available to degrade to DEA and/or MAE. DEA and MAE will also form carbamates in the presence of CO_2, and at high temperatures, will undergo condensation polymerization reactions (Polderman, 1956). In the case of

$DEACOO^-$, condensation polymerization will lead to the formation of HEOD. Section 9.4.1 provides a detailed review of the formation of HEOD in thermally degraded MDEA solvents, and the subsequent reactions that can occur with HEOD in the presence of PZ behaving as a strong nucleophile. The practical result of these additional reactions involving $DEACOO^-$ is the loss of DEA with time at high temperature, as evidenced by the DEA+MAE decrease exhibited in Figure 7.12.

The ammonium ion was detected and quantified in Th. No. 16 samples, and plotted as NH_3 in Figure 7.12. As with other species, NH_3 formed in the initial 25 days of the experiment, but decreased to ~0 mM/hr after ~50 days of thermal degradation. Although a pathway for the formation of ammonia through thermal degradation is not presented in Chapter 9, ammonia may be appearing in the experiment as a result of the fragmentation of amine degradation products such as MEA, MAE and DEA.

7.2.5.2 Mass balance in degraded 7 m MDEA/2 m PZ

A mass balance was performed on the final sample results from the thermally degraded 7 m MDEA/2 m PZ in Th. No. 16. In particular, it is of interest to know how much of the lost carbon and nitrogen as MDEA and PZ loss can be accounted for in the identified and quantified degradation products. These products include DEA+MAE, 1-MPZ, 1,4-DMPZ, AEP, FPZ, and NH_3, but the carboxylate ions also comprise a small portion of the overall carbon loss and are included in the mass balance. The percentage of carbon and nitrogen lost as both MDEA and PZ loss that each identified product comprises are listed in Table 7.5. The total recovered carbon and nitrogen in the final sample are also listed. The PZ derivatives comprise ~14% of the total carbon loss and ~9% of the nitrogen loss. The only other major amine(s) quantified in the thermally degraded blend is DEA+MAE which comprised 0.3% of both carbon and nitrogen loss.

Although ammonia was identified in the thermally degraded blend, it only made up 0.2% of the measured nitrogen loss.

Table 7.5: End sample carbon and nitrogen molar balance in 7 m MDEA/2 m PZ (α=0.25 mol CO_2/mol alkalinity) thermally degraded at 150 °C

Mass Balance for Th. No. 16:		
Product	% of C	% of N
DEA+MAE	0.3	0.3
1-MPZ	1.0	1.5
1,4-DMPZ	11.0	14.5
AEP	1.5	3.0
NH_3	0.0	0.2
Formate	0.3	0.0
Total	14.1	19.6

The data in Figure 7.12 and Figure 7.13 indicated that the mix of degradation products in thermally degraded 7 m MDEA/2 m PZ changes with time and the degree of degradation, with 1,4-DMPZ starting to form, but at ~175 mM versus its final concentration of nearly 400 mM in the experiment. In contrast, 1-MPZ has reached its highest concentration (~185 mM) at this point in time. A mass balance was performed on this sample (Table 7.6), with 1-MPZ and 1,4-DMPZ representing approximately the same amount (~5.5%) of carbon and nitrogen as lost MDEA and PZ. This result is in contrast to the observation of 1-MPZ representing only 1% of carbon in the final sample, whereas 1,4-DMPZ represented ~11% of carbon and 7% of nitrogen. The PZ derivatives in this case represent ~13% of carbon loss and ~12.5% of nitrogen loss, which is a slightly greater amount than they represent in the final sample of this experiment. Finally, DEA+MAE represents 2% of carbon and nitrogen loss, which is ~7X the percentage represented in the final sample.

The amount of carbon recovered as a percentage of the carbon lost for both MDEA and PZ loss is presented as a function of time in Figure 7.15. The amount of nitrogen recovered as a percentage of the lost nitrogen from MDEA and PZ loss is also presented in the figure. For both carbon and nitrogen, the percentage recovered is better towards the beginning of the experiment, but tends to level off within 50 days. When the zero time data point is ignored, the amount of nitrogen recovered trends downward, reflecting the loss of nitrogen (and alkalinity) from the solvent to compounds which have not been identified using the current methods.

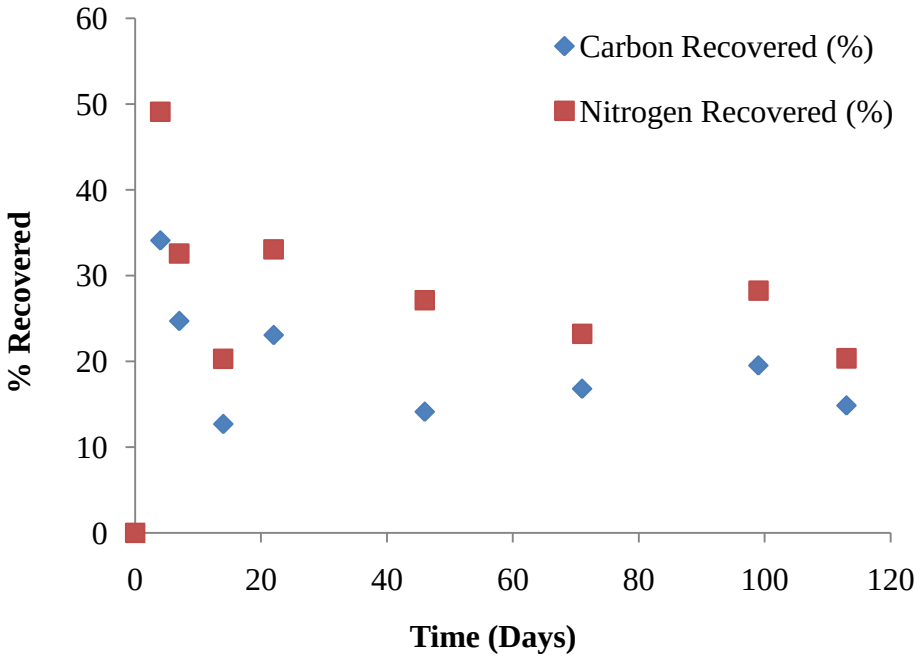

Figure 7.15: Carbon and nitrogen recovered as percentage of loss of initial amine (MDEA + PZ) in 7 m MDEA/2 m PZ (α=0.14 mol CO_2/mol alkalinity) cycled from 55 to 120 °C

Overall, the mass balance data reflect the trend for many of the initial degradation products to behave as intermediates, undergoing degradation to other products. For

example, 1-MPZ and DEA+MAE can be considered intermediate *and* final degradation products in the blend. Accounting for a greater percentage of the overall carbon and nitrogen loss in the Day 22 sample also reflects the tendency of the solvent to degrade following several different pathways, resulting in additional products, some of which have been identified, but many of which have not.

Table 7.6: Day 22 sample carbon and nitrogen molar balance in 7 m MDEA/2 m PZ (α=0.25 mol CO_2/mol alkalinity) thermally degraded at 150 °C

Mass Balance at t=22 days:		
Product	% of C	% of N
DEA+MAE	2.1	2.0
1-MPZ	5.7	11.0
1,4-DMPZ	5.4	10.5
AEP	1.6	4.7
NH_3	0.5	0.5
Formate	2.6	2.6
Total	18.8	32.0

7.2.5.3 Trends in acid-treated 7 m MDEA/2 m PZ

In experiment Th. No. 17, 7 m MDEA/2 m PZ was treated with acid at 0.1 mol H^+/mol alkalinity before the solvent was charged to the Swagelok® sample cylinders and placed in the ovens for thermal degradation. As stated in previous sections, the purpose of the experiment was to determine the type and quantity of products in the blend. In this section, the product concentrations are plotted, and a mass balance is presented to compare the effect of protonation on the mixture of products.

The concentrations of MDEA, PZ and degradation products of 7 m MDEA/2 m PZ in the acid-treated blend at an initial concentration of 0.1 mol H^+/mol alkalinity and thermally degraded at 150 °C are presented in Figure 7.16. In contrast to the findings of the thermally degraded CO_2-loaded blend, the concentration of DEA+MAE continued to

increase through the end of the experiment, indicating that the 1° and 2° amines were not being degraded from the solution at as high of a rate as was observed in the presence of CO_2. The protonation of MDEA in the absence of CO_2 avoided the formation of carbamates of these degradation products, preventing condensation polymerization reactions which lead to the formation of oxazolidone compounds (HEOD). The latter mentioned reactions lead to the degradation of compounds such as DEA and MAE.

The concentration of 1-MPZ increased immediately, and reached approximately 375 mM after 33 days as presented in Figure 7.16. The formation of 1,4-DMPZ experienced a lag time of approximately 8 days, after which the concentration increased to approximately that of 1-MPZ. The concentrations of both PZ derivatives ended the experiment at ~255 mM, indicating that the rate of S_N2 substitution reactions decreased.

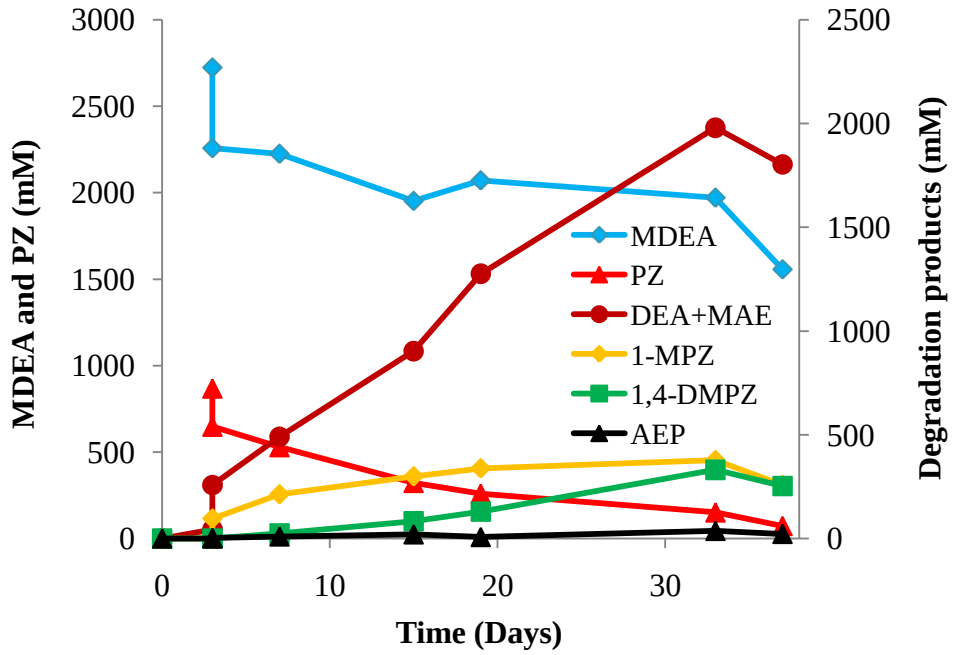

Figure 7.16: Concentration of MDEA, PZ and amine degradation products in thermally degraded (150 °C) 7 m MDEA/2 m PZ, acid treated at a concentration of 0.1 mol H^+/mol alkalinity

The degradation times for the data collected in the acid-treated experiment (Th. No. 17) were H^+ load-normalized to allow direct comparison to the data collected in the CO_2-loaded experiment at a nominal initial loading of 0.25 mol CO_2/mol alkalinity. Degradation times in the acid-treated experimental data, plotted on the x-axis in Figure 7.17, were multiplied by the ratio of 0.1/0.25 to normalize to the extent of protonation occurring in the CO_2-loaded solvent. The MDEA, PZ, and degradation product concentrations through ~15 days of degradation from both experiments are plotted in Figure 7.17, with solid lines used for the acid-treated blend and dashed lines used for the CO_2-loaded blend.

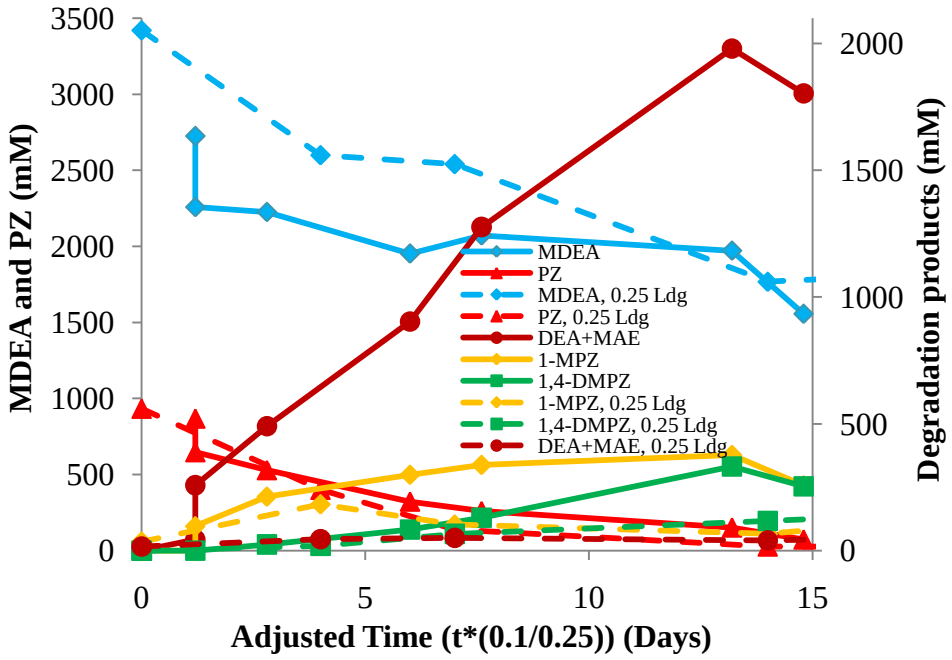

Figure 7.17: Comparison of 7 m MDEA/2 m PZ, initially loaded to 0.25 mol CO_2/mol alkalinity (dashed lines) and 0.1 mol H^+/mol alkalinity (solid lines), thermally degraded at 150 °C; time scale of acid treated experimental data adjusted by factor of 0.10/0.25 for H^+ loading

The data plotted in Figure 7.17 indicate that protonation of 7 m MDEA/2 m PZ results in loss rate and behavior of MDEA and PZ which are approximately the same as exhibited by the CO_2-loaded solvent. However, a contrast in degradation behavior is most evident in DEA+MAE formation, with the concentration in the acid-treated blend continuing to increase while in the CO_2-loaded solvent, DEA+MAE levels out at an approximate concentration of ~20 mM, which is ~1/100X the concentration exhibited by the acid-treated solvent. The absence of CO_2 allows the DEA+MAE to form without the degrading reactions associated with carbamate polymerization occurring. The concentrations of 1-MPZ and 1,4-DMPZ also exhibit contrasting behavior in this plot, with these compounds in the CO_2-loaded solvent (dashed lines) never able to form and stabilize at concentrations representing a significant portion of the overall carbon and nitrogen loss.

7.2.5.4 Mass balance in acid-treated 7 m MDEA/2 m PZ

A mass balance was performed on the degradation data from the acid-treated thermal degradation experiment with 7 m MDEA/2 m PZ (Th. No. 17) at 150 °C. As listed in Table 7.7, closure of the balance on the final sample (Day 37) from the experiment was achieved, with the data reflecting greater than 100% recovery of lost carbon (~103%) and nitrogen (105%). Although greater than 100% closure of the balance is not technically possible, the balance calculations do reflect the fact that much better closure is achievable in the acid treated blend. The concentration of DEA+MAE alone was ~1,800 mM in the final sample, and represented ~70% of lost carbon and ~65% of lost nitrogen. The PZ derivatives represent ~34% of carbon loss and 41% of nitrogen loss. The mass balance for recovered carbon and nitrogen is provided in Figure 7.18. Clearly, greater than 100% recovery of carbon and nitrogen as a percentage of

MDEA and PZ loss is not possible, but the data in the figure do reflect the fact that the acid treated solvent degraded following more straightforward behavior, resulting in DEA+MAE and PZ derivatives and small amounts of heat stable salts (formate). This result is in direct contrast to the findings of the CO_2-loaded cycling experiment at the same basic conditions. In the acid treated experiment, 100%+ recovery was achieved with the listed compounds in Table 7.7 within ~20 days.

As discussed above in reference to rates of degradation, MDEA and PZ degradation in the presence of CO_2 leads to the production of DEA and $DEACOO^-$, which will undergo condensation polymerization to HEOD, an oxazolidone compound. Oxazolidones can react with the strong nucleophile PZ to form other compounds, resulting in the irreversible loss of 1° and 2° amines, PZ and alkalinity in the solvent. When protonated with acid, 1° and 2° products of MDEA will not form carbamates or oxazolidone compounds at high temperature, leaving S_N2 reactions as the dominant reactions with PZ in the blend under acidified conditions. The S_N2 reactions will result in arm switching products, and may even reverse under the appropriate conditions as degradation proceeds. The products and their respective percentages listed in Table 7.7 reflect the less complex degradation environment of the acidified blend. In contrast to this data, the products and percentages listed in Table 7.6 reflect the fact that when loaded with CO_2, the majority of both carbon and nitrogen cannot be accounted for in the products quantified in this work. Additional effort to quantify the oxazolidone, imidazolidone, and urea products in the blend using HPLC methods would likely improve the mass balance.

Table 7.7: Carbon and nitrogen balance in 7 m MDEA/2 m PZ acid treated at 0.1 mol H^+/mol alkalinity and thermally degraded at 150 °C; balance performed on final sample (Day 37)

Product	% of Lost C	% of Lost N
DEA+MAE	69.9	65.3
1-MPZ	14.3	18.7
1,4-DMPZ	16.8	18.3
AEP	1.5	2.4
FPZ	1.2	1.6
Formate	0.01	0.0
Total	104	106

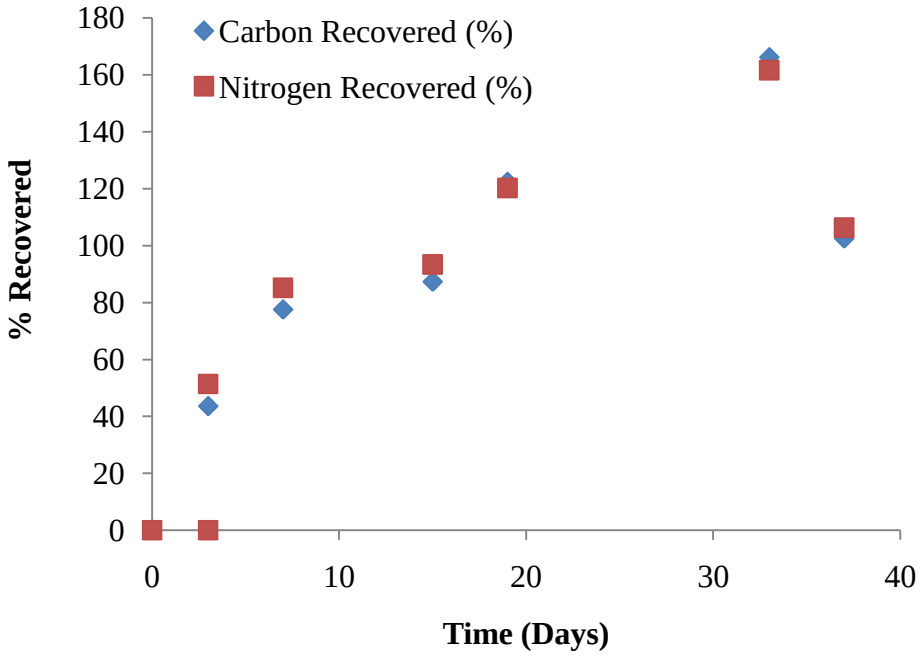

Figure 7.18: Carbon and nitrogen recovered as percentage of loss of initial amine (MDEA + PZ) in 7 m MDEA/2 m PZ (treated with 0.1 mol H^+/mol alkalinity) cycled from 55 to 120 °C

7.3 CYCLING OF 7 m MDEA/2 m PZ

As listed in Table 7.1, 7 m MDEA/2 m PZ was cycled in the ISDA in six separate experiments. The first three (C-21, C-22, and C-23) were conducted with the original (1.12 L) thermal reactor, while the last three (C-30, C-33, and C-34) were conducted with the redesigned (0.13 L) thermal reactor. With the exception of the last cycling experiment, the experiments were conducted with an initial loading of 0.14 mol CO_2/mol alkalinity. All cycling experiments were conducted with the oxidative reactor maintained at 55 °C, while the thermal reactor temperature was varied from 90 to 125 °C to provide a range of high temperature oxidation conditions. The last cycling experiment (C-34) was conducted on unloaded 7 m MDEA/2 m PZ, but with acid treatment at a concentration of 0.1 mol H^+/mol alkalinity; sulfuric acid was added to the solvent before being charged to the ISDA for cycling from 55 °C in the oxidative reactor to 125 °C in the thermal reactor.

After reviewing the compounds typically detected in cycled 7 m MDEA/2 m PZ, a complete analysis of the degradation data from one of the cycling experiments (C-21) is presented below. These data and analysis will then be compared to the data from experiment C-34 which entailed the cycling of acid-treated 7 m MDEA/2 m PZ. This comparison will be performed to understand the role of protonation in causing the degradation of the blend in the absence of CO_2 much the same way this same effect was investigated in the review of the thermal degradation data above.

7.3.1 Degradation products in cycled 7 m MDEA/2 m PZ

The degradation products observed in cycled 7 m MDEA are listed in Table 4.6. Many of those same products were observed in 7 m MDEA/2 m PZ. The products consistently observed in cycled 7 m MDEA/2 m PZ are listed in Table 7.8. Table 7.8 is not a comprehensive list of all compounds identified or suspected to exist in cycled 7 m MDEA/2 m PZ. For example, additional compounds observed in the cycled solvent

include HEOD and 4-methyl-1-piperazineethanamine. However, because they have been identified in a limited number of samples, and are suspected to be present at low concentrations, they are not of interest except for understanding the more complex degradation mechanisms and pathways occurring in the blend. Their identification did not include a method for quantification.

Table 7.8: Degradation products in cycled 7 m MDEA/2 m PZ

Compound	MW	Compound Type	Method
Formate	45	Carboxylate ion	Anion IC
Acetate	59	Carboxylate ion	Anion IC
Oxalate	89.1	Carboxylate ion	Anion IC
DMAE	89.1	1° and 2° amines	Cation IC, LC-MS
DEA+MAE	105.1/75.1	1° and 2° amines	Cation IC
1-MPZ	100.2	PZ derivative	Cation IC
1,4-DMPZ	114.2	PZ derivative	Cation IC
AEP	129.2	PZ derivative	Cation IC
N-formyl PZ	114.1	Amide	Cation IC
N-(2-hydroxyethyl)-N-methyl formamide	103.1	Amide	HPLC
N,N-bis-(2-hydroxyethyl) formamide	133.1	Amide	HPLC
Bicine	163.1	Amino acid	HPLC-AAA
HES	133.1	Amino acid	HPLC-AAA
Glycine	75.1	Amino acid	HPLC-AAA

Using HPLC, the formyl-amides of MAE (N-(2-hydroxyethyl)-N-methyl formamide) and DEA (N,N-bis-(2-hydroxyethyl) formamide) were identified in the cycled blend through comparison of hydrolyzed and unhydrolyzed samples injected in the system. In the unhydrolyzed samples, numerous peaks appear using the HPLC with UV detection. Many of those same peaks do not appear in hydrolyzed samples from the same experiment, providing evidence of amides (Chapter 2). The identification of amides other than the formyl amides of DEA and MAE was attempted, particularly in

regard to amides of PZ, but those efforts did not provide definitive results. Using a HILIC non-polar HPLC separation column on the Dionex HPLC system, separation of additional peaks with retention times between 18.0 and 28.0 minutes was achieved. Many of those same peaks were not present in the hydrolyzed samples. Although these peaks were identified as probable amides in the cycled blend, creating a match to these peaks with a known standard was not achieved. In conclusion, amides of degradation products other than DEA and MAE likely exist, and additional efforts to identify these compounds would assist in closing the carbon and nitrogen balance in the degraded blend.

The concentration of DEA+MAE was generally known and represented a significant percentage of the overall carbon and nitrogen loss. It can, therefore, be assumed that the two identified amides of DEA and MAE in cycled 7 m MDEA/2 m PZ represent the largest contribution to carbon and nitrogen loss of the amides formed in the cycled solvent. The concentrations of the amides were estimated by determining the extent of the conversion or loss of MAE in the synthesized standard using cation IC. Knowing the conversion in the reaction and the extent of dilution of the amide standards allowed the estimation of the concentration of amides in the cycled samples.

7.3.2 Cycling experiment C-21 with 7 m MDEA/2 m PZ in the ISDA

7 m MDEA/2 m PZ at an initial loading of ~0.14 mol CO_2/mol alkalinity was cycled from 55 °C in the oxidative reactor to 120 °C in the thermal reactor of the ISDA. A gas purge mixture of 98% O_2/2% CO_2 was continuously supplied to the headspace of the oxidative reactor during each of these experiments. Although the estimation of initial rates of MDEA and PZ loss and degradation product formation are the most valuable results from the cycling experiments, the solvent was cycled for 570 hours in C-21 to

allow the evaluation of second-order effects. The experiment was conducted with the original design of the ISDA which included the large thermal reactor. A full suite of analytical methods was used on the samples from this experiment soon after completion. Those methods included cation IC, anion IC, amino acid analysis using the HPLC-AAA method, total inorganic carbon (TIC), and titration for alkalinity. MS methods were also implemented on a subset of samples. Those methods included GC-MS and IC-MS. HPLC analysis of samples was completed approximately seven months after experiment completion due to the equipment and method not being available at the time of the experiment. All relevant data from C-21 are reviewed below.

7.3.2.1 Initial rates of MDEA and PZ loss

The initial rates of MDEA, PZ, and alkalinity loss were estimated using the methods described in earlier chapters, selecting the initial period of amine loss which exhibited linear behavior for regression of amine concentration or alkalinity data. The loss rates were regressed for all cycling experiments with 7 m MDEA/2 m PZ for comparison in Table 7.9. The data are arranged in the table from lowest (90 °C) thermal reactor temperature to highest (125 °C). The last rates entries are from the acid treated experiment (C-34). The initial rates were normalized to residence time in the thermal reactor, an exercise which was performed in Section 3.8 in the discussion related to the cycling of 7 m MDEA. The purpose in this normalization process is to put all the initial rate data on the same thermal reactor residence time basis to allow direct comparison. The rates measured in cycling experiments conducted with the redesigned thermal reactor of 0.13 L volume were divided by the factor of 0.13/1.2, or 0.12. The residence time normalized rates are listed in parentheses () in Table 7.9.

Table 7.9: Initial rates of MDEA, PZ, and alkalinity loss in cycled 7 m MDEA/2 m PZ and nominal initial loading of 0.14 mol CO_2/mol alkalinity, and oxidative reactor temperature of 55 °C; rates in parentheses () have been normalized to residence time in thermal reactor

Expt. No.	Th Rx T (°C)	Rx Size (L)	Loss rates (mM/hr)		
			MDEA	PZ	Alkalinity
C-22	90	1.12	1.6	0.8	3.2
C-33	90	0.13	0.5 ± 0.2 (4.2 ± 2.0)	0.1 ± 0.1 (0.8 ± 0.4)	0.1 ± 0.4 (0.8 ± 3.3)
C-23	100	1.12	2.8	0.7	1.2
C-21	120	1.12	2.7 ± 0.4	1.2 ± 0.1	2.5 ± 0.1
C-30	125	0.13	5 (41.7)	2.2 (18.3)	4.7 (39.2)
C-34*	125	0.13	3.7 ± 0.3 (30.8 ± 2.5)	1.5 ± 0.1 (12.5 ± 1.1)	3.5 ± 0.4 (29.2 ± 3.25)

* Acid-treated at 0.1 mol H^+/mol alk. Shaded experimental data conducted in redesigned thermal reactor

With the exception of the rates listed for C-22, the raw rates of MDEA, PZ, and alkalinity loss generally followed a pattern of increasing with thermal reactor temperature. The initial rate data from C-22 are outliers for all three parameters, and when compared directly to the initial rates measured in C-33, which was conducted with the smaller (0.13 L) thermal reactor, the nearly order of magnitude increase in all rates indicates that the greater residence time in the larger thermal reactor resulted in significantly higher overall degradation.

Normalization of the rates to thermal reactor residence time slightly improved the adherence to a trend of increase in rate with thermal reactor temperature. For example, when the rate measured in C-22 is ignored, the alkalinity loss rate follows a general pattern of increase with thermal reactor temperature. When the rate measured in C-33 is ignored, the MDEA loss rate follows a trend of increase with thermal reactor temperature. If the rate measured in C-23 is ignored, the PZ loss rate follows a pattern of increase with thermal reactor temperature.

A comparison of the rates measured in experiments C-30 and C-34, both conducted with a thermal reactor temperature of 125 °C, indicates that the protonation experiment (C-34) experienced 30 to 50% lower degradation rates. Both experiments were conducted with the smaller thermal reactor, and the normalized rates are provided for both in Table 7.9. These lower rates in the acid treated experiment are indicative of the more simplistic set of rate mechanisms occurring in the acidified blend, wherein protonation of the starting amines to $MDEAH^+$ and PZH^+ initiates the degradation processes in the absence of CO_2. In contrast, in C-30, the blend was initially loaded to 0.14 mol CO_2/mol alkalinity and cycled in the ISDA, and the degradation processes included the more complex reactions involving the condensation polymerization of carbamates of 1° and 2° amines in the presence of CO_2. These polymerization reactions lead to the formation of oxazolidones through the pathways discussed in Chapter 8. The end result of these more complex reactions is an increase in the loss rate of MDEA, PZ and alkalinity.

7.3.2.2 First-order rate constants in cycled 7 m MDEA/2 m PZ

The amine concentration data were plotted versus time (hours) on a semi-log plot to allow estimation of first-order loss rate constants for MDEA, PZ, and alkalinity in each of the 7 m MDEA/2 m PZ cycling experiments. The plot for experiment C-21 is presented here as Figure 7.19. The data provide a good fit in the linear regressions, with R^2 values of greater than 0.96 in all cases.

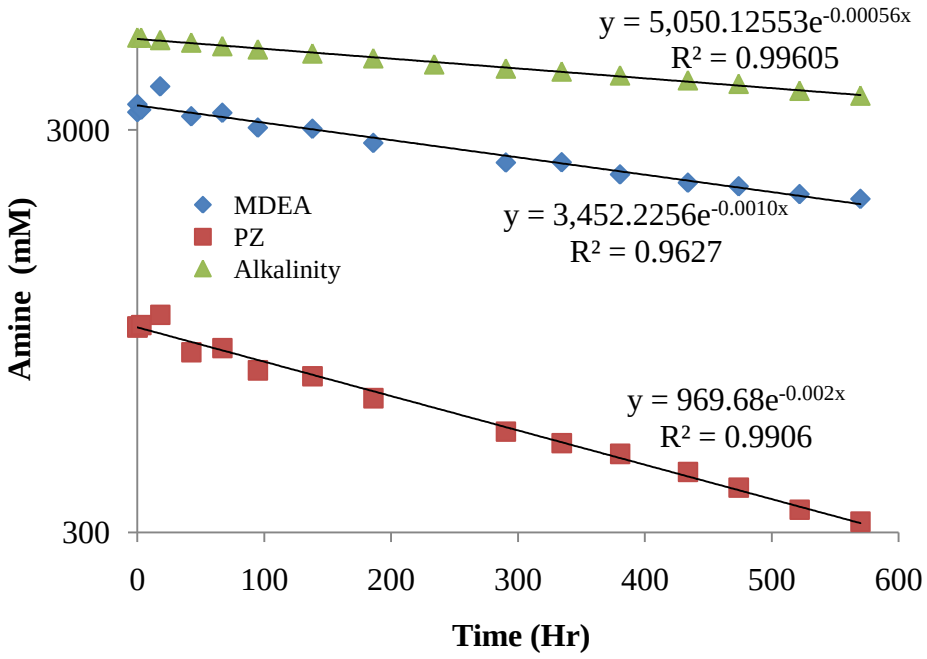

Figure 7.19: First-order rate constant estimation of MDEA, PZ and alkalinity loss in 7 m MDEA/2 m PZ cycled 55 to 120 °C in the ISDA

After normalizing the rate constants from the three cycling experiments conducted with the small thermal reactor for residence time in the thermal reactor, the rate constants were plotted as $\ln(k_{norm})$ versus 1/T (K) for each component to allow estimation of E_a for each (Figure 7.20). Linear regressions were performed for each, and the E_a for MDEA, PZ, and alkalinity were estimated at 65, 72, and 104 kJ/mol, respectively. The rate constants measured in the acid-treated experiment (C-34) when the solvent was cycled from 55 to 125 °C are also presented in the figure using open symbols. In general, the alkalinity loss rate constants exhibited a high degree of variability, with significant differences displayed between the two cycling experiments conducted with a thermal reactor temperature of 90 °C; the difference in those experiments was the thermal reactor size (1.12 and 0.13 L).

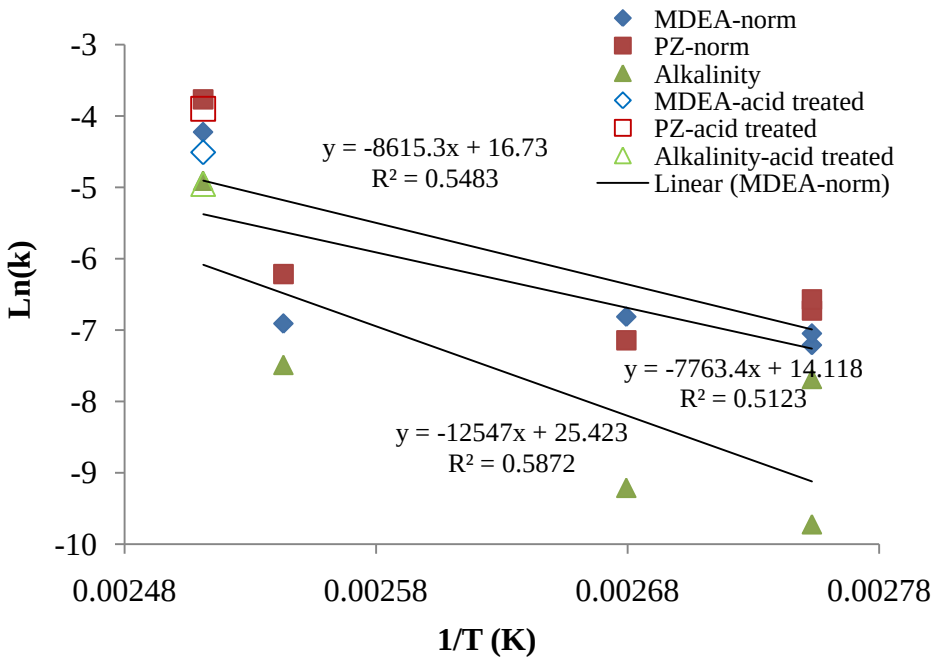

Figure 7.20: Estimation of activation energy (E_a) in cycled 7 m MDEA/2 m PZ; rate constants from experiments with smaller thermal reactor (C-30, C-33, and C-34) are normalized for thermal reactor residence time; acid-treated cycling experiment depicted with open symbols

The initial loss rates and E_a for MDEA, PZ and alkalinity loss for 7 m MDEA/2 m PZ can be compared to those values presented for 7 m MDEA in Chapter 4, and 8 m PZ presented in Chapter 6 (Table 7.10). In general, the lowest rates of amine and alkalinity loss were exhibited by 8 m PZ, followed by 7 m MDEA/2 m PZ and 7 m MDEA. 8 m PZ did exhibit a higher initial loss rate of PZ than the blend, but the blend experienced an accompanying MDEA loss rate of 2.7 mM/hr. The activation energies for MDEA and alkalinity loss in 7 m MDEA were the lowest of the three amines.

7.3.3 Normalization and combining of Low-gas and cycling data

As was performed with the 8 m PZ degradation data from both the Low-gas and the ISDA, the 7 m MDEA/2 m PZ Low-gas and cycling data can be combined in order to

collapse and create a data set for oxidation over the range of experimental temperatures. OD-9 was performed at 70 °C, while the cycling experiments with the blend were performed over the range of 90 to 125 °C. A Low-gas experiment was conducted with 7 m MDEA/2 m PZ with 100 mM Inh A at 55 °C, but these data were not incorporated into the body of oxidative data.

Table 7.10: Initial rates of amine loss and associated activation energies for loss mechanisms in 7 m MDEA/2 m PZ and other solvents cycled in the ISDA; initial rates quoted for cycling from 55 to 120 °C

Solvent	MDEA		PZ		Alkalinity	
	Init Rate* (mM/hr)	E_a (kJ/mol)	Init Rate* (mM/hr)	E_a (kJ/mol)	Init Rate* (mM/hr)	E_a (kJ/mol)
7 m MDEA/2 m PZ	2.7 ± 0.40	65	1.2	72	2.5	104
7 m MDEA	4.6 ± 1.9	32	-	-	4.7 ± 3.2	27
8 m PZ	-	-	1.6	100	1	76

* Initial rate for cycling from 55 to 120 °C in the ISDA.

Loss rates estimated from cycling experiments with the ISDA were normalized to residence time in the thermal reactor, taking into account the entire system volume. For example, in the original design of the ISDA, the total system volume was ~3.4 L while the thermal reactor volume was approximately 1.12 L. As such, the normalization factor was ~0.35 (1.12/3.4), and all rates estimated in experiments conducted with this design (C-21, C-22, and C-23) were normalized by dividing by this factor. The thermal reactor and total system volumes in the redesigned system were 0.13 and 2.3 L, respectively, so the rates from experiments performed with this system (C-30, C-33, and C-34) configuration were normalized by dividing by a factor of ~0.057. Applying these factors normalized the cycling experimental rates to those collected in the Low-gas reactor (OD-9). The rates were also normalized to the percentage of oxygen in the headspace of the

oxidative reactor. In all cycling experiments conducted with the ISDA, the gas mixture was 98% O_2/2% CO_2, which matched the CO_2 solubility condition in 7 m MDEA/2 m PZ at the oxidative reactor liquid temperature of 55 °C. The loss rates measured in these experiments were, therefore, normalized by dividing the rates by 98 kPa O_2. OD-9 was conducted in the Low-gas reactor with a headspace gas mixture of ~92.5% O_2/7.5% CO_2, which matched the CO_2 solubility condition in the blend at 70 °C. The loss rates measured in these experiments were, therefore, normalized by dividing the rates by 92.5 kPa O_2. As such, all normalized rates are quoted in units of mM/hr-kPa O_2 X 1000 in Table 7.11.

Table 7.11: Loss rates in 7 m MDEA/2 m PZ degraded in the ISDA and the Low-gas reactor systems; rates normalized to residence time in thermal reactor, and to oxygen content in headspace gas; 8 m PZ rates (Freeman, 2011)

			Rates (mM/hr-kPa O_2) X 1000		
Expt No.	T_{th} °C	Th Rx Size (L)	MDEA loss	PZ loss	Alk loss
OD-9	70	0.35	1.8	0.8	1.8
C-22	90	1.12	46.6	23.3	93.3
C-33	90	0.13	89.5	17.9	17.9
C-23	100	1.12	81.6	20.4	35.0
C-21	120	1.12	78.7	35.0	72.9
C-30	125	0.13	895.1	393.8	841.4
C-34*	125	0.13	662.4	268.5	626.6
C-16**	120	1.12	-	31.8	26.3

*Performed with acid-treated 7 m MDEA/2 m PZ.

**Cycling experiment with 8 m PZ.

The normalized rates for MDEA, PZ, and alkalinity loss listed in Table 7.11 exhibit improved adherence to expected trends, with C-22 data being an obvious exception. However, the data were used to estimate the activation energy for MDEA, PZ and alkalinity loss in 7 m MDEA/2 m PZ. The acid-treated data were not incorporated

into this analysis due to the difference in the extent of protonation (0.1 vs 0.14), and the previously established idea that protonation alone (absence of CO_2) will lead to a more simple set of reactions, which is not indicative of the degradation that can be expected in a flue gas capture application. The E_a estimated with the normalized data were 97, 100, and 98 kJ/mol for MDEA, PZ and alkalinity loss, respectively. These values can be compared to the activation energies estimated from the raw rates above of 65, 72, and 104 kJ/mol for MDEA, PZ, and alkalinity loss, respectively. These estimated E_a from the normalized data reflect the similarities in the overall loss rate mechanisms for the measured parameters.

7.3.4 Product formation rates in cycled 7 m MDEA/2 m PZ

The products which were consistently identified and quantified in cycled 7 m MDEA/2 m PZ include formate, total formate, bicine, DEA+MAE, and the PZ derivatives 1-MPZ, 1,4-DMPZ, and AEP. The amide N-formyl PZ (FPZ) was quantified in the more recent experiments with the ISDA, but data for this degradation product were not collected in all cycling experiments with the blend.

The rates of formation of formate, total formate, DEA+MAE, and bicine were estimated for all cycling experiments with 7 m MDEA/2 m PZ and are presented in Table 7.12. These products are generally indicative of the rate of oxidation of the solvent, while the PZ derivatives are more indicative of S_N2 substitution reactions in the blend. The product formation rates in cycled 7 m MDEA and 8 m PZ are also presented in the table to allow direct comparisons to be made. The Excel Linest statistics function was applied to a subset of the regressions to establish the average and standard deviation of the linear fit to the product formation rates. All rates presented in Table 7.12 are raw rates and have not been normalized to reactor system residence time.

Table 7.12: Product formation rates in cycling experiments with 7 m MDEA/2 m PZ; including cycled 7 m MDEA, Low-gas degradation of 7 m MDEA/2 m PZ, and cycled 8 m PZ

Expt No.	Solvent	T_{th} °C	Formation Rates (mM/hr)			
			Formate	Total Formate	DEA+MAE	Bicine
OD-9	7 m MDEA/2 m PZ	70	0.03 ± 0.00	0.08 ± 0.00	0.20 ± 0.01	0.04
C-22	7 m MDEA/2 m PZ	90	0.2	0.41	0.39 ± 0.02	0.22
C-33	7 m MDEA/2 m PZ	90	0.03	0.06	0.24 ± 0.01	0.03
C-23	7 m MDEA/2 m PZ	100	0.19	0.41	0.18 ± 0.01	0.22
C-21	7 m MDEA/2 m PZ	120	0.22 ± 0.01	0.48 ± 0.02	3.43 ± 0.25	0.14
C-30	7 m MDEA/2 m PZ	125	0.36	0.86	2.82 ± 0.16	0.39
C-34*	7 m MDEA/2 m PZ	125	0.67	1.49	2.60 ± 0.23	0.43
C-16	8 m PZ	120	0.05	0.13	0	0
C-6	7 m MDEA	120	0.28	0.34	2.12 ± 0.09	0.34

*Acid treated at 0.1 mol H^+/mol alkalinity.

As presented in previous sections, the initial rates of formate and total formate production in the blend are a fraction (~1/3 to 1/10X) the initial rates of DEA+MAE production at most thermal reactor temperatures. The bicine production rate tended to be on the order of that measured for formate. All rates exhibited a clear increase with temperature, but the rates measured in C-22 tended to represent the outliers for each parameter in terms of following a trend of increase with thermal reactor temperature. This result was the same as exhibited by the MDEA, PZ and alkalinity loss rates listed in Table 7.9. As was observed in the Low-gas data, the formate production rate in 7 m MDEA was generally slightly higher than the rate measured in the blend, but the total formate production rate was generally lower in 7 m MDEA. PZ and 1° and 2° amine degradation products in 7 m MDEA/2 m PZ have the ability to form amides, thus increasing the total formate production rate. MDEA, a 3° amine, will not form an amide, so the formation of amides in 7 m MDEA occurs only after the 1° and 2° amines are formed from MDEA degradation.

The rates measured in C-16 wherein 8 m PZ was cycled to 120 °C in the thermal reactor can be compared to both C-6 for 7 m MDEA and C-21 for 7 m MDEA/2 m PZ. 8 m PZ does not form measureable quantities of DEA+MAE or bicine, but will form formate and total formate. In both cases, the rates measured in 8 m PZ were below the rates measured in both other solvents. In terms of formate production, the cycled solvents can be ranked from highest to lowest rate as: 7 m MDEA>7 m MDEA/2 m PZ>8 m PZ. In terms of total formate, the cycled solvents can be ranked from highest to lowest rate as: 7 m MDEA/2 m PZ>7 m MDEA>8 m PZ.

The product formation rates were normalized to residence time in the thermal reactor, as was performed with the amine loss rate data earlier in this chapter. The normalization factor was ~0.35 (1.12/3.4) for all rates estimated in experiments conducted with the original design (C-21, C-22, and C-23). The rates from experiments performed with the redesigned system (C-30, C-33, and C-34) were normalized by dividing by a factor of 0.057. Applying these factors normalized the cycling experimental rates to those collected in the Low-gas reactor (OD-9). The rates were also normalized to the percentage of oxygen in the headspace of the oxidative reactor. In all cycling experiments conducted with the ISDA, the gas mixture was 98% O_2/2% CO_2, and the loss rates measured in these experiments were normalized by dividing the rates by 98 kPa O_2. OD-9 was conducted in the Low-gas reactor with a headspace gas mixture of ~92.5% O_2/7.5% CO_2, and rates from that experiment were normalized by dividing by a factor of 92.5 kPa O_2. The rates normalized to thermal reactor residence time and X1000 are listed in parentheses () in Table 7.13.

Table 7.13: Normalized rates of degradation product formation in cycled 7 m MDEA/2 m PZ; cycling rates normalized to thermal reactor residence time (Initial rate X V_{Tot}/V_{TR})

Expt No.	Solvent	Th Rx Size (L)	T_{th} °C	Formation Rates (mM/hr-kPa O_2) X 1000			
				Formate	Total Formate	DEA+MAE	Bicine
OD-9	7 m MDEA/2 m PZ	-	70	0.3	0.9	2.2	0.4
C-22	7 m MDEA/2 m PZ	1.12	90	5.8	12.0	11.4	6.4
C-33	7 m MDEA/2 m PZ	0.13	90	5.4	10.7	43.0	5.4
C-23	7 m MDEA/2 m PZ	0.13	100	5.5	12.0	5.2	6.4
C-21	7 m MDEA/2 m PZ	1.12	120	6.4	14.0	100.0	4.1
C-30	7 m MDEA/2 m PZ	0.13	125	64.4	154.0	504.8	69.8
C-34*	7 m MDEA/2 m PZ	0.13	125	119.9	266.7	465.4	77.0
C-16	8 m PZ	1.12	120	1.5	3.8	0.0	0.0
C-6	7 m MDEA	1.12	120	8.2	9.9	61.8	9.9

*Acid treated at 0.1 mol H^+/mol alkalinity. Shaded entries for redesigned thermal reactor.

The rates listed in Table 7.13 adhere to a pattern of increasing with an increase in reactor temperature from 70 to 90 °C, but then remain relatively flat when increased from 90 to 120 °C. However, for all degradation products, the increase in the measured rate from a thermal reactor temperature of 120 to 125 °C was generally an order of magnitude, which did not follow the pattern exhibited over the lower temperature range.

The total formate data were plotted as ln(Init $Rate_{norm}$) versus 1/T (K) to allow estimation of activation energy E_a. That plot is presented here as Figure 7.21. The plot reflects the flatness in measured rates over the temperature range of 90 to 120 °C. The normalized rates for total formate production in the acid treated experiment (■) and in the 7 m MDEA experiment (▲) are also included in the plot for comparison. The E_a for total formate production was estimated from the plot as 80 kJ/mol. This same analysis was performed for the other products, and the results for formate, total formate, DEA+MAE, and bicine are tabulated with the initial rates of formation measured at 120 °C in Table 7.14.

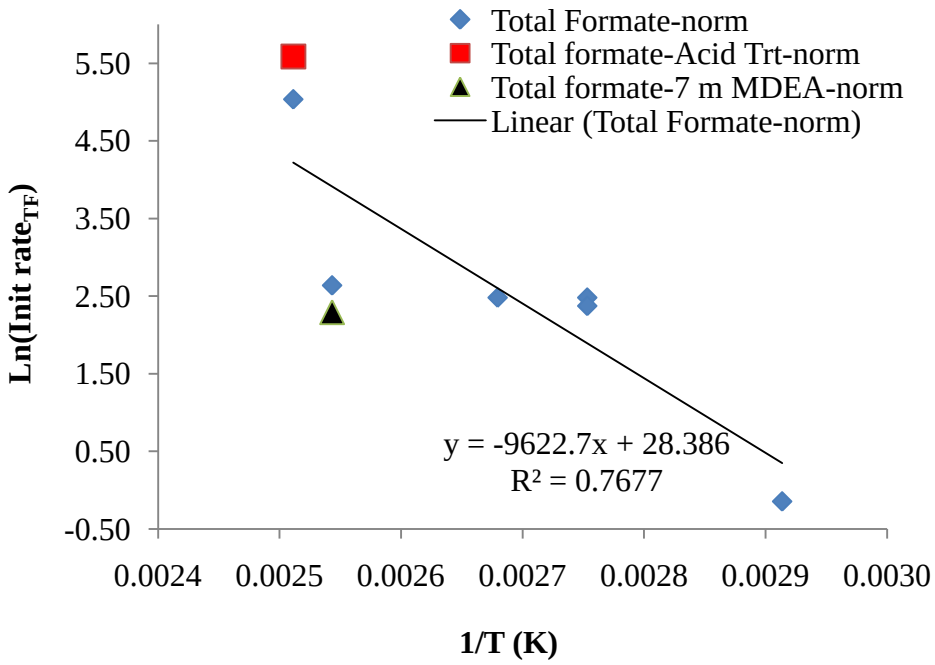

Figure 7.21: Plot of natural log of initial rate of total formate production versus inverse temperature (K); initial rates of total formate production have been normalized to thermal reactor residence time and partial pressure of oxygen in oxidative reactor headspace gas

The rates and activation energies for formate and total formate formation can be compared to those measured in the ISDA with other solvents including 7 m MDEA and 8 m PZ. The raw rates, normalized rates and E_a for formate and total formate measured in the ISDA are provided in Table 7.15. The formate and total formate production rate patterns exhibited by the three solvents have been explained previous to this section, but in general, the blend and 8 m PZ exhibit more amide production than 7 m MDEA due to MDEA being a 3° amine. The activation energies for both products are approximately the same (~80 kJ/mol) in 7 m MDEA/2 m PZ and 8 m PZ, but above the energies estimated in 7 m MDEA (~56-63 kJ/mol). Although the degradation of the blend is initiated predominantly by the protonation of MDEA and PZ, the presence of PZ in the blend alters the activation energy of the blend such that it behaves similar to 8 m PZ.

Table 7.14: Initial rates and activation energies of product formation in cycled 7 m MDEA/2 m PZ at an initial loading of 0.14 mol CO_2/mol alkalinity; initial rates measured at 120 °C, and normalized rates consider thermal reactor residence time

Parameter	Formate	Total formate	DEA+MAE	Bicine
Raw Rates at 120 °C (mM/hr)	0.22	0.48	3.43	0.14
Norm Rates (mM/hr-kPa O_2) X 1000	6.4	14	100	4.1
E_a (kJ/mol)	81	80	96	72

Table 7.15: Comparison of initial rates, normalized initial rates, and E_a for formate and total formate production measured in the ISDA in 7 m MDEA/2 m PZ, 7 m MDEA, and 8 m PZ; initial rates estimated for solvents cycled to 120 °C

Parameter	7 m MDEA/2 m PZ	7 m MDEA	8 m PZ
Init Rate-formate (mM/hr)	0.22 ± 0.01	0.28 ± 0.01	0.046
Norm rate-formate (mM/hr-kPa O_2) X 1000	6.4	-	1.3
E_a-formate (kJ/mol)	81	63	80
Init Rate-total formate (mM/hr)	0.48 ± 0.02	0.34 ± 0.01	0.13
Norm rate-total formate (mM/hr-kPa O_2) X 1000	14	-	3.8
E_a-total formate (kJ/mol)	80	56	81

7.3.5 Comparison/application of 7 m MDEA oxidative model to 7 m MDEA/2 m PZ

It is of interest to compare the 7 m MDEA oxidative model described in Chapter 5 to the degradation rates measured in 7 m MDEA/2 m PZ. In particular, it is useful to be able to predict and utilize the total formate production rate in the blend as was performed with 7 m MDEA. The data necessary to develop a completely separate 7 m MDEA/2 m PZ oxidation model does not exist, but the 7 m MDEA model will serve the purpose of predicting total formate production in the blend.

Recall that the isothermal PFR model developed in Chapter 5 is explicitly defined as follows:

$$\Delta[TF] = \frac{P_{O2} * S * Q * t}{K_H * V_{Tot}} \left(1 - \exp\left(\frac{(k_1(T) * V_{TR})}{Q}\right)\right) \tag{7.16}$$

This equation can be rearranged, with each side divided by a factor of $1/V_{TR}$:

$$\frac{\Delta[TF]}{t} * \frac{V_{Tot}}{V_{TR} * P_{O2}} = \frac{S * Q}{K_H * V_{TR}} \left(1 - \exp\left(\frac{(k_1(T) * V_{TR})}{Q}\right)\right) \tag{7.17}$$

The right-hand side of this equation, which predicts a normalized total formate production rate, can be plotted for the 7 m MDEA model against thermal reactor temperature, assuming a solvent flow rate of 200 mL/min (Figure 7.22). The model prediction was calculated using the converged values of S (0.14), E_a (151 kJ/mol) and k_{363} (3.3 hr^{-1}) from the 7 m MDEA model in Chapter 5 for the large and small reactor designs in the ISDA. The large thermal reactor model prediction is depicted with a dashed blue line, while the small thermal reactor model prediction is depicted with a solid red line.

Based on the knowledge that a solvent system will become oxygen solubility limited at higher temperatures in the ISDA design with the larger thermal reactor, the blue dashed line predicts a decrease in the total formate production rate at a lower temperature than predicted with smaller thermal reactor design. In the smaller thermal reactor, the total formate production rate is maintained in a kinetically limited mode up to much higher temperatures. This analysis serves to confirm the key conclusion related to the redesign of the ISDA and discussed in Chapter 3. In that chapter, it was stated that the redesign of the ISDA to a smaller thermal reactor allowed measurement of degradation rates in a kinetically controlled region of operation as opposed to an oxygen solubility limited region. The total formate production rates measured in the cycling experiments with 7 m MDEA/2 m PZ were plotted using the left-hand side of Equation 7.17, which provides a production rate normalized to reactor residence time and partial

pressure of oxygen. The solid symbols represent the total formate production in the blend in experiments with the larger thermal reactor, while the open symbols represent the total formate production in the blend in experiments with the smaller thermal reactor. The total formate production measured in the Low-gas reactor at 70 °C with 7 m MDEA/2 m PZ is plotted with the black symbol (■). In general, the total formate production in 7 m MDEA/2 m PZ with the larger thermal reactor is predicted well by the 7 m MDEA model at the higher experimental temperatures. However, at the lower temperature of 363.2 K, the measured rate in the blend was ~3X the predicted rate in 7 m MDEA. The total formate production rates measured with the smaller thermal reactor were consistently ~2 to 3X the predicted rates in 7 m MDEA. Finally, the rate measured in the Low-gas reactor at 70 °C (343.2 K) was also ~2 to 3X the rate predicted for 7 m MDEA. From this analysis, a k_{363} for total formate production in 7 m MDEA/2 m PZ can be estimated that is ~3X the value for 7 m MDEA. The rate constant will be 3 X 3.4 hr^{-1}, or ~10 hr^{-1}.

It is useful to relate the production of total formate to a practical limit to oxidation in 7 m MDEA/2 m PZ. This same analysis was performed in Chapter 5 for 7 m MDEA. A dissolved oxygen consumption limit in the piping passing through the heat exchanger and carrying solvent to the top of the stripper provides a good basis for performing this analysis. This limit can be related to a temperature limit for the solvent in this part of an absorber/stripper system. Equation 7.18 is the first-order relationship relating oxygen concentration in and out to the first-order rate constant and residence time. The estimate for k_{363} for total formate in 7 m MDEA/2 m PZ of 10 hr^{-1} was used in the Arrhenius relationship to provide the $k_1(T)$. An assumption was made that the solvent passes through this portion of the system in ~30 seconds for each pass through the system. The upper limit of temperature tolerance at 10, 20 and 50% of dissolved oxygen consumption

was calculated from the corresponding k_1 values returned by the model over the range of temperatures for total formate, and the temperature limits tabulated in Table 7.16.

$$\ln \frac{C_{in}}{C_{out}} = k(T) * t \tag{7.18}$$

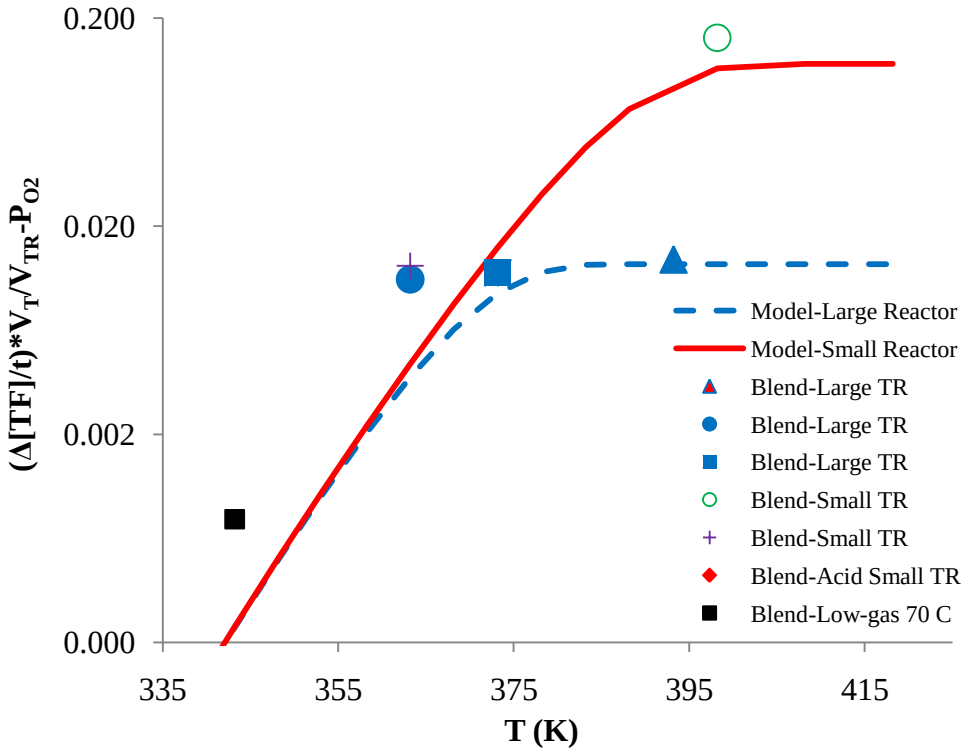

Figure 7.22: Total formate production from 7 m MDEA oxidative model based on isothermal PFR behavior in the ISDA; solid and dashed lines depict 7 m MDEA model predictions with k_{363} = 10 hr^{-1}; filled red symbols depict total formate production in 7 m MDEA/2 m PZ with large thermal reactor; open symbols depict total formate production in 7 m MDEA/2 m PZ with small thermal reactor

The results of the temperature tolerance calculation are provided in Table 7.16 for oxygen consumption levels of 10, 20, and 50% per pass based on 30 seconds of residence time in the high temperature section of absorber/stripper system. The values calculated

for 7 m MDEA (Chapter 5) and 8 m PZ (Chapter 6) are included in the table for comparison. It is unlikely that the 50% oxygen consumption level would be tolerable in an absorber/stripper system due to the demands this would place on solvent reclamation, but the 10% limit represents a realistic level of degradation tolerance. The solvent operation would, therefore, be able to tolerate an upper temperature limit of ~92 °C in the heat exchanger and piping to the stripper based on this analysis.

Table 7.16: Temperature tolerance in heat exchanger and piping based on total formate production at various O_2 consumption levels and τ = 30 seconds

Oxygen Consumed (%)	Temperature (°C)		
	7 m MDEA/2 m PZ	7 m MDEA	8 m PZ
10	92	101	112
20	97	106	123
50	106	115	145

The first-order rate constants for oxygen consumption and conversion of amine (MDEA + PZ) to total formate can be related to overall amine loss, and through an estimate of solvent CO_2 carrying capacity, the amount of amine loss per unit CO_2 captured. As with 7 m MDEA, this analysis was performed based on total formate production at an average temperature of 100 °C and a flue gas oxygen concentration of 5 kPa (5%). Other calculation parameters included the stoichiometric ratio S returned by the oxidative model for total formate (0.14 mol total formate/mol oxygen), a k_1 value of 38.3 hr^{-1} for 100 °C, and an average solvent capacity of 0.75 mol CO_2/kg solvent for the blend. The rate of total formate production was calculated as follows:

$$rate = \left(\frac{38.3}{hr}\right)\left(0.14\frac{mols\,TF}{mols\,O_2}\right)\left(\frac{0.05\,atm\,O_2}{5.45E10^4\,atm\,O_2}\frac{gmol\,O_2}{gmol\,solv}\right)\left(\frac{10^3\,mmol\,TF}{gmol\,TF}\right)\left(34.8\frac{gmol\,solv}{L\,solv}\right)$$

$$rate = 0.17\frac{mmolsTF}{L*hr}$$

Using the calculated rate in terms of moles total formate and an estimate of 7.5 moles MDEA loss per mol total formate formed from the ISDA experiments, we can relate to the CO_2 capture rate per mass solvent:

$$rate = \left(0.17 \frac{mmol\,TF}{L * hr}\right)\left(\frac{kg\,solv}{0.75\,mol\,CO_2}\right)(30s)\left(\frac{hr}{3600\,s}\right)\left(\frac{7.5\,mmol\,Am\,lost/L}{mmol\,TF/L}\right)\left(\frac{L}{1.08\,kg}\right)$$

$$rate = \left(1.32E10^{-2} \frac{mmol\,Am\,Lost}{mol\,CO_2 Captured}\right)\left(\frac{mol\,Am\,Lost}{10^3\,mmol\,Am\,Lost}\right)$$

$$rate = \left(3.4E10^{-6} \frac{mol\,Am\,Lost}{mol\,CO_2 Captured}\right)\left(\frac{1mol\,CO_2}{44\,gm\,CO_2}\right)\left(\frac{454\,gm\,CO_2}{lb\,CO_2}\right)\left(\frac{2000\,lb\,CO_2}{ton\,CO_2}\right)$$

The final calculation provides a rate of 0.27 mol amine lost/ton CO_2 captured, where mol amine accounts for moles MDEA + moles PZ. The capacity estimate of 0.75 mol CO_2 captured/kg solvent is based on a 90% CO_2 removal assumption. For a 500 MW power plant, if 90% CO_2 capture is assumed, the rate of CO_2 capture is estimated to be 1 ton CO_2/MW-hr. At 0.27 mol amine lost/ton CO_2 captured, the amine loss rate is estimated to be ~1.2 X 10^6 mol/year (calculation below), or ~1.3 X 10^5 kg/year.

$$Amine\,Loss = \left(\frac{0.27\,mol\,Am}{ton\,CO_2}\right)\left(\frac{1\,ton\,CO_2}{MW - hr}\right)(500\,MW)\left(\frac{365\,days}{yr}\right)\left(\frac{24\,hr}{day}\right)$$

A summary of the amine loss rates per ton CO_2 captured, and annual amine loss based on a 500 MW power plant operation for 7 m MDEA/2 m PZ, 7 m MDEA, and 8 m PZ is provided in Table 7.17. The amine loss rates for 8 m PZ are the lowest, with 7 m MDEA/2 m PZ and 7 m MDEA providing comparable amine loss.

Table 7.17: Summary of amine loss rates for solvents, assuming a first stage flash of 100 °C, 30 s of residence time at temperature, 5 kPa O_2 in flue gas, 90% CO_2 capture, and a 500 MW power plant

Solvent	Amine loss rate	Annual loss	Annual loss
	gmol amine/ton CO_2	gmol amine/year	Kg amine/year
7 m MDEA/2 m PZ	0.27	1.2×10^6	1.3×10^5
7 m MDEA	0.29	1.3×10^6	1.5×10^5
8 m PZ	0.15	6.7×10^5	5.7×10^4

7.3.6 Mass balance in cycled 7 m MDEA/2 m PZ

A mass balance was performed on endpoint samples of 7 m MDEA/2 m PZ from two cycling experiments. The first experiment is C-21 which entailed cycling the blend from 55 to 120 °C at an initial loading of 0.14 mol CO_2/mol alkalinity. The second experiment is C-34 which entailed cycling the blend from 55 to 125 °C, but at zero CO_2 loading; the solvent was treated with acid at 0.1 mol H^+/mol alkalinity. The similarity in experimental conditions allows the direct comparison of the mass balance data. The mass balance was performed on sample number C-21-15, which was collected after cycling 7 m MDEA/2 m PZ for 570 hours, and C-34-8, which was collected after cycling the acid-treated blend for 353 hours. The results of the mass balance for both samples are tabulated in Table 7.18. The listed numbers represent the percentage of lost carbon or nitrogen loss that the individual products comprise.

The balance demonstrated that a similar mix of compounds was observed in these two samples, with slightly more carbon recovery in the CO_2-loaded solvent (68 vs. 63%), but almost identical nitrogen recovery between the two (59 vs. 60%). DEA+MAE is the product(s) representing the largest percentage of both carbon and nitrogen, at ~27-28% of carbon and nitrogen in both samples. The second largest degradation product in terms of recovery of both carbon and nitrogen was 1-MPZ, at ~8.5-9% of carbon and ~12-13% of

nitrogen. The PZ derivatives represented ~13 and 19% of lost carbon and nitrogen, respectively, in the CO_2-loaded experiment. In the acid-treated experiment, the PZ derivatives represented ~12 and 16.5% of lost carbon and nitrogen, respectively.

The most significant differences in all of the products are the amount of carbon and nitrogen represented by the amino acids bicine and HES. Bicine represented 2X the amount of recovered carbon and nitrogen in the acid-treated experiment when compared to the CO_2-loaded experiment. In contrast, HES represented 3X the amount of recovered carbon and nitrogen in the CO_2-loaded experiment when compared to the acid-treated experiment. These differences are likely caused by a fundamental difference in the way the amino acids are being formed from the degradation intermediates of 7 m MDEA/2 m PZ, which are DEA and MAE. The mass balance comparison demonstrated that DEA+MAE represented approximately the same overall amount of lost carbon and nitrogen (~27%). But the individual amounts of these two products may differ enough to lead to the differences in the amount of carbon and nitrogen the amino acids comprise in the end samples of these two experiments. For example, the CO_2-loaded solvent may degrade in the cycled conditions to a greater proportion of MAE, whereas the acid-treated blend may degrade to a greater proportion of DEA. An oxidation pathway is postulated in Chapter 8 of this dissertation, but also presented here as Figure 7.23. The likelihood of an initial proton abstraction to occur on one of the hydroxyethyl group β-carbons of MDEA in the presence of oxygen and transition metal salts is greater than on the β-carbon of the methyl group. The reasons for this are discussed in Chapter 8, and can be summarized as follows: (1) there are two hydroxyethyl groups as opposed to one methyl group, creating 2X the number of chances for the abstraction to occur, and (2) the adjacent hydrogens on the hydroxyethyl groups will stabilize the formation of a free radical on the hydroxyethyl groups more than can be expected from hydrogens on the

methyl group. The protonation of the solvent through acid addition results in a greater propensity to abstract at the methyl group. The process for formation of bicine from an abstraction of a proton from DEA may be favored by the acidified solvent as opposed to the CO_2-loaded solvent. In general, the results presented in Table 7.18 indicate strong similarities in the mass balance between the two experiments. The differences associated with the amino acid composition are significant enough to lead to different conclusions about how the presence of CO_2 affects the overall degradation of the solvent.

Table 7.18: Mass balance in end samples of 7 m MDEA/2 m PZ cycling experiments (55 to 120 °C) for an initial loading of 0.14 mol CO_2/mol alkalinity (C-21) and 0.1 mol H^+/mol alkalinity (C-34)

Carbon & Nitrogen Balance Comparison - 7 m MDEA/2 m PZ				
Compound	% of C-Loss CO_2 Loaded	% of C-Loss Acid Trt	% of N-Loss CO_2 Loaded	% of N-Loss Acid Trt
DEA + MAE	27.5	26.5	27.5	27.5
1-MPZ	8.4	9.1	11.8	13.3
1,4-DMPZ	0.9	0.9	1	1.1
AEP	3.5	1.2	6.2	2.1
MAE Amide	3.4	3.5	3	3.2
DEA Amide	1.7	1.75	1.2	1.25
Other formyl amides	4	0.5	1.5	2.5
HSS (includes formate)	2.5	1.3	0	0
Bicine	5.3	10.4	3.1	6.3
HES	10.5	3.5	7.5	2.6
Total % =	68	59	63	60

7.4 ENVIRONMENTAL IMPLICATIONS OF 7 m MDEA/2 m PZ DEGRADATION

7 m MDEA/2 m PZ degrades to products which are both volatile and non-volatile. Further, some of these products are precursors to other amine degradation products. It is

helpful to understand the general environmental implications of these degradation products. The best way to perform this analysis is to review the properties the control their fate and transport in the environment. An equally important issue is their toxicity to human and environmental receptors. This section briefly reviews the properties associated with the major degradation products, and is not intended to be a comprehensive review of all environmental issues associated with the deployment of 7 m MDEA/2 m PZ for CO_2 capture purposes.

The principal degradation products of 7 m MDEA/2 m PZ identified in these studies were 2° amines including DEA and MAE, PZ derivative including 1-MPZ, 1,4-DMPZ, AEP, and FPZ, amino acids including bicine and HES, amides of 2° amines, and heat stable salts including formate and acetate. Ureas and oxazolidones were also detected in the solvent, but their true concentrations are as yet unknown. A handful of these products were consistently detected and quantified at a frequency and concentration to make them a concern for this analysis. However, this analysis is best performed by looking at classes of compounds detected in the degraded blend. Those classes include: (1) 1° and 2° amines, (2) PZ and PZ derivatives, (3) amino acids, (4) amides, and (5) heat stable salts. Some of these products are more volatile than others, which to a great extent controls their fate and transport. And some of these products exhibit very little toxicity, diminishing the concern(s) associated with their accumulation in a degraded solvent system.

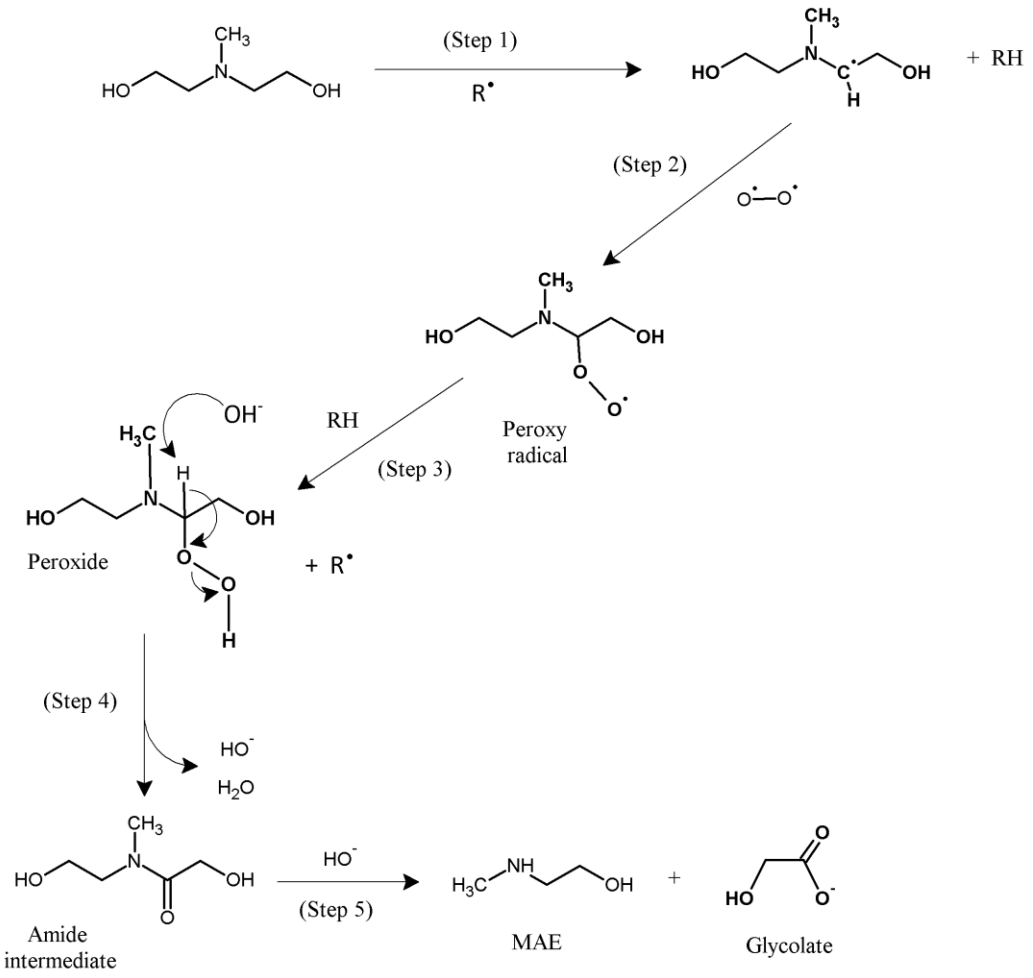

Figure 7.23: Pathway for formation of MAE from oxidation of MDEA in the presence of metal salts and free radicals

A list of the classes of compounds consistently identified in degraded 7 m MDEA/2 m PZ, and the environmental concerns associated with each is provided in Table 7.19. Note that environmental data related to many of these compounds is simply unavailable. For example, of the compounds listed, an Occupational Health and Safety Administration (OSHA) Permissible Exposure Limit (PEL) only exists for DEA and formamide (NIOSH, 2011). None of the compounds has an EPA Maximum Contaminant Level (MCL) for protection of drinking water. The Texas Commission on Environmental

Quality (TCEQ) Total-Soil-Combined standard for remediation of soil following a surface release to land has been included for the two compounds for which a standard was listed (DEA and formic acid). Those data reflect that soil impacted with DEA in an area less than 0.5 acres must be remediated to less than 33 mg/kg, while a release of formic acid would require remediation to a standard of 210 mg/kg. The derivation of a similar Protective Contaminant Level (PCL) for other released alkanolamines would be required by the TCEQ in the state of Texas should they be released to surface or soil or groundwater. The PCL would likely be of the same order of magnitude as the PCL for DEA of 33 mg/kg.

Performing a more in-depth analysis related to any one class or individual compound requires knowledge of the potential release mechanism and released quantity for the compound. For example, the potential environmental concerns associated with DEA are very different for two potential release scenarios: (1) a solvent inventory/storage tank rupture and subsequent release into the surrounding environment including into a major surface waterway containing an endangered species and or drinking water supply, or (2) a amine water wash system failure during active CO_2 capture system operations, resulting in the release of volatiles from the top of an absorber system. In the former case, a number of issues could trigger a major environmental concern including (i) an EPA NPDES discharge permit violation, (ii) exposure of an endangered species to solvent compounds at concentrations that are harmful, and (iii) contamination of a drinking water supply which may be either a surface waterway or a groundwater aquifer. The latter release mechanism could result in exposure of humans in the surrounding area to concentrations of compounds above OSHA PELs, and an air permit discharge violation. Both scenarios have a complex set of parameters which dictate their severity or importance, and an in-depth analysis is beyond the scope of this work.

The accumulation of these degradation products would require that some form of reclamation is implemented on an absorber/stripper system using 7 m MDEA/2 m PZ. From a quick review of the mass balance data listed in Table 7.18, the compounds representing the greatest overall quantity in the cycled blend were DEA+MAE, followed by amino acids and PZ derivatives. DEA+MAE can be reclaimed through vacuum distillation on a slipstream of solvent, while this method is not likely to be effective for the amino acids due to their low volatility. Vacuum distillation will be less effective at removing the PZ derivatives than the 2° amines. In summary, it is likely that the optimal operation of an absorber/stripper system with 7 m MDEA/2 m PZ for CO_2 capture purposes will require a combination of vacuum distillation and another method to remove both the amino acids and heat stable salts such as ion exchange.

7.5 SUMMARY OF 7 m MDEA/2 m PZ DEGRADATION

When 7 m MDEA/2 m PZ was oxidized in the Low-gas reactor, the measured initial rate of degradation, presented as formate production at 55 °C was 0.011 ± 0.002 mM/hr. At 70 °C, the rates of formate and total formate production were 0.031 and 0.075 mM/hr, respectively. The initial rate of formate production in 7 m MEA was 12X the rate measured in the blend. When the blend was augmented with 100 mM Inhibitor A, there was little effect on the initial rate of formate production in the Low-gas reactor. However, the initial rate of amine loss was ~0 mM/hr. In terms of formate production in the Low-gas reactor, the solvents can be ranked from greatest to least as follows: 7 m MEA>7 m MDEA/2 m PZ=7 m MDEA. For total formate production, the solvents can be ranked from greatest to least as follows: 7 m MEA>7 m MDEA/2 m PZ>7 m MDEA.

The degradation products which were quantified at the greatest concentration in the Low-gas reactor (55 to 70 °C) were DEA+MAE, bicine, and total formate.

Table 7.19: Summary of environmental information related to degradation products of 7 m MDEA/2 m PZ; information related to N-formyl PZ substituted with formamide data

Class	Example	Volatile (Y/N)	Toxicity (LD-50) (mg/kg)	OSHA PEL (ppm)	TCEQ* (mg/kg)	Health Effects
1° and 2° amines	DEA	Y	2000	3	33	skin/eye damage
PZ Derivatives	PZ	Y	3800	NA	NA	aquatic impacts
Amino acids	Bicine	N	3750	NA	NA	skin/eye irritant
Amides	Formamide	N	6000	20	NA	skin/eye irritant
Heat Stable Salts	Formate	N	NA	NA	210	NA

*Texas Commission on Environmental Quality Total Soil-Combined std for area <0.5 acres.

Thermal degradation of the blend in the Swagelok® sample cylinders at temperatures ranging from 120 to 150 °C caused a more varied mixture of degradation products including 1° and 2° amines, PZ derivatives, oxazolidones, and products of the reaction of strong nucleophiles such as PZ and oxazolidones. In the absence of CO_2, the blend was generally thermally stable up to 150 °C. However, at a loading of 0.25 mol CO_2/mol alkalinity, the blend experienced 50% PZ loss in 75 days at 150 ^oC, with MDEA and PZ loss rates of 0.17 and 0.24 mM/hr, respectively.

Two thermal degradation models were developed from the body of degradation data with 7 m MDEA/2 m PZ. The first model was based on the Arrhenius relationship for the change in first-order rate constant varying with temperature at a given activation energy. Rate constants for MDEA and PZ loss were estimated based on the thermal degradation data, and using a temperature-normalized time parameter, an average E_a for

both MDEA and PZ loss at each of the two loadings (0.1 and 0.25 mol CO_2/mol alkalinity) was estimated. At a loading of 0.1 mol CO_2/mol alkalinity, the average E_a was 138 kJ/mol, whereas at a loading of 0.25 mol CO_2/mol alkalinity, the average E_a was 95 kJ/mol. This model generally provided a good fit to the measured MDEA concentration in the degraded blend, but did not accurately predict the PZ concentration.

The second thermal degradation model is based on the derivation of a universal E_a for amine loss at all loadings and temperature in the blend. Key underlying assumptions of this model are that the loss of amine in the blend is first-order in [$MDEAH^+$], which is the rate limiting step, and the overall degradation of the blend is independent of [PZ]. The model assumes a relationship between MDEA and PZ loss as S, the stoichiometric factor, which is defined as: S=Init Rate PZ loss/Init Rate MDEA loss. Values for S were calculated from each of the degradation series, and an average was determined (1.13). The thermal degradation data for the blend over the range of experimental loadings and temperatures were normalized by residence time in the thermal reactor and initial loading, and regressed to determine an average E_a, which was 109 kJ/mol. The universal equation for predicting thermal degradation in the blend is expressed as (Equation 7.12):

$$\frac{d[MDEA]}{dt} = k_U(T) * [MDEA]_T * \alpha$$

An expression for $k_U(T)$ was developed as Equation 7.16 and restated here:

$$k_U(T) = k_{408}(1/hr) * exp\left\{-\frac{104{,}300\ J/mol}{8.314\ J/mol-K}\left(\frac{1}{408\ K}-\frac{1}{T_U}\right)\right\}$$

The relationship between MDEA loss and PZ loss can be stated here as follows:

$$\frac{d[PZ]}{dt} = 1.13 k_U(T) * [MDEA]_T * \alpha$$

When 7 m MDEA/2 m PZ was CO_2-loaded and degraded, the product formation trend was characterized by the rapid appearance of 1-MPZ, which quickly dropped off in concentration through the end of the experiment. However, the formation of 1,4-DMPZ slightly lagged the 1-MPZ concentration, but continued to increase in concentration through the end of the experiment, indicating that S_N2 substitution reactions resulting in methyl group switching were continuing to occur in the blend. In contrast to this result, in the acid-treated blend, 1-MPZ rapidly appeared at 150 °C, and leveled off over the remainder of the experiment. 1,4-DMPZ experienced a lag time in formation, but ended the experiment at approximately the same concentration as 1-MPZ (~350 mM). Another key difference was in the formation of DEA+MAE, which continued to increase in concentration in the acid-treated experiment. These contrasting results are attributed to the loss of 2° (DEA and MAE) amines and 1-MPZ in the presence of CO_2 through carbamate polymerization reactions which will not occur with 1,4-DMPZ, and are not possible in the absence of CO_2. The practical and important conclusion from this observation is that the CO_2-loaded solvent is prone to amine loss through carbamate polymerization, with degradation products of the initial amine being incorporated into the loss mechanism(s).

A mass balance was performed on the end sample from a CO_2-loaded solvent thermal degradation experiment at 150 °C, and ~14% of the lost carbon and ~20% of lost nitrogen recovered in the major quantified degradation products. When treated with acid, ~100% of both carbon and nitrogen were recovered in the end sample, with DEA+MAE comprising ~70% of lost carbon and~65% of lost nitrogen.

When 7 m MDEA/2 m PZ was cycled in the ISDA, the major degradation products included the heat stable salts formate, acetate, and oxalate, the PZ derivatives including 1-MPZ, 1,4-DMPZ, AEP, and FPZ, and the amino acids bicine and HES.

Amides other than FPZ observed in the degraded blend included the amide of MAE (N-(2-hydroxyethyl)-N-methyl formamide) and of DEA (N,N-bis-(2-hydroxyethyl) formamide).

The initial rates of loss of MDEA, PZ and alkalinity were combined with data collected from the Low-gas reactor at 70 °C in experiment OD-9, and normalized based on residence time in the thermal reactor for the cycling experiments, and the oxygen content in the headspace purge gas. When plotted together, the E_a for MDEA, PZ and alkalinity loss were estimated at 97, 100, and 98 kJ/mol, respectively.

The common degradation products of 7 m MDEA, 8 m PZ, and the blend include formate and total formate, which includes amides of amine products. The cycled solvents can be ranked from highest to lowest rate for formate production: 7 m MDEA>7 m MDEA/2 m PZ>8 m PZ. In terms of total formate production, the cycled solvents can be ranked from highest to lowest rate as: 7 m MDEA/2 m PZ>7 m MDEA>8 m PZ. The E_a for total formate production in cycled solvents was estimated as ~80 kJ/mol for 7 m MDEA/2 m PZ and 7 m MDEA, reflecting a similarity in degradation behavior due to the presence of PZ in the blend. In 7 m MDEA, the activation energy was ~56 kJ/mol.

A mass balance was performed on the degraded blend when both CO_2-loaded and when treated with acid. The experiments demonstrated that a similar mix of compounds was observed in these two samples, with slightly more carbon recovery in the CO_2-loaded solvent (68 vs. 63%), but similar nitrogen recovery between the two (59 vs. 60%). DEA+MAE represented the largest percentage of both carbon and nitrogen, at 27-28% of carbon and nitrogen in both samples. The PZ derivatives represented ~13 and 19% of lost carbon and nitrogen, respectively, in the CO_2-loaded experiment, while in the acid-treated experiment, the PZ derivatives represented ~12 and 16.5%. Significant differences existed in the amount of carbon and nitrogen represented by the amino acids

bicine and HES. Bicine represented 2X the amount of recovered carbon and nitrogen in the acid-treated experiment when compared to the CO_2-loaded experiment. HES represented 3X the amount of recovered carbon and nitrogen in the CO_2-loaded experiment when compared to the acid-treated experiment. These differences are likely caused by a fundamental difference in the way the amino acids are being formed from the degradation intermediates of 7 m MDEA/2 m PZ, which are DEA and MAE. The CO_2-loaded solvent may degrade in the cycled conditions to a greater proportion of MAE, whereas the acid-treated blend may degrade to a greater proportion of DEA. In general, the results presented in Table 7.18 indicate strong similarities in the mass balance between the two experiments.

The 7 m MDEA oxidation model developed in Chapter 5 was utilized to estimate the upper limit of temperature tolerance in 7 m MDEA/2 m PZ based on total formate production. A dissolved oxygen consumption limit in the piping passing through the heat exchanger and carrying solvent to the top of the stripper provided the basis for this analysis. The limit was related to a temperature limit for the solvent in this part of an absorber/stripper system. The estimate for k_{363} for total formate in 7 m MDEA/2 m PZ of 10 hr^{-1} was used in the Arrhenius relationship to provide the k(T). An assumption was made that the solvent passes through this portion of the system in ~30 seconds for each pass through the system. The upper limit of temperature tolerance at 10, 20 and 50% of dissolved oxygen consumption was calculated from the corresponding k_1 values returned by the model over the range of temperatures for total formate. The calculated temperature limits were 92, 97, and 106 °C for a 10, 20, and 50% oxygen consumption per solvent pass through the system. Those numbers were compared to the values calculated for 7 m MDEA and 8 m PZ using the same assumptions for total formate production. At the 10% oxygen consumption level, the estimated temperatures were 92,

101, and 112 °C for 7 m MDEA/2 m PZ, 7 m MDEA, and 8 m PZ. In terms of an upper limit of temperature tolerance assuming 10% oxygen consumption, the solvents can be ranked from most tolerant to least as follows: 8 m PZ>7 m MDEA=7 m MDEA/2 m PZ.

The first-order rate constants for oxygen consumption and conversion of amine (MDEA + PZ) to total formate can be related to overall amine loss, and through an estimate of solvent CO_2 carrying capacity, the amount of amine loss per unit CO_2 captured. This analysis was performed based on total formate production at an average temperature of 100 °C and a flue gas oxygen concentration of 5 kPa (5%). The final calculation provides a rate of 0.27 mol amine lost/ton CO_2 captured, where mol amine accounts for mol MDEA + mol PZ. This loss rate can be compared to the rate of 0.29 mol amine lost/ton CO_2 captured estimated for 7 m MDEA. For a 500 MW power plant, a solvent capacity for the blend of 0.75 mol CO_2 captured/kg solvent, 90% CO_2 capture, a rate of CO_2 capture of 1 ton CO_2/MW-hr, the amine loss rate is estimated to be ~1.2 X 10^6 mol/year (~1.3 X 10^5 kg/year). For 7 m MDEA and 8 m PZ, the estimated amine loss rates were ~1.3 X 10^6 mol/year and ~6.7 X 10^5 mol/year, respectively, for the same plant size and capture rate.

Chapter 8 - Oxidative Degradation Pathways/Mechanisms

This chapter presents proposed oxidative degradation pathways and mechanisms for 7 m MDEA/2 m PZ based on data collected from degradation of the solvent in the ISDA and the Low-gas oxidative degradation system. The proposed pathways and mechanisms are supported by data collected from the degradation of other solvents including 7 m MDEA, 7 m DEA, and 7 m MAE. Degradation experiments with 7 m MAE and 7 m DEA were also conducted based on preliminary findings that these 2° amines appear in the blend as degradation products, but likely function as reaction intermediates. Key experiments that support the proposed pathways are referenced in this chapter, and are listed in Table 8.1. However, the proposed pathways and mechanisms are generally consistent with all oxidative data collected as part of this research. A separate set of degradation pathways and mechanisms for thermal degradation of 7 m MDEA/2 m PZ is presented in Chapter 9. Note that all experiments discussed in this chapter in support of the proposed pathways and mechanisms were conducted with the stainless steel metals salts added at the beginning of the experiment before degradation occurred. Those salts were added to achieve concentrations of 0.4 mM Fe^{2+}, 0.1 mM Cr^{3+}, and 0.05 mM Ni^{2+}.

A summary of the important oxidative degradation products is first provided. Justification is provided for the effort made to explain the formation of these products through reaction pathways and mechanisms. Additional emphasis is placed on explaining the formation of products such as the 2° amines DEA and MAE, as they are believed to function as both reaction intermediates and end-products in the degraded blend. Their reactivity as intermediates requires added attention.

Pathways and mechanisms for key degradation products are then provided. These pathways were developed based on this work and the work of others (Sexton, 2008, Freeman, 2011), and provide a framework for understanding how 7 m MDEA/2 m PZ degrades. The pathways and mechanisms explain the production of the products identified in Table 8.1, but can also be used to explain the production of other, yet unidentified, products of the blend that fall into the same class of products.

Table 8.1 Experiments used in pathway analysis

Expt No.	Solvent*	Expt Type	Rx T	Purge Gas	Initial CO_2 Loading
			°C	% O_2/% CO_2	mol CO_2/mol alk
OD-6	7 m DEA	Low-gas	55	98/2	0.1
OD-7	7 m MAE	Low-gas	55	98/2	0.1
OD-8	7 m MDEA	Low-gas	70	92.5/7.5	0.1
OD-9	7 m MDEA/2 m PZ	Low-gas	70	92.5/7.5	0.14
C-6	7 m MDEA	ISDA	55/120	98/2	0.1
C-8	7 m MDEA	ISDA	55/120	98 N_2/0 O_2/2 CO_2	0.1
C-16	8 m PZ	ISDA	55/120	98/2	0.32
C-21	7 m MDEA/2 m PZ	ISDA	55/120	98/2	0.14
C-31	7 m MDEA/1 m MAE	ISDA	55/120	98/2	0.13
C-32	7 m MDEA/1 m DEA	ISDA	55/120	98/2	0.125
C-34	7 m MDEA/2 m PZ	ISDA	55/120	98/2	0.1 mol H^+/mol alk

*Stainless steel metals salts addedd to all expts; 0.4 mM Fe, 0.1 mM Cr, 0.05 mM Ni.

The presence of certain degradation products in degraded samples led to the preliminary formulation of reaction pathways, but not necessarily mechanisms. In this chapter, those pathways are described along with supporting data from the oxidative experiments, and proposed mechanisms. Morrison and Boyd (1973) stated the following about reaction mechanisms:

> "It is important for us to know not only *what* happens in a chemical reaction but also *how* it happens, that is, to know not only the *facts* but also the *theory*. ….*the detailed, step-by-step description of a chemical reaction, is called a* **mechanism**. It is only a hypothesis; it is advanced to account for the facts."

The authors go on to state:

> "It would be difficult to say that a mechanism has ever been *proved*. If, however, a mechanism accounts satisfactorily for a wide variety of facts; if we make predictions based upon this mechanism and find these predictions borne out; if the mechanism is consistent with mechanisms for other, related reactions; then the mechanism is said to be *well established*, and it becomes part of the theory of organic chemistry."

Mechanisms have been proposed that explain the presence of some of the key degradation products identified in this work. In some cases, the mechanisms are not completely consistent with the kinetics observed, and an explanation is provided. Note that the findings under thermal degradation conditions are presented in Chapter 9 and demonstrated some overlap in products formed (MAE, DEA, 1-MPZ and 1,4-MDPZ), but the proposed thermal pathways are more dependent on CO_2 as a catalyst for degradation due to protonation of MDEA and carbamate polymerization reactions. The similarity between the reaction mechanisms is generally limited to end-product commonality.

7 m MDEA was degraded extensively in this research in order to develop an understanding of its own pathways and mechanisms. 7 m MDEA generally degrades in the same fashion as when MDEA is combined with 2 m PZ in the 7 m MDEA/2 m PZ blend (Chapters 4 and 6). Because of this similarity, the following discussion reviews 7 m MDEA degradation first. When combined with PZ, the solvent degradation processes include the formation of PZ derivatives. Finally, oxidative degradation of 8 m PZ in the Low-gas system at 55 or 70 °C (Freeman, 2011) or the ISDA (Chapter 6) leads to the formation of very few products. The exceptions include ethylenediamine (EDA), formate, and the amino acid glycine. Of these compounds, EDA was generally not observed in cycled 7 MDEA or 7 m MDEA/2 m PZ, while glycine was observed in very

small amounts relative to other amino acids including hydroxyethyl sarcosine (HES) and bicine.

8.1 OXIDATIVE DEGRADATION PRODUCTS

8.1.1 7 m MDEA

The major oxidative degradation products of 7 m MDEA are listed in Table 8.2 by experiment from which they were identified. OD-6 and OD-7 products are also listed in Table 8.2 because the parent amines in these experiments are degradation products of 7 m MDEA, and their degradation products are directly relevant to the degradation of 7 m MDEA.

Table 8.2 Oxidation products in experiments relevant to 7 m MDEA

Expt No.	Amine	Expt Type	Degradation Product Type			
			Amines	Carboxylate Ions	Amino Acids	Amides
OD-6	7 m DEA	Low-gas	MEA	Formate	Bicine	N,N-bis-(2-hydroxyethyl) formamide
OD-7	7 m MAE	Low-gas	MEA	Formate	Bicine, HES	N-(2-hydroxyethyl)-N-methyl formamide
OD-8	7 m MDEA	Low-gas	MAE, DEA	Formate, Glycolate	Bicine, HES	N,N-bis-(2-hydroxyethyl) formamide, N-(2-hydroxyethyl)-N-methyl formamide
C-6	7 m MDEA	ISDA	MAE, DEA	Formate, Glycolate	Bicine	N,N-bis-(2-hydroxyethyl) formamide, N-(2-hydroxyethyl)-N-methyl formamide
C-8	7 m MDEA	ISDA**	-	Formate	-	Not measured

*Stainless steel metals salts added to all expts; 0.4 mM Fe, 0.1 mM Cr, 0.05 mM Ni.

**ISDA experiment run with N_2 headspace gas to eliminate oxidative degradation.

The major products indicate that pathways for the production of the 1° amine MEA and 2° amines MAE and DEA exist when oxidation of 7 m MDEA occurs. The presence of bicine and HES also indicate that pathways for degradation of MDEA to

these amino acids exist. Because both the amine degradation products and the amino acids were produced in Low-gas experiments at 55 to 70 °C as well as when cycled from 55 to 120 °C+ in the ISDA, the pathways for these products do not necessarily require the presence of heat. The formation of the carboxylate ions including formate and glycolate indicate the generation of carboxylic acids including formic and glycolic acid, although as reviewed in Chapters 4 through 6, the concentrations for these degradation products were generally much lower than for the amines and amino acids. The presence of formyl amides through the hydrolyzation of samples with NaOH was well established (Chapter 4). Morrison and Boyd (1973) explain that:

> "Tertiary amines, although basic, fail to yield amides, presumably because they cannot lose a proton…"

Two amides of 2° amines, N-(2-hydroxyethyl)-N-methyl formamide and N,N-bis-(2-hydroxyethyl) formamide, were identified and their concentrations estimated through synthesis efforts. Their presence confirms that a pathway(s) for the production of formyl amides in 7 m MDEA exist. By analogy, amides of glycolate ions may be formed from 1° and 2° amines due to the presence of the carboxylate ion glycolate in degraded 7 m MDEA. However, these amides were not present in significant concentrations based on measuring a very limited amount of glycolate in solution before and after hydrolyzation of degraded MDEA samples from the Low-gas and cycling reactors.

8.1.2 7 m MDEA/2 m PZ

The important degradation products of 7 m MDEA/2 m PZ are listed in Table 8.3. Lesser important products are also listed in the table, but a mechanism for their generation may not be provided. Because MDEA plays an important role in the degradation of the blend, many of the same products of 7 m MDEA degradation are listed in Table 8.3. In contrast, the presence of EDA in the blend was not observed, but the

amines 1-MPZ, 1,4-DMPZ and AEP were, indicating important differences in the pathways with which the blend degrades when compared to 8 m PZ.

Table 8.3 Important degradation products of 7 m MDEA/2 m PZ

Expt No	Solvent [a] (m)	Expt Type	Degradation Product Type			
			Amines	Carboxylate Ions	Amino Acids	Amides
OD-5 [b]	7 MDEA/ 2 PZ	Low-gas	NM [c]	Formate	NM	NM
OD-9	7 MDEA/ 2 PZ	Low-gas	MAE, DEA	Formate, Glycolate	Bicine, HES	Unidentified formyl amides
C-21	7 MDEA/ 2 PZ	ISDA	MAE, DEA, MPZ, DMPZ, AEP	Formate, Oxalate, Acetate	Bicine, HES	N,N-bis-(2-hydroxyethyl) formamide N-(2-hydroxyethyl)-N-methyl formamide FPZ, and other formyl amides
C-34	7 MDEA/ 2 PZ	ISDA	MAE, DEA, 1-MPZ, 1,4-DMPZ, AEP	Formate, Oxalate, Acetate	Bicine, HES	N,N-bis-(2-hydroxyethyl) formamide N-(2-hydroxyethyl)-N-methyl formamide FPZ, and other formyl amides

[a] Stainless steel metals salts added to all expts; 0.4 mM Fe, 0.1 mM Cr, 0.05 mM Ni.
[b] Solvent augmented with 1 mM Fe^{2+}, 100 mM Inh A instead of stainless steel metals salts.
[c] NM: not measured

The 2° amines MAE and DEA are present in significant quantities in degraded 7 m MDEA/2 m PZ from the Low-gas experiment OD-9. In contrast, these same 2° amines as well as cyclic diamines are present in cycled 7 m MDEA/2 m PZ (C-21 and C-34). The latter difference indicates that 7 m MDEA/2 m PZ likely must reach the higher temperature of the thermal reactor in order to generate the PZ derivatives observed in C-21. For example, in C-22, 7 m MDEA/2 m PZ was cycled from 55 °C in the oxidative reactor to 90 °C in the thermal reactor in the ISDA, and only 1-MPZ was observed at appreciable quantities (~60 mM after 593 hours of cycling). Neither 1,4-DMPZ nor AEP were observed in the blend in that experiment. This observation indicates that a different mechanism may be responsible for the generation of some or all of the PZ derivatives in the degraded blend. The proposed mechanisms must account for this observation.

In contrast, Freeman (2011) observed the presence of EDA, the formyl amide FPZ, oxalate, oxalyl amides, acetyl amides, and NH_4^+ in the Low-gas reactor maintained at 70 °C, but only after augmenting the solvent with 4 mM Cu^{2+} at the start of the

experiment (OE25). When conducting a comparable Low-gas experiment with 8 m PZ at 55 °C and a lean loading of 0.3 mol CO_2/mol alkalinity (OE18), but with the stainless steel metals salts only, the degradation products were primarily formate and total formate, with FPZ, EDA and oxalyl amides not detected. The observation of degradation products limited to carboxylate ions and amides in 8 m PZ at 55 °C indicates that PZ alone is responsible for a limited set of pathways and mechanisms. When blended with MDEA, the possibilities for new pathways expand, as discussed below.

8.2 Oxidation pathways and mechanisms – 1° and 2° amines

The 1° and 2° amines MEA, MAE and DEA have been identified in oxidized 7 m MDEA and 7 m MDEA/2 m PZ. Each of these amines represents the base structure of MDEA, but missing either a methyl group (DEA), an hydroxyethyl group (MAE), or a methyl and an hydroxyethyl group (MEA). This observation provides the foundation for explaining the pathway from MDEA to each of these products. The single carbon associated with the methyl group on MDEA represents one α–carbon with respect to the nitrogen, while the two carbons adjacent to the nitrogen on each of the hydroxyethyl groups also represent α–carbons. Each of the hydroxyethyl groups also has β-carbon (with respect to the nitrogen). In summary, MDEA has three α–carbons, two of which are located in identical positions in terms of adjacent bonds and atoms, and two β-carbons, identical in terms of adjacent atoms and bonds.

In the presence of dissolved salts of transition metals (Fe^{2+}, Cr^{3+}, and Ni^{2+}) dissolved oxygen which behaves as the di-radical di-oxygen ($O^{\bullet}$-$O^{\bullet}$), and free radicals, MDEA will initially go through an electron abstraction process at one of the five carbons. The five carbons on MDEA provide three distinct possibilities for which carbon

experiences the initial electron abstraction (Step 1); one of the three α–carbons which represent two different initial steps, or one of the two β-carbons, which represents only one distinct abstraction. This electron abstraction is a transition to a proton abstraction, resulting in three different free radical forms.

8.2.1 Formation of MAE

The pathway and mechanism for the initial electron abstraction from a hydroxyethyl α–carbon on MDEA, and ultimately the production of MAE and hydroxyl acetaldehyde is presented in Figure 8.1. The initial proton abstraction (Step 1) at one of these two α–carbons is considered to be the more likely abstraction to occur when compared to the methyl group abstraction for several reasons. The first is that two of these carbons exist, providing more opportunity for this abstraction to occur than at the single methyl group α–carbon. The second reason is that the formation of a radical form at this carbon is likely stabilized by electrons associated with the β-hydrogens through the phenomenon known as hyperconjugation. According to Parsons (2000), a methyl group radical is less stable than a primary carbon radical (bonded to at least one R-group). The R-group behaves as an electron-releasing alkyl group exerting a positive inductive effect on the radical. A pair of bonding electrons from the neighboring σ bond can be donated to the partly filled orbital of the radical, creating radical stability. The approximate C-H bond strength for methane is 440 kJ/mol versus 420 kJ/mol for a primary carbon C-H bond, making it slightly more difficult to abstract a methyl group proton. Additionally, Parsons (2000) notes the contribution due to steric crowding. The formation of a radical on the hydroxyethyl group results in a greater release of strain. The hydroxyethyl group represents a more bulky alkyl group than the methyl group, and radical formation at this α–carbon releases more strain.

In Figure 8.1, $R^{\bullet}$ represents a radical in the degraded solvent; note that the pathways presented in the next few figures all generally involve the production of radicals from the initial abstraction of a proton, peroxide radicals and radicals from the decomposition of peroxides. $R^{\bullet}$ represents all of these radicals. The formation of the initial radical in Figure 8.1 is followed by the production of a peroxy radical (Step 2), given the reactivity of the initial radical and the presence of dissolved oxygen in solution. In the aqueous basic environment of the degraded solvent, the peroxy radical will form a peroxide (Step 3) and a radical $R^{\bullet}$, with the peroxide group located on the α–carbon, and a radical. The peroxide form is an alkyl-hydro-peroxide, with the alkyl group bonded to a nitrogen. The hydro-peroxide will decompose (Step 4) through a heterolytic process, providing an oxygen-centered radical, and an $OH^{\cdot}$ radical. As written, Step 4 generates another radical (oxygen-centered) in solution. Step 5 involves the formation of a hemi-aminal from the oxygen-centered radical in the basic solution, and an $R^{\bullet}$. Finally, in Step 6, the hemi-aminal will hydrolyze to MAE and hydroxy acetaldehyde. This step is well understood (King, 2011). The presence of hydroxyl acetaldehyde has not been proven in these studies, but evidence of its existence comes in the form of other products requiring a reactive two-carbon intermediate such as this aldehyde, as presented in Section 8.3 below.

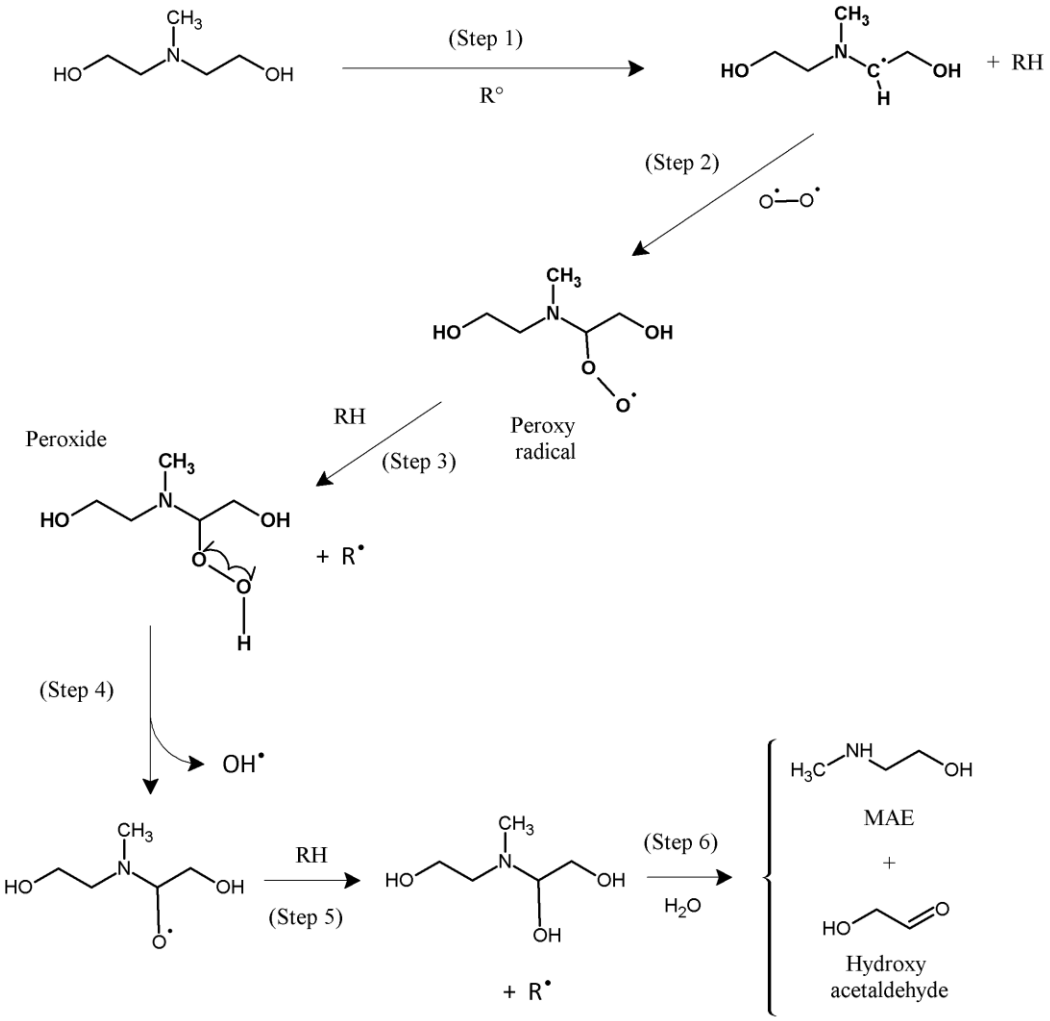

Figure 8.1: Pathway for formation of MAE

An alternative pathway and mechanism for the generation of MAE is presented in Figure 8.2. In that pathway, the basic mechanistic steps for creating the hydro-peroxide intermediate (Steps 1 – 3) are the same, starting with a proton abstraction at the α-carbon on one of the hydroxyethyl groups. Blanskby et al. (2002) demonstrated that alkyl hydro-peroxides will undergo a base-mediated heterolytic decomposition to lose an OH^- group and form a compound with a carbonyl (C═O) bond. However, in Step 4, the peroxide can undergo an internal rearrangement, ultimately resulting in dehydration of the

peroxide (Figure 8.2). Grigoryan (1983) demonstrated that complexes of amines with hydro-peroxides (RO-OH) will form in aqueous solutions, with conjugation occurring between the electrons at the nitrogen atom on the amine and oxygen-oxygen bond on the hydroperoxide. The author recognized the work of others demonstrating that the O-O bond in hydro-peroxides is weakened in amine solutions, with decomposition occurring at temperatures as low as 30 to 40 °C. Step 4 entails the dehydration of the alkyl hydro-peroxide in base solution (presence of hydroxide ion) to form water plus the amide intermediate. Finally, Step 5 involves the hydrolysis of the amide (hydroxyethylmethyl glycolamide) to form MAE and glycolate ion. Under alkaline conditions, hydrolysis involves attack by the strongly nucleophilic hydroxide ion on the amide, resulting in a nucleophilic substitution (Morrison and Boyd, 1973). As listed in Table 8.2 and Table 8.3, MAE and glycolate were detected in degraded 7 m MDEA and 7 m MDEA/2 m PZ. However, the observed concentrations of glycolate in oxidized 7 m MDEA/2 m PZ from Low-gas and cycling studies were relatively low (1/100X) when compared to other heat stable salts such as formate. Given this observation, the second mechanism has less support in the data from this work.

8.2.2 Formation of DEA

A pathway and mechanism for abstraction from the methyl α–carbon is presented in Figure 8.3. This pathway leads to the production of DEA and formaldehyde from MDEA degradation. The formaldehyde will be detectable in solution as the formate ion.

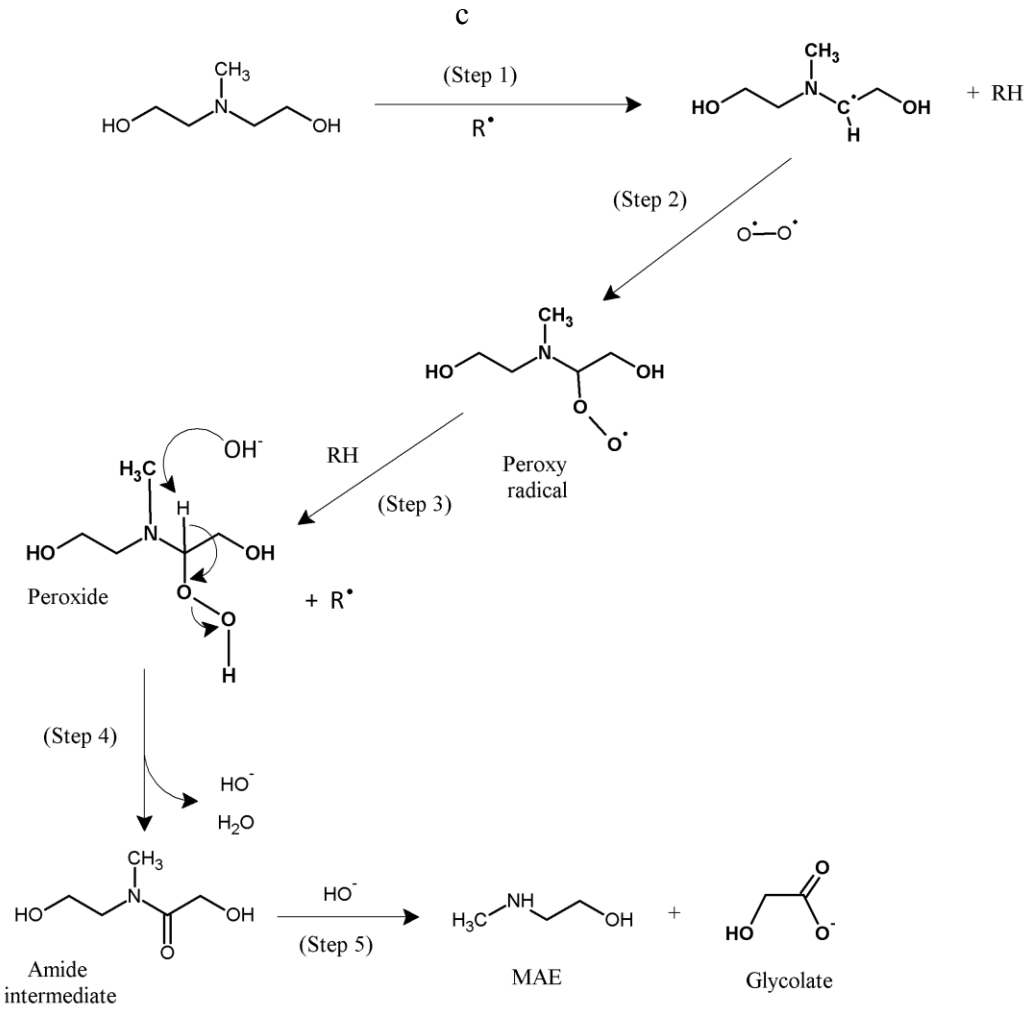

Figure 8.2: Alternative pathway for formation of MAE

Step 1 involves the proton abstraction from the methyl carbon in the presence of transition metal salts and free radicals ($R^{\bullet}$), resulting in the free radical centered on the methyl carbon. As mentioned above, the abstraction (Step 1) at the methyl α–carbon is considered to be less likely to occur when compared to the hydroxyethyl group abstraction. Among other reasons, the radical form at this carbon is characterized by less stability than the more stable α–carbon radicals on the hydroxyethyl groups, which are

stabilized by hyperconjugation of electrons from the β-carbons. However, despite the theoretical limitations associated with this mechanism, the data collected in this research demonstrate that DEA is formed when 7 m MDEA and 7 m MDEA/2 m PZ are oxidized in the Low-gas and the ISDA reactors.

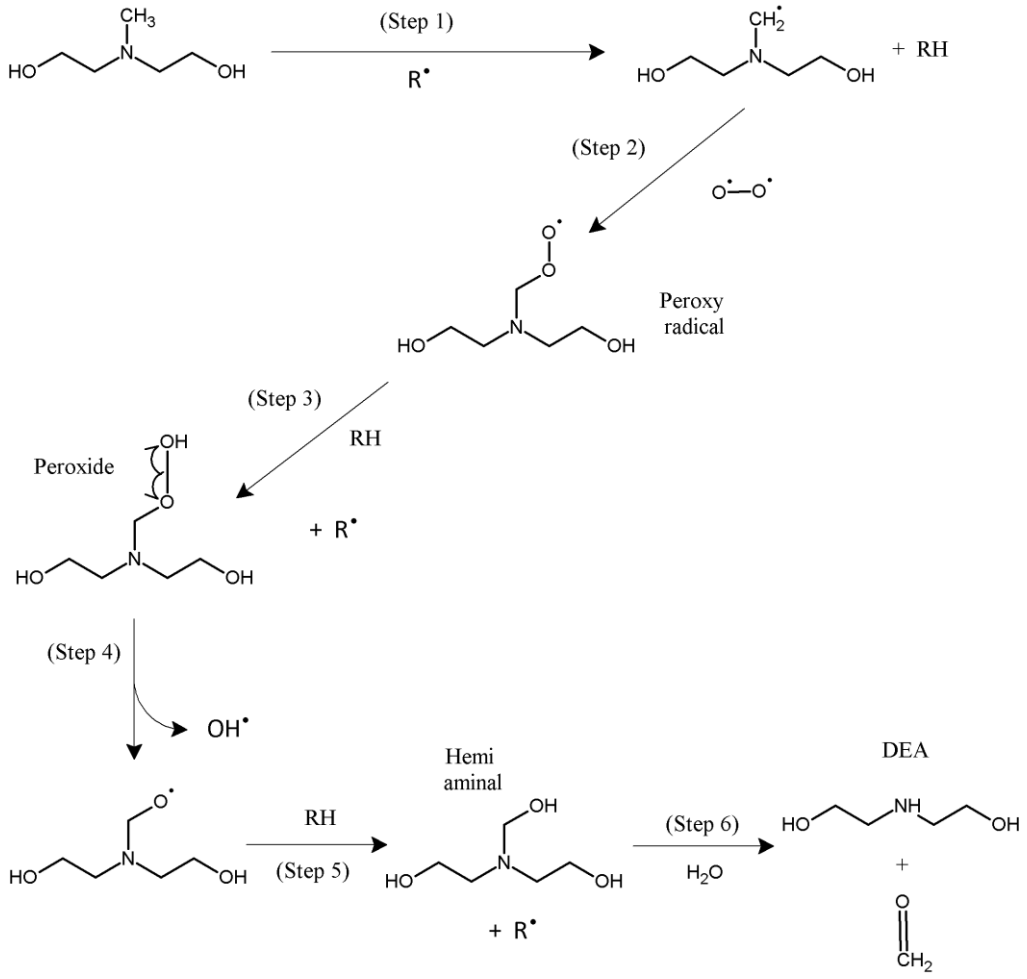

Figure 8.3: Pathway for formation of DEA from oxidation of MDEA

In the presence of dissolved oxygen, a peroxy radical is formed in Step 2. In Step 3, a peroxide and a radical are formed from the peroxy radical in the basic solution, represented as RH. As in section 8.2.1, the peroxide form is an alkyl-hydro-peroxide,

with the alkyl group bonded to a nitrogen. The hydro-peroxide will decompose (Step 4) for the same reasons discussed in section 8.2.1, with decomposition occurring as a heterolytic process, providing an oxygen-centered radical, and an $OH^{\bullet}$ radical. As written, Step 4 generates another radical in solution. Step 5 involves the formation of a hemi-aminal from the oxygen-centered radical in the basic solution, and an $R^{\bullet}$. Finally, in Step 6, the hemi-aminal will hydrolyze to DEA and formaldehyde. This step is well understood (King, 2011). DEA and the formate ion have been identified and measured in degraded 7 m MDEA and 7 m MDEA/2 m PZ. Formaldehyde will readily oxidize in an oxygen-rich environment to formic acid (Morrison and Boyd, 1973), which can be quantified as the anion formate.

The difference between the pathway for degradation to DEA depicted in Figure 8.3 and the pathway for the formation of MAE depicted in Figure 8.1 is the position where the initial electron abstraction takes place (α-carbon on methyl group versus α–carbon on hydroxyethyl group). The differences between the pathway and mechanism in Figure 8.3 and the pathway for MAE production depicted in Figure 8.2 include the position where the initial electron abstraction takes place (α-carbon on methyl group versus α–carbon on hydroxyethyl group), and the mechanism for decomposition of the peroxide intermediate. In the case of MAE production in Figure 8.2, this decomposition involves a heterolytic dehydration and loss of an OH^{-} ion, whereas in the case of DEA production, the peroxide undergoes a homolytic decomposition to form a reactive radical and $OH^{\bullet}$. The important difference in the formation of the two 2° amines is the location at which the electron abstraction takes place, with MAE formation favored as explained in section 8.2.1.

8.2.3 Formation of MEA

A pathway and mechanism for the formation of the 1° amine MEA and hydroxyl acetaldehyde from DEA is presented in Figure 8.4. The pathway involves an initial proton abstraction at the α-carbon on one of the hydroxyethyl groups (Step 1). The abstraction occurs due to the presence of transition metal salts in solution (M^{n+}) and free radicals ($R^{\bullet}$), and results in the formation of a radical. In Step 2, a peroxy radical is formed due to the presence of di-oxygen in solution. In the presence of amine (RH), a hydro-peroxide is formed in Step 3. In Step 4, decomposition of the peroxide occurs as a heterolytic process, providing an oxygen-centered radical, and an $OH^{\bullet}$ radical. Step 5 involves the formation of a hemi-aminal from the oxygen-centered radical in the basic solution, and an $R^{\bullet}$ radical. Finally, in Step 6, the hemi-aminal decomposes into MEA and hydroxy acetaldehyde.

8.3 FORMATION OF AMINO ACIDS

The formation of the amino acids hydroxyethyl sarcosine (HES) and bicine can be explained by similar pathways and mechanisms as those presented in Figure 8.1 through Figure 8.4 for the formation of amine products. The following section provides an explanation of those pathways.

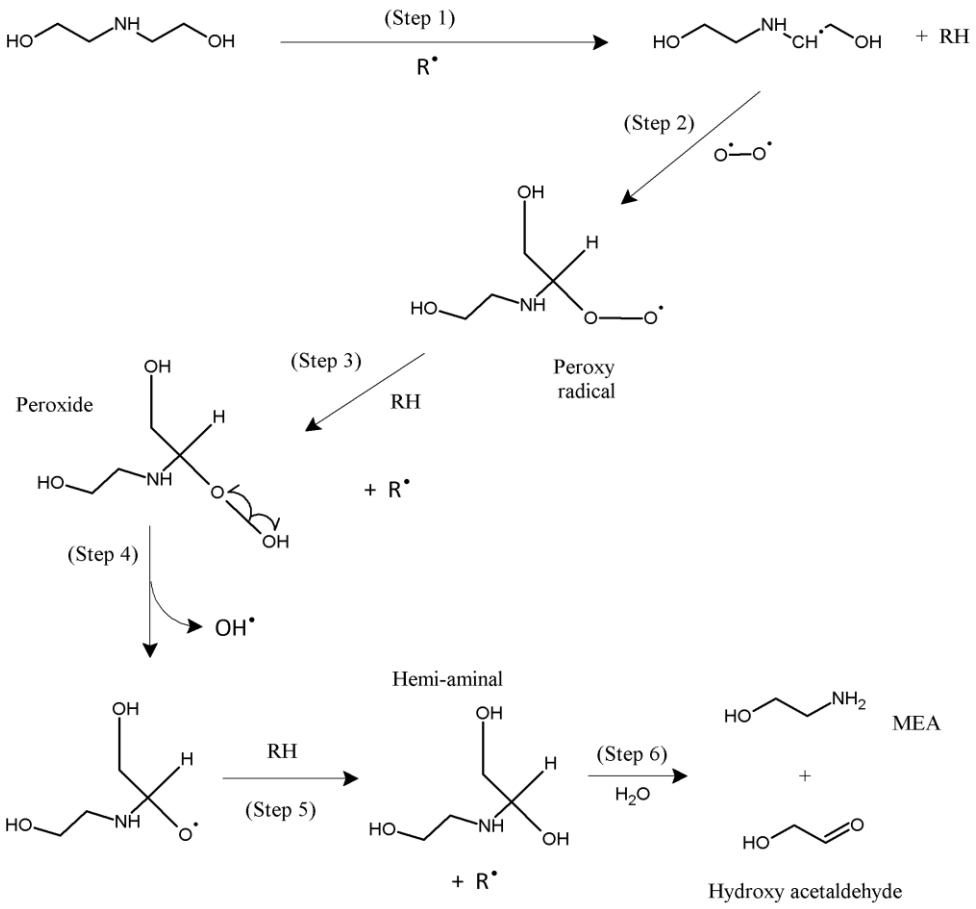

Figure 8.4: Pathway for formation of MEA and hydroxylacetaldehyde from DEA

8.3.1 Formation of hydroxyethyl sarcosine (HES)

The formation of HES can be explained by two different pathways and mechanisms. The first pathway presented in Figure 8.5 involves a nucleophilic substitution reaction between the 2° amine MAE and hydroxyacetaldehyde. Previous pathways have resulted in the formation of hydroxyacetaldehyde, so its presence in degraded solvent is explained. The strong nucleophile MAE will attack the carbonyl (C═O) bond of the aldehyde to form an intermediate; the carbonyl carbon is electron deficient while the carbonyl oxygen is electron-rich and exposed. The important step in a

nucleophilic substitution reaction is the formation of a bond to the electron-deficient (acidic) carbonyl carbon. The carbonyl group is most susceptible to attack by electron-rich, nucleophilic reagents (bases) (Morrison and Boyd, 1973) including 2° amines.

The formation of HES under oxidative conditions occurs in much the same way as MAE, with one important difference. The initial electron abstraction (Step 1) takes place on the β-carbon on either hydroxyethyl group. As with the formation of MAE, two possible β-carbons exist in MDEA, increasing the likelihood that the initial abstraction on a β-carbon will occur. Further, many of the same arguments regarding hyperconjugation and stress release associated with the loss of an H^+ from the α-carbon on each hydroxyethyl group are valid for the β-carbon on the two hydroxyethyl groups. Step 1 results in the formation of an intermediate with adjacent alcohol functionalities, which dehydrates in Step 2 into a tertiary enamine intermediate. Step 3 involves the rearrangement of the enamine form to a tertiary aldehyde. As discussed in Section 8.2, the aldehyde functionality will readily oxidize to a carboxylic acid group. In Step 4, the tertiary aldehyde will oxidize in the presence of dissolved oxygen in a multi-step fashion to form HES. Two arrows in series depict this multi-step oxidation to HES.

The pathway presented in Figure 8.5 is supported by the data from OD-7. In that Low-gas experiment, 7 m MAE was oxidized at 55 °C. HES was formed at over 200X the initial rate measured in all other Low-gas experiments starting with 7 m DEA, 7 m MDEA, and 7 m MDEA/2 m PZ. Starting with MAE in OD-7 eliminated the initial lag period required for MDEA to degrade to MAE under oxidative conditions.

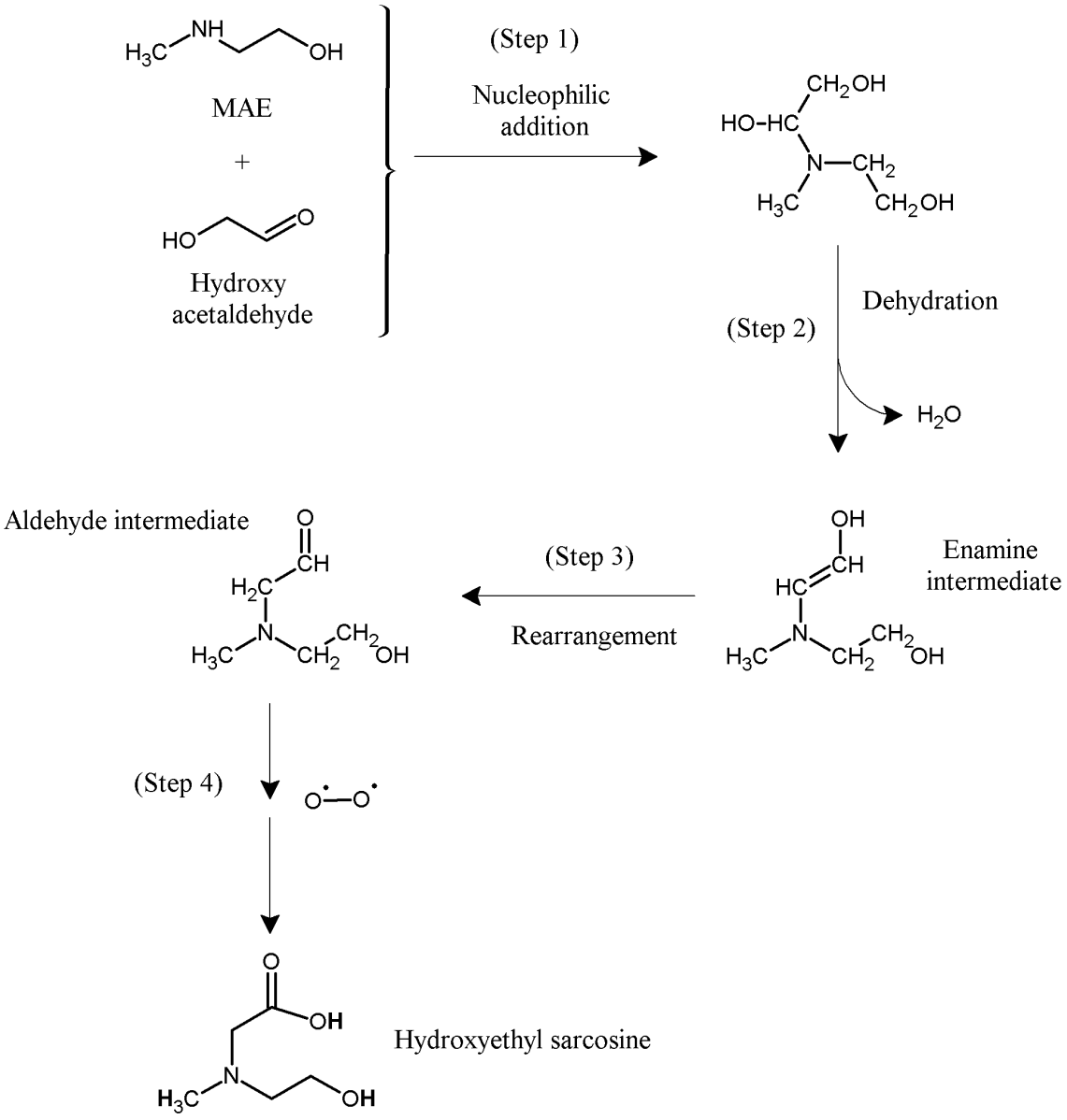

Figure 8.5: Pathway for formation of HES from MAE

An alternative pathway (Figure 8.6) for the production of HES starts with a proton abstraction from the β-carbon of one of the hydroxyethyl groups on MDEA (Step 1). Step 2 involves the formation of a peroxy radical in the presence of dissolved oxygen, which readily forms a peroxide in the presence of amine (Step 3). The peroxide then

rearranges to undergo a dehydration to form the amino acid HES in Step 4. The two key steps that differentiate this pathway from previous ones presented in this chapter are Step 1 which involves the initial proton abstraction at the β-carbon, and Step 4, the base-catalyzed dehydration of the peroxy group leading directly to the carboxylic acid functional group on HES and formation of another OH^- ion.

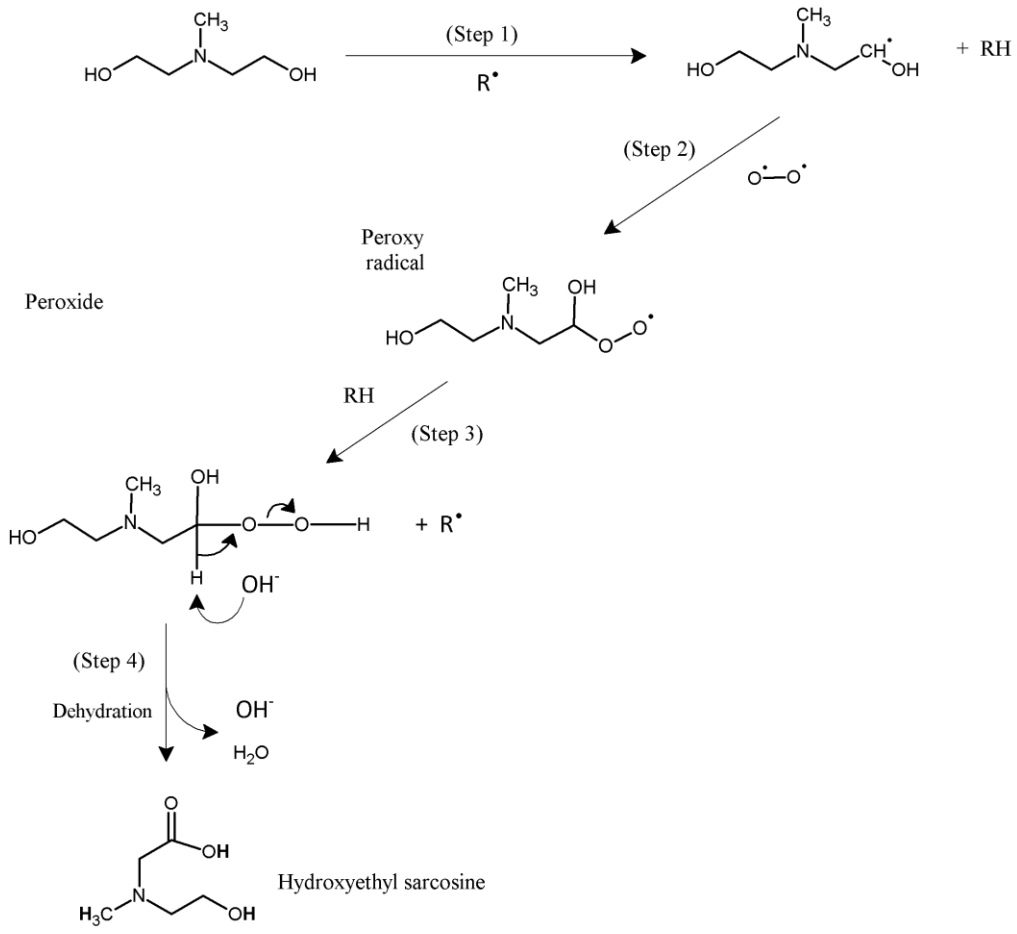

Figure 8.6: Alternative pathway for formation of HES from MDEA

This alternative pathway for the formation of HES is not as well supported by the data collected in this work as the MAE nucleophilic substitution pathway presented in Figure 8.5. For example, in OD-8, which entailed the oxidation of 7 m MDEA at 70 °C

in the Low-gas system, the rate of HES formation was two orders of magnitude less than measured in OD-7 conducted with 7 m MAE at the lower temperature of 55 °C. With all other conditions being the same, including the presence of dissolved metal salts and a purge gas of 92.5% oxygen, the lower temperature in the 7 m MAE Low-gas experiment generated a 100X greater amount of HES than in 7 m MDEA.

One other alternative pathway for the production of HES from MAE involves a pseudo-nucleophilic substitution reaction between the protonated form of oxidized DEA and MAE. In this pathway (Figure 8.7), the electron deficient β-carbon of $DEAH^+$ is attacked by the nucleophilic nitrogen on MAE (Step 2) to form an aminal intermediate by acquiring a methyl group, leaving MEA. The aminal is oxidized in a multi-step fashion (Step 3) to form HES.

8.3.2 Formation of bicine

The amino acid bicine has been identified through an HPLC method utilizing an electrochemical detector in samples from several experiments with both 7 m MDEA and 7 m MDEA/2 m PZ, and its presence has been reported in the literature (Critchfield and Jenkins, 1999) related to degraded/oxidized MDEA from tail gas treating units (TGTUs). A pathway and mechanism for its formation from DEA is proposed in Figure 8.8. Step 1 in this pathway is similar to Step 1 in Figure 8.5 for the formation of HES from MAE, involving a nucleophilic substitution on the carbonyl carbon of hydroxyacetaldehyde, resulting in a tertiary intermediate. The tertiary intermediate, which has three hydroxyethyl groups, one of which has a substituted alcohol group, will dehydrate to a tertiary aminal in Step 2. The aminal will rearrange in Step 3 to a tertiary aldehyde, which will then oxidize in the presence of dissolved oxygen in the solvent to the amino acid bicine.

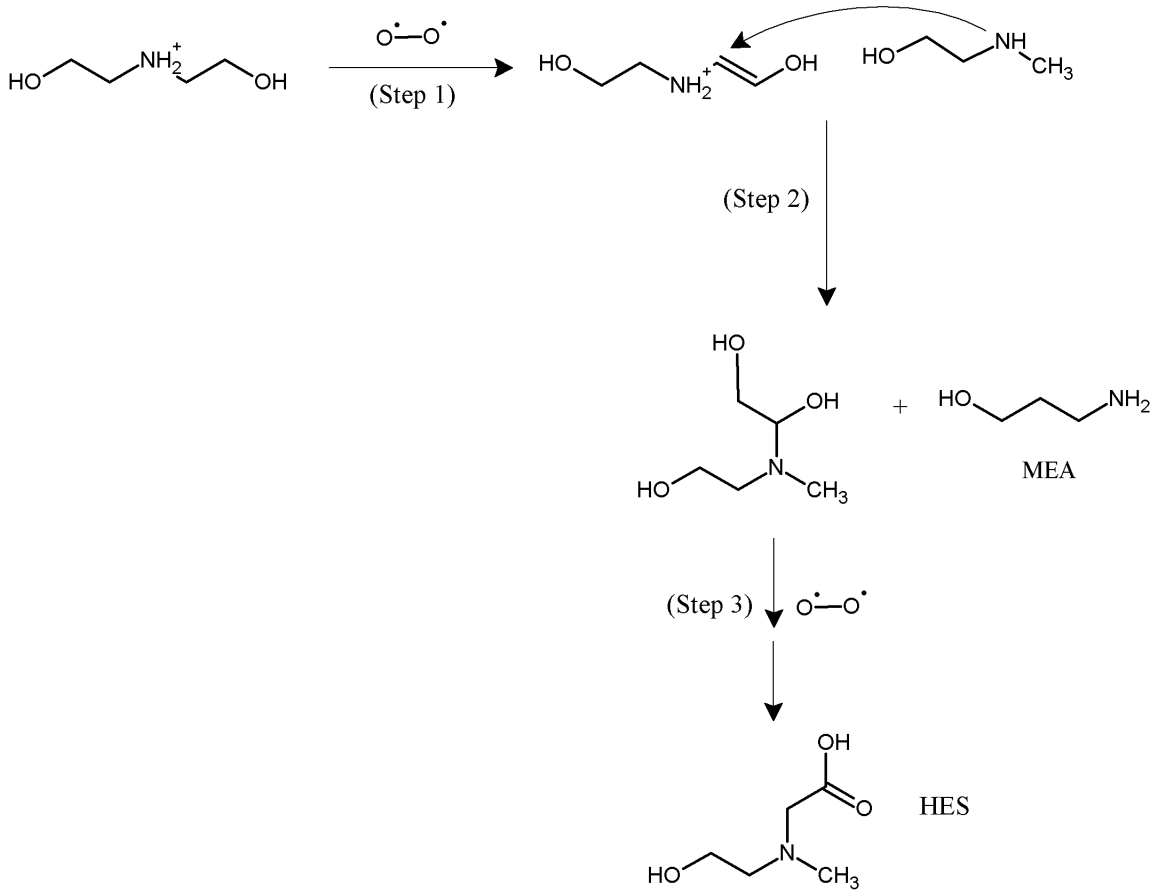

Figure 8.7: Alternative pathway for formation of HES from MAE through nucleophilic substitution at alpha-carbon of oxidized MDEA

Support for the pathway presented in Figure 8.8 comes from the results of Low-gas experiment OD-6 which entailed oxidizing 7 m DEA for 378 hours at 55 °C, resulting in the production of 490 mM bicine. This result is in contrast to the production of only 24 mM bicine in OD-8 which entailed oxidizing 7 m MDEA at 70 °C. The concentration of MDEA, MAE/DEA, and bicine are plotted in Figure 8.9 to demonstrate the lag time in generation of bicine in OD-8. This lag time of 50 to 60 hours of degrading the solvent is necessary to first degrade the MDEA to the 2° amine DEA, which can then undergo the nucleophilic substitution with hydroxyacetaldehyde, and subsequent

oxidation to bicine as depicted in Figure 8.8. There is also evidence of a short lag time in bicine production at the beginning of cycling experiments C-13 and C-26, which entailed cycling 7 m MDEA from 55 °C in the oxidative reactor to 120 and 130 °C, respectively, in the thermal reactor. An in depth discussion of those data is presented in Chapter 4.

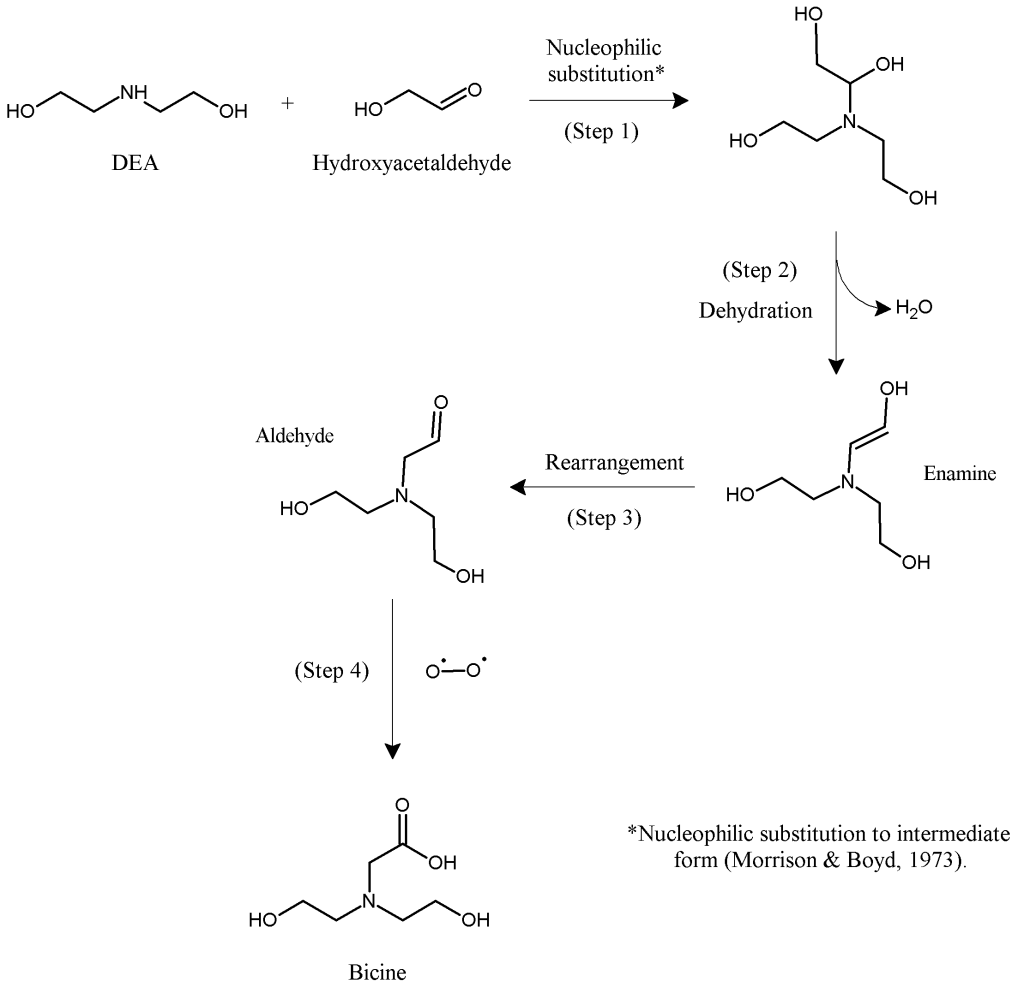

Figure 8.8 Formation of bicine from DEA following a nucleophilic substitution mechanism

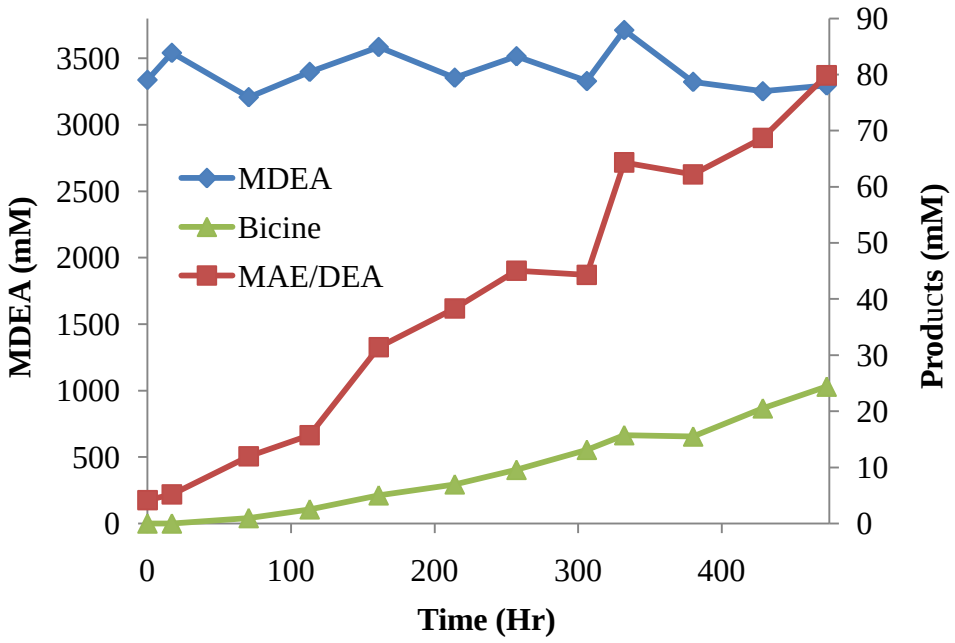

Figure 8.9: Oxidative degradation of 7 m MDEA at 70 °C

8.3.3 Formation of sarcosine

In an analogous fashion to the pathway presented in Figure 8.6 for the production of HES from MDEA, the amino acid sarcosine can be produced from the oxidative degradation of MAE. Like the mechanism presented in Figure 8.6, the initial electron abstraction takes place on the β-carbon of the hydroxyethyl group. Following the H^+ abstraction, the radical form is oxidized by di-oxygen to form the peroxy radical, and the subsequent formation of the hydro-peroxide. Finally, an internal rearrangement and dehydration results in the production of sarcosine. Evidence for this pathway does not exist in the degradation data from this work. A standard for sarcosine was obtained and injected on the HPLC AAA-Direct method, but a matching peak for sarcosine was never identified in degraded 7 m MDEA.

8.4 AMIDE PRODUCTION

As presented by Morrison and Boyd (1973), tertiary amines, although basic, fail to yield amides, presumably because they cannot lose a proton to stabilize the product. However, amides of 1° and 2° amines will form under oxidative conditions. Amides of 2° amines were identified and quantified in degraded samples of 7 m MDEA and 7 m MDEA/2 m PZ. This section presents pathways and mechanisms for the generation of three important amides formed in the degradation of 7 m MDEA/2 m PZ. These amides are N-(2-hydroxyethyl)-N-methyl formamide, an amide formed from MAE, N,N-bis-(2-hydroxyethyl) formamide, an amide formed from DEA, and N-formyl PZ (FPZ). In previous chapters of this document, the reader was introduced to evidence of MAE and DEA in oxidized 7 m MDEA and 7 m MDEA/2 m PZ. Further, in previous sections of this chapter, pathways for the production of MAE and DEA in these solvents have been provided. The proposed pathways for production of amides of these compounds, therefore, start with the respective 2° amines.

All amides of interest are believed to exist in equilibrium with an amine and an arm of degradation of the initial amines in solution. Recall that oxidized amine samples are hydrolyzed with NaOH to reverse the formation of amides in solution, allowing the recovery or quantification of an amine forming the backbone for that amide, and an arm on which the carbonyl carbon exists which is quantified as a carboxylate ion (i.e., formate). Amides exist in equilibrium with PZ and 1° and 2° amines in oxidized 7 m MDEA/2 m PZ, and their concentration depends on the pH of the solution. Some of these have been separated, identified, and quantified with HPLC, and others have not. The pathways presented in this section depict the fact that these amides exist in equilibrium with amines and carboxylate ions.

8.4.1 Pathway for production of N-(2-hydroxyethyl)-N-methyl formamide

The compound N-(2-hydroxyethyl)-N-methyl formamide was identified and quantified in oxidized 7 m MAE, 7 m MDEA, and 7 m MDEA/2 m PZ. This compound was synthesized as described in Chapter 2, and identified with HPLC based on retention time. A pathway for its formation through the oxidation of MAE is presented in Figure 8.10. MAE undergoes a nucleophilic substitution reaction with the carbonyl carbon of the formate ion in Step 1, leading to the generation of an intermediate. In the intermediate molecule, oxygen has accommodated the negative charge. The intermediate undergoes the loss of an hydroxyl ion to form N-(2-hydroxyethyl)-N-methyl formamide in Step 2. Two-way arrows are drawn to convey that the amide of MAE is known to exist in an equilibrium condition with MAE and formate.

In experiment C-34, 7 m MDEA/2 m PZ was treated with 0.1 mol H^+/mol alkalinity before being cycled in the ISDA from 55 to 125 °C. When the samples from that experiment were hydrolyzed with NaOH to reverse the formation of amides, the formate concentration increased by ~2.5X, indicating that protonation of the amine followed by cycling in an oxidizing environment led to the production of amides just as CO_2-loaded amine did. This finding was confirmed through HPLC analysis of samples in which the formyl amides of both MAE and DEA were detected and quantified.

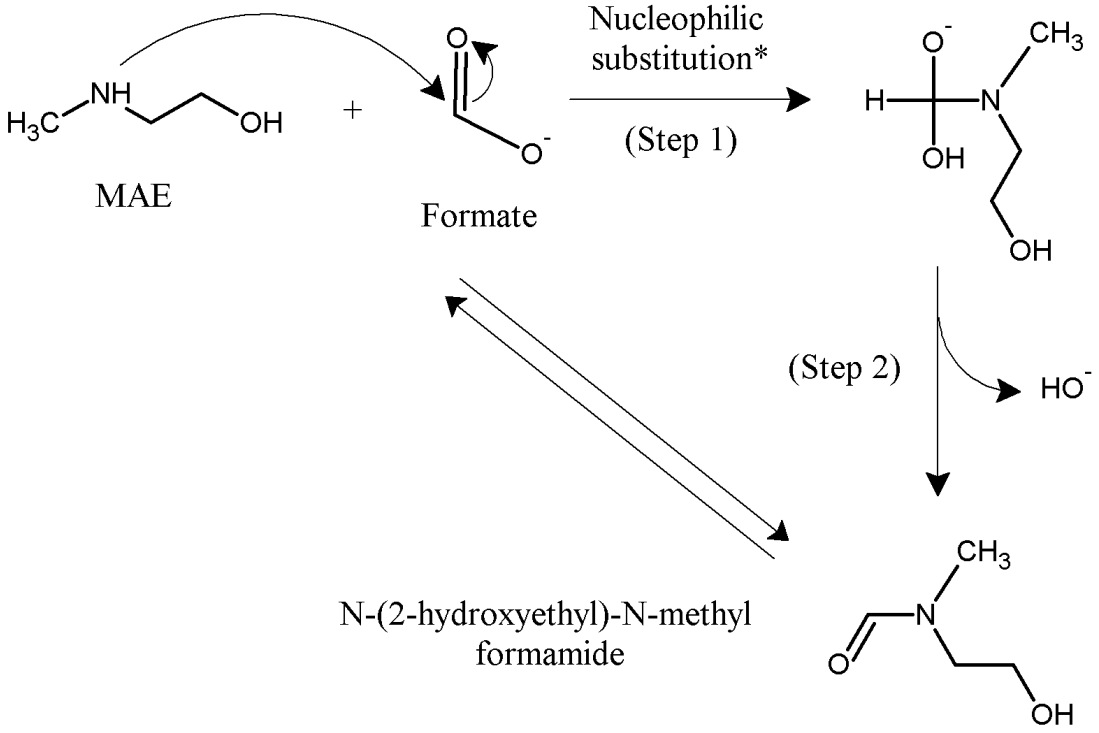

Figure 8.10: Pathway for production of N-(2-hydroxyethyl)-N-methyl formamide

8.4.2 Pathway for production of N,N-bis-(2-hydroxyethyl) formamide

A pathway for the production of N,N-bis-(2-hydroxyethyl) formamide from DEA is presented in Figure 8.11. This pathway starts with DEA, which undergoes a nucleophilic substitution reaction with the carbonyl carbon of the formate ion in Step 1, leading to the generation of the intermediate. As in the pathway presented for the formation of N-(2-hydroxyethyl)-N-methyl formamide, the intermediate loses an hydroxyl ion to form N,N-bis-(2-hydroxyethyl) formamide in Step 2. This pathway is also presented with two-way arrows reflecting the fact that the amide N-(2-hydroxyethyl)-N-methyl formamide is in equilibrium with DEA and formate. As noted above, N-(2-hydroxyethyl)-N-methyl formamide was identified in acid-treated 7 m MDEA/2 m PZ after oxidation in the ISDA (Experiment C-34).

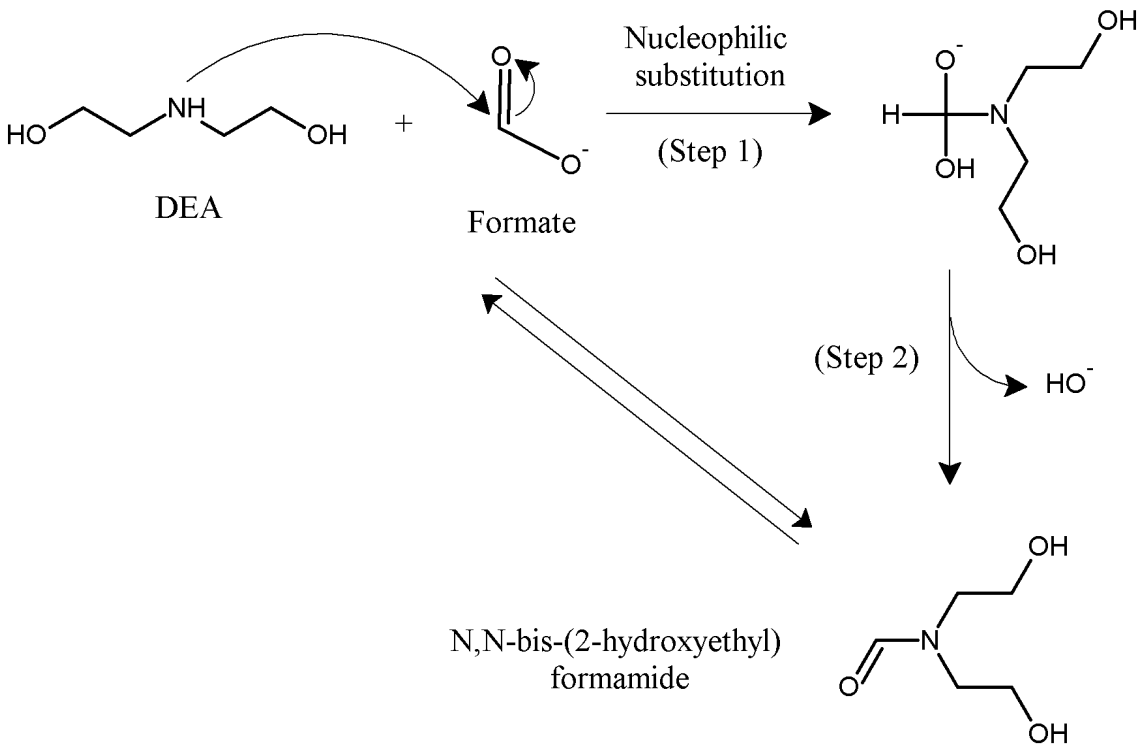

Figure 8.11: Pathway for production of N,N-bis-(2-hydroxyethyl) formamide

8.4.3 Pathway(s) for production of N-formyl PZ

A pathway for the production of FPZ is presented in Figure 8.12. This pathway also assumes that the formation of the formyl amide of PZ is initiated with the protonation of the amine, followed by the nucleophilic substitution reaction to form the intermediate in Step 1. The intermediate then undergoes dehydration in Step 2 to form the amide. Support for this pathway and mechanism lies in the identification of this compound in cycled samples from experiment C-21 using cation IC, GC-MS, and IC-MS analytical methods. The pathway is depicted with two-way arrows reflecting the fact that FPZ exists in equilibrium with PZ and formate in degraded solvent.

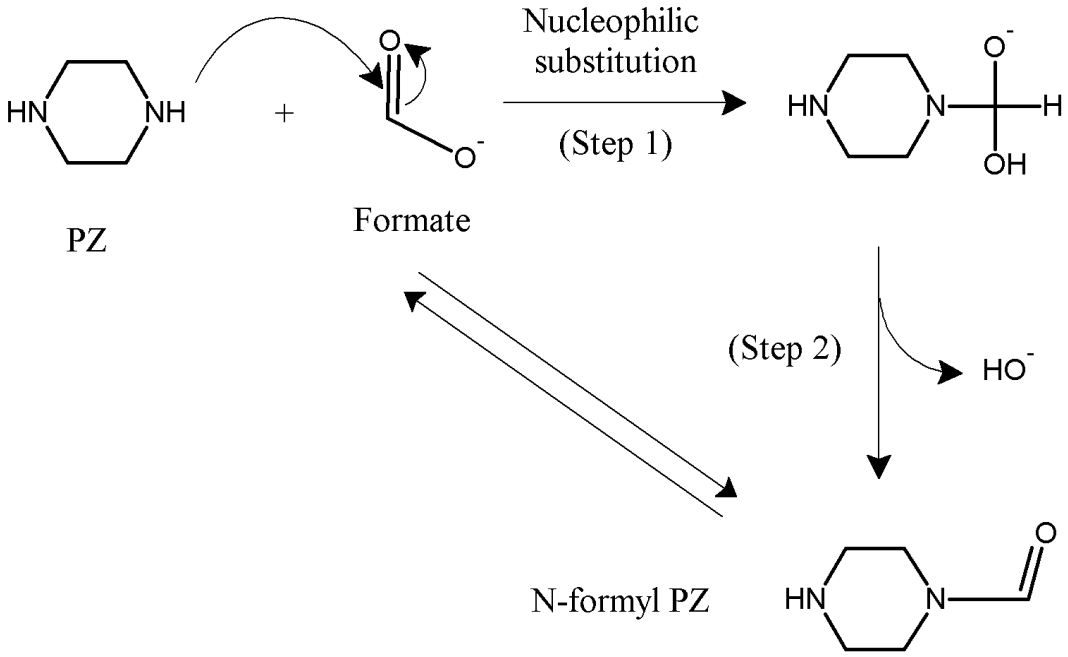

Figure 8.12: Pathway for production of N-formyl PZ in oxidized 7 m MDEA/2 m PZ

An alternate pathway for the formation of the amide of PZ (N-formyl PZ) is depicted in Figure 8.13. That pathway starts with the formation of a hemi-aminal from the reaction of the strong nucleophile PZ at the electron deficient carbonyl carbon of formaldehyde in Step 1, followed by the oxidation of the hemi-aminal to form FPZ in Step 2. This pathway is also depicted with two-way arrows to convey that the FPZ is in equilibrium with PZ and formaldehyde.

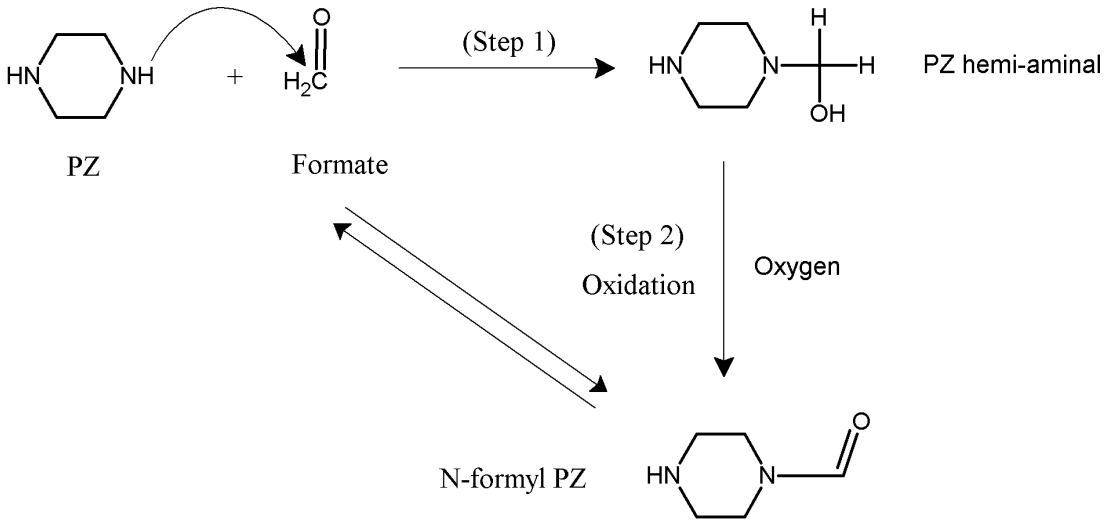

Figure 8.13: Alternate pathway for the formation of N-formyl PZ through initial formation of a hemi-aminal of PZ, followed by oxidation

Amine oxides are synthesized through the reaction of tertiary amines with hydrogen peroxide (Lawrence, 2004). Given the likelihood of having peroxides in the oxidized solvents in the Low-gas and ISDA reactors, the formation of amine oxides from MDEA and other tertiary amines formed in the degradation of 7 m MDEA/2 m PZ is considered a possibility. Amine oxides are usually depicted with a dative covalent bond between the amine nitrogen atom and the oxygen atom with formal positive and negative charges, as depicted on the left-hand side in Figure 8.14. According to Lawrence, the N-O bond has a relatively high dipole moment (4.3D), giving amine oxides their special character. Below pH 3 in aqueous solution, amine oxides exist in cationic form, and are capable of protonation reactions.

Reactions of amine oxides which were considered for degraded 7 m MDEA/2 m PZ include the Cope Elimination for aliphatic amines, the Meissenheimer Rearrangement for aliphatic amines without a β-carbon, and substitution reactions at low pH. The Cope Elimination reaction will occur at temperatures above 90 °C, and results in the

elimination of an arm. If R is an –OH group as would exist in MDEA, the reaction would result in the loss of a hydroxyethyl arm, and the formation of a dialkyl-hydroxylamine. According to White and Woodcock (1968), this reaction has found use in the synthesis of alkenes. No mention was made of this reaction with hydroxyethyl groups, where alcohol group may provide some resonance stability to the β-carbon, thereby preventing this reaction. The Meissenheimer Rearrangement will occur in amine-oxides without a β-carbon at 100 to 200 °C, and is catalyzed by the presence of a strong base. The rearrangement results in the formation of a tri-substituted hydroxylamine. This rearrangement does not result in the loss of an arm, and does not explain arm switching or the presence of many of the degradation products observed in the blend. Substitution reactions with amine-oxides occur from their protonation, and require low pH. Some amine-oxides will stabilize the proton positive charge through resonance, a factor which is greatest with benzylic compounds, then react with strong nucleophiles. In degraded amine solvent systems, the pH is not likely to be acidic, so these reactions are not considered possible.

Another possibility for reaction with an amine-oxide is through direct arm switching with a strong nucleophile under basic conditions. An example of this reaction is presented as Pathway 1 in Figure 8.14, which involves the amine-oxide of MDEA and PZ. The reaction results in the transfer of the methyl group to the PZ to form 1-MPZ, and $MDEAH^+$. If this reaction with the tertiary amine MDEA occurs under the oxidizing conditions of the ISDA, nucleophilic substitution reactions between $MDEAH^+$ and other strong nucleophiles including 1-MPZ, DEA, and MAE can be postulated. The end result of these reactions would be the formation of many of the same reaction products postulated as being formed under S_N2 substitution reactions as presented in Chapter 9. Those products include DEA, MAE, MEA, and the PZ derivatives.

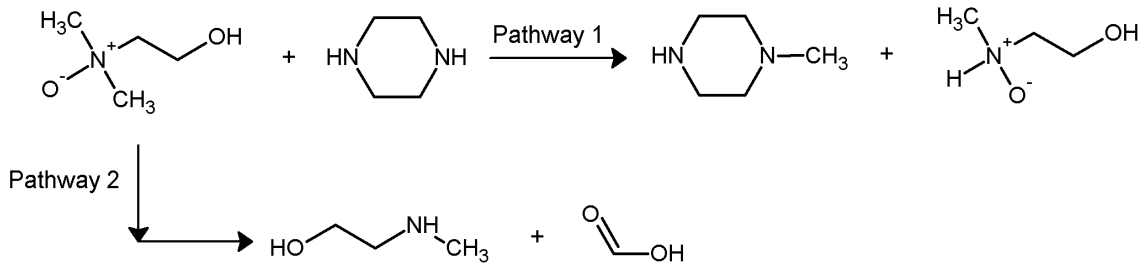

Figure 8.14: Reactions of MDEA amine-oxide: Pathway 1 is nucleophilic substitution with PZ resulting in loss of methyl group and formation of 1-MPZ; Pathway 2 is the direct decomposition of MDEA amine-oxide to form MAE and formic acid

One other possibility is the decomposition of the amine-oxide to form an amine and a carboxylic acid. In Pathway 2 of Figure 8.14, the decomposition of the MDEA oxide to MAE and formate is depicted. This decomposition is very similar to the equilibrium reaction between an amide, and the corresponding amine and carboxylate ion which are formed upon decomposition of the amide through hydrolysis with NaOH. No evidence for this reaction exists in the literature at this time, but one possible explanation is that the MAE and formic acid products represent more stable structures than the aliphatic amine oxide of MDEA.

8.6 PRODUCTION OF FORMATE

The oxidation of 7 m MDEA/2 m PZ leads to the production of formate, as was observed in other solvent systems including 7 m MEA and 7 m MDEA. One explanation for its formation in the Low-gas and cycling environment is the "oxidative fragmentation" mechanism described by Dennis et al (1967) for β-substituted amines. In that work, the oxidative fragmentation of triethylene diamine in the presence of the strong

oxidizing agent perchloryl fluoride leading to the production of PZ and two moles of formaldehyde was described. The authors showed that ethanolamines and diamines can oxidize by fragmentation, or carbon-carbon bond cleavage. In the case of MEA, the imine radical is oxidized to an unstable enamine, which hydrolyzes to two moles of formaldehyde and one mole of ammonia. In the case of triethylene diamine, the first fragmentation led to the loss of two carbons in the form of two formaldehydes, and the production of PZ. The second fragmentation step led to the opening of the PZ ring to form EDA, which oxidized to ammonia and formaldehyde.

The same mechanisms postulated in the work of Dennis and colleagues (1967) may likely explain the production of formaldehyde in oxidized 7 m MDEA/2 m PZ. The step-wise oxidation of hydroxyethyl arms of MDEA, and the opening of the PZ ring could both lead to the production of formaldehyde. The formaldehyde will rapidly oxidize to formic acid in the cycling reactor. The initial oxidation occurs on the α-carbon of one of the hydroxyethyl groups of MDEA to form an aminal structure. The two-carbon arm is then cleaved from the nitrogen, and the carbon-carbon bond itself is cleaved to form two formaldehyde molecules which will oxidize to formic acid in the oxidizing environment of the ISDA.

8.7 SUMMARY OF PATHWAYS

This chapter presented pathways and mechanisms for the production of amines, amino acids, and amides when oxidizing 7 m MDEA/2 m PZ. A summary of the major pathways and mechanisms for the production of these oxidative degradation products is presented in Figure 8.15. Through a proton abstraction step followed by oxidation to form peroxides, 1° and 2° amines, and carboxylate ions can be generated. The

abstraction can also be followed by base-catalyzed rearrangement and the loss of a hydroxyl ion (OH^-) to form an amino acid. The 1° and 2° amines can also participate in nucleophilic substitution reactions with aldehydes followed by dehydration and oxidation to form amino acids. Alternatively, the nucleophilic substitution can be followed by loss of a hydroxyl ion (OH^-) to form an amide.

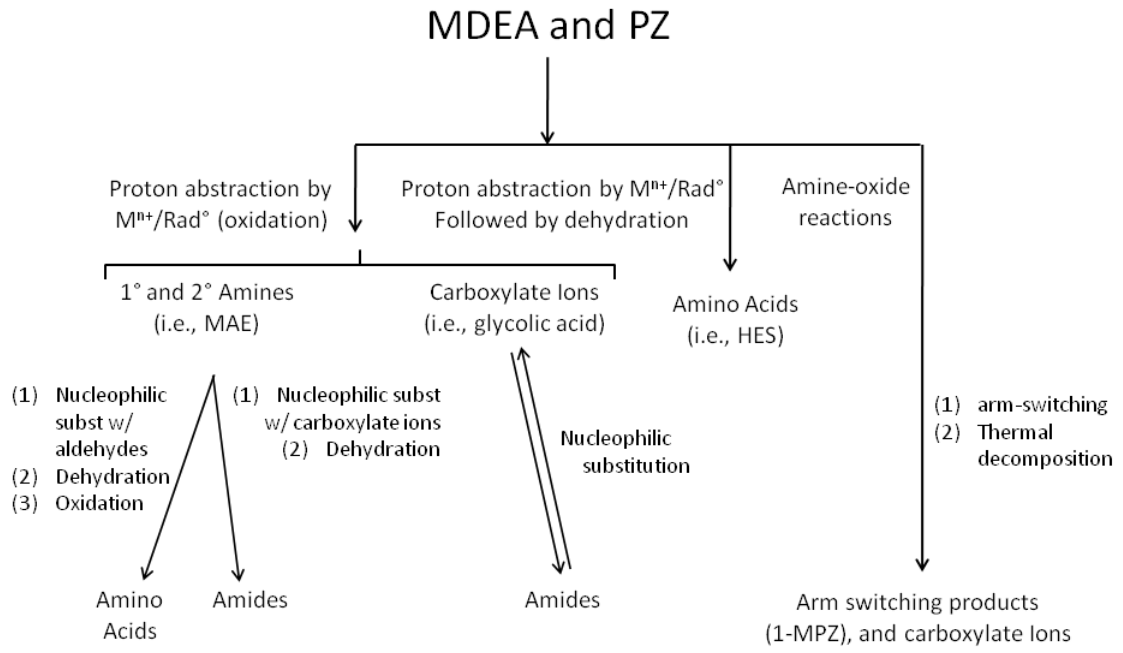

Figure 8.15: Summary of pathways leading to the oxidation of 7 m MDEA/2 m PZ

Note that the PZ derivatives observed in degraded 7 m MDEA/2 m PZ from the ISDA (C-21) are not accounted for in the proton abstraction pathways described in this chapter. Instead, pathways involving the initial formation of amine-oxides from tertiary amines in the presence of peroxides, followed by arm-switching and/or thermal decomposition to lose an arm as an aldehyde, have been postulated. The amine-oxide pathways explain the production of arm-switching products including DEA, MAE and

the PZ derivatives 1-MPZ and 1,4-DMPZ at elevated temperatures (100-120 °C), but do not involve the same S_N2 substitution reactions which explain the formation of these same products under thermal degradation conditions, as reviewed in Chapter 9.

Chapter 9 - Thermal Degradation Pathways/Mechanisms

Thermal degradation pathways and mechanisms for 7 m MDEA/2 m PZ have been developed based on data collected from degradation of the solvent using Swagelok® thermal degradation cylinders and the ISDA. These pathways are presented in this chapter. The proposed pathways and mechanisms are supported by data collected from the degradation of other solvents including 7 m MDEA, 8 m PZ, and blends of each with potential degradation products such as DEA and 1-MPZ.

The information presented in this chapter inherently overlaps and complements the oxidative pathway discussion provided in Chapter 8. The overlap is a result of the production of similar degradation products in cycling experiments with the ISDA and thermal degradation experiments with the Swagelok® thermal degradation cylinders. The vast majority of the cycling experiments were conducted with a high oxygen content (98 kPa) in the headspace purge gas, and at high solvent temperatures in the thermal reactor (≥120 °C). The overlap in products is likely a result of two factors: (1) an overlap in conditions in the ISDA, and (2) similar chemical mechanisms at play as the solvent undergoes degradation. The latter comment is due additional emphasis given that all cycling, Low-gas, and thermal degradation experiments have been conducted with CO_2 loaded solvents. Many of the thermal degradation pathways and mechanisms consider the formation of either a carbamate or protonated amine as an important first step in polymerization mechanisms. For example, Polderman (1956) proposed a pathway for the dehydration of DEA following the formation of DEA-carbamate ($DEACOO^-$) in loaded solutions exposed to heat to form 3-(2-hydroxyethyl) oxazolidone (HEOD). It was

assumed from the outset of conducting ISDA experiments that the formation of DEA and $DEACOO^-$ would lead to the observation of dehydration products such as HEOD.

9.1 REVIEW OF DEGRADATION PRODUCTS

A review of the major products observed in degraded 7 m MDEA and 7 m MDEA/2 m PZ in the Low-gas reactor, the ISDA, and the Swagelok® thermal degradation cylinders is provided in Table 9.1. The products which have been observed in the thermal cylinders and either of the other two degradation systems are listed in red. Several analytical methods have been used to identify degradation products in 7 m MDEA/2 m PZ over several experiments. The criteria for listing a compound in Table 9.1 include: (1) the positive identification of the compound using one or more of the methods described in Chapter 2, with emphasis placed on matches to retention time in ion chromatography or HPLC, and a match to molecular weight with MS, (2) the identification of the compound in multiple samples, and (3) the quantification of the compound at concentrations well above instrument background. Finally, the inclusion of products observed in degraded 7 m MDEA was made based on the observation that nearly all of these products have either been identified in the degraded blend, or are expected to be in the degraded blend.

The more volatile of the products listed in Table 9.1 were identified more frequently in condensate samples collected from the ISDA than in the corresponding liquid samples collected directly from the reactor in each experiment. For example, in some instances, DMAE and MEA were detected at large concentrations in condensate samples, while not being detected above background in reactor samples. An additional analyte, NH_4^+, was sometimes detected in condensate samples while not being detected in

reactor samples. The latter observation is a result of NH_3 evolution and volatilization from the reactor solvent, but condensing in the condensate tube.

Table 9.1: Major products in 7 m MDEA and 7 m MDEA/2 m PZ

Product	MW	Analytical Method(s)	Experiment Type		
			ISDA	Low-gas	Thermal Cylinders
Carboxylate Ions					
Formate		(a)	Y	Y	Y
Acetate		(a)	Y	N	N
Oxalate		(a)	Y	N	N
Glycolate		(a)	N	Y	N
Amines					
MEA	61	(b)	Cond	N	
MAE	75	(b)(e)(f)(g)	Y	Y	Y
DMAE	89	(b)(e)(g)	Y	N	Y
DEA	105	(b)(e)(f)(g)	Y	Y	Y
1-MPZ	100	(b)(e)(g)	Y	N	Y
1,4-DMPZ	114	(b)(e)(g)	Y	N	
AEP	129	(b)(e)(g)	Y	N	Y
Hydroxyethyl PZ (HEP)	130	(b)		N	Y
bis-hydroxyethyl PZ (bHEP)	174	(b)(e)(g)	Y	N	Y
1-(N-methylpiperazine) ethanol	144	(f)(g)	Y	N	Y
1-methyl-4-(2-aminoethyl) PZ	143	(g)		N	Y
Amino Acids					
Bicine	163	(d)(e)(f)(g)	Y	Y	N
Glycine	75	(d)	Y	N	N
HES	133	(d)	Y	Y	N
Amides					
N-(2-hydroxyethyl)-N-methyl formamide	103	(c)(g)	Y	N	P
N,N-bis-(2-hydroxyethyl) formamide	133	(c)(e)	Y	N	P
N-formyl PZ	114	(b)(g)	Y	Y	Y
N-acetyl PZ	128	(c)	Y	N	N
diformyl PZ	142	(c)	N	Y	N
Ureas/Oxazolidones					
3-(2-hydroxyethyl)-2-oxazolidone	131	(f)(g)	Y	NM	Y

Y=Yes, N=No, P=Possible

(a) Anion IC, (b) Cation IC, (c) HPLC, (d) HPLC-AAA, (e) IC-MS, (f) LC-MS, and (g) GC-MS

9.2 SPECIATION IN 7 m MDEA/2 m PZ

An Aspen model for 7 m MDEA/2 m PZ was developed by Frailie (2011) which provides the speciation for this solvent when loaded with CO_2 as shown in Table 9.2.

The species for the loaded solvent are plotted as mol fraction against loading (mol CO_2/mol alkalinity) and previously presented as Figure 2.1. At a lean loading (0.1 mol CO_2/mol alkalinity), the concentration of protonated MDEA ($MDEAH^+$) is ~0.007 mol/mol solvent, whereas the concentration of protonated PZ (PZH^+) is ~0.0085 mol/mol solvent. At the same loading, the free MDEA is ~0.1 mol/mol solvent while the free PZ mol fraction is approximately ~0.01 mol/mol solvent. At a rich loading (0.25 mol CO_2/mol alkalinity), the concentration of $MDEAH^+$ is 0.025 mol/mol solvent, whereas the concentrations of free MDEA and PZ are 0.09 and 0.0015 mol/mol solvent, respectively.

Table 9.2: Speciation in 7 m MDEA/2 m PZ (Frailie, 2011)

Species	Loading (mol CO_2/mol alkalinity)		
	0.1	0.15	0.25
Free MDEA	0.1	0.1	0.09
Free PZ	0.01	0.007	0.0015
$MDEAH^+$	0.007	0.01	0.025
PZH^+	0.0085	0.009	0.0009
$PZCOO^-$	0.006	0.004	0.0007
H^+PZCOO^-	0.003	0.007	0.03
$PZ*MDEAH^+$	0.0000700	0.0000700	0.0000375
$MDEA*MDEAH^+$	0.0007	0.001	0.00225
$(PZ*2+PZCOO^-)(MDEAH^+)$	0.00018	0.00018	0.00009

Three different degradation reaction rate mechanisms were considered in previous chapters when discussing the degradation of 7 m MDEA and 7 m MDEA/2 m PZ. These include the following: (1) rate is first order in [$MDEAH^+$], (2) rate is first order in [MDEA] and first order in [$MDEAH^+$], and (3) rate is first order in [MDEA] and first order in [PZ]. The thermal degradation experiments were limited to initial concentrations of amine 7 m MDEA and 2 m PZ in all cases. Because the initial amine concentrations

were not varied, the experiments do not allow a definitive assessment of the exact order of reaction. However, as explained in Chapter 7, a simple rate model considering first-order behavior in 7 m MDEA/2 m PZ provided a satisfactory fit to the thermal degradation data for the blend. A series of new thermal degradation experiments with 7 m MDEA accompanied by varied starting concentrations of PZ would assist in determining whether the overall reaction order is truly second-order overall.

If the reaction is second order, and varies as [$MDEAH^+$]*[MDEA], the predicted speciation in Table 9.2, suggests that the rate should vary a factor of 2.25 from a 0.1 to 0.25 loading, corresponding exactly to the empirical loading effect reported in Chapter 7. If the reaction actually followed first order dependence on [$MDEAH^+$] as in Equation 9.1, the rate would increase a factor of 3.55 from 0.1 loading to 0.25 loading, somewhat more than the empirical first order dependence on loading. If the kinetics depended on the product of free piperazine concentration and [$MDEAH^+$] ([PZ]*[$MDEAH^+$]), the speciation predicts that the rate would decrease a factor of 2 from 0.1 to 0.25 loading, in contradiction to the observed dependence on CO_2 loading. Therefore, it is most probable that the thermal degradation rate depends on the product, [MDEA]*[$MDEAH^+$].

$$r \cong -k\left[MDEAH^+\right] \tag{9.1}$$

In experiment Th. No. 17, 7 m MDEA/2 m PZ was thermally degraded in Swagelok® sample cylinders at temperatures of 120, 135, and 150 °C. The solvent was augmented with toluenesulfonic acid (TSA), a monoprotic acid with a pK_a of -2.8, at a concentration of 0.1 mol H^+/mol alkalinity. TSA is a strong organic acid which does not have an oxidizing tendency with amines. It is assumed that any interaction with the amines in the blend will be as two-electron transfer mechanisms, resulting in protonation.

At a temperature of 120 °C, the initial loss rates of MDEA and PZ were 0.14 and 0.1 mM/hr, respectively (Figure 9.1). These rates increased to 0.46 and 0.41 mM/hr for MDEA and PZ, respectively, when degraded at 135 °C. At 150 °C, the rates increased to 0.67 and 0.65 mM/hr, confirming that the protonation of the solvent plays an important factor in understanding its degradation.

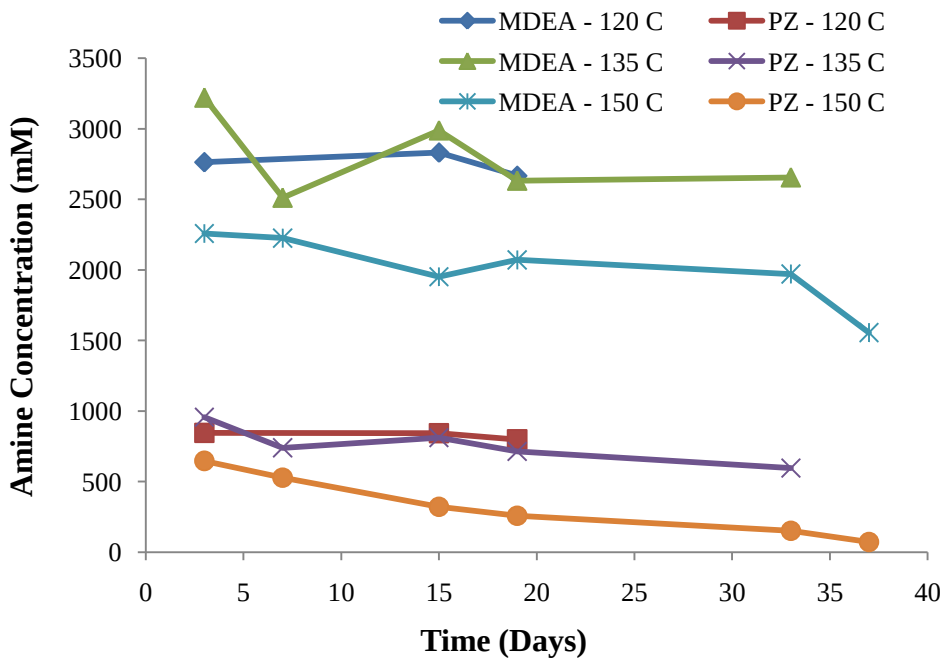

Figure 9.1: Thermally degraded 7 m MDEA/2 m PZ over range of 120 to 150 °C; 0.1 mol H^+/mol alkalinity (as TSA), no CO_2 loading

9.3 THERMAL DEGRADATION PATHWAYS AND MECHANISMS

This section introduces the proposed thermal degradation pathways and mechanisms for 7 m MDEA/2 m PZ. The purpose is to explain the pathways and mechanisms of formation for major degradation products not formed through the oxidative pathways reviewed in Chapter 8. In particular, the oxidative pathways did not

provide a basis for forming PZ derivatives including 1-MPZ, 1,4-DMPZ, AEP, HEP, bHEP, 1-(N-methylpiperazine)ethanol, and 1-methyl-4-(2-aminoethyl) PZ. FPZ is an amide of PZ, and a pathway for its formation was provided in section 8.4.3. The generally accepted pathway and mechanism (Polderman, 1956) for the formation of 3-(2-hydroxyethyl)oxazolidone (HEOD) from DEA is also reviewed in this section, as it provides the basis for understanding how other degradation products are formed in the blend.

9.3.1 S_N2 Substitution reactions

Substitution reactions between nucleophiles and protonated or quaternary amines can generally follow S_N2 reaction mechanisms. According to Morrison and Boyd (1973), S_N2 is a term for substitution nucleophilic bimolecular; the term bimolecular refers to the rate determining step which involves collision of two particles. These reactions generally follow second-order kinetics. As explained in Chapter 7, the reaction order for thermal degradation was adequately modeled considering first-order ($[MDEAH^+]$) behavior. Despite this result from a rate modeling standpoint, S_N2 substitution reactions do provide a basis for understanding the types of reactions that prevail in 7 m MDEA/2 m PZ.

Reactivity in S_N2 reactions is generally diminished by steric effects, including crowding caused by alkyl groups attached to the carbon at which the substitution is occurring. The same argument applies to S_N2 reactions centered at an α-nitrogen of an amine. Solomons (1992) states that simple alkyl halides show the following general order of reactivity in S_N2 reactions: methyl>primary>secondary>tertiary. The author goes on to state:

> "An S_N2 reaction requires an approach by the nucleophile to a distance within bonding range of the carbon atom bearing the leaving group. Because of this, bulky substituents at or *near* the carbon atom have a dramatic inhibiting effect…"

A stronger base will generally exhibit stronger nucleophilic activity towards the substrate. In the case of the MDEA/PZ blend, we can expect that free PZ will behave as the stronger nucleophile than MDEA to the surrounding substrate, including $MDEAH^+$. However, in the case of diminished free PZ concentration, which occurs as loading increases above 0.25 mol CO_2/mol alkalinity, free MDEA would serve as the nucleophile in solution, thus participating in the nucleophilic substitution reaction (arm switching). This propensity for MDEA to serve as the nucleophile would clearly be the primary mechanism for degradation in 7 m MDEA.

9.3.1.1 Pathway for loss of arm from quaternary amine

Bedell et al., (2010) demonstrated that MDEA systems will form quaternary amines when exposed to temperatures of 140 °C+ in stainless steel degradation cylinders, and that these quaternary amines will participate in S_N2 substitution reactions just as $MDEAH^+$ is believed to (Figure 9.2). Given this mechanism, the formation of multiple products can be explained mechanistically including DEA, TEA, and DMEA. Further, the mechanism results in the creation of a quaternary amine which can continue to propagate the S_N2 substitution process. Further, in 7 m MDEA/2 m PZ, other amines can participate in the S_N2 substitution process (Steps 1 and 3), resulting in a loss of starting amines (MDEA and PZ) and amines other than the starting amine products. For example, in Figure 9.3, the concentration of the PZ derivatives 1-MPZ, 1,4-DMPZ, and AEP collected from a thermal degradation experiment (Th. No. 16) conducted at 150 °C with the 7 m MDEA/2 m PZ are plotted against MDEA and PZ concentration. The data demonstrate the formation of the PZ derivative 1-MPZ, with subsequent loss as the experiment proceeds. However, the concentration of 1,4-DMPZ continues to increase throughout the experiment. These results are consistent with the participation of amine

products with nucleophilic behavior (1-MPZ) participating in further arm switching to other products (1,4-DMPZ) as degradation proceeds.

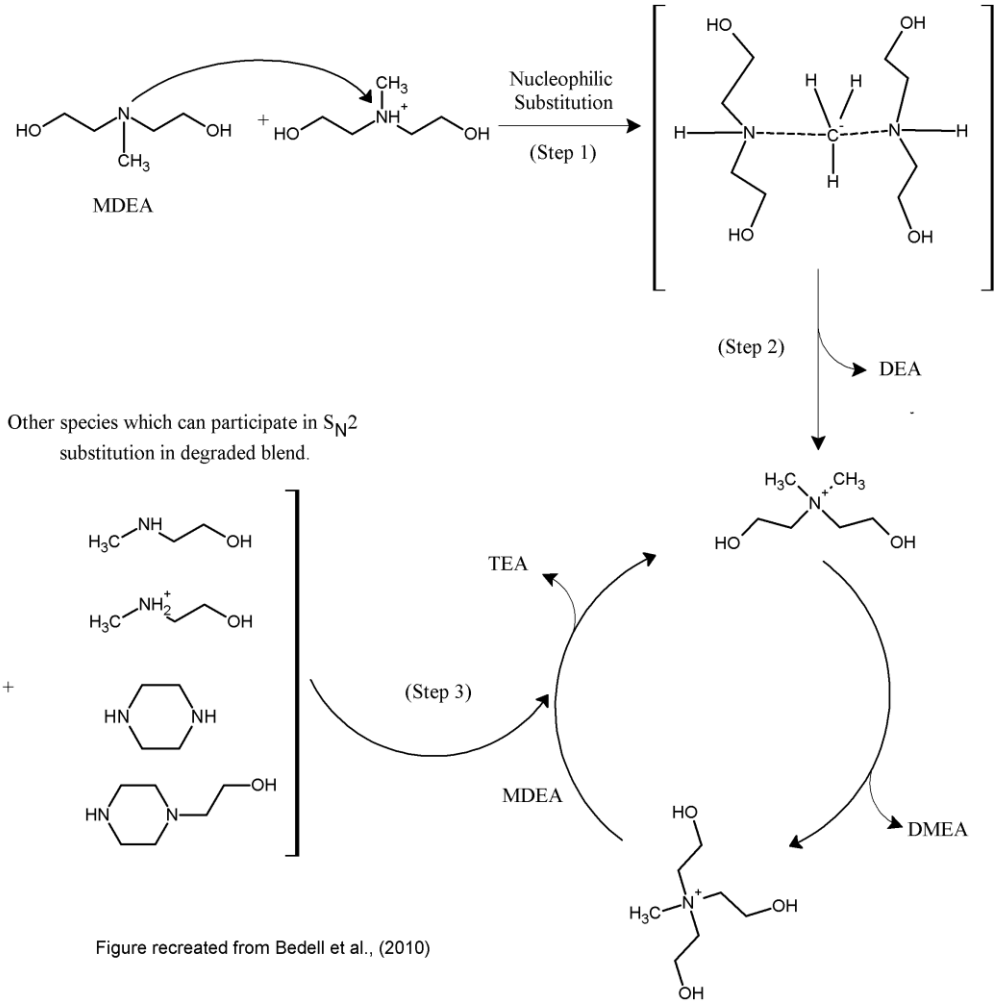

Figure 9.2 S_N2 substitution pathway and mechanism for arm switching between MDEA and $MDEAH^+$ in CO_2 loaded solutions of 7 m MDEA and blend; figure of Bedell (2010) adapted for blend

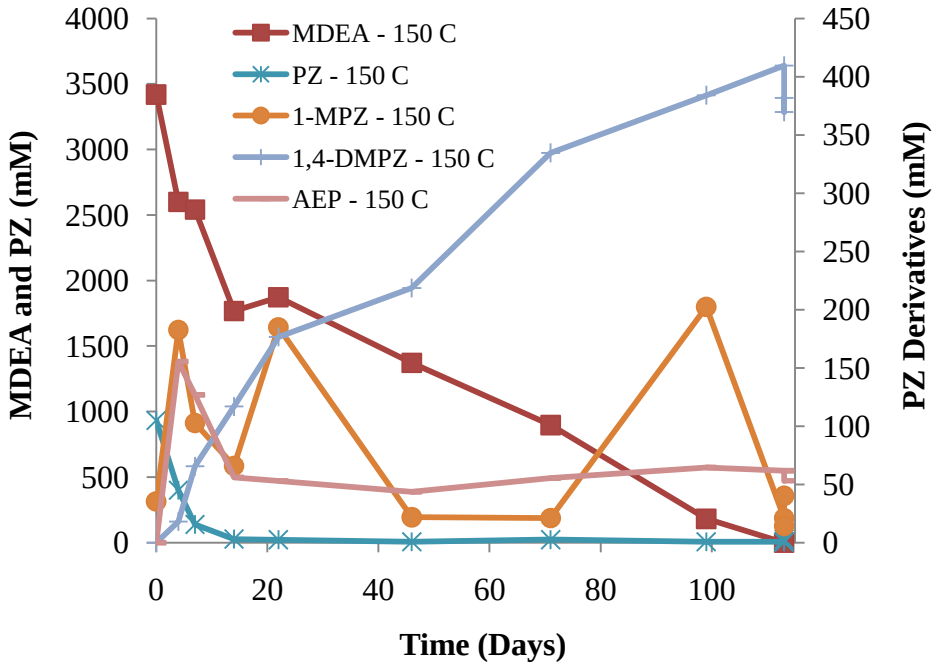

Figure 9.3: PZ derivatives in thermally degraded (150 °C) 7 m MDEA/2 m PZ; initial loading = 0.25 mol CO_2/mol alkalinity

9.3.1.2 Pathway for loss of methyl group from MDEA

A proposed pathway and S_N2 mechanism for the reaction between $MDEAH^+$ and PZ is presented in Figure 9.4. In Step 1 of the pathway, MDEA is protonated to form $MDEAH^+$. In Step 2, PZ behaves as a strong nucleophile, attacking the methyl group of $MDEAH^+$ to form the transition state noted in brackets; the transition state lasts the time required to undergo one molecular vibration (10^{-12} s) (Solomons, 1992). As presented, the "leaving group" in the mechanism is protonated DEA ($DEAH^+$). Because the transition state includes both nucleophile (PZ) and the substrate ($MDEAH^+$), the mechanism has second-order reaction kinetics. This mechanism can be repeated with $DEAH^+$ and PZ to remove an hydroxyethyl group and form HEP and MEA. A discussion related to the hydroxyethyl group behaving as a leaving group is presented below.

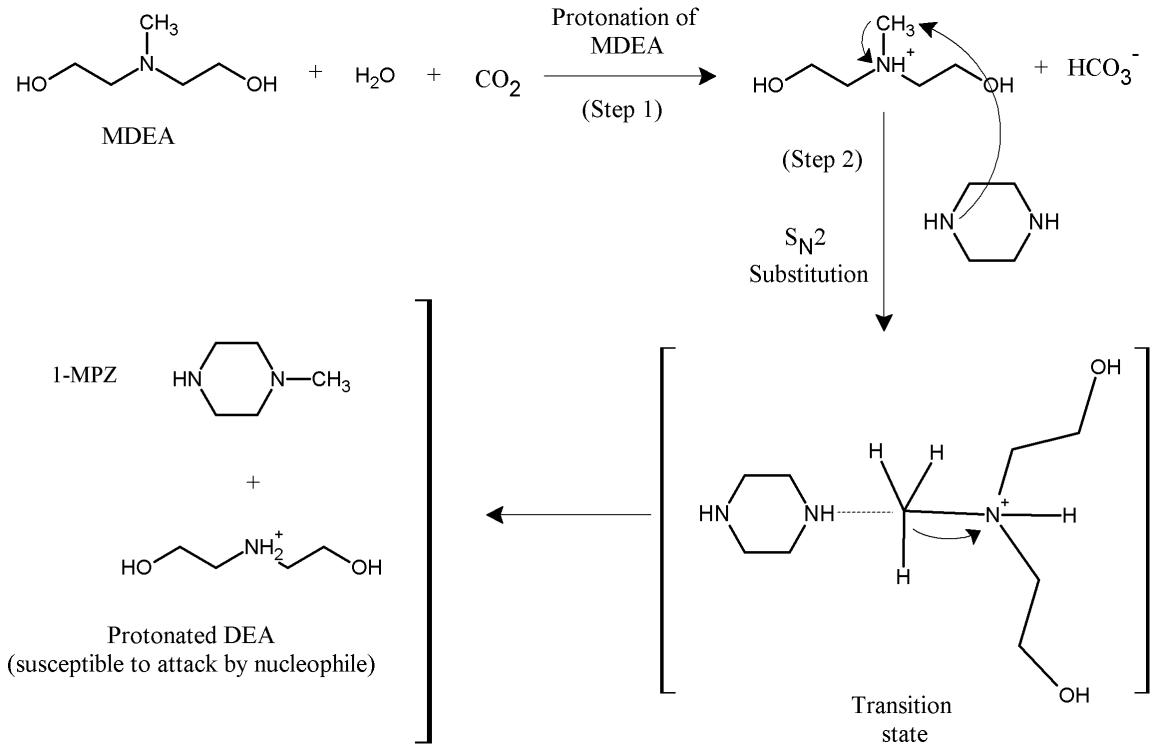

Figure 9.4: Pathway for S_N2 substitution reaction between $MDEAH^+$ and PZ resulting in production of 1-MPZ and $DEAH^+$

9.3.1.3 Pathway for loss of hydroxyethyl group from MDEA

A proposed pathway and S_N2 mechanism for the reaction between $MDEAH^+$ and PZ is presented in Figure 9.5. This pathway differs from the pathway presented in Figure 9.4. As before, MDEA is protonated to form $MDEAH^+$ in Step 1. However, in Step 2 of this pathway, PZ behaves as a strong nucleophile, attacking the hydroxyethyl group of $MDEAH^+$ to form the transition state noted in brackets. As presented, the "leaving group" in the mechanism is protonated MAE ($MAEH^+$). The key differences between this mechanism and the one presented in Figure 9.4 are the location of the attack (hydroxyethyl versus methyl group), and the leaving group ($MAEH^+$ versus $DEAH^+$).

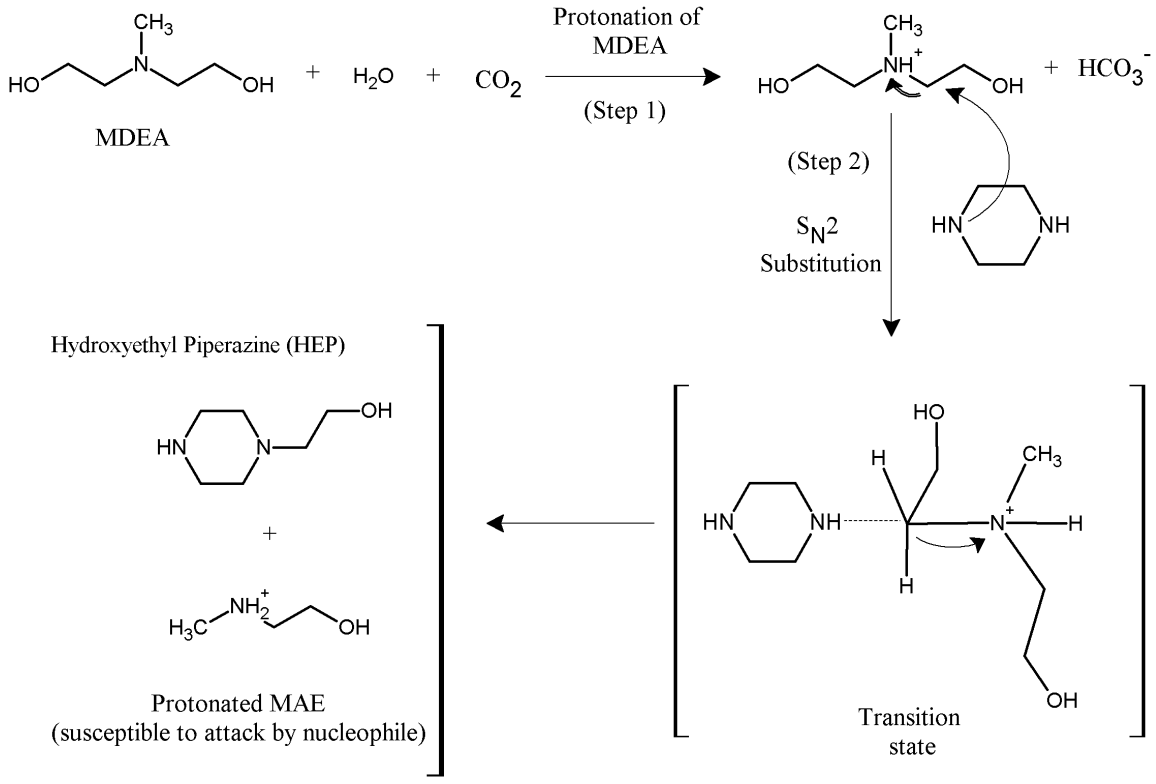

Figure 9.5: Thermal pathway for loss of hydroxyethyl group from MDEA

According to Huening and Baron (1956), a methyl group is the most likely leaving group from a quaternary ammonium salt in the presence of a nucleophile such as an amine. That work suggests that the pathway for loss of the methyl group (Figure 9.4) from MDEA is more likely to occur in thermal degradation than the loss of the hydroxyethyl group pathway presented in Figure 9.5. Willson (2009) indicated that the methyl group substitution could be expected to occur at least 90% of the time when PZ is present as the nucleophile. These reactions, as written, produce or propogate the presence of quaternary amines including $DEAH^+$ (Figure 9.4) and $MAEH^+$ (Figure 9.5). These quaternary amines will continue to participate in S_N2 reactions with nucleophiles including MDEA, PZ, 1-MPZ, HEP, and any other product with active amine functionality. The quaternary amines themselves likely undergo elimination reactions,

decomposing into products including ethylene glycol and methanol plus an amine. A discussion related to the quaternary amine decomposition mechanisms is presented in Section 9.4.

To test the consistency of the general mechanism of degradation being initiated by either a protonated amine or a quaternary amine, it is relevant to consider the behavior of 8 m PZ in thermal degradation experiments. Freeman (2011) demonstrated that CO_2-loaded 8 m PZ is thermally stable to 150 °C+. If the S_N2 mechanism were to hold for this solvent, it would suggest that PZ in the presence of PZH^+ and $PZCOO^-$ provides a "leaving group" that can accommodate the negative charge, and that sufficient free PZ is present in loaded solution to allow degradation to occur. The concentration of free PZ will be high up to its maximum practical loading range (0.4 mol CO_2/mol alkalinity), but the solvent is resistant to thermal degradation. It is likely that PZH^+ does not provide a satisfactory leaving group for direct interaction with PZ until higher temperatures are reached.

9.4 DECOMPOSITION OF QUATERNARY AMINES THROUGH ELIMINATION REACTIONS

The S_N2 reactions presented above generally result in the production of a substituted amine and a new quaternary amine. In that sense, they serve to propogate the overall S_N2 behavior of degradation in the solvent. However, it is likely that the quaternary amines will eventually decompose, and one possible pathway is through an elimination reaction in the presence of water at high temperature, resulting in a protonated amine plus an alcohol such as methanol or ethylene glycol. Two pathways for the quaternary amine decomposition reaction are presented in Figure 9.6. One quat decomposition results in a hydroxyethyl group loss to form ethylene glycol (Step 3a),

while a parallel quaternary amine decomposition could result in a methyl group loss resulting in the formation of a methanol (Step 3b). This decomposition of the quats is not a necessary or probable step. These other tertiary amines can degrade as MDEA did by reacting with MDEA to produce another quat. The quat decomposition pathways are also presented in parallel to the formation of DEA-carbamate ($DEACOO^-$) from DEA in Figure 9.6. The $DEACOO^-$ can proceed through the formation of HEOD through the condensation polymerization reaction described below in Section 9.6.1. Other decomposition pathways can be substituted for Step 3a and 3b which lead to the formation of either a new quat or a protonated amine in solution. Further, the decomposition process can be interrupted or reversed, with the reaction of the $DMAEH^+$ (formed in Step 3a) or $MDEAH^+$ (formed in Step 3b) with a strong nucleophile such as PZ to continue the nucleophilic substitution process.

9.5 DEHYDRATION REACTIONS

The presence of products such as HEOD in degraded 7 m MDEA/2 m PZ indicate that pathways other than those previously presented are responsible for degradation of the blend under thermal degradation conditions. Pathways for a few of those products are presented in this section. In general these pathways entail the formation of a 1° or 2° amine, followed by carbamate formation and condensate polymerization. Because MAE and DEA have been observed as degradation products in 7 m MDEA/2 m PZ, as reported in this work, these represent two obvious pathways for further degradation of the blend.

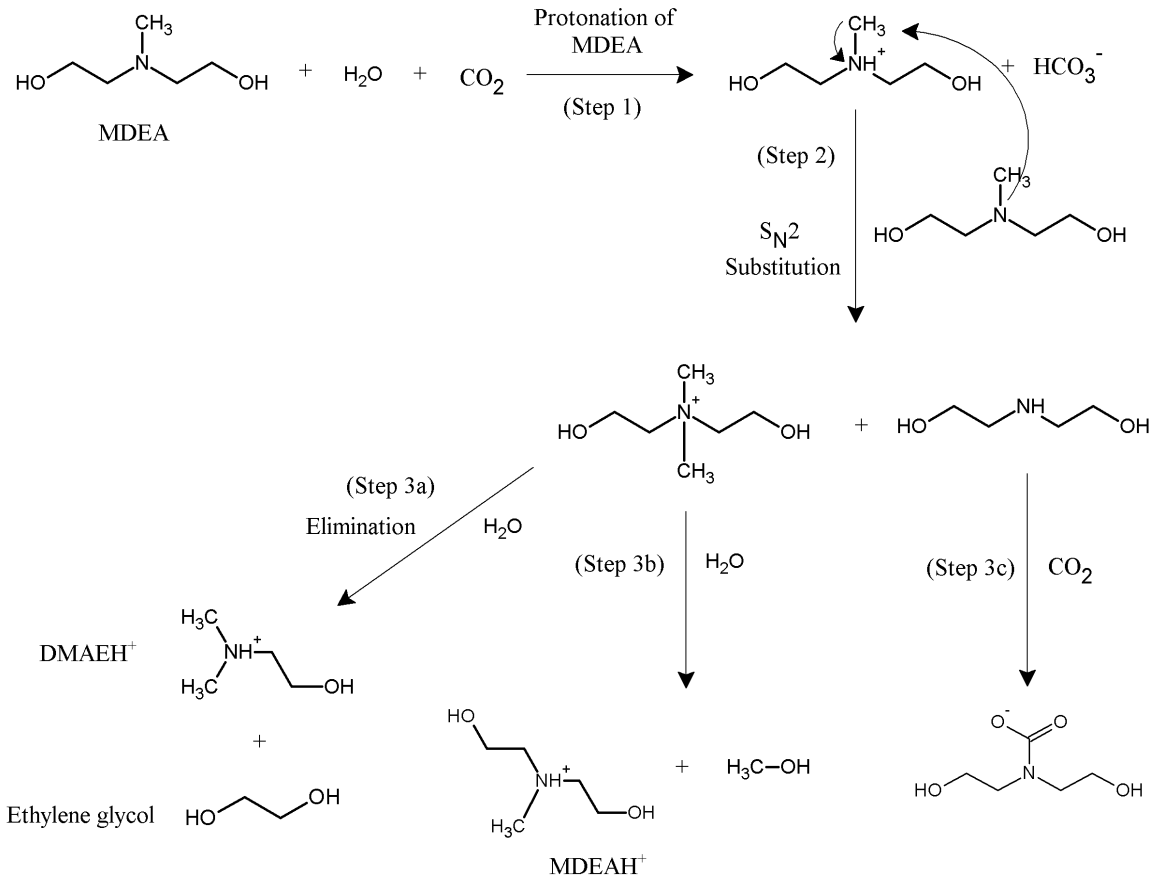

Figure 9.6: Quaternary amine elimination reactions following initial S_N2 substitution reaction resulting in loss of R-groups and new quaternary amine, accompanied by formation of DEA and $DEACOO^-$

9.6.1 Formation of HEOD from DEA

The presence of HEOD was confirmed in cycled 7 m MDEA (C-6-8) and thermally degraded 7 m MDEA/2 m PZ (α=0.25 mol CO_2/mol alkalinity, 150 °C) in this work (Th. No. 7). Its presence was confirmed with LC-MS (Th. No. 7) and GC-MS (cycling experiment C-6). A condensate polymerization pathway for the formation of this compound was first proposed by Polderman et al., (1956), and the pathway presented in Figure 9.7 expands on that understanding by presenting the formation of HEOD in

Steps 1 through 3, and considering follow-on reactions that can occur once HEOD is formed (Steps 4a and 4b).

9.6.2 Nucleophilic substitution reactions between HEOD and PZ derivatives

In Step 4a of Figure 9.7, PZ in the blend will behave as a strong nucleophile and react at the electron deficient carbon adjacent to the ester oxygen to open the oxazolidone ring and form 2-[[2-(1-piperazinyl)ethyl]amino]ethanol which has a molecular weight of 173.1. Assuming most of the free PZ has already reacted with protonated or quaternary species to form 1-MPZ, Step 4b would lead to the production of 2-[[2-(4-methyl-1-piperazinyl)ethyl]amino]ethanol with a molecular weight of 187.1. Step 4b might, therefore, be expected to occur to a greater extent after 7 m MDEA/2 m PZ has degraded. Steps 4a and 4b both lead to the production of CO_2 as the oxazolidone ring opens.

Two experiments were conducted in order to verify that these pathways do occur and these compounds are formed in thermally degraded 7 m MDEA/2 m PZ. The experiments were designed to expedite the formation of HEOD by thermally degrading DEA with 1-MPZ in experiment RPN-1, and DEA with PZ in RPN-2. By starting with DEA, the arm switching process associated with MDEA was avoided, along with other products of this mechanism. In RPN-1, 1 m DEA was combined with 1.5 m 1-MPZ in aqueous solution. The solvent mixture was then loaded to 0.2 mol CO_2/mol alkalinity, transferred to Swagelok® sample cylinders, and placed in ovens at 135, 150 and 175 °C to thermally degrade for up to two weeks. When analyzed with LC-MS, a peak and associated compound mass of 187.1 were present in samples degraded at 150 and 175 °C for only three days. From cation IC, it was determined that PZ loss was greater than 50% at 175 °C, confirming that PZ played a role in the degradation mechanisms. In RPN-2, 1 m DEA was combined with 1.5 m PZ, loaded to 0.25 mol CO_2/mol alkalinity, transferred

to Swagelok® sample cylinders, and placed in ovens at 135, 150 and 175 °C to thermally degrade. When the samples degraded at 150 to 175 °C were analyzed with LC-MS, a peak with an associated mass of 173.1 was observed. As with RPN-1, PZ loss was determined to be significant (>75%) after only two days of degradation at 175 °C using cation IC.

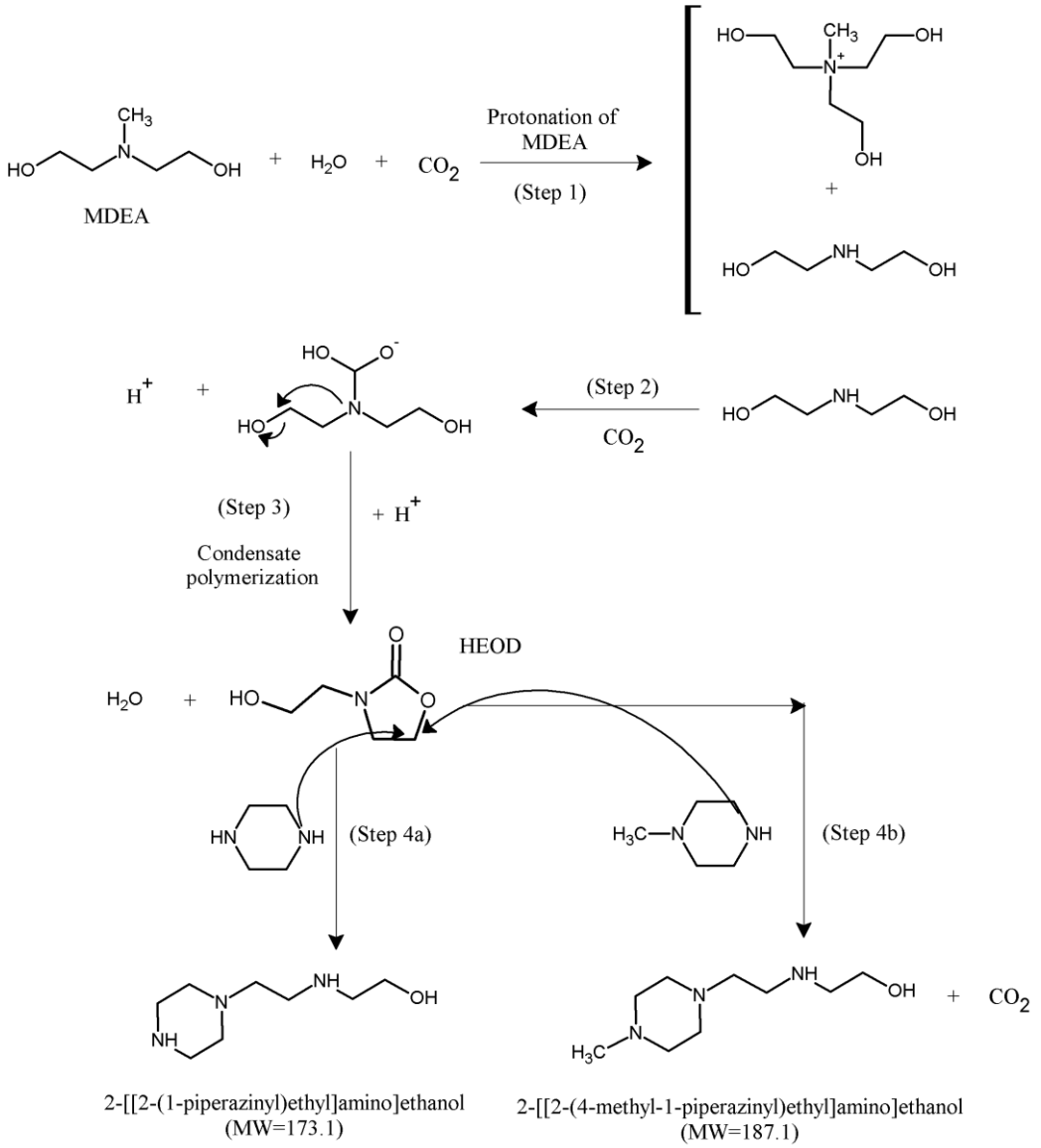

Figure 9.7: Thermal pathway for formation of HEOD in 7 m MDEA/2 m PZ

It is possible that other strong nucleophiles in the degraded blend could play the same role as PZ and 1-MPZ in Step 4 of the pathway presented in Figure 9.7. For example, MEA is considered to play the same role in the presence of 2-oxazolidone, the product of condensation polymerization of the MEA-carbamate ($MEACOO^-$). In that case, the product of the reaction is N-(2-hydroxyethyl)ethylenediamine (HEEDA). This product is known to further react in a dehydration reaction to form hydroxyethyl imidazolidone (HEI). As such, given the ability of MDEA to react to form DEA, MAE, and to a lesser extent MEA, the possibilities for condensation polymerization and follow-on dehydration reactions are many-fold.

9.6.3 Follow-on reactions to oxazolidone formation

The final degradation products depicted in Figure 9.7 will have some nucleophilic activity. In both cases, the product has a secondary amine functional group which can react with CO_2, or participate in a nucleophilic substitution reaction. The extent to which these follow-on reactions will occur is currently unknown, but speculation as to what products are possible provides some insight. The PZ-nitrogen of the secondary nitrogen on the arm on 2-[[2-(1-piperazinyl)ethyl]amino]ethanol could protonate, providing two avenues for reaction with another strong nucleophile and participation in follow-on S_N2 substitution reactions. Alternatively, either compound could serve as a nucleophile in degraded solution, extracting an arm from another protonated amine. This latter mechanism is less likely due to the bulky nature of the compounds and likely reduced pK_a of the 2° amines.

One other possibility for formation of degradation products in degraded 7 m MDEA/2 m PZ is the dehydration and ring closure of polymers of amine products to form imidazolidone products (ureas). None of these urea products have been identified in

degraded 7 m MDEA/2 m PZ, but their presence is likely, given that thermally degraded CO_2-loaded 7 m MEA will readily form these products at temperatures above 120 °C (Davis, 2009).

9.7 FORMATION OF CARBOXYLATE IONS (FORMATE)

In experiment Th. No. 16 with 7 m MDEA/2 m PZ, the carboxylate ion formate was identified and quantified as a product in the samples from all three temperature series (120, 135, and 150 °C). The concentration of formate increased with loading in all temperature series, as presented for the 150 °C series data in Figure 9.8. At a loading of 0.25 mol CO_2/mol alkalinity, the formate concentration was ~100 mM after 100 days of degradation. Freeman (2011) demonstrated that formate was produced in the thermal degradation of 8 m PZ, and through ^{13}C NMR, determined that the carbon in the generated formate was from CO_2 in the loaded experiments. The data plotted in Figure 9.8 are consistent with Freeman's findings that formate carbon originates with the CO_2 carbon; the formate concentration increased with increase in loading. The increased loading provided a greater source of carbon for formate production.

Freeman was unable to elucidate a mechanism for the generation of formate from CO_2 in thermally degraded 8 m PZ, but determined that an equilibrium relationship existed between the concentration of the protonated specie (HPZ^+) + formate, and FPZ + water. A similar relationship likely exists in the CO_2 loaded blend as thermal degradation proceeds (Figure 9.9). In the case of the degraded blend, the protonated species can include PZH^+, $DEAH^+$, $MDEAH^+$, while the amides may include those previously identified in other aspects of this work with the blend including FPZ, the DEA-amide, and the MAE-amide.

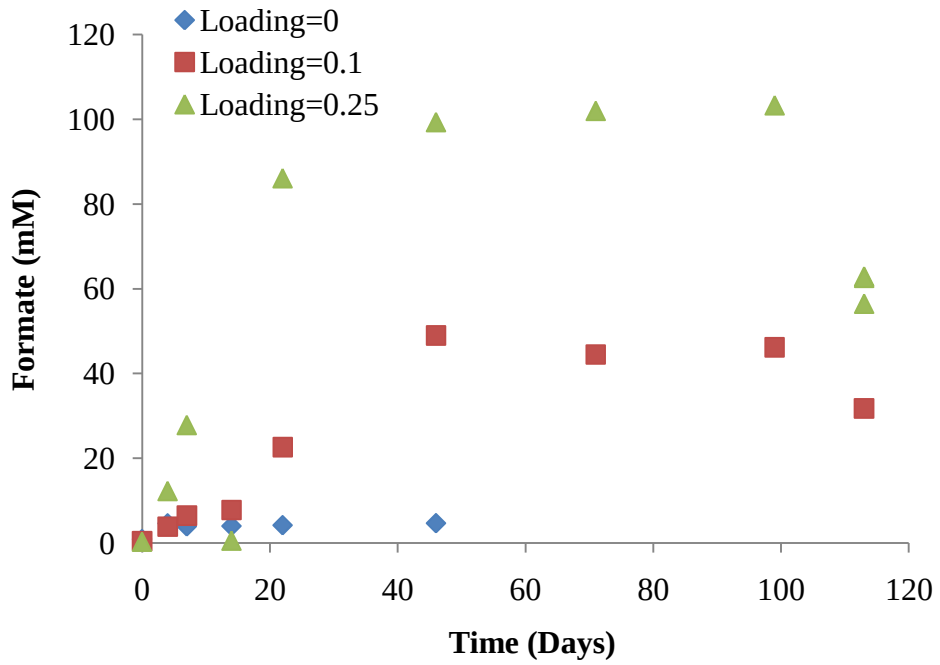

Figure 9.8: Formate concentration in 7 m MDEA/2 m PZ thermally degraded at 150 °C at loadings of 0.0, 0.1, and 0.25 mol CO_2/mol alkalinity

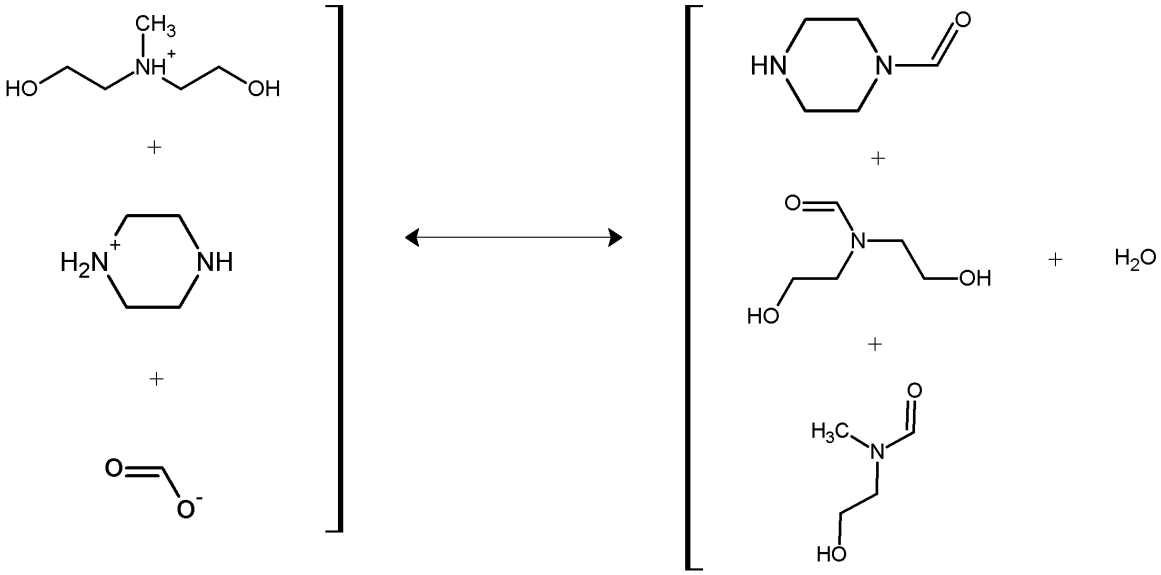

Figure 9.9: Equilibrium between formate and protonated species in degraded 7 m MDEA/2 m PZ, and commonly expected amides in the thermally degraded blend

9.5 THERMAL PATHWAYS SUMMARY

As depicted in Figure 9.10, the dominant reactions for the thermal degradation of 7 m MDEA/2 m PZ include S_N2 substitution reactions initiated by the formation of either a protonated amine ($MDEAH^+$) or a quaternary amine (Step 1). These reactions would preferentially lead to the extraction of a methyl group from MDEA (Step 2), but the loss of an hydroxyethyl group is also supported by thermal degradation data indicating that MAE and HEP are key amine products in degraded 7 m MDEA/2 m PZ. Bedell (2010) had demonstrated the presence and role of quaternary amines in the degradation of MDEA, and similar pathways and mechanisms are proposed for the blend. In the latter case, the participation of PZ, PZ derivatives, and 2° amines occurs in the blend, resulting in additional thermal degradation products. In parallel with the S_N2 substitution reactions is the decomposition of the quaternary amines to smaller quaternary and protonated amines + eliminated groups such as a hydroxyethyl group to form ethylene glycol or a methyl group to form methanol.

The production of 2° amines including DEA, MAE and MEA in the CO_2-loaded blend leads to the formation of oxazolidone compounds including HEOD through condensation polymerization reactions (Step 3). In Step 4 of Figure 9.10, HEOD will react with strong nucleophiles in the thermally degraded blend to open the oxazolidone ring structure and form other degradation products including the two polymers with ethanol functional groups as demonstrated in the pathways presented in Figure 9.7. Finally, although not confirmed in this work, polymer structures similar to the compounds formed in the pathways presented in Figure 9.7 can undergo dehydration and ring closure reactions to form imidazolidones, which are ureas (Step 5).

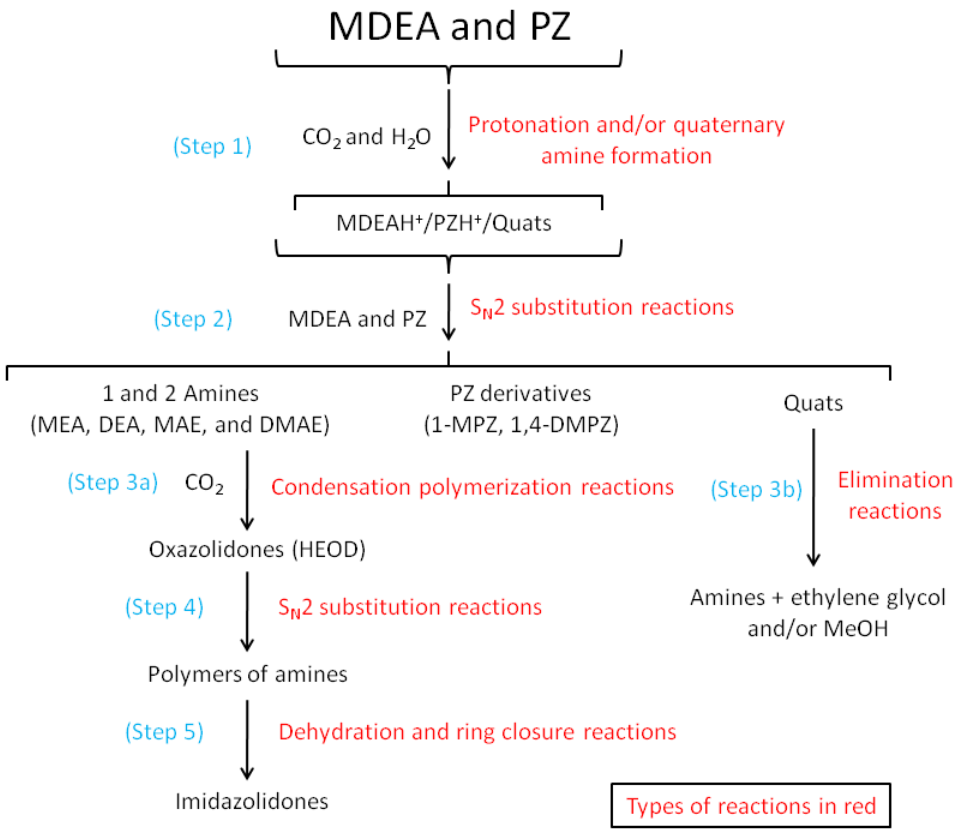

Figure 9.10: Overall thermal degradation pathways for 7 m MDEA/2 m PZ

Chapter 10 – Conclusions and Recommendations

This chapter provides a summary of key findings of this research into the degradation of 7 m methyldiethanolamine (MDEA)/2 m piperazine (PZ) when used for CO_2 capture in a flue gas application. Practical findings relevant to the use of any amine solvent for CO_2 capture are first provided. These findings are largely a result of the construction and operation of the Integrated Solvent Degradation Apparatus (ISDA) cycling system for investigating solvent degradation. Additional findings related specifically to the degradation of 7 m MDEA/2 m PZ are then provided. The chapter concludes with recommendations for additional work which will enhance the understanding of 7 m MDEA/2 m PZ degradation.

10.1 KEY FINDINGS

10.1.1 Practical findings

Construction and testing of the ISDA was an integral part of the investigative work summarized in this dissertation. The reactor system was initially tested with 7 m MDEA in 15 separate cycling experiments to understand the behavior of the system when compared to other degradation methods already in use including the Low-gas and Swagelok® degradation methods. These experiments provided valuable insight to the degradation of this tertiary solvent at varied conditions. Over the course of those initial characterization experiments, important practical findings were made, as discussed in this section. A list of the rates of degradation measured in the relevant characterization experiments conducted with 7 m MDEA in the ISDA is provided in Table 10.1. These rates are referenced in the ensuing discussion.

Table 10.1: Rates measured in characterization experiments with the ISDA cycling reactor; purge gas 98% O_2/2% CO_2; all rates in mM/hr

Expt No.	Th Rx T (°C)	Stir Rate (rpm)	MDEA Loss Rate	Alk Loss Rate	Formate Production	Total Formate Production
C-1	120	1,440	8.8	5.2	0.59	0.98
C-4	120	520	3.4	2.46	0.17	0.15
C-5	120	1,000	8.5	4.3	0.37	0.57
C-6	120	1,440	4.6	4.93	0.28	0.34
C-18	120	1,440	0	0.73	0.047	0.044
C-13	120	1,440	0.24	0.52	0.08	0.08
C-14	90	1,440	0.22	0.18	0.044	0.058
C-12	90	1,440	2.87	2.19	0.12	0.15
C-8	90	1,440	1.9	1.57	0.013	0

10.1.1.1 Dissolved oxygen increases oxidation rate; gas stripping mitigates the problem

Dissolved oxygen in solvent increases the rate of oxidation as the solvent is heated in the cross-exchanger and piping to the stripper. This dissolved oxygen can be stripped from the solvent before high temperature oxidation occurs. Several experiments including C-8 and C-9 which utilized a 98% N_2/2% CO_2 purge gas at 100 mL/min demonstrated that, when dissolved oxygen is eliminated from the headspace of the oxidative reactor, the rate of oxidation of solvent is reduced several orders of magnitude. The implication of these results is that dissolved oxygen resulting from solvent contact with flue gas will lead to oxidation.

Experiment C-18 incorporated the stripping of dissolved gases from the solvent with a 1 L/min N_2 gas purge in a modified bubble removal vessel, and demonstrated the success of this simple stripping method for minimizing oxidation in 7 m MDEA. All rates indicative of MDEA degradation decreased by an order of magnitude when compared to the rates measured in a comparable cycling experiment without the stripping

device (C-6). The oxidation rate reductions were on top of those reductions observed with entrained bubble removal, thereby demonstrating the benefit of removing dissolved oxygen in addition to entrained oxygen bubbles.

The experiments demonstrated the efficacy of a simple stripper in reducing oxidation by ~5 to 10X. The optimal stripping rate and conditions for stripping were not evaluated, but the simplicity and effectiveness of the stripping concept was demonstrated, warranting further consideration as an approach to minimizing oxidation in full-scale systems. A patent relating to the stripping of dissolved oxygen from solvents to prevent degradation has been awarded to Chakravarti (2001).

10.1.1.2 Entrained oxygen increases oxidation rate

Entrainment of gas bubbles high in oxygen content in solvent exiting the absorber will cause accelerated oxidation. When entrained oxygen bubbles containing 98% O_2 were observed in solvents passing out of the oxidative reactor of the ISDA (C-1 through C-5), the overall rate of oxidation measured as formate production was ~2X the rate measured when entrained gas bubbles were removed with a simple bubble removal vessel (C-6). A simple stir rate reduction in the oxidative reactor resulted in a reduction of the oxidation rate to 1/3X the original rate. The installation of a glass vessel containing a 1 and 1/4-inch bed of loose distillation packing at a location downstream of the solvent exit from the oxidative reactor resulted in the decrease in formate production rate by nearly 1/3 to 1/2X. These observations make it clear that gas bubble entrainment in solvent exiting the absorber results in a higher oxidation rate. In a flue gas application where the feed gas may consist of as much as 15% O_2, the entrainment effect on oxidation rate will be greater when compared to a natural gas application where the oxygen content is typically below 0.1%.

The bubble entrainment problem was easily solved in the ISDA reactor system with the bubble interception vessel with packing, which decreased degradation rates to 1/2X those rates observed without entrained bubble removal. In a full-scale absorber/stripper system, the use of packing to coalesce entrained bubbles in the absorber sump section may be sufficient to decrease bubble entrainment in solvent exiting the absorber, and the resulting oxidation rate. Bubbles may also be reduced by conventional design for adequate gas/liquid separation in the absorber sump.

10.1.1.3 Oxidation rate is directly related to thermal reactor (stripper) temperature

The rate of oxidation in solvent will increase with temperature as the solvent is heated in the heat exchanger and travels to the stripper. The ISDA characterization experiments demonstrated the effect of high temperature oxidation. Rates of MDEA and alkalinity loss increased by a factor of ~2X when the thermal reactor temperature was increased from 90 to 120 °C, as demonstrated by rates measured in experiments C-12 and C-6 listed in Table 10.1. The rates of formate and total formate production increased by ~3X when the thermal reactor temperature was increased from 90 to 120 °C.

These findings indicate that rates of solvent oxidation will increase as steam stripper temperature is increased to take advantage of the thermodynamic benefits of a higher heat of absorption. The steam stripper is a thermal swing process, and solvents with a higher heat of absorption such as 7 m MDEA/2 m PZ ($\Delta H \sim 68$ kJ/mol*K) will provide energy benefits in an optimized system. As absorber/stripper systems are designed for higher stripper temperatures, heat stable salt (carboxylate ion) and other degradation product formation rates will increase, resulting in an increased need for solvent reclaiming.

10.1.1.4 Higher purge gas oxygen content directly increases oxidation rate

The rate of oxidation of solvent is directly related to the concentration of oxygen in the dissolved gases in contact with the solvent. In experiment C-13 in the ISDA, the substitution of air for pure O_2 at 98% of purge gas composition reduced the degradation of 7 m MDEA measured as formate production by nearly 10X. When the headspace gas composition was reduced to zero oxygen by substitution with 98% N_2 (C-8), the loss rates decreased by 3X (compare to C-14). The implication of this finding for full-scale systems is that, when treating a flue gas high in oxygen content (5-15 kPa), the rate of oxidation can be expected to be much higher than in typical acid gas treating systems wherein the feed gas is likely to be <1% O_2. The designers of flue gas CO_2 scrubbing systems will need to consider feed gas composition when selecting the solvent, and specifying operating conditions.

10.1.2 Key findings with 7 m MDEA/2 m PZ degradation

10.1.2.1 Degradation products of thermally degraded 7 m MDEA/2 m PZ

The major products of thermally degraded 7 m MDEA/2 m PZ included diethanolamine (DEA), methylaminoethanol (MAE), and the PZ derivatives 1-methyl piperazine (1-MPZ), 1,4-dimethylpiperazine (1,4-DMPZ), and aminoethylpiperazine (AEP). The peaks for DEA and MAE were unseparable using cation IC, so a combined concentration for the two was reported throughout this dissertation. Important compounds also identified in the degraded blend, but at lesser concentrations, included 3-(2-hydroxyethyl) oxazolidone (HEOD), polymerization products of the attack of HEOD by PZ and 1-MPZ, and the carboxylate ion formate.

10.1.2.2 S_N2 substitution explains thermal degradation in 7 m MDEA/2 m PZ

S_N2 substitution reactions between protonated or quaternary amine species and strong nucleophiles such as PZ explain the production of many of the thermal degradation products identified in 7 m MDEA/2 m PZ. The S_N2 mechanism explains the reaction between $MDEAH^+$ and PZ to form 1-MPZ at temperatures of 120 to 150 °C. These reactions will continue to occur as long as a protonated or quaternary amine specie is present with a nucleophile, as evidenced by continued methyl-group arm switching resulting in the decrease in 1-MPZ concentration, and the increase in 1,4-DMPZ concentration.

By definition, the S_N2 substitution mechanism is a bimolecular (second-order) mechanism. Despite the fact that first-order kinetics adequately predicted the rates and concentrations of amine, the S_N2 mechanism explains the production of the key thermal degradation species in degraded solvent, including DEA, MAE, 1-MPZ, and 1,4-DMPZ.

10.1.2.3 PZ participates in reactions with multiple compounds

PZ participates in thermal degradation reactions with condensation polymerization products in the blend including HEOD. The presence of HEOD in degraded 7 m MDEA/2 m PZ was confirmed with GC-MS methods, and through targeted experiments and the utilization of IC- and LC-MS methods, two compounds with masses of 173.1 and 187.1 were identified. The presence of compounds with these masses was anticipated as a result of reactions between HEOD and strong nucleophiles. The strong nucleophile in the case of 2-[[2-(1-piperazinyl)ethyl]amino]ethanol (mass of 173.1) was PZ. In the case of 2-[[2-(4-methyl-1piperazinyl)ethyl]amino]ethanol with a mass of 187.1, the strong nucleophile was 1-MPZ. The identification of these products provided confirmation that nucleophilic attack of carbonyl carbon atoms of degradation products

by the nucleophiles PZ and 1-MPZ continues the degradation of the blend beyond simple S_N2 substitution reactions.

10.1.2.4 Thermal degradation rates in 7 m MDEA/2 m PZ increase with CO_2 loading

Unloaded 7 m MDEA/2 m PZ was generally thermally stable up to 150 °C, exhibiting very low loss rates. However, at a loading of 0.25 mol CO_2/mol alkalinity, loss rates of 0.17 ± 0.21 and 0.24 ± 0.06 mM/hr, respectively, for MDEA and PZ were measured. In contrast to these rates, the loss rates were ~0 for both amines in the unloaded blend.

10.1.2.5 Amine loss rates comparable between 7 m MDEA and 7 m MDEA/2 m PZ

At a temperature of 150 °C and a nominal loading of 0.25 mol CO_2/mol alkalinity, the loss rates of MDEA measured in 7 m MDEA and 7 m MDEA/2 m PZ were comparable, at 3.0 ± 0.7 and 3.6 mM/hr, respectively. In both cases, the concentration of PZ decreased to 0 mM, after which the MDEA concentration continued to decrease. However, the experimental series at this same loading but a temperature of 135 °C exhibited a different result. After complete loss of PZ in the blend, the MDEA concentration decreased at a slower rate. The comparable experiment with 7 m MDEA exhibited similar MDEA loss behavior, with a slowdown in loss rate after a higher initial loss period of ~25 days.

10.1.2.6 Thermal degradation data were modeled as first-order in [$MDEAH^+$]

A thermal degradation model for prediction of the MDEA and PZ concentrations with time was developed which assumed that the rate-limiting step for degradation in the blend was first-order in [$MDEAH^+$]. The model also assumed that the rate is independent of [PZ]. This "universal activation energy" model was developed by normalizing all of the MDEA and PZ loss data based on initial amine concentration and

initial loading from the thermal degradation experiments, and estimating a universal activation energy (~104 kJ/mol) which applied to the amine loss behavior for both amines across all experimental temperatures and loadings. Two equations were developed which described the amine loss behavior in the blend with temperature. The first equation is the Arrhenius relationship for predicting the first-order rate constant with temperature based on the universal E_a calculated from the entire data set, while the second equation relates the loss of PZ to the MDEA concentration and loading:

$$k_U(T) = k_{408}(1/hr) * \exp\left\{-\frac{104{,}300 J/mol}{8.314 J/mol - K}\left(\frac{1}{408K} - \frac{1}{T_U}\right)\right\}$$

$$\frac{d[PZ]}{dt} = -1.13 k_U(T) * [MDEA]_T * \alpha$$

10.1.2.7 Closure of mass balance in acid-treated 7 m MDEA/2 m PZ

When 7 m MDEA/2 m PZ was acid-treated to 0.1 mol H^+/mol alkalinity and thermally degraded at 150 °C, the mass balance on recovered thermal degradation products was ~100% of lost carbon and nitrogen as MDEA and PZ losses. This high recovery of lost carbon and nitrogen was due to the simpler degradation processes associated with S_N2 reactions in the absence of CO_2. The presence of CO_2 results in carbamate polymerization reactions, and the loss of carbon and nitrogen as unrecovered products including oxazolidone and urea compounds. At day 37 in the acid-treated experiment, ~70% of carbon and ~65% of nitrogen were accounted for in DEA+MAE, whereas, in the comparable experiment with CO_2-loaded blend, DEA+MAE accounted for 2% of carbon and nitrogen. The overall poor recovery in the CO_2-loaded experiment was due to the loss of carbon and nitrogen from CO_2 polymerization reactions involving compounds including DEA and MAE.

10.1.2.8 Oxidation rates in 7 m MDEA/2 m PZ << rates in 7 m MEA

When degraded in the Low-gas reactor at 55 °C, the rates of oxidation in 7 m MDEA/2 m PZ, measured as formate and total formate production, were ~1/20 to 1/10X the rates measured in 7 m MEA. The formate production rate in 7 m MDEA/2 m PZ was approximately the same as the rate measured in 7 m MDEA (~0.01 mM/hr), but the total formate production rate in the blend was ~3X the rate measured in 7 m MDEA (0.08 vs. 0.03 mM/hr). The latter observation reflects a common observation for blend degradation, which is the observance of more amides in oxidized 7 m MDEA/2 m PZ as compared to 7 m MDEA. The amides are partially a result of the formation of FPZ in the oxidized blend. In contrast, rates of formate and total formate production derived from the data of Sexton (2008) for oxidized 7 m MEA were ~10X the rates measured in either 7 m MDEA/2 m PZ or 7 m MDEA at 55 °C. In terms of amine loss and total formate production rates, the solvents can be ranked from greatest to least as follows: 7 m MEA>7 m MDEA/2 m PZ>7 m MDEA>8 m PZ.

10.1.2.9 Oxidation in the ISDA can be predicted using a PFR model

A plug-flow reactor (PFR) model was developed from the ISDA cycling data to accurately predict the rate of oxidation in 7 m MDEA. The ISDA behaved as an isothermal PFR, and using a series of cycling experiments over a range of thermal reactor temperatures, an oxidation model was developed which allows the prediction of formation rates of key indicators of oxidation including formate, total formate, and bicine. Due to complete consumption of dissolved oxygen at the higher temperatures when solvents were cycled with the original design of the thermal reactor, the Arrhenius relationship did not accurately predict the rate constants for degradation. The PFR model corrected for this anomaly by incorporating a stoichiometric factor (S), which was defined as $\Delta[Prod]/\Delta[O_2]$. Equation 5.14 from Chapter 5 defines the PFR model.

$$\Delta[\mathrm{Prod}] = \frac{P_{O_2} * S * Q * t}{K_H * V_{tot}} \left(1 - \exp(-\frac{k_1 * V_{TR}}{Q})\right)$$

A spreadsheet model was used to solve for k_o, E_a, and S for formate, total formate, and bicine, and the values for these degradation products in 7 m MDEA are listed in Table 10.2.

Table 10.2: PFR oxidative model results for degradation products in 7 m MDEA

Parameter	k_o (hr^{-1})	E_a (kJ/mol)	S (mol Prod/mol O_2)
Formate	2.6	151	0.09
Total formate	3.4	152	0.14
Bicine	0.32	244	0.35

Comparison of the activation energy E_a for formate production of 151 kJ/mol to the estimate of 46 kJ/mol from Chapter 4 indicates that the stoichiometric ratio S of degradation product formation to oxygen consumption is accounted for, the activation energy is 3X. With complete resaturation of the solvent upon each pass through the system, excess oxygen is available in the system. It is anticipated that the solvent exposure to oxygen would be the same in an absorber/stripper system designed for CO_2 capture from flue gas streams where the oxygen concentration could be as high as 15%. The stoichiometric ratio S for total formate production is 0.14, indicating that approximately 7.1 moles of oxygen are required for every mole of total formate produced.

The model was used to predict the rates of total formate production in small and large thermal reactor designs in the ISDA, and checked against data collected from both configurations (Figure 10.1). The predicted total formate production rates for the small thermal reactor design and for the large thermal reactor design are separately plotted in the figure. The solid filled symbols (♦) represent the measured rates of total formate

production in 7 m MDEA cycling experiments in the ISDA with the large thermal reactor, while the solid filled symbols (■) represent the measured rates of total formate production in 7 m MDEA cycling experiments in the ISDA with the small thermal reactor. All rates have been normalized to residence time in the Low-gas reactor.

The model provides a match for total formate production rates in the ISDA at the lower temperatures for the small and large thermal reactor designs. As the temperature rises beyond 100 °C, the predicted rates for the two thermal reactor designs diverge, with the large thermal reactor predicting a lower rate of total formate production. This divergence is a result of the oxygen solubility limited operation associated with the larger thermal reactor; at the greater residence times associated with the larger thermal reactor, insufficient dissolved oxygen is available to maintain a higher rate of total formate production. The smaller thermal reactor more accurately measures the degradation of 7 m MDEA in a kinetically controlled region. The two measured total formate production rates with the small reactor (■) match well with the oxidative model, while the measured rates with the large reactor (♦) match well at the higher temperatures, but diverge from the model at the lower temperature (55 °C).

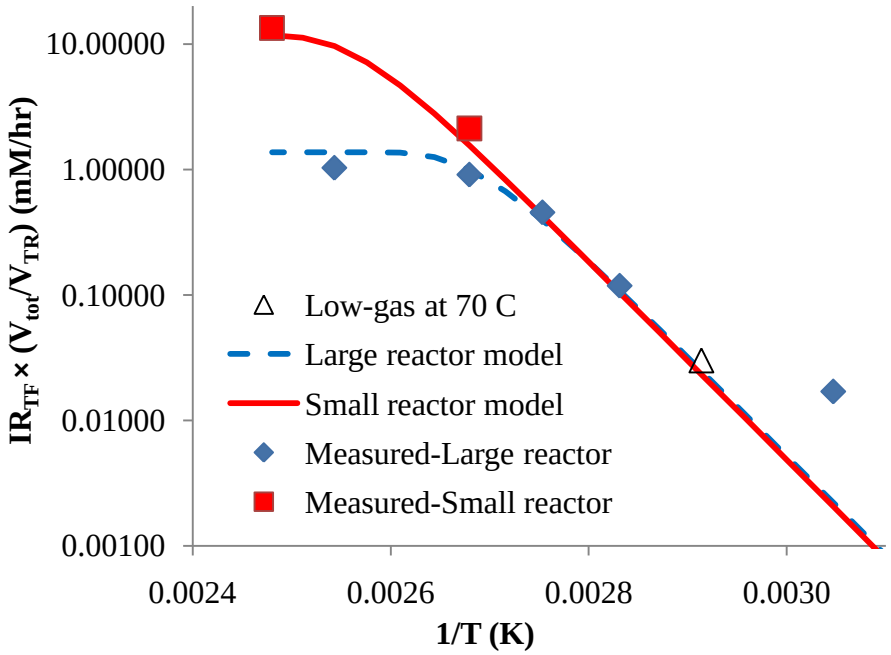

Figure 10.1: Initial rates of total formate production measured in 7 m MDEA in the ISDA; oxidative degradation model predicted values plotted for large thermal reactor (dashed blue line) and small thermal reactor (solid red line); (figure taken from Chapter 5)

10.1.2.10 Stripper temperature limit in 7 m MDEA predicted to be 104 °C

An average temperature limit of 104 °C in the stripper was estimated with the oxidative model for 7 m MDEA assuming 30 seconds of residence time and 10% oxygen consumption per pass. When we consider a dissolved oxygen consumption limit in the piping passing through the heat exchanger and carrying solvent to the top of the stripper, we can relate this limit to a temperature limit for the solvent in this part of an absorber/stripper system. Using Equation 5.15, which is the first-order relationship relating oxygen concentration in and out to the first-order rate constant and residence time, and an assumption that the solvent passes through this portion of the system in ~30 seconds for each pass through the system, the upper limit of temperature tolerance at 10, 20 and 50% of dissolved oxygen consumption was calculated from the corresponding k_1

values returned by the model over the range of temperatures for formate, total formate, and bicine. The temperature limits are tabulated in Table 10.3.

$$\ln \frac{C_{in}}{C_{out}} = k(T) * t$$

Table 10.3: 7 m MDEA oxidative model temperature analysis assuming 30 seconds of residence time at temperature

	Temperature (°C)			
Oxygen Consumed (%)	Formate	Total formate	Bicine	Average
10	102	101	108	104
20	107	106	111	108
50	117	115	117	116

The results indicate that 7 m MDEA can tolerate ~104 °C at the 10% oxygen consumption level based on an average across all three degradation products. The average temperature tolerance limit increases to 108 °C for a 20% oxygen consumption, and 116 °C for a 50% oxygen consumption level.

10.1.2.11 MDEA loss estimated to be 1.5 X 10^5 kg/yr for 100 °C stripper temperature

The MDEA loss rate was estimated to be ~1.5 X 10^5 kg/year based on total formate production at an average temperature of 100 °C, and a flue gas oxygen concentration of 5 kPa (5%). The first-order rate constant for oxygen consumption and conversion of MDEA to total formate was related to overall MDEA loss, and through an estimate of solvent CO_2 carrying capacity, the amount of MDEA loss per unit CO_2 captured. The analysis was performed based on total formate production at an average temperature of 100 °C, and a flue gas oxygen concentration of 5 kPa (5%). Using the calculated rate in terms of moles total formate, and an estimate of 15 moles MDEA loss per mol total formate formed from the ISDA experiments, the CO_2 capture rate per mass solvent was related as follows:

$$rate = \left(0.0594 \frac{mmol\ TF}{L\ solv * hr}\right)\left(\frac{kg\ solv}{0.5\ mols\ CO_2}\right)(30\ s)\left(\frac{hr}{3600s}\right)\left(\frac{15\ mmol\ MDEA\ lost/L}{mmol\ TF/L}\right)\left(\frac{L\ solv}{1.055\ kg\ solv}\right)$$

$$rate = \left(1.4E10^{-2}\ \frac{mmol\ MDEA\ Lost}{mol\ CO_2 Captured}\right)\left(\frac{mol\ MDEA\ Lost}{10^3\ mmol\ MDEA\ Lost}\right)$$

$$rate = \left(1.4E10^{-5}\ \frac{mol\ MDEA\ Lost}{mol\ CO_2 Captured}\right)\left(\frac{1\ mol\ CO_2}{44\ gm\ CO_2}\right)\left(\frac{454\ gm\ CO_2}{lb\ CO_2}\right)\left(\frac{2000\ lb\ CO_2}{ton\ CO_2}\right)$$

The final calculation provides a rate of 0.29 mol MDEA lost/ton CO_2 captured. The estimate of 0.5 mol CO_2 captured/kg solvent is based on a 90% CO_2 removal assumption. For a 500 MW power plant, if 90% CO_2 capture is assumed, the rate of CO_2 capture is estimated to be 1 ton CO_2/MW-hr. At 0.29 mol MDEA lost/ton CO_2 captured, the MDEA loss rate is estimated to be ~1.3 X 10^6 mol/year, or ~1.5 X 10^5 kg/year.

10.1.2.12 The stripper temperature limit in 7 m MDEA/2 m PZ estimated to be 92 °C

An average temperature limit of 92 °C in the stripper was estimated for 7 m MDEA/2 m PZ using the oxidative model for 7 m MDEA, and assuming 30 seconds of residence time and 10% oxygen consumption per pass with the blend. Using the same assumptions as were used in the estimate of temperature tolerance in 7 m MDEA, including ~30 seconds of residence time for each pass through the system, the upper limits of temperature tolerance at 10, 20 and 50% of dissolved oxygen consumption were calculated from the corresponding k_1 values returned by the model over the range of temperatures for total formate. The estimate for k_{363} for total formate in 7 m MDEA/2 m PZ of 10 hr^{-1} was used in the Arrhenius relationship to provide the $k_1(T)$. The temperature limits are tabulated with the values calculated for 7 m MDEA and 8 m PZ in

Table 10.4. 8 m PZ provides the greatest temperature tolerance, at 112 °C at the 10% oxygen consumption per pass level. 7 m MDEA/2 m PZ provides the lowest temperature tolerance, at 92 °C.

Table 10.4: Temperature tolerance in heat exchanger and piping based on total formate production at various O_2 consumption levels and τ = 30 seconds

Oxygen Consumed (%)	Temperature (°C)		
	7 m MDEA/2 m PZ	7 m MDEA	8 m PZ
10	92	101	112
20	97	106	123
50	106	115	145

10.1.2.13 Total amine loss rate in 7 m MDEA/2 m PZ was 1.3 X 10^5 kg/yr at 100 °C

The amine (MDEA+PZ) loss rate was estimated to be ~1.3 X 10^5 kg/year based on total formate production at an average temperature of 100 °C, and a flue gas oxygen concentration of 5 kPa (5%). The first-order rate constants for oxygen consumption and conversion of amine (MDEA + PZ) to total formate were related to overall amine loss at a stripper temperature of 100 °C and an assumed flue gas oxygen concentration of 5 kPa (5%). Using an estimated k_1 of 38.3 hr^{-1} for 100 °C for total formate production, and an average solvent capacity of 0.75 mol CO_2/kg solvent for the blend, the rate of total formate production in the blend was calculated to be 0.17 mmol total formate/L-hr. Using the calculated rate in terms of moles total formate and an estimate of 7.5 moles MDEA loss per moles total formate formed from the ISDA experiments, we related the CO_2 capture rate per mass solvent as follows:

$$rate = \left(0.17\frac{mmol\,TF}{L*hr}\right)\left(\frac{kg\,solv}{0.75\,mol\,CO_2}\right)(30s)\left(\frac{hr}{3600\,s}\right)\left(\frac{7.5\,mmol\,Am\,lost/L}{mmol\,TF/L}\right)\left(\frac{L}{1.08\,kg}\right)$$

$$rate = \left(1.32E10^{-2} \frac{mmol\ Am\ Lost}{mol\ CO_2 Captured} \right) \left(\frac{mol\ Am\ Lost}{10^3\ mmol\ Am\ Lost} \right)$$

$$rate = \left(3.4E10^{-6} \frac{mol\ Am\ Lost}{mol\ CO_2 Captured} \right) \left(\frac{1mol\ CO_2}{44\ gm\ CO_2} \right) \left(\frac{454\ gm\ CO_2}{lb\ CO_2} \right) \left(\frac{2000\ lb\ CO_2}{ton\ CO_2} \right)$$

The final calculation provides a rate of 0.27 mol amine lost/ton CO_2 captured, where moles amine accounts for moles MDEA + moles PZ. The capacity estimate of 0.75 mol CO_2 captured/kg solvent is based on a 90% CO_2 removal assumption. At 0.27 mol amine lost/ton CO_2 captured, the amine loss rate is estimated to be ~1.2 X 10^6 mol/year, or ~1.3 X 10^5 kg/year. A summary of the amine loss rates per ton CO_2 captured and annual amine loss based on a 500 MW power plant operation for 7 m MDEA/2 m PZ, 7 m MDEA, and 8 m PZ is provided in Table 10.5. The amine loss rates for 8 m PZ are the lowest, with 7 m MDEA/2 m PZ and 7 m MDEA providing comparable amine loss.

Table 10.5: Summary of amine loss rates for solvents, assuming a first stage flash of 100 °C, 30 s of residence time at temperature, 5 kPa O_2 in flue gas, 90% CO_2 capture, and a 500 MW power plant

Solvent	Amine loss rate	Annual loss	Annual loss
	gmol amine/ton CO_2	gmol amine/year	Kg amine/year
7 m MDEA/2 m PZ	0.27	1.2 X 10^6	1.3 X 10^5
7 m MDEA	0.29	1.3 X 10^6	1.5 X 10^5
8 m PZ	0.15	6.7 X 10^5	5.7 X 10^4

10.2 RECOMMENDATIONS FOR FUTURE WORK

This section provides a set of recommendations for additional work that should be performed to improve or enhance the understanding of the degradation rates and processes that occur in 7 m MDEA/2 m PZ when used in a flue gas CO_2 scrubbing

application. These recommendations can also be used for any other solvent system when cycled in the ISDA.

10.2.1 Improvement in mass balance closure in degraded 7 m MDEA/2 m PZ

More extensive use of synthesis and analytical methods should be used to close the mass balance in degraded 7 m MDEA/2 m PZ. The amount of carbon and nitrogen accounted for in degradation products quantified in this work in cycled CO_2-loaded 7 m MDEA/2 m PZ are less than 68 and 63%, respectively. The major products are primarily 1° and 2° amines, PZ derivatives, and amino acids. Attempts were made to identify additional degradation products including amino acids and amides. In both cases, synthesis of standards was successfully performed for compounds, which were subsequently identified and roughly quantified. However, some of these attempts were unsuccessful, and further synthesis efforts were not attempted.

Additional synthesis of amino acids may prove useful. A single large peak appearing before bicine in retention time using the HPLC amino acid method described in this work was observed. Identification of this peak would add to the recovered carbon and nitrogen in heavily degraded samples of the blend from the ISDA. Additional work to synthesize amides of degradation products including PZ derivatives may also prove successful. Hydrolyzed samples of heavily cycled 7 m MDEA/2 m PZ strongly indicate that several unidentified peaks appearing on the HPLC system and separated with the HILIC non-polar column are amides. The synthesis of likely degradation products of 7 m MDEA/2 m PZ may allow the identification and quantification of compounds corresponding to those peaks.

Additional efforts with HPLC and mass spectrometry (MS) methods coupled to both HPLC and gas chromatography would likely result in the identification of additional

degradation products of 7 m MDEA/2 m PZ. Few of the urea and oxazolidone compounds of the blend were positively identified with the current methods, and the deployment of HPLC and GC coupled to MS was never extensive enough to achieve adequate separation and identification of some suspected compounds with urea and oxazolidone structures. The exceptions to this include the identification of HEOD in many of the samples through GC-MS.

10.2.2 Modification of the ISDA to achieve continuous headspace gas sampling

The ISDA cycling system could be retrofitted with an oxidative reactor which allows the collection of all gases passing out of this reactor, and redirects them to a gas-phase analyzer such as a Fourier Transform Infrared (FTIR) analyzer, or gas chromatograph. This redesign would allow the identification and quantification of volatile degradation species that are generated as solvents are cycled and degraded in the ISDA.

The current design of the ISDA allows for the collection of liquid solvent samples directly from the oxidative reactor, as well as liquid condensate samples collected from gas passing out of the headspace of the oxidative reactor. The condensate samples are collected without sufficient knowledge of the gas flow rate passing through the condensate tube, and are diluted by condensed water vapor coming off the solvent. The condensate sample collection method, therefore, only allows for a semi-quantitative evaluation of volatile species generated as the solvent degrades. The recommended improvement to the glass oxidative reactor will enhance the collection of data, and knowledge of how solvents degrade during each experiment. Further, this improvement would allow for a much better mass balance closure. The current methods only allow for

the assessment of mass balance with liquid phase solvent samples directly from the reactor.

10.2.3 Implementation of cycling experiments at different loadings

7 m MDEA/2 m PZ should be cycled in the ISDA over a range of initial CO_2 loadings to better understand the effect of loading on degradation rates. The thermal degradation experiments exhibited a clear trend of increased degradation with increased initial loadings. The ISDA experiments completed for the work summarized in this document did not include CO_2 loadings across a range of initial conditions. The initial loading for all cycling experiments with 7 m MDEA/2 m PZ was 0.14 mol CO_2/mol alkalinity, which matched the solubility of CO_2 for a headspace gas composition of 98% O_2/2% CO_2.

A recommended matrix of experiments to better understand the degradation of 7 m MDEA/2 m PZ with loading changes would include nominal initial loadings of 0.02, 0.05, and a high loading of 0.26 mol CO_2/mol alkalinity, which corresponds to a rich loading. The headspace gas composition would need to be changed to accommodate the solubility condition at each of these loadings at 55 °C. The speciation of the blend is more complex than speciation in other single amine solvents, and degrading the solvent over a range of loadings would prove useful in better understanding how this solvent degrades in both a natural gas application as well as flue gas scrubbing application.

10.2.4 Modify the ISDA to run thermal reactor at 125+ °C

A final modification to the ISDA is the installation of a pump which generates a head pressure in excess of the total pressure of 7 m MDEA/2 m PZ at 125 °C so that cycling experiments with a thermal reactor setting of greater than 125 °C can be completed. The benefits associated with this recommendation include the ability to test

the more thermally resistant solvents such as 8 m PZ at a thermal reactor temperature where solvent degradation will occur in a shorter timeframe. This modification would potentially shorten all cycling experiments with the ISDA by accelerating oxidation.

The current hardware in the ISDA includes a Cole-Parmer pump which is capable of continuously producing no more than ~70 psig. It is anticipated that a pump with a head pressure capability of ~100 psig would extend the upper limit for the thermal reactor temperature to increase to 140+ °C.

10.2.5 Utilize a wider range of headspace gas compositions

Cycling experiments in the ISDA should utilize a wider variety of conditions in headspace gas composition. One recommended change includes performing experiments over a range of headspace gas compositions, including an oxygen content (e.g., 50%) between those conditions already tested in this work (0, 20, and 98%). A similar recommendation is the inclusion of gas-phase components which are typically present in flue gas streams, but have not been tested in the ISDA experiments. These include nitric oxide (NO) and nitrogen dioxide (NO_2) gas. Retrofitting of the system to include these gases will require consideration to health and safety of individuals working in the laboratory, and in the immediate vicinity of the ISDA fume hood.

Appendix A – Analytical Method Programs

A.1 Cation IC Method

```
; ECD.MSA =          22.0
; ECD.Recommended Current =       78
        Pressure.LowerLimit =       200
        Pressure.UpperLimit =       4000
        %A.Equate =  "6"
        %B.Equate =  "8"
        %C.Equate =  "55"
        %D.Equate =  "%D"
        Pump_InjectValve.LoadPosition
        Data_Collection_Rate =      2.0
        Temperature_Compensation =          1.7
        Oven_Temperature =  40
        Suppressor_Type =    CSRS_4mm
; ECD.H2SO4 =        0.0
; ECD.Other eluent =  0.0

        Suppressor_Current = 136

-3.000  Flow = 1.20
        Concentration =        1.1 [mM]
        Curve =        5

-2.400  Pump_relay_1.open

-2.300  Flow = 1.20
        Concentration =        1.1 [mM]
        Curve =        5
        Pump_Relay_1.Closed         Duration= 120

 0.000  Autozero
        Flow = 1.20
        Concentration =        1.1 [mM]
        Curve =        5
        ECD_1.AcqOn
        Pump_InjectValve.InjectPosition      Duration= 30
        Flow = 1.20
        Concentration =        1.1 [mM]
        Curve =        5
```

7.000 Flow = 1.20
Concentration = 1.65 [mM]
Curve = 5

7.001 Flow = 1.20
Concentration = 1.65 [mM]
Curve = 5

20.000 Flow = 1.20
Concentration = 2.75 [mM]
Curve = 5

20.001 Flow = 1.20
Concentration = 8.25 [mM]
Curve = 5

50.000 Flow = 1.20
Concentration = 16.5 [mM]
Curve = 5

55.000 ECD_1.AcqOff

End

A.2 ANION IC METHOD

Sampler.AcquireExclusiveAccess
Sampler_DiverterValve.Position_2
Column_TC.AcquireExclusiveAccess
Compartment_TC.AcquireExclusiveAccess
Pressure.LowerLimit = 200 [psi]
Pressure.UpperLimit = 3000 [psi]
MaximumFlowRamp = 6.00 [mL/min²]
%A.Equate = "%A"
CR_TC = On
Flush Volume = 250
Wait FlushState
NeedleHeight = 2 [mm]
CutSegmentVolume = 10 [µl]
SyringeSpeed = 4
CycleTime = 0 [min]
WaitForTemperature = False
Data_Collection_Rate = 5.0 [Hz]

```
          Temperature_Compensation =          1.7 [%/°C]
          CellHeater.Mode       = On
          CellHeater.TemperatureSet =         35.00 [°C]
          Column_TC.Mode =   On
          Column_TC.TemperatureSet =          30.00 [°C]
          Compartment_TC.Mode =     On
          Compartment_TC.TemperatureSet = 30.00 [°C]
          Suppressor2.Type =    ASRS_4mm
          Suppressor2.CurrentSet =      179 [mA]
          Flow =          1.600 [mL/min]
          Pump_2.Curve =        5
          Wait    SampleReady
          ;Wait  Column_TC.TemperatureState
          ;Wait Compartment_TC.TemperatureState
          ;Wait  Column_TC.TemperatureState
          ;Wait Compartment_TC.TemperatureState
          ; Suppressor1.Carbonate =     0.0
          ; Suppressor1.Bicarbonate =   0.0
          ; Suppressor1.Hydroxide =     45.0
          ; Suppressor1.Tetraborate =   0.0
          ; Suppressor1.Other eluent =  0.0
          ; Suppressor1.Recommended Current =        179

-6.100    Concentration =         45.00 [mM]
          EGC_1.Curve =         5

-6.000    Concentration =         2.00 [mM]
          EGC_1.Curve =         5

 0.000    CDet1.Autozero
          Load
          Wait    CycleTimeState
          Inject
          Wait    InjectState
          Pump_2_Pressure.AcqOn
          CD_1.AcqOn
          CD_1_Total.AcqOn
          Sampler.ReleaseExclusiveAccess
          Compartment_TC.ReleaseExclusiveAccess
          Column_TC.ReleaseExclusiveAccess

10.000    ;compartment_TC.ReleaseExclusiveAccess
          ;column_TC.ReleaseExclusiveAccess
```

17.000 Concentration = 2.00 [mM]
EGC_1.Curve = 5

25.000 Concentration = 45.00 [mM]
EGC_1.Curve = 5

35.000 Concentration = 45.00 [mM]
Pump_2_Pressure.AcqOff
CD_1.AcqOff
CD_1_Total.AcqOff
EGC_1.Curve = 5
End

A.3 AAA-DIRECT AMINO ACID METHOD

Sampler.AcquireExclusiveAccess
Sampler_DiverterValve.Position_1
Column_TC.AcquireExclusiveAccess
Compartment_TC.AcquireExclusiveAccess
Pressure.LowerLimit = 200 [psi]
Pressure.UpperLimit = 3900 [psi]
MaximumFlowRamp = 1.00 [mL/min²]
%A.Equate = "%A"
%B.Equate = "%B"
%C.Equate = "%C"
%D.Equate = "%D"
Flush Volume = 250
Wait FlushState
NeedleHeight = 2 [mm]
CutSegmentVolume = 10 [µl]
SyringeSpeed = 4
CycleTime = 0 [min]
WaitForTemperature = False
EDet1.Mode = IntAmp
EDet1.CellControl = On
Data_Collection_Rate = 1.00 [Hz]
pH.UpperLimit = 13.00
pH.LowerLimit = 10.00
WaveformName = "amino acids (ph,ag,agcl reference)"
WaveformDescription = "Amino Acids (pH/Ag/AgCl Ref.)"
Electrode = pH
Waveform Time = 0.000, Potential = 0.130, GainRegion = Off, Ramp = On, Integration = Off

Waveform Time = 0.040, Potential = 0.130, GainRegion = Off, Ramp = On, Integration = Off
Waveform Time = 0.050, Potential = 0.330, GainRegion = Off, Ramp = On, Integration = Off
Waveform Time = 0.210, Potential = 0.330, GainRegion = On, Ramp = On, Integration = On
Waveform Time = 0.220, Potential = 0.550, GainRegion = On, Ramp = On, Integration = On
Waveform Time = 0.460, Potential = 0.550, GainRegion = On, Ramp = On, Integration = On
Waveform Time = 0.470, Potential = 0.330, GainRegion = On, Ramp = On, Integration = On
Waveform Time = 0.560, Potential = 0.330, GainRegion = Off, Ramp = On, Integration = Off
Waveform Time = 0.570, Potential = -1.670, GainRegion = Off, Ramp = On, Integration = Off
Waveform Time = 0.580, Potential = -1.670, GainRegion = Off, Ramp = On, Integration = Off
Waveform Time = 0.590, Potential = 0.930, GainRegion = Off, Ramp = On, Integration = Off
Waveform Time = 0.600, Potential = 0.130, GainRegion = Off, Ramp = On, Integration = Off, LastStep = On
Column_TC.Mode = On
Column_TC.TemperatureSet = 30.00 [°C]
Compartment_TC.Mode = On
Compartment_TC.TemperatureSet = 30.00 [°C]
Wait SampleReady

-1.000 Flow = 0.250 [mL/min]
%B = 24.0 [%]
%C = 0.0 [%]
%D = 0.0 [%]
Curve = 5

0.000 Load
Inject
InjectValve_1.InjectPosition Duration=120.00
ED_1.AcqOn
ED_1_Total.AcqOn
Sampler.ReleaseExclusiveAccess
Compartment_TC.ReleaseExclusiveAccess
Column_TC.ReleaseExclusiveAccess

8.000 Flow = 0.250 [mL/min]
%B = 36.0 [%]
%C = 0.0 [%]
%D = 0.0 [%]
Curve = 8

11.000 Flow = 0.250 [mL/min]
%B = 36.0 [%]
%C = 0.0 [%]
%D = 0.0 [%]
Curve = 8

18.000 Flow = 0.250 [mL/min]
%B = 20.0 [%]
%C = 40.0 [%]
%D = 0.0 [%]
Curve = 8

21.000 Flow = 0.250 [mL/min]
%B = 16.0 [%]
%C = 44.0 [%]
%D = 0.0 [%]
Curve = 5

23.000 Flow = 0.250 [mL/min]
%B = 16.0 [%]
%C = 70.0 [%]
%D = 0.0 [%]
Curve = 8

42.000 Flow = 0.250 [mL/min]
%B = 16.0 [%]
%C = 70.0 [%]
%D = 0.0 [%]
Curve = 8

42.100 Flow = 0.250 [mL/min]
%B = 80.0 [%]
%C = 0.0 [%]
%D = 0.0 [%]
Curve = 5

44.100 Flow = 0.250 [mL/min]

%B = 80.0 [%]
%C = 0.0 [%]
%D = 0.0 [%]
Curve = 5

44.200 ED_1.AcqOff
ED_1_Total.AcqOff
Flow = 0.250 [mL/min]
%B = 24.0 [%]
%C = 0.0 [%]
%D = 0.0 [%]
Curve = 5

75.000 Flow = 0.250 [mL/min]
%B = 24.0 [%]
%C = 0.0 [%]
%D = 0.0 [%]
Curve = 5
End

A.4 HPLC PROGRAM

Column_A.ActiveColumn = No
TempCtrl = On
Temperature.Nominal = 30.0 [°C]
Column_B.ActiveColumn = No
Pressure.LowerLimit = 25 [bar]
Pressure.UpperLimit = 350 [bar]
MaximumFlowRampDown = Infinite
MaximumFlowRampUp = Infinite
%A.Equate = "%A"
%B.Equate = "%B"
%C.Equate = "%C"
%D.Equate = "%D"
DrawSpeed = 5.000 [µl/s]
DrawDelay = 3000 [ms]
DispSpeed = 20.000 [µl/s]
DispenseDelay = 0 [ms]
WasteSpeed = 32.000 [µl/s]
SampleHeight = 2.000 [mm]
InjectWash = NoWash
LoopWashFactor = 2.000

PunctureOffset = 0.0 [mm]
PumpDevice = "Pump"
InjectMode = Normal
SyncWithPump = On
Data_Collection_Rate = 2.5 [Hz]
TimeConstant = 0.60 [s]
ELS_1.Step = 0.10 [s]
ELS_1.Average = Off
UV_VIS_1.Wavelength = 210 [nm]
EvaporatorTemperature.Nominal = 50 [°C]
NebuliserTemperature = 90 [°C]
LightSourceIntensity = 85 [%]
CarrierFlow.Nominal = 1.60 [slm]
SmoothWidth = 20
PMTGain = 1.0
UV.LeakSensorMode = Disabled

-4.000 Flow = 1.000 [mL/min]
%B = 0.0[%]
%C = 0.0 [%]
%D = 0.0 [%]

0.000
UV.Autozero
ELSD.Autozero
Wait AZ_Done
Wait UV.Ready and ELSD.Ready
Inject
ELS_1.AcqOn
UV_VIS_1.AcqOn
Pump_Pressure.AcqOn

3.000 Flow = 1.000 [mL/min]
%B = 0.0 [%]
%C = 0.0 [%]
%D = 0.0 [%]

10.000 Flow = 1.000 [mL/min]
%B = 0.0 [%]
%C = 5.0 [%]
%D = 0.0 [%]

20.000 Flow = 1.000 [mL/min]
%B = 0.0 [%]
%C = 50.0 [%]
%D = 0.0 [%]

30.000 Flow = 1.000 [mL/min]
%B = 20.0 [%]
%C = 50.0 [%]
%D = 0.0 [%]

ELS_1.AcqOff
UV_VIS_1.AcqOff
Pump_Pressure.AcqOff

End

A.5 IC-MS METHOD

Jason3Auto-HalfmL_min.pgm:
Pressure.LowerLimit = 200 [psi]
Pressure.UpperLimit = 3000 [psi]
%A.Equate = "%A"
CR_TC = On
WaitForTemperature = False
Data_Collection_Rate = 5.0 [Hz]
CellTemperature.Nominal = 30.0 [°C]
ColumnTemperature.Nominal = 30.0 [°C]
Suppressor_Type = CSRS_4mm
Suppressor_Current = 77 [mA]
ECD_Total.Step = 0.20 [s]
ECD_Total.Average = Off
Pump_InjectValve.LoadPosition
Flow = 0.50 [mL/min]

0.000 Concentration = 5.50 [mM]
Autozero
Inject
ECD_1.AcqOn
ECD_Total.AcqOn
Concentration = 5.50 [mM]
Pump_ECD_Relay_2.Closed Duration=10.00

0.100 Pump_ECD_Relay_1.State Closed

1.000 Pump_ECD_Relay_1.State Open

2.300 Pump_InjectValve.InjectPosition Duration=60.00

16.400 Concentration = 5.50 [mM]

16.501 Concentration = 11.00 [mM]

26.400 Concentration = 11.00 [mM]

36.400 Concentration = 38.50 [mM]

47.400 Concentration = 38.50 [mM]

47.500 Concentration = 5.50 [mM]

50.000 ECD_1.AcqOff
ECD_Total.AcqOff
Concentration = 5.50 [mM]

End

A.6 GC-MS METHOD

0111-0539_100X_EI
TRACE GC Ultra
Oven Method
Initial Temperature (C): 60
Initial Time (min): 3.00
Number of Ramps: 1
Rate #1 (deg/min): 3.0
Final Temperature #1 (C): 280
Hold Time #1 (min): 5.00
Post Run Temperature: Off
Enable Cryogenics: Off
Maximum Temperature (C): 320
Prep Run Timeout (min): 10.00
Equilibration Time (min): 1.00

Right SSL Method

Base Temperature: On
Base Temperature (C): 250
Mode: Splitless
Split Flow: On
Split Flow Flow (mL/min): 30
Splitless Time (min): 1.00
Surge Pressure: Off
Surge Pressure (psi): 4.35
Surge Duration (min): 1.00
Constant Purge: On
Stop Purge At: (min): 0.00
Right Carrier Method
Mode: Constant Flow
Initial Value: On
Initial Value (mL/min): 1.50
Initial Time: 1.00
Gas Saver: Off
Gas Saver Flow (mL/min): 20
Gas Saver Time: 2.00
Vacuum Compensation: On

No Left Inlet

No Right Detector

No Left Detector

No Aux Detector

Aux Zones
Aux 1 MS Transfer Line: On
Aux 1 MS Transfer Line (C): 240
Aux 2 : Off
Aux 2 (C): 30

Run Table
External Event #1 Prep-Run Default: Off
External Event #2 Prep-Run Default: Off
External Event #3 Prep-Run Default: Off
External Event #4 Prep-Run Default: Off
External Event #5 Prep-Run Default: Off
External Event #6 Prep-Run Default: Off
External Event #7 Prep-Run Default: Off

Appendix B – ISDA Experimental Data

Table B.1: Summary of Experimental Data, C-1, 7 m MDEA, 55/120 °C

Sample No.	Time (hr)	MDEA (Cations) (mM)	α_{act} (mol CO_2 /mol alk)	Total Alk (mmol/kg)	Concentration (mM)								
							Heat Stable Salts Concentration					Amino Acids	
					DEA+MAE	EDA	Formate	Glycolate	Oxalate	Acetate	Sulfate	Bicine	Glycine
C-1-0	0	3717	0.103	3553	0	0	0.4	0.0	0.0	NM	NM	0.0	0.0
C-1-1	4	3696	0.093	3529	52	0	1.1	0.6	0.0	NM	NM	NM	NM
C-1-2	12	3587	0.086	3516	62	0	5.3	3.0	0.1	NM	NM	1.8	0.0
C-1-3	20	3361	0.078	3450	80	0	11.8	5.3	0.0	NM	NM	NM	NM
C-1-4	28	3484	0.074	3406	187	0	14.8	6.2	0.2	NM	NM	9.8	0.0
C-1-5	36	3355	0.071	3385	208	0	18.4	7.2	0.5	NM	NM	NM	NM
C-1-6	44	3514	0.068	3367	277	0	22.4	8.2	0.8	NM	NM	20.6	0.1
C-1-7	52	3040	0.066	3260	225	0	26.3	9.4	0.7	NM	NM	NM	NM
C-1-8	60	3220	0.069	3291	291	0	29.3	10.2	1.2	NM	NM	31.2	0.1

Table B.2: Summary of Experimental Data - Hydrolyzed, C-1, 7 m MDEA, 55/120 °C

Sample No.	Time (hr)	MDEA (Cations) (mM)	Hydrolyzed Concentration (mM)								
					Heat Stable Salts Concentration					Amino Acids	
			DEA+MAE	EDA	Formate	Glycolate	Oxalate	Acetate	Sulfate	Bicine	Glycine
C-1-0+NaOH	0	3717	0	0	11.1	6.8	0.0	NM	NM	NM	NM
C-1-1+NaOH	4	3703	0	0	9.3	6.9	0.1	NM	NM	NM	NM
C-1-2+NaOH	12	3714	0	0	20.3	11.6	0.2	NM	NM	NM	NM
C-1-3+NaOH	20	3602	80	0	32.7	20.5	0.0	NM	NM	NM	NM
C-1-4+NaOH	28	3413	97	0	37.6	25.8	0.3	NM	NM	NM	NM
C-1-5+NaOH	36	3138	90	0	48.4	32.4	0.0	NM	NM	NM	NM
C-1-6+NaOH	44	2798	107	0	52.0	35.0	0.8	NM	NM	NM	NM
C-1-7+NaOH	52	3203	94	0	46.6	28.5	1.3	NM	NM	NM	NM
C-1-8+NaOH	60	2952	149	0	52.0	30.0	1.4	NM	NM	NM	NM

Table B.3: Summary of Experimental Data, C-2, 7 m MDEA, 55/55 °C

Sample No.	Time (hr)	MDEA (Cations) (mM)	α_{act} (mol CO_2 /mol alk)	Total Alk (mmol/kg)	Concentration (mM)								
							Heat Stable Salts Concentration					Amino Acids	
					DEA+MAE	EDA	Formate	Glycolate	Oxalate	Acetate	Sulfate	Bicine	Glycine
C-2-0	0	4577	0.1	3676	NM	0	0.1	NM	NM	NM	NM	0.0	0.0
C-2-1	8	4515	0.078	3464	NM	0	0.9	NM	NM	NM	NM	NM	NM
C-2-2	16	4541	0.073	3503	NM	0	0.0	NM	NM	NM	NM	0.1	0.0
C-2-3	24	4541	0.079	3505	NM	0	0.0	NM	NM	NM	NM	NM	NM
C-2-4	32	4531	0.076	3507	NM	0	0.2	NM	NM	NM	NM	NM	NM
C-2-5	40	5385	0.075	3521	NM	0	0.2	NM	NM	NM	NM	NM	NM
C-2-6	48	4580	0.07	3503	NM	0	2.3	NM	NM	NM	NM	0.3	0.0
C-2-7	56	4869	0.067	3503	NM	0	0.0	NM	NM	NM	NM	NM	NM
C-2-8	64	4545	0.064	3514	NM	0	0.1	NM	NM	NM	NM	0.5	0.0

Table B.4: Summary of Experimental Data - Hydrolyzed, C-2, 7 m MDEA, 55/55°C

Sample No.	Time (hr)	MDEA (Cations) (mM)	Hydrolyzed Concentration (mM)								
					Heat Stable Salts Concentration					Amino Acids	
			DEA+MAE	EDA	Formate	Glycolate	Oxalate	Acetate	Sulfate	Bicine	Glycine
C-2-0+NaOH	0	4895	NM	0.0	11.6	NM	NM	NM	NM	NM	NM
C-2-1+NaOH	8	4708	NM	0.0	1.6	NM	NM	NM	NM	NM	NM
C-2-2+NaOH	16	5580	NM	0.0	1.2	NM	NM	NM	NM	NM	NM
C-2-3+NaOH	24	4928	NM	0.0	17.9	NM	NM	NM	NM	NM	NM
C-2-4+NaOH	32	4761	NM	0.0	0.8	NM	NM	NM	NM	NM	NM
C-2-5+NaOH	40	5295	NM	0.0	0.8	NM	NM	NM	NM	NM	NM
C-2-6+NaOH	48	4837	NM	0.0	16.5	NM	NM	NM	NM	NM	NM
C-2-7+NaOH	56	6280	NM	0.0	1.2	NM	NM	NM	NM	NM	NM
C-2-8+NaOH	64	4892	NM	0.0	0.0	NM	NM	NM	NM	NM	NM

Table B.5: Summary of Experimental Data, C-3, 7 m MDEA/2 m PZ, 55/55 °C, SSM

Sample No.	Time (hr)	MDEA (Cations) (mM)	α_{act} (mol CO_2 /mol alk)	Total Alk (mmol/kg)	Concentration (mM)								
							Heat Stable Salts Concentration					Amino Acids	
					DEA+MAE	EDA	Formate	Glycolate	Oxalate	Acetate	Sulfate	Bicine	Glycine
C-3-0	0	3826	0.103	3660	NM	NM	0.21	0.0	NM	NM	NM	NM	NM
C-3-0B	1	3859	0.1	3660	NM	NM	0.27	0.0	NM	NM	NM	NM	NM
C-3-1	9	3735	0.099	3609	NM	NM	0.25	0.0	NM	NM	NM	NM	NM
C-3-2	17	3747	0.091	3593	NM	NM	0.35	0.0	NM	NM	NM	NM	NM
C-3-3	25	3751	0.083	3588	NM	NM	0.20	0.0	NM	NM	NM	NM	NM
C-3-4	43	3869	0.071	3580	NM	NM	0.50	0.0	NM	NM	NM	NM	NM
C-3-5	51	3769	0.075	3575	NM	NM	0.40	0.0	NM	NM	NM	NM	NM
C-3-6	59	3745	0.069	3577	NM	NM	0.47	0.0	NM	NM	NM	NM	NM
C-3-7	67	3715	0.067	3563	NM	NM	0.65	0.0	NM	NM	NM	NM	NM
C-3-8	75	4517	0.059	3573	NM	NM	0.00	0.0	NM	NM	NM	NM	NM
C-3-9	83	4450	0.06	3581	NM	NM	0.21	0.0	NM	NM	NM	NM	NM

Table B.6: Summary of Experimental Data - Hydrolyzed, C-3, 7 m MDEA, 55/55 °C, SSM

Sample No.	Time (hr)	MDEA (Cations) (mM)	Hydrolyzed Concentration (mM)								
					Heat Stable Salts Concentration					Amino Acids	
			DEA+MAE	EDA	Formate	Glycolate	Oxalate	Acetate	Sulfate	Bicine	Glycine
C-3-0+NaOH	0	3717	NM	NM	2.20	0.0	NM	NM	NM	NM	NM
C-3-0B+NaOH	1	3716	NM	NM	1.43	0.0	NM	NM	NM	NM	NM
C-3-1+NaOH	9	3746	NM	NM	1.89	0.0	NM	NM	NM	NM	NM
C-3-2+NaOH	17	3796	NM	NM	1.80	0.0	NM	NM	NM	NM	NM
C-3-3+NaOH	25	3784	NM	NM	1.79	0.0	NM	NM	NM	NM	NM
C-3-4+NaOH	43	4248	NM	NM	1.98	0.0	NM	NM	NM	NM	NM
C-3-5+NaOH	51	3853	NM	NM	2.19	0.0	NM	NM	NM	NM	NM
C-3-6+NaOH	59	3846	NM	NM	1.69	0.0	NM	NM	NM	NM	NM
C-3-7+NaOH	67	4676	NM	NM	0.00	0.0	NM	NM	NM	NM	NM
C-3-8+NaOH	75	NM	NM	NM	0.00	0.0	NM	NM	NM	NM	NM

Table B.7: Summary of Experimental Data, C-4, 7 m MDEA, 55/120°C, Stir rate 520 rpm, SSM

Sample No.	Time (hr)	MDEA (Cations) (mM)	α_{act} (mol CO_2 /mol alk)	Total Alk (mmol/kg)	Concentration (mM)								
							Heat Stable Salts Concentration					Amino Acids	
					DEA+MAE	EDA	Formate	Glycolate	Oxalate	Acetate	Sulfate	Bicine	Glycine
C-4-0	0	3795	0.083	3639	NM	NM	0.78	0.00	0.17	NM	NM	NM	NM
C-4-0B	0	3788	0.095	3646	NM	NM	1.90	0.00	0.00	NM	NM	NM	NM
C-4-1	4	3774	0.091	3602	NM	NM	2.72	0.65	0.00	NM	NM	NM	NM
C-4-2	10	3604	0.086	3597	NM	NM	2.52	1.25	0.07	NM	NM	NM	NM
C-4-3	31	3612	0.076	3566	NM	NM	4.38	3.27	0.16	NM	NM	NM	NM
C-4-4	54	3590	0.067	3527	NM	NM	6.90	5.40	0.30	NM	NM	NM	NM
C-4-5	65	3795	0.069	3444	NM	NM	11.33	6.16	0.75	NM	NM	NM	NM

Table B.8: Summary of Experimental Data - Hydrolyzed, C-4, 7 m MDEA, 55/120°C, Stir rate 520 rpm, SSM

Sample No.	Time (hr)	MDEA (Cations) (mM)	Hydrolyzed Concentration (mM)								
					Heat Stable Salts Concentration					Amino Acids	
			DEA+MAE	EDA	Formate	Glycolate	Oxalate	Acetate	Sulfate	Bicine	Glycine
C-4-0+NaOH	0	NM	NM	NM	0.0	0.0	0.0	NM	NM	NM	NM
C-4-0B+NaOH	0	NM	NM	NM	2.75	0.12	0.00	NM	NM	NM	NM
C-4-1+NaOH	4	NM	NM	NM	3.28	0.82	0.00	NM	NM	NM	NM
C-4-2+NaOH	10	NM	NM	NM	3.85	1.37	0.00	NM	NM	NM	NM
C-4-3+NaOH	31	NM	NM	NM	6.57	3.51	0.23	NM	NM	NM	NM
C-4-4+NaOH	54	NM	NM	NM	10.21	5.62	0.57	NM	NM	NM	NM
C-4-5+NaOH	65	NM	NM	NM	12.52	6.21	0.67	NM	NM	NM	NM

Table B.9: Summary of Experimental Data, C-5, 7 m MDEA, 55/120°C, Stir rate 1000 rpm, SSM

Sample No.	Time (hr)	MDEA (Cations) (mM)	α_{act} (mol CO_2 /mol alk)	Total Alk (mmol/kg)	Concentration (mM)								
							Heat Stable Salts Concentration					Amino Acids	
					DEA+MAE	EDA	Formate	Glycolate	Oxalate	Acetate	Sulfate	Bicine	Glycine
C-5-0i	0	4874	0.099	3623	NM	NM	0.0	0.0	0.12	NM	0.71	NM	NM
C-5-1	3	4775	0.09	3560	NM	NM	2.3	0.4	0.06	NM	0.74	NM	NM
C-5-2	4	4604	0.09	3550	NM	NM	3.0	1.1	0.06	NM	0.84	NM	NM
C-5-3	10	4666	0.081	3565	NM	NM	7.9	3.5	0.16	NM	0.75	NM	NM
C-5-4	28	4437	0.081	3494	NM	NM	19.0	9.0	0.47	NM	0.70	NM	NM
C-5-5	35.5	4764	0.079	3447	NM	NM	21.4	10.4	0.56	NM	0.71	NM	NM
C-5-6	52	4267	0.076	3382	NM	NM	28.3	14.4	1.13	NM	0.74	NM	NM
C-5-7	59	4616	0.065	3351	NM	NM	28.5	12.4	1.54	NM	1.14	NM	NM
C-5-8	81	4126	0.063	3291	NM	NM	32.3	11.9	1.96	NM	1.11	NM	NM
C-5-9	82	4106	0.062	3250	NM	NM	34.3	11.9	1.83	NM	0.84	NM	NM
C-5-10	109	3721	0.061	3165	NM	NM	38.7	13.6	2.97	NM	1.11	NM	NM

Table B.10: Summary of Experimental Data - Hydrolyzed, C-5, 7 m MDEA, 55/120°C, Stir rate 1000 rpm, SSM

Sample No.	Time (hr)	MDEA (Cations) (mM)	Hydrolyzed Concentration (mM)								
					Heat Stable Salts Concentration					Amino Acids	
			DEA+MAE	EDA	Formate	Glycolate	Oxalate	Acetate	Sulfate	Bicine	Glycine
C-5-0i+NaOH	0	4778	NM	NM	5.6	0.0	0.13	NM	2.65	NM	NM
C-5-1+NaOH	3	4586	NM	NM	7.1	0.7	0.12	NM	1.94	NM	NM
C-5-2+NaOH	4	4769	NM	NM	7.3	1.0	0.17	NM	1.11	NM	NM
C-5-3+NaOH	10	6687	NM	NM	12.1	3.0	0.22	NM	1.13	NM	NM
C-5-4+NaOH	28	5955	NM	NM	30.6	9.3	0.61	NM	1.09	NM	NM
C-5-5+NaOH	35.5	4804	NM	NM	33.7	11.1	0.76	NM	1.04	NM	NM
C-5-6+NaOH	52	4254	NM	NM	41.5	12.5	1.62	NM	2.06	NM	NM
C-5-7+NaOH	59	4503	NM	NM	43.9	12.6	1.81	NM	2.01	NM	NM
C-5-8+NaOH	81	3824	NM	NM	59.0	15.7	2.83	NM	1.78	NM	NM
C-5-9+NaOH	82	3768	NM	NM	55.5	15.2	3.10	NM	1.88	NM	NM
C-5-10+NaOH	109	3870	NM	NM	61.5	16.1	3.37	NM	1.48	NM	NM

Table B.11: Summary of Experimental Data, C-6, 7 m MDEA, 55/120°C, Bubble vessel, SSM

Sample No.	Time (hr)	MDEA (Cations) (mM)	α_{act} (mol CO_2 /mol alk)	Total Alk (mmol/kg)	Concentration (mM)								
							Heat Stable Salts Concentration					Amino Acids	
					DEA+MAE	EDA	Formate	Glycolate	Oxalate	Acetate	Sulfate	Bicine	Glycine
C-6-0i	0	4565	0.104	3620	0.0	NM	0.18	0.00	0.17	NM	1.06	0.0	0.0
C-6-1	1	4534	0.097	3631	0.0	NM	0.28	0.10	0.07	NM	0.94	NM	NM
C-6-2	21	4391	0.086	3572	52.7	NM	6.32	3.93	0.33	NM	1.03	6.8	0.1
C-6-3	27	4323	0.082	3591	61.4	NM	8.30	4.95	0.46	NM	0.99	NM	NM
C-6-4	45	4404	0.075	3444	99.5	NM	12.84	7.01	0.90	NM	1.02	18.2	0.1
C-6-5	50.5	4621	0.071	3437	124.7	NM	13.82	7.37	1.03	NM	1.04	21.8	0.3
C-6-6	69.5	4093	0.066	3313	162.1	NM	17.96	9.29	1.63	NM	1.00	32.3	0.6
C-6-7	74.5	4466	0.052	3296	170.0	NM	18.87	9.69	1.79	NM	1.02	35.0	0.5
C-6-8	93	3980	0.049	3214	200.8	NM	21.85	10.86	2.41	NM	0.97	43.8	0.7
C-6-F	94	3983	0.049	3155	184.8	NM	21.29	10.15	2.35	NM	1.05	NM	NM

Table B.12: Summary of Experimental Data - Hydrolyzed, C-6, 7 m MDEA, 55/120°C, Bubble vessel, SSM

Sample No.	Time (hr)	MDEA (Cations) (mM)	Hydrolyzed Concentration (mM)								
					Heat Stable Salts Concentration					Amino Acids	
			DEA+MAE	EDA	Formate	Glycolate	Oxalate	Acetate	Sulfate	Bicine	Glycine
C-6-0+NaOH	0	4722	0.0	NM	1.37	0.11	0.12	NM	1.41	NM	NM
C-6-1+NaOH	1	4753	0.0	NM	1.59	0.24	0.10	NM	1.53	NM	NM
C-6-2+NaOH	21	4618	0.0	NM	8.33	3.60	0.46	NM	1.57	NM	NM
C-6-3+NaOH	27	4535	0.0	NM	10.81	4.58	0.68	NM	1.58	NM	NM
C-6-4+NaOH	45	4377	91.0	NM	16.41	6.00	1.13	NM	1.22	NM	NM
C-6-5+NaOH	50.5	4684	98.3	NM	16.73	6.81	1.38	NM	1.21	NM	NM
C-6-6+NaOH	69.5	4011	147.2	NM	20.84	7.98	1.96	NM	1.37	NM	NM
C-6-7+NaOH	74.5	4385	127.0	NM	22.12	8.48	2.23	NM	1.36	NM	NM
C-6-8+NaOH	93	3641	190.2	NM	25.98	9.50	2.94	NM	1.42	NM	NM

Table B.13: Summary of Experimental Data, C-7, 7 m MDEA, 55/120°C, Bubble vessel, SSM, 100 mM Inh A

Sample No.	Time (hr)	MDEA (Cations) (mM)	α_{act} (mol CO_2 /mol alk)	Total Alk (mmol/kg)	Concentration (mM)								
							Heat Stable Salts Concentration					Amino Acids	
					DEA+MAE	EDA	Formate	Glycolate	Oxalate	Acetate	Sulfate	Bicine	Glycine
C-7-0i	0	4582	0.097	3589	0.0	NM	0.27	0.00	0.02	NM	1.43	0.0	0.0
C-7-1	0	4586	0.097	3549	0.0	NM	0.51	0.00	0.00	NM	1.19	0.0	0.0
C-7-2	2	4542	0.095	3552	6.2	NM	0.96	0.64	0.00	NM	1.24	0.1	0.0
C-7-3	20	4342	0.083	3528	41.4	NM	5.43	3.71	0.41	NM	1.15	6.2	0.0
C-7-4	25.5	4496	0.077	3485	3.9	NM	6.22	3.93	0.72	NM	1.26	7.7	0.0
C-7-5	50	4455	0.069	3296	86.8	NM	12.35	6.42	1.76	NM	1.20	18.8	0.0
C-7-6	71	4035	0.062	3222	121.6	NM	16.85	7.79	2.72	NM	1.31	NM	0.0
C-7-7	94.5	4157	0.044	3102	153.1	NM	21.28	9.68	5.68	NM	1.65	NM	0.0
C-7-F	95	3837	0.046	3108	139.2	NM	21.32	9.93	3.92	NM	1.17	NM	0.0

Table B.14: Summary of Experimental Data - Hydrolyzed, C-7, 7 m MDEA, 55/120°C, Bubble vessel, SSM, 100 mM Inh A

Sample No.	Time (hr)	MDEA (Cations) (mM)	Hydrolyzed Concentration (mM)								
					Heat Stable Salts Concentration					Amino Acids	
			DEA+MAE	EDA	Formate	Glycolate	Oxalate	Acetate	Sulfate	Bicine	Glycine
C-7-0i+NaOH	0	4667	0.0	NM	2.17	0.00	0.00	NM	2.18	NM	NM
C-7-1+NaOH	0	4627	3.8	NM	1.82	0.00	0.00	NM	2.91	NM	NM
C-7-2+NaOH	2	4569	6.4	NM	2.30	0.65	0.00	NM	6.06	NM	NM
C-7-3+NaOH	20	4587	30.0	NM	8.14	3.64	0.59	NM	3.98	NM	NM
C-7-4+NaOH	25.5	4551	0.0	NM	10.95	4.17	0.56	NM	4.18	NM	NM
C-7-5+NaOH	50	4394	89.8	NM	17.20	6.59	2.32	NM	3.70	NM	NM
C-7-6+NaOH	71	4157	101.9	NM	24.66	7.45	2.70	NM	3.95	NM	NM
C-7-7+NaOH	94.5	4235	154.1	NM	28.65	9.03	4.61	NM	3.74	NM	NM

Table B.15: Summary of Experimental Data, C-8, 7 m MDEA/2 m PZ, 55/120°C, 98% N_2 Purge gas, SSM

Sample No.	Time (hr)	MDEA (Cations) (mM)	α_{act} (mol CO_2 /mol alk)	Total Alk (mmol/kg)	Concentration (mM)								
							Heat Stable Salts Concentration					Amino Acids	
					DEA+MAE	EDA	Formate	Glycolate	Oxalate	Acetate	Sulfate	Bicine	Glycine
C-8-0	0	4506	0.103	3618	NM	NM	0.85	0.20	0.00	NM	0.91	NM	NM
C-8-1	2.5	4674	0.104	3608	NM	NM	0.95	0.24	0.00	NM	0.93	NM	NM
C-8-2	25	4635	0.105	3551	NM	NM	1.50	0.35	1.51	NM	0.82	NM	NM
C-8-3	49	4595	0.105	3500	NM	NM	1.73	0.37	0.02	NM	0.87	NM	NM
C-8-4	68	4458	0.099	3481	NM	NM	1.96	0.49	0.00	NM	0.97	NM	NM
C-8-5	73.5	4814	0.11	3454	NM	NM	2.17	0.52	0.00	NM	0.92	NM	NM
C-8-6	97.5	4407	0.087	3415	NM	NM	1.97	0.48	0.02	NM	1.02	NM	NM
C-8-7	117	4740	0.094	3394	NM	NM	2.09	0.42	0.02	NM	1.13	NM	NM
C-8-8	148	4207	0.096	3354	NM	NM	2.22	0.71	0.04	NM	0.93	NM	NM

Table B.16: Summary of Experimental Data - Hydrolyzed, C-8, 7 m MDEA, 55/120°C, 98% N_2 Purge gas, SSM

Sample No.	Time (hr)	MDEA (Cations) (mM)	Hydrolyzed Concentration (mM)								
					Heat Stable Salts Concentration					Amino Acids	
			DEA+MAE	EDA	Formate	Glycolate	Oxalate	Acetate	Sulfate	Bicine	Glycine
C-8-0+NaOH	0	4833	NM	NM	2.59	0.19	0.00	NM	1.25	NM	NM
C-8-1+NaOH	2.5	4768	NM	NM	2.31	0.11	0.00	NM	1.34	NM	NM
C-8-2+NaOH	25	4797	NM	NM	2.31	0.17	0.00	NM	1.63	NM	NM
C-8-3+NaOH	49	4704	NM	NM	2.35	0.22	0.00	NM	1.29	NM	NM
C-8-4+NaOH	68	4771	NM	NM	2.32	0.29	0.00	NM	1.31	NM	NM
C-8-5+NaOH	73.5	4992	NM	NM	2.31	0.19	0.00	NM	1.34	NM	NM
C-8-6+NaOH	97.5	4709	NM	NM	2.07	0.39	0.00	NM	1.26	NM	NM
C-8-7+NaOH	117	4946	NM	NM	2.43	0.39	0.00	NM	1.52	NM	NM
C-8-8+NaOH	148	4501	NM	NM	2.14	0.41	0.00	NM	1.82	NM	NM
C-8-9+NaOH	167.5	4488	NM	NM	2.35	0.40	0.00	NM	1.53	NM	NM

Table B.17: Summary of Experimental Data, C-9, 7 m MDEA, 55/120°C, 98% N_2 Purge gas, No stirring, SSM

Sample No.	Time (hr)	MDEA (Cations) (mM)	α_{act} (mol CO_2 /mol alk)	Total Alk (mmol/kg)	Concentration (mM)								
							Heat Stable Salts Concentration					Amino Acids	
					DEA+MAE	EDA	Formate	Glycolate	Oxalate	Acetate	Sulfate	Bicine	Glycine
C-9-0	0	4741	0.102	3638	NM	NM	0.42	0.05	0.03	NM	0.64	NM	NM
C-9-1	1	4884	0.103	3593	NM	NM	0.34	0.12	0.03	NM	0.62	NM	NM
C-9-2	18	4872	0.1	3609	NM	NM	1.75	0.20	0.03	NM	0.66	NM	NM
C-9-3	27	4848	0.09	3571	NM	NM	1.81	0.22	0.02	NM	0.64	NM	NM
C-9-4	42	4724	0.082	3530	NM	NM	1.76	0.23	0.04	NM	0.60	NM	NM
C-9-5	48	4835	0.08	3472	NM	NM	1.82	0.27	0.03	NM	0.62	NM	NM
C-9-6	68	4466	0.074	3454	NM	NM	1.93	0.36	0.03	NM	0.73	NM	NM

Table B.18: Summary of Experimental Data - Hydrolyzed, C-9, 7 m MDEA, 55/120°C, 98% N_2 Purge gas, No stirring, SSM

Sample No.	Time (hr)	MDEA (Cations) (mM)	Hydrolyzed Concentration (mM)								
					Heat Stable Salts Concentration					Amino Acids	
			DEA+MAE	EDA	Formate	Glycolate	Oxalate	Acetate	Sulfate	Bicine	Glycine
C-9-0+NaOH	0	4948	NM	NM	1.76	0.10	0.05	NM	1.19	NM	NM
C-9-1+NaOH	1	5117	NM	NM	2.47	0.21	0.07	NM	1.04	NM	NM
C-9-2+NaOH	18	5197	NM	NM	2.47	0.19	0.06	NM	0.97	NM	NM
C-9-3+NaOH	27	5266	NM	NM	2.45	0.22	0.06	NM	0.98	NM	NM
C-9-4+NaOH	42	5177	NM	NM	2.20	0.25	0.04	NM	0.93	NM	NM
C-9-5+NaOH	48	5293	NM	NM	2.23	0.22	0.05	NM	0.99	NM	NM

Table B.19: Summary of Experimental Data, C-10, 7 m MDEA, 55/100°C, SSM

Sample No.	Time (hr)	MDEA (Cations) (mM)	α_{act} (mol CO_2 /mol alk)	Total Alk (mmol/kg)	Concentration (mM)								
							Heat Stable Salts Concentration					Amino Acids	
					DEA+MAE	EDA	Formate	Glycolate	Oxalate	Acetate	Sulfate	Bicine	Glycine
C-10-0	0	0.00	0.102	3555	0	NM	0.15	0.00	0.26	0.00	2.16	0.0	0.0
C-10-1	1	4440.00	0.098	3594	102	NM	0.24	0.07	0.31	0.05	2.39	0.0	0.0
C-10-2	18	3242.05	0.083	3492	101	NM	1.89	1.56	0.40	0.06	2.18	2.0	0.1
C-10-3	25	3234.96	0.078	3462	36	NM	3.48	2.09	0.51	0.06	2.21	4.1	0.2
C-10-4	41.5	2828.34	0.07	3385	57	NM	6.92	3.01	0.81	0.35	2.19	7.6	0.0
C-10-5	47.5	3015.19	0.068	3351	71	NM	8.27	3.58	0.98	0.43	2.21	10.4	0.0
C-10-6	68.5	2871.65	0.065	3275	91	NM	12.50	4.47	1.51	0.62	2.24	16.4	0.0
C-10-7	94	2873.25	0.06	3203	158	NM	16.86	5.28	2.16	0.28	2.20	31.5	0.0
C-10-8	115	2727.90	0.059	3181	136	NM	20.53	6.16	2.84	0.42	2.27	40.0	0.1
C-10-10	160	2612.80	0.059	3101	180	NM	24.14	6.62	3.60	0.44	2.28	42.4	0.0

Table B.20: Summary of Experimental Data - Hydrolyzed, C-10, 7 m MDEA, 55/100°C, SSM

Sample No.	Time (hr)	MDEA (Cations) (mM)	Hydrolyzed Concentration (mM)								
					Heat Stable Salts Concentration					Amino Acids	
			DEA+MAE	EDA	Formate	Glycolate	Oxalate	Acetate	Sulfate	Bicine	Glycine
C-10-0+NaOH	0	3254	0	NM	1.49	0.00	0.72	0.21	4.68	NM	NM
C-10-1+NaOH	1	3436	0	NM	1.28	0.00	0.73	0.21	4.81	NM	NM
C-10-2+NaOH	18	3320	0	NM	4.61	1.72	0.84	0.20	4.23	NM	NM
C-10-3+NaOH	25	3222	48	NM	6.67	2.17	1.04	0.25	6.55	NM	NM
C-10-4+NaOH	41.5	3547	47	NM	13.47	3.89	1.43	0.37	5.28	NM	NM
C-10-5+NaOH	47.5	3433	58	NM	15.05	3.97	1.70	0.20	4.62	NM	NM
C-10-6+NaOH	68.5	3073	100	NM	21.86	5.15	2.43	0.25	4.19	NM	NM
C-10-7+NaOH	94	3189	132	NM	29.13	0.00	3.35	0.66	3.93	NM	NM
C-10-8+NaOH	115	3070	143	NM	36.42	7.38	4.52	0.53	4.71	NM	NM
C-10-9+NaOH	137	0	192	NM	40.04	7.69	5.23	0.58	4.91	NM	NM
C-10-10+NaOH	160	0	186	NM	48.05	8.45	6.45	0.70	4.73	NM	NM

Table B.21: Summary of Experimental Data, C-11, 7 m MDEA, 55/80°C, SSM

Sample No.	Time (hr)	MDEA (Cations) (mM)	α_{act} (mol CO_2 /mol alk)	Total Alk (mmol/kg)	Concentration (mM)								
							Heat Stable Salts Concentration					Amino Acids	
					DEA+MAE	EDA	Formate	Glycolate	Oxalate	Acetate	Sulfate	Bicine	Glycine
C-11-0	0	3636	0.105	3584	0.0	NM	0.2	0.06	0.21	0.00	2.43	0.0	0.0
C-11-1	3	3885	0.101	3589	0.0	NM	0.2	0.07	0.21	0.09	2.40	0.4	0.0
C-11-2	25	3830	0.083	3540	0.0	NM	0.6	0.58	0.12	0.07	1.69	1.8	0.1
C-11-3	46.5	3696	0.071	3527	0.0	NM	1.2	0.95	0.15	0.24	1.61	1.4	0.3
C-11-4	67	3662	0.063	3509	0.0	NM	1.9	1.47	0.24	0.41	1.68	4.8	0.6
C-11-5	73.5	3872	0.058	3480	0.0	NM	2.0	1.48	0.30	0.41	1.51	5.5	0.5
C-11-6	91	3698	0.055	3514	0.0	NM	2.7	1.85	0.30	0.56	1.39	NM	NM
C-11-7	115	3791	0.04	3470	0.0	NM	3.5	2.45	0.32	0.39	1.70	NM	NM

Table B.22: Summary of Experimental Data - Hydrolyzed, C-11, 7 m MDEA, 55/80°C, SSM

Sample No.	Time (hr)	MDEA (Cations) (mM)	Hydrolyzed Concentration (mM)								
					Heat Stable Salts Concentration					Amino Acids	
			DEA+MAE	EDA	Formate	Glycolate	Oxalate	Acetate	Sulfate	Bicine	Glycine
C-11-0+NaOH	0	3954	NM	NM	1.4	0.05	0.42	0.36	2.31	NM	NM
C-11-1+NaOH	3	3978	NM	NM	1.4	0.10	0.42	0.03	2.44	NM	NM
C-11-2+NaOH	25	3017	NM	NM	2.2	0.55	0.41	0.07	2.47	NM	NM
C-11-3+NaOH	46.5	3467	NM	NM	2.9	1.06	0.44	0.20	2.45	NM	NM
C-11-4+NaOH	67	3459	NM	NM	3.6	1.40	0.41	0.21	3.31	NM	NM
C-11-5+NaOH	73.5	3892	NM	NM	4.0	1.73	0.95	0.32	3.57	NM	NM
C-11-6+NaOH	91	3319	NM	NM	5.1	2.17	0.99	0.33	3.46	NM	NM

Table B.23: Summary of Experimental Data, C-12, 7 m MDEA, 55/120°C, SSM

Sample No.	Time (hr)	MDEA (Cations) (mM)	α_{act} (mol CO_2 /mol alk)	Total Alk (mmol/kg)	Concentration (mM)								
							Heat Stable Salts Concentration					Amino Acids	
					DEA+MAE	EDA	Formate	Glycolate	Oxalate	Acetate	Sulfate	Bicine	Glycine
C-12-0	0	3452	0.120	3550	0.0	NM	0.00	0.00	0.00	0.00	16.36	0.0	0.0
C-12-1	2	3426	0.116	3611	0.0	NM	0.25	0.00	0.00	0.00	16.11	0.0	0.0
C-12-2	6.5	3466	0.113	3613	0.0	NM	0.35	0.00	0.00	0.00	18.61	0.0	0.0
C-12-3	23	3391	0.096	3551	0.0	NM	0.82	0.41	0.00	0.00	15.24	1.0	0.0
C-12-4	30	3430	0.089	3540	0.0	NM	1.08	0.76	0.00	0.00	15.13	1.5	0.0
C-12-5	47	3432	0.081	3500	0.0	NM	1.96	1.12	0.00	0.29	14.90	3.2	0.0
C-12-6	70.5	3319	0.068	3464	0.0	NM	5.83	3.32	0.00	0.00	15.95	6.1	0.1
C-12-7	97	3293	0.047	3392	52.1	NM	9.11	4.24	0.89	0.00	17.26	11.5	0.3
C-12-8	121	2887	0.044	3327	90.5	NM	13.12	5.12	1.28	0.16	14.42	15.9	0.5
C-12-9	148	3062	0.041	3275	115.0	NM	17.39	5.98	1.82	0.00	14.29	21.9	1.1
C-12-10	167	3071	0.040	3234	129.3	NM	21.05	6.69	2.10	0.34	14.16	27.0	1.5

Table B.24: Summary of Experimental Data - Hydrolyzed, C-12, 7 m MDEA, 55/120°C, SSM

Sample No.	Time (hr)	MDEA (Cations) (mM)	Hydrolyzed Concentration (mM)								
					Heat Stable Salts Concentration					Amino Acids	
			DEA+MAE	EDA	Formate	Glycolate	Oxalate	Acetate	Sulfate	Bicine	Glycine
C-12-0+NaOH	0	3707	0.0	NM	2.34	0.00	0.00	0.00	33.38	NM	NM
C-12-1+NaOH	2	3759	0.0	NM	2.52	0.20	0.00	0.00	28.02	NM	NM
C-12-2+NaOH	6.5	3794	0.0	NM	2.45	0.43	0.00	0.28	27.95	NM	NM
C-12-3+NaOH	23	3728	0.0	NM	4.19	1.18	0.00	0.17	28.04	NM	NM
C-12-4+NaOH	30	3671	0.0	NM	5.67	1.57	0.00	0.00	27.51	NM	NM
C-12-5+NaOH	47	3939	0.0	NM	7.70	2.39	0.00	0.23	27.64	NM	NM
C-12-6+NaOH	70.5	3608	0.0	NM	11.03	2.98	0.00	0.00	27.22	NM	NM
C-12-7+NaOH	97	3687	0.0	NM	15.91	4.53	1.54	0.25	27.12	NM	NM
C-12-8+NaOH	121	3346	0.0	NM	21.72	5.56	1.99	0.20	26.36	NM	NM
C-12-9+NaOH	148	3577	97.2	NM	29.88	6.79	2.32	0.11	23.78	NM	NM
C-12-10+NaOH	167	3418	131.4	NM	33.58	6.81	2.45	0.00	14.61	NM	NM

Table B.25: Summary of Experimental Data, C-13, 7 m MDEA, 55/120°C, 98% Air Purge gas, SSM

Sample No.	Time (hr)	MDEA (Cations) (mM)	α_{act} (mol CO_2 /mol alk)	Total Alk (mmol/kg)	Concentration (mM)								
							Heat Stable Salts Concentration					Amino Acids	
					DEA+MAE	EDA	Formate	Glycolate	Oxalate	Acetate	Sulfate	Bicine	Glycine
C-13-0 (unl)	0	3722	0.102	3579	0.0	NM	0	0	0	0	0	0.0	0.0
C-13-1	1.5	3672	0.102	3586	5.5	NM	0.67	0.11	0.19	0.00	1.27	0.1	0.0
C-13-2	17.5	3667	0.096	3556	13.4	NM	2.71	0.91	0.30	0.00	1.14	0.3	0.0
C-13-3	45	3596	0.085	3553	24.0	NM	5.24	2.15	0.32	0.32	1.19	1.3	0.0
C-13-4	65.5	3667	0.078	3548	29.2	NM	6.89	3.11	0.37	0.54	1.20	2.1	0.0
C-13-5	90	3774	0.085	3529	38.4	NM	8.27	3.81	0.47	0.57	1.07	3.4	0.1
C-13-6	113.5	3683	0.068	3523	40.5	NM	10.18	4.74	0.63	0.88	1.00	4.6	0.1
C-13-7	137.5	4093	0.051	3503	67.3	NM	11.12	5.29	0.75	0.51	1.18	6.2	0.1
C-13-8	163.5	3998	0.038	3483	57.4	NM	12.62	5.99	0.89	0.44	1.31	8.7	0.2
C-13-9	188	3475	0.036	3488	58.7	NM	14.96	7.18	1.11	0.92	1.51	9.9	0.2
C-13-10	213.5	3848	0.036	3509	71.0	NM	14.30	6.97	1.12	0.95	1.01	12.7	0.3
C-13-11	237.5	3929	0.036	3495	93.1	NM	17.00	8.44	1.42	1.22	1.23	15.0	0.3
C-13-12	257	3794	0.035	3434	75.4	NM	15.27	7.37	1.33	0.64	1.02	17.5	0.3
C-13-13	281	3574	0.034	3436	98.8	NM	17.52	8.68	1.52	1.40	1.32	19.3	0.4
C-13-14	305.5	3227	0.033	3428	74.7	NM	18.23	9.18	1.68	1.31	0.85	22.6	0.5
C-13-15	331	3597	0.026	3397	86.4	NM	19.49	10.04	2.82	1.72	1.09	26.5	0.5
C-13-16	352.5	3205	0.026	3400	110.5	NM	19.65	10.25	2.21	1.71	0.89	29.3	0.6
C-13-17	379.5	3893	0.024	3404	130.8	NM	18.82	9.85	2.14	1.67	1.05	34.5	0.6
C-13-18	401.5	3752	0.028	3355	114.5	NM	20.36	11.27	2.48	2.21	0.82	36.0	0.7
C-13-19	449.5	3759	0.025	3335	0.0	NM	21.09	11.77	2.92	2.11	1.56	41.9	0.8

Table B.26: Summary of Experimental Data - Hydrolyzed, C-13, 7 m MDEA, 55/120°C, 98% Air purge gas, SSM

Sample No.	Time (hr)	MDEA (Cations) (mM)	Hydrolyzed Concentration (mM)								
					Heat Stable Salts Concentration					Amino Acids	
			DEA+MAE	EDA	Formate	Glycolate	Oxalate	Acetate	Sulfate	Bicine	Glycine
C-13-0	0	4163	0.0	NM	3.02	0.00	0.28	0.00	1.87	NM	NM
C-13-1	1.5	4097	0.0	NM	2.93	0.00	0.32	0.79	1.53	NM	NM
C-13-2	17.5	3930	0.0	NM	3.77	0.56	0.35	0.00	1.09	NM	NM
C-13-3	45	3805	18.2	NM	7.08	1.59	0.47	0.41	1.40	NM	NM
C-13-4	65.5	4088	26.4	NM	9.53	2.46	0.55	0.74	1.22	NM	NM
C-13-5	90	4543	39.8	NM	11.67	3.08	0.67	0.53	1.32	NM	NM
C-13-6	113.5	3490	42.9	NM	13.31	4.01	0.80	0.53	0.97	NM	NM
C-13-7	137.5	4452	50.1	NM	14.50	4.56	0.97	0.48	1.15	NM	NM
C-13-8	163.5	4237	72.9	NM	16.19	5.31	1.16	0.44	1.20	NM	NM
C-13-9	188	3897	63.6	NM	18.09	6.11	1.28	0.88	1.24	NM	NM
C-13-10	213.5	3988	71.8	NM	19.78	6.73	1.48	0.98	1.58	NM	NM
C-13-11	237.5	3886	66.1	NM	20.35	7.03	1.62	0.75	1.21	NM	NM
C-13-12	257	3783	80.7	NM	22.97	7.71	1.75	0.00	1.51	NM	NM
C-13-13	281	3768	85.6	NM	22.75	7.92	1.87	0.79	1.22	NM	NM
C-13-14	305.5	3684	92.2	NM	25.05	8.75	2.16	2.11	3.09	NM	NM
C-13-15	331	3962	97.6	NM	24.84	9.20	2.56	1.26	1.52	NM	NM
C-13-16	352.5	3724	70.1	NM	24.56	9.34	2.37	1.06	1.05	NM	NM
C-13-17	379.5	3869	93.2	NM	27.42	9.89	2.83	2.24	2.91	NM	NM
C-13-18	401.5	3823	0.0	NM	25.40	9.58	2.78	1.51	1.47	NM	NM
C-13-19	449.5	3437	93.2	NM	27.43	10.73	3.10	1.90	2.06	NM	NM

Table B.27: Summary of Experimental Data, C-14, 7 m MDEA/2 m PZ, 55/90°C, 98% Air Purge gas, SSM

Sample No.	Time (hr)	MDEA (Cations) (mM)	α_{act} (mol CO_2 /mol alk)	Total Alk (mmol/kg)	Concentration (mM)								
							Heat Stable Salts Concentration					Amino Acids	
					DEA+MAE	EDA	Formate	Glycolate	Oxalate	Acetate	Sulfate	Bicine	Glycine
C-14-0	0	3480	0.104	3616	0.2	NM	0.14	0.00	0.34	0.00	1.25	0.0	0.0
C-14-1	3	3391	0.103	3616	3.0	NM	0.48	0.01	0.19	0.00	1.20	0.0	0.0
C-14-2a	19	3397	0.092	3617	4.5	NM	0.69	0.19	0.16	0.00	1.09	0.0	0.0
C-14-2b	19	3464	0.095	3615	1.4	NM	0.55	0.20	0.14	0.00	1.10	0.0	0.0
C-14-2c	19	3369	0.090	3631	0.0	NM	0.54	0.19	0.13	0.00	1.02	0.0	0.0
C-14-3	42.5	3709	0.076	3622	11.0	NM	0.60	0.20	0.14	0.00	1.07	0.0	0.0
C-14-4	66.5	3323	0.049	3600	4.4	NM	1.07	0.58	0.17	0.19	1.13	0.1	0.0
C-14-5	91	3395	0.036	3609	2.4	NM	1.99	1.06	0.20	0.70	1.58	0.3	0.0
C-14-6	121.5	3508	0.043	3589	0.5	NM	3.48	1.71	0.31	0.08	1.02	2.8	0.0
C-14-7	143.5	3485	0.035	3546	19.9	NM	5.07	2.24	0.45	0.14	1.06	4.0	0.0
C-14-8a	163	3386	0.036	3553	45.2	NM	6.24	2.56	0.55	0.14	1.15	5.8	0.0
C-14-8b	163	3387	0.043	3532	23.5	NM	6.95	2.81	0.66	0.10	1.08	7.0	0.0
C-14-8c	163	3316	0.104	0	9.3	NM	7.35	2.89	0.68	0.68	1.39	5.6	0.0
C-14-8-avg	163	3363		3562	0.0	NM	6.94	2.86	0.71	0.15	1.05	7.2	0.0
C-14-9sp	164	3328	0.041	3544	41.3	NM	7.08	2.85	0.68	0.31	1.17	6.6	0.0
C-14-10sp	187	6921	0.040	3549	755.7	NM	7.01	2.90	0.72	0.18	1.09	7.4	0.0
C-14-11sp	210.5	7061	0.033	3576	786.5	NM	8.38	3.14	0.83	0.34	1.15	7.7	2.1
C-14-12sp	234.5	3344	0.030	3527	2.1	NM	9.47	3.46	0.99	0.31	1.14	10.9	4.2
C-14-13sp	263.5	3490	0.033	3489	3.1	NM	10.10	4.23	1.33	0.30	1.48	12.9	0.0
C-14-14sp	305.5	3775	0.033	3616	44.7	NM	12.49	4.00	1.46	0.18	1.04	17.2	0.0

Table B.28: Summary of Experimental Data - Hydrolyzed, C-14, 7 m MDEA, 55/90°C, 98% Air Purge gas, SSM

Sample No.	Time (hr)	MDEA (Cations) (mM)	Hydrolyzed Concentration (mM)								
					Heat Stable Salts Concentration					Amino Acids	
			DEA+MAE	EDA	Formate	Glycolate	Oxalate	Acetate	Sulfate	Bicine	Glycine
C-14-0+NaOH	0	3417	0.0	NM	1.32	0.04	0.35	0.00	1.50	0.0	0.0
C-14-1+NaOH	3	3551	0.0	NM	1.41	0.07	0.44	0.18	1.58	0.0	0.0
C-14-2a+NaOH	19	3576	0.0	NM	1.55	0.26	0.35	0.00	1.54	0.0	0.0
C-14-2b+NaOH	19	3537	0.0	NM	1.46	0.27	0.34	0.09	1.47	0.0	0.0
C-14-2c+NaOH	19	3694	0.0	NM	1.54	0.25	0.31	0.00	1.46	0.0	0.0
C-14-2-avg	19	3602	0.0	NM	1.52	0.26	0.33	0.03	1.49	0.0	0.0
C-14-3+NaOH	42.5	3672	0.0	NM	1.88	0.63	0.33	0.00	1.44	0.0	0.0
C-14-4+NaOH	66.5	1948	0.0	NM	2.94	1.16	0.36	0.14	1.51	1.4	0.0
C-14-5+NaOH	91	3650	0.0	NM	5.22	1.86	0.59	0.05	1.40	1.8	0.0
C-14-6+NaOH	121.5	3506	0.0	NM	7.40	2.45	0.79	0.30	1.45	4.2	0.0
C-14-7+NaOH	143.5	3434	0.0	NM	8.60	2.61	0.87	0.27	1.42	5.9	0.0
C-14-8a+NaOH	163	3626	0.0	NM	9.69	2.94	0.93	0.23	1.41	7.8	0.0
C-14-8b+NaOH	163	3728	0.0	NM	10.04	2.88	1.00	0.30	1.77	7.6	0.0
C-14-8c+NaOH	163	11514	111.2	NM	9.76	3.11	0.97	0.23	1.67	7.4	0.0
C-14-8-avg	163	6290	0.0	NM	9.83	2.97	0.97	0.25	1.62	7.6	0.0
C-14-9sp+NaOH	164	17251	172.1	NM	11.35	3.07	0.96	0.44	1.96	7.8	5.6
C-14-10sp+NaOH	187	11660	135.9	NM	12.87	3.45	1.18	0.53	1.90	10.1	5.9
C-14-11sp+NaOH	210.5	4932	52.0	NM	12.85	3.35	1.32	0.43	1.71	11.9	0.0
C-14-12sp+NaOH	234.5	4998	57.9	NM	14.59	3.89	1.47	0.62	1.94	13.7	0.0
C-14-13sp+NaOH	263.5	4294	0.0	NM	17.54	4.27	1.85	0.44	1.74	17.2	0.0
C-14-14sp+NaOH	305.5	3917	54.4	NM	18.30	4.45	1.95	0.60	2.03	21.6	0.0

Table B.29: Summary of Experimental Data, C-15, 7 m MDEA, 55/90°C, 100 mM Inh A, SSM

Sample No.	Time (hr)	MDEA (Cations) (mM)	α_{act} (mol CO_2 /mol alk)	Total Alk (mmol/kg)	Concentration (mM)								
							Heat Stable Salts Concentration					Amino Acids	
					DEA+MAE	EDA	Formate	Glycolate	Oxalate	Acetate	Sulfate	Bicine	Glycine
C-15-0	0	3553	0.1	3545	0.0	NM	0.2	0.1	0.0	0.0	1.28	0.0	0.0
C-15-1	2	3476	0.098	3517	0.0	NM	0.6	0.1	0.0	0.1	1.50	0.0	0.0
C-15-2	18	3403	0.08	3525	0.0	NM	0.9	0.5	0.0	0.5	1.26	0.5	0.0
C-15-3	46.5	3446	0.07	3468	0.0	NM	3.1	1.7	0.0	0.0	1.15	6.2	0.0
C-15-4	66.5	3409	0.065	3418	0.0	NM	6.1	2.9	0.5	2.5	1.47	8.4	0.0
C-15-5	117.5	3379	0.056	3348	0.0	NM	14.5	4.9	1.5	5.2	1.46	23.2	0.2
C-15-6	137.5	3115	0.063	3313	0.0	NM	18.3	5.5	0.0	6.1	1.41	48.5	3.5
C-15-7	163.5	3118	0.041	3273	0.0	NM	25.1	6.9	2.9	8.5	1.38	42.3	0.5

Table B.30: Summary of Experimental Data - Hydrolyzed, C-15, 7 m MDEA, 55/90°C, 100 mM Inh A, SSM

Sample No.	Time (hr)	MDEA (Cations) (mM)	Hydrolyzed Concentration (mM)								
					Heat Stable Salts Concentration					Amino Acids	
			DEA+MAE	EDA	Formate	Glycolate	Oxalate	Acetate	Sulfate	Bicine	Glycine
C-15-0+NaOH	0	2863	0	NM	0.0	0.0	0.0	0.7	0.00	0.0	0.0
C-15-1+NaOH	2	2699	0	NM	2.3	0.0	0.0	0.3	0.00	0.0	0.0
C-15-2+NaOH	18	2584	0	NM	3.1	0.5	0.2	0.7	1.58	0.0	0.0
C-15-3+NaOH	46.5	5954	0	NM	6.9	2.1	0.5	1.6	1.51	4.9	0.4
C-15-4+NaOH	66.5	5648	0	NM	10.2	3.2	0.9	3.4	1.53	8.6	0.0
C-15-5+NaOH	117.5	5736	0	NM	24.1	5.7	2.6	6.1	1.54	31.4	2.1
C-15-6+NaOH	137.5	5022	0	NM	30.1	6.6	3.5	8.0	1.62	40.3	2.2
C-15-7+NaOH	163.5	5586	0	NM	37.1	7.4	4.8	0.0	1.54	55.2	3.3

Table B.31: Summary of Experimental Data, C-16, 8 m PZ, 55/120°C, SSM

Sample No.	Time (hr)	PZ (Cations) (mM)	α_{act} (mol CO_2 /mol alk)	Total Alk (mmol/kg)	Concentration (mM)								
							Heat Stable Salts Concentration					Amino Acids	
					DEA+MAE	EDA	Formate	Glycolate	Oxalate	Acetate	Sulfate	Bicine	Glycine
C-16-0	0	4013	0.316	4053	0.0	0.0	0.1	0.0	0.0	0.0	1.03	0.00	0.00
C-16-0B	0	4056	0.318	4086	0.0	0.0	0.1	0.0	0.0	0.0	0.31	0.00	0.00
C-16-1	4.5	4043	0.329	4029	0.0	0.0	0.2	0.0	0.0	0.0	1.01	0.00	0.00
C-16-2	21	3981	0.319	4007	0.0	0.0	0.9	0.1	0.0	0.0	0.97	0.00	0.15
C-16-3	48.5	3907	0.321	3993	0.0	7.0	2.2	0.3	0.0	0.0	1.00	0.00	0.58
C-16-4	70.5	4277	0.317	3941	0.0	13.3	3.5	0.3	0.1	0.0	1.03	0.00	1.12
C-16-5	93	3890	0.304	3918	0.0	16.7	4.7	0.4	0.1	0.0	0.95	0.00	1.50
C-16-6	118	4045	0.296	3897	0.0	25.7	6.3	0.4	0.2	0.0	0.93	0.00	1.82
C-16-7	141	3727	0.301	3880	0.0	25.0	7.0	0.5	0.2	0.0	0.90	0.00	2.05
C-16-8	190	3782	0.296	3866	0.0	33.8	8.6	0.5	0.4	0.0	0.93	0.00	2.96
C-16-9	242	3905	0.295	3717	0.0	37.3	11.4	0.5	0.7	0.0	1.06	0.94	3.59
C-16-10	288.5	3650	0.289	3766	0.0	52.2	13.1	0.6	1.0	0.0	0.95	1.35	3.88
C-16-11	334.5	3666	0.285	3762	0.0	59.5	14.8	0.5	1.6	0.0	0.93	1.70	4.45
C-16-12	358.5	3581	0.286	3730	0.0	53.9	16.4	0.8	1.9	0.0	0.94	1.82	4.01
C-16-cond-1		0	NM	NM	NM	NM	NM	NM	NM	NM	NM	NM	NM
C-16-cond-2		0	NM	NM	NM	NM	NM	NM	NM	NM	NM	NM	NM
C-16-cond-3		37	NM	NM	NM	NM	NM	NM	NM	NM	NM	NM	NM
C-16-cond-4		22	NM	NM	NM	NM	NM	NM	NM	NM	NM	NM	NM
C-16-cond-5		32	NM	NM	NM	NM	NM	NM	NM	NM	NM	NM	NM
C-16-cond-6		28	NM	NM	NM	NM	NM	NM	NM	NM	NM	NM	NM
C-16-cond-7		37	NM	NM	NM	NM	NM	NM	NM	NM	NM	NM	NM

Table B.32: Summary of Experimental Data - Hydrolyzed, C-16, 8 m PZ, 55/120°C, SSM

Sample No.	Time (hr)	PZ (Cations) (mM)	Hydrolyzed Concentration (mM)								
					Heat Stable Salts Concentration					Amino Acids	
			DEA+MAE	EDA	Formate	Glycolate	Oxalate	Acetate	Sulfate	Bicine	Glycine
C-16-0+NaOH	0	4345	0.0	0.0	0.5	0.0	0.0	0.0	0.53	0.00	0.00
C-16-0b+NaOH	0	4195	0.0	0.0	0.5	0.0	0.0	0.0	1.40	0.00	0.00
C-16-1+NaOH	4.5	4406	0.0	0.0	0.9	0.5	0.0	0.0	1.20	0.00	0.00
C-16-2+NaOH	21	4558	0.0	0.0	2.9	0.2	0.1	0.0	1.22	0.00	0.00
C-16-3+NaOH	48.5	4287	0.0	0.0	7.0	0.2	0.1	0.0	1.23	0.00	0.84
C-16-4+NaOH	70.5	3131	0.0	0.0	8.2	0.2	0.3	0.0	1.75	0.00	1.21
C-16-5+NaOH	93	4181	0.0	0.0	12.7	0.3	0.3	0.0	1.20	0.00	1.97
C-16-6+NaOH	118	4020	0.0	0.0	17.0	0.3	0.4	0.0	1.29	0.00	2.75
C-16-7+NaOH	141	4008	0.0	0.0	18.1	0.3	0.5	0.0	1.17	0.85	3.12
C-16-8+NaOH	190	4220	0.0	25.2	22.6	0.3	0.8	0.0	1.18	0.98	3.94
C-16-9+NaOH	242	3996	0.0	40.4	29.5	0.0	1.3	0.0	1.20	1.22	5.12
C-16-10+NaOH	288.5	3873	0.0	43.6	35.3	0.0	1.9	0.0	1.09	1.54	5.60
C-16-11+NaOH	334.5	3930	0.0	65.8	42.1	0.0	2.7	0.0	1.16	1.99	5.94
C-16-12+NaOH	358.5	0	0.0	0.0	46.7	0.0	3.9	0.0	1.38	2.45	6.64

Table B.33: Summary of Experimental Data, C-17, 90 °C m PZ, 55/90°C, SSM

Sample No.	Time (hr)	PZ (Cations) (mM)	α_{act} (mol CO_2 /mol alk)	Total Alk (mmol/kg)	Concentration (mM)								
							Heat Stable Salts Concentration					Amino Acids	
					DEA+MAE	EDA	Formate	Glycolate	Oxalate	Acetate	Sulfate	Bicine	Glycine
C-17-0	0	3617	NM	4071	0.0	0.0	0.31	0.00	0.01	0.00	0.22	0.00	0.00
C-17-1	4	3673	NM	4066	0.0	0.0	0.21	0.00	0.01	0.00	0.85	0.00	0.00
C-17-2	21.5	3740	NM	4025	0.0	0.0	0.48	0.00	0.01	0.00	0.82	0.00	0.00
C-17-3	45	3581	NM	4003	0.0	0.0	1.09	0.00	0.01	0.13	0.83	0.00	0.07
C-17-4	69	3700	NM	4002	0.0	0.0	1.32	0.00	0.02	0.14	0.87	0.00	0.17
C-17-5	93	3839	NM	4002	0.0	7.9	1.72	0.00	0.03	0.20	0.83	0.00	0.23
C-17-6	120	3605	NM	3994	0.0	11.0	2.10	0.00	0.03	0.23	0.86	0.00	0.30
C-17-7	165	3697	NM	3997	0.0	10.6	2.69	0.00	0.05	0.24	0.79	0.00	0.47
C-17-8	216	3531	NM	4003	0.0	13.9	3.20	0.00	0.07	0.38	0.88	0.00	0.51
C-17-9	261	3662	NM	4006	0.0	18.7	3.53	0.00	0.10	0.39	0.84	0.00	0.54
C-17-10	313	3634	NM	4006	0.0	23.2	4.43	0.00	0.12	0.59	1.31	0.00	0.73
C-17-11	358	3666	NM	3978	0.0	21.0	5.07	0.00	0.16	0.60	0.95	0.00	0.80
C-17-12	413	3623	NM	3984	0.0	30.5	5.72	0.00	0.20	0.77	1.08	0.00	1.13
C-17-13	429	3644	NM	3999	0.0	32.9	6.38	0.00	0.21	1.34	1.84	0.00	1.22

Table B.34: Summary of Experimental Data - Hydrolyzed, C-17, 90 °C m PZ, 55/90°C, SSM

Sample No.	Time (hr)	PZ (Cations) (mM)	Hydrolyzed Concentration (mM)								
					Heat Stable Salts Concentration					Amino Acids	
			DEA+MAE	EDA	Formate	Glycolate	Oxalate	Acetate	Sulfate	Bicine	Glycine
C-17-0+NaOH	0	4515	0.0	0.0	0.70	0.25	0.00	0.38	0.67	0.00	0.00
C-17-1+NaOH	4	4562	0.0	0.0	0.83	0.46	0.00	0.46	1.20	0.00	0.00
C-17-2+NaOH	21.5	4241	0.0	22.8	1.19	0.34	0.03	0.15	0.98	0.00	0.00
C-17-3+NaOH	45	4466	0.0	0.0	3.19	0.27	0.06	0.34	1.38	0.00	0.00
C-17-4+NaOH	69	4429	0.0	0.0	3.82	0.17	0.13	0.29	1.07	0.00	0.19
C-17-5+NaOH	93	4416	0.0	0.0	5.74	0.21	0.13	0.73	2.26	0.00	0.38
C-17-6+NaOH	120	4354	0.0	0.0	6.92	0.17	0.20	0.53	1.08	0.00	0.66
C-17-7+NaOH	165	4351	0.0	0.0	6.96	0.18	0.19	0.53	1.08	0.00	0.72
C-17-8+NaOH	216	4092	0.0	0.0	9.01	0.17	0.20	0.65	1.13	0.00	0.89
C-17-9+NaOH	261	4099	0.0	10.3	10.54	0.22	0.31	1.62	1.35	0.00	1.05
C-17-10+NaOH	313	4348	0.0	15.7	12.60	0.23	0.37	1.54	1.40	0.00	1.31
C-17-11+NaOH	358	4296	0.0	24.1	14.91	0.30	0.46	1.26	1.08	0.00	1.53
C-17-12+NaOH	413	4100	0.0	30.8	17.17	0.19	0.43	1.88	2.37	0.00	1.84
C-17-13+NaOH	429	4140	0.0	21.4	0.00	0.25	0.61	1.66	1.14	0.00	1.97

Table B.35: Summary of Experimental Data, C-18, 7 m MDEA 55/120°C, 1 L/min N_2 gas stripping, SSM

Sample No.	Time (hr)	MDEA (Cations) (mM)	α_{act} (mol CO_2 /mol alk)	Total Alk (mmol/kg)	Concentration (mM)								
							Heat Stable Salts Concentration					Amino Acids	
					DEA+MAE	EDA	Formate	Glycolate	Oxalate	Acetate	Sulfate	Bicine	Glycine
C-18-0	0	3002	0.125	3599	0.0	NM	0.35	0.10	0.00	0.00	0.69	0.0	0.0
C-18-1	20	3516	0.054	3663	14.2	NM	2.36	0.99	0.06	0.09	0.76	0.9	0.5
C-18-2	45	3274	0.039	3574	31.9	NM	4.08	2.44	0.11	0.25	0.79	2.7	0.6
C-18-3	65.5	3559	0.03	3681	18.0	NM	5.47	3.31	0.14	0.39	0.61	4.1	0.8
C-18-4	95.5	3374	0.028	3631	20.3	NM	6.33	4.32	0.23	0.65	0.69	6.2	1.0
C-18-5	113.5	3801	0.028	3556	33.9	NM	7.12	4.96	0.23	0.80	0.62	7.7	1.0
C-18-6	143.5	3349	0.029	3542	68.8	NM	8.54	6.12	0.29	1.06	0.63	10.4	1.3
C-18-7	161	3456	0.021	3495	0.0	NM	9.25	6.57	0.35	1.37	0.78	11.9	1.5

Table B.36: Summary of Experimental Data - Hydrolyzed, C-18, 55/120°C, 1 L/min N_2 gas stripping, SSM

Sample No.	Time (hr)	MDEA (Cations) (mM)	Hydrolyzed Concentration (mM)								
					Heat Stable Salts Concentration					Amino Acids	
			DEA+MAE	EDA	Formate	Glycolate	Oxalate	Acetate	Sulfate	Bicine	Glycine
C-18-0+NaOH	0	3474	0.0	NM	2.02	0.58	0.07	0.29	1.13	0.0	0.0
C-18-1+NaOH	20	3579	6.3	NM	3.16	1.67	0.10	0.16	1.15	1.2	0.8
C-18-2+NaOH	45	3891	27.0	NM	5.48	3.25	0.17	0.32	1.13	2.6	1.0
C-18-3+NaOH	65.5	3908	26.8	NM	6.38	4.01	0.21	0.49	1.15	3.8	1.1
C-18-4+NaOH	95.5	3950	24.8	NM	7.94	4.95	0.28	0.97	1.29	5.9	1.3
C-18-5+NaOH	113.5	5041	45.5	NM	9.19	5.68	0.32	1.57	1.35	7.6	1.4
C-18-6+NaOH	143.5	3272	53.7	NM	10.38	6.67	0.38	1.07	1.18	10.5	1.7
C-18-7+NaOH	161	3485	79.6	NM	10.83	6.83	0.27	1.29	1.06	11.9	1.9

Table B.37: Summary of Experimental Data, C-20, 7 m MDEA + 100 mM Formate, 55/120°C, SSM

Sample No.	Time (hr)	MDEA (Cations) (mM)	α_{act} (mol CO_2 /mol alk)	Total Alk (mmol/kg)	Concentration (mM)								
							Heat Stable Salts Concentration					Amino Acids	
					DEA+MAE	EDA	Formate	Glycolate	Oxalate	Acetate	Sulfate	Bicine	Glycine
C-20-0a	0	4118	0.095	3718	0.0	NM	0.8	0.0	0.0	0.0	0.77	0.0	0.0
C-20-0b	0	3987	0.092	3413	0.0	NM	175.8	0.0	0.0	0.6	0.67	0.0	0.0
C-20-1	1.5	3719	0.088	3389	0.0	NM	170.0	0.3	0.0	0.7	0.77	0.4	0.0
C-20-2	17.8	3632	0.073	3363	14.5	NM	150.6	2.3	0.2	0.7	0.75	13.9	0.0
C-20-3	46.8	3378	0.065	3350	35.9	NM	121.2	4.7	0.5	1.6	0.72	50.8	0.0
C-20-4	70.8	3472	0.063	3319	20.0	NM	103.4	6.2	0.8	2.4	0.78	81.1	0.0
C-20-5	95.8	3420	0.045	3289	55.7	NM	94.0	7.1	1.0	2.5	0.61	99.8	0.0
C-20-6	119.8	3372	0.031	3248	37.5	NM	84.3	8.0	1.3	2.8	0.63	119.9	0.0
C-20-7	138.8	3193	0.029	3259	26.6	NM	68.3	7.6	1.3	3.0	0.75	119.3	8.9
C-20-8	187.8	2933	0.032	3187	8.6	NM	64.4	10.2	2.1	4.2	0.69	178.5	17.0
C-20-9	213	2886	0.033	3148	44.7	NM	58.8	11.2	2.6	5.0	0.67	203.3	21.1
C-20-10	237	2703	0.029	3118	89.2	NM	57.0	11.6	2.9	5.4	0.68	218.6	23.1
C-20-11	261.8	2665	0.016	3114	26.0	NM	54.3	12.2	3.2	5.7	0.66	231.3	25.9
C-20-12	282.8	4118	0.031	3082	0.0	NM	50.1	12.8	3.6	6.7	0.68	248.7	32.7

Table B.38: Summary of Experimental Data - Hydrolyzed, C-20, 7 m MDEA + 100 mM Formate, 55/120°C, SSM

Sample No.	Time (hr)	MDEA (Cations) (mM)	Hydrolyzed Concentration (mM)								
					Heat Stable Salts Concentration					Amino Acids	
			DEA+MAE	EDA	Formate	Glycolate	Oxalate	Acetate	Sulfate	Bicine	Glycine
C-20-0a+NaOH	0	3899	0.0	NM	2.1	0.0	0.1	0.0	1.18	0.0	0.0
C-20-0b+NaOH	0	3558	0.0	NM	176.0	0.0	0.0	1.9	1.12	0.0	0.0
C-20-1+NaOH	1.5	3604	52.9	NM	175.2	0.5	0.1	1.5	0.97	0.0	0.0
C-20-2+NaOH	17.8	3464	39.6	NM	168.6	2.9	0.3	3.2	0.92	12.0	0.0
C-20-3+NaOH	46.8	3671	19.2	NM	143.2	5.1	0.6	1.7	1.07	46.4	0.0
C-20-4+NaOH	70.8	2908	39.4	NM	127.1	6.6	1.0	2.0	1.02	74.5	0.0
C-20-5+NaOH	95.8	3339	26.7	NM	118.9	7.5	1.3	4.8	1.53	94.7	4.9
C-20-6+NaOH	119.8	3849	20.1	NM	125.8	9.6	1.8	8.4	1.51	128.0	7.9
C-20-7+NaOH	138.8	3205	68.7	NM	104.9	10.1	1.9	3.4	0.91	124.0	7.4
C-20-8+NaOH	187.8	2953	78.1	NM	89.4	10.6	2.5	4.2	0.99	163.4	11.6
C-20-9+NaOH	213	2799	30.5	NM	82.9	11.3	3.0	5.0	0.84	180.5	12.8
C-20-10+NaOH	237	2548	71.5	NM	79.2	11.9	3.2	5.6	1.17	192.3	14.1
C-20-11+NaOH	261.8	2415	25.7	NM	75.3	12.4	3.5	6.1	0.79	206.3	15.9
C-20-12+NaOH	282.8	2554	45.4	NM	71.4	12.8	3.7	6.5	1.05	225.3	19.8

Table B.39: Summary of Experimental Data, C-21, 7 m MDEA/2 m PZ, 55/120°C, SSM

Sample No.	Time (hr)	MDEA (Cations) (mM)	PZ (Cations) (mM)	α_{act} (mol CO_2 /mol alk)	Total Alk (mmol/kg)	Concentration (mM)											
											Heat Stable Salt Concentration					Amino Acids	
						DEA+MAE	EDA	1-MPZ	1,4-DMPZ	AEP	Formate	Glycolate	Oxalate	Acetate	Sulfate	Bicine	Glycine
C-21-0b	0	3321	968	0.137	5090	15	0	0.0	0.0	0.0	0.3	0.0	0.1	0.2	1.1	0.0	0.0
C-21-1	3	3473	974	0.136	5086	18	0	0.4	0.0	0.0	0.6	0.0	0.1	0.1	1.1	0.0	0.0
C-21-2	18	3366	982	0.135	5017	30	0	1.1	0.0	0.0	1.5	0.0	0.1	0.1	1.2	0.0	0.0
C-21-3	42.5	3846	1042	0.137	4945	102	0	10.0	0.0	0.0	7.2	0.4	0.2	1.5	1.1	1.4	0.0
C-21-4	67	3242	841	0.134	4845	204	0	36.7	0.0	1.6	20.5	0.5	0.9	4.2	1.1	5.0	0.0
C-21-5	95	3308	861	0.129	4756	279	0	49.6	0.0	5.5	27.1	0.8	1.3	5.4	1.1	9.8	0.2
C-21-6	138	3040	758	0.118	4646	325	0	61.1	0.0	5.1	37.3	0.8	1.9	7.9	1.0	14.0	0.4
C-21-7	186	3020	733	0.108	4520	422	0	80.4	2.0	9.6	49.0	1.0	2.6	10.4	1.0	19.0	0.4
C-21-8	234	2785	647	0.11	4366	450	0	92.4	1.5	17.1	57.9	1.5	3.4	13.0	1.0	23.2	0.7
C-21-9	290.5	2490	534	0.107	4263	570	0	119.1	0.0	37.3	67.5	1.4	4.3	15.6	0.9	29.7	0.8
C-21-10	334.5	2494	500	0.103	4191	559	0	136.5	5.2	44.2	79.9	1.4	5.7	20.4	1.0	38.4	1.1
C-21-11	380.5	2327	470	0.091	4099	646	0	135.7	5.8	52.7	91.8	1.7	6.7	26.5	0.9	44.0	1.2
C-21-12	434	2220	424	0.09	3986	630	0	140.4	7.6	53.3	99.1	2.0	7.7	27.0	0.8	47.7	1.4
C-21-13	474	2174	388	0.096	3907	666	0	142.9	9.5	55.4	99.7	1.8	8.9	30.4	0.9	55.7	1.8
C-21-14	522	2079	342	0.1	3755	748	0	149.4	11.7	50.1	107.0	1.9	10.0	33.0	0.8	63.3	2.3
C-21-15	570	2023	319	0.09	3652	777	0	152.9	13.6	53.7	122.3	2.0	11.9	37.5	0.8	74.1	2.5

Table B.40: Summary of Experimental Data - Hydrolyzed, C-21, 7 m MDEA/2 m PZ, 55/120°C, SSM

Sample No.	Time (hr)	MDEA (Cations) (mM)	PZ (Cations) (mM)	Hydrolyzed Concentration (mM)											
						Heat Stable Salts Concentration								Amino Acids	
				DEA+MAE	EDA	1-MPZ	1,4-DMPZ	AEP	Formate	Glycolate	Oxalate	Acetate	Sulfate	Bicine	Glycine
C-21-0a+NaOH	0	3523.3	1040.6	17	0	0.6	0.0	0.0	2.1	0.0	0.1	0.0	1.3	0.0	0.0
C-21-0b+NaOH	0	3517.9	1034.1	29	0	3.4	0.0	1.7	3.0	0.0	0.5	0.0	1.3	0.0	0.0
C-21-1+NaOH	3	3458.1	1028.3	48	0	1.0	0.0	0.0	4.2	1.2	0.2	0.4	1.2	0.0	0.0
C-21-2+NaOH	18	3415.4	959.6	86	0	7.4	0.0	0.0	17.4	1.3	0.4	3.5	1.3	1.8	0.0
C-21-3+NaOH	42.5	3613.8	936.7	219	0	32.8	0.0	1.8	42.4	0.0	1.1	7.0	1.3	7.6	0.0
C-21-4+NaOH	67	3442.3	844.2	282	0	40.8	0.0	0.0	55.3	0.0	2.0	7.3	1.5	10.8	0.0
C-21-5+NaOH	95	3175.3	798.3	365	0	59.7	0.0	1.4	76.5	2.0	2.8	9.4	1.6	15.2	0.5
C-21-6+NaOH	138	3042.2	759.4	450	0	75.1	0.0	7.8	100.3	0.0	4.0	11.6	1.4	20.8	0.6
C-21-7+NaOH	186	2890.5	701.7	494	0	96.3	0.0	18.7	119.6	3.2	5.1	14.6	1.4	26.1	0.7
C-21-8+NaOH	234	2856.1	678.4	561	0	111.2	3.0	31.2	151.5	4.2	6.9	19.8	1.4	24.4	1.0
C-21-9+NaOH	290.5	2746.5	602.3	658	0	150.5	3.6	40.2	178.0	3.0	8.1	21.6	1.4	41.0	1.1
C-21-10+NaOH	334.5	2685.2	549.6	685	0	133.8	5.3	28.5	196.0	3.2	9.5	24.8	1.3	45.8	1.5
C-21-11+NaOH	380.5	2628.4	515.4	711	0	140.4	5.3	34.4	200.6	4.0	10.8	25.8	1.4	51.7	1.4
C-21-12+NaOH	434	2531.6	477.4	757	0	150.1	7.5	40.2	218.1	3.5	12.3	29.9	1.3	60.5	1.8
C-21-13+NaOH	474	2457.9	453.2	793	0	161.1	11.1	49.8	247.2	4.9	14.3	33.6	1.3	67.6	2.4
C-21-14+NaOH	522	2340.5	409.6	867	0	164.6	11.6	53.9	266.1	3.6	17.2	37.3	1.4	77.4	2.8
C-21-15+NaOH	570	2240.8	366.5	866	0	164.5	15.7	49.5	272.5	3.5	16.0	37.9	1.3	NM	NM

Table B.41: Summary of Experimental Data, C-22, 7 m MDEA/2 m PZ, 55/90°C, SSM

Sample No.	Time (hr)	MDEA (Cations) (mM)	PZ (Cations) (mM)	α_{act} (mol CO_2 /mol alk)	Total Alk (mmol/kg)	Concentration (mM)											
											Heat Stable Salts Concentration					Amino Acids	
						DEA+MAE	EDA	1-MPZ	1,4-DMPZ	AEP	Formate	Glycolate	Oxalate	Acetate	Sulfate	Bicine	Glycine
C-22-0	0	2618	867	0.125	7701	8.4	0	0.0	0.0	0.0	0.50	0.00	0.00	0.00	1.08	0.0	0.0
C-22-1	1.5	2508	888	0.128	7642	9.0	0	0.0	0.0	0.0	0.55	0.00	0.00	0.00	1.26	0.0	0.0
C-22-2	17.5	2540	875	0.126	7633	12.7	0	0.0	0.0	0.0	1.66	0.00	0.00	0.00	1.04	0.0	0.0
C-22-3	42.5	2499	845	0.124	7700	17.9	0	0.0	0.0	0.0	3.70	0.00	0.00	0.00	1.13	0.0	0.0
C-22-4	65	2412	854	0.118	7728	24.6	0	0.0	0.0	0.0	6.01	0.00	0.00	0.00	0.97	1.1	0.0
C-22-6	142	2617	849	0.11	7611	73.3	0	253.3	496.6	0.0	NM	NM	NM	NM	NM	3.1	0.0
C-22-7	186	2332	804	0.105	7705	89.1	0	12.7	0.0	0.0	13.70	0.00	0.09	0.00	1.04	11.5	0.0
C-22-8	235	2087	698	0.108	7338	105.6	0	18.3	0.0	0.0	26.57	0.00	0.78	0.00	1.20	24.8	0.0
C-22-9	284	2092	669	0.111	7123	120.8	0	27.5	0.0	0.0	38.21	0.00	1.53	0.00	0.99	37.8	0.0
C-22-10	330.5	1935	620	0.11	6836	120.0	0	33.8	0.0	0.0	54.17	0.00	2.56	0.00	1.07	50.2	0.0
C-22-11	383	1934	599	0.095	6690	143.5	0	49.7	0.0	0.0	60.95	0.00	3.38	0.00	0.84	57.3	0.0
C-22-12a	425	1860	535	0.092	6496	147.8	0	51.5	0.0	0.0	75.39	0.00	4.79	0.00	1.03	71.5	0.0
C-22-12b	425	1867	537	0.091	6373	146.2	0	52.0	0.0	0.0	79.27	0.00	5.73	0.00	1.05	79.1	0.0
C-22-12c	425	1846	524	0.098	6382	147.3	0	52.2	0.0	0.0	80.01	0.00	5.68	0.00	0.99	79.8	0.0
C-22-13	499	1766	497	0.099	6343	160.8	0	51.1	0.0	0.0	82.39	0.00	5.66	0.00	0.91	81.0	0.0
C-22-14	550.5	1764	474	0.092	6202	168.2	0	55.4	0.0	0.0	95.00	0.00	7.57	0.00	1.04	94.8	0.0
C-22-15	592.5	1718	461	0.089	6078	167.7	0	59.5	0.0	6.4	102.69	0.00	8.82	0.00	1.06	110.5	0.0

Table B.42: Summary of Experimental Data - Hydrolyzed, C-22, 7 m MDEA/2 m PZ, 55/90°C, SSM

Sample No.	Time (hr)	MDEA (Cations) (mM)	PZ (Cations) (mM)	Hydrolyzed Concentration (mM)											
									Heat Stable Salts Concentration					Amino Acids	
				DEA+MAE	EDA	1-MPZ	1,4-DMPZ	AEP	Formate	Glycolate	Oxalate	Acetate	Sulfate	Bicine	Glycine
C-22-0+NaOH	0	2901	NM	11	0	0.0	0.0	0.0	3.02	0.00	0.00	0.00	1.74	0.0	0.0
C-22-1+NaOH	1.5	2676	NM	10	0	0.0	0.0	0.0	3.62	0.00	0.06	0.00	1.45	0.0	0.0
C-22-2+NaOH	17.5	2753	NM	13	0	0.0	0.0	0.0	6.56	0.00	0.00	0.00	1.90	0.0	0.0
C-22-3+NaOH	42.5	2784	NM	22	0	0.0	0.0	0.0	9.86	0.00	0.00	0.00	1.48	0.0	0.0
C-22-4+NaOH	65	2996	NM	41	0	0.0	0.0	0.0	15.92	0.00	0.12	0.00	4.53	2.7	0.0
C-22-5+NaOH	92	3024	NM	50	0	376.1	138.0	0.0	19.92	0.00	0.00	7.29	2.57	4.3	0.0
C-22-6+NaOH	142	3053	NM	70	0	194.6	29.0	0.0	32.88	0.00	0.31	0.00	1.97	9.0	0.0
C-22-7+NaOH	186	2921	NM	113	0	11.7	0.0	0.0	61.11	0.00	1.96	0.00	1.86	17.9	0.0
C-22-8+NaOH	235	2593	NM	313	0	19.8	0.0	0.0	90.78	0.00	4.18	0.00	1.83	34.3	0.0
C-22-9+NaOH	284	1464	NM	113	0	28.8	0.0	0.0	120.86	0.00	6.15	0.00	1.97	48.2	0.0
C-22-10+NaOH	330.5	NM	NM	NM	0	55.2	0.0	0.0	132.44	0.00	7.27	0.00	1.70	50.4	0.0
C-22-11+NaOH	383	NM	NM	NM	0	60.3	0.0	0.0	156.58	0.00	9.62	0.00	1.69	66.1	0.0
C-22-12a+NaOH	425	NM	NM	NM	0	62.4	0.0	0.0	17.91	0.00	10.45	0.00	1.98	76.5	0.0
C-22-12b+NaOH	425	NM	NM	NM	0	48.3	0.0	0.0	168.78	0.00	10.03	0.00	1.49	76.5	0.0
C-22-12c+NaOH	425	NM	NM	NM	0	55.4	0.0	0.0	176.56	0.00	10.13	0.00	1.32	77.2	0.0
C-22-13+NaOH	499	NM	NM	NM	0	54.0	0.0	0.1	197.98	0.00	12.88	0.00	1.49	91.0	0.0
C-22-14+NaOH	550.5	NM	NM	NM	0	51.6	0.0	0.0	214.95	0.00	14.97	0.00	1.53	108.5	0.0
C-22-15+NaOH	592.5	NM	NM	NM	0	61.2	0.0	0.0	228.18	0.00	13.46	0.00	1.85	103.8	0.0

Table B.43: Summary of Experimental Data, C-23, 7 m MDEA/2 m PZ, 55/100°C, SSM

Sample No.	Time (hr)	MDEA (Cations) (mM)	PZ (Cations) (mM)	α_{act} (mol CO_2 /mol alk)	Total Alk (mmol/kg)	Concentration (mM)									
									Heat Stable Salts Concentration					Amino Acids	
						DEA+MAE	EDA	1-MPZ	Formate	Glycolate	Oxalate	Acetate	Sulfate	Bicine	Glycine
C-23-0	0	2936	967	0.129	7827	1.2	NM	0.0	0.32	0.00	0.13	0.13	0.74	0.0	0.0
C-23-1	3	2999	988	0.13	7614	2.0	NM	0.0	0.45	0.00	0.03	0.18	1.04	0.0	0.0
C-23-2	19	2931	1028	0.13	7891	2.0	NM	0.0	1.27	0.00	0.03	0.13	0.77	0.5	0.0
C-23-3	51.5	2843	890	0.128	7846	7.8	NM	11.4	3.98	0.11	0.07	0.19	0.71	3.8	0.0
C-23-4	67	2881	877	0.127	7662	11.6	NM	5.2	6.28	0.32	0.11	0.19	0.67	7.3	0.0
C-23-5	92.5	2905	1078	0.129	7599	19.1	NM	56.2	11.46	0.46	0.28	0.00	0.61	13.1	0.0
C-23-6	115.5	2546	841	0.121	7745	24.0	NM	20.7	20.92	0.71	0.66	0.00	0.66	22.9	0.0
C-23-7	169	2341	835	0.091	7699	29.1	NM	62.0	30.40	0.76	1.19	0.00	0.71	35.1	0.0
C-23-8	193	2473	849	0.085	7557	34.9	NM	66.7	35.73	0.87	1.49	0.00	0.76	42.2	0.0
C-23-9	211.5	2488	852	NA	7393	36.9	NM	70.4	39.08	0.94	1.73	0.00	0.57	45.6	0.0

Table B.44: Summary of Experimental Data - Hydrolyzed, C-23, 7 m MDEA/2 m PZ, 55/100°C, SSM

Sample No.	Time (hr)	MDEA (Cations) (mM)	PZ (Cations) (mM)	Hydrolyzed Concentration (mM)								
						Heat Stable Salts Concentration					Amino Acids	
				DEA+MAE	EDA	Formate	Glycolate	Oxalate	Acetate	Sulfate	Bicine	Glycine
C-23-0+NaOH	0	2858	1112	3.2	NM	4.77	1.23	0.08	0.00	0.98	0.0	0.0
C-23-1+NaOH	3	2916	1087	3.8	NM	4.30	1.28	0.07	0.00	0.86	0.0	0.0
C-23-2+NaOH	19	2920	1135	5.5	NM	5.95	1.49	0.09	0.00	0.81	0.0	0.0
C-23-3+NaOH	51.5	2782	992	4.8	NM	10.90	1.48	0.16	0.00	0.94	2.4	0.0
C-23-4+NaOH	67	2790	989	13.6	NM	17.53	1.50	0.30	0.40	1.33	4.9	0.0
C-23-5+NaOH	92.5	2860	999	18.7	NM	27.86	3.06	0.68	0.00	0.84	10.3	0.0
C-23-6+NaOH	115.5	2679	1117	28.1	NM	45.86	2.84	1.42	0.00	0.77	18.9	0.0
C-23-7+NaOH	169	2685	1070	36.5	NM	67.50	1.76	2.18	0.00	0.68	31.3	0.0
C-23-8+NaOH	193	2569	1009	36.0	NM	79.36	2.03	2.76	0.00	0.90	32.9	0.0
C-23-9+NaOH	211.5	2537	972	38.4	NM	87.53	2.08	3.13	0.00	0.94	36.2	0.0

Table B.45: Summary of Experimental Data, C-24, 7 m MDEA+100 mM DEA, 55/120°C, SSM

Sample No.	Time (hr)	MDEA (Cations) (mM)	α_{act} (mol CO_2 /mol alk)	Total Alk (mmol/kg)	Concentration (mM)									
								Heat Stable Salts Concentration					Amino Acids	
					DEA+MAE	EDA	1-MPZ	Formate	Glycolate	Oxalate	Acetate	Sulfate	Bicine	Glycine
C-24-0	0	3304	0.092	3751	13.1	0.0	0.0	0.6	0.0	0.0	0.0	0.8	0.0	0.0
C-24-1	3	3399	0.09	3696	14.6	0.0	0.0	1.3	0.2	0.0	56.1	0.7	2.0	0.0
C-24-2	21	3450	0.08	3656	22.4	0.0	0.0	8.3	1.3	0.2	56.0	0.6	20.9	0.0
C-24-3	47	3319	0.073	3594	30.7	0.0	0.0	19.2	2.9	0.7	0.0	0.6	57.8	0.0
C-24-4	69	3916	0.058	3548	37.6	0.0	0.0	25.6	3.7	1.1	0.0	0.5	79.6	0.0
C-24-5	118	4102	0.057	3406	50.2	0.0	0.0	43.1	5.9	2.2	0.0	0.7	130.0	0.5
C-24-6	140.5	3228	0.056	3322	46.5	0.0	0.0	62.9	7.2	3.1	0.0	0.7	147.3	0.8
C-24-7	165.5	3354	0.038	3277	48.3	0.0	0.0	62.7	7.6	3.4	0.0	0.7	171.2	1.6
C-24-8	188	3153	0.034	3237	47.3	0.0	0.0	69.0	8.1	3.8	0.0	0.6	182.2	1.3

Table B.46: Summary of Experimental Data - Hydrolyzed, C-24, 7 m MDEA+100 mM DEA, 55/120°C, SSM

Sample No.	Time (hr)	MDEA (Cations) (mM)	Hydrolyzed Concentration (mM)								
					Heat Stable Salts Concentration					Amino Acids	
			DEA+MAE	EDA	Formate	Glycolate	Oxalate	Acetate	Sulfate	Bicine	Glycine
C-24-0+NaOH	0	3860	19.1	0.0	2.4	0.0	0.0	0.0	0.8	0.0	0.0
C-24-1+NaOH	3	3511	19.8	0.0	3.5	0.0	0.1	0.0	0.6	0.0	0.0
C-24-2+NaOH	21	3413	27.4	0.0	14.2	0.0	0.3	0.0	0.6	15.3	0.0
C-24-3+NaOH	47	3410	35.0	0.0	31.5	4.1	1.1	0.0	1.0	56.1	0.0
C-24-4+NaOH	69	3342	39.0	0.0	37.6	4.8	1.5	109.9	1.0	78.3	0.0
C-24-5+NaOH	118	3374	50.0	0.0	61.0	6.7	2.9	127.4	0.9	134.2	0.0
C-24-6+NaOH	140.5	3171	52.5	0.0	73.4	7.6	3.7	126.0	1.0	156.5	0.7
C-24-7+NaOH	165.5	3228	54.6	0.0	71.2	7.3	3.6	124.9	0.7	184.2	0.9
C-24-8+NaOH	188	3112	54.7	0.0	71.8	7.5	4.0	129.6	1.2	193.6	0.9

Table B.47: Summary of Experimental Data, C-25, 7 m MDEA, New Thermal Reactor, 55/120°C, SSM

Sample No.	Time (hr)	MDEA (Cations) (mM)	α_{act} (mol CO_2 /mol alk)	Total Alk (mmol/kg)	Concentration (mM)								
							Heat Stable Salts Concentration					Amino Acids	
					DEA+MAE	EDA	Formate	Glycolate	Oxalate	Acetate	Sulfate	Bicine	Glycine
C-25-0a	0	3558	0.107	3591	15	NM	0.5	0.1	0.3	0.3	1.9	0.0	0.0
C-25-0b	0	3597	0.102	3549	10	NM	0.7	0.2	0.4	0.0	2.0	0.0	0.0
C-25-1	1.5	3479	0.097	3567	27	NM	0.6	0.7	0.3	0.0	2.0	0.0	0.0
C-25-2	18.5	3230	0.068	3552	109	NM	10.5	8.3	1.1	0.0	2.1	3.9	0.0
C-25-3	30	3165	0.054	3436	175	NM	23.3	12.1	3.1	0.5	2.0	29.0	0.0
C-25-4	54	2995	0.056	3335	242	NM	31.6	13.6	4.7	1.4	1.8	53.5	1.1
C-25-5	82	2763	0.051	3172	361	NM	45.2	0.0	9.6	0.0	2.0	130.1	0.9
C-25-6	104.5	2951	0.036	3066	424	NM	50.5	17.6	11.4	3.3	2.2	183.5	1.4
C-25-7	125.5	2551	0.04	2936	433	NM	53.4	17.9	13.3	4.6	2.0	129.2	1.1
C-25-8	152.5	2670	0.04	2915	470	NM	56.3	18.6	14.9	5.3	1.9	146.2	1.4
C-25-9	178.5	3558	0.036	2849	15	NM	0.5	0.1	0.3	0.3	1.9	0.0	0.0

Table B.48: Summary of Experimental Data - Hydrolyzed, C-25, 7 m MDEA, New Thermal Reactor, 55/120°C, SSM

Sample No.	Time (hr)	MDEA (Cations) (mM)	Hydrolyzed Concentration (mM)								
					Heat Stable Salts Concentration					Amino Acids	
			DEA+MAE	EDA	Formate	Glycolate	Oxalate	Acetate	Sulfate	Bicine	Glycine
C-25-0a+NaOH	0	2621	18	NM	3.5	1.1	0.4	0.5	2.9	0.0	0.0
C-25-0b+NaOH	0	2743	18	NM	3.5	1.2	0.3	0.5	2.5	0.0	0.0
C-25-1+NaOH	1.5	2521	11	NM	3.9	1.8	0.3	0.4	2.6	0.0	0.0
C-25-2+NaOH	18.5	3584	85	NM	16.1	7.9	1.4	0.1	2.2	0.0	0.0
C-25-3+NaOH	30	3325	163	NM	42.4	15.2	4.2	1.3	3.2	32.2	0.0
C-25-4+NaOH	54	3348	269	NM	NM	19.2	8.4	1.9	2.9	31.3	0.0
C-25-5+NaOH	82	3317	352	NM	80.5	20.4	12.4	3.2	3.3	73.5	0.0
C-25-6+NaOH	104.5	3026	379	NM	86.3	21.6	15.3	3.6	3.2	74.4	0.0
C-25-7+NaOH	125.5	3009	437	NM	89.7	20.7	16.0	4.0	2.4	114.8	0.0
C-25-8+NaOH	152.5	2983	490	NM	100.8	21.4	19.8	5.0	2.5	156.2	0.0
C-25-9+NaOH	178.5	2857	506	NM	87.9	17.6	18.5	4.9	2.7	187.1	0.0

Table B.49: Summary of Experimental Data, C-26, 7 m MDEA, New thermal reactor, 55/130°C, SSM

Sample No.	Time (hr)	MDEA (Cations) (mM)	α_{act} (mol CO_2 /mol alk)	Total Alk (mmol/kg)	Concentration (mM)									
								Heat Stable Salts Concentration					Amino Acids	
					DEA+MAE	NH_4^+	1-MPZ	Formate	Glycolate	Oxalate	Acetate	Sulfate	Bicine	Glycine
C-26-0a	0	3197	0.095	3715	0.0	0.0	0.0	0.2	0.0	0.3	0.0	1.3	0.0	0.0
C-26-0b	0	3392	0.092	3676	6.5	0.0	0.0	0.1	0.0	0.3	0.0	1.7	0.0	0.0
C-26-1	1	3627	0.089	3600	14.4	0.0	0.0	0.5	0.9	0.2	0.0	1.6	0.0	0.0
C-26-2	17	3270	0.074	3643	97.6	0.0	0.0	8.3	5.4	0.7	0.0	1.2	0.0	0.0
C-26-3	42	2966	0.061	3453	246.6	1482.9	0.0	15.7	7.9	1.7	0.4	1.0	40.6	0.0
C-26-4	68	2415	0.046	3359	212.3	0.0	0.0	29.2	13.7	4.2	2.0	1.9	131.7	0.0
C-26-5	97	0	0.045	3324	958.4	0.0	0.0	28.5	12.6	4.3	2.6	1.3	165.6	0.0
C-26-6	113.5	2359	0.034	3233	241.9	0.0	0.0	35.0	15.3	5.9	4.1	1.4	264.8	0.0
C-26-cond-1		0	NM	NM	6.0	27.3	0.0	NM	NM	NM	NM	NM	NM	NM
C-26-cond-2		0	NM	NM	0.0	53.7	0.0	NM	NM	NM	NM	NM	NM	NM

Table B.50: Summary of Experimental Data - Hydrolyzed, C-26, 7 m MDEA, New thermal reactor, 55/130°C, SSM

Sample No.	Time (hr)	MDEA (Cations) (mM)	Hydrolyzed Concentration (mM)								
					Heat Stable Salts Concentration					Amino Acids	
			DEA+MAE	NH_4^+	Formate	Glycolate	Oxalate	Acetate	Sulfate	Bicine	Glycine
C-26-0a+NaOH	0	2236	9.1	NM	1.8	0.0	0.3	0.0	2.1	0.0	0.0
C-26-0b+NaOH	0		4.8	NM	2.4	0.5	0.2	0.2	2.3	0.0	0.0
C-26-1+NaOH	1	2487	0.0	NM	2.7	1.4	0.2	0.0	2.3	0.0	0.0
C-26-2+NaOH	17	339	7.7	NM	18.8	8.6	1.4	0.3	2.6	0.0	0.0
C-26-3+NaOH	42	2259	120.4	NM	42.5	15.0	4.1	1.4	2.5	0.0	0.0
C-26-4+NaOH	68	3169	252.7	NM	50.5	16.4	5.5	2.1	2.2	39.9	0.0
C-26-5+NaOH	97	3265	353.9	NM	66.8	20.3	8.0	3.5	3.2	210.6	0.0
C-26-6+NaOH	113.5	2778	336.9	NM	63.5	18.6	7.9	4.1	2.0	189.3	0.0

Table B.51: Summary of Experimental Data, C-27, 7 m MDEA, New thermal reactor, 55/100°C, SSM

Sample No.	Time (hr)	MDEA (Cations) (mM)	α_{act} (mol CO_2 /mol alk)	Total Alk (mmol/kg)	Concentration (mM)									
								Heat Stable Salts Concentration					Amino Acids	
					DEA+MAE	EDA	1-MPZ	Formate	Glycolate	Oxalate	Acetate	Sulfate	Bicine	Glycine
C-27-0a	0	3049	0.100	3643	0.0	0.0	0.0	0.1	0.0	0.1	0.0	0.6	0.0	0.0
C-27-0b	0	3309	0.098	3644	0.0	0.0	0.0	0.1	0.0	0.1	0.0	0.6	0.0	0.0
C-27-1	3	3250	0.091	3646	0.0	0.0	0.0	0.1	0.2	0.1	0.0	0.6	0.0	0.0
C-27-2	21.5	3170	0.077	3646	13.6	0.0	0.0	0.7	1.0	0.1	0.0	0.6	0.0	0.0
C-27-3	42	3188	0.061	3622	28.1	0.0	0.0	1.9	1.9	0.1	0.0	0.6	0.0	0.0
C-27-4	66.5	3064	0.051	3582	44.9	0.0	0.0	4.2	2.9	0.2	0.0	0.6	8.0	0.0
C-27-5	97	3060	0.047	3507	80.2	0.0	0.0	8.6	4.0	0.4	0.0	0.6	16.9	0.0
C-27-7	120	2902	0.039	3418	125.5	0.0	0.0	13.3	4.8	0.7	0.0	0.5	27.4	0.0
C-27-8	141	2751	0.034	3354	163.6	0.0	0.0	17.5	5.4	1.0	0.0	0.5	38.4	0.0
C-27-9	163.5	2709	0.028	3343	212.2	0.0	0.0	23.4	5.9	1.5	0.0	0.5	53.6	0.1
C-27-10	188.5	2656	0.030	3338	231.4	0.0	0.0	26.4	6.1	1.7	0.0	0.5	60.6	0.6
C-27-11	212.5	2559	0.031	3260	247.4	0.0	0.0	29.6	6.4	2.0	0.0	0.5	70.1	0.7
C-27-12a	235.5	2616	0.029	3250	271.8	0.0	0.0	33.4	6.8	2.4	0.0	0.5	81.5	0.9
C-27-12b	235.5	2550	0.029	3180	267.1	0.0	0.0	33.0	6.7	2.3	0.0	0.5	79.6	0.9
C-27-12c	235.5	2548	0.029	3267	264.9	0.0	0.0	32.7	6.7	2.3	0.0	0.5	80.9	1.0
C-27-cond-1	-	0	0.100	3643	11.5	0.0	0.0	0.0	0.0	0.0	0.0	0.0	NM	NM
C-27-cond-2	-	0	0.098	3644	0.0	0.0	0.0	0.0	0.0	0.0	0.0	0.0	NM	NM

Table B.52: Summary of Experimental Data - Hydrolyzed, C-27, 7 m MDEA, New thermal reactor, 55/100°C, SSM

Sample No.	Time (hr)	MDEA (Cations) (mM)	Hydrolyzed Concentration (mM)									
						Heat Stable Salts Concentration					Amino Acids	
			DEA+MAE	EDA	1-MPZ	Formate	Glycolate	Oxalate	Acetate	Sulfate	Bicine	Glycine
C-27-0a+NaOH	0	3180	0.0	0.0	0.0	0.2	0.0	0.1	0.0	1.2	0.0	0.0
C-27-0b+NaOH	0	3263	0.0	0.0	0.0	0.4	0.0	0.1	0.0	1.2	0.0	0.0
C-27-1+NaOH	3	3236	0.0	0.0	0.0	0.3	0.3	0.1	0.0	1.1	0.0	0.0
C-27-2+NaOH	21.5	3238	0.0	0.0	0.0	1.6	2.1	0.2	0.0	1.2	0.0	0.0
C-27-3+NaOH	42	3149	27.6	0.0	0.0	3.8	3.8	0.3	0.0	1.2	6.8	0.0
C-27-4+NaOH	66.5	3124	52.0	0.0	0.0	8.7	5.9	0.4	0.0	1.2	0.0	0.0
C-27-5+NaOH	97	3135	93.0	0.0	0.0	18.1	8.2	0.8	0.0	1.2	36.7	0.1
C-27-7+NaOH	120	2852	119.7	0.0	0.0	27.2	9.8	1.4	0.0	1.1	59.8	0.2
C-27-8+NaOH	141	2864	167.4	0.0	0.0	35.4	11.0	2.0	0.0	1.1	82.5	0.3
C-27-9+NaOH	163.5	2763	222.5	0.0	0.0	47.6	12.0	3.0	0.0	1.0	109.0	0.3
C-27-10+NaOH	188.5	2780	223.0	0.0	0.0	53.0	12.3	3.5	0.0	1.0	116.9	1.1
C-27-11+NaOH	212.5	2736	269.4	0.0	0.0	49.3	8.4	3.0	0.0	0.6	57.1	0.0
C-27-12a+NaOH	235.5	2650	281.0	0.0	0.0	53.8	0.0	3.4	0.0	0.7	71.1	0.2
C-27-12b+NaOH	235.5	2671	286.1	0.0	0.0	54.0	0.0	3.4	0.0	0.6	72.0	0.2
C-27-12c+NaOH	235.5	2574	289.9	0.0	0.0	53.8	0.0	3.3	0.0	0.7	71.3	0.2
C-27-cond-1+NaOH	-	0	0	0.0	0.0	0.0	0.0	0.0	0.0	0.0	0.0	0.0

Table B.53: Summary of Experimental Data, C-28, 8 m PZ, New thermal reactor, 55/110°C, SSM

Sample No.	Time (hr)	PZ (Cations) (mM)	α_{act} (mol CO_2 /mol alk)	Total Alk (mmol/kg)	Concentration (mM)									
								Heat Stable Salts Concentration					Amino Acids	
					EDA	1-MPZ	NH_4^+	Formate	Glycolate	Oxalate	Acetate	Sulfate	Bicine	Glycine
C-28-0a	0	4329	0.287	4238	0.0	0.0	0.0	0.1	0.0	0.0	0.0	0.4	0.0	0.0
C-28-0b	0	4001	0.29	4153	0.0	0.0	0.0	0.1	0.0	0.0	0.0	0.5	0.0	0.0
C-28-1	17	4006	0.284	4104	0.0	0.0	0.0	0.2	0.0	0.0	0.0	0.4	0.0	0.0
C-28-2	46	3833	0.278	4068	0.0	0.0	0.0	0.6	0.5	0.0	0.0	0.4	0.0	0.0
C-28-3	64.5	3837	0.28	3991	0.0	0.0	0.0	0.9	0.0	0.0	0.0	0.4	0.0	0.3
C-28-4	94.5	3781	0.281	4031	0.0	0.0	0.0	1.5	0.5	0.0	0.0	0.5	0.0	0.7
C-28-5	120.5	4214	0.271	3896	10.1	0.0	26.5	1.8	0.0	0.0	0.0	0.4	0.0	0.7
C-28-6	137	4148	0.273	3951	9.8	0.0	0.0	2.1	0.0	0.1	0.0	1.0	0.0	0.7
C-28-7	161.5	4026	0.267	3962	13.2	0.0	13.6	3.0	0.5	0.1	0.0	0.5	0.0	0.9
C-28-8	183.5	3846	0.262	3969	17.3	0.0	0.0	3.5	0.4	0.1	0.0	0.4	0.0	1.0
C-28-9	214.5	3580	0.266	3863	17.6	0.0	0.0	4.2	0.4	0.1	0.0	0.4	0.0	1.3
C-28-10	256.5	3546	0.259	3832	14.9	0.0	0.0	5.0	0.4	0.1	0.0	0.4	0.0	1.6
C-28-11	304.5	4449	0.271	3831	45.5	0.0	0.0	6.6	0.4	0.2	0.0	0.6	0.0	2.2
C-28-cond-1	-	0	NM	NM	0.01	0.0	0.0	0.0	0.0	0.0	0.0	0.0	NM	NM
C-28-cond-2	-	0	NM	NM	0.02	0.0	0.0	0.0	0.0	0.0	0.0	0.0	NM	NM
C-28-cond-3	-	0	NM	NM	0.03	0.0	0.0	0.0	0.0	0.0	0.0	0.0	NM	NM
C-28-cond-4	-	7	NM	NM	0.01	0.0	0.0	0.0	0.0	0.0	0.0	0.0	NM	NM
C-28-cond-5	-	10	NM	NM	0.05	0.0	0.0	0.0	0.0	0.0	0.0	0.0	NM	NM
C-28-cond-6	-	0	NM	NM	0		0.0	0.0	0.0	0.0	0.0	0.0	NM	NM

Table B.54: Summary of Experimental Data - Hydrolyzed, C-28, 8 m PZ, New thermal reactor, 55/110°C, SSM

Sample No.	Time (hr)	PZ (Cations) (mM)	Hydrolyzed Concentration (mM)									
						Heat Stable Salts Concentration					Amino Acids	
			EDA	1-MPZ	NH_4^+	Formate	Glycolate	Oxalate	Acetate	Sulfate	Bicine	Glycine
C-28-0a+NaOH	0	4210	0.0	0.0	0.0	0.0	0.0	0.0	0.0	0.6	0.0	0.0
C-28-0b+NaOH	0	3882	0.0	0.0	0.0	0.0	0.0	0.0	0.0	0.6	0.0	0.0
C-28-1+NaOH	17	3765	0.0	0.0	0.0	0.1	0.0	0.0	0.0	0.6	0.0	0.0
C-28-2+NaOH	46	4036	0.0	0.0	24.5	2.4	0.0	0.1	0.0	0.6	0.0	0.0
C-28-3+NaOH	64.5	NM	28.1	0.0	0.0	3.2	0.0	0.1	0.0	0.6	0.0	0.3
C-28-4+NaOH	94.5	4069	0.0	0.0	183.4	5.0	0.0	0.1	0.0	0.6	0.0	0.7
C-28-5+NaOH	120.5	4481	0.0	0.0	0.0	7.0	0.0	0.2	0.0	0.6	0.0	0.7
C-28-6+NaOH	137	3732	0.0	0.0	0.0	7.0	0.0	0.2	0.0	0.6	0.0	0.7
C-28-7+NaOH	161.5	3849	0.0	0.0	0.0	8.7	0.0	0.2	0.5	0.6	0.0	0.9
C-28-8+NaOH	183.5	3802	0.0	0.0	0.0	10.1	0.0	0.3	0.6	0.5	0.0	1.0
C-28-9+NaOH	214.5	4168	23.7	0.0	0.0	13.0	0.0	0.3	0.0	0.5	0.0	1.3
C-28-10+NaOH	256.5	3953	18.3	0.0	0.0	16.3	0.0	0.4	0.7	0.6	0.0	1.6
C-28-11+NaOH	304.5	3981	28.0	0.0	0.0	19.9	0.0	0.4	0.8	0.7	0.0	2.2

Table B.55: Summary of Experimental Data, C-29, 8 m PZ, New thermal reactor, 55/125°C, SSM

Sample No.	Time (hr)	PZ (Cations) (mM)	α_{act} (mol CO_2 /mol alk)	Total Alk (mmol/kg)	Concentration (mM)									
								Heat Stable Salts Concentration					Amino Acids	
					EDA	FPZ	NH_4^+	Formate	Glycolate	Oxalate	Acetate	Sulfate	Bicine	Glycine
C-29-0a	0	5288	0.23	4070	0.0	0.0	0.0	0.2	0.0	0.0	0.0	0.60	0.0	0.0
C-29-0b	0	3519	0.215	4071	0.0	0.0	0.0	0.0	0.0	0.0	0.0	0.39	0.0	0.0
C-29-1	4	3465	0.227	4070	0.0	0.0	0.0	0.1	0.0	0.0	0.0	0.39	0.0	0.0
C-29-2	22.5	3470	0.232	4026	0.0	0.0	0.0	0.7	0.5	0.0	0.0	0.38	0.0	0.0
C-29-3	48	3442	0.212	4021	0.0	0.0	0.0	1.5	0.6	0.0	0.0	0.36	0.0	0.4
C-29-4	71	3804	0.268	3969	0.0	0.0	0.0	3.0	0.6	0.0	0.0	0.43	0.0	0.9
C-29-5	98	3318	0.267	3968	26.7	0.0	6.0	4.2	0.5	0.1	0.0	0.35	0.0	1.5
C-29-6	115	3441	0.251	3939	35.6	0.0	4.0	7.3	0.5	0.1	0.0	0.39	0.0	1.7
C-29-7	140.5	3265	0.265	3923	43.9	18.8	6.0	7.3	0.5	0.2	0.0	0.36	0.0	2.3
C-29-8	165	3132	0.278	3774	58.8	28.7	5.3	8.7	0.0	0.3	0.0	0.35	0.0	2.9
C-29-9	187.5	3204	0.276	3898	67.6	35.2	26.1	10.3	0.4	0.4	0.0	0.35	0.0	3.5
C-29-10	211	3039	0.282	3866	65.8	41.7	18.7	12.0	0.0	0.5	0.0	0.35	0.0	4.0
C-29-11	240.5	2998	0.245	3849	75.8	50.5	24.8	14.3	0.0	0.8	0.0	0.38	0.0	4.6
C-29-12	267	2966	0.267	3816	93.4	57.1	45.2	16.3	0.0	1.0	0.0	0.36	0.0	5.2
C-29-13	283	3030	0.267	3845	0.0	64.9	66.3	17.7	0.0	1.2	0.0	0.35	0.0	5.4
C-29-cond-1	-	0.0	NM	NM		0.0	0.0	0.0	0.0	0.0	0.0	0.00	0.0	0.0

Table B.56: Summary of Experimental Data - Hydrolyzed, C-29, 7 m MDEA/2 m PZ, 55/120°C, SSM

Sample No.	Time (hr)	PZ (Cations) (mM)	Hydrolyzed Concentration (mM)									
						Heat Stable Salts Concentration					Amino Acids	
			EDA	FPZ	NH_4^+	Formate	Glycolate	Oxalate	Acetate	Sulfate	Bicine	Glycine
C-29-0a+NaOH	0	3622	0.0	0.0	0.0	0.0	0.0	0.0	0.0	0.36	0.00	0.00
C-29-0b+NaOH	0	3849	0.0	0.0	0.0	0.0	0.0	0.0	0.0	0.37	0.00	0.00
C-29-1+NaOH	4	3657	0.0	0.0	0.0	0.1	0.0	0.0	0.0	0.35	0.00	0.00
C-29-2+NaOH	22.5	3725	0.0	0.0	0.0	1.3	0.0	0.0	0.0	0.43	0.00	0.00
C-29-3+NaOH	48	3873	8.2	0.0	0.0	5.0	0.0	0.1	0.0	0.39	0.00	0.00
C-29-4+NaOH	71	3870	17.9	0.0	0.0	8.9	0.0	0.1	0.0	0.35	0.00	0.96
C-29-5+NaOH	98	0	0.0	0.0	0.0	0.0	0.0	0.1	0.0	0.05	0.00	0.00
C-29-6+NaOH	115	3964	32.1	0.0	0.0	18.1	0.0	0.4	0.0	0.35	0.00	2.10
C-29-7+NaOH	140.5	3600	45.1	0.0	0.0	24.6	0.0	0.7	0.0	0.36	0.00	3.16
C-29-8+NaOH	165	3420	41.5	0.0	2.3	29.6	0.0	0.7	0.0	0.37	0.00	4.18
C-29-9+NaOH	187.5	3386	65.4	0.0	5.8	35.6	0.0	0.9	0.0	0.34	0.00	4.51
C-29-10+NaOH	211	3342	71.5	0.0	0.0	41.9	0.0	1.1	0.0	0.34	0.00	5.74
C-29-11+NaOH	240.5	3381	83.5	0.0	6.6	50.3	0.0	1.7	0.0	0.39	0.05	8.50
C-29-12+NaOH	267	3152	55.4	0.0	31.3	57.5	0.0	2.2	0.0	0.35	0.07	7.75
C-29-13+NaOH	283	3258	98.8	0.0	18.1	62.6	0.0	2.0	0.0	0.38	0.30	8.34

Table B.57: Summary of Experimental Data, C-30, 7 m MDEA/2 m PZ, New thermal reactor, 55/125°C, SSM

Sample No.	Time (hr)	MDEA (Cations) (mM)	PZ (Cations) (mM)	α_{act} (mol CO_2 /mol alk)	Total Alk (mmol/kg)	Concentration (mM)											
											Heat Stable Salts Concentration					Amino Acids	
						DEA+MAE	EDA	1-MPZ	FPZ	NH_4^+	Formate	Glycolate	Oxalate	Acetate	Sulfate	Bicine	Glycine
C-30-0a	0	3259	980	0.151	5104	3.0	0.0	0.0	0.0	0.0	0.00	0.00	0.12	0.00	0.67	0.0	0.0
C-30-0b	0	3248	983	0.153	5173	4.2	0.0	0.0	0.0	0.0	0.02	0.00	0.00	0.02	0.76	0.0	0.0
C-30-1	5.5	3198	971	0.152	5330	9.6	0.0	0.0	0.0	0.0	0.48	0.00	0.01	0.00	0.74	0.0	0.0
C-30-2	20.5	3325	987	0.149	5343	44.7	0.0	87.7	0.0	0.0	4.47	0.41	0.05	0.00	0.79	0.0	0.0
C-30-3	44.5	3012	895	0.145	5175	175.4	0.0	128.8	11.8	0.0	15.87	0.68	0.52	0.00	0.63	13.0	0.0
C-30-4	69.5	2920	876	0.139	5053	264.8	0.0	160.4	23.2	2.5	25.61	0.90	1.16	0.00	0.66	23.7	0.0
C-30-5	99.5	2704	794	0.133	4883	341.6	0.0	182.3	30.0	3.9	37.59	1.05	2.16	0.00	0.78	37.3	0.0
C-30-6	121.5	2603	740	0.104	4785	399.4	0.0	198.3	37.9	5.2	45.33	1.13	2.99	0.00	0.65	46.7	0.0
C-30-7	149.5	2483	638	0.092	4612	423.9	0.0	199.5	35.9	5.8	53.27	1.30	3.93	4.43	0.63	54.7	0.0
C-30-8	164	2414	611	0.093	4524	450.4	0.0	207.5	45.5	8.8	57.51	1.37	4.47	5.08	0.62	61.1	0.0
C-30-9	189.5	2444	605	0.091	4447	523.2	0.0	224.4	51.5	9.2	66.10	1.55	5.61	6.52	0.60	72.1	0.0
C-30-cond-1																	

Table B.58: Summary of Experimental Data - Hydrolyzed, C-30, 7 m MDEA/2 m PZ, New thermal reactor, 55/125°C, SSM

Sample No.	Time (hr)	MDEA (Cations) (mM)	PZ (Cations) (mM)	Hydrolyzed Concentration (mM)											
									Heat Stable Salts Concentration					Amino Acids	
				DEA+MAE	EDA	1-MPZ	FPZ	NH_4^+	Formate	Glycolate	Oxalate	Acetate	Sulfate	Bicine	Glycine
C-30-0a+NaOH	0	3414	1114	0.0	0.0	0.0	0.0	0.0	0.03	0.00	0.03	0.00	0.47	0.0	0.0
C-30-0b+NaOH	0	3441	1129	0.0	0.0	0.0	0.0	0.0	0.00	0.00	0.03	0.00	0.40	0.0	0.0
C-30-1+NaOH	5.5	3280	1247	11.5	0.0	0.0	0.0	0.0	0.02	0.00	0.03	0.12	0.24	0.0	0.0
C-30-2+NaOH	20.5	3343	916	50.4	0.0	0.0	0.0	0.0	0.00	0.00	0.03	0.00	0.48	0.0	0.0
C-30-3+NaOH	44.5	3199	846	172.0	0.0	222.6	0.0	0.0	42.74	0.00	1.21	1.02	0.98	9.6	0.0
C-30-4+NaOH	69.5	3048	794	256.6	0.0	257.4	0.0	0.0	65.94	0.00	2.31	1.70	0.90	17.8	0.0
C-30-5+NaOH	99.5	2919	735	359.4	0.0	298.3	0.0	0.0	96.28	0.00	4.12	3.41	0.94	28.9	0.0
C-30-6+NaOH	121.5	2894	718	454.4	0.0	310.1	0.0	0.0	115.65	0.00	4.81	3.84	0.84	37.5	0.0
C-30-7+NaOH	149.5	2669	669	467.5	0.0	327.5	0.0	0.0	130.20	0.00	6.04	5.10	0.90	43.5	0.0
C-30-8+NaOH	164	2661	605	484.5	0.0	337.4	0.0	0.0	146.21	0.00	6.96	5.88	0.87	54.6	0.0
C-30-9+NaOH	189.5	4943	1161	1063.8	0.0	481.8	107.2	13.6	139.08	0.00	11.80	13.55	2.75	151.6	0.0

Table B.59: Summary of Experimental Data, C-31, 6 m MDEA/1 m MAE, New thermal reactor, 55/120°C, SSM

Sample No.	Time (hr)	MDEA (Cations) (mM)	α_{act} (mol CO_2 /mol alk)	Total Alk (mmol/kg)	Concentration (mM)														
												Heat Stable Salts Concentration					Amino Acids	
					DEA+MAE	EDA	DMAE	MEA	1-MPZ	1,4-DMPZ	NH_4^+	Formate	Glycolate	Oxalate	Acetate	Sulfate	Bicine	Glycine
C-31-0a	0	3048	0.133	3677	637	0.0	0.0	0.0	0.0	0.0	3.3	0.26	0.00	0.02	0.00	NM	0.00	0.0
C-31-0b	0	3045	0.130	3829	637	0.0	0.0	0.0	0.0	0.0	4.3	0.01	0.00	0.02	0.00	NM	0.00	0.0
C-31-1	2.5	2996	0.128	3871	630	0.0	0.0	0.0	0.0	0.0	0.0	0.00	0.00	0.02	0.00	NM	0.00	0.0
C-31-2	18	2553	0.120	3798	600	0.0	0.0	0.0	0.0	0.0	17.6	0.87	0.00	0.02	0.00	NM	0.00	0.0
C-31-3	42.5	3001	0.100	3776	719	0.0	0.0	0.0	0.0	0.0	1.8	5.17	0.00	0.54	0.49	NM	0.00	0.0
C-31-4	66.5	2757	0.091	3692	666	0.0	0.0	0.0	0.0	0.0	1.5	11.49	0.00	0.70	0.98	NM	2.74	0.0
C-31-5	94	2698	0.081	3586	709	0.0	0.0	0.0	0.0	0.0	2.9	18.94	0.00	1.26	1.18	NM	21.08	0.0
C-31-6	118	2717	0.083	3377	722	0.0	0.0	0.0	4.4	0.0	3.0	24.45	0.00	1.64	1.41	NM	27.72	0.0
C-31-7	138	2543	0.090	3474	716	0.0	0.0	0.0	0.0	0.0	1.7	30.06	0.00	2.33	1.83	NM	52.03	0.0
C-31-8	162	2588	0.091	3317	769	0.0	0.0	0.0	0.0	0.0	1.5	39.01	0.00	3.51	2.76	NM	81.01	0.0
C-31-9	186	2420	0.091	3257	742	0.0	0.0	0.0	0.0	0.0	2.1	45.03	0.00	4.53	3.56	NM	102.33	0.0
C-31-10	210	2374	0.093	2999	756	0.0	0.0	0.0	1.2	0.0	2.8	51.22	0.00	0.00	4.19	NM	130.22	0.0
C-31-cond-1		10			93	0.0	0.0	12.0	0.0	0.0	4.7	0.02	0.00	0.00	0.00	NM	0.00	0.0
C-31-cond-2		0			119	0.0	0.0	0.0	0.0	0.0	7.5	0.06	0.00	0.00	0.00	NM	NM	NM

Table B.60: Summary of Experimental Data - Hydrolyzed, C-31, 6 m MDEA/1 m MAE, New thermal reactor, 55/120°C, SSM

Sample No.	Time (hr)	MDEA (Cations) (mM)	Hydrolyzed Concentration (mM)								
					Heat Stable Salts Concentration					Amino Acids	
			DEA+MAE	EDA	Formate	Glycolate	Oxalate	Acetate	Sulfate	Bicine	Glycine
C-31-0a+NaOH	0	3238	644	0.0	0.9	0.0	0.0	0.0	NM	0.0	0.0
C-31-0b+NaOH	0	3183	638	0.0	1.0	0.0	0.0	0.0	0.0	0.0	0.0
C-31-1+NaOH	2.5	3200	632	0.0	1.3	0.0	0.0	0.0	0.0	0.0	0.0
C-31-2+NaOH	18	3170	655	0.0	5.1	0.0	0.0	0.0	0.0	0.0	0.0
C-31-3+NaOH	42.5	3097	706	0.0	16.3	0.0	0.0	0.0	0.0	0.0	0.0
C-31-4+NaOH	66.5	2985	733	0.0	32.3	0.0	0.0	0.0	0.0	0.0	0.0
C-31-5+NaOH	94	3009	769	0.0	44.5	0.0	0.0	0.0	0.0	11.8	0.0
C-31-6+NaOH	118	2805	732	0.0	55.3	0.0	0.0	0.0	0.0	16.9	0.0
C-31-7+NaOH	138	2723	765	0.0	70.6	0.0	0.0	0.0	0.0	23.6	0.0
C-31-8+NaOH	162	2663	814	0.0	88.0	0.0	0.0	0.0	0.0	65.0	0.0
C-31-9+NaOH	186	2597	820	0.0	99.0	0.0	0.0	0.0	0.0	0.0	0.0
C-31-10+NaOH	210	2519	844	0.0	NM	0.0	0.0	0.0	0.0	110.6	0.0

All samples: NH4+, 1-MPZ, 1,4-DMPZ, and HEP = 0.0

Table B.61: Summary of Experimental Data, C-32, 6 m MDEA/1 m DEA, New thermal reactor, 55/90°C, SSM

Sample No.	Time (hr)	MDEA (Cations) (mM)	α_{act} (mol CO_2 /mol alk)	Total Alk (mmol/kg)	Concentration (mM)								
							Heat Stable Salts Concentration					Amino Acids	
					DEA+MAE	MEA	Formate	Glycolate	Oxalate	Acetate	Sulfate	Bicine	Glycine
C-32-0a	0	3081	0.125	3896	498	0.0	0.5	0.0	0.0	0.2	1.8	0.0	0.0
C-32-0b	0	3124	0.122	3881	482	0.3	0.3	0.1	0.0	0.4	0.6	0.0	0.0
C-32-1	3.5	3132	0.117	3884	495	1.6	0.2	0.0	0.0	0.1	0.7	0.0	0.0
C-32-2	19.5	3125	0.106	3823	490	0.3	0.4	0.0	0.0	0.1	0.6	0.0	0.0
C-32-3	35	3132	0.089	3841	512	0.4	0.7	0.1	0.0	0.1	0.7	2.6	0.0
C-32-4	84.5	3085	0.067	3835	509	0.5	1.3	0.1	0.0	0.6	0.6	9.6	0.0
C-32-5	127.5	3069	0.066	3750	520	0.7	2.1	0.1	0.0	0.1	0.6	17.5	0.0
C-32-6	176.5	3140	0.061	3535	544	0.6	2.9	0.2	0.0	0.8	0.6	23.0	0.0
C-32-7	231	2959	0.063	3672	513	0.4	4.5	0.6	0.1	0.2	0.6	38.3	0.0
C-32-8	247.5	2933	0.062	3680	518	0.6	4.9	0.3	0.1	0.1	0.6	42.0	0.0
C-32-cond-1	-	0	NM	NM	0	0.1	0.0	0.0	0.0	0.0	0.1	0.0	0.0
C-32-cond-2	-	34	NM	NM	0	0.2	0.0	0.0	0.0	0.0	0.1	0.0	0.0
C-32-cond-3	-	0	NM	NM	0	0.1	0.0	0.0	0.0	0.0	0.2	0.0	0.0

Table B.62: Summary of Experimental Data - Hydrolyzed, C-32, 6 m MDEA/1 m DEA, New thermal reactor, 55/90°C, SSM

Sample No.	Time (hr)	MDEA (Cations) (mM)	Hydrolyzed Concentration (mM)								
					Heat Stable Salts Concentration					Amino Acids	
			DEA+MAE	MEA	Formate	Glycolate	Oxalate	Acetate	Sulfate	Bicine	Glycine
C-32-0a+NaOH	0	3275	520	1.5	2.3	0.9	0.0	1.4	0.9	0.0	0.0
C-32-0b+NaOH	0	3402	544	0.8	2.6	1.2	0.0	1.4	1.1	0.0	0.0
C-32-1+NaOH	3.5	3255	503	2.9	2.5	1.2	0.0	1.6	0.8	0.0	0.0
C-32-2+NaOH	19.5	3236	519	1.7	3.4	1.9	0.0	1.8	1.0	0.0	0.0
C-32-3+NaOH	35	3193	496	0.0	3.2	1.5	0.0	1.2	1.0	0.0	0.0
C-32-4+NaOH	84.5	3204	526	1.0	4.7	2.0	0.0	1.2	0.8	0.0	0.0
C-32-5+NaOH	127.5	3373	575	0.0	12.6	3.5	0.1	0.1	1.0	0.0	0.0
C-32-6+NaOH	176.5	3143	549	0.0	9.9	2.7	0.1	0.3	0.8	23.0	0.0
C-32-7+NaOH	231	3079	538	0.0	11.1	2.7	0.1	0.5	0.9	25.7	0.0
C-32-8+NaOH	247.5	3068	539	1.2	11.0	2.7	0.2	0.3	0.9	35.6	0.0

Table B.63: Summary of Experimental Data, C-33, New thermal reactor, 7 m MDEA/2 m PZ, 55/90°C, SSM

Sample No.	Time (hr)	MDEA (Cations) (mM)	PZ (Cations) (mM)	α_{act} (mol CO_2 /mol alk)	Total Alk (mmol/kg)	Concentration (mM)											
								Heat Stable Salts Concentration								Amino Acids	
						DEA+MAE	MEA	1-MPZ	1,4-DMPZ	NH_4^+	Formate	Glycolate	Oxalate	Acetate	Sulfate	Bicine	Glycine
C-33-0a	0	3285	712	0.133	7606	4.0	0.0	0.0	0.0	0.0	0.1	0.0	0.0	0.1	0.6	0.0	0.0
C-33-0b	0	3333	681	0.139	7879	3.5	0.0	0.0	0.0	0.0	0.3	0.0	0.0	0.1	0.7	0.0	0.0
C-33-1	4.5	3307	681	0.136	7857	4.2	0.0	0.0	0.0	0.0	0.2	0.0	0.0	0.1	0.6	0.0	0.0
C-33-2	21	3317	680	0.137	7904	28.7	0.0	0.0	0.0	0.0	0.5	0.0	0.0	0.1	0.6	0.0	0.0
C-33-3	68	3245	660	0.129	7615	18.4	0.0	0.0	0.0	0.0	1.7	0.1	0.0	0.1	0.5	0.6	0.0
C-33-4	120.5	3379	681	0.121	7854	31.3	0.0	0.0	0.0	0.0	3.1	0.1	0.0	0.1	0.6	1.4	0.0
C-33-5	165.5	3235	659	0.114	7925	40.3	0.0	0.0	0.0	0.0	4.6	0.1	0.0	0.1	0.7	2.6	0.0
C-33-6	214	3527	732	0.086	7958	55.0	0.0	0.0	0.0	0.0	6.6	0.2	0.0	0.1	0.5	4.8	0.0
C-33-7	261	3357	666	0.085	7946	66.5	0.0	3.8	0.0	0.0	7.9	0.2	0.0	0.1	0.6	5.6	0.0
C-33-8	315.5	3126	636	0.088	7869	81.6	0.0	7.2	0.0	0.0	10.1	0.4	0.0	0.1	0.5	7.2	0.0
C-33-9	356.5	3088	634	0.077	7513	92.1	0.0	9.9	0.0	0.0	11.5	0.3	0.1	0.1	0.5	8.8	0.0
C-33-10	381.5	3083	624	0.081	NM	101.8	2.3	12.3	0.0	0.0	12.3	0.4	0.1	0.1	0.5	9.1	0.0
C-33-cond-1	-	2	0			0.0	0.0	0.0	0.1	2.2	0.1	0.0	0.0	0.1	0.3	0.0	0.0
C-33-cond-2	-	3	0			0.0	0.0	0.0	0.1	8.9	0.1	0.0	0.0	0.1	0.3	0.0	0.0
C-33-cond-3	-	3	0			0.0	0.0	0.0	0.1	5.6	0.1	0.0	0.0	0.1	0.3	0.0	0.0
C-33-cond-4	-	3	1			0.0	0.0	0.1	0.1	8.0	0.2	0.0	0.0	0.1	0.8	0.0	0.0
C-33-cond-5	-	5	1			0.0	0.0	0.2	0.1	15.0	0.0	0.0	0.0	0.0	0.2	0.0	0.0
C-33-cond-6	-	4	1			0.0	0.1	0.3	0.1	18.4	0.1	0.0	0.0	0.0	0.2	0.0	0.0
C-33-cond-7	-	4	1			0.0	0.3	0.4	0.1	23.7	0.2	0.0	0.0	0.1	0.2	0.0	0.0

Table B.64: Summary of Experimental Data - Hydrolyzed, C-33, New thermal reactor, 7 m MDEA/2 m PZ, 55/90°C, SSM

Sample No.	Time (hr)	MDEA (Cations) (mM)	PZ (Cations) (mM)	Hydrolyzed Concentration (mM)									
							Heat Stable Salts Concentration					Amino Acids	
				DEA+MAE	MEA	1-MPZ	Formate	Glycolate	Oxalate	Acetate	Sulfate	Bicine	Glycine
C-33-0a+NaOH	0	3506	707	9.5	0.0	0.0	5.0	2.2	0.0	0.3	0.8	0.0	0.0
C-33-0b+NaOH	0	3518	702	10.8	0.0	0.0	5.2	2.2	0.0	0.3	0.9	0.0	0.0
C-33-1+NaOH	4.5	3529	701	10.9	0.0	0.0	5.7	2.3	0.0	0.3	0.8	0.0	0.0
C-33-2+NaOH	21	3516	706	15.0	0.0	0.0	6.9	2.5	0.0	0.2	0.8	0.0	0.0
C-33-3+NaOH	68	3483	685	20.3	0.0	0.0	8.5	2.0	0.0	0.3	0.9	0.0	0.0
C-33-4+NaOH	120.5	3410	682	32.9	0.0	0.0	13.6	3.5	0.0	0.5	0.7	1.0	0.0
C-33-5+NaOH	165.5	3780	725	41.7	0.0	0.0	12.3	1.4	0.0	0.2	0.8	2.0	0.0
C-33-6+NaOH	214	3705	725	54.8	0.0	0.0	15.0	1.3	0.1	0.2	0.7	2.6	0.0
C-33-7+NaOH	261	3266	662	56.4	0.0	0.0	17.8	0.8	0.1	0.2	0.7	3.8	0.0
C-33-8+NaOH	315.5	3196	640	73.4	0.0	5.9	22.1	0.8	0.1	0.2	0.7	5.8	0.0
C-33-9+NaOH	356.5	3175	649	83.0	3.7	9.7	27.6	0.7	0.2	1.2	0.7	7.2	0.0
C-33-10+NaOH	381.5	3193	692	89.7	0.0	12.5	27.3	0.5	0.1	1.0	0.7	7.8	0.0

All samples: NH_4^+, DMAE, and 1,4-DMPZ = 0.0

Table B.65: Summary of Experimental Data, C-34, New thermal reactor, 7 m MDEA/2 m PZ, 55/125°C, Acid-treated at 0.1 mol H^+/mol alkalinity, SSM

Sample No.	Time (hr)	MDEA (Cations) (mM)	PZ (Cations) (mM)	α_{act} (mol CO_2 /mol alk)	Total Alk (mmol/kg)	Concentration (mM)												
												Heat Stable Salts Concentration					Amino Acids	
						DEA+MAE	1-MPZ	1,4-DMPZ	AEP	FPZ	NH_4^+	Formate	Glycolate	Oxalate	Acetate	Sulfate	Bicine	HES
C-34-0a	0	3454	919	0.011	4819	4.5	0.0	0.0	0.0	0.0	0.0	0.0	0.0	0.0	0.0	269.4	0.0	0.0
C-34-0b	0	3451	920	0.001	4821	3.5	0.0	0.0	0.0	0.0	13.5	0.0	0.0	0.0	0.0	273.8	0.0	0.0
C-34-1	1	3409	919	0.001	4856	15.2	0.0	0.0	0.0	0.0	0.0	0.5	0.0	0.0	0.0	276.0	0.0	0.0
C-34-2	20.5	3345	817	0.006	4733	47.0	1.9	0.0	0.0	3.2	0.0	11.8	0.4	0.0	0.0	279.2	1.7	4.1
C-34-3	41	3134	758	0.013	4590	117.1	10.8	0.0	0.0	16.6	0.0	27.2	0.9	0.0	0.0	277.9	9.1	9.6
C-34-4	92	2928	688	0.009	4155	282.5	58.4	0.0	0.0	36.8	0.0	61.4	1.8	2.0	1.7	271.3	38.8	26.2
C-34-5	139	2619	589	0.016	4159	340.3	84.7	2.7	0.0	39.4	4.1	73.5	2.0	3.5	2.4	269.8	60.4	32.3
C-34-6	209.5	2586	521	0.019	3994	451.7	127.4	6.3	13.0	42.4	9.4	91.3	2.4	5.6	4.5	266.6	93.5	45.8
C-34-7	281	2327	446	0.021	3588	487.3	141.0	9.0	14.7	42.9	9.2	101.2	2.8	7.8	6.5	266.2	124.0	56.5
C-34-8	353	2181	390	0.026	3716	544.5	155.1	13.4	16.5	42.9	20.7	111.5	3.0	9.9	8.5	266.3	146.8	59.5
C-34-cond-1	-	21	8	NM	NM	0.8	0.2	0.0	0.0	0.0	5.1	0.0	0.0	0.0	0.0	0.6	0.0	0.0
C-34-cond-2	-	0	17	NM	NM	0.6	3.2	0.5	0.0	0.0	29.1	0.2	0.0	0.0	0.1	1.1	0.0	4.4
C-34-cond-3	-	0	3	NM	NM	0.4	4.0	1.8	0.0	1.7	53.7	0.2	0.0	0.0	0.1	1.0	0.0	2.7
C-34-cond-4	-	0	2	NM	NM	0.2	5.7	5.6	0.0	0.0	0.0	0.2	0.0	0.0	0.1	0.6	0.0	1.7
C-34-cond-5	-	0	2	NM	NM	0.2	5.5	7.7	0.0	0.0	0.0	0.2	0.0	0.0	0.1	0.3	0.0	0.0
C-34-cond-6	-	0	1	NM	NM	0.2	6.0	11.9	0.0	0.0	0.0	0.2	0.0	0.0	0.0	0.5	0.0	0.0
C-34-cond-7	-	0	0	NM	NM	0.2	6.8	1.1	0.0	0.0	0.0	0.2	0.0	0.0	0.0	0.6	0.0	0.0
All samples: Glycine, EDA = 0																		

Table B.66: Summary of Experimental Data - Hydrolyzed, C-34, New thermal reactor, 7 m MDEA/2 m PZ, 55/125°C, Acid-treated at 0.1 mol H^+/mol alkalinity, SSM

Sample No.	Time (hr)	MDEA (Cations) (mM)	PZ (Cations) (mM)	Hydrolyzed Concentration (mM)									
							Heat Stable Salts Concentration					Amino Acids	
				DEA+MAE	1-MPZ	AEP	Formate	Glycolate	Oxalate	Acetate	Sulfate	Bicine	HES
C-34-0a+NaOH	0	3560	1008	0.0	0.0	0.0	3.0	0.9	0.0	0.0	254.8	0.0	0.0
C-34-0b+NaOH	0	4284	1248	0.0	0.0	0.0	3.3	0.7	0.0	0.0	258.2	0.0	0.0
C-34-1+NaOH	1	3517	929	0.0	0.0	0.0	5.4	1.0	0.0	0.0	262.1	0.0	0.0
C-34-2+NaOH	20.5	3467	898	0.0	0.0	0.0	30.0	1.4	0.0	0.0	260.5	0.9	3.2
C-34-3+NaOH	41	3262	807	0.0	9.3	0.0	66.0	2.2	0.0	0.0	260.1	6.8	9.6
C-34-4+NaOH	92	2969	696	266.8	58.3	0.0	139.3	2.5	3.5	3.1	254.4	30.6	23.8
C-34-5+NaOH	139	0	0	0.0	0.0	NM	216.5	3.1	7.9	7.2	249.9	0.0	0.0
C-34-6+NaOH	209.5	2585	556	492.8	135.0	0.0	244.7	3.6	10.8	10.1	247.8	82.8	45.9
C-34-7+NaOH	281	2393	0	536.9	160.6	17.0	275.6	3.6	13.4	12.5	246.2	105.5	51.2
C-34-8+NaOH	353	2226	415	611.3	173.8	18.4	3.0	0.9	0.0	0.0	254.8	144.8	61.6

All samples, Glycine, FPZ, MEA, NH_4^+ = 0

Appendix C – Low-gas Experimental Data

Table C.1: Summary of Experimental Data, OD-1, 7 m MDEA/2 m PZ, 55 °C, α=0.3 mol CO_2/mol alkalinity, 1 mM Fe^{2+}

Sample No.	Time (Days)	MDEA (Cations) (m)	PZ (Cations) (m)	Formate (mM)
-	0	7.00	2.00	NM
-	2	7.18	2.15	0.6
-	4	7.62	2.25	1.9
-	8	7.61	2.16	2.0
-	10	7.93	2.26	2.4
-	12	7.08	1.94	2.6
-	14	7.20	2.01	3.7

Table C.2: Summary of Experimental Data, OD-2, 7 m MDEA, 55 °C, α=0.1 mol CO_2/mol alkalinity, 1 mM Fe^{2+}

Time (Days)	MDEA (Cations) (mM)	Formate (mM)
0	7.00	NM
4	6.52	1.69
6	7.54	1.84
8	6.52	2.93
10	6.79	3.56
12	6.58	4.08
14	6.52	4.49

Table C.3: Summary of Experimental Data, OD-3, 7 m MDEA/2 m PZ, 55 °C, α=0.24 mol CO_2/mol alkalinity, 0.1 mM Fe^{2+}, 0.6 mM Cr^{3+}, 0.1 mM Ni^{2+}

Time (Days)	MDEA (Cations) (m)	PZ (Cations) (m)	Formate (mM)	Sulfate (ppm)
0	7.00	2.00	1.30	38.4
2	6.82	1.90	1.24	36.6
4	7.99	2.80	1.09	35.0
6	7.90	2.65	2.98	21.5
8	1.94	0.45	2.42	42.6
10	8.87	3.00	4.19	57.6

Table C.4: Summary of Experimental Data, OD-4, 7 m MDEA/2 m PZ, 55 °C, α=0.24 mol CO_2/mol alkalinity, 0.1 mM Fe^{2+}, 5 mM Cu^{2+}

Time (Days)	MDEA (Cations) (mM)	PZ (Cations) (mM)	Formate (mM)	Sulfate (ppm)
0	NM	NM	0.28	0.0
2	NM	NM	1.35	23.8
4	NM	NM	2.38	44.0
6	NM	NM	5.25	10.9
8	NM	NM	3.95	10.4
10	NM	NM	3.50	9.2

Table C.5: Summary of Experimental Data, OD-5, 7 m MDEA/2 m PZ, 55 °C, α=0.242 mol CO_2/mol alkalinity, 1 mM Fe^{2+}, 100 mM Inh A

Time (Days)	MDEA (Cations) (mM)	PZ (Cations) (mM)	Formate (mM)	Nitrate (mM)	Nitrite (mM)
0	3237	1032	0.32	0.06	0.00
2	2803	912	0.41	0.55	0.00
4	3247	977	0.85	0.00	0.00
6	3387	1013	1.45	4.43	0.00
8	3326	1080	1.78	0.00	1.01
10	3431	1092	2.17	0.00	0.75
12	3451	1092	3.50	0.00	2.75
14	3406	1088	3.40	0.00	0.00
16	3299	1041	3.73	0.00	0.95
18	3269	1046	4.25	0.00	0.16
20	3215	1050	4.85	0.03	0.58

Table C.6: Summary of Experimental Data, OD-6, 7 m DEA, 55 °C, SSM

Sample No.	Time (hr)	DEA+MAE (Cations) (mM)	Hydrolyzed Concentration (mM)												
						Heat Stable Salts Concentration							Amino Acids		
			MEA	HEP	NH_4^+	Formate	Glycolate	Oxalate	Acetate	Sulfate	Nitrate	Nitrite	Bicine	Glycine	HES
OD-6-0	0	3724	2.7	0.9	1.5	0.4	0.1	0.0	2.8	0.6	0.0	0.0	0.0	0.0	0.0
OD-6-1	17.5	3404	60.3	1.4	1.0	2.9	1.2	0.0	1.8	0.6	0.0	0.3	0.0	0.0	0.0
OD-6-2	41.5	2887	196.4	1.0	11.6	11.8	3.9	0.2	2.6	1.0	0.5	3.7	19.1	0.0	0.0
OD-6-3	93	2271	219.7	0.5	8.0	22.7	6.8	0.8	2.6	0.7	2.3	13.8	139.0	1.4	0.0
OD-6-4	137	2247	242.1	1.8	6.8	30.0	6.3	1.6	2.4	0.8	3.7	17.9	227.4	1.8	7.1
OD-6-5	186	1993	229.6	1.9	5.7	38.7	5.2	2.6	3.6	0.8	4.9	19.6	314.8	1.9	11.0
OD-6-6	237	2091	283.0	1.1	3.8	45.1	3.5	3.8	3.9	0.0	5.7	18.9	398.3	2.3	9.9
OD-6-7	286	1962	238.1	1.8	2.5	51.5	2.8	5.1	3.6	0.0	6.6	18.5	431.6	2.5	7.5
OD-6-8	329	1932	224.3	2.4	2.3	55.7	2.5	6.1	4.3	0.8	7.0	17.2	476.7	2.8	6.5
OD-6-9	378	1907	226.0	1.9	2.2	57.7	2.2	6.7	3.6	0.8	7.3	16.6	484.8	2.8	5.9

All samples, DMAE, 1-MPZ, 1,4-DMPZ, AEP, and FPZ = 0

Table C.7: Summary of Experimental Data, OD-6 - Hydrolyzed, 7 m DEA, 55 °C, SSM

Sample No.	Time (hr)	DEA+MAE (Cations) (mM)	Concentration (mM)												
						Heat Stable Salts Concentration							Amino Acids		
			MEA	HEP	NH_4^+	Formate	Glycolate	Oxalate	Acetate	Sulfate	Nitrate	Nitrite	Bicine	Glycine	HES
OD-6-0+NaOH	0	3601	0.9	1.9	0.0	5.5	4.3	0.0	2.6	0.8	0.1	0.2	0.0	0.0	0.0
OD-6-1+NaOH	17.5	3404	46.6	1.6	0.0	22.4	45.2	0.1	7.3	0.0	0.0	0.5	0.0	0.0	0.0
OD-6-2+NaOH	41.5	4600	282.3	2.2	57.5	58.3	110.9	2.5	9.8	0.9	0.6	3.6	16.4	0.0	0.0
OD-6-3+NaOH	93	2573	285.5	3.4	0.0	128.5	155.0	10.8	12.2	0.0	2.2	12.4	139.5	2.4	0.0
OD-6-4+NaOH	137	3068	4.8	5.8	0.0	172.7	152.8	19.5	13.9	0.0	3.3	16.3	248.5	3.2	0.0
OD-6-5+NaOH	186	2365	312.6	5.2	0.0	226.6	85.7	25.9	13.7	1.0	4.5	18.2	360.6	3.7	0.0
OD-6-6+NaOH	237	2354	291.3	5.7	0.0	260.1	37.3	26.5	10.5	0.9	5.3	17.8	419.3	2.9	0.0
OD-6-7+NaOH	286	2265	281.8	1.8	0.0	289.3	42.8	30.1	14.0	0.0	6.0	17.6	485.1	3.5	0.0
OD-6-8+NaOH	329	2328	294.7	1.6	0.0	281.5	27.9	31.7	5.0	0.0	6.4	16.5	529.3	3.9	0.0
OD-6-9+NaOH	378	2073	262.9	1.7	0.0	298.2	26.1	33.4	9.3	0.0	6.4	15.2	517.8	3.7	0.0

All samples, DMAE, 1-MPZ, 1,4-DMPZ, AEP, and FPZ = 0

Table C.8: Summary of Experimental Data, OD-7, 7 m MAE, 55 °C, SSM

Sample No.	Time (hr)	DEA+MAE (Cations) (mM)	α_{act} (mol CO_2 /mol alk)	Total Alk (mmol/kg)	Concentration (mM)											
					Heat Stable Salts Concentration										Amino Acids	
					MEA	HEP	NH_4^+	Formate	Glycolate	Oxalate	Acetate	Sulfate	Nitrate	Nitrite	Bicine	HES
OD-7-0	0	5708	0.098	4545	0.0	0.0	1.4	0.3	0.1	0.0	3.8	0.7	0.0	0.0	0.0	15.6
OD-7-1	17.5	5968	0.160	4317	93.1	1.9	269.0	2.7	0.6	0.0	0.6	0.7	0.1	0.6	0.0	160.0
OD-7-2	41.5	4511	0.229	3832	153.0	1.7	53.3	11.7	1.9	0.2	2.8	1.1	0.4	5.7	0.0	0.0
OD-7-3	93	3796	0.298	3281	100.7	3.8	74.2	21.0	2.4	0.9	0.9	0.8	1.2	16.0	0.0	192.8
OD-7-4	137	3677	0.284	3093	207.1	3.9	27.3	30.7	2.5	1.8	1.2	0.9	1.8	19.1	0.0	189.7
OD-7-5	186	3357	0.261	2758	185.7	0.0	15.7	41.6	1.7	2.7	1.4	0.7	2.0	18.9	11.0	174.8
OD-7-6	237	3340	0.236	2896	195.4	0.0	0.0	54.2	1.9	3.6	0.0	0.5	2.3	17.8	22.9	167.4
OD-7-7	286	3191	0.230	2588	173.9	0.0	7.0	62.7	1.7	4.8	2.4	0.7	2.4	16.2	35.1	134.9
OD-7-8	329	3149	0.229	2572	162.1	0.0	5.4	71.1	1.4	5.7	3.5	0.7	2.6	14.8	32.6	176.1
OD-7-9	378	3078	0.221	2680	178.8	0.0	2.8	73.7	1.5	6.2	2.4	0.6	2.6	14.0	31.2	183.4

All samples, Glycine = 0

Table C.9: Summary of Experimental Data - Hydrolyzed, OD-7, 7 m MAE, 55 °C, SSM

Sample No.	Time (hr)	DEA+MAE (Cations) (mM)	Hydrolyzed Concentration (mM)										
						Heat Stable Salts Concentration							Amino Acids
			MEA	HEP	NH_4^+	Formate	Glycolate	Oxalate	Acetate	Sulfate	Nitrate	Nitrite	Bicine
OD-7-0+NaOH	0	5452	0.0	0.6	0.0	0.1	0.1	0.0	0.0	0.6	0.0	0.0	0.0
OD-7-1+NaOH	17.5	5206	91.9	0.0	0.0	0.4	0.4	0.0	0.0	0.7	0.0	0.0	0.0
OD-7-2+NaOH	41.5	4555	223.8	0.7	22.1	1.7	1.4	0.0	0.0	0.7	0.0	0.0	0.0
OD-7-3+NaOH	93	3893	107.4	3.3	51.4	2.7	2.0	0.0	0.0	0.7	0.0	0.0	0.0
OD-7-4+NaOH	137	3802	229.7	0.0	0.0	3.9	2.5	0.1	0.0	0.6	0.0	0.0	21.8
OD-7-5+NaOH	186	3688	210.5	0.0	0.0	5.5	2.9	0.1	0.0	0.6	0.0	0.0	35.8
OD-7-6+NaOH	237	3665	209.2	0.0	0.0	6.9	3.2	0.2	0.0	0.6	0.0	0.0	36.7
OD-7-7+NaOH	286	3433	217.3	0.0	1.6	10.1	4.0	0.3	0.2	0.6	0.0	0.0	38.6
OD-7-8+NaOH	329	3428	202.9	0.0	0.0	10.4	3.9	0.4	0.1	0.6	0.1	0.0	41.7
OD-7-9+NaOH	378	3284	173.4	0.0	0.0	11.7	4.1	0.5	0.1	0.6	0.1	0.0	34.7

Table C.10: Summary of Experimental Data, OD-8, 7 m MDEA, 70 °C, SSM

Sample No.	Time (hr)	MDEA (Cations) (mM)	α_{act} (mol CO_2 /mol alk)	Total Alk (mmol/kg)	Concentration (mM)										
							Heat Stable Salts Concentration							Amino Acids	
					DEA+MAE	NH_4^+	Formate	Glycolate	Oxalate	Acetate	Sulfate	Nitrate	Nitrite	Bicine	HES
OD-8-0	0	3338	0.121	3913	3.6	0.0	0.1	0.1	0.0	0.0	0.6	0.0	0.0	0.0	0.0
OD-8-1	17	3541	0.065	3820	4.5	0.0	0.4	0.4	0.0	0.0	0.7	0.0	0.0	0.0	0.0
OD-8-2	70.5	3207	0.055	4089	10.4	0.0	1.7	1.4	0.0	0.0	0.7	0.0	0.0	1.0	1.4
OD-8-3	113	3398	0.059	4019	13.7	0.0	2.7	2.0	0.0	0.0	0.7	0.0	0.0	2.5	2.4
OD-8-4	161	3585	0.058	4047	27.3	0.0	3.9	2.5	0.1	0.0	0.6	0.0	0.0	5.0	4.4
OD-8-5	214	3354	0.056	4018	33.3	3.6	5.5	2.9	0.1	0.0	0.6	0.0	0.0	7.0	5.9
OD-8-6	257	3516	0.055	3694	39.1	0.0	6.9	3.2	0.2	0.0	0.6	0.0	0.0	9.6	6.7
OD-8-7	306	3329	0.059	3841	38.4	1.6	10.1	4.0	0.3	0.2	0.6	0.0	0.0	13.1	7.0
OD-8-8	332	3713	0.053	3792	55.8	6.2	10.4	3.9	0.4	0.1	0.6	0.1	0.0	15.7	9.3
OD-8-9	380	3323	0.053	3863	54.0	0.0	11.7	4.1	0.5	0.1	0.6	0.1	0.0	15.5	10.1
OD-8-10	428.5	3252	0.053	3816	59.6	0.0	12.6	4.2	0.6	0.1	0.6	0.1	0.0	20.5	13.2
OD-8-11	473	3295	0.050	3823	69.3	0.0	0.1	0.1	0.0	0.0	0.6	0.0	0.0	24.4	13.8

All samples, Glycine, DMAE, MEA, 1-MPZ, 1,4-DMPZ, AEP, FPZ, and HEP = 0

Table C.11: Summary of Experimental Data - Hydrolyzed, OD-8, 7 m MDEA, 70 °C, SSM

Sample No.	Time (hr)	MDEA (Cations) (mM)	Hydrolyzed Concentration (mM)											
						Heat Stable Salts Concentration							Amino Acids	
			DEA+MAE	MEA	NH_4^+	Formate	Glycolate	Oxalate	Acetate	Sulfate	Nitrate	Nitrite	Bicine	HES
OD-8-0+NaOH	0	3454	5.5	0.0	0.0	2.8	0.8	0.0	0.6	0.9	0.1	0.0	0.0	0.0
OD-8-1+NaOH	17	3519	6.2	0.0	0.0	3.4	1.4	0.0	0.4	1.0	0.1	0.0	0.0	0.0
OD-8-2+NaOH	70.5	3511	8.8	0.0	0.0	4.3	2.2	0.0	0.2	1.0	0.1	0.0	0.0	0.0
OD-8-3+NaOH	113	3484	22.2	0.0	0.0	7.4	3.0	0.1	0.2	0.9	0.0	0.0	1.7	3.2
OD-8-4+NaOH	161	3608	26.3	0.0	30.5	8.0	3.5	0.1	0.1	0.8	0.0	0.0	4.8	0.0
OD-8-5+NaOH	214	3432	32.7	0.0	0.0	9.0	3.8	0.2	0.2	0.7	0.0	0.0	7.1	0.0
OD-8-6+NaOH	257	0	44.3	57.0	0.0	14.9	4.9	0.4	0.2	0.9	0.1	0.0	7.8	6.3
OD-8-7+NaOH	306	2117	24.2	3.2	0.0	14.3	4.6	0.4	0.2	0.8	0.0	0.0	12.2	12.3
OD-8-8+NaOH	332	3354	48.0	0.0	0.0	15.7	4.8	0.5	0.1	0.8	0.1	0.0	12.0	8.3
OD-8-9+NaOH	380	3332	48.0	0.0	0.0	16.4	4.4	0.6	0.1	0.9	0.1	0.0	14.2	10.1
OD-8-10+NaOH	428.5	3261	55.9	0.0	0.0	16.7	4.6	0.7	0.1	0.6	0.1	0.0	16.4	10.4
OD-8-11+NaOH	473	3333	65.2	0.0	0.0	2.8	0.8	0.0	0.6	0.9	0.1	0.0	19.0	11.0

All samples, Glycine, DMAE, 1-MPZ, 1,4-DMPZ, AEP, FPZ, and HEP = 0

Table C.12: Summary of Experimental Data, OD-9, 7 m MDEA/2 m PZ, 70 °C, SSM

Sample No.	Time (hr)	MDEA (Cations) (mM)	PZ (Cations) (mM)	α_{act} (mol CO_2 /mol alk)	Total Alk (mmol/kg)	Concentration (mM)										
								Heat Stable Salts Concentration								Amino Acids
						DEA+MAE	NH_4^+	Formate	Glycolate	Oxalate	Acetate	Sulfate	Nitrate	Nitrite	Bicine	HES
OD-9-0	0	3058	1016	0.135	5442	4.3	0.0	0.1	0.0	0.0	0.0	0.6	0.1	0.0	0.0	0.0
OD-9-1	17	3110	1021	0.147	5529	5.2	0.0	0.4	0.0	0.0	0.0	0.6	0.0	0.0	0.0	0.0
OD-9-2	70.5	2846	1032	0.150	5490	14.5	0.0	1.8	0.1	0.0	0.1	0.6	0.1	0.0	0.4	2.64
OD-9-3	113	3086	1046	0.150	5501	25.1	0.0	3.1	0.1	0.0	0.1	0.6	0.1	0.0	1.2	3.80
OD-9-4	161	2980	1086	0.148	5506	36.1	0.0	4.6	0.1	0.0	0.1	0.6	0.0	0.0	1.8	5.17
OD-9-5	214	2476	1016	0.145	5588	39.2	0.0	6.6	0.1	0.0	0.1	0.6	0.1	0.0	3.0	6.12
OD-9-6	257	3176	1051	0.152	5614	57.1	0.0	7.9	0.2	0.0	0.1	0.6	0.1	0.0	4.3	7.70
OD-9-7	306	2956	974	0.146	5425	62.5	0.0	9.5	0.2	0.0	0.1	0.5	0.1	0.0	6.1	11.18
OD-9-8	332	2972	1021	0.143	5452	69.9	0.0	10.4	0.2	0.0	0.1	0.6	0.1	0.0	7.8	12.21
OD-9-9	380	2988	1010	0.144	5565	77.1	0.0	11.6	0.3	0.1	0.1	0.5	0.2	0.0	8.9	13.65
OD-9-10	428.5	2937	1024	0.141	5577	87.2	0.0	13.2	0.3	0.1	0.1	0.5	0.2	0.0	10.9	17.68
OD-9-11	473	2926	995	0.142	5207	98.1	0.0	14.8	0.3	0.1	0.1	0.6	0.1	0.0	0.0	-

All samples, other cations ~0

Table C.13: Summary of Experimental Data - Hydrolyzed, OD-9, 7 m MDEA/2 m PZ, 70 °C, SSM

Sample No.	Time (hr)	MDEA (Cations) (mM)	PZ (Cations) (mM)	Hydrolyzed Concentration (mM)									
						Heat Stable Salts Concentration							Amino Acids
				DEA+MAE	MEA	Formate	Glycolate	Oxalate	Acetate	Sulfate	Nitrate	Nitrite	Bicine
OD-9-0+NaOH	0	3113	1160	5.2	0.0	0.0	0.0	0.0	0.0	0.5	0.0	0.0	0.0
OD-9-1+NaOH	17	3179	1179	6.8	0.0	0.0	0.0	0.0	0.0	0.5	0.0	0.0	0.0
OD-9-2+NaOH	70.5	3132	1177	11.9	0.0	0.0	0.0	0.0	0.0	0.5	0.0	0.0	0.0
OD-9-3+NaOH	113	3694	1258	0.0	0.0	11.4	1.5	0.0	0.2	0.8	0.0	0.0	0.5
OD-9-4+NaOH	161	3530	1244	35.8	0.0	12.8	0.8	0.0	0.2	0.8	0.1	0.0	1.2
OD-9-5+NaOH	214	3064	1158	36.0	0.0	16.2	0.8	0.1	0.2	0.8	0.1	0.0	2.1
OD-9-6+NaOH	257	3214	1231	44.3	0.0	18.7	0.5	0.1	0.2	0.7	0.1	0.0	2.9
OD-9-7+NaOH	306	3083	1172	59.3	1.5	22.7	1.2	0.1	0.4	0.7	0.1	0.0	3.9
OD-9-8+NaOH	332	3124	1208	68.8	0.0	23.5	0.6	0.1	0.3	0.7	0.1	0.0	4.8
OD-9-9+NaOH	380	3070	1189	71.1	0.0	27.6	1.1	0.2	0.3	0.8	0.2	0.0	6.3
OD-9-10+NaOH	428.5	3066	1198	82.4	0.0	31.1	0.9	0.2	0.3	0.9	0.2	0.0	8.9
OD-9-11+NaOH	473	3068	1207	94.4	0.0	34.2	0.5	0.2	0.3	0.6	0.1	0.0	9.4

All samples, Glycine, HES, NH_4^+, DMAE, 1-MPZ, 1,4-DMPZ, AEP, FPZ, and HEP = 0

Appendix D – Thermal Degradation Experimental Data

Table D.1: Summary of Experimental Data, Th. No. 3, 7 m MDEA, 100 °C, α=0.1, 0.21

Time (Days)	MDEA (Cations) (mM)
α=0.1, T=100 °C	
0	7.00
7	7.33
14	7.86
35	6.70
42	7.24
49	7.01
57	7.44
63	6.64
α=0.21, T=100 °C	
0	7.00
7	6.80
14	5.96
35	6.72
42	6.29
49	6.20
57	7.03
63	6.21

Table D.2: Summary of Experimental Data, Th. No. 3, 7 m MDEA, 120 °C, α=0.1, 0.21

Time (Days)	MDEA (Cations) (m)
α=0.1, T=120 °C	
0	7.00
7	6.69
14	6.65
35	6.66
42	6.02
49	7.96
63	6.50
α=0.21, T=120 °C	
0	7.00
7	6.62
14	9.09
35	6.11
42	6.09
49	6.97
57	5.27
63	5.65

Table D.3: Summary of Experimental Data, Th. No. 4, 7 m MDEA/2 m PZ, 100 °C, α=0.09, 0.19 mol CO_2/mol alk

Time (Days)	MDEA (Cations) (m)	PZ (Cations) (m)
α=0.09, T=100 °C		
0	7.00	2.00
7	6.89	1.91
14	7.79	2.25
22	7.00	1.97
28	5.55	1.57
35	6.32	1.70
42	7.27	2.08
49	7.11	1.98
54	6.98	1.93
α=0.19, T=100 °C		
0	7.00	2.00
7	7.33	2.04
14	7.70	2.15
22	6.78	1.92
28	7.05	1.93
35	6.76	1.80
42	7.08	1.91
49	6.59	1.88
54	6.50	1.81

Table D.4: Summary of Experimental Data, Th. No. 4, 7 m MDEA/2 m PZ, 120 °C, α=0.09, 0.19 mol CO_2/mol alk

Time (Days)	MDEA (Cations) (m)	PZ (Cations) (m)
α=0.09, T=120 °C		
0	7.00	2.00
7	6.50	1.76
14	6.94	1.93
22	7.03	1.91
28	5.41	1.47
35	6.72	1.73
42	6.76	1.72
49	6.92	1.72
54	5.67	1.40
α=0.19, T=120 °C		
0	7.00	2.00
7	6.46	1.78
14	6.08	1.69
22	6.23	1.63
28	6.85	1.86
35	6.48	1.59
42	7.00	1.77
49	6.50	1.45
54	7.00	2.00

Table D.5: Summary of Experimental Data, Th. No. 5, 7 m MDEA/2 m PZ, 100, 120 °C, α=0.176 mol CO_2/mol alk, 1 mM Fe^{2+}

Time (Days)	MDEA (Cations) (m)	PZ (Cations) (m)
α=0.176, T=100 °C		
0	7.00	2.00
7	6.28	1.74
14	6.97	1.97
22	6.65	1.88
33	6.90	2.00
42	10.16	3.26
α=0.176, T=120 °C		
0	7.00	2.00
7	7.69	2.23
14	6.10	1.77
22	7.44	2.17
33	6.42	1.62
49	6.80	1.65

Table D.6: Summary of Experimental Data - Th. No. 7, 7 m MDEA/2 m PZ, 135, 150 °C, α=0.11 & 0.26, no metals salts added

Cyl. No.	Time (hr)	MDEA (Cations) (mM)	PZ (Cations) (mM)	Cyl No.	Time (hr)	MDEA (Cations) (mM)	PZ (Cations) (mM)
α=0.11 and T=135 °C				**α=0.26 and T=135 °C**			
Stock Soln	0	3628	1039	Stock Soln	0	3516	1005
1	3	3515	994	30	3	3151	899
2	7	3569	960	31	7	3074	806
3	7	3597	987	33	7	3156	822
5	15	3462	825	34	15	2814	531
6	28	3288	683	35	21	2889	346
7	28	3396	713	36	21	2519	318
8	28	3295	692	37	21	2821	340
9	42	3329	489	38	35	2762	158
12	57	3076	0	41	69	2251	20
10	57	2926	0	43	69	2322	0
13	57	3303	0	39	69	1717	0
14	69	3036	140	42	69	2379	187
				45	99	1887	27
				46	99	1823	72
				44	99	1803	71
				47	120	1715	0

Table D.7: Summary of Experimental Data - Th. No. 7, 7 m MDEA/2 m PZ, 135, 150 °C, α=0.11 & 0.26, no metals salts added

Cyl. No.	Time (Days)	MDEA (Cations) (mM)	PZ (Cations) (mM)	Cyl. No.	Time (Days)	MDEA (Cations) (mM)	PZ (Cations) (mM)
α=0.11 and T=150 °C				**α=0.26 and T=150 °C**			
Stock Soln	0	3628	1039	Stock Soln	0	3516	1005
1	3	3515	994	30	3	3151	899
2	7	3569	960	31	7	3074	806
3	7	3597	987	33	7	3156	822
5	15	3462	825	34	15	2814	531
6	28	3288	683	35	21	2889	346
7	28	3396	713	36	21	2519	318
8	28	3295	692	37	21	2821	340
9	42	3329	489	38	35	2762	158
12	57	3076	0	41	69	2251	20
10	57	2926	0	43	69	2322	0
13	57	3303	0	39	69	1717	0
14	69	3036	140	42	69	2379	187
				45	99	1887	27
				46	99	1823	72
				44	99	1803	71
				47	120	1715	0

Table D.8: Summary of Experimental Data, Th. No. 8, 7 m MDEA/2 m PZ, 135, 150 °C, α=0.0, 0.019, and 0.299 mol CO_2/mol alk

Cyl. No.	Time (Days)	MDEA (Cations) (mM)	PZ (Cations) (mM)
α=0.0, T=135 °C			
	0	4308	3945
3	7	4576	938
14	35	9332	1102
α=0.016, T=135 °C			
	0	4510	1054
31	4	3761	873
32	7	4824	1124
33	14	2491	839
38	42	4017	922
41	73	4450	744
α=0.299, T=135 °C			
	0	3922	893
40	4	4039	806
52	7	3956	735
53	14	3183	446
61	21	3312	336

Table D.9: Summary of Experimental Data - Th. No. 8, 7 m MDEA/2 m PZ, 135, & 150 °C

Cyl. No.	Time (Days)	MDEA (Cations) (mM)	PZ (Cations) (mM)
α=0.0, T=150 °C			
	0	4308	3945
4	4	4019	844
20	7	4000	838
132	35	3709	711
α=0.016, T=150 °C			
	0	4550	949
29	4	3754	769
23	7	4136	820
30	21	4383	745
35	35	3884	583
α=0.299, T=150 °C			
	0	3943	897
51	7	3073	306
54	35	1580	1270
49	42	2334	293

Table D.10: Summary of Experimental Data, Th. No. 10, 7 m MDEA, 120, 135, and 150 °C, α=0.1 and 0.2 mol CO_2/mol alkalinity

Cyl. No.	Time (Days)	MDEA (Cations) (mM)	Formate (mM)
α=0.1, T=120 °C			
	0	4250	0.00
32	3	4508	0.03
1	7	3790	0.03
30	21	4291	0.04
31	35	5206	0.05
33	45	4106	0.06
45	69	4381	0.00
54	108	4250	0.00
α=0.2, T=120 °C			
	0	4773	0.00
38	3	4364	0.04
136	7	4813	0.04

Table D.11: Summary of Experimental Data - Th. No. 10, 7 m MDEA, 120, 135, and 150 °C, α=0.1 and 0.2 mol CO_2/mol alkalinity

Cyl. No.	Time (Days)	MDEA (Cations) (mM)	Formate (mM)
α=0.1, T=135 °C			
	0	4250	0.00
4	3	4288	1.93
34	7	4021	2.75
49	21	4018	4.31
57	35	4347	5.98
α=0.2, T=135 °C			
	0	4773	0.00
53	3	4469	2.96
55	7	3228	4.47
50	7	3091	19.64
58	21	3783	10.61
46	35	3359	14.82
50	45	3289	29.19
48	69	3174	43.22
51	108	4773	0.00

Table D.12: Summary of Experimental Data, Th. No. 10, 7 m MDEA, 120, 135, and 150 °C, α=0.1 and 0.2 mol CO_2/mol alkalinity

Cyl. No.	Time (Days)	MDEA (Cations) (mM)	Formate (mM)
α=0.1, T=150 °C			
Stock Soln	0	4250	NA
68	3	0	NA
47	3	4570	NA
61	21	4190	NA
65	35	3714	NA
132	69	687	NA
α=0.2, T=150 °C			
Stock Soln	0	4773	NA
59	3	4050	NA
41	7	3680	NA
69	35	381	NA
70	69	0	NA

Table D.13: Summary of Experimental Data - Th. No. 13, 7 m DEA, 150 °C, α=0.2 mol CO_2/mol alkalinity

Cyl. No.	Time (Days)	DEA (Cations) (mM)	Heat Stable Salts Concentration (mM)			
			Formate	Glycolate	Oxalate	Sulfate
α=0.0	0	3203	0.95	0.02	0.02	0.15
#1	6	3037	1.54	0.05	0.04	0.15
#40	13	2983	1.98	0.05	0.04	0.15
α=0.2	0	2876	1.02	0.01	0.01	0.13
#70	2	913	2.32	0.06	0.05	0.14
#101	6	299	13.58	0.01	0.01	0.13
#124	13	72	39.17	0.01	0.01	0.20

Table D.14: Summary of Experimental Data - Th. No. 14, 7 m MDEA + 0.35 m Quat, 150 °C, α=0.0 and 0.2 mol CO_2/mol alkalinity

Sample	Time (Days)	MDEA (Cations) (mM)	Heat Stable Salts Concentration			
			Formate	Glycolate	Oxalate	Sulfate
Series 1: α=0.0, No quat, T=150 °C						
FC105	12	3808	1.49	0.05	0.04	0.20
FC116	12	3634	1.68	0.04	0.03	0.16
114	19	3813	1.48	0.04	0.03	0.23
FC102	26	4091	1.56	0.05	0.04	0.28
Series 2: α=0.0, 0.35 m Quat, T=150 °C						
FC 94	7	2756	1.28	0.02	0.02	0.18
61	12	2859	1.42	0.03	0.02	0.17
FC 107	19	2706	1.44	0.02	0.02	0.36
FC 118	26	2702	1.53	0.02	0.02	0.47
Series 4: α=0.2, 0.35 m Quat, T=150 °C						
FC 117	7	2357	18.77	0.02	0.02	0.20
54	12	2177	27.47	0.08	0.06	0.16
FC 12	19	1990	37.04	0.03	0.03	0.19
FC 108	26	1931	43.60	0.05	0.04	0.43
FC 104	30	NM	48.38	0.09	0.08	0.24

Table D.15: Summary of Experimental Data – Th. No. 15, 7 m MDEA + 1 m Quat, T= 150°C, α=0.2 mol CO_2/mol alkalinity

Cyl. No.	Time (Days)	MDEA (Cations) (mM)	Quat (Cations) (mM)	α_{act} (mol CO_2 /mol alk)	Concentration (mM)									
										Heat Stable Salts Concentration				
					DEA+MAE	bHEP	1-MPZ	AEP	NH_4^+	Formate	Glycolate	Oxalate	Acetate	Sulfate
0.2 mol CO_2/mol alkalinity, T=150 °C, No quat														
Initial	0	NM	NM	NM	NM	NM	NM	NM	NM	NM	NM	NM	NM	NM
12	3	3427	0.0	0.253	118.7	0.0	20.6	0	0.0	13.6	0.7	0.0	0.0	1.8
13	3	2916	0.0	0.16	110.1	0.0	18.3	0	0.0	18.8	0.9	0.0	0.0	2.0
FC-13	8	2823	5.2	0.169	166.8	6.6	32.9	2.3	7.3	33.9	1.2	0.0	0.0	1.9
0.2 mol CO_2/mol alkalinity, T=150 °C, 1 m quat														
FC-19	3	3271	625.1	0.144	142.1	63.7	9.0	0.0	46.5	15.4	0.0	0.0	0	1.8
35	3	2901	467.3	0.197	156.8	62.8	21.2	4.7	57.4	30.5	0.0	0.0	0	1.6
54	8	1122	170.8	0.205	65.5	17.1	7.8	1.8	0.0	31.8	0.0	0.0	0	1.8
FC-101	9	2845	474.6	0.207	153.4	60.9	23.2	7.4	228.9	38.1	0.0	0.0	0	0.0
FC-106	11	731	106.4	0.161	43.7	13.2	6.3	1.5	70.5	32.0	0.0	0.0	0	1.5
FC-112	13	2097	356.6	0.161	124.2	48.8	25.8	6.3	0.0	31.7	0.0	0.0	0	0.0
FC-114	19	2448	417.5	0.156	137.5	130.5	52.7	20.1	18.4	58.5	0.0	0.0	0	1.6
FC-118	63	2190	388.7	0.163	121.8	132.2	50.3	24.4	27.0	55.0	1.3	0.0	0	0.0

Table D.16: Summary of Experimental Data – Th. No. 16, 7 m MDEA, T= 120, 135, and 150°C, α=0.0, 0.11, and 0.26 mol CO_2/mol alkalinity

Cyl. No.	Time (Days)	MDEA (Cations) (mM)	PZ (Cations) (mM)	Concentrations (mM)						
				DEA+MAE	bHEP	1-MPZ	1,4-DMPZ	AEP	NH_4^+	FPZ
α=0.0, T=120 °C										
-	0	4174	1054	18.9	0.0	30.6	0.0	0.0	4.1	4.0
48	4	3479	943	21.2	0.0	35.4	0.0	0.0	52.0	3.7
54	7	3669	971	23.8	0.0	24.8	0.0	0.0	35.8	3.8
57	22	3491	983	25.7	0.0	34.7	0.0	0.0	15.6	3.6
58	46	3832	991	25.1	0.0	21.1	0.0	0.0	11.3	3.9
60	71	3820	1022	25.9	0.0	0.0	0.0	0.0	0.0	3.7
α=0.1, T=120 °C										
-	0	3499	943	16.8	0.0	31.2	0.0	0.0	0.0	3.7
22	4	3216	855	28.0	0.0	56.1	0.0	1.8	44.9	3.8
α=0.25, T=120 °C										
-	0	3419	933	15.7	0.0	35.4	0.0	0.0	6.4	3.7
FC-102	7	3317	905	30.2	0.0	43.2	0.0	4.1	45.1	3.7
FC-103	14	4948	1294	49.9	0.0	101.8	0.0	26.4	33.5	3.8
FC-104	22	3273	854	44.5	0.0	149.9	0.0	55.8	21.3	3.8
FC-106	46	3209	645	39.3	0.0	206.6	5.2	102.8	47.5	5.0
FC-109	113	2998	302	31.6	0.0	226.1	41.4	132.3	4.4	9.9
FC-110	113	2762	292	26.2	0.0	178.4	32.3	130.8	0.0	9.4

Table D.16: Summary of Experimental Data – Th. No. 16, 7 m MDEA, T= 120, 135, and 150°C, α=0.0, 0.11, and 0.26 mol CO_2/mol alkalinity (Continued)

Cyl. No.	Time (Days)	MDEA (Cations) (mM)	PZ (Cations) (mM)	Concentration (mM)						
				DEA+MAE	bHEP	1-MPZ	1,4-DMPZ	AEP	NH_4^+	FPZ
α=0.0, T=135 °C										
-	0	4174	1054	18.9	0.0	30.6	0.0	0.0	4.1	4.0
13	4	879	239	5.3	0.0	17.6	0.0	0.0	0.0	3.7
30	7	4159	1070	28.5	0.0	14.7	0.0	0.0	0.0	3.9
31	14	4053	1079	29.0	0.0	35.5	0.0	0.0	0.0	3.8
36	22	3811	985	27.8	0.0	28.2	0.0	0.0	0.0	3.9
40	46	3696	951	30.7	0.0	16.3	0.0	0.0	0.0	3.9
α=0.11, T=135 °C										
-	0	3499	943	16.8	0.0	31.2	0.0	0.0	0.0	3.7
FC-112	4	3174	817	42.7	0.0	140.2	0.0	14.5	59.3	3.9
FC-113	7	3189	729	63.8	0.0	171.1	4.5	85.8	38.8	4.4
FC-115	14	3587	825	70.7	0.0	277.9	4.3	97.8	43.0	4.3
FC-119	22	3354	610	76.6	0.0	280.6	17.9	137.5	6.4	5.5
FC-120	46	3059	295	58.8	0.0	176.0	65.4	142.1	27.5	10.4
FC-121	71	2904	100	47.2	0.0	88.0	138.4	99.8	19.0	29.0
FC-122	99	2567	9	39.0	0.0	130.0	171.6	51.4	9.0	275.7
FC-123	113	2721	43	39.3	0.0	137.5	155.6	78.1	5.6	62.7
FC-124	113	2763	49	33.7	0.0	15.5	148.8	73.6	5.0	56.6

Table D.16: Summary of Experimental Data – Th. No. 16, 7 m MDEA, T= 120, 135, and 150°C, α=0.0, 0.11, and 0.26 mol CO_2/mol alkalinity (Continued)

Cyl. No.	Time (Days)	MDEA (Cations) (mM)	PZ (Cations) (mM)	Concentration (mM)						
				DEA+MAE	bHEP	1-MPZ	1,4-DMPZ	AEP	NH_4^+	FPZ
α=0.26, T=135 °C										
-	0	3419	933	15.7	0.0	35.4	0.0	0.0	6.4	3.7
FC-3	4	1381	350	18.6	0.0	74.6	0.0	12.1	45.4	3.9
FC-7	7	1930	424	24.0	0.0	203.0	0.0	55.9	63.9	4.5
FC-12	14	2959	501	43.9	0.0	218.4	11.2	144.8	35.6	5.9
FC-13	22	2883	327	39.2	0.0	121.3	51.0	140.7	25.3	8.8
FC-15	50	NM	NM	NM	NM	NM	NM	NM	NM	NM
FC-17	50	2611	35	40.3	0.0	236.8	97.1	82.8	40.0	75.4
α=0.0, T=150 °C										
-	0	4174	1054	18.9	0.0	30.6	0.0	0.0	4.1	4.0
521	7	3498	922	30.2	0.0	27.1	0.0	0.0	41.8	3.8
522	14	3728	1016	35.1	0.0	44.4	0.0	0.0	25.1	3.7
523	22	3559	973	45.5	0.0	68.9	0.0	1.9	24.3	3.7
524	46	3654	911	51.8	0.0	NM	66.8	0.0	58.3	4.0

Table D.16: Summary of Experimental Data – Th. No. 16, 7 m MDEA, T= 120, 135, and 150°C, α=0.0, 0.11, and 0.26 mol CO_2/mol alkalinity (Continued)

Cyl. No.	Time (Days)	MDEA (Cations) (mM)	PZ (Cations) (mM)	Concentration (mM)						
				DEA+MAE	bHEP	1-MPZ	1,4-DMPZ	AEP	NH_4^+	FPZ
α=0.1, T=150 °C										
-	0	3499	943	16.8	0.0	31.2	0.0	0.0	0.0	3.7
511	4	1657	358	39.4	0.0	255.8	3.9	45.2	51.7	4.6
512	7	3378	566	79.6	0.0	226.6	19.2	161.8	41.5	6.0
513	14	2070	174	49.5	0.0	143.6	55.7	123.5	33.8	11.9
515	22	2670	68	49.4	0.0	47.4	123.5	107.0	43.4	39.3
517	46	2358	11	55.8	0.0	56.3	210.5	35.5	31.3	205.6
518	71	2163	17	55.8	0.0	51.3	291.9	41.2	22.1	127.7
519	99	1745	3	40.7	0.0	NM	284.5	32.3	10.8	606.6
520	113	1798	13	38.8	0.0	22.2	345.5	37.0	7.6	138.4
α=0.26, T=150 °C										
-	**0**	3419	933	15.7	0.0	35.4	0.0	0.0	6.4	3.7
500	4	2599	400	45.2	0.0	182.6	18.1	155.4	58.0	6.5
501	7	2541	139	50.0	0.0	102.6	65.7	126.8	33.6	18.3
502	14	1767	27	40.1	0.0	65.9	116.8	56.1	47.8	64.4
503	22	1872	23	67.6	0.0	184.8	176.6	52.9	63.7	81.9
504	46	1373	7	53.7	0.0	21.8	218.5	43.6	76.3	196.4
505	71	897	23	52.1	0.0	21.1	334.6	55.5	0.0	38.7
506	99	182	7	21.5	0.0	202.4	384.1	64.4	0.0	24.6
508	113	0	7	26.6	0.0	21.2	409.5	61.6	7.0	0.0
509	113	0	27	16.0	0.0	14.4	369.7	61.9	0.0	0.0
510	113	0	5	18.1	0.0	40.2	381.8	53.1	12.3	0.0

Table D.17: Summary of Experimental Data – Th. No. 17, 7 m MDEA/2 m PZ + 0.1 mol H^+/mol alkalinity, T= 120, 135, and 150°C

Cyl. No.	Time (Days)	MDEA (Cations) (mM)	PZ (Cations) (mM)	Concentration (mM)						
				DEA+MAE	bHEP	1-MPZ	1,4-DMPZ	AEP	NH_4^+	FPZ
T=120 °C										
Initial	0	NM	NM	0.0	0.0	0.0	0.0	0.0	0.0	0.0
35	3	3111	960	53.2	0.0	0.0	0.0	0.0	91.3	3.2
45	3	2763	846	68.9	0.0	10.3	0.0	0.0	143.6	3.3
48	7	1412	440	51.9	0.0	11.2	0.0	0.0	90.7	3.2
53	15	2831	843	124.3	0.0	42.0	0.0	0.0	0.0	3.4
54	19	2667	799	133.4	0.0	42.5	0.0	0.0	0.0	3.3
T=135 °C										
Initial	0	NM	NM	0.0	0.0	0.0	0.0	0.0	0.0	0.0
61	3	3807	1152	65.5	0.0	0.0	0.0	8.2	0.0	3.3
63	3	3221	957	112.2	0.0	33.7	0.0	0.0	0.0	3.4
65	7	2511	740	168.5	0.0	65.7	0.0	0.0	0.0	3.4
100	15	2989	812	327.8	0.0	142.1	0.0	6.4	90.7	3.7
FC-102	19	2632	714	401.6	0.0	166.2	9.7	5.8	0.0	3.7
FC-114	33	2656	596	642.6	0.0	258.4	32.3	8.7	0.0	4.5

Table D.17: Summary of Experimental Data – Th. No. 17, 7 m MDEA/2 m PZ + 0.1 mol H^+/mol alkalinity, T= 120, 135, and 150°C (Continued)

Cyl. No.	Time (Days)	MDEA (Cations) (mM)	PZ (Cations) (mM)	Concentration (mM)						
				DEA+MAE	bHEP	1-MPZ	1,4-DMPZ	AEP	NH_4^+	FPZ
T=150 °C										
Initial	0	NM	NM	0.0	0.0	0.0	0.0	0.0	0.0	0.0
FC-116	3	2725	868	43.7	0.0	0.0	0.0	0.0	13.9	3.1
501	3	2258	647	257.6	0.0	96.2	0.0	3.4	0.0	3.5
511	7	2225	529	490.7	0.0	212.9	24.1	10.0	0.0	4.2
512	15	1952	322	903.2	0.0	299.3	83.2	20.3	12.9	6.1
514	19	2071	259	1276.2	0.0	338.1	129.7	7.4	0.0	8.0
516	33	1971	151	1979.7	0.0	377.3	331.2	37.1	23.3	13.0
521	37	1556	73	1803.1	0.0	257.4	252.9	22.5	0.0	21.4

Appendix E –Master Rate Table

Table E.1: Master Rate Table for All Cycling and Low-Gas Experiments

Expt	Solvent (m)	T_{th} (°C)	Stir Rate (rpm)	Purge Gas	Other Conditions [1]	Alk Loss (mM/kg-solv*hr)	Loss Rate (mM/hr)		Generation Rate (mM/hr)								
							MDEA	PZ	DEA	Formate	Total Formate	Bicine	Glycine	EDA	MAE	MEA	DEA+MAE
C-8	7 MDEA	120	1440	N_2/CO_2	SSM; bubble vessel	1.57	1.9	NA	0	0.013	0.001	0	0	NM	NM	NM	NM
C-9	7 MDEA	120	0	N_2/CO_2	SSM; bubble vessel	2.62	4.1	NA	0	0.024	0.002	0	0	NM	NM	NM	NM
C-13	7 MDEA	120	1440	Air/CO_2	SSM; bubble vessel	-0.52	0.24	NA	0.37	0.084	0.08	0.061	0.001	NM	NM	NM	0.3
C-14	7 MDEA	90	1440	Air/CO_2	SSM; bubble vessel	-0.18	0.22	NA	0.08	0.044	0.058	0.062	~0	NM	NM	NM	0.1
C-18	7 MDEA	120	1440	O_2/CO_2	SSM; 1 L/min N_2 purge	-0.73	0	NA	0.39	0.047	0.044	0.088	0.01	NM	NM	NM	0.3
C-4	7 MDEA	120	520	O_2/CO_2	SSM	2.46	3.4	NA	NM	0.17	0.15	NM	NM	NM	NM	NM	NM
C-5	7 MDEA	120	1000	O_2/CO_2	SSM; bubble removal	3.95	8.5	NA	NM	0.37	0.57	NM	NM	NM	NM	NM	NM
C-1	7 MDEA	120	1440	O_2/CO_2	Original design/no mods	4.78	8.8	NA	NM	0.59	0.98	0.48	0.001	NM	NM	NM	NM
C-2	7 MDEA	55	1440	O_2/CO_2	Original design/no mods	0	~0.0	NA	NM	0.0052	~0	~0	~0	NM	NM	NM	NM
C-15	7 MDEA	90	1440	O_2/CO_2	SSM; Inh A	-1.63	2.37	NA	0	0.15	0.23	0.27	0.004	NM	NM	NM	0.0
C-7*	7 MDEA	120	1440	O_2/CO_2	SSM; Inh A	5.03	5	NA	1.8	0.22	0.29	0.35	~0	NM	NM	NM	1.5
C-3	7 MDEA	55	1440	O_2/CO_2	SSM	0.91	0.9	NA	0	0.005	0.01	0.002	0	NM	-	NM	0
C-11	7 MDEA	80	1440	O_2/CO_2	SSM; bubble vessel	0.97	0.91	NA	0	0.034	0.039	0.027	0.009	NM	-	NM	0
C-12	7 MDEA	90	1440	O_2/CO_2	SSM; bubble vessel	2.19	2.87	NA	1.55	0.12	0.15	0.084	0.006	NM	-	NM	1.3
C-10	7 MDEA	100	1440	O_2/CO_2	SSM; bubble vessel	3.1	4.1	NA	1.64	0.18	0.31	0.22	0.007	NM	-	NM	1.4
C-6	7 MDEA	120	1440	O_2/CO_2	SSM; bubble vessel	4.93	4.6	NA	2.56	0.28	0.34	0.34	0.007	NM	-	NM	2.2
C-17	8 PZ	90	1440	O_2/CO_2	SSM; bubble vessel	0.087	NA	0.11	0.07	0.013	0.038	0	0.003	0.07	0	NM	0.1
C-16	8 PZ	120	1440	O_2/CO_2	SSM; bubble vessel	0.91	NA	1.1	0	0.046	0.130	0	0.013	0.17	0	NM	0.0
C-28	8 PZ	110	1440	O_2/CO_2	SSM; bubble vessel, new thermal reactor	1.02	NA	1.63	0	0.021	0.06	0	0.005	0	0	NM	0.0
C-29	8 PZ	125	1440	O_2/CO_2	SSM; bubble vessel, new thermal reactor	0.89	NA	3.64	0	0.061	0.22	0	0.02	0.36	0	NM	0.0
C-22	7 MDEA/	90	1440	O_2/CO_2	SSM; bubble vessel	3.2	1.6	0.79	1.23	0.2	0.41	0.22*	0	0	-	NM	0.39 ± 0.02

	2 PZ																
C-33	7 MDEA/ 2 PZ	90	1440	O_2/CO_2	SSM; bubble vessel; new thermal reactor	0.051	0.45	0.11	0.28	0.032	0.06	0.025	0	0	0.28	0	0.24 ± 0.01

[1] SSM: Stainless Steel Metals Mixture (0.4 mM Fe^{2+}, 0.1 mM Cr^{3+}, 0.05 mM Ni^{2+}); Inh A: 100 mM Inhibitor A
[2] Bracketed rates are measured after lag time.

Table E.1: Master Rate Table for All Cycling and Low-Gas Experiments (Continued)

Expt	Solvent (m)	T_{th} (°C)	Stir Rate (rpm)	Purge Gas	Other Conditions [1]	Alk Loss (mM/kg-solv*hr)	Loss Rate (mM/hr)		Generation Rate [2] (mM/hr)								
							MDEA	PZ	DEA	Formate	Total Formate	Bicine	Glycine	EDA	MAE	MEA	DEA+MAE
C-23	7 MDEA/ 2 PZ	100	1440	O_2/CO_2	SSM; bubble vessel	1.2	2.82	0.72	2.9	0.19	0.41	0.22		0	-	NM	0.18 ± 0.01
C-21	7 MDEA/ 2 PZ	120	1440	O_2/CO_2	SSM; bubble vessel	2.5	2.7	1.2	1.5 (4*)	0.22	0.50	0.14	0.005	0	-	NM	1.26 ± 0.11
C-30	7 MDEA/ 2 PZ	125	1440	O_2/CO_2	SSM; bubble vessel, new thermal reactor	4.7	5	2.19	?	0.36	0.86	0.39	0	0	2.41	NM	2.82 ± 0.16
C-34	7 MDEA/ 2 PZ	125	1440	O_2	SSM; bubble vessel, new thermal reactor (acid treat)	3.5	3.7	1.5	0	0.67	1.49	0.43	0	0	2.57	0	2.6 ± 0.23
C-25	7 MDEA	120	1440	O_2/CO_2	SSM; bubble vessel, new thermal reactor	4.4	5.1	NM	3.1	0.61	0.96	1.25	0.011	0	-	NM	2.6
C-26	7 MDEA	130	1440	O_2/CO_2	SSM; bubble vessel, new thermal reactor	3.67	15.6	NM	-	0.31	0.28	0.95	0	0	2.73	NM	3.2
C-27	7 MDEA	100	1440	O_2/CO_2	SSM; bubble vessel, new thermal reactor	1.88	3.16	NM	0	0.105	0.11	*0 (0.44)*	0	0	1.07	NM	0.0
C-20	7 MDEA	120	1440	O_2/CO_2	100 mM Formate; SSM; bubble vessel	1.08	3.96	NA	0.18	-0.4	-0.37	0.89	0.1	0	-	NM	0.2
C-24	7 MDEA	120	1440	O_2/CO_2	100 mM DEA; SSM; bubble vessel	2.7	0.99	NM	3.63	0.38	0.50	1	0.008	0	-	NM	3.1
C-31	6 MDEA/ 1 MAE	120	1440	O_2/CO_2	SSM; bubble vessel, new thermal reactor	3.4	2.73	NA	0	0.28	0.55	*0 (0.74)*	0	0	0.55	0.027	0.6
C-32	6 MDEA/ 1 DEA	90	1440	O_2/CO_2	SSM; bubble vessel, new thermal reactor	0.9	0.59	NA	0.155	0.016	0.04	0.17	0	0	0	0.0001	0.1
OD-6	7 DEA	55	1440	O_2/CO_2	Low-gas	3.9	NA	NA	-18.2	0.157	1.03	1.46	0.008	0	0	*4.73 (0)*	-15.6
OD-7	7 MAE	55	1440	O_2/CO_2	Low-gas	4.9	NA	NA	0	0.206	1.03	0	0	0	-20	*3.61*	-23.4

												(0.11)				*(0)*	
OD-8	7 MDEA	70	1440	O_2/CO_2	Low-gas (TOR)	0.37	0.12	NA	-	0.028	0.03	0.051	0	0	0.12	0	0.1
OD-9	7 MDEA/ 2 PZ	70	1440	O_2/CO_2	Low-gas (TOR)	0.17	0.166	0.065	0	0.032	0.08	0.0377	0	0	0.172	0	.2 +/- 0.005

[1] SSM: Stainless Steel Metals Mixture (0.4 mM Fe^{2+}, 0.1 mM Cr^{3+}, 0.05 mM Ni^{2+}); BR: DEFINITION; Inh A: 100 mM Inhibitor A
[2] Italicized text means ###, Bracketed rates are ###

References

Aaron D, C Tsouris (2005). “Separation of CO_2 From Flue Gas: A Review”, *Separation Science and Technology*, 40:1, 321 – 348.

Appl M, Wagner U, Henrici HJ, Kuessner K, Volkamer K, Fuerst E (1982). "Removal of CO_2 and/or H_2S and/or COS from Gases Containing These Constituents." BASF GmbH, Germany. US Patent 4,336,233.

Astarita, G, Savage D, Bisio A (1983). Gas Treating With Chemical Solvents, J. Wiley & Sons, New York, New York.

Bedell S, Worley CM, Darst K, Simmons K (2010). “Thermal and oxidative disproportionation in amine degradation-O_2 stoichiometry and mechanistic implication.” *International Journal of Greenhouse Gas Control*.

Blachly CH, Ravner H (1964). "The stabilization of monoethanolamine solutions for submarine carbon dioxide scrubbers." AD609888, NRL-6189; US Naval Research Laboratory: Washington D.C. U. S. Naval Research Laboratory: Washington D.C.

Blanskby SJ, Ellison GB, Bierbaum VM, and Kato S (2002). “Direct Evidence for Base-Mediated Decomposition of Alkyl Hydroperoxides (ROOH) in the Gas Phase.” *Journal of the American Chemical Society*, 124, 3196-3197.

Bottoms RR (1930). "Separating acid gases." Girdler Corporation, Louisville, KY. US Patent 1,783,901.

Chakma A, Meisen A (1988). “Identification of Methyl Diethanolamine Degradation Products by Gas Chromatography and Gas Chromatography-Mass Spectrometry”, *Journal of Chromatography,* 457, 287-297.

Chakma A, Meisen A (1997). "Methyl-diethanolamine degradation - Mechanism and kinetics." *Canadian Journal of Chemical Engineering*. **75** (5): 861-871.

Chakravarti S, Gupta A (2001). “Carbon Dioxide Recovery Plant”, Patent Appl. No. 09/774,031.

Critchfield J, Jenkins J (1999). “Evidence of MDEA degradation in tail gas treating units.” Petroleum Technology Quarterly, Spring, 1999.

Davis J (2009). “Thermal Degradation of Aqueous Amines Used for Carbon Dioxide Capture.” The University of Texas at Austin. Ph.D. Dissertation. 2009: 278.

Dawodu OF, Meisen A (1996). "Degradation of alkanolamine blends by carbon dioxide." *Canadian Journal of Chemical Engineering*. 74 (6): 960-966.

Dennis WH Jr., Hull LA, Rosenblatt, DH (1967). “Oxidation of Amines IV. Oxidative Fragmentation.” *Journal of Organic Chemistry*. 32 (12): 3783.

Energy Information Administration, US (2009). Downloaded February 2011 from: http://www.eia.gov/cneaf/coal/page/special/feature.html.

EPA Fact Sheet (2010). “Settlement Agreement to Address Greenhouse Gas Emissions From Electric Generating Units and Refineries Fact Sheet.” Downloaded May 2011 from: http://www.epa.gov/ttn/atw/nsps/electric/elecgenpg.html.

Fayette Power Plant Unit 3 (2008). E-mail communication to GT Rochelle, September 17, 2008. CO_2 and O_2 concentrations in LCRA's Fayette Power Plant Unit 3 for June, 2008.

Frailie P, Rochelle GT, Chen X, Xu Q, Nguyen T (2011). "Modeling energy performance of aqueous methyldiethanolamine/piperazine for CO_2 capture". Presented at Trondheim CO_2 Capture, Transport, and Storage Conference. Trondheim, NO. June 14-16, 2011.

Freeman, SA, Dugas R, Van Wagener, DH, Nguyen T, Rochelle, GT (2010). "Carbon dioxide capture by concentrated, aqueous piperazine." *International Journal of Greenhouse Gas Control*, 4 (2010) 119–124.

Freeman, SA (2011). "Thermal Degradation and Oxidation of Aqueous Piperazine for Carbon Dioxide." The University of Texas at Austin. Ph.D. Dissertation. 2011: 791.

Girdler Corporation (1950). "Carbon Dioxide Absorbents." Contract No. 50023. Girdler Corporation, Gas Processing Division: Louisville, KY.

Goff GS (2005). *Oxidative Degradation of Aqueous Monoethanolamine in CO_2 Capture Processes: Iron and Copper Catalysts, Inhibition, and O_2 Mass Transfer*. The University of Texas at Austin. Ph.D. Dissertation. 2005: 263.

Grigoryan SK (1983). "Reactions of Hydroperoxides with Amines and Aminoalcohols in Aqueous Solutions in the Presence and Absence of Metal Ions." Russian Chemical Reviews, 52 (6), Translated from *Uspekhi Khimii*, 52 936-952.

Hamborg ES, Versteeg GF (2009). "Dissociation Constants and Thermodynamic Properties of Amines and Alkanolamines from (293 to 353) K." *Journal of Chemical and Engineering Data*. 54 (4): 1318-1328.

Hilliard MD (2008). *A Predictive Thermodynamic Model for an Aqueous Blend of Potassium Carbonate, Piperazine, and Monoethanolamine for Carbon Dioxide Capture from Flue Gas*. The University of Texas at Austin. Ph.D. Dissertation. 2008: 1083.

Hofmeyer BG, Scholten HG, Lloyd WG (1956). Contamination and corrosion in monoethanolamine gas treating systems. National Meeting of the American Chemical Society. Dallas, TX.

Holland CD, Anthony RG (1979). Fundamentals of Chemical Reaction Engineering. Prentice-Hall, Inc., Edgewood Cliffs, New Jersey.

Holub PE, Critchfield JE, Su W-Y (1998). "Amine Degradation Chemistry in CO_2 Service". Presented at Laurence Reid Gas Conditioning Conference, Norman, OK.

Huning S, Baron W (1956). "Decomposition of Quaternary Ammonium Salts with Ethanolamine, I." Dissertation, Marburg University.

Kennard ML, Meisen A (1980). "Control DEA Degradation." Hydrocarbon Processing, Gas Processing Developments, April, 1980, 103-106.

Kim, CJ, Sartori, G (1984). "Kinetics and Mechanism of Diethanolamine Degradation in Aqueous Solutions Containing Carbon Dioxide", International Journal of Chemical Kinetics, Vol. 16, 1257-1266, 1984.

King (2011). Personal communication via telephone conversation. Dow Chemical, Freeport, Texas, May 2011.
Kvamsdal, H, Rochelle, G (2008). "Effects of the Temperature Bulge in CO_2 Absorption From Flue Gas by Aqueous Monoethanolamine", Ind. Eng. Chem. Res., 47 (3), 867-876, 2008.
Lawrence, SA (2004). Amine Synthesis, Properties and Applications. Cambridge University Press, Cambridge, UK.
Lepaumier H, Picq D, Carrette PL (2009). "Degradation study of new solvents for CO_2 capture in post-combustion, Energy Procedia, 1, 893-900, 2009.
Morrison RT, Boyd RN (1973). Organic Chemistry. 3rd Edition, Allyn and Bacon, Boston, MA.
National Institute of Standards and Technology (NIST) Library (2011). NIST/EPA/NIH NIST 11 Mass Spectral Library.
National Institute for Occupational Safety and Health, The (2011). OSHA Permissible Exposure Limits (PELs). Downloaded from website: http://www.cdc.gov/niosh/
Parsons AF (2000). An Introduction to Free Radical Chemistry. Blackwell Science, Oxford, UK.
Perry RH, Green DW (1997). Perry's Chemical Engineers' Handbook. New York, McGraw-Hill.
Polderman LD, Dillon CP, Steele AB (1955). "Why MEA Breaks Down in Gas-Treating Service." *The Oil and Gas Journal*, May 1955, p 180-183.
Polderman LD, Steele AB (1956). "Why Diethanolamine Breaks Down in gas-treating service." The Oil and Gas Journal, June 1956, p 206-214.
Ramezan M, Skone TJ, Res and Dev Solutions, LLC (2007). "Carbon Dioxide Capture From Existing Coal-Fired Power Plants." DOE/NETL-401/110907.
Rawlings JB, Ekerdt JG (2002). Chemical Reactor Analysis and Design. Nob Hill Publishing, LLC, Madison, WI.
Rochelle, GT, Bishnoi S, Chi S, Dang H, Santos J (2001). "Research Needs for CO_2 Capture from Flue Gas by Aqueous Absorption/Stripping." Final report for P.O. No. DE-AF26-99FT01029, US Dept. of Energy.
Rochelle GT et al. "CO_2 Capture by Aqueous Absorption, Fourth Quarterly Progress Report 2010." Luminant Carbon Management Program. The University of Texas at Austin. 2010.
Rochelle GT (2009). "Amine Scrubbing for CO_2 Capture." *Science*. 325 (5948): 1652-1654.
Rooney PC, DuPart MS, Bacon TR (1998). "Oxygen's role in alkanolamine degradation." *Hydrocarbon Processing*. **77** (7): 109-113.
Sexton AJ. "Amine Oxidation in CO_2 Capture Processes." The University of Texas at Austin. Ph.D. Dissertation. 2008: 262.
Skoog DA, West DM (1979). Analytical Chemistry. 3rd Edition, Holt, Rinehart and Winston, New York, New York.
Small, H (1989). Ion Chromatography. Plenum Press, New York.

Solomons G (1992). Organic Chemistry. 5th Edition, John Wiley & Sons, Inc., New York, New York.

Strazisar BR, Anderson RR, White CM (2003). "Degradation Pathways for Monoethanolamine in a CO_2 Capture Facility", Energy & Fuels, Vol. 17, 1034-1039.

Texas Commission on Environmental Quality (TCEQ) (2011). Texas Risk Reduction Program (TRRP), Screening Level Critieria, Total-soil-combined criteria, 0.5-acre release. Downloaded August 6, 2011 from: http://www.tceq.state.tx.us/.

Thermo Finnigan (2003). TSQ® Quantum Discovery Hardware Manual. Thermo Finnigan Corporation.

Vahidi M, Matin NS, Goharrokhi M, Jenab MH, Abdi MA, Najib SH (2009) "Correlation of CO_2 solubility in N-methyldiethanolamine + piperazine aqueous solutions using extended Debye–Hückel model." *J Chem Thermodynamics*, 41 (2009) 1272-1278.

Van Wagener D (2011). "Stripper modeling for CO_2 removal using monoethanolamine and piperazine solvents." The University of Texas at Austin. Ph.D. Dissertation.

White EH, Woodcock DJ, Patai S (Editor) (1968). "Cleavage of the carbon-nitrogen bond." Interscience Publishers, Surrey, England.

Willson GT (2009). Personal communication on May 19, 2009, Welch Hall, Austin, Texas.